Etude des mécanismes de la perception des visages à l'aide des enregistrements intracérébraux, de la stimulation électrique corticale et de la stimulation visuelle périodique

Jacques Jonas

UNIVERSITÉ DE LORRAINE

Mémoire d'Habilitation à Diriger des Recherches

Présenté et soutenu publiquement par

Jacques Jonas

Etude des mécanismes de la perception des visages à l'aide des enregistrements intracérébraux, de la stimulation électrique corticale et de la stimulation visuelle périodique

Le 26 Novembre 2020 à Nancy

Membres du jury

Rapporteurs	Frédérique Bonnet-Brilhault	PU-PH	Tours
	Nathalie George	DR CNRS	Paris
	Simon Thorpe	DR CNRS	Toulouse
Examinateurs	Pierre Burbaud	PU-PH	Bordeaux
	Bruno Chenuel	PU-PH	Nancy
	Louis Maillard	PU-PH	Nancy
	Bruno Rossion	DR CNRS	Nancy

Table des matières

Liste des abréviations

ATL : Anterior temporal lobe (lobe temporal antérieur)

BTLA : Basal Temporal Language Area (aire temporale basale du langage)

ECOG : Electro-corticographie

EEG : Electro-encéphalographie

iEEG : EEG intracrânien

FFA : Fusiform Face Area

FPVS : Fast Periodic Visual Stimulation (stimulation visuelle périodique rapide)

IRM : Imagerie par résonance magnétique

IRM fonctionnelle : Imagerie par résonance magnétique fonctionnelle

latFG : section latérale du gyrus fusiforme moyen

MNI : Montreal Neurological Institute

MVPA : Multi-Voxel Patern Analysis

OFA : Occipital Face Area

SEEG : Stéréo-électroencéphalographie

SSVEP : Steady-State Visual Evoked Potentials

TEP : Tomographie par émission de positons

VOTC : Ventral occipito-temporal cortex (cortex occipito-temporal ventral)

VWFA : Visual Word Form Area

Résumé

Ce mémoire présente une synthèse de mes activités cliniques, de recherche et pédagogiques, centrées sur la neurophysiologie clinique et fondamentale. La première partie est consacrée à mon parcours et curriculum vitae, jusqu'à ma nomination en 2017 en tant que MCU-PH de Physiologie à la faculté de médecine de Nancy et dans le service de Neurologie du CHRU de Nancy. La deuxième partie présente mes activités de recherche centrées sur l'exploration de mécanismes cérébraux de la reconnaissance visuelle des visages chez l'Homme. La reconnaissance des visages est une fonction essentielle pour la vie en société chez l'Homme, représente un défi pour le système visuel par sa complexité et par conséquent permet de servir de modèle pour la compréhension du système visuel de haut niveau dans sa globalité. Cette recherche se base en grande partie sur l'enregistrement de réponses électrophysiologiques du cortex visuel à l'aide d'une approche originale combinant d'une part les enregistrements intracérébraux réalisées chez des patients épileptiques (stéréo-électroencéphalographie ou SEEG) et d'un autre part sur une méthode présentation périodique des stimuli visuels (stimulation visuelle périodique rapide ou FPVS). Cette combinaison permet l'enregistrement de réponses objectives et quantifiables avec une très grande résolution spatiale. Cette recherche se base également sur les stimulations électriques intracérébrales réalisées pendant la SEEG qui permettent l'identification des régions critiques pour la reconnaissance des visages. Nous avons ainsi rapporté, à travers plusieurs études, une cartographie exhaustive des régions impliquées dans la reconnaissance des visages le long du cortex occipito-temporal ventral. Par rapport aux précédentes études et notamment en IRM fonctionnelle, cette cartographie a montré le caractère vaste et distribué de ces régions et a mis en lumière des régions méconnues comme le gyrus fusiforme antérieur droit. La troisième partie présenté mes activités pédagogiques notamment avec l'enseignement de neurophysiologie à la faculté de médecine de Nancy, ainsi que mes responsabilités administratives dans ce domaine. La quatrième partie est consacrée à la présentation de mes activités cliniques au sein de service de Neurologie, centrées sur le diagnostic et le traitement des patients atteints d'épilepsie, et notamment de mon activité de référence avec la prise en charge chirurgicale des épilepsies focales pharmaco-résistantes dans laquelle la SEEG joue un rôle crucial. Cette partie montre également les apports potentiels de notre recherche fondamentale pour la prise en charge chirurgicale des patients épileptiques : la réalisation de cartographies des différentes fonctions cérébrales à l'aide de réponses fiables et objectives par combinaison de la SEEG et de FPVS représente un outil prometteur afin de mieux prédire le devenir neuropsychologique de ces patients en post-opératoire. La cinquième partie est consacrée à la recherche de financement, avec les financements acquis et refusés. La sixième

partie est consacrée à mes activités d'encadrements de la recherche (master 2, thèse d'exercice, diplôme d'études spécialisées), avec une présentation détaillée de mon travail de co-encadrant d'une thèse d'Université, étudiant la contribution des structures temporales postérieures et antérieures dans les mécanismes de perception visuelle de haut et dans la mémoire sémantique, à l'aide de la SEEG-FPVS et des stimulations électriques intracérébrales. La septième partie liste mes contributions scientifiques (articles, chapitres de livre, présentations orales). Enfin, la dernière partie envisage les perspectives de recherche à court, moyen et long terme. A très long terme, ces recherches viseront à obtenir une vision globale du système, notamment par des cartographies réalisées à travers toutes les bandes de fréquences (réponses électrophysiologiques de basses et hautes fréquences) et par l'étude des réponses à tous les niveaux d'enregistrements dont nous disposons (neurone unique, population de neurones, réseau de neurones, EEG de surface). Nous espérons que ces travaux apporteront des informations essentielles afin de mieux comprendre les aspects mécanistiques du système visuel de haut niveau.

Chapitre 1 : Parcours et Curriculum Vitae

1.1 Mon parcours en quelques mots

J'ai fait mes études de médecine à la Faculté de Médecine de Strasbourg (1998-2005). Durant mes études, j'ai été initié à la recherche par l'acquisition d'une Maitrise de Sciences Biologiques et Médicales, l'équivalent du Master 1 actuel. Pour mon internat, j'ai choisi la spécialité neurologie et la faculté de Médecine de Nancy. Ma formation à la neurophysiologie et à la recherche a débuté réellement lors d'un stage d'internat dans l'unité d'épileptologie du service de Neurologie du CHRU de Nancy en 2007 (Pr Louis Maillard). J'y ai grandement apprécié l'intérêt de cette équipe pour la recherche clinique et fondamentale (équipe ESPACE du CRAN). J'ai été aussi fasciné par le potentiel incroyable de la stéréo-électroencéphalographie (SEEG) pour la compréhension des grandes fonctions cognitives. J'y ai effectué un travail de recherche clinique sur l'effet de l'hyperventilation à déclencher des crises d'épilepsie et cela m'a familiarisé avec les travaux de publications (Jonas et al., 2011, *Journal of Neurology, Neurosurgery, and Psychiatry*). J'ai ensuite réalisé un Master 2 de Neurosciences Cognitives (dans le cadre de l'année-recherche, 2009-2010) à l'Université Aix-Marseille avec un stage de recherche dans l'Unité INSERM U751 du Pr Patrick Chauvel. Dans cette unité, j'ai été initié à la recherche sur les mécanismes de la perception visuelle des visages à l'aide de l'électro-encéphalographie (EEG) et de le SEEG. De retour à Nancy, j'ai eu la chance de poursuivre mon travail sur la perception des visages dans le cadre de ma thèse de médecine, par l'étude de 2 patientes dont la stimulation électrique en SEEG avait provoqué une incapacité transitoire à reconnaître les visages (patientes KV et CD). Afin d'approfondir l'étude de ces 2 cas, nous avions été amenés à contacter Bruno Rossion, chercheur internationalement reconnu pour ses travaux en électrophysiologie appliqués à la perception des visages (Université Catholique de Louvain, Belgique). Cela a été le début d'une fructueuse collaboration. J'ai défendu ma thèse de médecine en 2011.

J'ai ensuite fait mon clinicat dans l'unité d'épileptologie du Pr Louis Maillard (2011-2013) durant lequel j'ai débuté une thèse d'Université en neurosciences sur le thème des bases neurophysiologiques de la perception des visages à l'aide des enregistrements intracérébraux chez les patients épileptiques. Cette thèse s'est organisée en cotutelle entre l'Université de Lorraine (CRAN, Pr Louis Maillard) et l'Université Catholique de Louvain (Institute of Neuroscience et Institute of Psychological Research, Bruno Rossion). Après la fin de mon clinicat, j'ai poursuivi cette thèse par une mobilité de 4 ans dans le laboratoire de Bruno Rossion à l'Université Catholique de Louvain (financée par une bourse de recherche neuroscience belge du Fonds de la Recherche Scientifique - FNRS d'une durée de 4 ans). L'originalité de ces travaux de recherche est de réunir deux éléments novateurs : d'une part

les enregistrements intracérébraux (domaine d'expertise du Pr Louis Maillard et du CRAN, UMR 7039 CNRS-Université de Lorraine) et d'autre part la stimulation visuelle périodique rapide ou FPVS pour fast periodic visual stimulation (domaine d'expertise de Bruno Rossion et de son laboratoire). Ces activités de recherche ont été marquées par la publication de travaux dans des revues internationales (Jonas et al., *Neuroscience*, 2012 ; Jonas et al., *Human Brain Mapping*, 2014 ; Jonas et al., *Neurology*, 2014 ; Jonas et al., *Neuroimage*, 2014 ; Jonas et al., *Cortex*, 2015 ; Jonas et al., *PNAS*, 2016) mais aussi par la réalisation de plusieurs communications orales dans des congrès internationaux (USA et UK) qui ont permis de faire découvrir nos travaux sur le plan international. Cette thèse d'Université a été soutenue avec succès le 4 juillet 2016.

En septembre 2017, j'ai été nommé Maître de Conférences – Praticien Hospitalier section Physiologie (44.02) à l'Université de Lorraine (Faculté de Médecine) et au CHRU de Nancy (service de Neurologie). Sur le plan de l'enseignement (département de Physiologie, Pr Bruno Chenuel), je participe à une grande partie des enseignements de Neurophysiologie fondamentale et clinique pour les FGSM3 (cours magistraux et travaux pratiques dématérialisés). Sur le plan de la clinique, mon activité est partagée entre la prise en charge des patients épileptiques au sein de l'Unité d'Epileptologie du service de Neurologie (Centre de Référence des Epilepsies Rares, Pr Louis Maillard) et l'interprétation EEG et des potentiels évoqués au sein des Explorations Fonctionnelles Neurologiques. Sur le plan de la recherche, je poursuis mes travaux de recherche sur la neurophysiologie de la perception visuelle et plus particulièrement des visages au sein de l'Equipe Neurosciences des Systèmes et de la Cognition (CRAN UMR 7039 CNRS-Université de Lorraine) dirigée par Bruno Rossion (qui a rejoint Nancy en tant que Directeur de Recherche CNRS au sein du CRAN).

1.2 Curriculum Vitae

Etat Civil

-Mr Jacques Jonas

-Né le 13 Avril 1980

-Nationalité : française

-Adresse professionnelle : CRAN, Pavillon Krug, Hôpital Central, CHRU de Nancy

29, Avenue du Maréchal de Lattre de Tassigny, 54000 Nancy, France

-Courriel : j.jonas@chru-nancy.fr ; jacques.jonas@univ-lorraine.fr

-Tel. professionnel : 03 83 85 15 68

-Tél. portable : 06 98 41 42 13

Fonctions actuelles

-Depuis 2017 : Maître de Conférences des Universités – Praticien Hospitalier (Département de Physiologie, Faculté de Médecine de Nancy – Service de Neurologie, CHRU de Nancy)

-Depuis 2017 : Membre titulaire de l'équipe Neurosciences des Systèmes et de la Cognition (CRAN, UMR 7039, CNRS-Université de Lorraine)

Fonctions antérieures

-2016-2017 : Post-doctorant en Neurosciences (Université Catholique de Louvain)

-2012-2016 : Doctorant en Neurosciences (cotutelle Université Catholique de Louvain et Université de Lorraine)

-2010-2013 : Assistant des Hôpitaux – Chef de Clinique des Universités (Unité d'épileptologie, Service de Neurologie, CHU de Nancy et Faculté de Médecine de Nancy)

-2009-2010 : Etudiant en Master 2 Neurosciences (Unité INSERM U751, Marseille)

-2006-2011 : Interne de Neurologie des Hôpitaux de Nancy (CHU de Nancy)

Titres et diplômes

Titres hospitaliers

-2011-2013 : Chef de Clinique des Universités – Assistant des Hôpitaux

-2006-2011 : Interne des Hôpitaux de Nancy

Diplômes universitaires

-2016 : Doctorat d'Université en Sciences de la Vie et de la Santé (Université de Lorraine) et Sciences Médicales (Université Catholique de Louvain)

-2013 : DIU de Pédagogie Médicale (Université de Lorraine)

-2011 : Doctorat en Médecine, DES de Neurologie (Université de Lorraine)

-2011 : DIU d'Epileptologie (Université de Lorraine)

-2010 : Master 2 Neurosciences Cognitives et Intégratives (Aix-Marseille Université)

-2009 : DIU de Neurophysiologie Clinique (UV EEG et PE) (Université Lille II)

-2007 : Maîtrise de Sciences Biologiques et Médicales (Université de Lorraine)

-2005 : Diplôme de fin de 2ème cycle des études médicales (Université de Strasbourg)

Activités de Recherche

Publications *(liste au Chapitre 7)*

-34 publications internationales

-Points SIGAPS : 557

-Index H : 15 (730 citations selon Google Scholar)

Mobilités

-2013 – 2017 : Université Catholique de Louvain, Belgique (Pr Bruno Rossion) dans le cadre d'un doctorat en neurosciences (financement par une bourse de thèse neurosciences du FNRS)

-2009 – 2010 : unité INSERM U751 Epilepsie et Cognition, Université Aix-Marseille, (Pr Patrick Chauvel) dans le cadre du Master 2 Neurosciences (financement au titre de l'année-recherche)

Prix et récompenses

-Prix de la meilleure communication orale, 1ère journée interrégionale « Recherche et Neuroscience », Dijon (2013)

-Bourse pour une thèse en neurosciences pour une durée de 4 ans, Fonds de la Recherche Scientifique – FNRS, Belgique (2013)

-Elsevier/Vision Research Travel Award (VSS Student Travel Award), Vision Sciences Society, USA (2013)

-Prix Sciences et Techniques de l'Académie Nationale de Metz pour la thèse de Doctorat en Médecine (2012)

Activité d'enseignement

Cours

-Neurophysiologie fondamentale pour les étudiants en médecine (PACES et FGSM3)

-DIU d'Epileptologie

-DIU de Neurophysiologie Clinique

-DIU de Pédagogie Médicale

-Master 2 Recherche de Neuropsychologie Cognitive et Clinique, Université de Strasbourg

Pédagogie médicale

-Responsable de la commission de Docimologie (Faculté de Médecine)

-Référent docimologie pour la Neurologie à la Faculté de Médecine

Intérêt général

Responsabilités collectives

-Responsable médical de l'unité d'explorations fonctionnelles neurologiques du service de Neurologie du CHRU de Nancy

-Responsable de la commission de docimologie de la Faculté de Médecine de Nancy

-Membre du bureau de la Commission des Jeunes Epileptologues de la Ligue Française Contre l'Epilepsie (LFCE)

-Membre de Conseil Scientifique de la Fondation Française pour la Recherche sur l'Épilepsie (FFRE)

Sociétés savantes

-Membre de la « Society for Neuroscience » (SFN)

-Membre de la Société de Neurophysiologie Clinique de Langue Française (SNCLF)

-Membre de la Ligue Française Contre L'Épilepsie (LFCE)

-Membre de la Société de Physiologie

Activité éditoriale (relecture d'articles)

Journal of Neuroscience, Cerebral Cortex, Neuropsychologia, Neuroimage, Human Brain Mapping, Social Cognitive and Affective Neuroscience, Brain Structure and Function, Neurophysiologie Clinique / Clinical Neurophysiology, Brain and Behavior, Brain Research, Nature Communications

Chapitre 2 : Activités de Recherche

2.1. Introduction

Le visage joue un rôle crucial dans les interactions sociales. Le visage transmet une foule d'informations sur un individu, son identité, son âge, son genre, son état d'esprit, ses émotions, son origine ethnique, etc. Toutes ces informations contenues dans les visages sont extraites instantanément lorsque nous interagissons avec quelqu'un.

Parmi toutes ces informations, l'identité occupe une place à part. A l'opposé de la très grande majorité des autres espèces animales, l'Homme est un animal social qui vit au sein de structures sociales complexes dans lesquelles la détermination de l'identité de chaque individu est essentielle aux interactions entre ses membres, c'est-à-dire les caractéristiques qui font que chaque individu est différent de tous les autres, et semblable à lui-même, même à travers son évolution dans le temps. Chez l'Homme, il existe plusieurs moyens de déterminer l'identité d'un individu (le visage, le son de la voix, la démarche ou l'allure générale, les vêtements, etc.), mais le visage est de loin le moyen le plus efficace, pour deux raisons principales. Premièrement, au cours de l'évolution, le visage est devenu un signal qui code pour l'identité des individus notamment grâce à une variation phénotypique très élevée qui fait que chaque visage est unique (Sheehan et al., 2014). Deuxièmement, l'Homme est un expert en perception des visages, notamment par l'acquisition au fil de l'évolution d'un système cérébral de perception des visages extrêmement efficace, c'est-à-dire permettant la perception de l'identité de manière fiable, rapide, malgré la similitude visuelle entre les visages et les changements d'apparence visuelle qui s'opèrent dans un environnement naturel (orientation de la tête, taille relative, niveau d'éclairage, vision partielle, expression des émotions, etc.).

La perception[1] des visages repose sur un système extrêmement complexe, comme en témoigne son efficacité malgré la difficulté des fonctions qui lui sont assignées. Cette complexité explique que ce système occupe une grande partie de la voie visuelle ventrale et repose sur une vaste zone corticale s'étendant ventralement du lobe occipital au lobe temporal antérieur (VOTC pour « ventral occipito-temporal cortex ») avec une prédominance droite. La compréhension des mécanismes cérébraux de la perception des visages est un enjeu essentiel pour les neurosciences, notamment par sa complexité, son importance dans la vie

[1] Dans ce document, il n'y a pas de distinction entre perception et mémoire. De notre point de vue, il n'y a pas de perception sans mémoire et la mémoire est présente à toutes étapes du processus de perception.

sociale de l'Homme et par sa vocation à être un modèle pour la compréhension de l'ensemble des fonctions de perception visuelle.

2.2 Méthodologie

Notre approche pour mieux comprendre les mécanismes cérébraux de la perception des visages est basée sur une méthodologie originale, dont la clé de voûte est la SEEG (Bancaud et Talairach, 1973). La SEEG correspond à l'implantation d'électrodes profondes chez des patients épileptiques en bilan pré-chirurgical de leur épilepsie, permettant des enregistrements intracérébraux d'une grande précision spatiale, tout le long du VOTC (Figure 1A). Ces électrodes se composent d'une rangée de sites d'enregistrements indépendants distribués le long de l'électrode, appelés contacts, permettant l'enregistrement de toutes les structures cérébrales traversées par l'électrode, du point de pénétration dans le cerveau, jusqu'à la cible profonde de l'électrode (cortex latéral et structures internes, sillons et gyri). La SEEG fait partie des techniques d'EEG intracrâniens (iEEG) avec l'électro-corticographie ou ECOG (implantation d'électrodes sur la surface corticale avec retrait du crâne, ne permettant pas l'enregistrement des structures profondes et des sillons).

Le premier axe de notre méthodologie originale consiste en la combinaison de la SEEG et d'une méthode particulière de présentation des stimuli visuels (Figure 1B), appelée FPVS, dans laquelle les stimuli visuels sont présentés de manière périodique, c'est-à-dire à une fréquence fixe. Cette méthode est connue depuis longtemps sous le nom de steady-state visuel evoked potential ou SSVEP (Adrian et Matthews, 1934 ; Regan, 1966) avec l'utilisation de stimuli visuels simples. L'originalité de notre approche est nous avons appliqué la SSVEP à l'étude de la vision de haut niveau (Rossion, 2014). Le principe de la FPVS est la suivante : la présentation de stimuli à une fréquence fixe et rapide génère une réponse EEG périodique à la même fréquence dans les régions cérébrales impliquées dans la perception de ces stimuli. Les réponses sont ensuite identifiées, non pas le domaine temporel, mais dans le domaine fréquentiel (des stimuli présentés à 6 Hz, c'est-à-dire à 6 images par sonde, génèrent une réponse électrophysiologique à 6 Hz dans le cortex visuel, qui sera identifiée à 6Hz dans le domaine fréquentiel après transformation de Fourier du signal électrophysiologique). Les avantages de cette méthode sont : (1) l'enregistrement de réponses avec un très haut rapport signal/bruit (les réponses d'intérêt sont concentrées sur une fréquence alors que le bruit est réparti sur tout le spectre fréquentiel) ; (2) son objectivité (les réponses sont identifiées à la fréquence d'intérêt déterminée par l'expérimentateur et donc connue a priori) ; (3) sa faible sensibilité aux artéfacts (les réponses d'intérêt sont concentrées sur une fréquence donnée alors que les artéfacts sont répartis sur une bande fréquentielle plus large et ont peu de chance de se concentrer spécifiquement sur la fréquence d'intérêt) ; et (4) l'enregistrement de

réponses facilement quantifiables, notamment grâce à l'objectivité et au haut rapport signal/bruit des réponses obtenues (en pratique il s'agit de sommer l'amplitude mesurée dans le spectre fréquentiel sur la fréquence d'intérêt et ses harmoniques).

Les avantages de la combinaison de la SEEG et de la FPVS ont été explicités dans un article de revue récent rédigé par notre équipe (Rossion, Jacques, et Jonas, in press, *Ann N Y Acad Sci*).

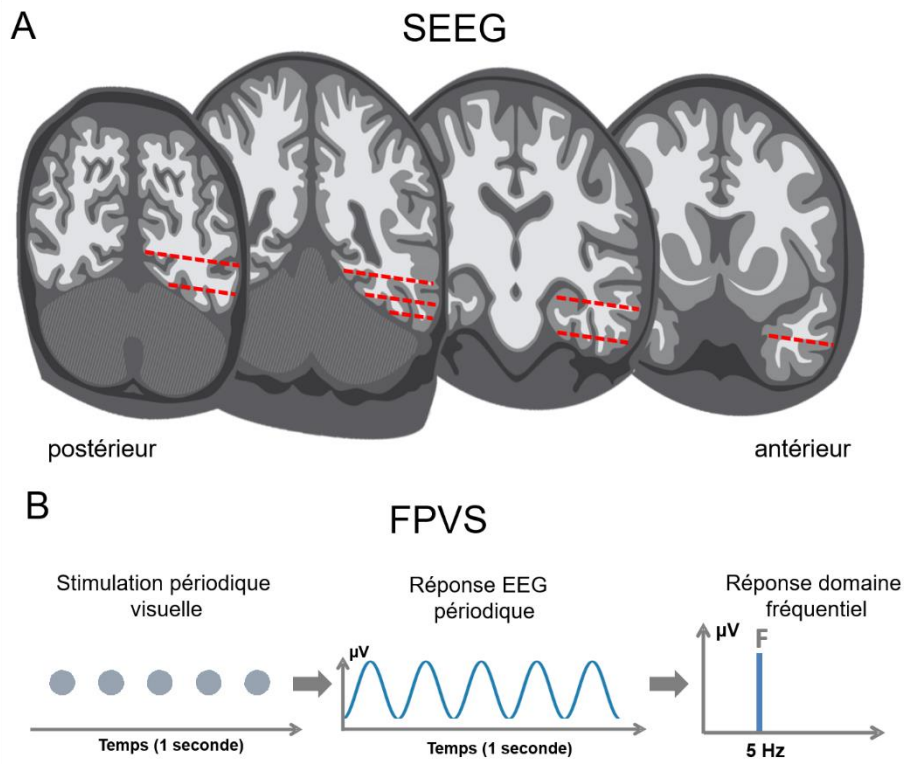

Figure 1. Combinaison de la SEEG et de la FPVS. A. Représentation schématique de la position des électrodes de SEEG le long du VOTC. Les électrodes (en rouge) sont composées de sites d'enregistrement indépendants distribués tout le long de l'électrode, appelés contacts, et représentés par les rectangles rouges. B. Principe de la FPVS. La présentation visuelle périodique d'un stimulus à 5 Hz va produire une réponse EEG à 5 Hz qui va être identifiée dans le domaine fréquentiel à la même fréquence que la fréquence de stimulation.

Le deuxième axe de notre méthodologie est l'utilisation de stimulations électriques corticales lors de la SEEG (Jonas, 2018). Il s'agit de délivrer un faible courant électrique entre 2 contacts d'une électrode intracérébrale afin de désorganiser temporairement la fonction de la région cérébrale stimulée. Les conséquences de cette stimulation sont visibles directement sur le patient. Les stimulations électriques sont couramment utilisées en clinique afin de réaliser une cartographie fonctionnelle avant chirurgie de l'épilepsie. L'hypothèse couramment admise est que la stimulation électrique détecte les régions critiques (ou essentielles) pour une fonction et qui par conséquent doivent être épargnées durant la résection chirurgicale (par

exemple, si la stimulation provoque un trouble du langage, c'est que la résection de cette région peut également entraîner un trouble du langage). Notre originalité est d'avoir appliqué cette méthode à l'étude de la perception des visages afin de déterminer les régions critiques (ou essentielles) pour cette fonction.

2.3 Cartographie des réponses sélectives aux visages

Notre premier axe de recherche concerne l'étude des bases neurales de la perception des visages. La détermination des bases neurales de la perception des visages est un prérequis essentiel à la compréhension des mécanismes de perception des visages. Les recherches dans ce domaine ont débuté il y a plusieurs décennies mais les résultats de ces études restent encore incomplets. L'imagerie structurelle des patients prosopagnosiques (patients incapables de reconnaître les personnes à partir de leur visage suite à une lésion cérébrale) a montré l'importance d'un vaste territoire au sein du VOTC, du lobe occipital jusqu'au lobe temporal antérieur, avec une prédominance droite (Barton et al., 2008 ; Bodamer, 1947 ; Bouvier et Engel, 2006 ; Busigny et al., 2014 ; Damasio et al., 2002 ; Rossion et al., 2003). Les études d'imagerie par résonnance magnétique (IRM) fonctionnelle chez des sujets sains et les études iEEG chez les patients épileptiques s'appuient sur l'enregistrement des réponses sélectives aux visages (plus amples pour les visages par rapport autres aux objets visuels) pour déterminer les régions impliquées dans la perception des visages. L'IRM fonctionnelle a mis en évidence des réponses sélectives aux visages regroupées dans des régions circonscrites du VOTC (organisation en « clusters » des réponses sélectives aux visages). Les 2 aires les plus connues sont l'OFA dans le gyrus occipital inférieur droit (« Occipital Face Area » ; Gauthier et al., 2000) et la FFA dans la section latérale du gyrus fusiforme moyen (« Fusiforme Face Area » ; Kanwisher et al., 1997). Ces réponses ont été principalement enregistrées dans la partie postérieure du VOTC (Weiner et Grill-Spector, 2010), comme l'OFA et la FFA, car l'IRM fonctionnelle est limitée dans sa capacité à étudier le lobe temporal antérieur en raison d'artéfacts de susceptibilité magnétique (notamment liés au canal auditif) qui réduisent le signal dans les parties antérieures du lobe temporal (« signal drop-out » ; Axelrod et Yovel, 2013). Les études iEEG réalisées chez les patients épileptiques sont une opportunité unique d'enregistrer l'activité neuronale directe avec un très haut rapport signal/bruit, du lobe occipital jusqu'au lobe temporal antérieur. Au contraire des études IRM fonctionnelle, les études iEEG ont enregistré des réponses sélectives aux visages de manière dispersée dans le VOTC, sans organisation en « clusters » (Allison et al., 1999 ; Davidesco et al., 2014, Engell et McCarthy, 2011, Jacques et al., 2016 ; Rangarajan et al., 2014, Sato et al., 2014 ; Tanji et al., 2012 ; Vidal et al., 2010). L'obstacle majeur de ces études iEEG a été le manque d'objectivité pour la définition des réponses sélectives aux visages, ce qui a limité leur quantification. En effet, les réponses sélectives aux visages ont pu être enregistrées dans

différentes fenêtres temporelles et dans différentes fenêtres fréquentielles (en basses fréquences ou potentiels évoqués et en hautes fréquences ou activité gamma).

Afin de rapporter une cartographie et une quantification globale des réponses sélectives aux visages à travers tout le VOTC, du lobe occipital au lobe temporal antérieur, nous avons utilisé la combinaison de la SEEG et de la FPVS chez 28 patients (Jonas et al, 2016, *PNAS*). Cette étude a été réalisée alors que j'étais affecté au laboratoire de Bruno Rossion à l'Université Catholique de Louvain et a été effectuée en proche collaboration avec un post-doctorant du laboratoire, Corentin Jacques (co-premier auteur de l'article) et avec Louis Maillard (CRAN, CHRU de Nancy). Nous avons utilisé un paradigme FPVS dit « face-localizer » construit afin d'identifier des réponses sélectives aux visages (Rossion et al., 2015). Pendant l'enregistrement SEEG, les patients ont visualisé des séquences FPVS d'images d'objets variables (visages, chaises, fruits, chiens, lampes, etc.) présentées à une fréquence fixe et rapide (6 Hz c'est-à-dire 6 images par seconde). Au sein des séquences, un visage était présenté toutes les 5 images (Figure 2A). La fréquence des visages a donc été fixée à 1,2 Hz (6 Hz/5). L'analyse du signal SEEG a été réalisée dans le domaine fréquentiel. Les réponses sélectives aux visages ont été identifiées et quantifiées dans le domaine fréquentiel à la fréquence de 1, 2 Hz et aux différentes harmoniques (voir Figure 2B pour un exemple chez un patient).

Nous donc rapporté une cartographie globale des réponses sélectives aux visages sur tout le VOTC (Figure 2C). Nous avons fait les observations suivantes. Premièrement, les réponses sélectives aux visages les plus amples se localisent dans une région précise, la section latérale du gyrus fusiforme moyen droit (latFG), ce qui valide par enregistrement neuronal direct 2 décennies d'études IRM fonctionnelle (qui retrouvent des réponses sélectives maximales dans cette région, correspondant à la FFA droite ; Kanwisher et al., 1997 ; Rossion et al., 2012). Les autres régions très sélectives aux visages sont le gyrus occipital inférieur droit et le gyrus fusiforme antérieur droit. Deuxièmement, nous avons retrouvé à la fois une répartition spatiale vaste et distribuée des réponses sélectives aux visages dans tout le VOTC et un regroupement spatial des réponses les plus amples en amas (ou « clusters ») dans certaines régions circonscrites (comme le gyrus fusiforme ou le gyrus occipital inférieur). Cela montre que le réseau de perception des visages est très vaste (ce grand espace cérébral est probablement nécessaire pour que l'identification du visage soit réalisée avec une telle efficacité) et que ce réseau repose également sur des nœuds critiques bien localisés, identifiés par ces « clusters » de réponses. Enfin, nous avons rapporté une cartographie précise des régions anatomiques sélectives aux visages dans le lobe temporal antérieur ou ATL pour « Anterior Temporal Lobe » (sillon collatéral antérieur, gyrus fusiforme antérieur, sillon occipito-temporal antérieur), dont l'étude est très limitée en IRM fonctionnelle

pour des raisons méthodologiques. En particulier, le gyrus fusiforme antérieur et sillon occipito-temporal antérieur n'ont pratiquement jamais été décrits comme étant sélectifs aux visages dans les études d'IRM fonctionnelle.

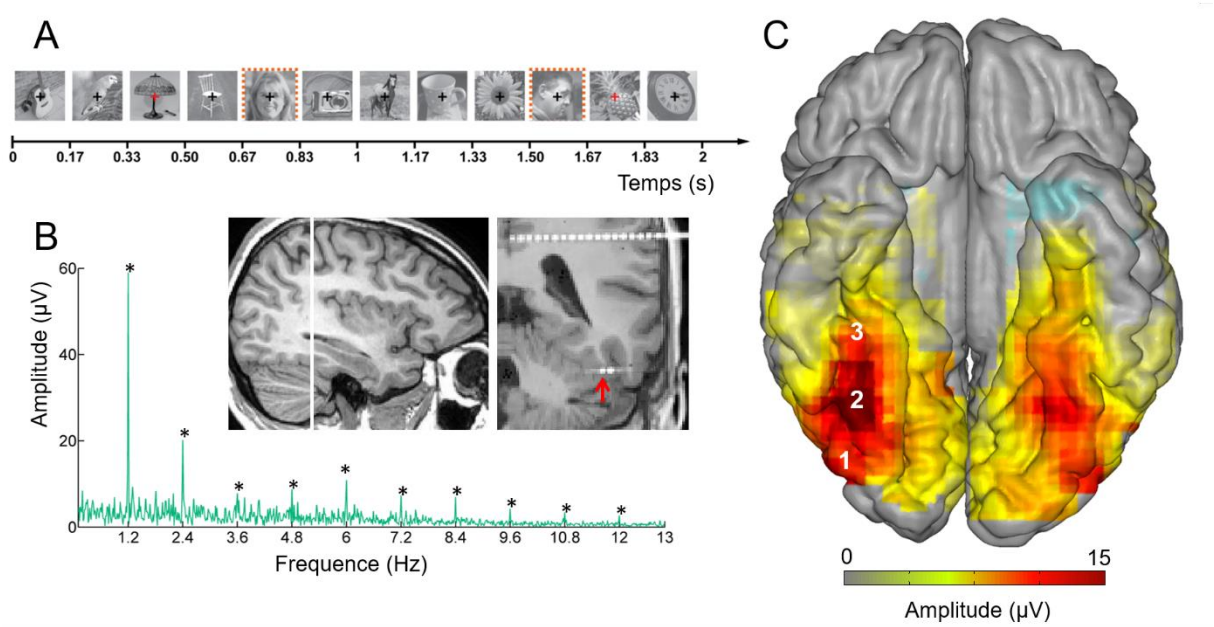

Figure 2. Réponses sélectives aux visages enregistrées en SEEG dans le VOTC (Jonas et al., 2016, *PNAS*). A. Paradigme FPVS dit « face-localizer » ou de « sélectivité aux visages » pour l'enregistrement de réponses sélectives aux visages. Des images d'objets sont présentées à une fréquence 6 Hz (6 objets par seconde) avec une image de visage insérée toutes les 5 images. B. Exemple de réponse sélective aux visages dans le domaine fréquentiel enregistrée dans le latFG droit chez un patient (contact d'enregistrement indiqué par une flèche rouge). Les réponses à 1.2 Hz et harmoniques (2.4, 3.6, 4.8 Hz, etc.) correspondent aux réponses sélectives aux visages (sauf les réponses à 6 Hz et 12 Hz qui correspondent à la fréquence de stimulation de base). C. Cartographie des réponses sélectives aux visages à travers les 28 patients et représentée dans l'espace MNI (Montreal Neurological Institute). Les réponses sélectives aux visages sont quantifiées sur chaque contact (somme de l'amplitude aux différentes harmoniques) et projetées sur la surface corticale. Les chiffres indiquent la localisation des régions anatomiques avec les réponses sélectives aux visages les plus amples (1 : gyrus occipital inférieur ; 2 : latFG ; 3 : gyrus fusiforme antérieur).

2.4 Traitement de l'individuation des visages

L'une des grandes fonctions de la voie visuelle ventrale est de déterminer l'identité des visages. L'une des étapes cruciales de ce processus est de déterminer quelles sont les caractéristiques visuelles propres du visage d'une personne donnée, en l'absence d'informations sémantiques (individuation des visages). Les bases neurales de ce processus restent pour l'instant débattues, notamment parce que les études en IRM fonctionnelle montrent des résultats discordants, avec notamment 2 techniques différentes en IRM

fonctionnelle, adaptation et MVPA (Multi-Voxel Patern Analysis), qui mettent en évidence des régions différentes (adaptation : Gauthier et al., 2000; Schiltz et Rossion, 2006; Ewbank et al., 2013 ; MVPA : Kriegeskorte et al., 2007; Natu et al., 2010; Nestor et al., 2011; Anzellotti et al, 2014; Goesaert and Op de Beeck, 2013). Notre objectif est de rapporter une cartographie complète des régions impliquées dans l'individuation des visages à l'aide de la combinaison SEEG-FPVS. Cette étude, que j'ai coordonnée, a été réalisée en collaboration avec Bruno Rossion, Louis Maillard et Corentin Jacques (Université Catholique de Louvain). Cette étude fait l'objet d'une publication et dont je suis le dernier auteur (Jacques, (….), Jonas, in press, *Neuroimage*). Nous avons inclus 69 patients implantés en SEEG et utilisé un paradigme FPVS permettant d'identifier les régions impliquées dans l'individuation des visages (Liu-Shuang et al., 2014). Dans ce paradigme (Figure 3A), un visage inconnu de la même identité est présenté à 6 Hz et un visage d'une identité différente est présenté toutes les 5 images, de sorte que la fréquence du changement d'identité a été fixée à 1.2 Hz (6 Hz/5). Nous avons 2 conditions, avec des séquences dont l'ensemble des visages sont à l'endroit et des séquences avec l'ensemble de visages à l'envers. La sensibilité à l'individuation des visages est mesurée à cette fréquence et aux différentes harmoniques dans le domaine fréquentiel (voir la Figure 3B pour un exemple de réponse sur un contact individuel).

Nous avons montré qu'une bande de cortex à droite, comprenant le gyrus occipital inférieur, le latFG et le gyrus fusiforme antérieur joue un rôle très important dans le traitement de l'identité. En effet, ces régions montraient des réponses d'individuation plus amples et plus fréquentes pour les visages à l'endroit par rapport aux visages à l'envers (Figure 3C). Cette étude montre qu'une partie de l'ATL (le gyrus fusiforme antérieur droit), joue un rôle dans l'individuation des visages, de manière indépendante de la mémoire sémantique, ce qui est conforme à nos observations précédentes (Jonas et al., 2015, *Cortex* ; patient DN, voir paragraphe 6.4.1). De manière surprenante, malgré un échantillonnage très important des régions plus antérieures dans l'ATL (notamment dans le pôle temporal), nous n'avons enregistré que très peu de réponses dans ces régions. Cela suppose que ces régions ne jouent pas un rôle dans l'individuation des visages mais plutôt dans la mémoire sémantique, ce qui en accord avec les travaux d'Angélique Volfart (dont je co-dirige les travaux de thèse) sur les performances neuropsychologiques en perception des visages des patients avec une épilepsie temporo-mésiale (étude ATENA-F, Volfart, Jonas, et al., in press, *Neuropsychologia*, voir paragraphe 6.4.1) et sur les bases neurales de l'intégration visages-noms (Volfart, Jonas, et al., 2020, *Plos Biology*, voir paragraphe 6.4.1).

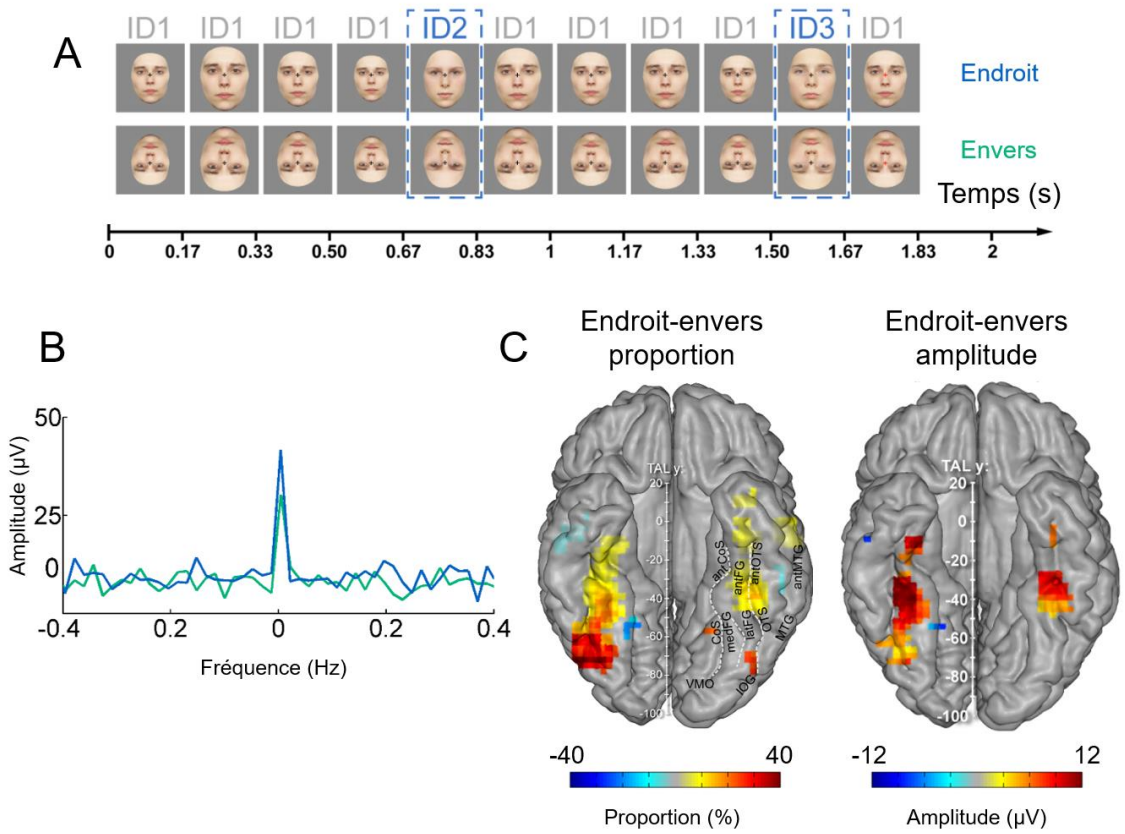

Figure 3. Réponses d'individuation des visages. A. Paradigme FPVS pour l'enregistrement de réponses d'individuation des visages. Des visages inconnus d'une identité donnée (ID1) sont présentés à une fréquence 6 Hz (6 objets par seconde) avec un visage d'identité différente (ID2, ID3, etc.) inséré toutes les 5 images**.** B. Exemple d'un contact chez un patient dans le gyrus occipital inférieur droit enregistrant une réponse d'individuation des visages, plus ample à l'endroit qu'à l'envers. La fréquence du changement d'identité est à 0 Hz (somme des réponses à 1.2 Hz et harmoniques centrée sur 0). C. Cartographies des réponses d'individuation des visages plus amples à l'endroit qu'à l'envers, à travers les 37 patients inclus dans l'étude, représentées dans l'espace Talairach. A gauche, cartographie des régions montrant une proportion de réponses à l'endroit plus importante que la proportion de réponses à l'envers, sur l'ensemble des contacts enregistrés (en jaune-rouge). A droite, cartographie des régions montrant des réponses plus amples à l'endroit qu'à l'envers (en jaune-rouge).

2.5 Relation entre la perception des visages et les autres catégories visuelles

Le VOTC n'est pas exclusif à la perception des visages et il joue également un rôle dans la perception des autres catégories visuelles (mots, objets, espaces extérieurs, etc.). Une question importante est de savoir quelle est la relation spatiale et fonctionnelle entre ces différents systèmes et notamment s'ils partagent certaines fonctions. Nous avons réalisé une étude SEEG-FPVS enregistrant les réponses sélectives aux visages et aux maisons (espaces visuels extérieurs) chez 78 patients en SEEG (Hagen, (….), Jonas, 2020, *Cereb Cortex*). Cette étude, que j'ai coordonnée et dont je suis le dernier auteur, a été réalisée en collaboration

avec Simen Hagen (post-doctorant au sein de l'équipe Neurosciences des Systèmes et de la Cognition du CRAN), Bruno Rossion, et Louis Maillard.

Pour cela nous avons testé les patients avec le paradigme dit « face-localizer » (Jonas et al., 2016, *PNAS*) et une autre version de ce paradigme dans lequel les visages sont remplacés par des maisons, ce qui permet d'enregistrer des réponses sélectives aux maisons, c'est-à-dire plus amples pour les maisons par rapport aux objets (Figure 4A). Nous avons enregistré des réponses sélectives aux visages (Figure 4B) de manière similaire à l'étude précédente (Jonas et al., 2016, *PNAS*), c'est-à-dire avec des réponses surtout dans le gyrus occipital inférieur, le latFG et le gyrus fusiforme antérieur avec une prédominance droite (Figure 4C). Les réponses sélectives aux maisons (Figure 4B) ont été enregistrées dans des régions plus médiales (Figure 4C), c'est-à-dire dans le gyrus fusiforme médial, le sillon collatéral, et le gyrus parahippocampique, comme cela a déjà été rapporté en IRM fonctionnelle ou en iEEG dans la partie postérieure du VOTC (Weiner and Grill-Spector 2010 ; Spiridon et al. 2006 ; Nasr et al. 2011 ; Tootell et al. 2008 ; Gomez et al. 2015 ; Kadipasaoglu et al. 2016). Cette confirmation des études précédentes montre bien que les réponses périodiques enregistrées par la FPVS reflètent des processus physiologiques, spécifiques de la fonction étudiée et non pas des processus aspécifiques de détection d'évènements rares dans une séquence ou de détection d'évènements périodiques. L'originalité de ce travail repose sur plusieurs points. Premièrement, nous avons montré que cette dissociation spatiale (réponses sélectives aux maisons plus médiales que les réponses aux visages) persiste même en avant dans l'ATL, zone dont l'étude est très limitée en IRM fonctionnelle (Figure 4C). Deuxièmement, nous avons montré que ces 2 réponses, sélectives aux visages et aux maisons, ne sont pas corrélées en amplitude. Ces 2 résultats montrent que ces 2 systèmes de perception sont spatialement et fonctionnellement dissociés tout le long du VOTC, même en avant dans l'ATL. Enfin nous avons montré que dans le lobe temporal antérieur, le nombre de réponses sélectives aux visages surclasse largement le nombre de réponses sélectives aux maisons (Figure 4C, cartographies en proportion), probablement en raison de la richesse sémantique liée aux visages et du rôle de l'ATL dans la mémoire sémantique (voir Volfart, Jonas, et al., 2020, *Plos Biology*).

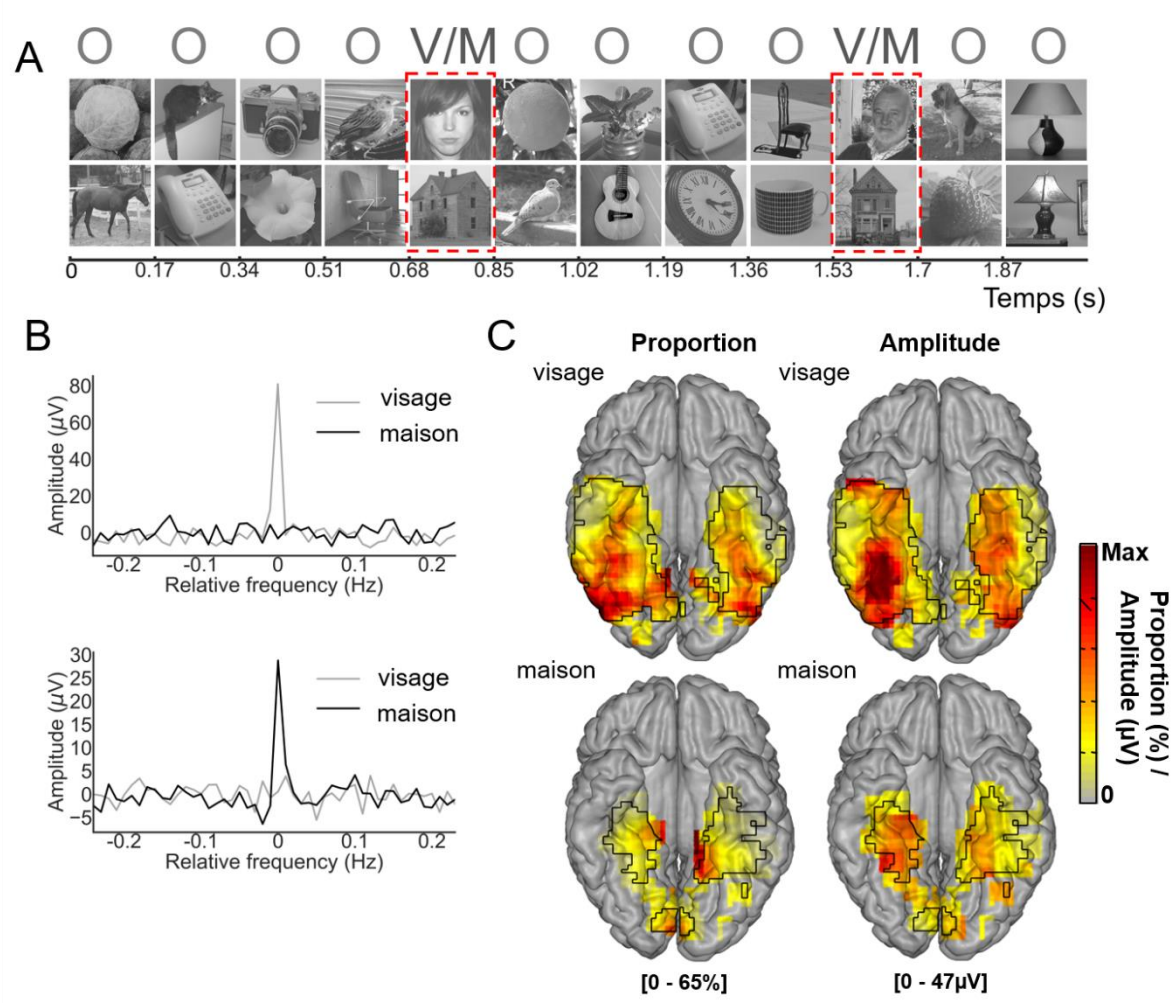

Figure 4. Réponses sélectives aux visages et aux maisons enregistrées en SEEG dans le VOTC (Hagen et al., 2020, *Cereb Cortex*). A. Paradigme FPVS pour l'enregistrement de réponses sélectives aux visages et aux maisons. Des images d'objets sont présentées à une fréquence 6 Hz (6 objets par seconde) avec une image de visage ou de maison insérée tous les 5 images. B. Exemple de réponse sélective aux visages dans le domaine fréquentiel enregistrée dans le latFG droit chez un patient (en haut), et de réponse sélective aux maisons dans le gyrus parahippocampique antérieur droit chez un autre patient (en bas). La fréquence sélective aux visages et aux maisons est à 0 Hz (somme des réponses à 1.2 Hz et harmoniques centrée sur 0). C. Cartographies des réponses sélectives aux visages et aux maisons à travers les 78 patients et représentées dans l'espace Talairach, en proportion (nombre de contacts avec réponses sélectives sur nombre de contacts enregistrés) et amplitude (réponses sélectives quantifiées et projetées sur la surface corticale). Noter la dissociation spatiale entre les réponses sélectives aux visages (latérales) et les réponses sélectives aux maisons (médiales), tout le long du VOTC jusqu'à l'ATL.

2.6 Cartographie des régions critiques pour la perception des visages

Au-delà de l'enregistrement de réponses sélectives aux visages dans des régions cérébrales spécifiques, une question cruciale est de savoir lesquelles jouent un rôle causal (ou critique) dans la perception des visages. La désorganisation de la fonction d'une aire avec un rôle causal entraîne immédiatement des conséquences sur la perception des visages, qui peuvent être rapportées par le sujet ou évaluées par des tests neuropsychologiques. A l'inverse, une région sélective aux visages sans rôle causal peut être désorganisée sans conséquence directe sur la fonction (ce qui ne sous-entend pas qu'elle joue aucun rôle).

Les études de cas de prosopagnosie ont montré que les régions impliquées de manière causale dans la perception des visages sont localisées dans le VOTC, avec une prédominance droite. En effet, suite à des lésions dans le VOTC, ces patients sont devenus incapables de reconnaître les visages (Barton et al., 2008 ; Bodamer, 1947 ; Bouvier et Engel, 2006 ; Busigny et al., 2014 ; Damasio et al., 2002 ; Rossion et al., 2003). Mais la localisation de ces lésions est très variable d'un patient à l'autre et est souvent très étendue et bilatérale, ce qui a empêché de déterminer précisément les régions critiques pour la perception des visages. Une autre approche a été utilisée : la stimulation électrique corticale. Cette méthode consiste à délivrer un courant électrique de faible intensité au niveau d'électrodes SEEG implantées chez des patients épileptiques afin de produire un signe clinique en rapport avec la fonction de la région stimulée. Cette méthode est utilisée en clinique afin de localiser la zone de départ des crises et de réaliser une cartographie fonctionnelle des régions critiques avant chirurgie. Les études de stimulation ont rapporté des difficultés à dénommer des visages célèbres ou des distorsions visuelles de visages lors de la stimulation électrique de certaines régions sélectives aux visages du VOTC (Allison et al., 1994 ; Puce et al., 1999 ; Parvizi et al., 2012). Mais aucune étude n'a rapporté de troubles du traitement de l'identité des visages lors des stimulations. Nous avons rapporté, à travers plusieurs études (Jonas et al., 2012, *Neuroscience ;* Jonas et al., 2014, *Neuroimage ;* Jonas et al., 2015, *Cortex ;* Jonas et al., 2018, *Cortex*) une cartographie des régions critiques pour le traitement de l'identité des visages à l'aide des stimulations électriques corticales (Figure 5).

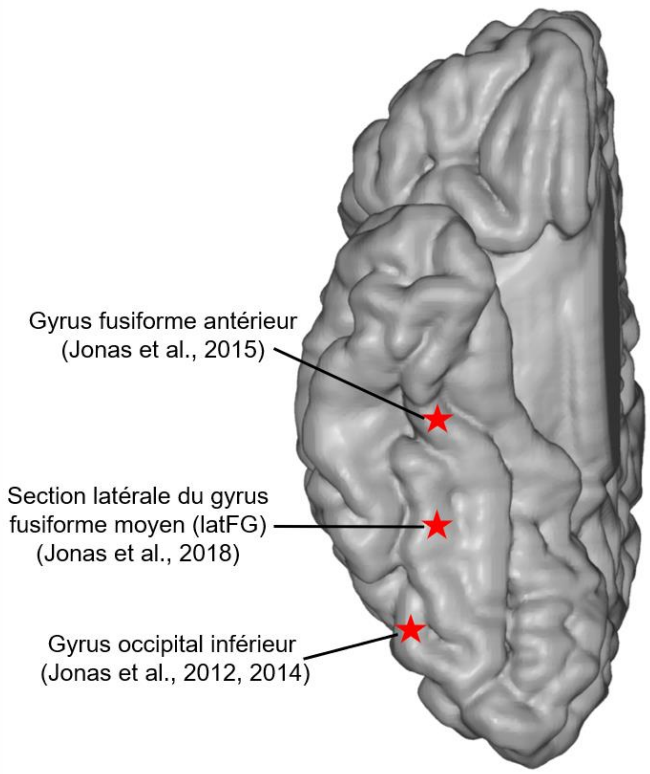

Figure 5. Représentation schématique de la localisation des régions dont la stimulation électrique corticale a provoqué un trouble du traitement de l'identité des visages (Jonas et al., 2012, 2014, 2015, 2018). Noter que toutes les régions sont localisées au niveau de l'hémisphère droit.

2.6.1 Le gyrus occipital inférieur droit

La première région à laquelle nous nous sommes intéressés a été une aire sélective dans le gyrus occipital inférieur droit (appelée OFA ou « Occipital Face Area » dans la littérature IRM fonctionnelle). Chez une patiente explorée en SEEG (KV), une électrode a été implantée par chance au sein de l'OFA droite, définie a posteriori par IRM fonctionnelle (Figure 6A). Cette électrode a permis de réaliser des stimulations électriques et d'enregistrer l'activité électrophysiologique au sein de l'OFA droite. Cette étude (Jonas et al., 2012, *Neuroscience*) a été réalisée en collaboration avec Bruno Rossion, Médéric Descoins (membre de l'équipe INSERM U751 dans laquelle j'avais fait mon stage de Master 2) et Louis Maillard. Il faut noter que c'est cette étude qui a permis de débuter notre collaboration avec Bruno Rossion. Pendant les stimulations électriques, il a été demandé à la patiente de reconnaître des photographies de visages célèbres (Figure 6A). Les stimulations électriques de sites sélectifs aux visages dans le gyrus occipital inférieur droit (attestés par potentiels évoqués lors de la SEEG et par IRM fonctionnelle après la SEEG) ont provoqué une incapacité transitoire à reconnaître les visages (contacts O6-O7 et O7-O8, Figure 6A). Pendant le temps de la stimulation, la patiente a été incapable de nommer les visages ou de donner d'autres informations biographiques.

Pour certaines stimulations, la patiente a rapporté percevoir les éléments des visages dans le désordre et pour d'autres, une difficulté à percevoir ces éléments de manière simultanée, sans déformation des éléments du visage. Ce résultat a été : (1) reproductible (6 sur 7 stimulations de l'OFA) ; (2) spécifique aux visages (pas de déficit lors de la reconnaissance d'objets ou de lieux célèbres) ; (3) spécifique de l'OFA droite (pas de déficit lors de la stimulation d'autres régions cérébrales).

Dans cette dernière étude (Jonas et al., 2012, *Neuroscience*), nous avons montré que l'OFA joue un rôle dans la perception de l'identité des visages familiers mais nous n'avons pas fourni d'informations quant au rôle précis que pourrait jouer l'OFA dans ce processus. Nous souhaitions donc adresser la question du rôle critique de l'OFA droite dans la discrimination de l'identité faciale, de manière indépendante aux informations sémantiques liées aux visages célèbres. Cela a été rendu possible par une deuxième SEEG réalisée chez la patiente KV avec à nouveau une électrode similaire qui traverse l'OFA droite (Figure 6B). Cette étude (Jonas et al., 2014, Neuroimage) a été réalisée en collaboration avec Bruno Rossion, Corentin Jacques (Université Catholique de Louvain) et avec Louis Maillard. Nous avons construit une tâche de discrimination de l'identité des visages inconnus que la patiente devait réaliser lors de la stimulation de l'OFA droite (Figure 6B). Cette tâche comprenait des paires de visages inconnus qui étaient soit identiques (de la même identité) ou légèrement différents (d'identité différente). Il a été demandé à la patiente KV de déterminer si les paires de visages appartenaient à une même identité ou à des identités différentes. En dehors de la stimulation, la patiente a montré de très bonnes performances (91% de réponses correctes, 49/54, pas de différence significative avec un groupe de sujets contrôles). Lors de la stimulation de l'OFA droite (contacts D5-D6, Figure 6B), ses performances ont chuté à 0%. Pour 6 des 6 stimulations de l'OFA droite, la patiente a répondu que les visages étaient identiques alors que les visages présentés étaient différents (6 réponses incorrectes sur 6). Elle n'a rapporté aucune distorsion des visages mais a déclaré que les visages apparaissaient identiques. Les stimulations électriques de l'OFA droite ont donc provoqué une incapacité transitoire à discriminer visuellement les visages.

De manière indépendante aux stimulations, nous avons mesuré la sensibilité de l'OFA droite à l'identité faciale grâce à un paradigme FPVS (Rossion et Boremanse, 2011). La patiente KV a visualisé des séquences FPVS comportant des séquences de visages identiques ou différents, à l'endroit ou à l'envers, présentés à une fréquence fixe et rapide (6 Hz : 6 visages par seconde) (Figure 6B). Dans plusieurs régions du VOTC droit nous avons enregistré une forte réponse à 6 Hz. Certaines régions ont montré un effet d'adaptation pour l'identité, c'est-à-dire une réduction de la réponse à 6 Hz pour les visages identiques par rapport aux visages différents. Grâce à la méthode FPVS, cet effet d'adaptation a pu être

quantifié sur chaque contact intracérébral. De manière remarquable, l'effet d'adaptation le plus ample et le plus spécifique des visages à l'endroit a été enregistré dans l'OFA droite, précisément sur le contact intracérébral impliqué lors des stimulations électriques provoquant une incapacité à discriminer les visages (contact D5, Figure 6B).

Cette étude montre que l'OFA droite est impliquée de manière causale dans la discrimination de l'identité faciale de manière indépendante des informations sémantiques, c'est-à-dire dans le traitement des caractéristiques visuelles qui rendent un visage unique. Ce résultat va à l'encontre des modèles qui assignent à l'OFA un rôle relativement bas dans le traitement hiérarchique de la perception des visages, généralement restreint au traitement des éléments du visage de manière isolée (comme les yeux, le nez, la bouche) (Haxby et al., 2000 ; Picher et al., 2011). Cette étude est aussi marquée par une convergence de preuves, les résultats en stimulation électrique étant corroborés par les enregistrements intracérébraux réalisés à l'aide de la méthode FPVS. Cette convergence renforce nos résultats et montre la pertinence fonctionnelle de la méthode FPVS qui a été capable de mettre en évidence de manière indépendante les régions critiques pour la discrimination de l'identité faciale.

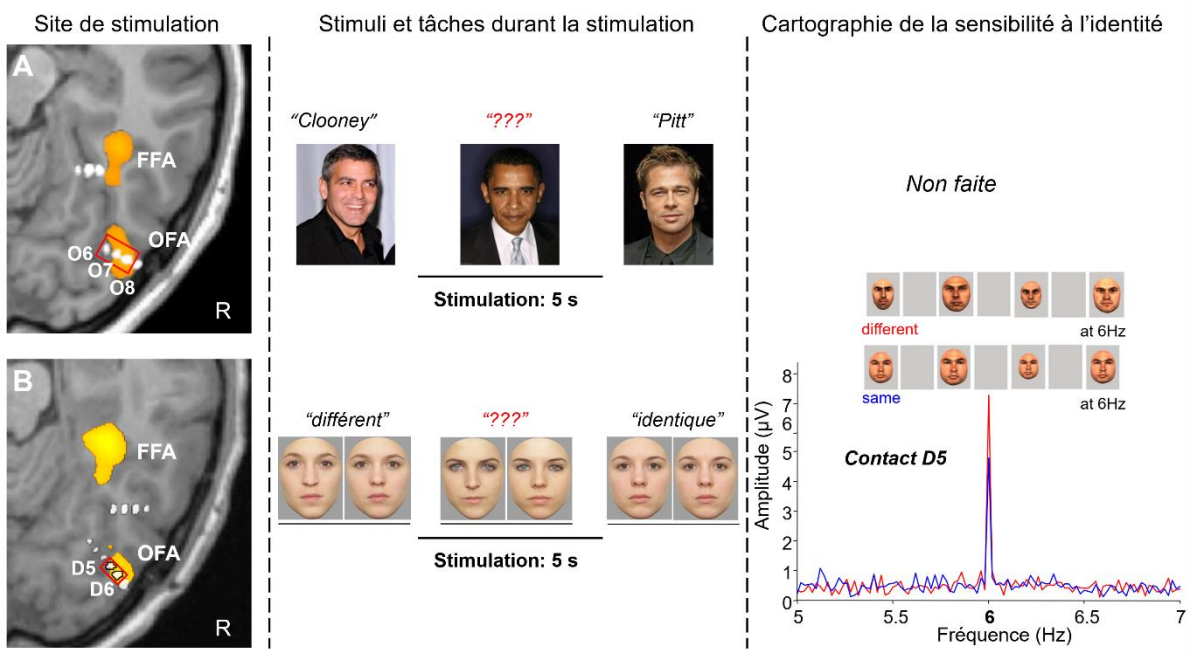

Figure 6. La stimulation du gyrus occipital inférieur droit induit une incapacité transitoire de reconnaissance des visages (sujet KV). A. Étude de Jonas et al., 2012, *Neuroscience*. B. Étude de Jonas et al., 2014, *Neuroimage*. Pour les deux études, le panneau de gauche montre les activations sélectives du visage en IRM fonctionnelle dans le VOTC droit (coupes axiales) avec les électrodes SEEG superposées (points blancs) ; le panneau du milieu montre les stimuli présentés pendant la procédure de stimulation ; le panneau de droite montre les enregistrements SEEG pendant un paradigme FPVS mesurant la sensibilité à l'identité des visages. Dans Jonas et al. (2012), les contacts éloquents O6, O7 et O8 (mis en évidence par un rectangle rouge) sont situés dans le cortex occipital inférieur droit sélectif aux visages comme le montre l'IRM fonctionnelle (OFA). La stimulation de ces contacts a induit une incapacité transitoire à reconnaître des visages célèbres. Dans Jonas et al. (2014) nous avons profité d'une deuxième SEEG réalisée sur le même sujet avec l'implantation d'une électrode similaire dans le gyrus occipital inférieur droit. La stimulation de deux contacts (D5-D6) a évoqué une incapacité transitoire à discriminer les identités de visages inconnus. Au cours de la SEEG, nous avons testé le sujet KV avec un paradigme d'adaptation FPVS mesurant la sensibilité à l'identité des visages et comprenant des séquences de visages à l'endroit ou à l'envers et présentés à une fréquence rapide et fixe de 6 Hz. Sur le contact D5, nous avons enregistré une réponse significativement plus grande pour des visages différents par rapport aux visages identiques (effet d'adaptation pour l'identité).

2.6.2 Le gyrus fusiforme antérieur droit

Le rôle de l'ATL dans la perception des visages et dans le traitement de l'identité faciale fait actuellement l'objet d'intenses recherches (Collins et Olson, 2014). De rares études IRM fonctionnelle ont mis en évidence des régions sélectives aux visages dans cette région, principalement dans le sillon collatéral antérieur (Nasr et Tootell, 2012 ; Rajimehr et al., 2009 ; Rossion, et al., 2012 ; Tsao, et al, 2008). Malheureusement nous disposons actuellement de très peu d'informations sur cette région, notamment parce que l'IRM fonctionnelle est limitée dans l'exploration de cette région en raison d'un artefact de susceptibilité magnétique qui réduit très fortement le signal enregistré dans cette région (Axelrod et Yovel, 2013 ; Ojemann et al., 1997). En utilisant la combinaison SEEG-FPVS, nous avons rapporté une cartographie précise des régions sélectives aux visages dans le lobe temporal antérieur (Jonas et al, 2016, *PNAS*), mais le caractère critique de ces régions reste à déterminer.

Une patiente (CD) a été implantée en SEEG avec une électrode traversant le gyrus fusiforme antérieur droit, et lors de la stimulation de cette électrode (contacts F3-F4, F4-F5, F5-F6, Figure 7A) il a été demandé à la patiente de reconnaître des photographies de visages célèbres pendant les stimulations électriques (de manière similaire à la première étude chez la patiente KV ; Jonas et al., 2012, *Neuroscience*). Cette étude (Jonas et al., 2015, *Cortex*) a été réalisée en collaboration avec Bruno Rossion, Corentin Jacques (Université Catholique de Louvain), Gabriela Hossu (CIC-IT, CHRU de Nancy) et Louis Maillard (CHRU de Nancy). Les stimulations électriques du gyrus fusiforme antérieur ont provoqué une incapacité transitoire de la patiente à reconnaître des visages célèbres (prosopagnosie transitoire). La patiente n'a jamais rapporté de modification visuelle des visages. Ce résultat a été : (1) reproductible (8 sur 8 stimulations) ; (2) spécifique des visages (pas de déficit lors de la reconnaissance d'objets) ; (3) spécifique du gyrus fusiforme antérieur droit (pas de déficit lors de la stimulation d'autres régions cérébrales).

Pendant la SEEG, nous avons réalisé une cartographie fonctionnelle des régions sélectives aux visages en enregistrant les réponses électrophysiologiques aux visages et aux objets à l'aide d'une stimulation visuelle classique non périodique (en potentiels évoqués et en activité gamma). A cette date, nous ne disposions pas encore de la FPVS (la patiente a été explorée en 2011). Nous avons montré que les stimulations ont intéressé une région sélective pour les visages dans le gyrus fusiforme antérieur droit (réponses sélectives aux visages en potentiels évoqués et en activité gamma, précisément sur les contacts impliqués durant les stimulations). Après la SEEG, nous avons également réalisé une cartographie des aires sélectives aux visages en IRM fonctionnelle (Figure 7A). L'IRM fonctionnelle a permis de faire 2 observations importantes : (1) le site de stimulation dans le gyrus fusiforme antérieur est

situé en avant de la FFA droite, localisé dans le latFG droit ; (2) aucune activation IRM fonctionnelle sélective pour les visages n'a été retrouvée dans la région du site de stimulation, malgré l'enregistrement de réponses électrophysiologiques sélectives aux visages en intracérébral. En effet, la superposition spatiale de la position de l'électrode et de l'amplitude du signal brut acquis pendant cette IRM fonctionnelle a montré que l'électrode est localisée au sein d'une zone comprenant très peu de signal en raison d'un artefact de susceptibilité magnétique lié au canal auditif (« signal drop-out », Figure 7A), ce qui explique l'absence de réponses sélectives aux visages retrouvées en IRM fonctionnelle dans cette région.

Cette étude a montré qu'au moins une région dans l'ATL droit, le gyrus fusiforme antérieur, est impliquée de manière causale dans le traitement de l'identité des visages. Cette étude met aussi en évidence une région méconnue, le gyrus fusiforme antérieur. Cette région n'a été que très rarement identifiée comme sélective aux visages en IRM fonctionnelle en raison d'un artefact de susceptibilité magnétique qui affecte le lobe temporal antérieur et particulièrement le gyrus fusiforme antérieur (voir notre article de revue Rossion, Jacques et Jonas, 2018, *Ann N Y Acad Sci*). Cette région a été aussi mise en évidence dans notre étude de groupe SEEG-FPVS (Jonas et al, 2016, *PNAS*) comme étant l'une des plus sélectives aux visages de tout le VOTC (après le latFG droit et le gyrus occipital inférieur droit). Ces différents résultats illustrent aussi l'apport de la SEEG par rapport aux méthodes plus classiques comme l'IRM fonctionnelle. Une des limites de cette étude est que nous avons utilisé uniquement des visages célèbres. Le trouble observé ici pourrait être expliqué par un défaut d'accès à la mémoire sémantique et non pas par un trouble spécifique du traitement des visages. Récemment, nous avons adressé cette limite en étudiant un autre patient (DN) dont la stimulation électrique du gyrus fusiforme antérieur droit a provoqué un trouble du traitement de l'identité des visages célèbres sans trouble de la reconnaissance des noms célèbres, ce qui exclut une participation de la mémoire sémantique aux troubles observés lors de la stimulation de cette région. Cette étude se fait en collaboration avec Angélique Volfart (doctorante que j'encadre actuellement au sein de l'équipe Neurosciences des Systèmes et de la Cognition du CRAN) et Bruno Rossion, et fait l'objet d'un article actuellement soumis (voir paragraphe 6.4.1).

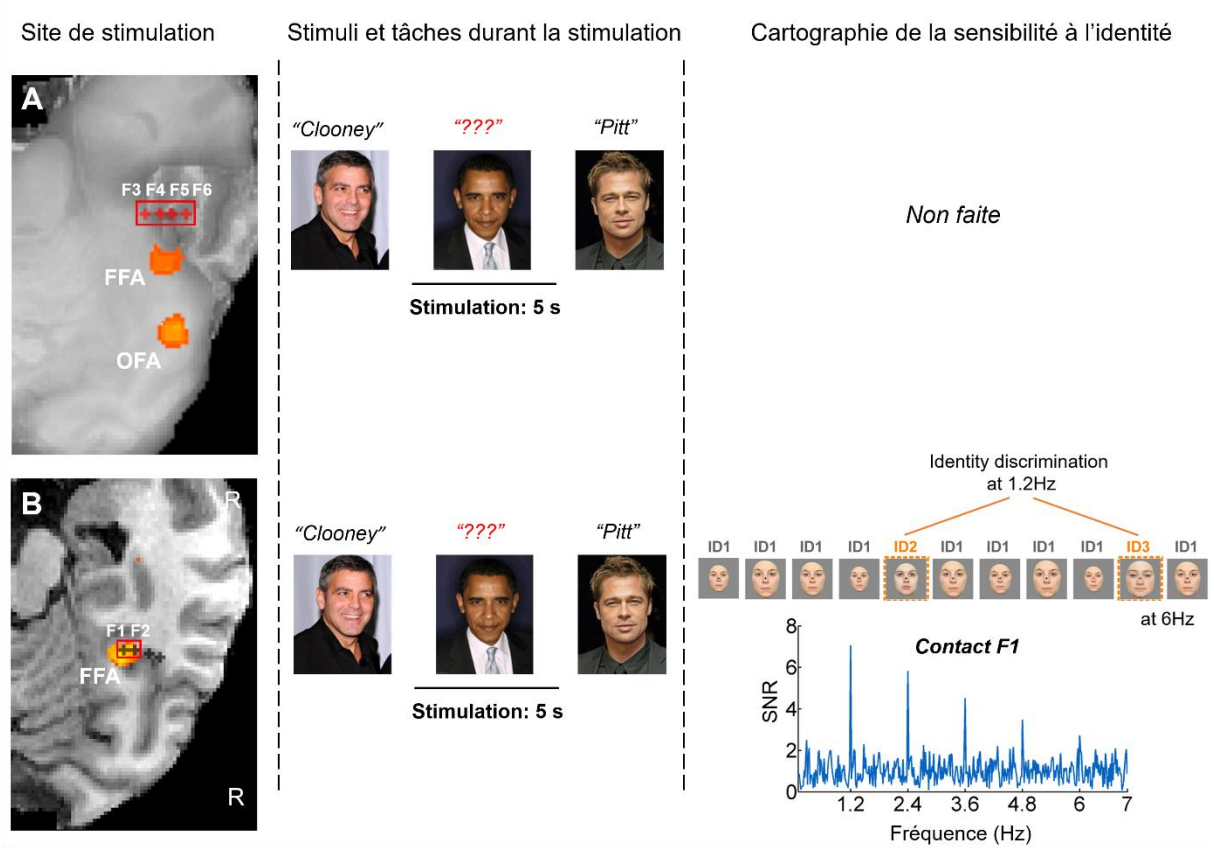

Figure 7. La stimulation du gyrus fusiforme droit induit une incapacité transitoire de reconnaissance des visages. A. Étude de Jonas et al., 2015, *Cortex* dans le gyrus fusiforme antérieur droit (sujet CD). B. Étude de Jonas et al., 2015, *Cortex* dans le latFG droit (sujet MB). Pour les deux études, le panneau de gauche montre les activations sélectives du visage IRM fonctionnelle dans le VOTC droit (coupes axiales) avec les électrodes SEEG superposées (croix noires ou rouges) ; le panneau du milieu montre les stimuli présentés pendant la procédure de stimulation ; le panneau de droite montre les enregistrements SEEG pendant un paradigme FPVS mesurant la sensibilité à l'identité du visage. Dans Jonas et al. (2015), les contacts éloquents (F3 à F6) étaient localisés dans le gyrus fusiforme antérieur droit, en avant de la FFA. Bien que nous ayons enregistré sur ces contacts des réponses sélectives pour les visages dans des bandes de fréquences basses et gamma, nous n'avons pas trouvé d'activations sélectives aux visages en IRM fonctionnelle autour de ces contacts en raison d'une importante perte de signal affectant la gyrus fusiforme antérieur droite (le panneau de gauche montre le signal IRM fonctionnelle brute en gris clair, avec les contacts éloquents au sein de cette région avec un signal IRM fonctionnelle très faible). La stimulation de ces contacts a induit une incapacité transitoire à reconnaître des visages célèbres. Dans Jonas et al. (2018), les contacts éloquents (F1 et F2) ont été localisés dans le latFG sélectif aux visages («FFA») comme le montre l'IRM fonctionnelle . La stimulation de ces contacts a induit une palinopsie faciale transitoire avec un mélange d'identités faciales différentes. Au cours du SEEG, le sujet MB a été testé avec un paradigme FPVS «oddball» mesurant la sensibilité à l'identité des visage et contenant des séquences avec une même identité de visage inconnu présentée à une fréquence rapide de 6 Hz, avec des visages d'identités différentes insérés toutes les 5 images (fréquence de changement d'identité = 1,2 Hz, soit 6 Hz / 5). Sur le contact F1, nous avons enregistré de grandes réponses de discrimination d'identité (le panneau de droite montre des réponses de discrimination d'identité enregistrées sur ce contact à 1,2 Hz et harmoniques dans le domaine fréquentiel). De tous les 137 contacts enregistrés dans le cerveau de MB, le contact F1 a enregistré, de loin, la plus grande amplitude de réponse.

2.6.3 Le gyrus fusiforme moyen droit

Après le gyrus occipital inférieur et le fusiforme antérieur, nous nous sommes intéressés au latFG droit. Il s'agit de la région la plus sélective aux visages (Jonas et al, 2016, *PNAS*) et contenant l'aire sélective aux visages définie par IRM fonctionnelle la plus connue et la plus étudiée (FFA). Même si cette région a été intensément étudiée depuis deux décennies maintenant, le rôle causal de cette région dans le traitement de l'identité des visages restait à déterminer. En 2012, il a été rapporté que la stimulation électrique en ECOG de la FFA droite provoque des distorsions visuelles de visages (Parvizi et al., 2012 ; voir aussi Rangarajan et al., 2014 pour une étude sur plus de patients). Si cette étude montre que la FFA est impliquée dans la perception des visages, elle ne montre pas que la FFA joue un rôle causal dans le traitement de l'identité des visages.

Nous avons étudié une patiente (MB) en SEEG, dont une électrode a été implantée dans le latFG droit. Durant les stimulations électriques de cette région (contacts F1-F2, Figure 7B), il a été demandé à la patiente de reconnaître des visages célèbres, des objets usuels et des lieux célèbres, et parfois de simplement regarder passivement ces images ou le visage du médecin présent dans la chambre lors des stimulations. Cette étude (Jonas et al., 2018, *Cortex*) a été réalisée en collaboration avec Bruno Rossion, Corentin Jacques (Université Catholique de Louvain), et Louis Maillard. Spécifiquement lors de la stimulation du latFG droit et en présence de visages, la patiente MB a rapporté un phénomène visuel caractérisé par le mélange de visages d'identités différentes. Selon elle, les éléments d'un visage donné (soit issu de sa mémoire, soit issu d'images montrées peu de temps avant) étaient intégrés dans le visage perçu lors de la stimulation, le tout formant un nouveau visage cohérent, non déformé. Sur le site de stimulation éloquent ont été enregistrées des fortes réponses sélectives aux visages en utilisant le paradigme FPVS dit « face-localizer » (Figure 2A). Une IRM fonctionnelle réalisée après la SEEG a montré que l'électrode était implantée dans la FFA droite.

Comme dans une autre étude de stimulation électrique (Jonas et al., 2014, *Neuroimage*), nous avons mesuré de manière indépendante aux stimulations la sensibilité du site de stimulation à l'identité faciale grâce à un paradigme FPVS, mais cette fois-ci en utilisant un autre paradigme FPVS (Liu-Shuang et al., 2014 ; Jacques, (….), Jonas, in press, *Neuroimage*). Dans ce paradigme, un visage inconnu de la même identité est présenté à 6 Hz et un visage d'une identité différente est présenté toutes les 5 images, de sorte que la fréquence du changement d'identité a été fixée à 1.2 Hz (6 Hz/5) (Figure 7B, voir aussi paragraphe 2.4). La sensibilité à l'identité des visages a été mesurée à cette fréquence et aux différentes harmoniques dans le domaine fréquentiel. Nous avons enregistré sur le site de

stimulation qui a provoqué ce phénomène de mélange d'identités (contact F1) les réponses de sensibilité à l'identité des visages les plus fortes parmi tous les sites d'enregistrement chez cette patiente (Figure 7B).

Cette étude montre que la FFA droite est impliquée de manière causale dans le traitement de l'identité des visages. Encore une fois, nous avons apporté deux sources de preuves convergentes, la stimulation électrique et les enregistrements FPVS. De plus, la FPVS a été capable de mettre en évidence les régions critiques pour l'identité, ce qui montre la pertinence fonctionnelle de cette méthode. Une des limites de cette étude est que la patiente MB a toujours été capable de reconnaître les visages malgré ce phénomène visuel de mélange d'identités. Récemment (en mai 2019), nous avons adressé cette limite en étudiant une autre patiente (CJ) dont la stimulation électrique du latFG droit a provoqué un déficit objectivable de la perception des visages (incapacité à détecter un visage célèbre parmi 2 inconnus). Cette étude est en préparation et se fait en collaboration avec Angélique Volfart et Bruno Rossion.

2.6.4 Autres études de stimulation électrique corticale

Nous avons appliqué la méthode des stimulations électriques corticales à d'autres fonctions du système visuel.

En 2014, nous avons rapporté les phénomènes subjectifs (hallucinations et illusions visuelles) évoqués par stimulation électrique du cortex visuel chez 22 patients en SEEG. Cette étude (Jonas et al., 2014, *Human Brain Mapping*) est basée sur la thèse d'exercice de Solène Frismand, interne en neurologie, dont j'ai encadré le travail, en collaboration avec Louis Maillard. Nous avons fait 2 observations importantes. Premièrement, nous avons montré une organisation postéro-antérieure de la qualité des phénomènes visuels, avec des phénomènes simples (flashs ou points) évoqués par la stimulation du VOTC postérieur et des phénomènes complexes (formes géométriques et objets visuels réels) par la stimulation du VOTC antérieur. Deuxièmement, nous avons montré que la probabilité d'évoquer un phénomène visuel est plus élevée par stimulation de l'hémisphère droit que par stimulation de l'hémisphère gauche. De plus, cette prédominance droite s'accentue le long de l'axe postéro-antérieur, avec une différence maximale droite-gauche pour les régions antérieures du VOTC. Ce résultat est en faveur d'une prédominance de l'hémisphère droit dans toutes les fonctions visuelles et surtout dans les fonctions visuelles les plus élevées, et ceci de manière indépendante de la tâche ou de l'implication des fonctions attentionnelles (aucune tâche n'était demandée aux patients).

La même année, nous nous sommes intéressés plus particulièrement à un phénomène visuel tout à fait particulier appelé hallucination autoscopique (Blanke et al., 2005). L'hallucination autoscopique est surtout rencontrée lors des crises d'épilepsie impliquant les régions postérieures et fait partie du groupe d'illusions caractérisées par une duplication de

son propre corps dans l'espace extra-personnel (avec l'héautoscopie et les phénomènes de sortie hors du corps). L'hallucination autoscopique est caractérisée par une hallucination visuelle de son propre visage en face de soi. Ce phénomène est interprété comme le reflet de la désorganisation des systèmes de représentation du soi. Les bases neurales des processus du soi sous-tendant l'hallucination autoscopique sont encore débattues. Nous avons rapporté le cas de 2 patients, dont la stimulation d'une région précise du cortex visuel, le sillon occipito-pariétal droit et le précunéus postérieur droit, a évoqué une hallucination de leur propre visage, en face d'eux, dans l'hémichamp visuel gauche. Cette étude (Jonas et al., 2014, *Neurology*) a été réalisée en collaboration avec le Dr Jean-Pierre Vignal (service de neurologie du CHRU de Nancy) et Louis Maillard. Le fait que l'hallucination autoscopique soit évoquée par une région du cortex visuel suggère qu'une représentation visuelle de notre visage est stockée dans le système visuel, et que cette représentation pourrait jouer un rôle dans la cognition sociale (préférence sexuelle de partenaires sexuels peu ressemblants de nous afin d'augmenter le métissage génétique ou renforcement des liens envers les personnes qui nous ressemblent comme les membres de notre famille).

2.7 Relations surface-profondeur des activités électrophysiologiques des visages

La perception des visages a bien entendu été étudiée principalement avec des méthodes non invasives, et en ce qui concerne les méthodes électrophysiologiques, l'EEG est de loin la méthode la plus utilisée pour l'étude de cette fonction. En EEG, il a été mis en évidence un potentiel évoqué, sélectif aux visages, négatif dans la région occipito-temporale droite et atteignant son pic d'amplitude aux alentours de 170 ms, la N170 (Rossion et Jacques, 2011). La N170 est considérée comme reflétant les mécanismes de perception des visages dans la partie postérieure du VOTC, et des centaines d'études ont été consacrées à ce potentiel. Néanmoins, la localisation des générateurs contribuant à la N170 enregistrée sur le scalp reste débattue.

Dans notre unité d'épileptologie du CHRU de Nancy, nous avons l'opportunité d'enregistrer des activités EEG de scalp de manière simultanée avec la SEEG (pose d'électrodes d'EEG de scalp après l'implantation des électrodes SEEG). Chez la patiente KV (décrite dans Jonas et al., 2012, *Neuroscience* et Jonas et al., 2014, *Neuroimage*) nous avons pu enregistrer la N170 à la fois en EEG scalp et en SEEG (Jacques et al., 2019, *Human Brain Mapping*). Cette étude, dont je suis 2ème auteur, a été réalisée en collaboration avec Corentin Jacques (Université Catholique de Louvain), Louis Maillard, Laurent Koessler (chargé de recherche CNRS dans l'équipe Neurosciences des Systèmes et de la Cognition du CRAN) et Bruno Rossion. Nous avons montré que le générateur principal de la N170 était le gyrus occipital inférieur droit et non le gyrus fusiforme, comme que cela est suggéré souvent. Cela

montre l'importance du gyrus occipital inférieur dans la perception des visages, région qui est souvent attachée à tort à des traitements précoces et peu complexes dans certains modèles hiérarchiques (Haxby et al., 2000 ; Pitcher et al., 2011).

Etant donné l'importance de l'EEG en recherche fondamentale, la compréhension des relations entre les activités EEG et leurs sources intracérébrales est cruciale. Récemment, nous avons montré que la FPVS est un outil particulièrement efficace pour comprendre ces relations. Nous avons présenté à la patiente citée plus haut (KV) un paradigme FPVS comportant des séquences de visages différents à l'endroit à 6 Hz (Rossion et Boremanse, 2011) alors qu'elle bénéficiait d'un enregistrement simultané SEEG-EEG (Jacques et al., 2020, *Human Brain Mapping*). Cette étude, dont je suis 2ème auteur, a été réalisée en collaboration avec Corentin Jacques, Louis Maillard, Laurent Koessler et Bruno Rossion. Grâce à différentes analyses (quantification de l'amplitude, estimation de la phase, corrélation des signaux dans le domaine temporel), nous avons pu précisément quantifier la contribution des différents générateurs intracérébraux dans le VOTC à l'activité projetée sur le scalp.

2.8. Applications à d'autres fonctions visuelles

Au cours de recherches, nous avons été amenés à nous intéresser à d'autres fonctions visuelles, notamment liées au langage (lecture et dénomination visuelle), en utilisant les méthodologies précédemment décrites (combinaison SEEG-FPVS et stimulations électriques corticales).

2.8.1 La lecture

Nous avons appliqué la combinaison SEEG-FPVS à l'étude des bases neurales de la lecture (Lochy, (…), Jonas, 2018, *PNAS*). Une des grandes questions est savoir s'il existe une région cérébrale purement lexicale (contenant un stock des mots connus), et si oui, où elle est localisée. La région connue sous le nom de VWFA (Visual Word Form Area ou aire de la forme visuelle des mots), mise en évidence par l'équipe de Stanislas Dehaene et Laurent Cohen (Cohen et al., 2002), est aujourd'hui considérée comme pré-lexicale (sensible à la structure orthographique fréquemment rencontrée dans les mots) plutôt que purement lexicale. Dans le cadre de cette étude, j'ai été amené à encadrer une post-doctorante du laboratoire de Bruno Rossion à l'Université Catholique de Louvain, Aliette Lochy, spécialiste des mécanismes de la lecture (1ère auteure de l'article). Aliette Lochy a apporté ses connaissances sur les mécanismes de lecture et j'ai apporté mon expertise dans la méthode SEEG-FPVS. Nous avons présenté à 37 patients implantés en SEEG des mots de manière périodique (1 fois sur 5) au sein de différentes séquences à 10 Hz contenant des stimuli variant selon leur proximité avec des mots (pseudo-lettres ou séries de lettres découpées et réarrangées spatialement ; non-mots ou séries de lettres non prononçables ; pseudo-mots ou séries de lettres

prononçables) (Figure 8A). Les réponses de discrimination aux mots ont été identifiées à la fréquence de 2 Hz et harmoniques (10 Hz/ 5). Nous avons enregistré des contacts avec des réponses purement lexicales, c'est-à-dire avec des réponses de discrimination de mots dans les 3 conditions, même dans la condition avec des pseudo-mots (Figure 8B). Ces réponses purement lexicales étaient concentrées au niveau du gyrus fusiforme moyen et antérieur gauche, c'est-à-dire en avant de la WVFA classiquement décrite (Figure 8C). Cette région n'avait pas été précédemment décrite car elle est située dans une zone où le signal enregistré est très faible en IRM fonctionnelle, en raison d'artéfacts méthodologiques. Ce résultat est en faveur d'une organisation hiérarchique des mécanismes de la lecture dans le VOTC, avec des processus de plus en plus complexes dans l'axe postero-antérieur, aboutissant à une région purement lexicale dans le gyrus fusiforme moyen et antérieur gauche. Cette étude illustre le fait que la combinaison de la SEEG et de la FPVS n'est pas limitée à l'étude des mécanismes de la perception des visages et peut être appliquée aux autres fonctions de la voie visuelle ventrale.

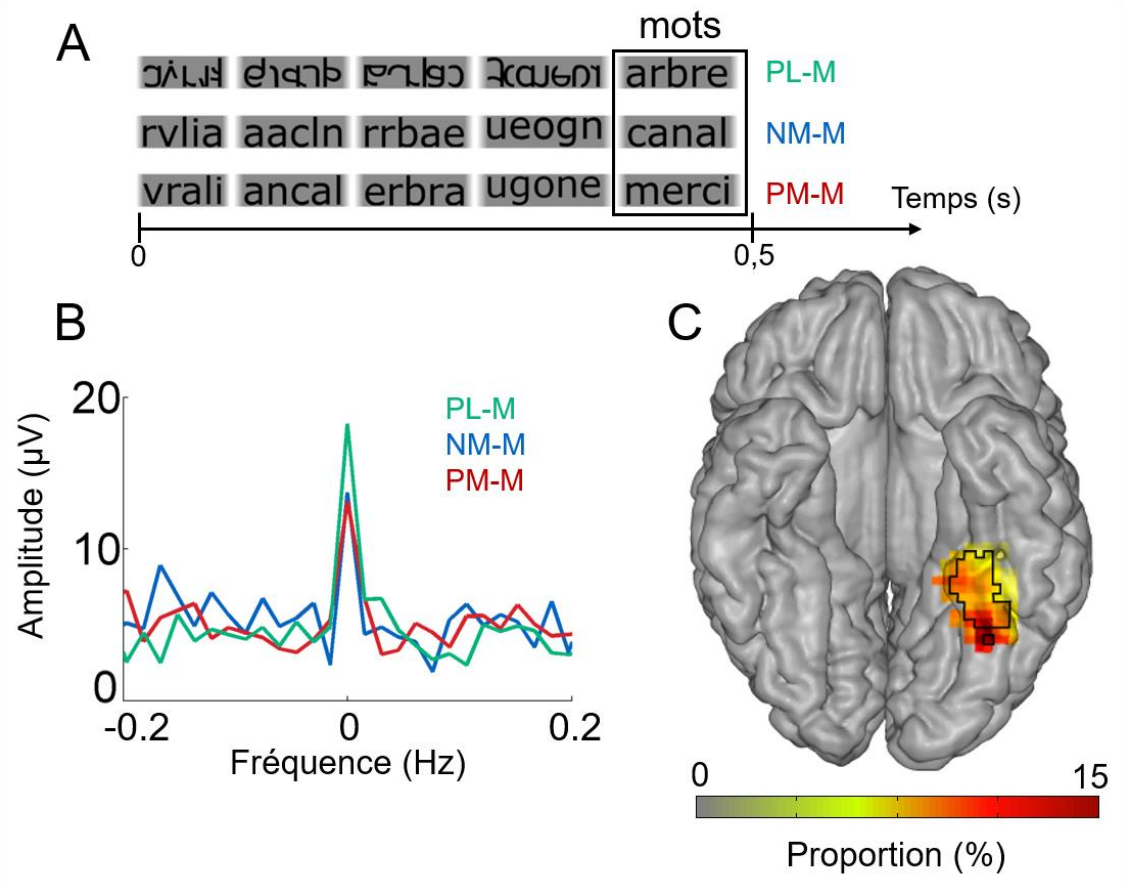

Figure 8. Réponses FPVS purement lexicales (Lochy et al., 2018, *PNAS*). A. Paradigme FPVS pour l'enregistrement de réponses sélectives aux mots. Des mots sont présentés de manière périodique (1 fois sur 5) au sein de séquences à 10 Hz contenant soit des pseudo-lettres (condition PL-M), des non-mots (NM-M) ou des pseudo-mots (PM-M), c'est-à-dire avec une fréquence de 2 Hz (10 Hz/5). B. Exemple d'un contact chez un patient dans le gyrus fusiforme antérieur gauche enregistrant une

réponse purement lexicale, avec une réponse à toutes les conditions. La fréquence des mots est à 0 Hz (somme des réponses à 2 Hz et harmoniques centrée sur 0). C. Proportion de contacts avec une réponse purement corticale sur l'ensemble des contacts enregistrés à travers les 37 patients inclus dans l'étude, représentée dans l'espace MNI.

2.8.2 La dénomination visuelle

La dénomination est une problématique importante dans les épilepsies du lobe temporal car les patients se plaignent très souvent de difficultés à trouver les mots et ces difficultés sont généralement aggravées par le traitement chirurgical, c'est-à-dire la lobectomie temporale antérieure. Les régions impliquées dans la dénomination dans le lobe temporal ont été historiquement identifiées grâce à la stimulation corticale (Lüders et al., 1991). En effet, la stimulation électrique du cortex temporal ventral gauche entraîne un trouble de la dénomination avec des anomies et des paraphasies. Cette région a été appelée BTLA (« Basal Temporal Language Area » ou aire temporale basale du langage). Notre objectif était de mieux déterminer la localisation de la BTLA et de mieux comprendre son rôle. Cette étude (Bédos Ulvin, Jonas et al., 2017, *Brain and Langage*) est basée sur la thèse d'exercice de Line Bédos Ulvin, interne en neurologie, dont j'ai encadré le travail, en collaboration avec Louis Maillard. Nous avons rapporté les résultats des stimulations électriques du cortex temporal droit et gauche pendant une tâche de dénomination d'images (ou dénomination visuelle) chez 23 patients implantés en SEEG. Nous avons rapporté une cartographie précise de la BTLA, en incluant également les sillons. Nous avons fait 2 observations importantes. Premièrement, nous avons montré que la BTLA est strictement latéralisée dans un seul hémisphère chez un patient donné (droit ou gauche). Ce résultat suggère que les stimulations électriques de la BTLA pourraient être utiles afin de déterminer la latéralisation hémisphérique du langage chez les patients implantés en SEEG (des études menées sous la direction de Louis Maillard sont actuellement en cours afin de confirmer ce point). Deuxièmement, le rôle de la BTLA est encore débattu. Une hypothèse serait qu'elle est impliquée dans la récupération lexicale (une tâche purement langagière), une autre hypothèse serait qu'elle fait partie de la mémoire sémantique et que les anomies observées seraient en fait liées à un défaut d'accès à la mémoire sémantique et non pas à un défaut d'accès au nom. Pour certains sites de stimulation évoquant une anomie, nous avons à nouveau stimulé ces sites en utilisant cette fois-ci une tâche sémantique. Nous n'avons jamais observé de troubles sémantiques, ce qui est en faveur d'un rôle de la BTLA dans la récupération lexicale.

2.9 Résilience du réseau de perception des visages après résection

Le modèle le plus reconnu du réseau de perception des visages est un modèle strictement hiérarchique (Haxby et al., 2000), dans lequel l'ensemble du réseau est dépendant

du traitement réalisé dans ce qui considéré comme la porte d'entrée du réseau l'OFA. Selon ce modèle, une lésion de l'OFA affectera toutes les aires situées en aval, en particulier la FFA. Nous avons testé ce modèle à l'aide d'une patiente épileptique (SP) dont la résection chirurgicale comprenait l'OFA droite et chez qui nous avons mesuré les activations sélectives aux visages en IRM fonctionnelle avant et après chirurgie (Weiner, Jonas et al., 2016, *Journal of Neuroscience*). Cette étude dont je suis 2ème auteur, a été réalisée en collaboration avec Bruno Rossion et avec Kevin Weiner et Kalanit Grill-Spector de l'Université de Stanford. Nous avons montré que la résection de l'OFA droite ne modifie pas le reste du réseau c'est-à-dire les autres activations sélectives aux visages, même celles situées en aval (OFA gauche, FFA droite et FFA gauche). Nous avons également montré grâce à une analyse en tractographie que cette résilience est probablement due à des faisceaux qui relient directement le cortex visuel primaire à la FFA sans passer par l'OFA, ce qui est en accord avec des études récentes de connectivité (Wang et al., in press). Ces résultats sont en faveur d'un modèle non strictement hiérarchique du réseau de la perception des visages (Rossion et al., 2008).

Chapitre 3 : Activités Pédagogiques

3.1 Formation à la pédagogie

J'ai obtenu en 2013 le DIU de Pédagogie Médicale (Faculté de Médecine de Nancy) qui m'a permis d'acquérir les connaissances de base en pédagogie. Le mémoire de validation de ce DIU a porté sur la création d'une vidéo d'e-learning pour l'apprentissage de l'annonce diagnostique de crises psychogènes non-épileptiques. Cette vidéo est toujours en ligne et est souvent visionnée par des médecins, des internes ou des patients (https://www.canal-u.tv/video/canal_u_medecine/annonce_d_un_diagnostic_de_crises_non_epileptiques_psychogenes.12726).

3.2 Charge d'enseignement

Depuis septembre 2017 et ma nomination en tant que MCU-PH de Physiologie, mes enseignements concernent principalement la neurophysiologie fondamentale et appliquée à la clinique pour la formation initiale des médecins (PACES : 2h par an, FGSM3 : 13h), pour différents DIU (DIU de neurophysiologie clinique options EEG et PE, DIU d'épileptologie, environ 4h par an), pour les formations paramédicales (IFSI, école d'orthophonie, école d'ergothérapie, école des manipulateurs en électroradiologie, école de kinésithérapie, environ 10h par an) et pour différents masters (M1 Santé de la Faculté de Médecine de Nancy, Master 2 de Neuropsychologie Cognitive et Clinique de l'Université de Strasbourg, environ 6h par an). Je participe également aux enseignements de la neurologie pour la formation initiale des médecins (4h par an en FGSM3).

Mon enseignement de neurophysiologie pour la formation initiale de médecins est caractérisé à la fois par la hiérarchisation des notions fondamentales qui sont essentielles aux médecins dans leur pratique quotidienne et par l'initiation des étudiants à la recherche en neurosciences. En ce qui concerne les notions essentielles, il est important que les étudiants disposent : (1) des notions fondamentales qui expliquent les signes cliniques d'une pathologie, les effets d'un traitement ou les résultats d'un examen neurophysiologique ; (2) des notions essentielles dans chaque sous-discipline (anatomie, moléculaire, cellulaire, génétique, histologie, psychologie, cognition) et de leur articulation, afin d'avoir une vision d'ensemble d'un système (et non d'avoir des connaissances poussées dans une sous-discipline). En ce qui concerne l'initiation à la recherche en neurosciences, cet enseignement illustre sur certains points les limites des connaissances actuelles et les recherches actuellement en cours au niveau international mais aussi au niveau local dans notre laboratoire (équipe Neurosciences

des Systèmes et de la Cognition, CRAN UMR 7039 CNRS-Université de Lorraine)**.** Il est important que les étudiants soient conscients que les neurosciences représentent actuellement un énorme champ de recherche au niveau international et que cette recherche se développe également au niveau local.

3.3 Responsabilité de la commission de docimologie

Depuis 2019, je suis responsable de la commission de docimologie de la Faculté de Médecine de Nancy. Mon rôle en tant que responsable est la bonne marche de cette commission dont l'objectif principal est de s'assurer que les épreuves proposées par les enseignants aux examens facultaires (de FGSM3 à FASM3) soient de bonne qualité sur le plan de la forme et respectent les programmes. L'autre objectif de la commission est d'accompagner la réforme actuelle du 2ème cycle des études médicales avec l'introduction de nouveaux types de questions (QCM à contexte riche, « key-features problem » et les tests de concordance de script). Cela implique la formation des rédacteurs et des correcteurs à ces nouvelles modalités.

La responsabilité de la commission de docimologie m'a amené à m'intéresser aux méthodes d'écriture des questions (QCM ou dossier progressif), aux critères de qualité nécessaires pour la construction des questions, aux différentes modalités d'écriture des questions avec chacune leurs avantages et leurs inconvénients (voir par exemple Pugh et al., 2018). Je participe dans ce cadre à l'enseignement du DIU de Pédagogie Médicale de la Faculté de Médecine de Nancy (3h par an).

3.4 Innovation pédagogique

Depuis 2017, je participe à un projet innovant en pédagogie. Il s'agit du développement de l'e-learning en physiologie et neurophysiologie, notamment avec la réalisation de travaux pratiques dématérialisés via la plateforme d'e-learning KuraCloud (AD Instruments) dans le cadre d'un projet faisant partie de l'Hôpital Virtuel de Lorraine (Pr Bruno Chenuel). La physiologie est une discipline fondamentale, dont l'enseignement est basé en partie sur l'observation directe par les étudiants des phénomènes de la vie. Cette partie de l'enseignement reposait classiquement sur les travaux pratiques. Malheureusement, l'augmentation du nombre d'étudiants en médecine ne permet plus la réalisation des travaux pratiques sous leur forme classique (en laboratoire). L'e-learning permet de pallier ce problème.

Via cette plateforme d'e-learning, j'ai construit des travaux pratiques dématérialisés de neurophysiologie pour les FGSM3. Le but de ces travaux pratiques est d'apprendre l'origine du signal électrophysiologique recueilli lors des examens complémentaires de

neurophysiologie (EEG, EMG et PE). L'originalité est que les étudiants manipulent et analysent de vraies données électrophysiologiques, pour la plupart recueillies dans le service de Neurologie du CHRU de Nancy (Figure 9) A partir de leurs analyses, les étudiants doivent faire leurs propres observations et répondre à des questions. Une séance de correction en présentiel permet aux étudiants de poser des questions et de renforcer l'enseignement par de l'interactivité.

Cette méthode pédagogique est appréciée des étudiants (cela est attesté par un questionnaire de satisfaction en ligne). Elle a fait l'objet d'une présentation orale au Congrès National de Physiologie et de Biologie Intégrative en 2019 (en collaboration avec le Pr Bruno Chenuel).

Figure 9. Exemple de présentation de données réelles (EEG) via la plateforme d'e-learning KuraCloud.

Chapitre 4 : Activités Cliniques

Mon activité clinique de neurologue est centrée sur la neurophysiologie, soit à travers le diagnostic et le traitement l'épilepsie, soit l'interprétation des explorations fonctionnelles neurologiques (EEG et potentiels évoqués). J'exerce ces 2 activités dans le service de neurologie du CHRU de Nancy (dirigé par le Pr Marc Debouverie), respectivement dans l'unité d'épileptologie (dirigée par le Pr Louis Maillard) et dans l'unité d'explorations fonctionnelles neurologiques (dont j'ai la responsabilité).

4.1. Diagnostic et traitement de l'épilepsie

4.1.1 Prise en charge des patients épileptiques de manière générale

En tant que neurologue spécialisé dans l'épilepsie, je participe à la prise en charge de tous les patients épileptiques, avec la réalisation de consultations d'épileptologie, la participation à l'activité de l'unité d'épileptologie (visite du secteur, interprétation des vidéo-EEG), l'interprétation des EEG des patients épileptiques, et la prise en charge des patients ayant présenté une première crise d'épilepsie (supervision des consultations « première crise » réalisées par les internes, supervision des hospitalisations de jour pour « première crise » avec réalisation d'une vidéo-EEG de 3 heures).

Dans ce cadre, je participe beaucoup à la formation des internes afin de leur transmettre les connaissances et les compétences de base pour le diagnostic et le traitement des épilepsies (en plus du DIU d'Epileptologie dans lequel je suis enseignant).

4.1.2 Activité de référence : les épilepsies focales pharmaco-résistantes

Mon activité de référence en épilepsie concerne la prise en charge des épilepsies rares et pharmaco-résistantes. Cette activité se fait au sein de l'Unité d'Epileptologie du service de Neurologie qui est Centre de Référence des Epilepsie Rares (centre constitutif, responsable : Pr Louis Maillard). Notre centre est centre multidisciplinaire comprenant 5 neurologues titulaires (Pr Louis Maillard, Pr Louise Tyvaert, Dr Jean-Pierre Vignal, Dr Jacques Jonas et Dr Olivier Aron à 40%), 1 neurochirurgien (Pr Sophie Colnat-Coulbois), 1 psychiatre (Dr Coraline Hingray), une neurologue spécialisée en neuro-génétique (Dr Mathilde Renaud), 3 neuropsychologues (Hélène Brissart, Natacha Forthoffer, Mylène Meyer).

Mon activité de référence concerne en particulier la prise en charge chirurgicale des épilepsies focales pharmaco-résistantes de l'adulte. Pour ces patients, les crises d'épilepsie persistent malgré de nombreux traitements antiépileptiques et une solution chirurgicale peut

être proposée. Cette chirurgie repose sur le principe que le retrait chirurgical de la zone cérébrale nécessaire et suffisante pour déclencher des crises (zone épileptogène) permettra la guérison de l'épilepsie. Avant de réaliser cette chirurgie, il est donc nécessaire de délimiter avec le plus de précision possible cette zone. Ce bilan pré-chirurgical repose en grande partie sur la réalisation d'un examen hautement spécifique, la SEEG. La SEEG correspond à la mise en place d'électrodes intracérébrales afin de localiser très précisément la zone de départ des crises et donc la zone à retirer chirurgicalement. Cet examen n'est réalisé que dans une dizaine de CHU en France. Le CHRU de Nancy est la seule structure avec le CHU de Strasbourg à porter cette activité dans l'inter-région Est. En termes de nombre de SEEG réalisées (environ 35 par an), le CHRU de Nancy est le 2ème centre en France (derrière la Fondation Rothschild, centre spécialisé dans la SEEG chez l'enfant) et le premier pour l'activité adulte.

4.1.3 Lien clinique-recherche : le pronostic neuropsychologique

Les épilepsies focales résistantes au traitement médicamenteux peuvent relever d'un traitement chirurgical. La résection chirurgicale a pour but de retirer la zone de déclenchement des crises (zone épileptogène) mais cette résection pourra également intéresser des zones cérébrales fonctionnelles, critiques pour certaines fonctions cérébrales, soit parce qu'elles font partie de la zone épileptogène, soit parce qu'elles se situent dans son voisinage ou sur la voie d'abord chirurgicale. Avant toute chirurgie de l'épilepsie, il est donc essentiel de réaliser une cartographie fonctionnelle de la zone épileptogène et des régions avoisinantes afin de déterminer si une résection est envisageable ou non sur le plan fonctionnel et si oui, de prédire le devenir neuropsychologique post-opératoire.

L'IRM fonctionnelle peut être utilisée pour réaliser une cartographie fonctionnelle per-opératoire, notamment pour le langage et la motricité. La limite de l'IRM fonctionnelle est que cette méthode ne montre que les régions qui sont activées par une tâche, et non pas spécifiquement celles qui sont critiques, c'est-à-dire celles dont la résection va effectivement entraîner un déficit post-opératoire. L'autre moyen est d'utiliser la SEEG pour réaliser la cartographie per-opératoire, soit en utilisant les stimulations électriques corticales (voir Jonas, 2018 pour une revue de littérature sur ce point), soit en utilisant les enregistrements électrophysiologiques (par potentiels évoqués classiques ou par FPVS).

Les études SEEG mentionnées dans le Chapitre 2 (utilisant la stimulation électrique ou les enregistrements FPVS) ont pour but la cartographie fonctionnelle des fonctions visuelles. Les données issues de ces patients sont parfois utilisées afin guider la résection chirurgicale (éviction des régions critiques pour la vision). Par exemple, la patiente KV (Jonas et al., 2012, *Neuroscience* ; Jonas et al., 2014, *Neuroimage*) dont les stimulations et les

enregistrements FPVS ont montré une région critique pour le traitement de l'identité des visages dans le gyrus occipital inférieur droit, proche de la zone épileptogène située dans le gyrus lingual, a été longtemps contre-indiquée pour la chirurgie (de 2010 à 2018) en raison du risque de prosopagnosie en cas de résection dans le lobe occipital droit (la patiente a finalement été opérée en 2018 avec une résection comprenant le gyrus occipital inférieur droit, et les résultats post-opératoires sur ses capacités de perception des visages sont équivoques et sont en cours d'interprétation).

Notre objectif dans l'avenir est de valider l'intérêt des stimulations et des enregistrements par des études sur un grand nombre de patients. Par exemple, un article de notre équipe dont je suis co-auteur explore l'intérêt de la cartographie de la BTLA par stimulation électrique sur le pronostic neuropsychologique post-opératoire en langage. Ce travail est fait en collaboration avec Louis Maillard et Chifaou Abdallah (ancienne Chef de Clinique dans l'unité d'épileptologie du CHRU de Nancy). Nous avons étudié 20 patients avec une épilepsie temporale qui ont bénéficié d'une cartographie de la BTLA par stimulations électriques en SEEG puis d'une lobectomie temporale antérieure. Nous avons montré qu'une résection d'une partie de la BTLA était prédictif d'une chute des performances en dénomination à 6 mois post-opératoire. Par contre, les performances en dénomination chez ces patients s'amélioraient à 23 mois post-opératoire, probablement grâce à des mécanismes de compensation ou de plasticité. Cela montre l'importance d'inclure une dimension temporelle lorsqu'il s'agit de prédire le devenir neuropsychologique. En d'autres termes, les mécanismes de compensation ou de plasticité font que la valeur prédictive d'une donnée ou d'un test varie en fonction du délai post-opératoire (dans cette étude, la résection d'une partie de la BTLA est prédictive d'une baisse des performances à 6 mois mais pas à 23 mois).

4.2. Explorations fonctionnelles neurologiques

4.2.1 Activité clinique

Mon autre activité clinique est centrée sur l'interprétation des EEG et des potentiels évoqués au sein de l'unité d'Explorations Fonctionnelles Neurologiques dont j'ai la responsabilité médico-administrative. Dans ce cadre, je suis impliqué dans l'interprétation des EEG standards (EEG adultes du CHRU, EEG des Hôpitaux périphériques comme Bar-le-Duc, Verdun, Neufchâteau), les astreintes EEG, l'interprétation des potentiels évoqués en laboratoire (potentiels évoqués somesthésiques), l'interprétation des potentiels évoqués en réanimation pour le pronostic de réveil des comas (Pôle réanimation du CHRU de Nancy) et l'interprétation des potentiels évoqués au bloc opératoire pour la surveillance électrophysiologique de la moelle épinière lors de la chirurgie rachidienne et médullaire (Pôle enfants du CHRU de Nancy).

Je suis impliqué dans l'enseignement de l'EEG et des potentiels évoqués auprès des internes de neurologie (en plus du DIU de Neurophysiologie Clinique dans lequel je suis enseignant). J'ai également mis en place une formation continue pour les infirmières de l'unité d'Explorations Fonctionnelles Neurologiques, avec des séances hebdomadaires de cours et des discussions autour des EEG réalisés récemment.

4.2.2 Lien clinique-recherche

Un autre élément important afin de prédire le devenir neuropsychologique post-opératoire en chirurgie de l'épilepsie consiste en une évaluation précise des capacités neuropsychologiques des patients avant chirurgie. Actuellement, ce bilan est réalisé par des tests neuropsychologiques classiques où il est demandé aux patients de réaliser des tâches évaluant la mémoire, le langage, la vision, les fonctions exécutives, les fonctions attentionnelles, etc. Malheureusement, ces tests sont parfois peu fiables et peu reproductibles en raison des biais attentionnels ou de motivation qui peuvent interférer. Par exemple, un patient qui a des troubles attentionnels ou qui a peu de motivation pour faire les tests pourra avoir des scores déficitaires dans plusieurs fonctions, sans que ces fonctions soient réellement déficitaires.

Comme mentionné plus haut, la FPVS est un outil prometteur afin d'évaluer de manière fiable les performances d'un sujet dans certains domaines (langage et perception visuelle principalement) et pourrait être utilisée afin de prédire le pronostic neuropsychologique post-opératoire après neurochirurgie de l'épilepsie. En effet, les réponses obtenues par FPVS ont plusieurs caractéristiques essentielles pour cet objectif : (1) les réponses sont objectives et facilement quantifiables ; (2) les réponses sont reproductibles dans le temps chez un même sujet ; (3) les réponses ont une valeur fonctionnelle. Concernant ce dernier point, plusieurs études d'EEG de scalp utilisant la FPVS ont montré une relation entre la valeur d'amplitude de la réponse et les performances (pour la lecture, voir Lochy et al., 2016 ; pour la perception des visages, voir Liu-Shuang et al., 2016).

Dans l'avenir, nous souhaiterions envisager le remplacement de certaines évaluations neuropsychologiques pré-opératoires classiques par une mesure électrophysiologique objective et quantifiable en combinant l'EEG de scalp et la FPVS (voir paragraphe 8.3.8). A terme, une partie du bilan neuropsychologique pré-opératoire ne se ferait plus par un bilan neuropsychologique classique, mais à l'aide d'un EEG réalisé dans l'unité d'explorations fonctionnelles neurologiques. Afin de valider cette approche, nous avons une étude en cours évaluant les capacités en perception des visages et les capacités de lecture chez des patients et des sujets témoins appariés, en utilisant à la fois le bilan neuropsychologique classique et l'EEG couplé à la FPVS. Pour cette étude, nous avons obtenu le financement d'un assistant

de recherche (Pierre Riff) en 2018 par une bourse Fondation Française pour la Recherche sur l'Épilepsie, FFRE (90912€).

Chapitre 5 : Financement de la Recherche

5.1 Financements obtenus

5.1.1 CPRC

En 2012, nous avons obtenu un financement de 20 000 € pour une étude intitulée « Evaluation des conséquences neuropsychologiques de l'épilepsie temporale antérieure pharmaco-résistante et de la lobectomie temporale antérieure sur la perception des visages » (ATENA-F) de la part du CHRU de Nancy via un CPRC (Contrat Programme de Recherche Clinique). Même s'il s'agit de ma thématique personnelle de recherche, je n'ai pas pu être investigateur principal de cette étude car je ne disposais pas à cette époque de statut de titulaire au CHRU (Assistant-Chef de Clinique). Le Pr Louis Maillard est donc investigateur principal de cette étude. Cette étude, que je coordonne en pratique, a été réalisée en collaboration avec Bruno Rossion, Hélène Brissart (neuropsychologue dans le service de neurologie) et Angélique Volfart dont je co-encadre la thèse d'Université. Cette étude est actuellement terminée et a fait l'objet d'un article publié (Volfart, Jonas, et al., in press, *Neuropsychologia*).

5.1.2 Bourse de thèse FNRS

En 2013, j'ai obtenu une bourse de thèse du FNRS (Fonds National de la Recherche Scientifique, Belgique) pour la réalisation d'une thèse de neurosciences. Cette bourse m'a permis de réaliser un séjour de 4 ans dans le laboratoire de Bruno Rossion (Institute of Neuroscience et Institute of Psychological Research) pour la préparation de ma thèse d'Université. Cette bourse comprenait un salaire mensuel de 2000 € et une bourse pour des frais divers de 10 000 €.

5.1.3 Système d'acquisition micro-électrodes

En 2013, nous avons obtenu un financement pour l'achat d'un système d'acquisition micro-électrodes afin de réaliser des enregistrements de neurones uniques chez l'Homme via la SEEG (voir paragraphe 8.2.2). Nous avons obtenu 171 000 € de la Fédération pour la Recherche sur le Cerveau (Appel d'Offres Exceptionnel « Espoir en tête ») et 340 000 € du Conseil régional de Lorraine 2013. Le Pr Louis Maillard est le porteur du projet et je suis l'un des investigateurs associés.

5.1.4 Bourse de voyage Nancy-Louvain-la-Neuve

Afin de prendre en charge mes déplacements entre Nancy et Louvain-la-Neuve (ma thèse d'Université s'est déroulée en cotutelle entre l'Université de Lorraine et l'Université

Catholique de Louvain, et de plus l'ensemble des acquisitions de données SEEG se faisaient au CHRU de Nancy tandis que le traitement des données se faisait principalement dans le laboratoire de Bruno Rossion), j'ai demandé et obtenu en 2015 une bourse de voyage du Conseil de Recherche de l'Université Catholique de Louvain d'un montant de 4180 €.

5.1.5 Bourse de voyage Israël

En 2015, j'ai obtenu une bourse de voyage du FNRS (Belgique) afin d'assister à une réunion scientifique (« workshop ») à Jérusalem d'une valeur de 500 € (Person Recognition Workshop, Jérusalem, 2015).

5.1.6 Contrat doctoral d'Angélique Volfart

En 2017, nous avons obtenu un contrat doctoral MENSR (école doctorale BIOSE, Université de Lorraine) pour Angélique Volfart, doctorante dans l'équipe Neurosciences des systèmes et de la cognition (CRAN, UMR 7039, CNRS-Université de Lorraine) et dont je co-encadre la thèse d'Université.

5.1.7 Contrat doctoral de Marie-Alphée Laurent

En 2020, nous avons obtenu un contrat doctoral (co-financement école doctorale BIOSE - Région Grand Est) pour le financement de la thèse de Marie-Alphée Laurent dont je suis le co-encadrant avec Bruno Rossion.

5.2 Demandes de financement refusées

5.2.1 ANR

En 2014, nous avons soumis une demande d'ANR intitulée « Cartographie intracérébrale humaine par stimulation visuelle périodique » (IPER-STIM) avec comme coordinateur Louis Maillard, et avec Bruno Rossion et moi-même dans le consortium. Le but scientifique de cette demande était de mieux comprendre les mécanismes de la perception visuelle en utilisant la SEEG, la FPVS et les stimulations électriques corticales. Cette demande a été refusée.

En 2015, nous avons soumis une demande similaire mais retravaillée, intitulée « Cartographie cérébrale humaine multimodale et multi-échelle par stimulation visuelle périodique rapide » (M3-STIM) avec comme coordinateur Louis Maillard, et avec Bruno Rossion et moi-même dans le consortium. Cette demande a été refusée.

En 2018, j'ai soumis en tant que coordinateur principal un appel à projets générique JCJC, avec dans le consortium Louis Maillard et Bruno Rossion, intitulé « Bases neurales de la reconnaissance faciale à l'aide des enregistrements intracérébraux » (NEUFI). Le but

scientifique de cette demande était de mieux comprendre les mécanismes du traitement de l'identité des visages en utilisant la SEEG, la FPVS, les stimulations électriques corticales et les enregistrements de neurones uniques. Cette demande a été refusée.

En 2019, nous avons soumis une demande d'ANR, dont je faisais partie du consortium (20%), intitulée « The neural basis of Primate Face Recognition: a comparative multimodal approach » (PREFER) avec comme coordinateurs Bruno Rossion et Benoit Cottereau (CerCo, UMR 5549 CNRS/Université Paul Sabatier, Toulouse III). Le but scientifique de cette demande était de comparer les bases neuronales de la perception des visages entre l'Homme et son modèle le plus utilisé pour étudier cette fonction, le macaque, en utilisant les mêmes paradigmes FPVS et les mêmes méthodes d'enregistrement (EEG de scalp, IRM fonctionnelle, enregistrements unitaires de neurones individuels). Cette demande a été refusée.

5.2.2 APJ

En 2019, nous avons postulé pour un APJ (Appel à Projet Jeune Chercheur) du GIRCI Est (Groupement Interrégional de Recherche Clinique et d'Innovation de l'Est). Cette demande s'intitulait « Cartographie fonctionnelle pré-opératoire du lobe temporal antérieur grâce à l'utilisation de techniques innovantes en IRM fonctionnelle chez des patients épileptiques pharmaco-résistants » (CARTA) et j'en étais l'investigateur principal. Cette demande a été réalisée en collaboration avec Gabriela Hossu (CIC-IT du CHRU de Nancy). Cette demande a été refusée.

Chapitre 6 : Encadrement de Projets de Recherche

6.1 Master 2 recherche

J'ai encadré 5 étudiants en Master 2, dans le cadre du Master 2 Recherche de Neuropsychologie Cognitive et Clinique, Université de Strasbourg : Mylène Romilly en 2013, Julie Gamper en 2013, Clémentine Castro en 2014, Marion Beringer en 2014 et Angélique Volfart en 2016.

6.2 Thèse d'exercice

En 2013, j'ai co-encadré avec Louis Maillard la thèse de Solène Frismand (alors interne de neurologie au CHRU de Nancy) sur le thème des stimulations électriques corticales dans le cortex visuel (voir paragraphe 2.6.4). Ce travail a fait l'objet d'une publication (Jonas J, Frismand S, Vignal JP, Colnat-Coulbois S, Koessler L, Vespignani H, Rossion B, Maillard L. Right hemispheric dominance of visual phenomena evoked by intracerebral stimulation of the human visual cortex. Human Brain Mapping. 2014;35:3360-71).

En 2013, j'ai co-encadré avec Louis Maillard la thèse de Nicolas Carpentier (alors interne de neurologie au CHRU de Nancy) sur le thème des activités électrophysiologiques enregistrées dans l'hippocampe à l'aide de la SEEG. Ce travail a fait l'objet d'une publication (Carpentier N, Cecchin T, Koessler L, Louis-Dorr V, Jonas J, Vignal JP, Carpentier M, Szurhaj W, Bourgin P, Maillard L. Stereo electroencephalography identifies N2 sleep and spindles in human hippocampus. Clin Neurophysiol. 2017;128:1696-1706.)

En 2016, j'ai co-encadré avec Louis Maillard la thèse de Line Bédos Ulvin (alors interne de neurologie au CHRU de Reims) sur le thème des stimulations électriques corticales induisant des troubles de la dénomination dans le cortex temporal ventral (voir paragraphe 2.8.2). Ce travail a fait l'objet d'une publication (Bédos Ulvin L, Jonas J, Brissart H, Colnat-Coulbois S, Thiriaux A, Vignal JP, Maillard L. Intracerebral stimulation of left and right ventral temporal cortex during object naming. Brain Lang. 2017;175:71-76).

En 2019, j'ai co-encadré avec le Pr Marc Debouverie (service de Neurologie, CHRU de Nancy) la thèse de Marion Selton (alors interne de neurologie au CHRU de Nancy) sur le thème de l'influence des crises d'épilepsie sur le pronostic de la sclérose en plaques. Un article est en cours de préparation dont je suis le dernier auteur.

6.3 Mémoire de Diplôme d'Etudes Spécialisées

En 2013, j'ai co-encadré avec Louis Maillard le mémoire de Diplôme d'Etudes Spécialisées (DES) de Neurologie de Nicolas Carpentier (alors interne de neurologie au CHRU de Nancy) sur le thème de l'adhésion au traitement anti-épileptique des patients avec une épilepsie focale pharmaco-résistante. Ce travail a fait l'objet d'une publication (Carpentier N, Jonas J, Frismand S, Vignal JP, Rikir E, Baumann C, Lapicque F, Saint-Marcoux F, Vespignani H, Maillard L. Direct evidence of non-adherence to antiepileptic medication in refractory focal epilepsy. Epilepsia. 2013;54:e20-e23).

6.4 Thèse d'Université

Depuis 2017, je suis co-encadrant (ACT) de la thèse d'Université d'Angélique Volfart, avec Bruno Rossion (Université de Lorraine) et Valérie Goffaux (Université Catholique de Louvain). Cette thèse est réalisée en cotutelle entre l'Université de Lorraine (équipe Neurosciences des systèmes et de la cognition, CRAN, UMR 7039, CNRS-Université de Lorraine) et l'Université Catholique de Louvain. Cette thèse s'intitule « Etude du système visuel ventral dans l'épilepsie du lobe temporal à partir d'une nouvelle approche en électrophysiologie ».

6.4.1 Résumé de la thèse

Le but de la thèse est de mieux comprendre les mécanismes de perception visuelle au sein du VOTC, et notamment de clarifier la contribution des structures temporales postérieures et antérieures dans les mécanismes de perception visuelle de haut et dans la mémoire sémantique. Pour cela, cette thèse s'appuie sur l'utilisation de la neuropsychologie, de la FPVS, des enregistrements en EEG de scalp et SEEG, de patients épileptiques et de sujets sains non-épileptiques.

La première étude a pour but d'évaluer les capacités de perception des visages chez des patients avec une épilepsie temporo-mésiale, à l'aide de tests neuropsychologiques. Cette étude a été supportée par le CHRU de Nancy par un financement de 20 000 € dans le cadre d'un CPRC en 2012 (étude ATENA-F). Nous avons inclus 42 patients et 42 sujets témoins appariés. Nous avons montré que les patients ont un déficit de mémoire sémantique et épisodique des visages (difficultés à reconnaître et dénommer des visages célèbres et à apprendre explicitement des nouveaux visages). En revanche, les patients ont des mécanismes perceptifs d'individuation des visages normaux (capacité à discriminer 2 visages différents sur base de leurs caractéristiques visuelles). Ces résultats montrent que les patients avec une épilepsie temporo-mésiale ont des mécanismes d'individuation des visages normaux et des troubles en mémoire épisodique et sémantique en rapport avec la localisation de leur

épilepsie (atteinte de l'hippocampe et du cortex temporal très antérieur et du pôle temporal, avec préservation d'une grande partie de la voie visuelle ventrale, notamment la partie moyenne et postérieure du VOTC). Cette étude supporte également la validité du modèle du cerveau épileptique pour l'étude des mécanismes de perception des visages à l'aide de la SEEG. Ce travail fait l'objet d'une publication (Volfart, Jonas, et al., in press, *Neuropsychologia*).

Une deuxième étude concerne le rôle du gyrus fusiforme antérieur droit dans la perception des visages. Nous avions montré que cette région est fortement sélective aux visages (Jonas et al., 2016, *PNAS*) et que la stimulation électrique de cette aire entraîne un trouble du traitement de l'identité des visages (Jonas et al., 2015, *Cortex*). Pour cette dernière étude, nous avions utilisé uniquement des visages célèbres, et par conséquent, le trouble observé lors de la stimulation pouvait être expliqué par un défaut de traitement spécifique des visages (individuation) mais aussi par un défaut d'accès à la mémoire sémantique. Nous avons étudié un patient implanté en SEEG (DN) avec une électrode dans le gyrus fusiforme antérieur droit en utilisant d'autres tâches lors des stimulations. Nous avons construit une tâche de pointage dans laquelle le patient devait pointer un item célèbre parmi 2 inconnus, en utilisant soit des visages, soit des noms (3 visages dont 1 célèbre, ou 3 noms dont 1 célèbre). Spécifiquement durant la stimulation électrique du gyrus fusiforme antérieur doit, le patient était incapable de pointer le visage célèbre, mais restait capable de pointer le nom célèbre. Cela montre que le gyrus fusiforme antérieur droit a un rôle crucial dans l'individuation des visages mais pas dans la mémoire sémantique. En d'autres termes, même située dans l'ATL, cette région reste impliquée dans des processus visuels de haut niveau et pas dans la mémoire sémantique. Par ailleurs, comme pour la patiente CD (Jonas et al., 2015, *Cortex*), nous avons montré que cette région est localisée dans une zone de susceptibilité magnétique en IRM fonctionnelle, avec une absence de signal et de réponses sélectives aux visages dans cette région. En revanche, en utilisant la FPVS durant la SEEG, nous avons enregistré des réponses sélectives aux visages très amples spécifiquement sur les sites de stimulation évoquant un trouble de l'identité des visages. Cela montre encore une fois la valeur fonctionnelle de la méthode FPVS. Ce travail fait l'objet d'un article dont je suis dernier auteur et qui a été soumis (Volfart A, Yan X, Maillard L, Rossion B, Jonas J, Intracerebral electrical stimulation and electrophysiology identifies the right anterior fusiform gyrus as key node of thehuman face identity recognition network).

La troisième étude concerne les bases neurales de la mémoire sémantique, et plus précisément de l'association visages-noms pour des personnes célèbres. Nous avons construit un paradigme FPVS permettant de mettre en évidence cette association. L'avantage de la FPVS est que cette méthode nous permet de mettre en évidence de manière directe des

réponses reflétant le processus d'association entre un visage et un nom (la réponse ne peut être générée uniquement si l'association a été réalisée), à l'opposé des études précédentes qui ont étudié de manière indirecte ce processus d'association, en comparant les réponses évoquées séparément par les visages et par les noms. Après avoir validé ce paradigme à l'aide de l'EEG de scalp chez des sujets sains, nous avons testé 7 patients implantés en SEEG avec des électrodes dans le lobe temporal gauche. Cette étude, dont je suis 2ème auteur, a été faite en collaboration avec Bruno Rossion (codirecteur de la thèse) et Louis Maillard (Volfart, Jonas, et al., 2020, *Plos Biology*). Nous avons mis évidence des sites avec des réponses « pures » d'association visages-noms, qui ne répondent pas aux visages isolément, ni aux noms isolément, mais uniquement à l'association des deux. Ces sites étaient tous localisés dans le lobe temporal antérieur. Leur faible nombre ne permettait pas une cartographie précise, mais un recrutement de plus de patients est en cours afin de rendre possible la cartographie fonctionnelle de cette fonction d'association. Cette étude montre que le lobe temporal gauche est un site d'intégration des visages et des noms au sein d'une représentation unifiée amodale.

En conclusion, ce travail de thèse montre que les processus de perception visuelle de haut niveau (dont l'individuation des visages), occupent une grande partie du VOTC, jusqu'au niveau du gyrus fusiforme antérieur dans l'ATL. En avant, les régions sont plus impliquées dans la mémoire sémantique, et en particulier dans l'intégration des visages et des noms au sein d'une représentation unifiée amodale. Les patients avec une épilepsie temporo-mésiale (type d'épilepsie focale la plus fréquente en SEEG et en chirurgie de l'épilepsie) montrent une atteinte de la mémoire sémantique sans atteinte des mécanismes d'individuation des visages (en accord avec la localisation de leur épilepsie), ce qui valide le modèle du cerveau épileptique pour l'étude par la SEEG des mécanismes de perception visuelle de haut niveau des visages.

6.4.2 Valorisation de la thèse

Cette thèse a été valorisée avec plusieurs communications affichées :

-Volfart, A., Yan, X., Maillard, L., Rossion, B. & Jonas, J. Intracerebral electrical stimulation of the right anterior fusiform gyrus elicits a transient face-specific impairment in recognizing famous people. Journées de Neurophysiologie Clinique, Nancy, France (2019).

-Volfart, A., Jonas, J., Maillard, L., Rossion, B. & Brissart, H. Typical unfamiliar face discrimination ability in anterior temporal lobe epilepsy. Vision Sciences Society, St Pete Beach, USA (2019).

-Volfart, A., Jonas, J., Maillard, L., Colnat-Coulbois, S. & Rossion, B. Evidence for integrated face-name representations in the left ventral anterior temporal cortex. Groupement de Recherche (GDR) Vision, Paris, France (2018).

Cette thèse a été valorisée par une communication orale dans un congrès international :

-Volfart, A., Jonas, J., Maillard, L., Rossion, B. & Brissart, H. Face discrimination abilities in patients with temporal lobe epilepsy. European Conference on Visual Perception, Louvain, Belgique (2019).

Chapitre 7 : Bibliographie

7.1 Liste des publications référencées PubMed

1. Volfart A, **Jonas J**, Maillard L, Busigny T, Rossion B, Brissart H. Typical visual unfamiliar face individuation in left and right mesial temporal epilepsy [published online ahead of print, 2020 Aug 7]. Neuropsychologia. 2020;147:107583. doi:10.1016/j.neuropsychologia.2020.107583
2. Jacques C, Rossion B, Volfart A, Brissart H, Colnat-Coulbois S, Maillard L, **Jonas J**. The neural basis of rapid unfamiliar face individuation with human intracerebral recordings [published online ahead of print, 2020 Jul 16]. Neuroimage. 2020;117174.
3. Volfart A, **Jonas J**, Maillard L, Colnat-Coulbois S, Rossion B. Neurophysiological evidence for crossmodal (face-name) person-identity representation in the human left ventral temporal cortex. PLoS Biol. 2020;18(4):e3000659.
4. Hagen S, Jacques C, Maillard L, Colnat-Coulbois S, Rossion B, **Jonas J**. Spatially Dissociated Intracerebral Maps for Face- and House-Selective Activity in the Human Ventral Occipito-Temporal Cortex. Cereb Cortex. 2020;30(7):4026-4043.
5. Jacques C, **Jonas J**, Maillard L, Colnat-Coulbois S, Rossion B, Koessler L. Fast periodic visual stimulation to highlight the relationship between human intracerebral recordings and scalp electroencephalography. Hum Brain Mapp. 2020;41(9):2373-2388.
6. Lochy A, Jacques C, Maillard L, Colnat-Coulbois S, Rossion, B, **Jonas J**. Selective visual representation of letters and words in the left ventral occipito-temporal cortex with intracerebral recordings. Proc Natl Acad Sci U S A. 2018;115:E7595-E7604.
7. Rossion B, Jacques C, **Jonas J**. Mapping face categorization in the human ventral occipitotemporal cortex with direct neural intracranial recordings. Ann N Y Acad Sci. 2018. In press
8. **Jonas J**, Brissart H, Hossu G, Colnat-Coulbois S, Vignal JP, Rossion B, Maillard L. A face identity hallucination (palinopsia) generated by intracerebral stimulation of the face-selective right lateral fusiform cortex. Cortex. 2018;99:296-310.
9. Salado AL, Koessler L, De Mijolla G, Schmitt E, Vignal JP, Civit T, Tyvaert L, **Jonas J**, Maillard LG, Colnat-Coulbois S. sEEG is a Safe Procedure for a Comprehensive Anatomic Exploration of the Insula: A Retrospective Study of 108 Procedures Representing 254 Transopercular Insular Electrodes. Oper Neurosurg. 2018;14:1-8.
10. Bédos Ulvin L, **Jonas J**, Brissart H, Colnat-Coulbois S, Thiriaux A, Vignal JP, Maillard L. Intracerebral stimulation of left and right ventral temporal cortex during object naming. Brain Lang. 2017;175:71-76.
11. Abdallah C, Maillard LG, Rikir E, **Jonas J**, Thiriaux A, Gavaret M, Bartolomei F, Colnat-Coulbois S, Vignal JP, Koessler L. Localizing value of electrical source imaging: Frontal lobe, malformations of cortical development and negative MRI related epilepsies are the best candidates. Neuroimage Clin. 2017;16:319-329.
12. Krieg J, Koessler L, **Jonas J**, Colnat-Coulbois S, Vignal JP, Bénar CG, Maillard LG. Discrimination of a medial functional module within the temporal lobe using an effective connectivity model: A CCEP study. Neuroimage. 2017;161:219-231.
13. Carpentier N, Cecchin T, Koessler L, Louis-Dorr V, **Jonas J**, Vignal JP, Carpentier M, Szurhaj W, Bourgin P, Maillard L. Stereo-electroencephalography identifies N2 sleep and spindles in human hippocampus. Clin Neurophysiol. 2017;128:1696-1706.
14. Nozaradan S, Mouraux A, **Jonas J**, Colnat-Coulbois S, Rossion B, Maillard L. Intracerebral evidence of rhythm transform in the human auditory cortex. Brain Struct Funct. 2017;222:2389-2404.
15. Weiner KS, **Jonas J**, Gomez J, Maillard L, Brissart H, Hossu G, Jacques C, Loftus D, Colnat-Coulbois S, Stigliani A, Barnett MA, Grill-Spector K, Rossion B. The Face-Processing Network Is Resilient to Focal Resection of Human Visual Cortex. J Neurosci. 2016;36:8425-40.

16. **Jonas J**, Jacques C, Liu-Shuang J, Brissart H, Colnat-Coulbois S, Maillard L, Rossion R. A face-selective ventral occipito-temporal map of the human brain with intracerebral potentials. Proc Natl Acad Sci U S A. 2016;113:E4088-97.
17. **Jonas J**, Rossion B, Brissart H, Frismand S, Jacques J, Hossu G, Colnat-Coulbois S, Vespignani H, Vignal JP, Maillard L. Beyond the core face-processing network: intracerebral stimulation of a face-selective area in the right anterior fusiform gyrus elicits transient prosopagnosia. Cortex. 2015;72:140-55.
18. Alexandre V, Mercedes B, Valton L, Maillard L, Bartolomei F, Szurhaj W, Hirsch E, Marchal C, Chassoux F, Petit J, Crespel A, Nica A, Navarro V, Kahane P, De Toffol B, Thomas P, Rosenberg S, Denuelle M, **Jonas J**, Ryvlin P, Rheims S. Risk factors of postictal generalized EEG suppression in generalized convulsive seizures. Neurology. 2015;85:1598-603.
19. Koessler L, Cecchin T, Colnat-Coulbois S, Vignal JP, **Jonas J**, Vespignani H, Ramantani G, Maillard LG. Catching the Invisible: Mesial Temporal Source Contribution to Simultaneous EEG and SEEG Recordings. Brain Topogr. 2015;28:5-20.
20. Carpentier N, **Jonas J**, Schaff JL, Koessler L, Maillard L, Vespignani H. The feasibility of home polysomnographic recordings prescribed for sleep-related neurological disorders: a prospective observational study. Neurophysiol Clin. 2014;44:251-5.
21. Monfort V, Pfeuty M, Klein M, Collé S, Brissart H, **Jonas J** , Maillard L. Distortion of time interval reproduction in an epileptic patient with a focal lesion in the right anterior insular/inferior frontal cortices. Neuropsychologia. 2014;64C:184-194.
22. **Jonas J**, Rossion B, Krieg J, Koessler K, Colnat-Coulbois S, Vignal JP, Vespignani H, Jacques C, Brissart H, Maillard L. Intracerebral electrical stimulation of a face-selective area in the right inferior occipital cortex impairs individual face discrimination. NeuroImage. 2014;99:487-97.
23. **Jonas J**, Maillard L, Frismand F, Colnat-Coulbois S, Vespignani H, Rossion R, Vignal JP. Self-face hallucination evoked by electrical stimulation of the human brain. Neurology. 2014;83:336-8.
24. **Jonas J**, Frismand S, Vignal JP, Colnat-Coulbois S, KoesslerL , Vespignani H, Rossion B, Maillard L. Right hemispheric dominance of visual phenomena evoked by intracerebral stimulation of the human visual cortex. Human Brain Mapping. 2014;35:3360-71.
25. Bourion-Bédès S, Hingray C, Faust C, Vignal JP, Vespignani H, Schwan R, **Jonas J**, Maillard L. Pitfalls in the diagnosis of new-onset frontal lobe seizures. Epilepsy Behav Case Rep. 2014;2:1-3.
26. Carpentier N, **Jonas J**, Gambier N, Vignal JP, Maillard L, Vespignani H. Adherence to medication and epilepsy: a current issue. Therapie. 2013;68:297-301.
27. Carpentier N, **Jonas J**, Frismand S, Vignal JP, Rikir E, Baumann C, Lapicque F, Saint-Marcoux F, Vespignani H, Maillard L. Direct evidence of non-adherence to antiepileptic medication in refractory focal epilepsy. Epilepsia. 2013;54:e20-e23.
28. Ramantani G, Koessler L, Colnat-Coulbois S, Vignal JP, Isnard J, Catenoix H, **Jonas J**, Zentner J, Schulze-Bonhage A, Maillard LG. Intracranial evaluation of the epileptogenic zone in regional infrasylvian polymicrogyria. Epilepsia. 2013;54:296-304.
29. Richard S, Idrissi AL, **Jonas J**, Vuillemet F, Toussaint-Hacquard M, Ducrocq X. Two cases of cervical artery dissection with cerebral ischemic recurrences due to heparin-induced thrombocytopenia. Platelets. 2013;24:248-9.
30. **Jonas J**, Descoins M, Koessler L, Colnat-Coulbois S, Guye M, Sauvée M, Vignal JP, Vespignani H, Rossion B, Maillard L. Focal intracerebral stimulation of a face-sensitive cortical area causes transient specific impairment in face recognition. Neuroscience. 2012;222:281-8.
31. Maillard L, **Jonas J**, Boyer R, Frismand S, Mathey G, Vignal JP, Guillemin F, Maignan M, Vespignani H. One year outcome after a first clinically possible epileptic seizure: predictive value of clinical classification and early EEG. Neurophysiol Clin. 2012;42:355-62.
32. **Jonas J**, Vignal JP, Baumann C, Anxionnat JF, Muresan M, Vespignani H, Maillard L. Effect of hyperventilation on seizure activation: potentiation by antiepileptic drug tapering. J Neurol Neurosurg Psychiatry. 2011;82:928-30.

33. Kaminsky P, Acquaviva-Bourdain C, **Jonas J**, Pruna L, Chalhoub G, Rigal O, Grignon Y, Vianey-Saban C. Subacute myopathy in a mature patient due to multiple acyl-CoA dehydrogenase deficiency. Muscle Nerve. 2011;43:444-6.
34. Maillard L, Vignal JP, Boyez R, **Jonas J**, Hubsch C, Vespignani H. Risk of epilepsy after a first epileptic seizure in adults: Can we predict the future? Rev Neurol. 2009;165:782-8.

7.2 Chapitre de livre

1. **Jonas J**. Prédiction du devenir fonctionnel postopératoire en chirurgie de l'épilepsie grâce aux stimulations électriques corticales. Dans : Hélène Brissart et Louis Maillard, Neuropsychologies des épilepsies de l'adulte, Louvain-La-Neuve, Editions De Boeck Supérieur, 2018, pp. 109-131.

7.3 Communications orales dans des conférences internationales

1. **Jonas J**. Understanding face categorization with intracerebral recording and stimulation in the human ventral occipito-temporal cortex. The organisational principles of the visual ventral stream, Experimental Psychology Society, Cambridge, 2019.
2. **Jonas J**. A comprehensive cartography of selective responses to letters and words in the left ventral temporal cortex with direct recordings of neural activity. Society for Neuroscience Annual Meeting, Washington DC, USA, 2017.
3. **Jonas J**. Beyond the core face-processing network: intracerebral stimulation of a face-selective area in the right anterior fusiform gyrus elicits transient prosopagnosia. Neurocog, Leuven, Belgique, 2016.
4. **Jonas J**. Beyond the core face-processing network: intracerebral stimulation of a face-selective area in the right anterior fusiform gyrus elicits transient prosopagnosia. Visual Sciences Society Annual Meeting, St. Pete Beach, USA, 2016.
5. **Jonas J**. Understanding human face perception using intracerebral recordings and electrical stimulation. Séminaires du pôle Cognition et Systèmes, Institute of Neuroscience, Université Catholique de Louvain, Belgique, 2015.
6. **Jonas J**. A gradual increase of face-selectivity along the human ventral visual pathway: direct evidence from intracerebral recordings with fast periodic visual stimulation. Society for Neuroscience Annual Meeting, Washington DC, USA, 2014.
7. **Jonas J**. Neural Coding of Individual Faces in the Human Right Inferior Occipital Cortex: Direct Evidence from Intracerebral Recordings and Stimulations. Society for Neuroscience Annual Meeting, San Diego, USA, 2013.
8. **Jonas J**. Functional relevance of intracerebral steady-state VEPs using face stimuli. Horizons in clinical neurophysiology, An European Chapter of the IFCN conference (British Society for Clinical Neurophysiology and Société de Neurophysiologie Clinique de Langue Française), Oxford, UK, 2013.
9. **Jonas J**. Neural coding of individual faces in the human right inferior occipital cortex: direct evidence from intracerebral recordings and stimulations. Visual Sciences Society Annual Meeting, Naples, USA, 2013.
10. **Jonas J**. Role and time-course of the right occipital face area: Evidence from intracerebral stimulations and recordings. Society For Neuroscience Annual Meeting, New Orleans, USA, 2012
11. **Jonas J**. Intra-cerebral electrical stimulation of a face sensitive cortical area causes transient specific impairment in face recognition. Visual Sciences Society Annual Meeting, Naples, USA, 2012.

7.4 Communications orales dans des conférences nationales

1. **Jonas J**. Utilisation d'une plateforme d'e-learning pour la réalisation de travaux pratiques de physiologie. Congrès National de Physiologie et de Biologie Intégrative, Montpellier, 2019.

2. **Jonas J**. A comprehensive cartography of selective responses to letters and words in the left ventral temporal cortex with direct recordings of neural activity. GDR Vision, Paris, 2018.
3. **Jonas J**. Stimulation corticale et prosopagnosie. Journées de Neurophysiologie Clinique, Nancy, 2019.
4. **Jonas J**. Codage de la reconnaissance visuelle à l'échelle des populations deones. Journées de Neurophysiologie Clinique, Lille, 2018.
5. **Jonas J**. Lorsque les crises sont psychogènes, du diagnostic à la prise en charge. Journées Françaises de l'Epilepsie, Marseille, 2017.
6. **Jonas J**. Hallucinations et illusions dans les crises d'épilepsie. Journées Françaises de l'Epilepsie, Toulouse, 2016.
7. **Jonas J**. Nouvelle approche électrophysiologique de la perception visuelle par la stimulation visuelle périodique rapide. Congrès de la Société de Neurophysiologie Clinique de Langue Française (SNCLF), Angers, 2014.
8. **Jonas J**. Neural Coding of Individual faces in the Human Right Inferior Occipital Cortex: Direct Evidence from Intracerebral Recordings and Stimulations. 1ère journée interrégionale « Recherche et Neuroscience », Dijon, France, 2013.
9. **Jonas J**. « Docteur, je ne vous reconnais plus ! ». Journées Françaises de l'Epilepsie, Bordeaux, 2011
10. **Jonas J**. Préhension et manipulation des objets durant une crise du cortex préfrontal gauche. Journées Françaises de l'Epilepsie, Marseille, 2009.

Chapitre 8 : Perspectives

8.1 Perspectives à court terme

8.1.1 Contribution des informations de bas niveau

De nombreuses études actuelles suggèrent que la perception des visages repose sur les informations visuelles de bas niveau (Honey et al., 2008 ; VanRullen, 2006 ; Crouzet and Thorpe, 2011 ; Andrews et al., 2010 ; Rice et al., 2014 ; Coggan et al., 2016), c'est-à-dire sur les informations contenues dans l'image (contraste, luminance, fréquences spatiales). Le système de perception ne serait alors qu'un simple analyseur d'image. Une autre vision suppose que la perception des visages est en grande partie basée sur notre expérience personnelle de ce qu'est un visage. Dans ce schéma, la mémoire jouerait un rôle important dans le processus de perception. Nous avons réalisé une étude sur 61 patients en SEEG-FPVS qui compare les réponses sélectives aux visages lorsque les visages sont intacts et lorsqu'ils ont été brouillés (perte de la structure du visage avec préservation des informations de bas niveau). Cette étude, que j'ai coordonnée, a été réalisée en collaboration avec Bruno Rossion, Louis Maillard et Corentin Jacques (Université Catholique de Louvain). Cette étude fait l'objet d'un article qui est actuellement soumis et dont je suis le dernier auteur (Jacques C, Rossion B, Maillard L, Colnat-Coulbois S, Jonas J. Minimal contribution of low-level properties to intracerebral face-selective responses in ventral occipitotemporal cortex). Pour cela nous avons testé les patients avec le paradigme dit « face-localizer » dans lequel les images étaient intactes et le même paradigme mais dans lequel toutes les images étaient brouillées (Figure 10A). Dans la condition intacte, nous avons enregistré des réponses sélectives aux visages très fortes et notamment à droite (Figure 10C). En revanche, nous n'avons presque pas enregistré de réponses dans la condition brouillée. Tous les 790 contacts (sauf 2) ont montré une réponse dans la condition intacte mais pas dans la condition brouillée (pour un exemple de contact, voir Figure 10B). De plus, en quantifiant l'amplitude des réponses surtout les contacts, quelle que soit leur significativité, nous avons observé une baisse dramatique des amplitudes pour la condition brouillée (Figure 10C). Ces résultats montrent que les informations de bas niveau seules ne sont pas suffisantes pour générer une réponse sélective aux visages et vont donc à l'encontre d'un rôle majeur des informations visuelles de bas niveau dans la perception des visages.

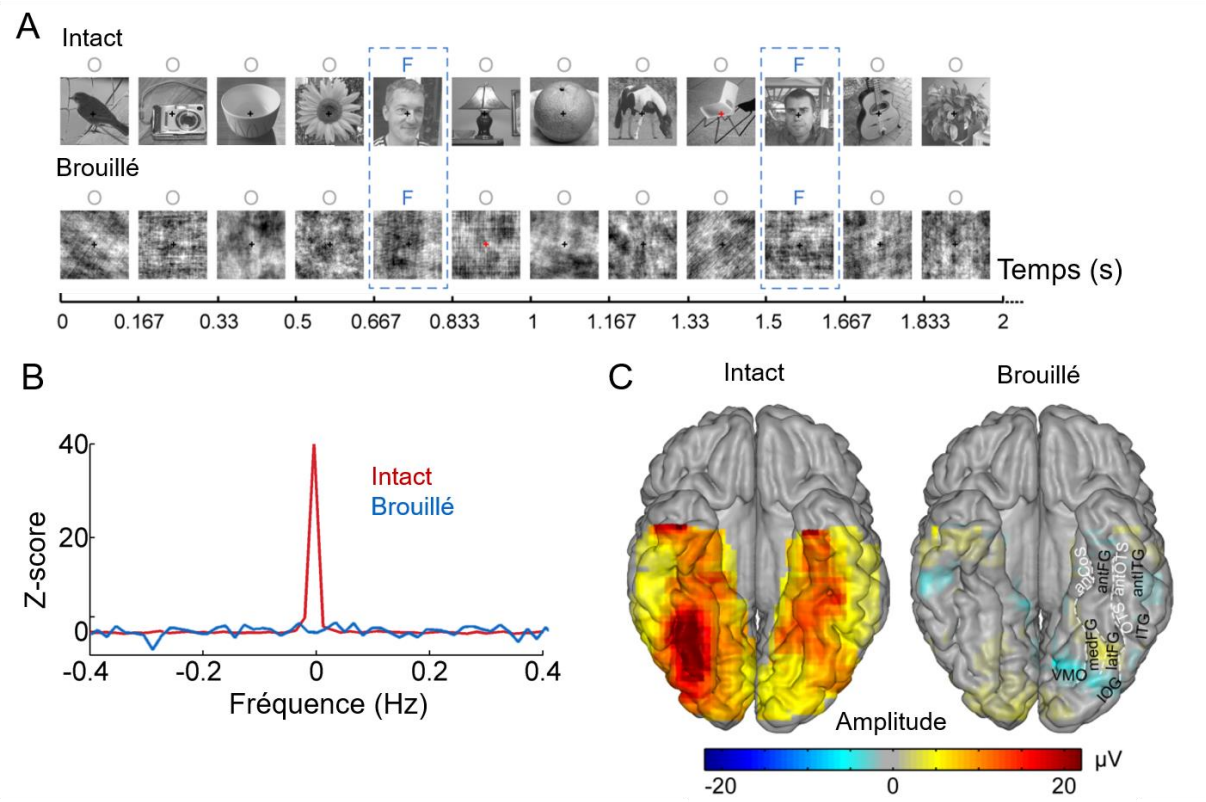

Figure 10. Absence de réponses sélectives aux visages uniquement sur la base des informations visuelles de bas niveau. A. Paradigme FPVS dit « face-localizer » en condition intacte et en condition brouillée. La fréquence des visages était déterminée à 1.2 Hz pour les 2 conditions. B. Exemple d'un contact représentatif chez un patient dans le latFG droit enregistrant une réponse dans la condition intacte mais pas dans la condition brouillée (pattern de réponses retrouvé sur les 790 contacts sélectifs aux visages en condition intacte, sauf 2 avec une réponse en condition brouillée). La fréquence de sélectivité aux visages est à 0 Hz (somme des réponses à 1.2 Hz et harmoniques centrée sur 0). C. Cartographies d'amplitude des réponses aux visages dans la condition intacte et la condition brouillée, sur tous les contacts enregistrés chez les 61 patients inclus dans l'étude, dans l'espace Talairach. Notez la baisse dramatique de l'amplitude en condition brouillée.

Nous avons également débuté une étude SEEG-FPVS utilisant le phénomène de paréidolie ou tendance naturelle du cerveau humain à percevoir des visages là où il n'y en a pas, notamment dans des objets ou des paysages, malgré l'absence d'informations de bas niveau en commun avec les visages (puisque ce ne sont pas des visages). Nous avons construit un paradigme FPVS dans lequel des objets qui évoquent des visages sont insérés périodiquement dans des séquences d'objets qui n'évoquent pas des visages. Si notre hypothèse se confirme, et que la perception des visages ne dépend pas des informations de bas niveau mais de l'expérience que nous avons des visages, nous devrions enregistrer des réponses fortes dans les régions sélectives aux visages. Nous avons commencé à inclure des patients et je coordonne cette étude.

8.1.2 Perception des visages et lecture

Dans quelle mesure le système de perception des visages et le système de la lecture partagent des régions corticales dans le VOTC pour leur fonctionnement est actuellement débattu. Il a été proposé que les visages et les mots partagent certaines fonctions et certains circuits neuronaux dans le VOTC, par exemple car ils nécessitent tous les 2 une vison fovéale et une discrimination individuelle au sein leur catégorie (Behrmann et Plaut, 2013; Nestor et al., 2012; Robinson et al., 2017). Nous avons réalisé une étude SEEG-FPVS enregistrant les réponses sélectives aux visages (paradigme « face-localizer » de l'étude Jonas et al., 2016, *PNAS*, voir Figure 2A) et aux mots (condition PL-M de l'étude de Lochy, (…), Jonas, 2018, *PNAS*, voir Figure 8A) chez 37 patients en SEEG. Ces patients ont aussi été testés avec le paradigme FPVS pour l'enregistrement de réponses sélectives aux maisons (Hagen, (….), Jonas, 2020, *Cereb Cortex*, voir Figure 4A) et celui-ci a servi de condition contrôle. Cette étude, que j'ai coordonnée avec Bruno Rossion et dont je suis l'avant dernier auteur, a été réalisée en collaboration avec Simen Hagen, Aliette Lochy (Université du Luxembourg), et Louis Maillard. Cette étude fait l'objet d'un article qui est actuellement soumis (Hagen S, Lochy A, Jacques C, Maillard L, Colnat-Coulbois S, Jonas J, Rossion B. Dissociated face- and word-selective intracerebral responses in the human ventral occipito-temporal cortex).

Dans cet article, nous apportons plusieurs arguments montrant que les visages et les mots sont dissociés spatialement et fonctionnellement. Sur le plan spatial, les visages sont fortement latéralisés à droite et les mots à gauche. Visages et mots sont également séparés dans l'axe médio-latéral et dans l'axe postérieur-antérieur au sein d'un même hémisphère. Sur le plan fonctionnel, les réponses aux visages sont très faiblement corrélées en amplitude aux réponses aux mots. De plus, cette corrélation visages-mots est similaire à celle qui existe entre les réponses aux visages et aux maisons, alors que cette dernière catégorie est connue pour ne partager aucune fonction avec les visages (comme cela a été aussi montré dans l'étude de Hagen, (….), Jonas, 2020, *Cereb Cortex*).

8.2 Perspectives à moyen terme

8.2.1 Relation entre les réponses à travers les différentes bandes de fréquence

Les enregistrements électrophysiologiques donnent accès à différents types de réponses en fonction de la bande fréquence étudiée (basses fréquences en dessous de 30Hz et hautes fréquences au-dessus de 30Hz ou réponses gamma). Cette richesse pose de nombreux problèmes en neurosciences actuellement. A partir d'une question scientifique, quel type de réponse faut-il étudier ? S'il existe plusieurs types de réponses, sont-elles superposables, ou reflètent-elles des processus différents ? Quelles sont les bases neurophysiologiques de chaque type de réponses ? Si une cartographie d'une fonction doit

être réalisée, est-ce que les hautes fréquences permettront des résultats plus précis sur le plan spatial, comme cela est parfois suggéré (Miller et al., 2007) ? Il est donc crucial de comprendre les relations entre ces différents types de réponses, pour notre domaine de recherche mais aussi pour les autres domaines en neurosciences utilisant des enregistrements électrophysiologiques.

Notre méthode SEEG-FPVS est particulièrement bien appropriée afin de comparer des réponses issues de 2 bandes de fréquences différentes. Premièrement, la FPVS permet d'identifier et de quantifier les réponses dans les hautes fréquences (Figure 11). Pour les hautes fréquences, il suffit d'ajouter une analyse temps-fréquence avant la transformée de Fourier. L'analyse temps-fréquence permet de visualiser des bouffées ou « bursts » périodiques d'activité gamma. Après un moyennage fréquentiel à travers les hautes fréquences, une transformée de Fourier permet de mettre en évidence cette activité périodique gamma dans le domaine fréquentiel, de la même manière que les basses fréquences. Deuxièmement, les avantages de la FPVS (sensibilité, objectivité et réponses facilement quantifiables) sont un atout lorsqu'il s'agit de comparer 2 types de réponses. Par rapport aux méthodes classiques de présentation non-périodique, nous évacuons la subjectivité liée à la définition a priori de la fenêtre temporelle à étudier ou le choix arbitraire d'un composant (ou potentiel évoqué) à analyser pour la comparaison.

Nous avons commencé à étudier les réponses FPVS sélectives aux visages dans les basses et hautes fréquences chez 90 patients en SEEG. Cette étude, que je coordonne, est réalisée en collaboration avec Bruno Rossion, Louis Maillard et Corentin Jacques (Université Catholique de Louvain). A ce stade, nous avons fait les observations suivantes. Premièrement, les réponses basses fréquences sont beaucoup plus fréquentes que les réponses gamma (rapport de 1/5). Deuxièmement, les cartographies en basses fréquences et en gamma sont similaires dans la partie postérieure du VOTC (mêmes régions sélectives aux visages, prédominance du latFG droit). Dans ces régions postérieures, il existe une forte corrélation d'amplitude entre ces 2 réponses. Cependant, les réponses gamma sont rares dans l'ATL alors qu'elles sont fréquentes en basses fréquences (voir Jonas et al., 2016, *PNAS*). Des analyses sont en cours afin de comprendre la raison d'une telle diminution des réponses gamma dans l'ATL. A ce stade, ces résultats suggèrent qu'une cartographie en gamma manquerait de mettre en évidence les régions sélectives aux visages dans l'ATL. D'autres études en ECOG ont également échoué à montrer des réponses gamma sélectives aux visages dans l'ATL (Kadipasaoglu et al. 2016 ; Schrouff et al., 2020). Enfin, nos analyses spatiales montrent que les réponses gamma ne sont pas plus précises spatialement que les réponses basses fréquences (même pattern de propagation spatiale des réponses autour des réponses les plus amples). Au total, ces résultats préliminaires suggèrent à ce stade un

avantage à cartographier les régions sélectives aux visages avec des réponses dans les basses fréquences (réponses plus fréquentes, cartographie de l'ATL, pas de supériorité du gamma dans la précision spatiale). Des études ultérieures seront menées afin de mieux comprendre les relations fonctionnelles entre ces 2 types de réponses, au-delà de leurs relations spatiales.

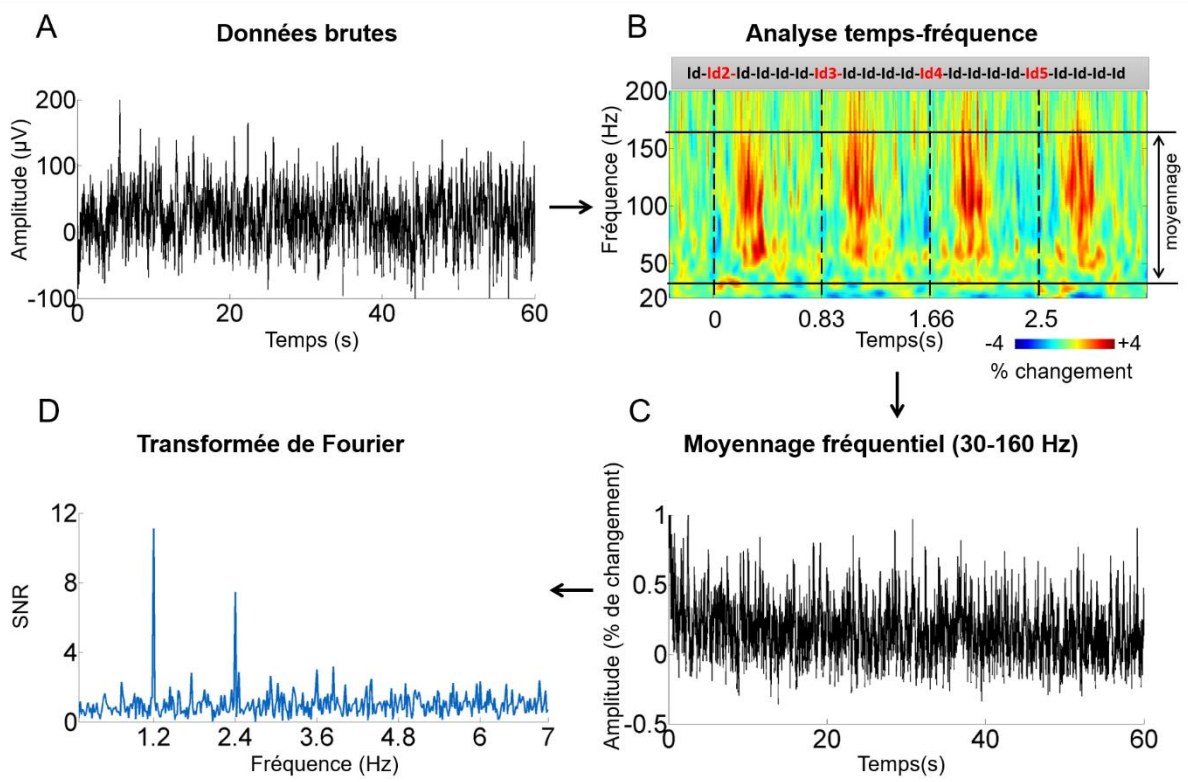

Figure 11. Identifier des réponses périodiques dans les hautes fréquences (gamma). Ici est représentée une analyse sur un contact implanté dans le latFG droit d'un patient pour le paradigme FPVS sur l'individuation des visages à l'endroit (voir Figure 3A). A. Données brutes enregistrées sur ce contact pendant l'expérience. B. Analyse temps-fréquence (dans un souci de clarté, ici est représenté un grand moyennage sur 4 cycles et non pas une analyse temps-fréquence sur toute la séquence). Nous observons des bouffées d'activité périodique dans la bande gamma. Ces activités suivent les changements d'identité (Id2, Id3, etc.) qui apparaissent de manière périodique à la fréquence de 1,2 Hz. C. Moyennage fréquentiel de l'analyse temps-fréquence dans la bande gamma (de 30 Hz à 160 Hz). D. Résultats obtenus après transformée de Fourier. Les réponses à 1,2 Hz et à ses harmoniques correspondent à des réponses de discrimination individuelle de l'identité des visages dans la bande gamma.

8.2.2 Traitement des visages au niveau cellulaire

L'une des grandes théories en neurosciences est que le neurone est la brique élémentaire du cerveau et que la compréhension du cerveau ne peut passer uniquement par l'étude de ces briques prises isolément (« neural doctrine », Barlow, 1972). Cette théorie a été

le point de départ de nombreuses recherches. Chez le singe, des enregistrements de neurones individuels ont été réalisés dans la voie visuelle ventrale et il a été découvert dans les années 1970 des neurones sélectifs aux visages, c'est-à-dire répondant uniquement aux visages (Gross et al., 1972). Ces recherches chez le singe se sont poursuivies jusqu'à une étude récente prétendant avoir découvert le « code » permettant de reconnaître les visages (Chang & Tsao, 2017). Cependant, cette espèce n'est pas très efficace en perception d'identité faciale et ne possède pas les structures cérébrales similaires à l'Homme (notamment le gyrus fusiforme) pour réaliser cette fonction, rendant ce modèle animal particulièrement inadéquat (Rossion et Taubert, 2019). Chez l'Homme, les enregistrements de neurones individuels sont beaucoup plus rares et réalisés presque uniquement dans l'hippocampe pour des raisons méthodologiques. Ces enregistrements ont tout de même permis la découverte de neurones « concepts » dans l'hippocampe, ne répondant qu'à un seul concept sémantique bien défini (par exemple à Jennifer Aniston ou à Star Wars ; Quiroga et al., 2005). Ces neurones jouent un rôle crucial dans la mémoire et non pas dans la perception des visages. Actuellement un énorme champ de recherche s'ouvre avec la possibilité d'enregistrer des neurones individuels dans le cortex chez l'Homme (et non pas uniquement dans l'hippocampe). Plusieurs équipes ont déjà réussi à enregistrer des neurones sélectifs aux visages chez l'Homme (Axelrod et al., 2019 ; Khuvis et al., 2019). Nous avons la chance au CHRU de Nancy d'avoir également cette possibilité.

Nous avons obtenu en 2013 un financement de plus de 500 000 € (FRC et Conseil Régional de Lorraine) afin d'acheter un système d'acquisition pour réaliser des enregistrements unitaires chez les patients épileptiques implantés en SEEG via des microélectrodes (système Blackrock). Le CHRU de Nancy s'est porté promoteur de cette étude (étude REUNIE, investigateur principal : Pr Louis Maillard). Pour la mise en place pratique des enregistrements, nous avons bénéficié de la collaboration de l'un des experts mondiaux dans le domaine (Rodrigo Quian Quiroga, University of Leicester). Afin d'enregistrer des réponses au niveau des neurones uniques, nous avons combiné l'enregistrement des microélectrodes et la FPVS. Actuellement, nous avons inclus et enregistré 20 patients. L'analyse de ces signaux étant particulière par rapport aux enregistrements classiques, cette recherche se fait en collaboration avec Pauline Jurczynski, ingénieur de formation et doctorante au sein de l'équipe Neurosciences des Systèmes et de la Cognition (CRAN UMR 7039 CNRS-Université de Lorraine), encadrée par Bruno Rossion et Radu Ranta (CRAN), et dont la thèse est centrée sur les aspects traitement du signal des enregistrements unitaires. En ce qui concerne l'étude des implications neurocognitives de ces enregistrements, nous avons obtenu un contrat doctoral en 2020 (co-financement école doctorale BIOSE - Région Grand Est) pour le

financement de la thèse de Marie-Alphée Laurent dont je suis le co-encadrant avec Bruno Rossion.

Nos résultats préliminaires sont très prometteurs et ont déjà permis de faire plusieurs observations. Premièrement, nous avons enregistré dans le latFG des neurones uniques sélectifs aux visages, c'est-à-dire des neurones qui déchargent des potentiels d'action de manière périodique, uniquement pour la présentation d'un visage (voir Figure 2A pour le paradigme FPVS). Nous avons également enregistré d'autres neurones dont la sélectivité aux visages se matérialise de manière inverse, c'est-à-dire par une diminution sélective du nombre de potentiels d'action à chaque présentation de visages. Cela montre qu'il existe différents patterns de sélectivité aux visages, soit des activations sélectives, soit des désactivations sélectives. Deuxièmement, nous avons enregistré des neurones spécifiquement dédiés au traitement de l'identité des visages dans le latFG, c'est-à-dire répondant uniquement lors des changements d'identité (voir Figure 7A pour le paradigme FPVS), avec un important effet d'inversion (diminution drastique de l'amplitude des réponses d'individuation lorsque les visages sont présentés à l'envers). Cette dernière observation montre qu'une partie du traitement de l'identité des visages est réalisée localement dans le latFG et non pas uniquement dans le lobe temporal antérieur comme cela est suggéré par d'autres études (Kriegeskorte et al., 2007; Anzellotti et al., 2014). Ce résultat corrobore également nos enregistrements intracérébraux classiques (obtenus sur des populations de neurones) qui ont montré des réponses d'individuation très amples et avec un fort effet d'inversion dans la même région, le latFG (Figure 3C, Jacques, (….), Jonas, in press, *Neuroimage*). Les réponses évoquées par d'autres paradigmes FPVS sont en cours d'analyse.

Cette recherche a un potentiel théorique énorme dans le domaine de la perception visuelle (quel est le rôle d'un neurone individuel dans la perception ? quels sont les traitements qui sont réalisés au niveau local ?) mais aussi de manière générale en neurosciences (quel type d'information porte un neurone unique ?).

8.2.3 Influence de la méthode de référence pour les cartographies intracérébrales

Nos cartographies SEEG-FPVS concernant les visages (Jonas et al., 2016, *PNAS*), les visages et les maisons (Hagen, (….), Jonas, 2020, *Cereb Cortex*) et les mots (Lochy, (….), Jonas, 2018, *PNAS*) ont été obtenues à l'aide de réponses enregistrées entre un contact SEEG actif et une électrode de référence dite monopolaire (référence à distance, soit une électrode EEG de scalp FpZ, soit un contact SEEG localisé dans la substance banche). Une question est de savoir si l'utilisation d'une méthode de référence locale permet d'améliorer nos cartographies, c'est-à-dire de renforcer les réponses réellement générées localement et d'éliminer les réponses issues de la diffusion biophysique des activités électriques (Li et al.,

2018). Nous avons étudié les réponses sélectives aux visages (paradigme dit « face-localizer, Figure 2A) obtenues chez 93 patients et comparé les cartographies obtenues avec notre méthode de référence monopolaire (électrode de référence à distance) avec des méthodes de référence locale (soit référence bipolaire, 1 contact actif et référence par un contact adjacent ; soit référence laplacienne, 1 contact actif et référence par la moyenne des 2 contacts adjacents de part et d'autre du contact actif). Cette étude, que je coordonne est réalisée en collaboration avec Simen Hagen, Radu Ranta et Bruno Rossion.

Les résultats préliminaires montrent que les cartographies de réponses sélectives aux visages varient assez peu en fonction de la méthode de référence utilisée. Les mêmes conclusions concernant les bases neuronales de la perception des visages sont tirées quelle que soit la méthode de référence. Néanmoins, il existe quelques différences. Par rapport à la méthode de référence monopolaire, les méthodes de référence locale permettent : (1) de diminuer le nombre de réponses sélectives aux visages dans des régions considérées comme non critiques (surtout dans le gyrus temporal inférieur et le gyrus parahippocampique), probablement par diminution des effets de la diffusion biophysique du signal, et (2) d'augmenter significativement le nombre de réponses sélectives aux visages dans l'ATL, grâce à une amélioration du rapport signal/bruit surtout due à une réduction importante du bruit. Dans nos futurs projets de recherche, une référence locale pourra être utilisée afin de maximiser nos chances d'identifier des réponses dans l'ATL. Par ailleurs, ce dernier résultat souligne le fait que l'enregistrement de réponses sélectives aux visages dans l'ATL est très dépendant du rapport signal/bruit et qu'une méthode sensible comme la SEEG-FPVS est nécessaire pour enregistrer ces réponses (Jonas et al. 2016, *PNAS* ; pour des réponses aux maisons dans l'ATL, voir Hagen, (….), Jonas, 2020, *Cereb Cortex*). La plupart des études iEEG n'ont pas rapporté de réponses sélectives aux visages dans l'ATL en basses fréquences, malgré le haut rapport signal/bruit des enregistrements intracrâniaux (pour de rares études avec des réponses dans l'ATL, voir Allison et al., 1999 ; Tanji et al., 2012). Pour la SEEG-FPVS, l'utilisation d'une référence locale permet d'améliorer la détection de ces réponses dans l'ATL, qui sont déjà détectables avec une référence monopolaire.

8.2.4 Traitement des visages familiers

Le but final de la perception des visages est de permettre une reconnaissance complète de la personne (avec son nom et les informations sémantiques associées). Cette reconnaissance complète peut être étudiée avec des visages connus, comme les visages de célébrités. Nous avons débuté une étude SEEG-FPVS permettant de mettre en évidence les régions répondant différentiellement aux visages connus (célèbres) et aux visages inconnus. Nous avons à ce stade inclus 31 patients. Cette étude se fait en collaboration avec Angélique

Volfart et Bruno Rossion. Les résultats préliminaires montrent que les régions qui répondent aux visages familiers sont situées dans l'ATL, précisément celles qui sont sensibles à l'association visages-noms (Volfart, Jonas, et al., 2020, *Plos Biology*) mais pas à l'individuation des visages inconnus (Jacques, (….), Jonas, in press, *Neuroimage*). Sans tomber dans l'excès de certaines théories modulaires, l'ensemble de ces résultats suggèrent que les processus visuels impliqués dans l'individuation des visages sont supportés par la partie postérieure du VOTC, tandis que les régions plus antérieures jouent un rôle dans la mémoire sémantique.

8.3 Perspectives à long terme

8.3.1 Poursuite des stimulations électriques intracérébrales

Dans l'avenir, je poursuivrai la recherche des aires cérébrales critiques pour la perception des visages grâce aux stimulations électriques intracérébrales appliquées au VOTC durant des tâches de perception des visages. L'objectif sera de réaliser une cartographie aussi complète que possible de ces aires critiques, et de déterminer le rôle de chacune de ces aires. L'observation d'une stimulation positive entrainant un déficit de perception des visages est aléatoire et dépend de plusieurs facteurs non modifiables, comme la position exacte des électrodes, la localisation des aires de perception des visages au niveau individuel, etc. Afin de maximiser nos chances de détecter ces aires, nous analysons le jour même les résultats des paradigmes FPVS « face-localizer » (Figure 2A) et d'individuation des visages (Figure 3A), et nous réalisons des stimulations électriques avec tâches de perception des visages en priorité sur les sites avec les réponses FPVS les plus amples.

8.3.2 Conséquences de la lobectomie temporale antérieure sur la perception des visages

L'étude ATENA-F a montré que les patients avec une épilepsie temporo-mésiale ont des mécanismes d'individuation des visages normaux par rapport aux sujets contrôles (Volfart, Jonas, et al., in press, *Neuropsychologia*). Cette étude comprend également une évaluation prospective de leurs capacités en perception des visages en post-opératoire, après lobectomie temporale antérieure. Nous avons à ce stade inclus 26 patients et 26 témoins appariés. Conformément aux résultats de nos études précédentes, nous prédisons que la chirurgie du lobe temporal antérieur impactera la mémoire sémantique et la mémoire épisodique liées aux visages, mais pas les capacités d'individuation des visages.

8.3.3 Traitement des émotions dans l'amygdale

L'amygdale joue un rôle important dans la discrimination des émotions faciales. Mais le rôle du VOTC et en particulier du latFG est plus débattu. Nous avons construit un paradigme FPVS permettant l'enregistrement de réponses de discrimination d'émotions faciales

(Dzhelyova et al., 2017). Nous avons appliqué ce paradigme à 30 patients SEEG implantés dans l'amygdale, dont 21 également dans le latFG. Les résultats préliminaires montrent des réponses de discrimination des émotions dans l'amygdale mais également dans le latFG. Dans le latFG, les réponses sont caractérisées par une très forte amplitude et par un fort effet d'inversion (réponses plus amples à l'endroit qu'à l'envers), ce qui montre que cette région joue un rôle très important dans la discrimination visuelle des émotions faciales. Une hypothèse serait que l'amygdale joue un rôle dans la valence à assimiler à chaque émotion, plutôt qu'à la discrimination visuelle des émotions. Cette étude est réalisée en collaboration avec Bruno Rossion et Stéphanie Caharel (laboratoire 2LPN, EA 7489, Université de Lorraine).

8.3.4 Dynamique temporelle de la perception des visages

La dynamique temporelle du processus de perception des visages reste encore méconnue, notamment parce les études en IRM fonctionnelle (qui sont dominantes sur ce thème) sont limitées par une faible résolution temporelle. Même si la plupart de nos études en SEEG-FPVS ont consisté en la quantification de l'amplitude des réponses dans le domaine fréquentiel, la méthode FPVS permet également une analyse des réponses dans le domaine temporel, comme pour des potentiels évoqués classiques (Liu-Shuang et al., 2014 ; Rossion et al., 2015). Dans l'avenir, nous souhaitons analyser dans le domaine temporel les réponses de sélectivité aux visages (Figure 2A) et de discrimination individuelle des visages (Figure 3A) acquises en SEEG chez un grand nombre de patients (plus de 100), afin d'avoir une vision globale de la dynamique temporelle de ces processus tout le long du VOTC. Il faut noter que l'interprétation de ces réponses dans le domaine temporel n'est pas facile pour plusieurs raisons : important chevauchement temporel des réponses (voir par exemple Barbeau et al., 2008), difficulté à déterminer avec objectivité le début exact de la réponse (quel critère statistique choisir ?), difficulté à déterminer les critères à retenir pour caractériser l'activation d'une région (début de la réponse ou pic de la réponse ?), importante variabilité inter-individuelle (ce qui augmente encore le chevauchement spatial des réponses lors du moyennage à travers les sujets), etc. Ce travail se fera en collaboration avec Bruno Rossion et Corentin Jacques.

8.3.5 Relation entre sélectivité aux visages et individuation des visages

Une question encore débattue est de savoir si une région impliquée dans l'individuation des visages doit être nécessairement sélective aux visages, c'est-à-dire montrer une réponse plus ample pour les visages par rapport aux objets (voir par exemple Kriegeskorte et al., 2007 et Nestor et al., 2011 pour des réponses d'individuation en dehors des régions sélectives aux visages). Nos cartographies de sélectivité pour les visages (Figure 2) et d'individuation des

visages (Figure 3) montrent qu'il existe, au niveau du groupe, un chevauchement spatial important entre ces 2 fonctions, notamment dans la partie postérieure du VOTC. Nous souhaitons à l'avenir obtenir des informations plus précises concernant ce chevauchement en analysant les patients qui ont bénéficié des 2 paradigmes FPVS : pourcentage de chevauchement de manière globale et en fonction des régions, chevauchement au niveau individuel, corrélation d'amplitude etc. Nous souhaitons également comparer la dynamique temporelle entre ces 2 fonctions. Ce travail se fera en collaboration avec Bruno Rossion et Corentin Jacques.

8.3.6 Relations entre la voie visuelle ventrale et l'hippocampe

Les informations visuelles sont traitées tout le long de la voie visuelle ventrale (anatomiquement dans le VOTC) puis envoyées dans l'hippocampe pour être encodées en mémoire épisodique. La méthode SEEG-FPVS permet l'enregistrement de réponses à la fois dans le VOTC et l'hippocampe chez un même patient. Afin de mieux comprendre les relations entre ces 2 structures, nous souhaitons dans l'avenir comparer les réponses enregistrées en SEEG-FPVS dans ces 2 structures, à l'aide de différents paradigmes FPVS (sélectivité aux visages, individuation des visages, discrimination de visages célèbres, etc.), dans les domaines fréquentiel et temporel, dans les basses et les hautes fréquences. Ce travail se fera en collaboration avec Bruno Rossion et Corentin Jacques.

8.3.7 Relations surface-profondeur

Dans l'unité d'épileptologie, nous avons la chance de réaliser, pour la plupart des patients implantés en SEEG, des enregistrements simultanés SEEG-EEG, c'est-à-dire que les patients bénéficient de la pose d'électrodes EEG de scalp après l'implantation des électrodes SEEG (Koessler et al., 2015). Cette méthodologie nous fournit une opportunité pour mieux comprendre les relations complexes entre les générateurs intracérébraux et les activités projetées sur le scalp (voir par exemple Jacques, Jonas et al., 2019, *Human Brain Mapping* et Jacques, Jonas et al., in press, *Human Brain Mapping* pour des études réalisées chez 1 patient). Dans l'avenir, nous souhaitons poursuivre ces analyses sur un grand nombre de patients avec des enregistrements simultanés SEEG-EEG et testés avec des paradigmes FPVS. Ce travail se fera en collaboration avec Bruno Rossion et Laurent Koessler.

8.3.8 Evaluation des capacités en perception des visages par EEG de surface

L'étude ATENA-F a pour but d'évaluer les capacités de perception des visages chez des patients avec une épilepsie temporo-mésiale à l'aide de tests neuropsychologiques (Volfart, Jonas, et al., in press, *Neuropsychologia*). Le défaut des tests neuropsychologiques est que les performances sont dépendantes de facteurs comme la motivation, l'attention, le

niveau de compréhension des consignes, etc., indépendants de la fonction étudiée et qui peuvent donc biaiser l'évaluation de celle-ci. Afin de pallier ce problème, nous envisageons l'utilisation d'une méthode implicite pour l'évaluation des capacités en individuation des visages des patients avec une épilepsie focale pharmaco-résistante : l'EEG de scalp combiné avec le paradigme FPVS d'individuation des visages (Figure 3A). Cette méthode permet l'enregistrement en quelques minutes de réponses objectives d'individuation des visages (Liu-Shuang et al., 2014), avec une très bonne reproductibilité dans le temps (Dzhelyova et al., 2019) et avec une très bonne valeur fonctionnelle (réponse abolie en cas de trouble du traitement de l'identité des visages comme dans les cas de prosopagnosie, Liu-Shuang et al., 2016). Nous avons pour l'instant testé une vingtaine de patients et leurs témoins appariés. En accord avec les résultats de l'étude en ATENA-F (Volfart, Jonas, et al., in press, *Neuropsychologia*), nous prédisons que les réponses EEG d'individuation des visages chez les patients avec une épilepsie temporo-mésiale ne différeront pas de celles enregistrées chez les sujets témoins. Pour cette étude, nous avons obtenu le financement d'un assistant de recherche (Pierre Riff) en 2018 par une bourse de la Fondation Française pour la Recherche sur l'Épilepsie, FFRE (90912€). Ce travail se fera en collaboration avec Bruno Rossion et Hélène Brissart (neuropsychologue au CHRU de Nancy, Equipe Neurosciences des Systèmes et de la Cognition, CRAN UMR 7039 CNRS-Université de Lorraine). Dans un second temps, cette méthode sera appliquée à d'autres fonctions cognitives. A terme, certaines évaluations neuropsychologiques en préopératoire pourront être remplacées par des mesures électrophysiologiques objectives en EEG-FPVS, ce qui permettra d'améliorer l'objectivité des évaluations et la prédiction du devenir neuropsychologique après chirurgie de l'épilepsie.

8.3.9 Cartographie fonctionnelle préopératoire par IRM fonctionnelle

L'EEG intracrânien (avec notamment les stimulations électriques) et l'IRM fonctionnelle sont les 2 principales méthodes de cartographie fonctionnelle en préopératoire dans la chirurgie de l'épilepsie et sont souvent complémentaires. En ce qui concerne l'épilepsie temporo-mésiale, l'IRM fonctionnelle est très limitée en raison d'un artefact de susceptibilité magnétique qui rend presque invisible l'ATL (Jonas et al., 2015, *Cortex* ; Rossion, Jacques, et Jonas, 2018, *Ann N Y Acad Sci*). Dans l'avenir, nous envisageons l'utilisation de séquences innovantes (séquences multi-écho) afin d'améliorer la détection des aires fonctionnelles dans l'ATL de patients avec une épilepsie temporo-mésiale en cours de bilan pré-chirurgical (aires fonctionnelles de la perception des visages, de la dénomination et de la mémoire sémantique qui sont connues pour être localisées dans l'ATL). Nous souhaitons ensuite évaluer l'intérêt de la détection de ces aires pour la prédiction du devenir neuropsychologique après chirurgie de l'épilepsie, en perception des visages, en dénomination et en mémoire sémantique. Ce travail se fera en collaboration avec Bruno Rossion et Gabriela Hossu (CIC-IT CHRU de

Nancy, IADI Inserm U1254). Une demande de financement par CPRC sera prochainement soumise au CHRU de Nancy, dont je serai l'investigateur principal.

8.4 Perspectives à très long terme

Sur le plan de la recherche fondamentale, j'espère, dans les 10 années à venir, arriver à une meilleure compréhension des mécanismes de perception des visages chez l'Homme. Comme notre recherche repose sur plusieurs modalités et plusieurs niveaux d'étude différents, je pense qu'une meilleure compréhension passera par la synthèse de l'ensemble des résultats que nous avons obtenus et que nous obtiendrons prochainement (SEEG, EEG, neurone unique ; potentiels d'action, hautes fréquences, basses fréquences ; électrophysiologie, neuropsychologie, imagerie fonctionnelle ; sujets sains et sujets avec lésions ; sujets avant et après chirurgie).

Premièrement, mon objectif sera d'obtenir différentes cartographies fonctionnelles du VOTC en utilisant la méthode SEEG-FPVS pour chaque aspect de la perception des visages, ainsi qu'une cartographie aussi complète que possible des régions critiques pour les visages en utilisant la stimulation électrique. Si possible, ces cartographies devront intégrer l'étude de la dynamique temporelle des réponses et l'étude des réponses dans les différentes bandes de fréquences (basses et hautes fréquences). Des cartographies par IRM fonctionnelle seront également intégrées si nous parvenons à obtenir des réponses fiables dans l'ATL. Ensuite, il sera nécessaire de comparer ces différentes cartes afin d'avoir une vision globale du processus de perception des visages.

Deuxièmement, mon objectif sera de mettre en lien les résultats obtenus grâce aux différents niveaux d'enregistrements dont nous disposons : neurone unique par enregistrement micro-électrodes, population de neurones par SEEG, population de neurones plus large par EEG de scalp. L'objectif sera d'avoir une compréhension à toutes les échelles du processus de perception des visages (neurone unique, population de neurone, réseau ou système neuronal). Je ne pense pas que les enregistrements au niveau du neurone unique puissent se suffire à eux-mêmes, même s'il existe un fort courant de pensée suggérant que tout mécanisme cérébral ne peut être compris qu'avec une étude au niveau cellulaire (Barlow, 1972 ; Chang & Tsao, 2017). C'est pourquoi je souhaite que les résultats des enregistrements au niveau cellulaire soient intégrés avec les enregistrements réalisés au niveau des populations de neurones.

J'espère également que ces recherches permettront d'éclaircir des problématiques plus vastes, dépassant le cadre de la perception des visages : compréhension du fonctionnement global de la voie visuelle ventrale et ses liens avec la mémoire épisodique et la mémoire sémantique, compréhension du rôle de l'ATL, compréhension des relations entre

les générateurs intracérébraux et l'activité projetée sur le scalp, compréhension des relations entre les différents types de signaux électrophysiologiques (potentiel d'action, activité de haute fréquence ou gamma, activité de basse fréquence), meilleure prédiction du devenir neuropsychologique après chirurgie de l'épilepsie.

Sur le plan de la recherche clinique, mon objectif sera de synthétiser toutes les observations réalisées chez les patients épileptiques en pré-opératoire (SEEG, EEG, neuropsychologie, imagerie fonctionnelle) afin de déterminer les informations qui permettent de prédire avec le plus de fiabilité le devenir neuropsychologie après chirurgie de l'épilepsie, en perception des visages mais aussi en langage (dénomination, lecture). Même s'il faut prudent lorsque l'on projette d'appliquer des connaissances fondamentales à la pratique clinique, j'espère tout de même dans l'avenir améliorer la prédiction du devenir neuropsychologique après chirurgie de l'épilepsie et donc améliorer la prise en charge des patients épileptiques.

Ce projet se réalisera bien entendu au sein de l'Equipe Neurosciences des Systèmes et de la Cognition (CRAN UMR 7039 CNRS-Université de Lorraine) avec la collaboration des membres suivants : Bruno Rossion (chef d'équipe), Laurent Koessler (relations surface-profondeur), Louis Maillard (épileptologie), Hélène Brissart (neuropsychologie), Sophie Colnat-Coulbois (neurochirurgie), Radu Ranta (traitement des signaux). Ce projet bénéficiera également de la collaboration de personnes extérieures au CRAN : Stéphanie Caharel pour le traitement des émotions (2LPN, EA 7489, Université de Lorraine), Gabriela Hossu pour l'IRM fonctionnelle (CIC-IT CHRU de Nancy, IADI Inserm U1254), Corentin Jacques pour les enregistrements SEEG-FPVS (Université Catholique de Louvain).

Références

Adrian ED, Matthews, BHC. The Berger rhythm: Potential changes from the occipital lobes in man. Brain. 1934;4:355–385.

Allison T, Ginter H, McCarthy G, Nobre AC, Puce A, Luby M, Spencer DD. Face recognition in human extrastriate cortex. J Neurophysiol. 1994;71:821-825.

Allison T, Puce A, Spencer DD, McCarthy G. Electrophysiological studies of human face perception I: Potentials generated in occipitotemporal cortex by face and non-face stimuli. Cereb Cortex. 1999;9:415-430.

Andrews TJ, Clarke A, Pell P, Hartley T.Selectivity for low-level features of objects in the human ventral stream. Neuroimage. 2010;49:703-711.

Anzellotti S, Fairhall SL, Caramazza A.Decoding representations of face identity that are tolerant to rotation. Cereb Cortex. 2014;24:1988-1995.

Axelrod V, Yovel G. The challenge of localizing the anterior temporal face area: a possible solution. Neuroimage. 2013;81:371-380.

Axelrod V, Rozier C, Malkinson TS, Lehongre K, Adam C, Lambrecq V, Navarro V, Naccache L. Face-selective neurons in the vicinity of the human fusiform face area. Neurology. 2019;92:197-198.

Bancaud J, Talairach J. Methodology of stereo EEG exploration and surgical intervention in epilepsy. Rev Otoneuroophtalmol. 1973;45:315-28.

Barbeau EJ, Taylor MJ, Regis J, Marquis P, Chauvel P, Liégeois-Chauvel C. Spatio temporal dynamics of face recognition. Cereb Cortex. 2008;18:997-1009.

Barlow HB. Single units and sensation: a neuron doctrine for perceptual psychology? Perception. 1972;1:371-394.

Barton JJ: Structure and function in acquired prosopagnosia: lessons from a series of 10 patients with brain damage. J Neuropsychol. 2008;2:197-225.

Bédos Ulvin L, Jonas J, Brissart H, Colnat-Coulbois S, Thiriaux A, Vignal JP, Maillard L.Intracerebral stimulation of left and right ventral temporal cortex during object naming. Brain Lang. 2017;175:71-76.

Behrmann M, Plaut DC. Distributed circuits, not circumscribed centers, mediate visual recognition. Trends Cogn Sci. 2013;17:210-219.

Blanke O, Mohr C. Out-of-body experience, heautoscopy, and autoscopic hallucination of neurological origin: implications for neurocognitive mechanisms of corporeal awareness and self-consciousness. Brain Res Brain Res Rev. 2005;50:184–199.

Bodamer J: Die-Prosop-agnosie Arch Psychiatr Nervenkrankh. 1947;179:6-54.

Bouvier SE, Engel SA. Behavioral deficits and cortical damage loci in cerebral achromatopsia. Cereb Cortex. 2006;16:183-191.

Busigny T, Van Belle G, Jemel B, Hosein A, Joubert S, Rossion B. Face-specific impairment in holistic perception following focal lesion of the right anterior temporal lobe. Neuropsychologia. 2014 ;56:312-333.

Chang L, Tsao DY. The Code for Facial Identity in the Primate Brain. Cell. 2017;169:1013-1028.e14.

Coggan DD, Liu W, Baker DH, Andrews TJ. Category-selective patterns of neural response in the ventral visual pathway in the absence of categorical information. Neuroimage. 2016;135:107-114.

Cohen L, Lehéricy S, Chochon F, Lemer C, Rivaud S, Dehaene S.Language-specific tuning of visual cortex? Functional properties of the Visual Word Form Area. Brain. 2002;125:1054-1069.

Crouzet SM, Thorpe SJ. Low-level cues and ultra-fast face detection. Front Psychol. 2011;2:342.

Damasio AR, Damasio H, Van Hoesen GW. Prosopagnosia: anatomic basis and behavioral mechanisms. Neurology. 1982;32:331-341.

Davidesco I, Zion-Golumbic E, Bickel S, Harel M, Groppe DM, Keller CJ, Schevon CA, McKhann GM, Goodman RR, Goelman G, Schroeder CE, Mehta AD, Malach R. Exemplar selectivity reflects perceptual similarities in the human fusiform cortex. Cereb Cortex. 2014;24:1879-1893.

Dzhelyova M, Jacques C, Rossion B. At a Single Glance: Fast Periodic Visual Stimulation Uncovers the Spatio-Temporal Dynamics of Brief Facial Expression Changes in the Human Brain. Cereb Cortex. 2017;27:4106-4123.

Engell AD, McCarthy G: The relationship of gamma oscillations and face-specific ERPs recorded subdurally from occipitotemporal cortex. Cereb Cortex. 2011;21:1213-1221.

Ewbank MP, Henson RN, Rowe JB, Stoyanova RS, Calder AJ. Different neural mechanisms within occipitotemporal cortex underlie repetition suppression across same and different-size faces. Cereb. Cortex. 2013;23:1073–1084.

Gauthier I, Tarr MJ, Moylan J, Skudlarski P, Gore JC, Anderson AW.The fusiform "face area" is part of a network that processes faces at the individual level. J Cogn Neurosci. 2000;12:495-504.

Goesaert E, Op de Beeck HP. Representations of facial identity information in the ventral visual stream investigated with multivoxel pattern analyses. J Neurosci. 2013;33:8549-58.

Gomez J, Pestilli F, Witthoft N, Golarai G, Liberman A, Poltoratski S, Yoon J, Grill-Spector K.Functionally defined white matter reveals segregated pathways in human ventral temporal cortex associated with category-specific processing. Neuron. 2015;85:216-227.

Gross CG, Rocha-Miranda CE, Bender DB. Visual properties of neurons in inferotemporal cortex of the Macaque. J Neurophysiol. 1972;35:96-111..

Hagen S, Jacques C, Maillard L, Colnat-Coulbois S, Rossion B, Jonas J. Spatially dissociated intracerebral maps for face- and house-selective activity in the human ventral occipito-temporal cortex. Cereb Cortex. In press.

Haxby JV, Hoffman EA, Gobbini MI. The distributed human neural system for face perception. Trends Cogn Sci. 2000;4:223-233.

Honey C, Kirchner H, VanRullen R. Faces in the cloud: Fourier power spectrum biases ultrarapid face detection. J Vis. 2008;8:9.1-13.

Jacques C, Witthoft N, Weiner KS, Foster BL, Rangarajan V, Hermes D, Miller KJ, Parvizi J, Grill-Spector K. Corresponding ECoG and fMRI category-selective signals in human ventral temporal cortex. Neuropsychologia. 2016;83:14-28.

Jacques C, Jonas J, Maillard L, Colnat-Coulbois S, Koessler L, Rossion B. The inferior occipital gyrus as a major cortical source of the face-evoked N170: evidence from simultaneous scalp and intracerebral human recordings. Hum Brain Mapp. 2019;40:1403-1418.

Jacques C, Jonas J, Maillard L, Colnat-Coulbois S, Rossion B, Koessler L. Fast periodic visual stimulation to highlight the relationship between human intracerebral recordings and scalp electroencephalography. Hum Brain Mapp. 2020;41(9):2373-2388.

Jacques C, Rossion B, Volfart A, Brissart H, Colnat-Coulbois S, Maillard L, Jonas J. The neural basis of rapid unfamiliar face individuation with human intracerebral recordings [published online ahead of print, 2020 Jul 16]. Neuroimage. 2020;117174.

Jonas J, Vignal JP, Baumann C, Anxionnat JF, Muresan M, Vespignani H, Maillard L. Effect of hyperventilation on seizure activation: potentiation by antiepileptic drug tapering. J Neurol Neurosurg Psychiatry. 2011;82:928-30.

Jonas J, Descoins M, Koessler L, Colnat-Coulbois S, Sauvée M, Guye M, Vignal JP, Vespignani H, Rossion B, Maillard L. Focal electrical intracerebral stimulation of a face-sensitive area causes transient prosopagnosia. Neuroscience. 2012;222:281-288.

Jonas J, Rossion B, Krieg J, Koessler K, Colnat-Coulbois S, Vignal JP, Vespignani H, Jacques C, Brissart H, Maillard L. Intracerebral electrical stimulation of a face-selective area in the right inferior occipital cortex impairs individual face discrimination. NeuroImage. 2014;99:487-97.

Jonas J, Maillard L, Frismand F, Colnat-Coulbois S, Vespignani H, Rossion R, Vignal JP. Self-face hallucination evoked by electrical stimulation of the human brain. Neurology. 2014;83:336-8. 1;99:487-497.

Jonas J, Frismand S, Vignal JP, Colnat-Coulbois S, Koessler L, Vespignani H, Rossion B, Maillard L.Right hemispheric dominance of visual phenomena evoked by intracerebral stimulation of the human visual cortex. Hum Brain Mapp. 2014;35:3360-3371.

Jonas J, Rossion B, Brissart H, Frismand S, Jacques C, Hossu G, Colnat-Coulbois S, Vespignani H, Vignal JP, Maillard L. Beyond the core face-processing network:

Intracerebral stimulation of a face-selective area in the right anterior fusiform gyrus elicits transient prosopagnosia. Cortex. 2015;72:140-155.

Jonas J, Jacques C, Liu-Shuang J, Brissart H, Colnat-Coulbois S, Maillard L, Rossion R. A face-selective ventral occipito-temporal map of the human brain with intracerebral potentials. Proc Natl Acad Sci U S A. 2016;113:E4088-97.

Jonas J, Brissart H, Hossu G, Colnat-Coulbois S, Vignal JP, Rossion B, Maillard L. A face identity hallucination (palinopsia) generated by intracerebral stimulation of the face-selective right lateral fusiform cortex. Cortex. 2018;99:296-310.

Jonas J. Prédiction du devenir fonctionnel postopératoire en chirurgie de l'épilepsie grâce aux stimulations électriques corticales. Dans : Hélène Brissart et Louis Maillard, Neuropsychologies des épilepsies de l'adulte, Louvain-La-Neuve, Editions De Boeck Supérieur, 2018, pp. 109-131.

Kanwisher N, McDermott J, Chun M M. The fusiform face area: a module in human extrastriate cortex specialized for face perception. J Neurosci. 1997;17:4302-4311.

Kadipasaoglu CM, Conner CR, Whaley ML, Baboyan VG, Tandon N.Category-Selectivity in Human Visual Cortex Follows Cortical Topology: A Grouped icEEG Study.PLoS One. 2016;11:e0157109.

Khuvis S, Yeagle EM, Norman Y, Grossman S, Malach R, Mehta AD. Face-selective units in human ventral temporal cortex reactivate during free recall. bioRxiv 2019 487686.

Koessler L, Cecchin T, Colnat-Coulbois S, Vignal JP, Jonas J, Vespignani H, Ramantani G, Maillard LG. Catching the invisible: mesial temporal source contribution to simultaneous EEG and SEEG recordings. Brain Topogr. 2015;28:5-20.

Kriegeskorte N, Formisano E, Sorger B, Goebel R. Individual faces elicit distinct response patterns in human anterior temporal cortex. Proc Natl Acad Sci USA. 2007;104:20600-20605.

Li G, Jiang S, Paraskevopoulou SE, Wang M, Xu Y, Wu Z, Chen L, Zhang D, Schalk G. Optimal referencing for stereo-electroencephalographic (SEEG) recordings. Neuroimage. 2018;183:327-335.

Liu-Shuang J, Norcia AM, Rossion B. An objective index of individual face discrimination in the right occipito-temporal cortex by means of fast periodic oddball stimulation. Neuropsychologia. 2014;52:57-72.

Liu-Shuang J, Torfs K, Rossion B. An objective electrophysiological marker of face individualisation impairment in acquired prosopagnosia with fast periodic visual stimulation. Neuropsychologia. 2016;83:100-113.

Lochy A, Jacques C, Maillard L, Colnat-Coulbois S, Rossion, B, Jonas J. Selective visual representation of letters and words in the left ventral occipito-temporal cortex with intracerebral recordings. Proc Natl Acad Sci U S A. 2018;115:E7595-E7604.

Miller KJ, Leuthardt EC, Schalk G, Rao RP, Anderson NR, Moran DW, Miller JW, Ojemann JG. Spectral changes in cortical surface potentials during motor movement. J Neurosci. 2007;27:2424-2432.

Nasr S, Liu N, Devaney KJ, Yue X, Rajimehr R, Ungerleider LG, Tootell RB. Scene-selective cortical regions in human and nonhuman primates. J Neurosci. 2011;31: 13771-13785.

Nasr S, Tootell RB. Role of fusiform and anterior temporal cortical areas in facial recognition. Neuroimage. 2012;63:1743-1753.

Natu VS, Jiang F, Narvekar A , Keshvari S, Blanz V, O'Toole AJ. Dissociable neural patterns of facial identity across changes in viewpoint. J. Cogn. Neurosci. 2010;22:1570–1582. https://doi.org/10.1162/jocn.2009.21312

Nestor A, Plaut, DC, Behrmann M. Unraveling the distributed neural code of facial identity through spatiotemporal pattern analysis. Proc. Natl. Acad. Sci. U. S. A. 2011;108: 9998–10003.

Nestor A, Behrmann M, Plaut DC.The neural basis of visual word form processing: a multivariate investigation. Cereb Cortex. 2013;23:1673-1684.

Parvizi J, Jacques C, Foster BL, Witthoft N, Rangarajan V, Weiner KS, Grill-Spector K. Electrical stimulation of human fusiform face-selective regions distorts face perception. J Neurosci. 2012;32:14915-14920.

Ojemann JG, Akbudak E, Snyder AZ, McKinstry RC, Raichle ME, Conturo TE. Anatomic localization and quantitative analysis of gradient refocused echo-planar fMRI susceptibility artifacts. Neuroimage. 1997;6:156-167.

Pitcher D, Walsh V, Duchaine B.The role of the occipital face area in the cortical face perception network.Exp Brain Res. 2011;209:481-493.

Puce A, Allison T, McCarthy G. Electrophysiological studies of human face perception. III: Effects of top-down processing on face-specific potentials. Cereb Cortex. 1999;9:445-458.

Pugh D, De Champlain A, Touchie C.Plus ça change, plus c'est pareil: Making a continued case for the use of MCQs in medical education. Med Teach. 2019;41:569-577.

Quiroga RQ, Reddy L, Kreiman G, Koch C, Fried I. Invariant visual representation by single neurons in the human brain. Nature. 2005;435:1102-1107.

Rajimehr R, Young JC, Tootell RB.An anterior temporal face patch in human cortex, predicted by macaque maps. Proc Natl Acad Sci U S A. 2009;106(6):1995-2000.

Rangarajan V, Hermes D, Foster BL, Weiner KS, Jacques C, Grill-Spector K, Parvizi J. Electrical stimulation of the left and right human fusiform gyrus causes different effects in conscious face perception. J Neurosci. 2014;34:12828-12836.

Regan, D. Some characteristics of average steady-state and transient responses evoked by modulated light. Electroencephalography and Clinical Neurophysiology. 1966;20: 238–248.

Rice GE, Watson DM, Hartley T, Andrews TJ. Low-level image properties of visual objects predict patterns of neural response across category-selective regions of the ventral visual pathway. J Neurosci. 2014;34:8837-8844.

Robinson AK, Plaut DC, Behrmann M. Word and face processing engage overlapping distributed networks: Evidence from RSVP and EEG investigations. J Exp Psychol Gen. 2017;146:943-961.

Rossion B, Caldara R, Seghier M, Schuller AM, Lazeyras F, Mayer E. A network of occipitotemporal face-sensitive areas besides the right middle fusiform gyrus is necessary for normal face processing. Brain. 2003;126;2381-2395.

Rossion B. Constraining the cortical face network by neuroimaging studies of acquired prosopagnosia. Neuroimage. 2008;40:423-426.

Rossion B, Boremanse A. Robust sensitivity to facial identity in the right human occipito-temporal cortex as revealed by steady-state visual-evoked potentials. J Vis. 2011;11(2).

Rossion B, Jacques C. The N170: Understanding the time-course of face perception in the human brain. 2011. In S. Luck & E. Kappenman (Eds.), The Oxford handbook of ERP components. Berlin: Oxford University Press.

Rossion B, Hanseeuw B, Dricot L. Defining face perception areas in the human brain: a large-scale factorial fMRI face localizer analysis. Brain Cogn. 2012;79:138–157.

Rossion B. Understanding individual face discrimination by means of fast periodic visual stimulation. Exp Brain Res. 2014;232:1599-1621.

Rossion B, Torfs K, Jacques C, Liu-Shuang J. Fast periodic presentation of natural images reveals a robust face-selective electrophysiological response in the human brain. J Vis. 2015;15:15.1.18.

Rossion B, Jacques C, Jonas J. Mapping face categorization in the human ventral occipitotemporal cortex with direct neural intracranial recordings. Ann N Y Acad Sci. In press

Rossion B, Taubert J. What can we learn about human individual face recognition from experimental studies in monkeys? Vision Res. 2019 157:142-158.

Sato W, Kochiyama T, Uono S, Matsuda K, Usui K, Inoue Y, Toichi M. Rapid, high-frequency, and theta-coupled gamma oscillations in the inferior occipital gyrus during face processing. Cortex. 2014;60:52-68.

Schiltz C, Rossion B. Faces are represented holistically in the human occipito-temporal cortex. Neuroimage. 2006;32:1385–1394.

Schrouff J, Raccah O, Baek S, Rangarajan V, Salehi S, Mourão-Miranda J, Helili Z, Daitch AL, Parvizi J. Fast temporal dynamics and causal relevance of face processing in the human temporal cortex. Nat Commun. 2020;11:656.

Sheehan MJ, Nachman MW. Morphological and population genomic evidence that human faces have evolved to signal individual identity. Nat Commun. 2014 ;5:4800.

Spiridon M, Fischl B, Kanwisher N. Location and spatial profile of category-specific regions in human extrastriate cortex. Hum Brain Mapp. 2006;27:77-89.

Tanji K, Iwasaki M, Nakasato N, Suzuki K. Face specific broadband electrocorticographic spectral power change in the rhinal cortex. Neurosci Lett. 2012;515:66-70.

Tootell RB, Devaney KJ, Young JC, Postelnicu G, Rajimehr R, Ungerleider LG. fMRI mapping of a morphed continuum of 3D shapes within inferior temporal cortex. Proc Natl Acad Sci U S A. 2008;105: 3605-3609.

Tsao DY, Moeller S, Freiwald WA. Comparing face patch systems in macaques and humans. Proc Natl Acad Sci USA. 2008;105:19514-19519.

VanRullen R. On second glance: still no high-level pop-out effect for faces. Vision Res. 2006;46:3017-3027.

Vidal JR, Ossandón T, Jerbi K, Dalal SS, Minotti L, Ryvlin P, Kahane P, Lachaux JP. Category-Specific Visual Responses: An Intracranial Study Comparing Gamma, Beta, Alpha, and ERP Response Selectivity. Front Hum Neurosci. 2010;4:195.

Volfart A, Jonas J, Maillard L, Colnat-Coulbois S, Rossion B. Neurophysiological evidence for crossmodal (face-name) person-identity representation in the human left ventral temporal cortex. PLoS Biol. 2020;18(4):e3000659.

Volfart A, Jonas J, Maillard L, Busigny T, Rossion B, Brissart H. Typical visual unfamiliar face individuation in left and right mesial temporal epilepsy [published online ahead of print, 2020 Aug 7]. Neuropsychologia. 2020;147:107583. doi:10.1016/j.neuropsychologia.2020.107583

Wang Y, Metoki A, Smith DV, Medaglia JD, Zang Y, Benear S, Popal H, Lin Y, Olson IR.Multimodal mapping of the face connectome. Nat Hum Behav. In press.

Weiner KS, Grill-Spector K. Sparsely-distributed organization of face and limb activations in human ventral temporal cortex. Neuroimage. 2010;52:1559-1573.

Weiner KS, Jonas J, Gomez J, Maillard L, Brissart H, Hossu G, Jacques C, Loftus D, Colnat-Coulbois S, Stigliani A, Barnett MA, Grill-Spector K, Rossion B. The Face-Processing Network Is Resilient to Focal Resection of Human Visual Cortex. J Neurosci. 2016;36:8425-40.

Publications principales

Neuroscience 222 (2012) 281–288

FOCAL ELECTRICAL INTRACEREBRAL STIMULATION OF A FACE-SENSITIVE AREA CAUSES TRANSIENT PROSOPAGNOSIA

J. JONAS, [a,b,f*] **M. DESCOINS,** [c,d†] **L. KOESSLER,** [b†] **S. COLNAT-COULBOIS,** [e] **M. SAUVÉE,** [a] **M. GUYE,** [c,d] **J.-P. VIGNAL,** [a,b] **H. VESPIGNANI,** [a,b,f] **B. ROSSION** [g] **AND L. MAILLARD** [a,b]

[a] *Service de Neurologie, Centre Hospitalier Universitaire de Nancy, 29 Avenue du Maréchal de Lattre de Tasssigny, 54000 Nancy, France*

[b] *Centre de Recherche en Automatique de Nancy (CRAN), UMR CNRS 7039, Université de Lorraine, Campus Sciences, BP 70239, 54506 Vandoeuvre-lès-Nancy, France*

[c] *INSERM U751 Epilepsie & Cognition, 27 Boulevard Jean Moulin, 13385 Marseille, France*

[d] *Centre de Résonance Magnétique Biologique et Médicale (CRMBM), UMR CNRS 6612, Aix-Marseille Université, 27 Boulevard Jean Moulin, 13385 Marseille, France*

[e] *Service de Neurochirurgie, Centre Hospitalier Universitaire de Nancy, 29 Avenue du Maréchal de Lattre de Tasssigny, 54000 Nancy, France*

[f] *Faculté de Médecine de Nancy, Université de Lorraine, 9 Avenue de la Forêt de Haye, 54500 Vandoeuvre-lès-Nancy, France*

[g] *Université Catholique de Louvain, 1 Place de l'Université, L0.01.09 B-1348 Louvain-la-Neuve, Belgium*

Abstract—Face perception is subtended by a large set of areas in the human ventral occipito-temporal cortex. However, the role of these areas and their importance for face recognition remain largely unclear. Here we report a case of transient selective impairment in face recognition (prosopagnosia) induced by focal electrical intracerebral stimulation of the right inferior occipital gyrus. This area presents with typical face-sensitivity as evidenced by functional neuroimaging right occipital face area (OFA). A face-sensitive intracerebral N170 was also recorded in this area, supporting its contribution as a source of the well-known N170 component typically recorded on the scalp. Altogether, these observations indicate that face recognition can be selectively impaired by local disruption of a single face-sensitive area of the network subtending this function, the right OFA.

Key words: face perception, OFA, electrical stimulation, prosopagnosia, N170.

INTRODUCTION

Face perception is an extremely important social function that is subtended by a set of widely distributed brain areas in human (Sergent et al., 1992; Allison et al., 1994, 1999; Kanwisher et al., 1997; Haxby et al., 2000; Ishai, 2008; Rossion et al., 2012) and non-human primates (Tsao et al., 2008), with a right hemisphere advantage. Despite intense research, important debates remain about the degree of face-specificity, and the functional organization of the areas of the ventral occipito-temporal cortex that are preferentially activated when perceiving faces as compared to other object categories (Wiggett and Downing, 2008; Weiner and Grill-Spector, 2010; Rossion et al., 2012). In particular, whether all of the right hemisphere face-sensitive occipito-temporal areas are necessary for normal face recognition remain unknown. In humans, the localization of lesions causing prosopagnosia – classically the impairment of face recognition following brain damage (Bodamer, 1947) – can potentially provide information about the necessity of occipito-temporal areas and their putative connections for face recognition (Hécaen and Angelergues, 1962; Damasio et al., 1982; Barton et al., 2002; Thomas et al., 2008). However, while there is a much higher prevalence of lesions in the right than the left hemisphere causing prosopagnosia, these patients usually have large and variable lesions that can encompass the lingual, fusiform, and parahippocampal gyri, and even the anterior part of the inferior temporal cortex (Barton et al., 2002; Bouvier and Engel, 2006; Bukach et al., 2006; Sorger et al., 2007), preventing to draw firm conclusions about the necessity of a given area for face recognition. Moreover, brain areas that may appear structurally intact and thus not considered to be critically associated with face recognition in a patient with prosopagnosia may in fact be functionally depressed because they do not receive normal inputs from lesioned areas ('diaschisis', see Price and Friston, 2002; see also Thomas et al., 2008). Another issue related to the functional organization of the cortical face network concerns the relative time-course of these areas: when and along

*Correspondence to: J. Jonas, Service de Neurologie, Hôpital Central, Centre Hospitalier Universitaire de Nancy, 29 Avenue du Maréchal de Lattre de Tassigny, 54000 Nancy, France. Tel: +33-3-83-85-14-41; fax: +33-3-83-85-29-45.
E-mail addresses: j.jonas@chu-nancy.fr (J. Jonas), mederic.descoins@gmail.com (M. Descoins), laurent.koessler@univ-lorraine.fr (L. Koessler), s.colnat@chu-nancy.fr (S. Colnat-Coulbois), m.sauvee@chu-nancy.fr (M. Sauvée), Maxime.GUYE@ap-hm.fr (M. Guye), jp.vignal@chu-nancy.fr (J.-P. Vignal), h.vespignani@chu-nancy.fr (H. Vespignani), bruno.rossion@uclouvain.be (B. Rossion), l.maillard@chu-nancy.fr (L. Maillard).
† These authors contributed equally to this study.
Abbreviations: ERP, evoked related potential; FFA, fusiform face area; SEEG, stereo-electroencephalographic; TMS, transcranial magnetic stimulation; MRI, magnetic resonance imaging; CT, computed tomography; TE, echo time; TR, repetition time.

0306-4522/12 $36.00
http://dx.doi.org/10.1016/j.neuroscience.2012.07.021

which time-course do they show face-sensitive responses (e.g., Jiang et al., 2011; Sadeh et al., 2010) and contribute to the face-sensitive N170 response recorded on the human scalp (Bentin et al., 1996; for reviews see Eimer, 2011; Rossion and Jacques, 2011).

In the present study we had a unique opportunity to test the role and time-course of the most posterior face-sensitive area that has been consistently reported, namely the right occipital face area ('rOFA', e.g., Gauthier et al., 2000; for a recent review see Pitcher et al., 2011). This opportunity was offered to us in the clinical context of a young human patient with a rare medically intractable right occipital epilepsy related to a focal cortical dysplasia involving the right inferior occipital gyrus. The patient had normal familiar face recognition and face perception outside of the epileptic seizures, as assessed by behavioral tests. Intra-cerebral electrodes were stereotactically implanted in the patients' occipito-temporal region in order to localize the zone of seizure onset, and to determine the post-surgical neuropsychological outcome. As part of her pre-surgical investigation, focal intracerebral electrical stimulations were performed to directly test the role of this region in face recognition, and the patient underwent a functional magnetic resonance examination contrasting the presentation of faces and objects. We also had the unique opportunity of recording intracerebral potentials to visual stimulation of faces and non-face objects in this cortical region, allowing testing for the time-course of its contribution to face recognition.

EXPERIMENTAL PROCEDURES

Case description

The patient is a 32-year-old right-handed woman (K.V.) who has rare medically intractable right occipital epilepsy related to a focal cortical dysplasia involving the right inferior occipital gyrus. She has never complained of difficulties in face recognition, even during seizures. Neuropsychological evaluations performed before the intracerebral exploration revealed a normal performance on intellect, memory, visual perception, and most importantly face and object perception (Table 1). She also has a normal pattern of performance in paradigms measuring integration of local facial features into a global ('holistic/configural') representation (face inversion effect, Fig. 1 and composite face effect, Fig. 2), as tested 6 months after the intracerebral exploration. She gave written consent to participate in these procedures, monitored by the appropriate ethics committee.

Stereo-electroencephalographic (SEEG) placement of intracerebral electrodes

SEEG recording was performed in order to define the epileptogenic zone (Talairach and Bancaud, 1973). The electrode implantation sites were chosen according to non-invasive data collected during the earlier phase of the investigation in order to localize and delineate the zone of epileptic seizure onset and early propagation (Maillard et al., 2009). Stereotactic placement of the intracerebral electrodes (Dixi Medical, Besançon, France), consisting of 5–18 contiguous contacts of 2-mm long separated by 1.5 mm, was performed as follows: after induction of general anesthesia, the Leksell G-frame (Elekta S.A., Stockholm, Sweden) was positioned on the patient's head and a stereotactic MRI (3D SPGR T1 weighted-sequence, TR: 20 ms, TE: 6 ms; matrix 512×512, with double injection of gadolinium, Signa 1.5 Tesla; General Electric Medical System, Milwaukee, United States) was carried out. MRI was imported into a computer-assisted stereotactic module (Leksell Surgiplan; Elekta S.A., Stockholm, Sweden), and electrode trajectories were calculated according to pre-operative planning, with careful avoidance of vascular structures. A post-operative stereotactic CT-scan was then carried out and fused with pre-operative MRI to determine the exact position of each electrode according to the Talairach and Tournoux coordinates. The signal was recorded at a 512-kHz sampling rate on a 128-channels amplifier (2 SD LTM 64 Headbox; Micromed, Italy). The reference electrode was a prefrontal–central surface electrode (FPz).

Eight electrodes were placed in the right hemisphere targeting the calcarine fissure (electrode Ca, containing 12 contacts), ventral-occipital cortex (electrode O, containing 10 contacts), middle ventral temporal cortex (electrode F containing 15 contacts), occipito-parietal junction (electrode S, containing 18 contacts), collateral fissure and the middle temporal gyrus (electrode TM, containing 15 contacts), entorhinal cortex and inferior temporal gyrus (electrode TB, containing 15 contacts), superior temporal gyrus (electrode T, containing 5 contacts) and hippocampus (electrode B, containing 12 contacts). Four electrodes were placed in the left hemisphere, exploring the ventral occipital cortex (electrode O′, containing 12 contacts), the middle ventral temporal cortex (electrode F′, containing 15 contacts), occipito-parietal junction (electrode S′, containing 18 contacts) and hippocampus (electrode B′, containing 15 contacts).

Cortical stimulations

Bipolar electrical intracerebral stimulations were applied between two contiguous contacts along one common electrode and performed at 50 Hz during 5 s at intensities ranging from 1 to 1.8 mA (usual stimulation settings in SEEG). Impulsion was diphasic and 1050 μs width. Trains of stimulation of electrodes targeting the right occipital lobe and the ventral-temporal cortex bilaterally (electrodes Ca, O, O′, F, F′) were carried out during naming photographs of famous faces, objects, and famous visual scenes that she has correctly named before the procedure. For a given category, the patient had to name a set of 3 stimuli, one before, one during and one after the stimulation (Fig. 3). Using this procedure we performed 33 stimulations (19 sets of famous faces, 10 sets of objects and 4 sets of famous scenes) at 12 different sites (Table 2). We used 10 different famous faces, 10 different objects and 10 different famous scenes. The patient never had to name the exact same set of 3 stimuli for 2 given stimulations. She was not aware of the stimulation onset and termination, the stimulation site and the potential evoked perceptual changes.

To ensure that the face task does not differ in difficulty from the non-face task, the patient was tested at the face and non-face (objects and famous scenes) recognition tasks the day before the stimulations. She named easily all famous faces, objects and famous scenes that were presented.

Functional mapping

Brain regions of interest for face perception were mapped using fMRI and intracerebral evoked related potentials (intracerebral ERPs) by contrasting responses to pictures of faces and objects (Allison et al., 1994; Bentin et al., 1996; Kanwisher et al., 1997). fMRI was performed 1 month after the SEEG exploration. No seizure occurred in 24 h before ERP recordings and fMRI procedure.

Intracerebral event-related potentials. The material consisted of 60 grayscale pictures of unknown faces and of 45 grayscale pictures of non-living objects extracted from the oral naming

Table 1. Summary of visual functions of KV

	Score
Visual field	Normal
Visual acuity	1.0 bilaterally
Benton line orientation	26
Rey–Osterrieth complex figure test	
Copy	33/36
Visual Object and Space Perception Battery (VOSP)	
Object perception	
Screening test	20/20
Incomplete letters (test 1)	20/20
Silhouettes (test 2)	21/30
Object decision (test 3)	18/20
Progressive silhouettes (test 4)	6/16
Space perception	
Dot counting (test 5)	10/10
Position discrimination (test 6)	18/20
Number location (test 7)	10/10
Cubes analysis (test 8)	10/10
Visual Agnosia Battery (PEGV)	
Entangled figure	10/10
Figure decision	9/10
Functional matching	10/10
Categorial matching	10/10
Benton face recognition test (electronic version, as in de Heering et al. (2012))	43/54, 5′17″ duration for whole test
Warrington face recognition test	39/50, normal
Old/new face recognition (experiment 3 in Busigny et al. (2010))	82%, within one SD of normal controls

DO 80 test (Deloche and Hannequin, 1997). Male and female faces were equally represented. All faces showed a frontal view with a neutral background and neutral or mildly positive expressions. The patient seated in a hospital bed facing a computer screen placed 70 cm from her face. The 60 pictures of faces and the 45 pictures of objects were presented two times randomly on the center of the screen using Bq-Evoque v1.0.3 software (Micromed, Italy). Stimulus duration was 396 ms. Interstimulus interval was filled by a black screen and varied randomly between 2000 and 3000 ms. The task consisted of pressing a mouse button with the right hand at a designated repeated checkerboard (presented 19 times at random).

Off-line processing of SEEG data was performed with BrainVision Analyzer® software (Brain Products GmbH, Munich, Germany). A Butterworth filter with a low pass of 0.1 Hz (24 dB/oct) and a high band pass of 30 Hz (48 dB/oct) were applied to the raw data. Epochs were created beginning 200 ms before stimulus onset and lasting until 1000 ms post-stimulus. Channels of epochs containing artifacts were individually removed using a semi-automatic thresholding of potential values. A baseline correction was applied between −200 and 0 ms. Averaging was computed separately for faces and objects. Amplitude differences between faces and objects ERPs were assessed with a two-tailed *t*-test ($p < 0.05$ two-tailed, 10 consecutive time points at least).

fMRI. The material consisted of 60 grayscale photographs of unknown faces and of 60 grayscale drawings of objects. Male and female faces were equally represented. All faces showed a frontal view with a neutral background. Presented faces showed neutral or mildly positive expressions. fMRI activations were studied using a block design. Nine epochs of each experimental condition (faces and objects) were performed. Epochs of face and object presentations (14.4 s; 4 TR) were counterbalanced and separated by baseline epochs (fixation cross; 14.4 s; 4 TR). In each face/object epoch, 18 stimuli were randomly presented for 500 ms, followed by a fixation cross (300 ms). The patient was required to perform a one-back task (detection of immediate repetition of an item) by pressing a response key.

Imaging was performed on a 3T wide-bore scanner (Verio, Siemens, Engerlingen, Germany), using 32-channel head coil. A gradient echo, echo-planar sequence (TE = 27 ms; TR = 3600 ms; field of view = 244 cm; pixel size = 2 × 2 mm; slice thickness = 2.5 mm; TA = 9 min 48 s) was used for the fMRI data acquisition. The images were acquired in the axial plane covering the whole brain. The high resolution T1-weighted anatomical reference images were acquired as a set of 100 contiguous sagittal slices using 3-dimensional magnetization-pre-

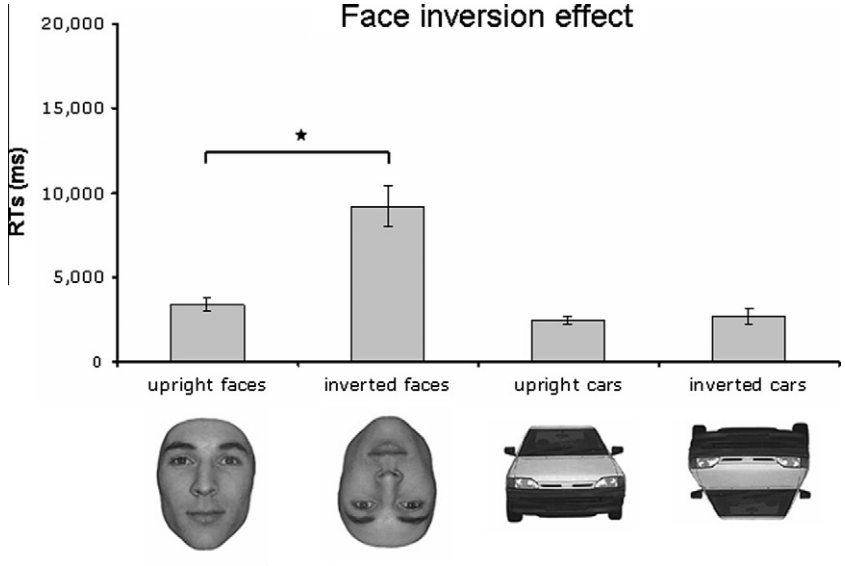

Fig. 1. Average responses times (RTs, ± SEs) of the patient KV for correct trials in a simultaneous match-to-sample task across viewpoint changes for faces and cars. All methods are described in the study of Busigny and Rossion (2010), experiment 3. The patient made only two mistakes (inverted faces conditions) and showed a typical inversion effect for faces in RTs.

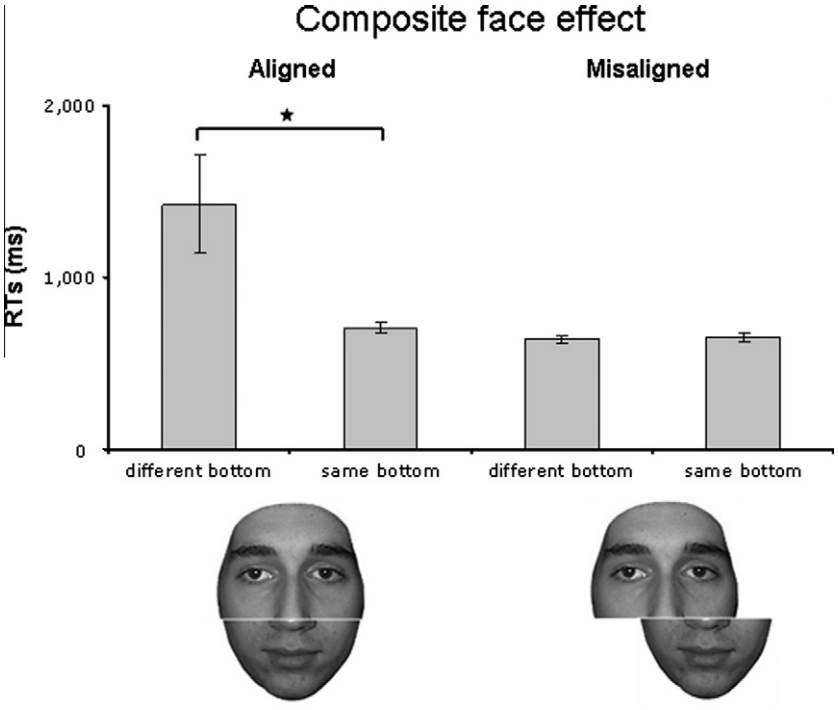

Fig. 2. Average responses times (RTs, ±SEs) of the patient KV for correct trials in a composite face-matching task. All methods are described in the study of Busigny et al. (2010), experiment 24. The patient had to match the top halves of two consecutively-presented faces and made only four mistakes in total (three in the critical ''bottom different'' condition). She was significantly slowed down when the bottom halves were different and aligned with the top halves, showing a typical composite face effect.

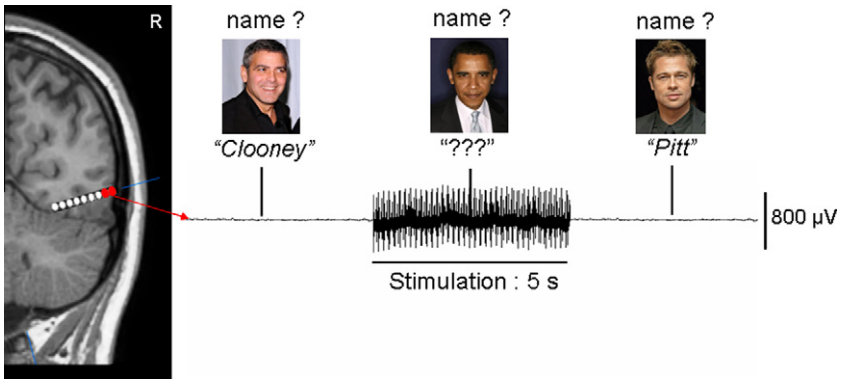

Fig. 3. Typical example of famous face recognition paradigm during intracerebral stimulation in the lateral section of the inferior occipital gyrus between two contiguous contacts along one common electrode.

pared rapid acquisition gradient echo (TE = 2.2 ms; TR = 1900 ms; flip angle = 9°; field of view = 260 cm; pixel size = 1 × 1 mm; slice thickness = 1 mm; TA = 2 min 26 s).

Data processing and statistical analysis were performed using Brain Voyager QX (2.3, Brain Innovation, Maastricht, The Netherlands) running on MacOS 10.6. Preprocessing consisted of a linear trend removal for excluding scanner-related signal, a temporal high-pass filtering applied to remove temporal frequencies lower than 3-cycles per run, and a correction for small inter-scan head movements by a rigid body algorithm rotating and translating each functional volume in 3D space (the patient had almost head movements during recordings). The data were corrected for the difference between the scan times of the different slices. Data were smoothed in the spatial domain (FWHM 4 mm, all three directions), and spatially coregistered with the 3D T1-weighted scans (automatic coregistration in Brain Voyager QX, verified manually). Subsequently, the functional data were analyzed using a multiple regression model (General Linear Model; GLM) consisting of two predictors, which corresponded to the particular experimental conditions (faces, objects). The predictor time courses used were computed on the basis of a linear model of the relation between neural activity and hemodynamic response, assuming a rectangular neural response during phases of visual stimulation (Boynton et al., 1996). A conservative (Bonferroni-corrected, $p < 0.05$) statistical threshold was used to define face-sensitive areas (faces – objects), corresponding to *t*-values above 5.095. The statistical map was then interpolated on a cubic grid of resolution 0.5 mm using trilinear interpolation for the coregistration with the CT-scan using a custom-based application.

Table 2. Locations of intracerebral electrical stimulations and the number of stimuli for each set used, for each location. Each stimulation location is defined by the name of the two contiguous contact involved in the stimulation, by its anatomical location and if possible by its functional location. (IOG, inferior occipital gyrus; MOTS, medial occipito-temporal sulcus; LOTS, lateral occipito-temporal sulcus)

Locations of stimulations	Sets of stimuli		
	Famous faces	Objects	Famous scenes
O6–O7 Right IOG, within rOFA	3	1	1
O7–O8 Right IOG, within rOFA	4	1	1
O3–O4 Right MOTS	1	1	
O4–O5 Right LOTS	1	1	
Ca5–Ca6 Right lateral and posterior occipital cortex	1	1	
Ca7–Ca8 Right lateral and posterior occipital cortex	1	1	
F5–F6 Right fusiform gyrus, at the edge of the rFFA	2		
F3–F4 Right fusiform gyrus	1		1
F4–F5 Right fusiform gyrus	1	1	
O′5–O′6 Left MOTS	1	1	
O′9–O′10 Left IOG	1	1	1
F′5–F′6 Left fusiform gyrus	2	1	

RESULTS

Six of the 7 stimulations involving one common contact of electrode O (named O7, Fig. 4) located within the right inferior occipital gyrus reproducibly induced a transient inability to recognize the face, that is prosopagnosia. The patient could not name the face and provide any semantic information about the faces (see Movies 1 and 2). This impairment completely recovered immediately upon termination of the stimulation. Stimulations at this eloquent contact never produced visual distortions, deficit in object and scene recognition (4 objects and 2 visual scenes correctly recognized out of 6 stimulations) or epileptic discharges. When she was asked to name objects and scenes during stimulations of the contact O7, the patient named them immediately and correctly without reporting any perceptual changes. When present, afterdischarges were always limited to the immediate vicinity of the stimulated site. Stimulation of contacts of other electrodes (Ca, O′, F, F′) did not elicit prosopagnosia or deficit in object and scene recognition. The epileptogenic zone and the focal–cortical dysplasia were respectively located 2 cm medially (lingual gyrus) and 0.5 cm posteriorly to contact O7.

For 5 out of 6 stimulations producing transient prosopagnosia, the patient spontaneously and reproducibly reported two types of face perception deficits. First, she described a disturbance in perceiving the spatial relationship of facial elements (stimulations number 1, 3, 4, 7). She stated: "*the facial elements were mixed*" (stimulation 1), "*the facial elements were in disarray*" (stimulation 4), "*the mouth was in the place of the forehead and the nose was in the place of the mouth*" (stimulation 7), "*the nose was not in its place*" (stimulation 7), (see Movie 1 for stimulation number 7). Second, she reported that she was unable to perceive the face as a whole (stimulations number 1, 3, 6). She stated: "*the face does not appear to me as a single entity*" (stimulation 1), "*the entity of the face was altered*" (stimulation 3), "*the overview of the face is not forthcoming*" (stimulation 6), "*the name didn't come to me because I didn't assimilate the face as a whole*" (stimulation 6), (see Movie 2 for stimulation number 6). She never reported such distortion for objects and scenes.

The eloquent contact O7 was located within the functionally face-sensitive area in the right inferior occipital gyrus (rOFA; see Fig. 4), which extended more laterally to contacts O8 and O9. This area had a size of 447 voxels at a threshold of $p < 0.05$ (Bonferroni corrected), and is known as the most posterior face-sensitive area in the human brain (e.g., Rossion et al., 2003; Pitcher et al., 2011).

A N170 potential was recorded at the same contact O7 and at O9 with a phase reversal (P170). N170 and P170 potentials recorded on contacts O7 and O9 were much larger in response to faces than objects, as observed on the scalp at the exact same latency in numerous studies (Bentin et al., 1996; for a review see Rossion and Jacques, 2011), but also in intracranial recordings of the ventral occipito-temporal cortex most often in more anterior locations (N200: Allison et al., 1994, 1999; Puce et al., 1999; N160: Mundel et al., 2003; N170: Rosburg et al., 2010; see also Halgren et al., 1994; Barbeau et al., 2008 for SEEG recordings of a P180/P160 respectively in the fusiform gyrus). Here, importantly, the phase reversal observed between

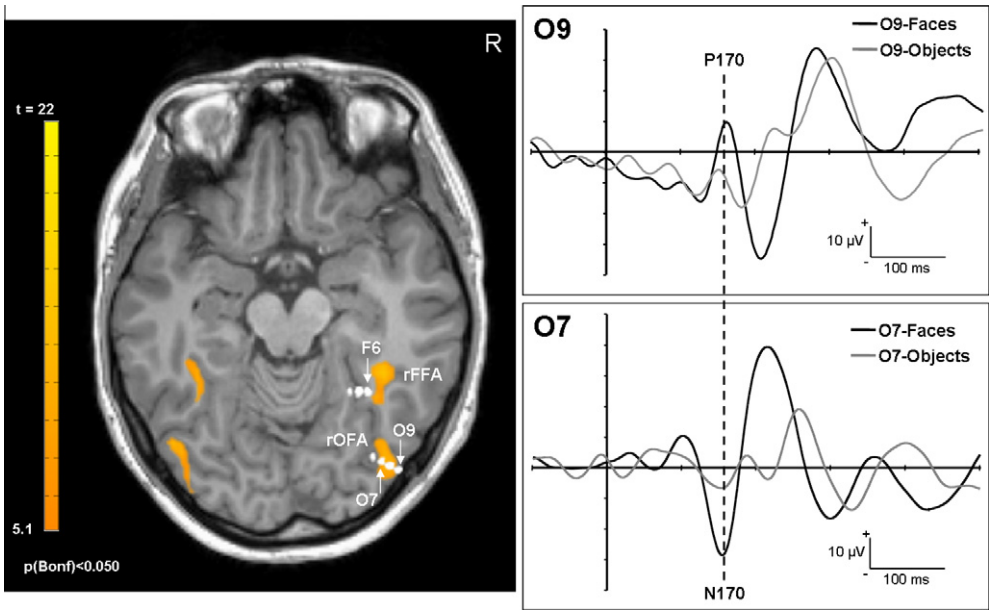

Fig. 4. Anatomical and functional location of the eloquent stimulation site whose stimulation induced transient prosopagnosia (contact O7). Left: Fusion between fMRI and post-operative CT-scan with implanted depth electrodes. fMRI disclosed classical face-selective regions in the right inferior occipital gyrus (most posterior activation, right OFA, Talairach coordinates: $x = 39$ mm, $y = -78$ mm, $z = -17$ mm, 447 voxels) comprising the contacts O7 to O9 and in the right fusiform gyrus (most anterior activation, right FFA, $x = 33$, $y = -43$, $z = -21$, 3162 voxels). Homologous regions in the left hemisphere were also disclosed at this threshold (left OFA: 145 voxels, $x = -44$ mm, $y = -72$ mm, $z = -17$ mm; left FFA: 291 voxels, $x = -36$ mm, $y = -47$ mm, $z = -14$ mm). Note that the Talairach coordinate were obtained after standardization in the Talairach space, but the non-normalized image is displayed here. Right: Visual potentials evoked by faces and objects on contacts O7 and O9. A face sensitive N170/P170 potential (latency: 160 ms) was recorded on contacts O7 and 09. The polarity reversal observed for the face sensitive N170/P170 potential between these two close contacts suggests a local generator of this face-sensitive component.

contacts O7 and O9 (more lateral) suggests a local generator of the face sensitive N170 recorded within the right inferior occipital gyrus (Fig. 4). A face-selective P170 potential was also recorded at a contact of electrode F (named F6) located at the edge of the well-known right fusiform face area (FFA; Kanwisher et al., 1997), albeit with a much lower signal-to-noise ratio. However, stimulation at this latter contact did not evoke prosopagnosia, probably because the contact was located at the edge of the right FFA as shown by its anatomical location and

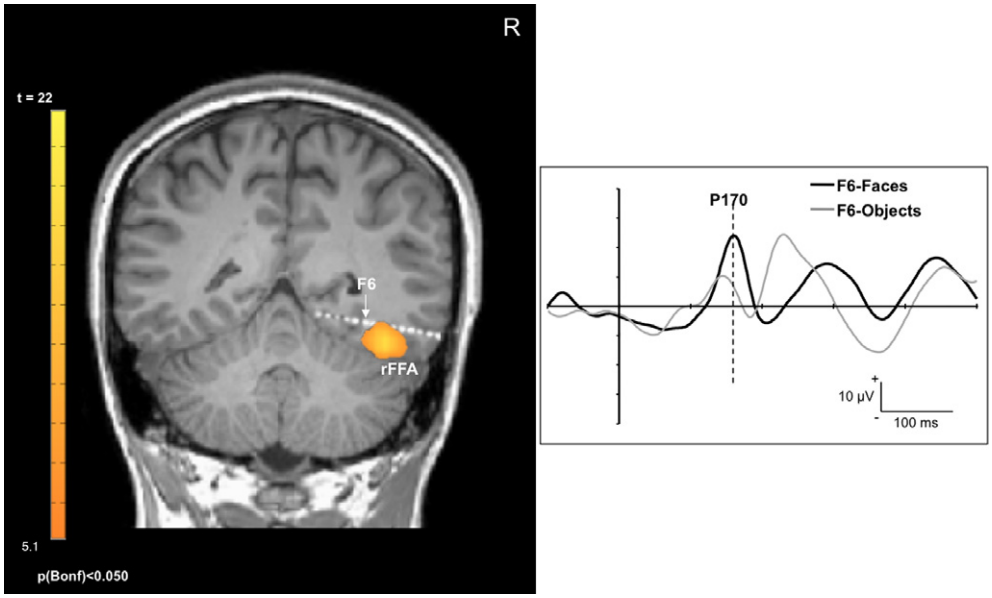

Fig. 5. Anatomical and functional location of the contact F6 on a coronal slice. Left: Fusion between fMRI and post-operative CT-scan with implanted depth electrodes. fMRI disclosed the classical rFFA in the right fusiform gyrus. Contact F6 was located at the edge of the rFFA. Note that more lateral contacts F7, F8, and F9 that were closer to the rFFA than F6 were not recorded because they were located in the white matter. Right: Visual potentials evoked by faces and objects on contact F6. A face sensitive P170 potential (latency: 160 ms) was recorded on contact F6, albeit with a low signal-to-noise ratio.

the low signal-to-noise ratio of the face-selective P170 potential recorded at this location (Fig. 5). No other face-selective N170 or P170 potentials were recorded on other contacts.

DISCUSSION

In a unique patient, we found that focal stimulation of the right inferior occipital gyrus elicited a specific and reproducible transient prosopagnosia. Transient impairments in face recognition, or face-name association (''person, or face, anomia'') have been previously reported following electrical stimulations of the fusiform gyrus using grids of subdural electrodes (Allison et al., 1994; Puce et al., 1999). In some cases, object naming was reported as normal or near-normal (Puce et al., 1999). However, these reports were only anecdotally mentioned in studies that rather focused on detailed electrophysiological investigations. Consequently the tests were limited to 1 or 2 items, without information about the procedure and the face processing abilities of the epileptic patients outside of the electrical stimulation. Most importantly, rare stimulations of the lateral inferior occipital cortex and inferior temporal gyrus (Puce et al., 1999) produced either no deficits in face recognition or deficits that were not specific, including very general deficits in sentence reading (alexia) and distorsions of any viewed image, suggestive of a general perceptual deficit.

In the present case, the specificity of the induced prosopagnosia for electrical stimulation outside of the fusiform gyrus was most likely due to several factors. First, stimulation was performed in a face-selective area, as defined in fMRI (see also Murphey et al., 2009 for FFA stimulation). Here, the coordinates of the stimulated region, and most importantly the fMRI and electrophysiological mapping provide decisive evidence that the disrupted functional area is the right OFA. Second, in contrast to subdural grids as used in previous stimulation studies (Allison et al., 1994, 1999; Puce et al., 1999; Mundel et al., 2003), the Stereo-EEG method (Talairach and Bancaud, 1973) relies on intra-cerebral electrodes which allow us to use low voltage-electrical currents resulting in a very focal effect (e.g., 10 mA in Allison et al. (1994) and Puce et al. (1999) for 1 to 1.8 mA in the present study). Supporting this claim, high frequency intracerebral stimulation at low voltage is thought to evoke experiential phenomena through the disruption of the neural function near the stimulating electrode (Halgren and Chauvel, 1993).

Our stimulation findings provide direct evidence that the right OFA is necessary for normal face perception as a critical node within a bilateral occipito-temporal network of face-sensitive areas (Haxby et al., 2000; Rossion et al., 2003; Pitcher et al., 2011). In line with these observations, it has been recently shown that scalp transcranial magnetic stimulation (TMS) above the right OFA may transiently and selectively disrupt the matching/discrimination of individual faces (Pitcher et al., 2008). However, such disruptive effects are relatively small and the effects of cortically-localized TMS need not be necessarily limited to the cortical area directly under the coil (Sack and Linden, 2003). In addition, the nature of the disturbance in face perception reported by the patient here could be speculatively described as holistic/configural perception (integration of multiple facial elements into a whole; e.g., Tanaka and Farah, 1993). Therefore, and although this is purely based on a subjective report, our observations may suggest a critical role of the right OFA in holistic/configural processing, a fundamental process of human face recognition.

Finally, our recording of a N170 directly in the human right OFA has implications for the understanding of the sources of the N170 typically recorded on the scalp (Bentin et al., 1996; see Rossion and Jacques, 2011 for a review), and more largely for the spatio-temporal course of face perception. Many studies have recorded face-specific or face-sensitive potentials around that latency in the fusiform gyrus (N200: Allison et al., 1994, 1999; P180: Halgren et al., 1994; N200: McCarthy et al., 1999; Puce et al., 1999; N160: Mundel et al., 2003; P160: Barbeau et al., 2008), including one study with fMRI functional co-localization in the FFA (Puce et al., 1997). However, such potentials have been only rarely reported in the lateral occipital region (N200: Allison et al., 1999; N170: Rosburg et al., 2010) and without any functional co-localization in fMRI. The present observation of a face sensitive N170/P170 within the rOFA, with a phase reversal between two closed-by contacts, is informative because it strongly suggests that rather than being associated with earlier low-level face-sensitive P1 response (Sadeh et al., 2010), this area is an important generator of the face-sensitive N170 recorded on the human scalp, in line with other indirect sources of evidence (e.g., Bötzel et al., 1995; Herrmann et al., 2005; Deffke et al., 2007).

REFERENCES

Allison T, McCarthy G, Nobre A, Puce A, Belger A (1994) Human extrastriate visual cortex and the perception of faces, words, numbers, and colors. Cereb Cortex 4:544–554.

Allison T, Puce A, Spencer DD, McCarthy G (1999) Electrophysiological studies of human face perception. I: potentials generated in occipitotemporal cortex by face and non-face stimuli. Cereb Cortex 9:415–430.

Barbeau EJ, Taylor MJ, Regis J, Marquis P, Chauvel P, Liégeois-Chauvel C (2008) Spatio temporal dynamics of face recognition. Cereb Cortex 18:997–1009.

Barton JJ, Press DZ, Keenan JP, O'Connor M (2002) Lesions of the fusiform face area impair perception of facial configuration in prosopagnosia. Neurology 58:71–78.

Bentin S, Allison T, Puce A, Perez E, McCarthy G (1996) Electrophysiological studies of face perception in humans. Cogn Neurosci 8:551–565.

Bodamer J (1947) Die Prosop-Agnosie. Arch Psychiatr Nervenkr Z Gesamte Neurol Psychiatr 118:6–53.

Bötzel K, Schulze S, Stodieck SR (1995) Scalp topography and analysis of intracranial sources of face-evoked potentials. Exp Brain Res 104:135–143.

Bouvier SE, Engel SA (2006) Behavioral deficits and cortical damage loci in cerebral achromatopsia. Cereb Cortex 16:183–191.

Boynton GM, Engel SA, Glover GH, Heeger DJ (1996) Linear systems analysis of functional magnetic resonance imaging in humanV1. J Neurosci 16:4207–4221.

Bukach CM, Bub DN, Gauthier I, Tarr MJ (2006) Perceptual expertise effects are not all or none: spatially limited perceptual expertise for faces in a case of prosopagnosia. J Cogn Neurosci 18:48–63.

Busigny T, Joubert S, Felician O, Ceccaldi M, Rossion B (2010) Holistic perception of the individual face is specific and necessary: evidence from an extensive case study of acquired prosopagnosia. Neuropsychologia 48:4057–4092.

Busigny T, Rossion B (2010) Acquired prosopagnosia abolishes the face inversion effect. Cortex 46:965–981.

Damasio AR, Damasio H, Van Hoesen GW (1982) Prosopagnosia: anatomic basis and behavioral mechanisms. Neurology 32:331–341.

de Heering A, Rossion B, Maurer D (2012) Developmental changes in face recognition during childhood: evidence from upright and inverted faces. Cogn Dev 27:17–27.

Deffke I, Sander T, Heidenreich J, Sommer W, Curio G, Trahms L, Lueschow A (2007) MEG/EEG sources of the 170-ms response to faces are co-localized in the fusiform gyrus. Neuroimage 35:1495–1501.

Deloche G, Hannequin D (1997) Test de dénomination orale d'images DO80. Paris: Les éditions du Centre de Psychologie appliquée.

Eimer M (2011) The face-sensitivity of the n170 component. Front Hum Neurosci 5:119.

Gauthier I, Tarr MJ, Moylan J, Skudlarski P, Gore JC, Anderson AW (2000) The fusiform ''face area'' is part of a network that processes faces at the individual level. J Cogn Neurosci 12:495–504.

Halgren E, Baudena P, Heit G, Clarke JM, Marinkovic K, Clarke M (1994) Spatio-temporal stages in face and word processing. I. Depth-recorded potentials in the human occipital, temporal and parietal lobes. J Physiol Paris 88:1–50.

Halgren E, Chauvel P (1993) Experimental phenomena evoked by human brain electrical stimulation. Adv Neurol 63:123–140.

Haxby JV, Hoffman EA, Gobbini MI (2000) The distributed human neural system for face perception. Trends Cogn Sci 4:223–233.

Hécaen H, Angelergues R (1962) Agnosia for faces (prosopagnosia). Arch Neurol 7:92–100.

Herrmann MJ, Ehlis AC, Muehlberger A, Fallgatter AJ (2005) Source localization of early stages of face processing. Brain Topogr 18:77–85.

Ishai A (2008) Let's face it: it's a cortical network. Neuroimage 40:415–419.

Jiang F, Dricot L, Weber J, Righi G, Tarr MJ, Goebel R, Rossion B (2011) Face categorization in visual scenes may start in a higher order area of the right fusiform gyrus: evidence from dynamic visual stimulation in neuroimaging. J Neurophysiol 106:2720–2736.

Kanwisher N, McDermott J, Chun MM (1997) The fusiform face area: a module in human extrastriate cortex specialized for face perception. J Neurosci 17:4302–4311.

MacCarthy G, Puce A, Belger A, Allison T (1999) Electrophysiological studies of human face perception. II: response properties of face-specific potentials generated in occipitotemporal cortex. Cereb Cortex 9:431–444.

Maillard L, Koessler L, Colnat-Coulbois S, Vignal JP, Louis-Dorr V, Marie PY, Vespignani H (2009) Combined SEEG and source localisation study of temporal lobe schizencephaly and polymicrogyria. Clin Neurophysiol 120:1628–1636.

Mundel T, Milton JG, Dimitrov A, Wilson HW, Pelizzari C, Uftring S, Torres I, Erickson RK, Spire JP, Towle VL (2003) Transient inability to distinguish between faces: electrophysiologic studies. J Clin Neurophysiol 20:102–110.

Murphey DK, Maunsell JH, Beauchamp MS, Yoshor D (2009) Perceiving electrical stimulation of identified human visual areas. Proc Natl Acad Sci U S A 106:5389–5393.

Pitcher D, Walsh V, Duchaine B (2011) The role of the occipital face area in the cortical face perception network. Exp Brain Res 209:481–493.

Pitcher D, Walsh V, Yovel G, Duchaine B (2008) TMS evidence for the involvement of the right occipital face area in early face processing. Curr Biol 17:1568–1573.

Price CJ, Friston KJ (2002) Functional imaging studies of neuropsychological patients: applications and limitations. Neurocase 8:345–354.

Puce A, Allison T, McCarthy G (1999) Electrophysiological studies of human face perception. III: effects of top-down processing on face-specific potentials. Cereb Cortex 9:445–458.

Puce A, Allison T, Spencer SS, Spencer DD, McCarthy G (1997) Comparison of cortical activation evoked by faces measured by intracranial field potentials and functional MRI: two case studies. Hum Brain Mapp 5:298–305.

Rosburg T, Ludowig E, Dümpelmann M, Alba-Ferrara L, Urbach H, Elger CE (2010) The effect of face inversion on intracranial and scalp recordings of event-related potentials. Psychophysiology 47:147–157.

Rossion B, Jacques C (2011) The N170: understanding the time-course of face perception in the human brain. In: Luck, Kappenman E, editors. The Oxford Handbook of ERP components. Oxford: University Press. p. 115–142.

Rossion B, Caldara R, Seghier M, Schuller AM, Lazeyras F, Mayer E (2003) A network of occipito-temporal face-sensitive areas besides the right middle fusiform gyrus is necessary for normal face processing. Brain 126:2381–2395.

Rossion B, Hanseeuw B, Dricot L (2012) Defining face perception areas in the human brain: a large-scale factorial fMRI face localizer analysis. Brain Cogn 79:138–157.

Sack AT, Linden DE (2003) Combining transcranial magnetic stimulation and functional imaging in cognitive brain research: possibilities and limitations. Brain Res Brain Res Rev 43:41–56.

Sadeh B, Podlipsky I, Zhdanov A, Yovel G (2010) Event-related potential and functional MRI measures of face-selectivity are highly correlated: a simultaneous ERP-fMRI investigation. Hum Brain Mapp 31:1490–1501.

Sergent J, Ohta S, MacDonald B (1992) Functional neuroanatomy of face and object processing. A positron emission tomography study. Brain 115:15–36.

Sorger B, Goebel R, Schiltz C, Rossion B (2007) Understanding the functional neuroanatomy of prosopagnosia. Neuroimage 35:836–852.

Talairach J, Bancaud J (1973) Stereotaxic approach to epilepsy: methodology of anatomo-functional stereotactic investigations. Prog Neurol Surg 5:297–354.

Tanaka JW, Farah MJ (1993) Parts and wholes in face recognition. Q J Exp Psychol A 46:225–245.

Thomas C, Avidan G, Humphreys K, Jung KJ, Gao F, Behrmann M (2008) Reduced structural connectivity in ventral visual cortex in congenital prosopagnosia. Nat Neurosci 12:29–31.

Tsao DY, Moeller S, Freiwald WA (2008) Comparing face patch systems in macaques and humans. Proc Natl Acad Sci U S A 105:19514–19519.

Wiggett AJ, Downing PE (2008) The face network: overextended? (Comment on: ''Let's face it: It's a cortical network'' by Alumit Ishai). Neuroimage 40:420–422.

Weiner KS, Grill-Spector K (2010) Sparsely-distributed organization of face and limb activations in human ventral temporal cortex. Neuroimage 52:1559–1573.

APPENDIX A. SUPPLEMENTARY DATA

Supplementary data associated with this article can be found, in the online version, at http://dx.doi.org/10.1016/j.neuroscience.2012.07.021.

(Accepted 7 July 2012)
(Available online 17 July 2012)

◆ Human Brain Mapping 35:3360–3371 (2014) ◆

Right Hemispheric Dominance of Visual Phenomena Evoked by Intracerebral Stimulation of the Human Visual Cortex

Jacques Jonas,[1,2,3,5,6]* Solène Frismand,[1] Jean-Pierre Vignal,[1,2,6] Sophie Colnat-Coulbois,[3,4] Laurent Koessler,[2,6] Hervé Vespignani,[1,2,3,6] Bruno Rossion,[5] and Louis Maillard[1,2,3,6]

[1]*Service de Neurologie, Centre Hospitalier Universitaire de Nancy, Nancy, France*
[2]*Université de Lorraine, CRAN, UMR 7039, Nancy, France*
[3]*Faculté de Médecine de Nancy, Université de Lorraine, Nancy, France*
[4]*Service de Neurochirurgie, Centre Hospitalier Universitaire de Nancy, Nancy, France*
[5]*Université Catholique de Louvain, IPSY, IoNS, Louvain-la-Neuve, Belgique*
[6]*CNRS, CRAN, UMR 7039, Nancy, France*

Abstract: Electrical brain stimulation can provide important information about the functional organization of the human visual cortex. Here, we report the visual phenomena evoked by a large number (562) of intracerebral electrical stimulations performed at low-intensity with depth electrodes implanted in the occipito-parieto-temporal cortex of 22 epileptic patients. Focal electrical stimulation evoked primarily visual hallucinations with various complexities: simple (spot or blob), intermediary (geometric forms), or complex meaningful shapes (faces); visual illusions and impairments of visual recognition were more rarely observed. With the exception of the most posterior cortical sites, the probability of evoking a visual phenomenon was significantly higher in the right than the left hemisphere. Intermediary and complex hallucinations, illusions, and visual recognition impairments were almost exclusively evoked by stimulation in the right hemisphere. The probability of evoking a visual phenomenon decreased substantially from the occipital pole to the most anterior sites of the temporal lobe, and this decrease was more pronounced in the left hemisphere. The greater sensitivity of the right occipito-parieto-temporal regions to intracerebral electrical stimulation to evoke visual phenomena supports a predominant role of right hemispheric visual areas from perception to recognition of visual forms, regardless of visuospatial and attentional factors. *Hum Brain Mapp 35:3360–3371, 2014.* © 2013 Wiley Periodicals, Inc.

Key words: stereo-electroencephalography; electrical stimulation; hallucination; prosopagnosia; recognition; hemispheric asymmetry

Jacques Jonas and Solène Frismand equally contributed to the study.

*Correspondence to: Dr. Jacques Jonas, Service de Neurologie, Hôpital Central, Centre Hospitalier Universitaire de Nancy, 29, Avenue du Maréchal de Lattre de Tassigny, 54000 Nancy, France. E-mail: j.jonas@chu-nancy.fr

Received for publication 18 March 2013; Revised 7 August 2013; Accepted 11 September 2013.

DOI 10.1002/hbm.22407

Published online 25 November 2013 in Wiley Online Library (wileyonlinelibrary.com).

INTRODUCTION

The portion of the human visual cortex dedicated to visual form perception and recognition extends from the posterior medial occipital cortex to the anterior temporal cortex [Grill-Spector and Malach, 2004]. Electrical cortical stimulation studies in epileptic patients have provided important information about the spatial and functional organization of the human visual cortex [e.g., Lee et al., 2000, Murphey et al., 2009, Penfield and Rasmussen, 1957]. Stimulation of the occipital cortex mainly induces elementary hallucinations such as phosphenes (spot of light) or more complex forms (e.g., stars, balls), which are sometimes colored or in motion [Bak et al., 1990, Brindley and Lewin, 1968, Lee et al., 2000, Murphey et al., 2009, Penfield and Jasper, 1954, Penfield and Rasmussen, 1957]. However, stimulations of more anterior sites in the visual cortex are rare, and the few studies published to date have reported discrepant observations. Stimulations of the temporal lobe evoked either complex hallucinations [Ishibashi et al., 1964, Lee et al., 2000, Puce et al., 1999], visual illusions [Lee et al., 2000], or no detectable percept or elementary hallucinations [Murphey et al., 2009]. Likewise, stimulation studies have yielded contradictory results regarding a postero-anterior hierarchical organization of the visual cortex [DeYoe and Van Essen, 1988; Hubel and Wiesel, 1962, Lee et al., 2000, Murphey et al., 2009]. For instance, Lee et al. (2000) showed an increasing complexity of electrically induced visual phenomena along a postero-anterior axis. In contrast, Murphey et al. (2009) reported only elementary hallucinations evoked by stimulating equally low-level and high-level visual areas defined by fMRI.

Another important issue regarding functional organization of the visual system is its functional hemispheric asymmetry. Studies of split-brain patients have supported a right hemispheric dominance for visuospatial processing [Corballis, 2003]. Scalp ERP studies have suggested that this asymmetry could be related to the processing of specific material such as abstract pictures or faces [see Maillard et al., 2011; Rossion et al., 2003 respectively]. However, cortical stimulation studies have not addressed this issue of hemispheric lateralization so far [Lee et al., 2000; Murphey et al., 2009].

Here, we report the visual phenomena evoked by a large set of electrical stimulations (562) of the visual cortex, carried out over the past five years in 22 epileptic patients implanted for presurgical delineation of epileptogenic zones and functional mapping of the occipito-temporal and parietal regions. Importantly, while previous electrical stimulation studies of the visual cortex relied on subdural electrodes on the cortical surface [Lee et al., 2000; Murphey et al., 2009], our approach relies on intracerebral recordings with depth electrodes [Talairach and Bancaud, 1973]. The subdural electrode approach has the advantage of offering an extensive superficial spatial coverage, but has several limitations compared to intracerebral recordings with depth electrodes as used here: (i) electrical fields evoked by subdural electrical stimulations are less focal because of higher intensities of stimulations (usually more than 5 mA), larger electrodes and inter-electrodes distances, and the spreading of current through cerebrospinal fluid [Nathan et al., 1993]; (ii) subdural electrodes do not allow direct stimulation of deep sulcal cortex; (iii) the sampling of medial structures is difficult and less systematic with subdural electrodes.

In contrast, our investigations were conducted using intracerebral electrodes that provided coverage of all the structures encountered in their trajectories, from their site of penetration to their final impact point [e.g., Jonas et al., 2012; Kahane et al., 2003]. Therefore, electrical stimulations were performed not only within the cortical surface, but also in sulci and medial cortical structures that are essential to visual perception (i.e., calcarine sulcus, precuneus, lingual gyrus). In addition, our procedure was based on intracortical stimulations delivered in bipolar mode through close adjacent contacts (1.5 mm) with low intensities (0.5–2 mA), and so is very effective in producing localized current flows. The effectiveness of this focal low intensity stimulation results partly from the fact that the stimulated contacts are not located on the pia-arachnoid, but inside the cortex, avoiding shunting of the current through cerebrospinal fluid [Nathan et al., 1993]. In addition, intracerebral stimulations has been shown to produce visual percepts at much lower intensities than subdural grid stimulation [Bak et al., 1990], thus preventing afterdischarges, epileptic discharges, and remote effects.

The main purpose of this study was to explore the functional organization of the visual system by using intracerebral electrical stimulations, with a specific emphasis on hemispheric lateralization and postero-anterior functional gradient. We analyzed the visual phenomena provoked by intracortical electrical stimulations of the human temporo-parieto-occipital cortex. The originality of this study relies on both the use of intracerebral depth electrodes implanted for stereo-electroencephalography (SEEG) and the similar distribution of electrical stimulations between the left and right hemispheres, allowing comparison of their sensitivity and properties.

Abbreviations

CT	computed tomography
ERP	event-related potential
FFA	fusiform face area
fMRI	functional magnetic resonance imaging
LO	lateral occipital
MRI	magnetic resonance imaging
MT	middle temporal
OFA	occipital face area
PPA	parahippocampal place area
SEEG	stereo-electroencephalography

MATERIALS AND METHODS

Patients

The study included 22 patients (11 men and 11 women) undergoing intracerebral evaluation (SEEG) for refractory

partial epilepsy between 2007 and 2011, in the Epilepsy Unit of the Department of Neurology (University Hospital of Nancy). Inclusion criterion was the presence of intracerebral electrodes implanted in occipital, temporal, or parietal lobes. All 22 patients gave written consent to participate to the study. All patients were right-handed attested by the Edinburgh Handedness Inventory [Oldfield, 1971]. Mean age at the time of SEEG was 36 years (+/−9). Three out of 22 patients reported visual phenomena during epileptic seizures: two patients presented visual illusions characterized by blurring, with additional change of color in one; one patient reported complex visual hallucinations (e.g., landscape, animals). Eleven out of the 22 patients presented a brain lesion identified by structural MRI. Brain lesions were right hippocampal sclerosis (1 patient), left hippocampal sclerosis (5 patients), left anterior temporal focal dysplasia (1 patient), right temporal lobe schizencephaly (1 patient), left temporal lobe schizencephaly (1 patient), left temporo-occipital schizencephaly (1 patient), and right occipital focal dysplasia (1 patient). None of the patients, including the two with occipital lesions (i.e., right occipital dysplasia and left temporo-occipital schizencephaly), had visual field defects.

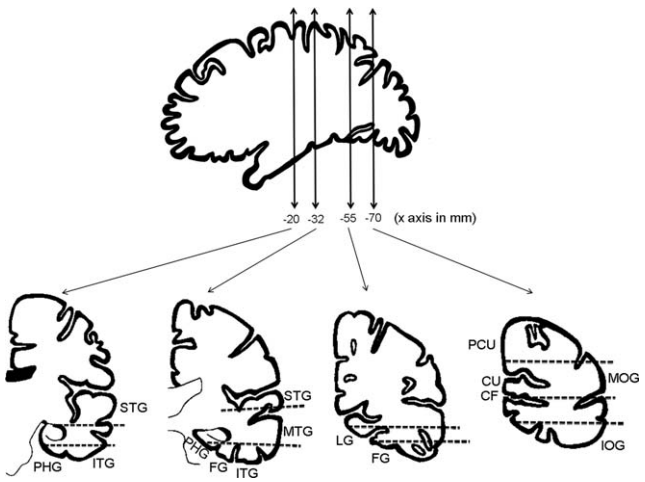

Figure 1.

Schematic representation of usual trajectories of depth electrodes implanted in occipital, temporal, and parietal lobes. (IOG: inferior occipital gyrus; MOG: middle occipital gyrus; CU: cuneus; PCU: precuneus; FG: fusiform gyrus; LG: lingual gyrus; ITG: inferior temporal gyrus; MTG: middle temporal gyrus; STG: superior temporal gyrus; PHG: parahippocampal gyrus; CF: calcarine sulcus).

Stereotactic Placement of Intracerebral Electrodes and SEEG Recording

Intracerebral electrodes (0.8 mm diameter, Dixi Medical, Besançon, France) were stereotactically implanted in the occipito-temporo-parietal regions to delineate the epileptogenic zone and to determine the postsurgical neuropsychological outcome [Talairach and Bancaud, 1973]. The electrode implantation sites were chosen according to noninvasive data collected during an earlier phase of the investigation. Stereotactic placement of the intracerebral electrodes, consisting of 5–18 contiguous contacts of 2 mm in length, separated by 1.5 mm, was performed as follows: after induction of general anesthesia, the Leksell G-frame was positioned on the patient's head and stereotactic MRI was carried out [Maillard et al., 2009]. MRI data was imported into a computer-assisted stereotactic module and electrode trajectories were calculated according to pre-operative planning with careful avoidance of vascular structures. The signal was recorded at a 512 kHz sampling rate on a 128 channel amplifier (2 SD LTM 64 Headbox; Micromed, Italy). The reference electrode was a prefrontal medial surface electrode (FPz). Overall 222 intracerebral electrodes (total number of contacts: 2,553) were implanted in the 22 patients, corresponding to 80–140 contacts per patient. Figure 1 illustrates the typical trajectories of electrodes implanted in occipital, temporal and parietal lobes.

Intracerebral Stimulations

The clinical goal of intracerebral stimulations was to reproduce usual epileptic seizures to map functionally eloquent areas that should be spared during surgery. Bipolar electrical intracerebral stimulations were applied between two contiguous contacts and performed at 50 Hz during 5 s, at intensities ranging from 0.5 to 2 mA. The intensities were set to elicit visual phenomena and other clinical symptoms without afterdischarges (usually between 1 and 1.5 mA). Impulsion was diphasic with 500 μs width on each phase. Patients were sitting in their bed, facing the video camera, with eyes opened.

Depending on the expected clinical response, they were asked either to look at a white wall in front of them, or to perform language and visual recognition tests. These tests comprised naming famous faces, famous scenes, usual objects, and reading words. Patients were not aware of the stimulation onset and termination, the stimulation site, or the potential perceptual changes elicited by stimulation. They were asked to report any symptoms as soon as they experienced them and were immediately questioned on these symptoms. When visual hallucinations were evoked, they were asked to report their color, their form, their motion, and their location in the visual field. When complex visual phenomena were evoked, patients were asked if the visual phenomena comprised a familiar scene or corresponded to a personal memory. Stimulations that produced remote afterdischarges or epileptic discharges were not considered in the analysis. Stimulations that were accompanied by an afterdischarge limited to the immediate vicinity of the stimulated site (i.e., in the same anatomical structure) were included in the analysis.

Overall, the lingual gyrus, cuneus, inferior, middle and superior occipital gyri, fusiform gyrus, parahippocampal

TABLE I. Number of stimulated sites, number of positive sites (site where a visual phenomenon was evoked), and probability to evoke a visual phenomenon (%) in each anatomical structure

	Left Hemisphere			Right Hemisphere		
Anatomical structure	Number of stimulated sites	Number of positive sites	%	Number of stimulated sites	Number of positive sites	%
Calcarine sulcus	0	0	/	6	4	67
Lateral occipital cortex	2	0	0	14	10	71
Precuneus	0	0	/	4	3	75
Cuneus/Parieto-occipital sulcus	13	7	54	14	10	71
Lingual gyrus	12	7	58	12	12	100
Fusiform gyrus	45	8	18	40	20	50
ITG	37	0	0	13	0	0
CoS	8	0	0	10	3	30
OTS	14	0	0	10	0	0
MTG	27	0	0	17	1	6
STG	38	0	0	56	1	2
PHG	12	0	0	16	4	25
Rhinal cortex	36	0	0	22	2	9
Hippocampus	55	3	6	29	0	0
Total	299	25	8	263	70	27

CoS: collateral sulcus; ITG: inferior temporal gyrus; MTG: middle temporal gyrus; OTS: occipito-temporal sulcus; PHG: parahippocampal gyrus; STG: superior temporal gyrus.

gyrus, inferior, middle, and superior temporal gyri, rhinal cortex, and hippocampus were stimulated bilaterally (Table I). The calcarine sulcus and the precuneus were explored and stimulated only in the right hemisphere because none of the enrolled patients had a presumed seizure onset or early propagation zone in these regions within the left hemisphere.

Probability of Evoking a Visual Phenomenon

To compare data among patients and to calculate the probability of evoking a visual phenomenon, the coordinates of all stimulated contacts in all patients were normalized and represented within the standard Talairach space [Talairach and Tournoux, 1988]. We calculated the percentage of contacts producing visual phenomena in right and left hemispheres, every 10 mm along the x (medial-lateral) and y (antero-posterior) axis, and for each anatomical structure (calcarine sulcus, lingual gyrus, cuneus, lateral occipital cortex precuneus, fusiform gyrus, parahippocampal gyrus, inferior, middle, and superior temporal gyri, rhinal cortex, and hippocampus). For each region, we computed the percentage of "positive sites," that is, the number of contacts producing visual phenomena divided by the total number of stimulated contacts, multiplied by 100.

Visual Phenomena Quality

Visual phenomena were defined as visual hallucinations, visual illusions or visual perceptive impairments (e.g., prosopagnosia). Hallucinations were classified as follows [Lee et al., 2000]: (i) elementary hallucinations were defined as a spot or a blob; (ii) intermediary hallucinations were defined as geometric forms (e.g., kaleidoscope, square, triangle, star, diamond); (iii) complex hallucinations were defined as meaningful visual hallucinations (e.g., face, landscape, animal, body parts). For all hallucinations, the color, the form, the character of movement and the location in the visual field of the hallucinations were reported. Visual perceptive impairments were defined by a transient inability to name a picture (face, object, or scene) that was not due to a language problem (e.g., prosopagnosia for faces). Dreamy states (i.e., "déjà vécu" and reminiscence) were excluded from our analysis because they may have resulted from disturbance of the autobiographic memory system involving medial temporal structures outside of the visual stream [Vignal et al., 2007]. The precise anatomical locations of the stimulated contacts were provided by coregistration of the postoperative stereotactic CT-scan and the preoperative MRI for each patient.

Statistical Analyses

To compare stimulation results between the right and left hemispheres, we performed chi-square analyses or Fisher's exact test for small samples. A P value of <0.05 was considered statistically significant.

RESULTS

Global Results

From a total of 562 stimulated sites in the occipito-parieto-temporal cortex (678 stimulations in total), 95 sites

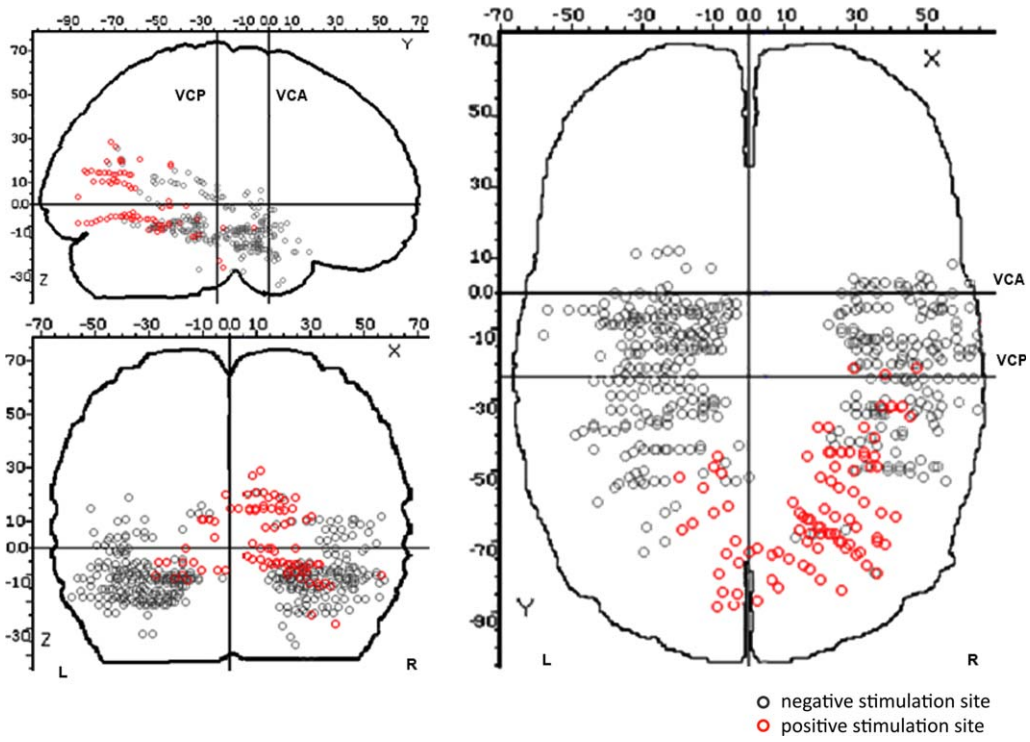

Figure 2.
Spatial distribution of positive stimulation sites (i.e., sites where stimulation evoked a visual phenomenon) and negative stimulation sites (i.e., sites where stimulation did not elicit a visual phenomenon) on a schematic brain representation (Talairach and Tournoux coordinates). [Color figure can be viewed in the online issue, which is available at wileyonlinelibrary.com.]

evoked a visual phenomenon (125 visual phenomena in total; Fig. 2). Some sites were stimulated several times to ensure that the evoked phenomena were reproduced, but a site was counted only once for analysis in this case. Visual phenomena, which were all reproduced when stimulating several times, were comprised of 104 visual hallucinations (82 sites), 8 visual illusions (8 sites), and 13 visual perceptive impairments (5 sites; Table II, Fig. 5). Visual hallucinations were classified by quality, resulting in the count of 61 elementary hallucinations (54 sites), 29 intermediary hallucinations (21 sites), and 14 complex hallucinations (7 sites).

Mean intensity of stimulation did not differ between stimulations that produced visual phenomena and those that did not (1.30 mA +/−0.34 vs. 1.26 mA +/−0.35, Student t test, ns.). Additionally, mean intensity of stimulation producing a visual phenomenon did not differ between types of visual phenomena (hallucinations: 1.25 mA +/−0.34; illusions: 1.51 mA +/−0.23; visual perceptive impairments: 1.3 mA +/−0.4; Student t test, ns.). All 22 patients presented either transient anomia/alexia from stimulating the left temporo-basal cortex or no anomia/alexia from stimulating the right temporo-basal cortex, thus reflecting their left hemispheric dominance for language.

Probability of Evoking a Visual Phenomenon

Overall, the probability of evoking a visual phenomenon was significantly higher in the right (70/263, 26.6%) than in the left hemisphere (25/299, 8.4%), irrespective of the distance to the occipital pole, along a postero-anterior axis (χ^2 test, $P < 0.0001$) and in each stimulated anatomical structure (Table I, Figs. 2–5). Mean intensity of stimulation producing a visual phenomenon did not differ between the right and left hemispheres (1.29 mA +/−0.27 vs. 1.27 mA +/−0.36, respectively; Student t test, ns.). There was a striking relationship between the position of the contacts along the postero-anterior axis (y-axis) and medio-lateral axis (x-axis) and the probability to evoke a visual phenomenon: the probability to evoke visual phenomena dramatically decreased with increasing distance from the occipital pole along the postero-anterior axis (y-axis; Fig. 3). This decrease was more pronounced in the left hemisphere than in the right hemisphere. Along the medio-lateral axis (x-axis), the probability to evoke visual phenomena was maximal in the medial part of both hemispheres and decreased laterally (Fig. 4). Again, this decrease was more pronounced in the left than in the right hemisphere.

To ensure that this right predominance was not related to a lack of sampling in critical visual regions in the left

TABLE II. Distribution of evoked visual phenomena in function of the stimulated structures and the type of hallucinations

	Positive sites for elementary hallucinations		Positive sites for intermediary hallucinations		Positive sites for complex hallucinations		Illusions		Visual perceptive impairments	
Anatomical structure	Right	Left	Right	Left	Right	Left	Right	Left	Right	Left
Calcarine sulcus	2	/	2	/	0	/	0	/	0	/
Lateral occipital cortex	4	0	4	0	0	0	0	0	2	0
Precuneus	0	/	2	/	1	/	0	/	0	/
Cuneus/Parieto-occipital sulcus	1	7	4	0	5	0	0	0	0	0
Lingual gyrus	10	5	2	2	0	0	0	0	0	0
Fusiform gyrus	10	7	4	1	1	0	2	0	3	0
ITG	0	0	0	0	0	0	0	0	0	0
CoS	1	0	0	0	0	0	2	0	0	0
OTS	0	0	0	0	0	0	0	0	0	0
MTG	1	0	0	0	0	0	0	0	0	0
STG	1	0	0	0	0	0	0	0	0	0
PHG	1	0	0	0	0	0	3	0	0	0
Rhinal cortex	1	0	0	0	0	0	1	0	0	0
Hippocampus	0	3	0	0	0	0	0	0	0	0

CoS: collateral sulcus; ITG: inferior temporal gyrus; MTG: middle temporal gyrus; OTS: occipito-temporal sulcus; PHG: parahippocampal gyrus; STG: superior temporal gyrus.

hemisphere, we defined three volumes of interest in the right hemisphere that were highly sensitive to stimulations and we considered the corresponding volumes in the left hemisphere. Based on the visual analysis of Figure 2, we defined the Talairach coordinates of three volumes in the right hemisphere: one in the medial occipital cortex, one in the ventral occipito-temporal cortex and one in the anterior temporal cortex. We then defined the corresponding volumes in the left hemisphere that were symmetric according to the y-axis. Results are shown in Table III. There was an undersampling of the left medial occipital cortex compared to the right (13 vs. 38), so no conclusion about lateralization effects could be drawn for this region (Fisher's exact test: $P = 0.3$). However, there was an equivalent sampling of more anterior critical regions (ventral occipito-temporal cortex: 35 vs. 36; anterior temporal cortex: 77 vs. 78), and for both regions the proportion of evoked visual phenomena was significantly larger in the right than in the left hemisphere (ventral occipito-temporal cortex, $\chi^2 = 7.3$, $P = 0.007$; anterior temporal cortex, Fisher's exact test: $P = 0.003$). Therefore, with the exception of the medial occipital cortex, the right hemisphere predominance cannot be accounted for by a lack of sampling of left hemisphere critical regions.

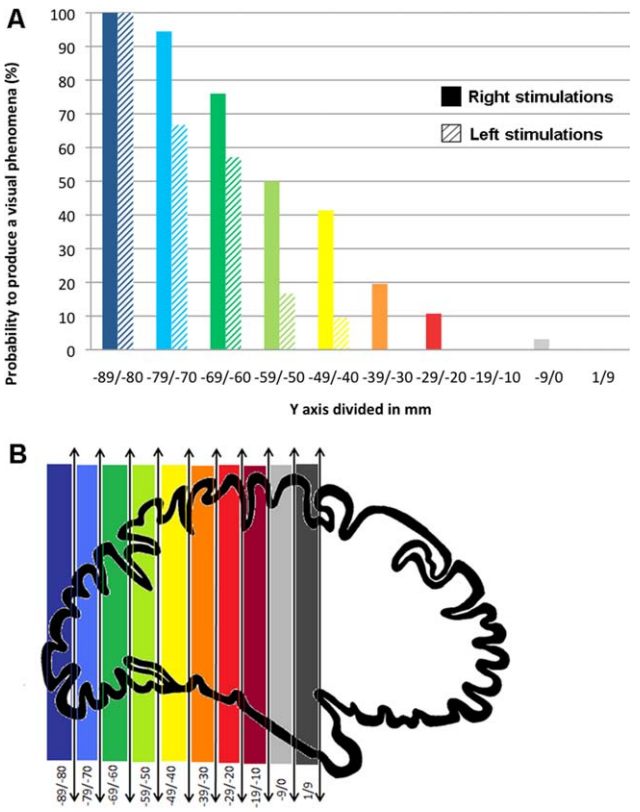

Figure 3.
Probability to produce a visual phenomenon along the posterior-anterior (y) axis. [Color figure can be viewed in the online issue, which is available at wileyonlinelibrary.com.]

Visual Phenomena Quality

Visual hallucinations

The spatial distribution of the types of hallucinations evoked by stimulation is shown in Figure 5 and Table II. Eighty-five percent of elementary hallucinations were

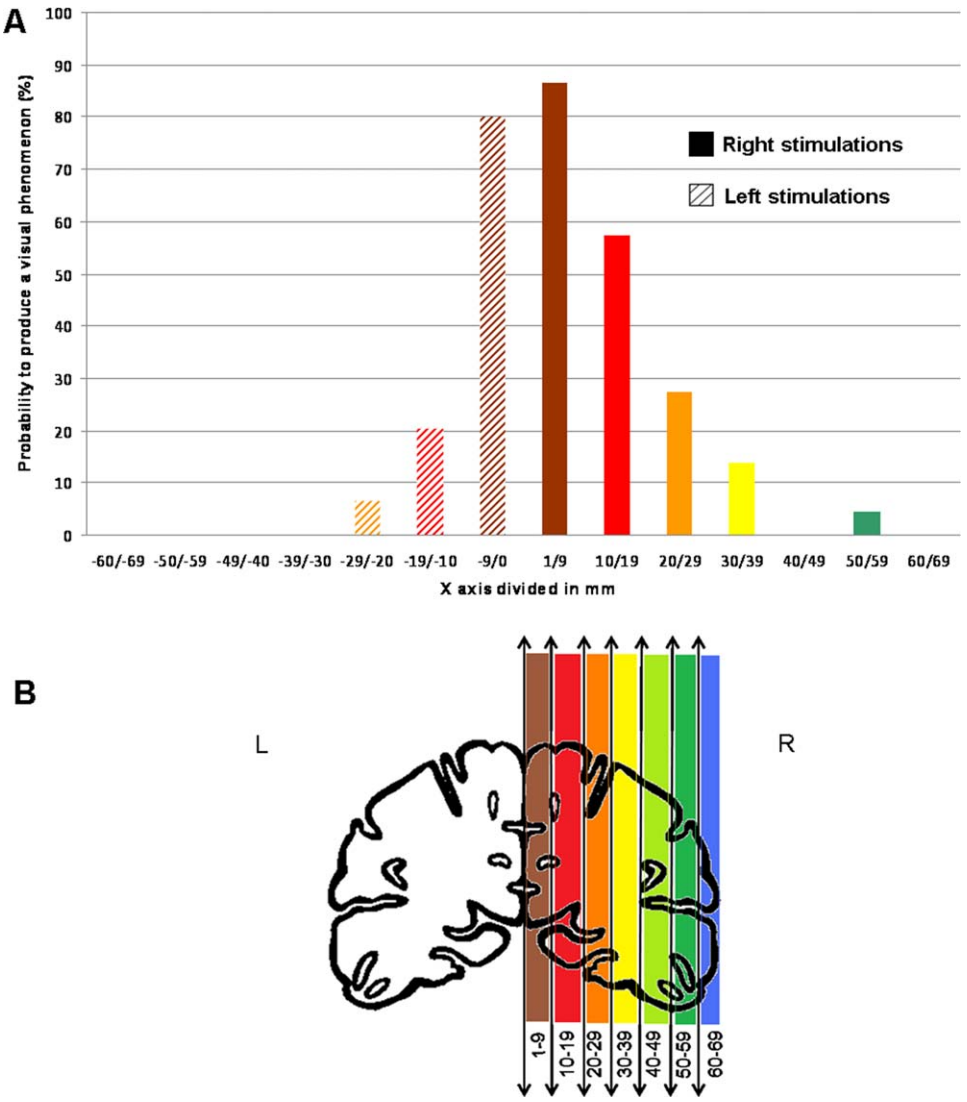

Figure 4.
Probability to produce a visual phenomenon along the medial-lateral (x) axis. [Color figure can be viewed in the online issue, which is available at wileyonlinelibrary.com.]

induced by stimulating the calcarine sulcus, the lingual gyrus, the lateral occipital cortex, the fusiform gyrus and the cuneus/parieto-occipital sulcus (46/54 sites). All intermediary hallucinations were induced by stimulating the same structures as those eliciting elementary hallucinations (21/21 sites). However, compared to elementary hallucinations, intermediary hallucinations were evoked at more anterior sites in infra-calcarine occipital structures and in the ventral temporal region (Fig. 5). Complex hallucinations were hallucinations of faces induced by stimulating the cuneus/parieto-occipital sulcus (5/7 sites), the precuneus (1/7 sites) and the fusiform gyrus (1/7 sites).

Most elementary and intermediary hallucinations were colored and moving. There were only few sites on which motionless (4/75, 5%) or colorless (15/75, 20%) elementary and intermediary hallucinations were evoked. Elementary and intermediary hallucinations were all located in the contralateral visual hemifield of the stimulation side, except those elicited by stimulations of the calcarine sulcus, which were located in the center of the visual field.

Visual illusions

Eight visual illusions were produced at eight different sites, all characterized by a change of color or by a spatial modification of the visual background. Illusions were all elicited by stimulating the right hemisphere, in the rhinal cortex, parahippocampal gyrus, collateral sulcus, and fusiform gyrus (see Fig. 5).

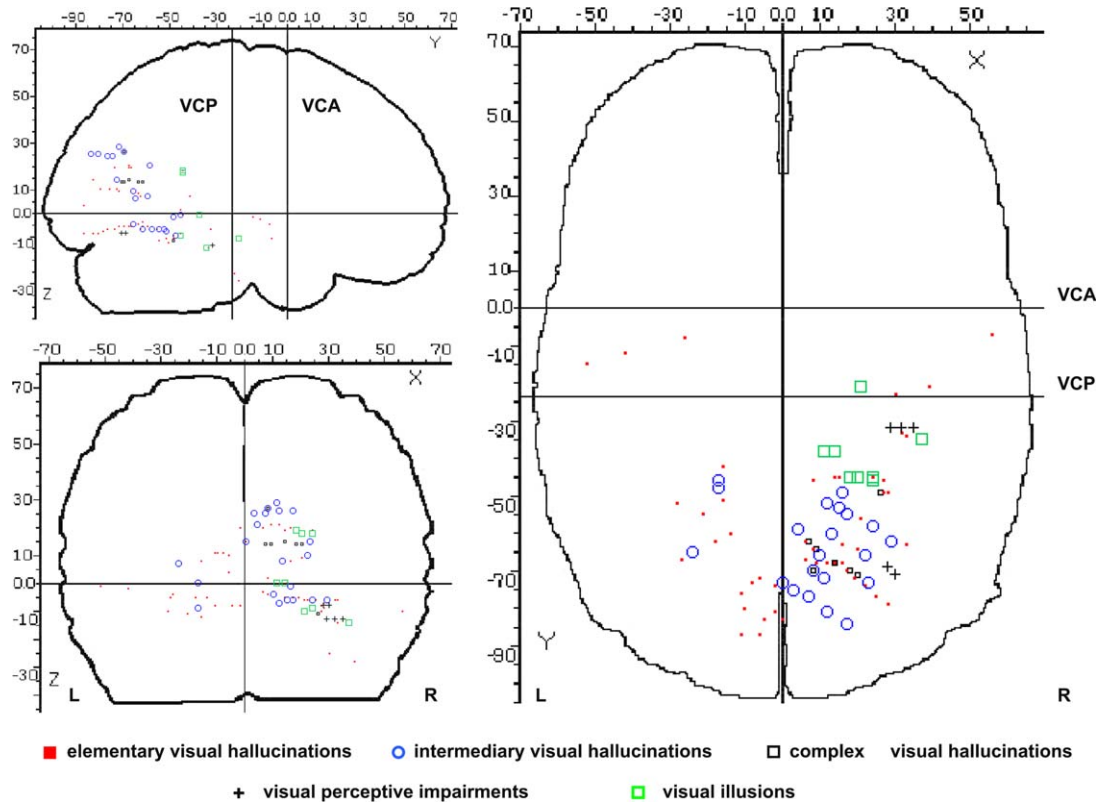

Figure 5.

Spatial distribution of types of visual phenomena evoked by stimulation, represented on a schematic brain representation (Talairach and Tournoux coordinates). [Color figure can be viewed in the online issue, which is available at wileyonlinelibrary.com.]

Visual perceptive impairments

We evoked transient impairment in two patients exclusively by stimulating the right hemisphere. In both patients, the impairments consisted of transient prosopagnosia [i.e., specific impairment of face recognition; Bodamer, 1947; Busigny et al., 2010] during stimulation. This was found by asking these two patients to name photographs of famous faces, famous scenes, and usual objects, before, during, and after stimulations [the full procedure is described in Jonas et al., 2012]. Prosopagnosia was evoked by the stimulation of the right inferior occipital gyrus in the first patient (reproduced six times at two sites of stimulation) and by the stimulation of the right middle fusiform gyrus in the second patient (reproduced seven times at three sites of stimulation). The patients were unable to name famous faces, whereas they were able to recognize objects and famous scenes during stimulation of these sites. Prosopagnosia completely recovered immediately upon termination of the stimulation. The first patient

TABLE III. Number of stimulated sites, number of positive sites (site where a visual phenomenon was evoked), and probability to evoke a visual phenomenon (%) in each defined volume: in the medial occipital cortex (*x*: 0/±30; *y*: −90/−60; *z*: −10/30), in the ventral occipito-temporal cortex (*x*: ±10/±40; *y*: −60/−35; *z*: −20/0), and in the anterior temporal cortex (*x*: ±20/±50; *y*: −35/−10; *z*: −30/0)

	Left Hemisphere			Right Hemisphere		
	Number of stimulated sites	Number of positive sites	%	Number of stimulated sites	Number of positive sites	%
Anterior temporal cortex	77	0	0%	78	9	11%
Ventral occipito-temporal cortex	35	6	17%	36	17	47%
Medial occipital cortex	13	13	100%	45	38	84%

(K.V.) is fully described in Jonas et al. (2012). The stimulated site was located in a high-level visual area involved in face perception in the right inferior occipital gyrus (right "occipital face area," right OFA) as defined by fMRI and intracerebral ERPs. For the second patient, face sensitive ERPs were recorded on the stimulated sites (manuscript in preparation, data not shown here).

Spatial Organization of Visual Phenomena Types

Visual analysis of the spatial organization of visual phenomena evoked from the infra-calcarine occipital structures to the ventral temporal region ($z < 0$ mm) showed a trend toward a postero-anterior gradient (Fig. 5) with a predominance of elementary hallucinations at the most posterior sites, a mix of elementary and intermediary hallucinations more anteriorly and illusions at the most anterior sites in the temporo-basal cortex. However, the location of the stimulated sites along the antero-posterior axis (x-axis) did not differ between the three different qualities of evoked visual phenomena (one-way ANOVA, $F_{2,48} = 1.29$; $P = 0.28$). No spatial organization was found for visual phenomena evoked from the supra-calcarine occipital structures to the parietal region ($z > 0$ mm). However, there were few depth electrodes implanted in these structures.

The right hemispheric predominance was more pronounced for complex visual phenomena (Fig. 6). Elementary hallucinations were evoked with a slight right predominance but with no statistical significance (32 positive sites in the right hemisphere vs. 22 in the left hemisphere, $\chi^2 = 3.7$, $P = 0.053$). Intermediary hallucinations showed a significant right predominance (18 positive sites in the right hemisphere vs. 3 in the left hemisphere, Fisher's exact test: $P < 0.001$). Complex hallucinations, illusions, and visual perceptive impairments were exclusively evoked by stimulating the right hemisphere (20 positive sites in the right hemisphere vs. 0 in the left hemisphere, Fisher's exact test: $P < 0.0001$).

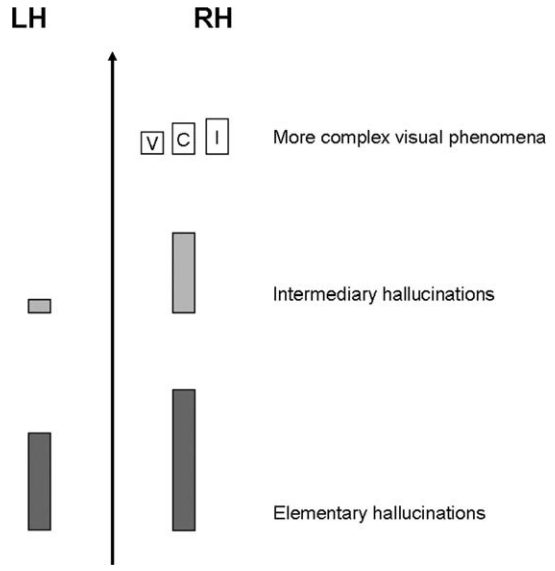

Figure 6.
Schematic representation of the number of visual phenomena evoked in the left and right hemispheres along a gradient of complexity (LH: left hemisphere, RH: right hemisphere, V: visual perceptive impairments, C: complex hallucinations, I: illusions). The number of visual phenomena is represented by the height of the bars.

DISCUSSION

Taken altogether, our data showed a general organization of evoked visual phenomena consisting of: (i) a decreasing probability to evoke visual phenomena along the posterior-anterior axis; (ii) a trend towards posterior-anterior gradient in terms of complexity of visual phenomena; and (iii) a clear functional hemispheric asymmetry with right hemisphere predominance. The right visual cortex showed a greater sensitivity to electrical stimulation for each stimulated structure and each type of evoked visual phenomenon, except for occipital medial structures and elementary visual phenomena. Moreover, this hemispheric asymmetry increased along the postero-anterior axis: the decreasing probability to evoke a visual phenomenon along the postero-anterior axis was less pronounced in the right hemisphere, and the right hemispheric predominance was significant for complex and intermediary but not for elementary visual phenomena.

Hierarchical Organization of the Visual System

Our observations suggest that there is a posterior-anterior gradient regarding visual phenomena quality in the ventral visual pathway (i.e., infracalcarine occipital structures to the ventral temporal region). Intermediary hallucinations were roughly localized anteriorly to elementary hallucinations, and illusions were all localized anteriorly to intermediary hallucinations. Although it was not statistically significant because of low statistical power, these observations are consistent with a previous stimulation study that showed a postero-anterior distribution of simple, intermediate, and complex forms, respectively [Lee et al., 2000]. Overall, these observations are consistent with a hierarchical organization of visual areas along the occipito-temporal pathway in which visual information is first represented in a localized and simple form, and is then transformed into more complex representations through a sequence of processes [DeYoe and Van Essen, 1988; Grill-Spector and Malach, 2004; Hubel and Wiesel, 1962].

Our results showed a decreasing probability of eliciting visual phenomena from posterior to anterior sites. This decrease may arise from a postero-anterior gradient in the functional connectivity of visual areas. The greater

sensitivity to electrical stimulation of posterior and low-level visual areas might be related to their greater extrinsic connectivity compared to anterior, higher level visual areas [Murphey et al., 2009; Tolias et al., 2005]. However, compared to a previous stimulation study [Murphey et al., 2009], our study showed qualitative differences between visual percepts evoked by the stimulation of posterior, as opposed to anterior, sites: the increasing complexity of evoked visual phenomena along the posterior-anterior axis paralleled the decreasing probability to evoke visual phenomena. Altogether, these results support the view of a hierarchical posterior-anterior organization of visual system.

Right Hemispheric Predominance

The most original and important observation of the present study is the greater sensitivity to electrical stimulation found in the right hemisphere, compared to the left hemisphere, from the ventral occipito-temporal cortex to more anterior temporal regions (Figs. 2 and 5). The probability of evoking a visual phenomenon was significantly higher in the right than the left hemisphere, except for the medial occipital cortex. Intermediary hallucinations were predominantly elicited by right hemisphere stimulation, whereas complex hallucinations, illusions, and visual perceptive impairments were elicited exclusively by right hemisphere stimulation (Figs. 5 and 6).

This right hemispheric predominance of electrically evoked visual phenomena has scarcely been reported in previous studies, and then only for visual illusions [Mullan and Penfield, 1959]. Interestingly, epileptic complex visual hallucinations (e.g., faces, objects, bodies) or illusions were also reported to be associated with a right epileptic focus in a retrospective study of medically intractable occipital epilepsy [Salanova et al., 1992]. In most previous visual cortex stimulation studies, this functional hemispheric asymmetry has not been specifically addressed [Lee et al., 2000; Lesser et al., 1998; Murphey et al., 2009]. Our original observations can be tentatively related to the use of depth electrodes, as opposed to subdural electrodes used in previous studies. Depth electrodes indeed allow eliciting phenomena with low stimulation intensities (mean intensity of 1.29 mA, as compared to 4.75 mA in Lee et al., (2000), for instance). Thus, the depth electrode approach is very effective in producing localized low intensity current flows, preventing afterdischarges and spread to homologous contralateral sites through corpus callosum connections.

The increased sensitivity of the right hemisphere to produce electrically induced visual phenomena is consistent with the long-standing view of right hemisphere specialization in processing visual or nonverbal stimuli [Jackson, 1874]. This view has been supported by studies of patients with temporal lobe damage or surgical resection [Kimura, 1963, 1966; Milner, 1958], occipito-temporo-parietal damage [Humphreys and Riddoch, 1984; Warrington and Taylor, 1978; Warrington, 1982] and studies of split-brain patients [Bogen and Gazzaniga, 1965, Gazzaniga et al., 1965]. More specifically, the right hemisphere would be superior to the left in visual tasks requiring spatial judgment [Corballis et al., 2002; Funnel et al., 1999] or spatial attention [for a review see Karim and Kojima, 2010]. However, this right hemispheric general superiority in visuospatial processing or in spatial attention cannot easily account for its greater sensitivity to evoke visual phenomena, because: (i) during electrical stimulation, patients were not engaged in spatial or attentional tasks; (ii) evoked visual phenomena were described by the patients as vivid and clear after stimulation of both hemispheres, making it very unlikely that the right predominance resulted from an attentional bias; and (iii) the greater sensitivity of the right hemisphere to evoke visual phenomena was reported for several anatomical structures and for very different types of visual phenomena, suggesting that this greater sensitivity of the right hemisphere reflects the general function of the visual system, rather than a specific involvement of visuospatial processes.

Hemispheric asymmetry also increased along the posterior-anterior axis. The decreasing probability of evoking a visual phenomenon along the posterior-anterior axis was indeed less pronounced in the right hemisphere and paralleled the right hemispheric predominance for more complex visual phenomena. These results suggest a progressive and increasing postero-anterior specialization of the right hemisphere in visual processing from the occipito-temporal ventral cortex to the more anterior temporal areas.

These results are consistent with the view that asymmetries in visual processing are likely to arise relatively late in the visual system, and in areas with bilateral receptive fields. ''Low-level'' or ''early'' visual areas are constituted of neurons with small receptive fields, responding to spatially limited visual stimuli localized in the contralateral visual hemifield. These receptive fields get progressively larger and more bilateral in "higher-level" and more anterior visual areas. At early levels of processing, in each hemisphere, the representation of the contralateral visual field is unique; therefore, asymmetries in early visual processing are unlikely to arise. At higher level of processing, the representation of the visual field is redundant in both hemispheres. At these higher stages, visual representations might therefore be favored in one hemisphere (for instance in the right) over the other. This right hemispheric dominance at higher levels of processing is also reflected by the larger amplitude of visual evoked potential over the right ventral occipito-temporal region between 150 and 200 ms during face or abstract pictures processing [Maillard et al., 2011; Rossion et al., 2003].

Face-Selective Regions

We evoked specific visual perceptive impairments (i.e., prosopagnosia, impairment in face recognition) during

stimulation of face-sensitive areas in two patients. The first patient (K.V.) is fully described in Jonas et al. (2012). In that article, we showed that transient prosopagnosia was induced by stimulating a high-order visual area involved in face perception in the right inferior occipital gyrus (right OFA). This observation indicated that a specific process (here, face recognition) could be selectively disrupted by stimulating a high-order and functionally specific visual area. In a second patient, we also induced transient prosopagnosia by stimulating a face sensitive site localized in the right middle fusiform gyrus. Previous electrical stimulation studies that did not use specific visual stimuli during stimulations have not found visual perceptive impairments during stimulations of anterior sites in the temporal lobe or functionally defined high-level areas [Lee et al., 2000; Lesser et al., 1998; Murphey et al., 2009]. In particular, Murphey et al. (2009) reported only elementary visual hallucinations, even after stimulation of fMRI-defined high-level areas (V8, MT, PPA, FFA, LO). Our study shows that presenting real face stimuli during electrical cortical stimulations allows the establishment of a causal relationship between face-selective regions and face perception.

CONCLUSIONS

Overall, our depth electrode stimulation study contributes to the understanding of the functional organization of the human visual cortex, as reflected by its heterogeneous but organized sensitivity to electrical stimulation. Specifically, we found a clear right hemispheric functional predominance that cannot easily be accounted for by a task-related or a material-specific bias. Rather, this right hemispheric dominance seems to reflect the general function of the visual system.

REFERENCES

Bak M, Girvin JP, Hambrecht FT, Kufta CV, Loeb GE, Schmidt EM (1990): Visual sensations produced by intracortical microstimulation of the human occipital cortex. Med Biol Eng Comput 28:257–259.

Bodamer J (1947): Die Prosop-Agnosie. Arch Psychiatr Nervenkr Z Gesamte Neurol Psychiatr 118:6–53.

Bogen JE, Gazzaniga MS (1965): Cerebral commissurotomy in man: Minor hemisphere dominance for certain visuospatial functions. J Neurosurg 23:394–399.

Brindley GS, Lewin WS (1968): The sensations produced by electrical stimulation of the visual cortex. J Physiol (Lond) 196: 479–493.

Busigny T, Joubert S, Felician O, Ceccaldi M, Rossion B (2010): Holistic perception of the individual face is specific and necessary: Evidence from an extensive case study of acquired prosopagnosia. Neuropsychologia 48:4057–4092.

Corballis PM (2003): Visuospatial processing and the right-hemisphere interpreter. Brain Cogn 53:171–176.

Corballis PM, Funnell MG, Gazzaniga MS (2002): Hemispheric asymmetries for simple visual judgments in the split brain. Neuropsychologia 40:401–410.

DeYoe EA, Van Essen DC (1988): Concurrent processing streams in monkey visual cortex. Trends Neurosci 11:219–226.

Funnell MG, Corballis PM, Gazzaniga MS (1999): A deficit in perceptual matching in the left hemisphere of a callosotomy patient. Neuropsychologia 37:1143–1154.

Gazzaniga MS, Bogen JE, Sperry RW (1965): Observations on visual perception after disconnection of the cerebral hemispheres in man. Brain 88:221–236.

Grill-Spector K, Malach R (2004): The human visual cortex. Annu Rev Neurosci 27:649–677.

Hubel DH, Wiesel TN (1962): Receptive fields, binocular interaction and functional architecture in the cat's visual cortex. J Physiol 160:106–154.

Humphreys GW, Riddoch MJ (1984): Routes to object constancy: Implications from neurological impairments of object constancy. Q J Exp Psychol A 36:385–415.

Ishibashi T, Hori H, Endo K, Sato T (1964): Hallucinations produced by electrical stimulation of the temporal lobes in schizophrenic patients. Tohoku J Exp Med 82:124–139.

Jackson JH (1874): On the nature of the duality of the brain. Medical Press Cricular 1:19–63.

Jonas J, Descoins M, Koessler L, Colnat-Coulbois S, Sauvée M, Guye M, Vignal JP, Vespignani H, Rossion B, Maillard L (2012): Focal electrical intracerebral stimulation of a face-sensitive area causes transient prosopagnosia. Neuroscience 222:281–228.

Kahane P, Hoffmann D, Minotti L, Berthoz A (2003): Reappraisal of the human vestibular cortex by cortical electrical stimulation study. Ann Neurol 54:615–624.

Karim AK, Kojima H (2010): The what and why of perceptual asymmetries in the visual domain. Adv Cogn Psychol 6:103–115.

Kimura D (1963): Right temporal-lobe damage: Perception of unfamiliar stimuli after damage. Arch Neurol 8:264–271.

Kimura D (1966): Dual functional asymmetry of the brain in visual perception. Neuropsychologia 4:275–285.

Lee HW, Hong SB, Seo DW, Tae WS, Hong SC (2000): Mapping of functional organization in human visual cortex: electrical cortical stimulation. Neurology 54:849–854.

Lesser RP, Arroyo S, Crone N, Gordon B (1998): Motor and sensory mapping of the frontal and occipital lobes. Epilepsia 39 Suppl 4:S69–80.

Maillard L, Koessler L, Colnat-Coulbois S, Vignal JP, Louis-Dorr V, Marie PY, Vespignani H (2009): Combined SEEG and source localisation study of temporal lobe schizencephaly and polymicrogyria. Clin Neurophysiol 120:1628–1636.

Maillard L, Barbeau E, Baumann C, Koessler L, Bénar C, Chauvel P, Liegeois-Chauvel C (2011): From perception to recognition memory: Time course and lateralization of neural substrates of word and abstract picture processing. J Cogn Neurosci 23:782–800.

Milner B (1958): Psychological defects produced by temporal lobe excision. Proc Ass Res Nerv Ment Dis 36:244–257.

Mullan S, Penfield W (1959): Illusions of comparative interpretation and emotion; production by epileptic discharge and by electrical stimulation in the temporal cortex. AMA Arch Neurol Psychiatry 81:269–284.

Murphey DK, Maunsell JH, Beauchamp MS, Yoshor D (2009): Perceiving electrical stimulation of identified human visual areas. Proc Natl Acad Sci U S A 106:5389–5393.

Nathan SS, Sinha SR, Gordon B, Lesser RP, Thakor NV (1993): Determination of current density distributions generated by electrical stimulation of the human cerebral cortex. Electroencephalogr Clin Neurophysiol 86:183–192.

Oldfield RC (1971): The assessment and analysis of handedness: The Edinburgh inventory. Neuropsychologia 9:97–113.

Penfield W, Jasper H. 1954. Epilepsy and the functional anatomy of the human brain. Boston: Little, Brown.

Penfield WR, Rasmussen T. 1957. The Cerebral Cortex of Man: A Clinical Study of Localization of Function. New York: Macmillan.

Puce A, Allison T, McCarthy G (1999): Electrophysiological studies of human face perception. III: Effects of top-down processing on face-specific potentials. Cereb Cortex 9:445–458.

Rossion B, Joyce CA, Cottrell GW, Tarr MJ (2003): Early lateralization and orientation tuning for face, word, and object processing in the visual cortex. Neuroimage 20:1609–1624.

Salanova V, Andermann F, Olivier A, Rasmussen T, Quesney LF (1992): Occipital lobe epilepsy: Electroclinical manifestations, electrocorticography, cortical stimulation and outcome in 42 patients treated between 1930 and 1991. Surgery of occipital lobe epilepsy. Brain 115:1655–1680.

Talairach J, Bancaud J (1973): Stereotaxic approach to epilepsy: Methodology of anatomo-functional stereotactic investigations. Prog Neurol Surg 5:297–354.

Talairach J, Tournoux P. 1988. Coplanar stereotaxic atlas of the human brain: 3-dimensional proportional system: An approach to cerebral imaging. Stuttgart: Thieme.

Tolias AS, Sultan F, Augath M, Oeltermann A, Tehovnik EJ, Schiller PH, Logothetis NK (2005): Mapping cortical activity elicited with electrical microstimulation using FMRI in the macaque. Neuron 48:901–911.

Vignal JP, Maillard L, McGonigal A, Chauvel P (2007): The dreamy state: Hallucinations of autobiographic memory evoked by temporal lobe stimulations and seizures. Brain 130: 88–99.

Warrington EK (1982): Neuropsychological studies of object recognition. Philos Trans R Soc Lond B Biol Sci 298:15–33.

Warrington EK, Taylor AM (1978): Two categorical stages of object recognition. Perception 7:695–705.

Self-face hallucination evoked by electrical stimulation of the human brain

Jacques Jonas, MD
Louis Maillard, MD, PhD
Solène Frismand, MD
Sophie Colnat-Coulbois, MD, PhD
Hervé Vespignani, MD
Bruno Rossion, PhD
Jean-Pierre Vignal, MD

Correspondence to Dr. Jonas: j.jonas@chu-nancy.fr

ABSTRACT

Objectives: Self-face hallucination (autoscopic hallucination or AH) has been reported in patients with widespread brain damage or retrospectively after epileptic seizures. The neural basis and the self-processing operations underlying AH remain unknown.

Methods: We report the results of intracerebral electrical stimulations of the right medial occipitoparietal cortex (right precuneus and occipitoparietal sulcus) in 2 patients with epilepsy who underwent a stereo-EEG.

Results: Immediately after the onset of the stimulation, the 2 patients reported seeing their current own face, facing themselves, in their left visual field.

Conclusions: Our study shows that the medial occipitoparietal junction has a key role in generating AH. This region has been shown to have a central role in various self-processing operations and especially in self-face recognition. Our observations further reveal that this region is involved in a visual representation of our own face, which is generated during the pathologic phenomenon of AH. This visual representation of our own face may be useful for self-face recognition and social cognition processes involving judgment of self-facial resemblance to others. *Neurology*® 2014;83:336–338

GLOSSARY

AH = autoscopic hallucination; **OBE** = out-of-body experience.

The conscious experience of the self is one of the most astonishing features of the human brain and comprises different facets (the sense that I exist separately from others, my autobiographical memories, the awareness of my own body, what I look like, etc.). One of the most important elements of our sense of identity is the appearance of our own face. Notably, although we are rarely confronted with our own face compared with others in everyday life, we are quicker at identifying our own face than other people's faces. This has been interpreted as reflecting the existence of a robust neural self-face representation.

One of the most fascinating phenomena related to the disturbance of the neural processes underlying the representation of the self is autoscopic hallucination (AH). AH is characterized by the visual hallucination of one's own face, sometimes including the upper parts of one's body. AH is part of a heterogeneous class (autoscopic phenomena) of pathologic visual illusory reduplication of one's own body in the extrapersonal space, which also contains out-of-body experiences (OBEs) and heautoscopy.[1–3] While the neural basis and the self-processing operations underlying OBEs and heautoscopy have been well documented (i.e., temporoparietal junction, disturbance of the awareness of our own body), these aspects remain debated for AH.[1] Here we report the first description of AH evoked by focal electrical stimulation of the human brain.

METHODS

Case descriptions. We report the cases of 2 right-handed patients with epilepsy who never experienced AH during their seizures. Patient 1 is a 46-year-old man and patient 2 is a 24-year-old woman. Both patients underwent a stereo-EEG, which delineated the epileptogenic zone in the right medial temporal lobe for patient 1 and in the right posterior insula for patient 2.

Supplemental data at Neurology.org

From Service de Neurologie (J.J., L.M., S.F., H.V., J.-P.V.) and Service de Neurochirurgie (S.C.-C.), Centre Hospitalier Universitaire de Nancy; CRAN, UMR 7039 (J.J., L.M., H.V., J.-P.V.), Université de Lorraine and CNRS, Nancy; Faculté de Médecine de Nancy (J.J., L.M., S.C.-C., H.V.), Université de Lorraine, Nancy, France; and Université Catholique de Louvain (J.J., B.R.), Louvain-la-Neuve, Belgique.

Go to Neurology.org for full disclosures. Funding information and disclosures deemed relevant by the authors, if any, are provided at the end of the article.

Cortical stimulations. Stereotactic placement of the intracerebral electrodes consisted of 5 to 18 contiguous 2-mm-long contacts separated by 1.5 mm. Intracerebral stimulations were performed to localize the epileptogenic zone and to map functionally relevant areas. Bipolar electrical intracerebral stimulations were applied between 2 contiguous contacts and performed at 50 Hz over 5 seconds, at intensities ranging from 0.5 to 2 mA. Patients were not aware of the stimulation onset and termination, the stimulation site, or the potential evoked perceptual changes.

RESULTS **Patient 1.** Patient 1 reported transient visual hallucinations of his own face during stimulations of 2 different sites in the posterior bank of the right occipitoparietal sulcus (figure). One site was located in the medial part of the right occipitoparietal sulcus (contacts O1-O2, 1 mA, 2 of 6 stimulations) and the other site was located in the lateral part of the sulcus (contacts O4-O5, 1.2 mA, 2 of 4 stimulations). Immediately after stimulation onset, the patient reported seeing a face in his left visual field ("I see a face"). When asked whose face it was, the patient spontaneously responded: "it seems to be my face," "I think it's my face." When asked if he saw any other parts of his body, the patient stated that he also saw his bust. Stimulations of the most medial contacts of electrode O in the occipitoparietal sulcus (contacts O1-O2) evoked garish, colored hallucinations of his own face (video 1 on the *Neurology*® Web site at Neurology.org). When asked if the hallucinated face was his current own face, he responded directly: "my face, yes." Four additional stimulations at this site produced hallucination of faces that were not spontaneously recognized as his own face. Stimulations of intermediate contacts of electrode O located in the white matter evoked either hallucinations of unknown faces (O2-O3, 2 stimulations) or elementary visual hallucinations (O3-O4, 1 stimulation). Notably, stimulations of more lateral contacts of electrode O located within the lateral part of the right occipitoparietal sulcus evoked hallucinations of the patient's own face again (contacts O4-O5, 2 stimulations). At this site, the patient saw his own face with the bandage that he was currently wearing during stereo-EEG (video 2). Stimulations of the most lateral contacts outside the occipitoparietal sulcus evoked hallucinations of unknown faces (O5-O6 and O6-O7, 2 stimulations).

Patient 2. Stimulation of one site in the right posterior precuneus at the edge of the occipitoparietal sulcus evoked a transient hallucination of the patient's own face (PP2-PP3, 1.2 mA; figure). During the stimulation train and the local after-discharge limited to the immediate vicinity of the stimulated site, the patient reported vertigo ("I am dizzy") and visual hallucination

Figure **Anatomical locations of relevant contacts that produced autoscopic hallucination at stimulation**

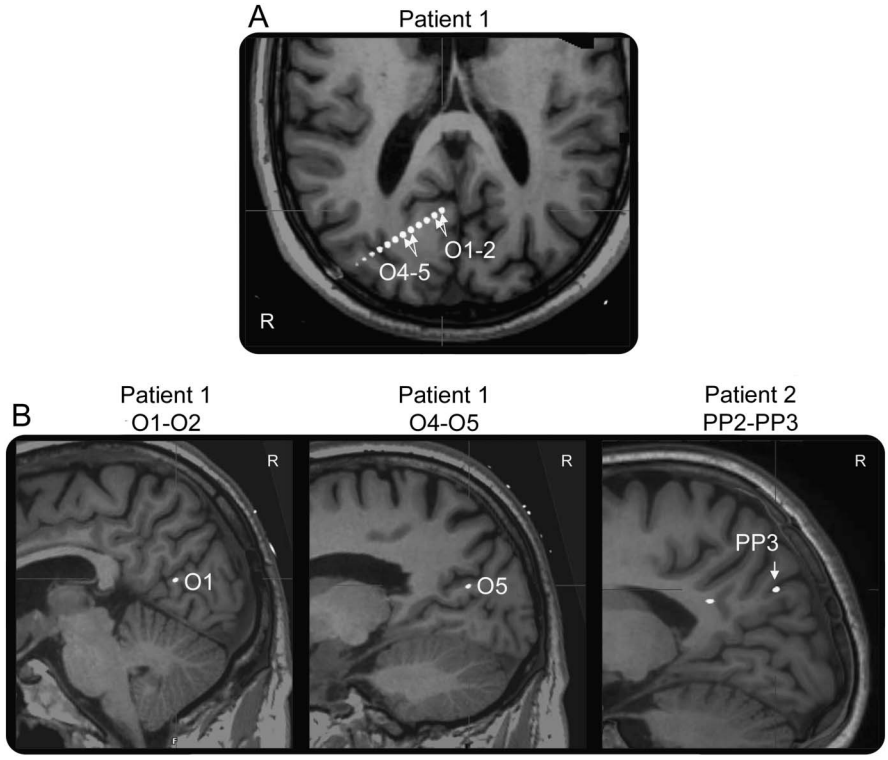

(A) Axial view of electrode O in patient 1 (bipolar stimulations of contacts O1-O2 and contacts O4-O5). Note that only stimulations of contacts located within the right occipitoparietal sulcus induced autoscopic hallucination. (B) Sagittal view of relevant contacts in patient 1 (bipolar stimulations of contacts O1-O2 and contacts O4-O5) and in patient 2 (bipolar stimulations of contacts PP2-PP3). For each pair of contacts, only one contact is represented.

in the left visual field ("there is something in front of my left eye"). She spontaneously reported: "I saw myself like in a mirror," "I saw my face," "I recognized myself like in a mirror," "there was something metallic like a mirror, I looked and I saw myself," "it was on my left," "I was colored like in a mirror" (video 3). Three subsequent stimulations at this site performed at lower intensities (0.8 and 1 mA) only evoked vertigo and elementary colored hallucinations in the left visual field.

Standard protocol approvals, registrations, and patient consents. Ethics committee approval was not requested because we only report results that were obtained in a clinical context. Also note that patients are not recognizable in the text or the videos.

DISCUSSION To our knowledge, we report the first 2 cases of self-face visual hallucination evoked by electrical stimulation of the human brain. In contrast to previous brain stimulation studies evoking autoscopic phenomena (OBEs) with subdural electrodes applied over the cortical surface,[4,5] our investigations used intracerebral depth electrodes. In this approach, the stimulations are not only performed in the lateral cortex but also in the sulci and in deep and medial cortical structures that are essential to self-processing (e.g., precuneus, cingulate cortex, medial prefrontal cortex).[6]

Phenomenologically, these hallucinations are similar to the pathologic AH described in various cerebral diseases causing damage to the right occipital and/or the parietal region. However, the heterogeneous and widespread localization of brain lesions has prevented establishing firm conclusions concerning the critical region(s) generating AH.[2,3] A recent study showed an overlap of these lesions in the right occipital lobe (cuneus, and the right superior occipital gyrus).[1] Focal electrical stimulation findings reported here provide a more accurate anatomo-functional correlation pointing toward the right precuneus and right parieto-occipital sulcus. Moreover, electrical stimulations further provide a causal link between the stimulated brain areas (right medial occipitoparietal junction) and the occurrence of AH.

Our current observations are consistent with functional neuroimaging studies in healthy subjects that showed a central role of the occipitoparietal sulcus and the precuneus in various self-processing operations.[7] More specifically, the right precuneus has been shown to have a role in self-face processing within a widespread cortical network involving the left fusiform gyrus, and bilateral middle and inferior frontal gyri.[8] Our results emphasize the crucial role of the right precuneus and occipitoparietal sulcus within this large cortical network.

The present observations show the key role of the right precuneus and occipitoparietal sulcus in representing self-face visual information within a distributed neural network dedicated to self-face processing. We suggest that AH may represent an abnormal activation of a visual internal template of our own face. Such a visual internal template of our own face may be useful for self-face recognition and judgment of self-facial resemblance of others, a function that is very important for social cognition, including trusting behavior, prosocial perceptions, and sexual preferences.[9] However, because our face changes with age and experience, such a template has to be a malleable construct and updated by recent visual experience of our own face.[10] This may explain why both patients reported seeing their current face (with his bandage for patient 1 and "like in a mirror" for patient 2).

AUTHOR CONTRIBUTIONS

J.J. wrote the article, L.M. performed the stimulations and wrote the article, S.F. wrote the article, S.C.-C. implanted the intracerebral electrodes and provided the figures, H.V. wrote the article, B.R. wrote the article, and J.-P.V. performed the stimulations and wrote the article.

STUDY FUNDING

No targeted funding reported.

DISCLOSURE

The authors report no disclosures relevant to the manuscript. Go to Neurology.org for full disclosures.

Received March 6, 2014. Accepted in final form April 17, 2014.

REFERENCES

1. Heydrich L, Blanke O. Distinct illusory own-body perceptions caused by damage to posterior insula and extrastriate cortex. Brain 2013;136:790–803.
2. Blanke O, Mohr C. Out-of-body experience, heautoscopy, and autoscopic hallucination of neurological origin: implications for neurocognitive mechanisms of corporeal awareness and self-consciousness. Brain Res Brain Res Rev 2005;50:184–199.
3. Maillard L, Vignal JP, Anxionnat R, Taillandier L, Vespignani H. Semiologic value of ictal autoscopy. Epilepsia 2004;45:391–394.
4. Blanke O, Ortigue S, Landis T, et al. Stimulating illusory own-body perceptions. Nature 2002;419:269–270.
5. De Ridder D, Van Laere K, Dupont P, Menovsky T, Van de Heyning P. Visualizing out-of-body experience in the brain. N Engl J Med 2007;357:1829–1833.
6. Northoff G, Bermpohl F. Cortical midline structures and the self. Trends Cogn Sci 2004;8:102–107.
7. Cavanna AE, Trimble MR. The precuneus: a review of its functional anatomy and behavioural correlates. Brain 2006;129:564–583.
8. Platek SM, Wathne K, Tierney NG, Thomson JW. Neural correlates of self-face recognition: an effect-location meta-analysis. Brain Res 2008;1232:173–184.
9. DeBruine LM, Jones BC, Watkins CD, et al. Opposite-sex siblings decrease attraction, but not prosocial attributions, to self-resembling opposite-sex faces. Proc Natl Acad Sci USA 2011;108:11710–11714.
10. Hauber ME, Sherman PW. Self-referent phenotype matching: theoretical considerations and empirical evidence. Trends Neurosci 2001;24:609–616.

NeuroImage 99 (2014) 487–497

Contents lists available at ScienceDirect

NeuroImage

journal homepage: www.elsevier.com/locate/ynimg

Intracerebral electrical stimulation of a face-selective area in the right inferior occipital cortex impairs individual face discrimination

Jacques Jonas [a,b,c,d,e,*], Bruno Rossion [e], Julien Krieg [b,c], Laurent Koessler [b,c], Sophie Colnat-Coulbois [d,f], Hervé Vespignani [a,b,c,d], Corentin Jacques [e], Jean-Pierre Vignal [a,b,c], Hélène Brissart [a], Louis Maillard [a,b,c,d]

[a] Service de Neurologie, Centre Hospitalier Universitaire de Nancy, 29 Avenue du Maréchal de Lattre de Tassigny, 54000 Nancy, France
[b] Université de Lorraine, CRAN, UMR 7039, Campus Sciences, Boulevard des Aiguillettes, 54500 Vandœuvre-lès-Nancy, France
[c] CNRS, CRAN, UMR 7039, Campus Sciences, Boulevard des Aiguillettes, 54500 Vandœuvre-lès-Nancy, France
[d] Faculté de Médecine de Nancy, Université de Lorraine, 9 Avenue de la Forêt de Haye, 54500 Vandœuvre-lès-Nancy, France
[e] Université Catholique de Louvain, 10 Place du Cardinal Mercier, 1348 Louvain-La-Neuve, Belgium
[f] Service de Neurochirurgie, Centre Hospitalier Universitaire de Nancy, 29 Avenue du Maréchal de Lattre de Tassigny, 54000 Nancy, France

ARTICLE INFO

Article history:
Accepted 6 June 2014
Available online 14 June 2014

Keywords:
Intracerebral recordings
Individual face discrimination
Repetition suppression
Electrical brain stimulation
Occipital face area
Fast periodic visual stimulation

ABSTRACT

During intracerebral stimulation of the right inferior occipital cortex, a patient with refractory epilepsy was transiently impaired at discriminating two simultaneously presented photographs of unfamiliar faces. The critical electrode contact was located in the most posterior face-selective brain area of the human brain (right "occipital face area", rOFA) as shown both by low- (ERP) and high-frequency (gamma) electrophysiological responses as well as a face localizer in fMRI. At this electrode contact, periodic visual presentation of 6 different faces by second evoked a larger electrophysiological periodic response at 6 Hz than when the same face identity was repeated at the same rate. This intracerebral EEG repetition suppression effect was markedly reduced when face stimuli were presented upside-down, a manipulation that impairs individual face discrimination. These findings provide original evidence for a causal relationship between the face-selective right inferior occipital cortex and individual face discrimination, independently of long-term memory representations. More generally, they support the functional value of electrophysiological repetition suppression effects, indicating that these effects can be used as an index of a necessary neural representation of the changing stimulus property.

Introduction

One of the most impressive functions of the human brain is its ability to differentiate complex visual forms (DiCarlo and Cox, 2007). The human face constitutes the most familiar, socially relevant, and complex visual form, so that discriminating individual faces requires elaborate and refined perceptual skills called for by few other categories of objects. Despite the high similarity among faces and their complex configuration of several parts (eyes, nose, mouth, etc.), adults attain a high degree of proficiency with these skills. Yet, to date, the neural basis of individual face discrimination in the human brain remains by and large a mystery.

In humans, there is a large bilateral network of occipito-temporal areas responding preferentially to faces (i.e., face-selective areas), with right hemispheric dominance (e.g., Allison et al., 1994; Calder and Young, 2005; Haxby et al., 2000; Rossion et al., 2012a; Sergent et al., 1992; Weiner and Grill-Spector, 2010). To investigate sensitivity to individual faces of these areas, functional magnetic resonance imaging (fMRI) studies have taken advantage of the reduction of neural activity following repetition of the same stimulus (repetition suppression, also referred to fMR-adaptation or habituation; Grill-Spector and Malach, 2001; Grill-Spector et al., 2006). The rationale of this approach is that populations of neurons sensitive to differences between individual faces show a smaller response when the same face identity is repeated compared to the presentation of different face identities. Many fMRI studies have reported such decreases to individual face repetition in face-selective areas of the ventral occipito-temporal cortex (e.g., Gauthier et al., 2000; Grill-Spector and Malach, 2001; Andrews and Ewbank, 2004; Schiltz et al., 2006; Gilaie-Dotan and Malach, 2007; Davies-Thompson et al., 2009; Xu and Biederman, 2010; Ewbank et al., 2013). Multivariate pattern analyses of fMRI data have also identified various clusters of voxels in the ventral occipito-temporal cortex that are sensitive to individual faces (Goesaert and Op de Beeck, 2013; Kriegeskorte et al., 2007; Nestor et al., 2011). Taken together, the observations of these studies point to a distributed representation of individual face information in the ventral occipito-temporal cortex, with a right hemispheric advantage. However, the relationship between these effects – in particular the face identity repetition suppression effects in neuroimaging – and behavioral performance at individual face

* Corresponding author at: Service de Neurologie, Hôpital Central, Centre Hospitalier Universitaire de Nancy, 29 Avenue du Maréchal de Lattre de Tassigny, 54000 Nancy, France.
E-mail address: j.jonas@chu-nancy.fr (J. Jonas).

http://dx.doi.org/10.1016/j.neuroimage.2014.06.017
1053-8119/

discrimination remains unknown. Moreover, these neuroimaging studies are not in a position to clarify the extent to which these identified brain regions encode *critical* information for individual face discrimination behavior.

This question can be tackled with other approaches. For instance, studies of neuropsychological patients with prosopagnosia – typically impairment in face recognition following brain damage – suggest that multiple regions of the right ventral occipito-temporal cortex play an important role in individual face discrimination (e.g., Barton, 2008; Bouvier and Engel, 2006; Rossion et al., 2003; Sergent and Signoret, 1992). However, patients with acquired prosopagnosia usually have large cortical lesions (e.g., Barton, 2008; Busigny et al., 2010a) preventing firm conclusions to be drawn about the critical role of a given cortical area in this process. Transcranial magnetic stimulation (TMS) on the scalp above a right face-selective area of the lateral occipital cortex (right "occipital face area", "OFA") may also impair individual face discrimination (Pitcher et al., 2007). Yet, it is fair to say that the TMS disruptive effects on individual face discrimination are relatively small (e.g., Solomon-Harris et al., 2013) and not always observed (Pitcher et al., 2008). More generally, these effects are of limited localizing value because TMS cannot be applied to other face-selective areas of the ventral visual stream, and the TMS effects are not necessarily limited to the cortical area directly under the coil (Sack and Linden, 2003).

In a recent study, we reported a transient inability to recognize photographs of famous faces during intracerebral electrical stimulation of the right occipital cortex in an epileptic patient implanted with depth electrodes (Jonas et al., 2012). Since the stimulated area was located in the right OFA, this study provided evidence for a causal link between this face-selective area and face recognition (Jonas et al., 2012; see also Vignal et al., 2000 and Parvizi et al., 2012 for reports of a distortion of the physician's face following electrical stimulation of the prefrontal cortex and fusiform gyrus respectively). Here we report the results of a second intracerebral exploration performed a year later in the same patient (KV, Jonas et al., 2012). Since this second exploration also involved intracerebral electrodes in the right inferior occipital cortex, it provided a unique opportunity to test the causal link between the right OFA and behavioral individual face discrimination. To do so, we designed an experimental paradigm with unfamiliar rather than familiar faces during intracerebral stimulation, testing individual face discrimination independently from memory factors. To test the relationship between repetition suppression/adaptation effects and individual face discrimination behavior, we measured repetition suppression by means of a fast periodic visual stimulation (FPVS) paradigm with trains of either identical faces or different faces (Rossion and Boremanse, 2011; Rossion et al., 2012b). This approach has the advantage of providing high signal-to-noise ratio repetition suppression effects for face identity within a few minutes of stimulation, a factor that is particularly important in a clinical context with limited testing time.

Materials and methods

Case description

The patient is a 32-year-old right-handed female (KV) who has rare refractory right occipital epilepsy related to a focal cortical dysplasia involving the right inferior occipital gyrus. Her case was previously reported as evidence of a transient inability to recognize famous faces following intracerebral electrical stimulation of the right inferior occipital gyrus (Jonas et al., 2012). Because she was contraindicated to conventional resection based on this first stereo-electroencephalography (SEEG; Talairach and Bancaud, 1973), the patient underwent a second SEEG about a year later (December 2011) in order to perform radiofrequency-thermolesions of the epileptic focus (Catenoix et al., 2008). To date, the patient did not have surgery. All of the SEEG and behavioral data reported in the present paper study come from this second electrode implantation and have never been reported.

The patient never reported face recognition difficulties, between and during seizures and had preserved memory and preserved visual perception (including faces and objects), as shown by neuropsychological evaluations (Jonas et al., 2012). She gave written informed consent for this study, which was approved by the ethical committee of the Nancy University Hospital.

Intracerebral electrode placement and SEEG recordings

Stereotactic placement of 3 intracerebral electrodes, consisting of 8–11 contiguous contacts of 2 mm in length, separated by 1.5 mm, was performed according to a well-defined and previously described procedure (Maillard et al., 2009). Intracerebral EEG was recorded at a 512 kHz sampling rate with a 128 channel amplifier (2 SD LTM 64 Headbox; Micromed, Italy). The reference electrode was a prefrontal midline surface electrode (FPz). All three electrodes were placed in the right ventral occipito-temporal cortex (see Fig. 1). Electrodes D (8 contacts, D1 to D8) targeted the right ventral occipital cortex, from the lateral part of the inferior occipital gyrus to the posterior collateral sulcus. Electrode F (11 contacts, F1 to 11) was located more anteriorly in the ventral occipito-temporal junction, from the right inferior temporal gyrus to the lingual gyrus. Electrode L (8 contacts, L1 to L8) was located between electrodes D and F, also in the right occipital cortex but slightly above these electrodes. Note that this kind of electrode implantation is very rare in clinical practice, where most epileptic patients are implanted with more anterior electrodes to sample the temporal cortex.

Cortical stimulation: individual face discrimination task

Since typical clinical settings in SEEG do not allow performing a large number of electrical stimulations and the patient was only implanted with intracerebral electrodes during 3 days which were mainly dedicated to clinical investigations, we first identified the relevant electrode contacts for face processing, in order to test these contacts with a well-controlled individual discrimination task limited to the category of faces. Therefore, we first screened the effect of electrical stimulation on recognition of famous faces, scenes, and everyday objects, for most of the contacts (recognition task; Table 1). This allowed us to select relevant electrode contacts whose stimulation evoked perceptual or recognition disturbances specifically for faces (i.e., no recognition difficulties for visual scenes or object pictures). Then, we tested the effect of electrical stimulation on individual face discrimination only on these selected electrode contacts (individual face discrimination task; Table 1).

Stimuli

Pictures of unfamiliar faces of 48 Caucasian undergraduate students were used. Faces were cropped along the face contour, so that no hair or external cues were visible. All images were obtained under identical conditions (distance, lighting, position). Photo Morpher v3.10 (Morpheus, Santa Barbara, CA, USA) was used to create 48 morph continua by morphing each face with two other faces of the same sex. For each face, 300 points were placed on the critical features (i.e., pupils, iris, eye bulbs, eyelids, eyebrows, mouth, nose, and overall facial contour) to allow smooth transitions between the 11 stimuli defining each morph continuum (two original faces representing the extremes, with consecutive increments of 10%). For each of the continua, two stimuli that differed from each of the two original faces (0% and 100%) by 40% (i.e., 30% and 70%) were selected. We constructed pairs of stimuli that consisted of two identical faces (two 30% or two 70%) or two different faces (one 30% and one 70%) presented next to each other (Fig. 2). For each continuum, there were thus 3 kinds of trials ($3 \times 48 = 144$). Then, we constructed 28 sets of 5 pairs of photographs. Out of the 28 potential sets, the patient was eventually shown 13 sets (65 pairs) in total. In the majority of sets (11/13), there were three pairs of different faces and two pairs of identical faces. The size of the presented faces was 8 cm in height × 6 cm in width (roughly 8° × 6° at a distance of 60 cm).

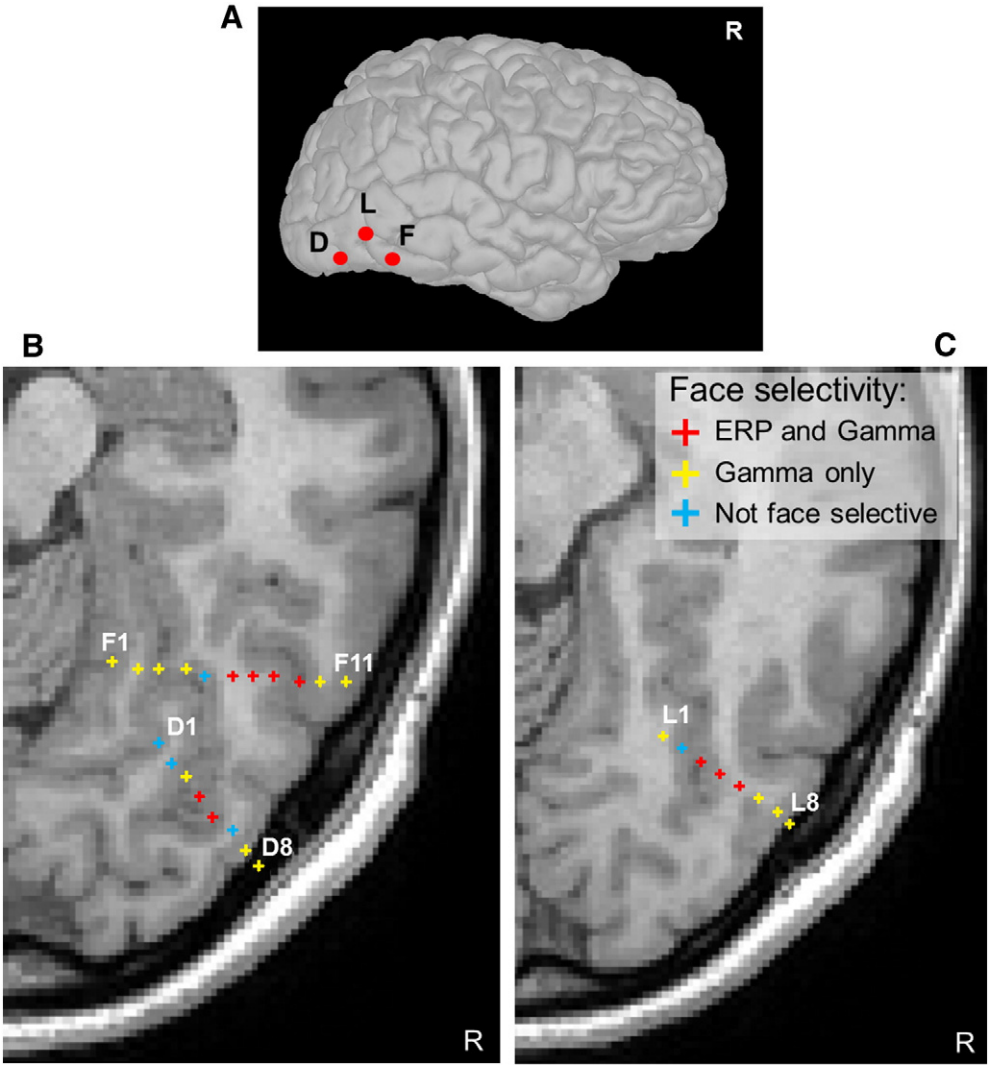

Fig. 1. Anatomical locations of the 3 intracerebral electrodes implanted in the right inferior occipito-temporal cortex (electrodes, D, L and F) and face selectivity results on each contact. **A.** Schematic locations of enter points of the 3 electrodes shown on a segmented brain of patient KV. **B and C.** Schematic locations of the electrodes and all contacts along these electrodes on MRI axial slices. Each contact is represented by a cross. The color of the cross indicates face selectivity responses recorded on each contact. Only the most medial and the most lateral contacts of each electrode are named. Electrode L is located slightly above electrodes F and D. Contact D8 is the most lateral contact of electrode D and was not located inside the brain but sitting on the surface of the lateral occipital cortex.

Procedure

Bipolar electrical intracerebral stimulations were applied between two contiguous contacts along a common electrode (50 Hz over 5 s at intensities ranging from 1 to 2 mA; Jonas et al., 2012). During the recognition task, the patient was shown with sets of 5 colored photographs of a same category (famous faces, famous scenes or objects that she correctly recognized before the stimulation procedure) presented one by one. The patient had to name each photograph in turn. For each set, the stimulation was triggered randomly during the presentation of one of the 5 photographs (1 s before the presentation). During the individual discrimination task, each face pair was presented one by one, with 5 pairs presented consecutively. Stimulations were triggered randomly during the presentation of only one pair of each set, beginning 1 s before the onset of that pair (Fig. 2). Within a set (i.e., 5 pairs presented consecutively), each pair of faces was presented for 2000 ms, with an interstimulus interval varying randomly between 4100 ms and 4500 ms (black screen of 300 ms followed by a central fixation cross randomized between 3800 ms and 4200 ms). One face was located in the center of the screen and the other face on the right side, so that the patient's first fixation fell onto a face rather than between the two faces. For each pair of faces the patient was instructed to decide whether the faces were identical or different. A video camera and sound recorder recorded the patient performing the experiment and an experimenter sitting behind the patient in the room also recorded her oral response. Electrical stimulation was applied only on a pair of different faces because we hypothesized that the effect of stimulation would disrupt the perception of the information that differs between different faces rather than making identical faces look different. The patient was not aware of the stimulation onset, stimulation offset, or the localization of the stimulation site. The patient was seated in a chair in her hospital room, facing the computer screen placed 60 cm away from her face. Visual stimuli were presented on a computer screen using E-Prime v2.0. For two sets of 5 pairs, the patient was also asked to perform the matching task without any electrical stimulation.

Face-selectivity: fMRI face localizer

The comprehensive method used for this fMRI localizer study was previously reported in detail (Jonas et al., 2012) and will only be briefly summarized here. Nine epochs [duration 14.4 s; 4 repetition time (TR)] of two conditions (faces and objects) were presented alternatively during fMRI recording. In each epoch, 18 stimuli were presented, each

Table 1
Number of electrical stimulations performed at each stimulation site and type of stimulus sets used. For each stimulation, the patient was presented with a set of 5 successive images of the same category, 4 images without stimulation and 1 image during stimulation. In brackets are indicated the corresponding number of stimulations which evoked difficulties in recognizing visual objects for the recognition task and incorrect responses for the individual face discrimination task. Each stimulation location is defined by the name of the 2 contiguous contacts involved in the stimulation, by its anatomical location, and if possible by its functional location (OTS: occipito-temporal sulcus; CoS: collateral sulcus, rOFA: right occipital face area).

	Number of sets			
	Recognition task			Individual face discrimination task
Locations of stimulations	Famous faces	Objects	Famous scenes	Morphs of unknown faces
D2–D3 Right CoS	1 (0)			
D3–D4 Right CoS	1 (0)			
D4–D5 Right CoS, within rOFA	1 (0)	1 (0)		
D5–D6 Right CoS, within rOFA	2 (2)		1 (0)	6 (6)
D6–D7 Right lateral occipital cortex, within rOFA	2 (2)		1 (0)	1 (0)
L1–L2 Right CoS		1 (0)		
L2–L3 Right CoS	1 (0)			
L4–L5 Right CoS	2 (0)			
L6–L7 Right lateral occipital cortex	5 (3)		2 (0)	4 (2)
L7–L8 Right lateral occipital cortex	1 (0)			
F1–F2 Right lingual gyrus	1 (0)			
F2–F3 Right CoS		1 (0)		
F3–F4 Right CoS	2 (0)			
F4–F5 Right CoS	1 (0)	1 (0)		
F5–F6 Right CoS	1 (0)			
F6–F7 White matter	1 (0)			
F7–F8 Right OTS	1 (0)			
F9–F10 Right OTS		1 (0)		

stimulus being presented for 500 ms followed by a fixation cross (300 ms). The patient was required to perform a one-back task (detection of immediate repetition of an item) by pressing a response key.

Imaging was performed on a 3 T wide-bore scanner (Verio, Siemens, Engerlingen, Germany), using 32-channel head coil. Both a high resolution T1-weighted anatomical image (100 contiguous sagittal slices, echo time (TE) = 2.2 ms; TR = 1900 ms; flip angle = 9°; field of view (FOV) = 260 cm; pixel size = 1 × 1 mm; slice thickness = 1 mm) and a gradient echo, echo-planar sequence (TE = 27 ms; TR = 3600 ms; FOV = 244 cm; pixel size = 2 × 2 mm; slice thickness = 2.5 mm; acquisition time (TA) = 9 min 48 s) were acquired. Data processing (linear trend removal, slice scan time correction, high-pass filtering of >3-cycles/run, and head motion correction) and statistical analysis were performed using Brain Voyager QX. The fMRI data were spatially smoothed (full width at half maximum of 4 mm, all three directions), and coregistered with the 3D T1-weighted scans. Functional data were analyzed using a General Linear Model with two predictors (faces, objects). Predictors' time courses were computed on the basis of a linear model of the relation between neural activity and hemodynamic response, assuming a rectangular neural response during phases of visual stimulation. A conservative statistical threshold (Bonferroni-corrected, $p < 0.05$) was used to define face-selective areas (faces–objects), corresponding to t-values above 5.095. The statistical map was then interpolated on a cubic grid of resolution 0.5 mm using trilinear interpolation for the coregistration with the computed tomography (CT)-scan using a custom-based application.

Face-selectivity: intracerebral ERP and gamma activity

Face-selectivity of the electrode contacts was determined by comparing the response to faces, objects, and phase-scrambled stimuli, exactly as in a scalp event-related potential (ERP) study (Rossion and Caharel, 2011). Color photographs of full-front segmented faces and cars were used, in addition to their phase-scrambled versions. All stimuli subtended approximately 6.52° × 7.44° of visual angle at a distance of 60 cm.

Procedure

The patient was seated in a chair in her hospital room facing a computer screen placed 60 cm from her face. In each trial, a fixation point was displayed at the center of the screen for 100 ms, followed approximately 300 ms (200–400 ms) later by the test stimulus for 300 ms. An inter-trial interval of about 1700 ms (1600–1800 ms) was used. The patient was asked to judge whether the presented stimulus was an object (face or car) or a "texture" (scrambled versions), by pressing one of two response keys with her right hand. The patient performed two blocks of 86 trials (172 trials in total with 43 trials per condition, randomized).

ERP analysis

Stereo-electroencephalographic ERPs were analyzed using *Letswave* (Mouraux and Ianetti, 2008) and MATLAB v7.9 (The Mathworks, Inc.). The analysis consisted of: (i) bandpass filtering (0.1–48 Hz, 24 dB/oct), (ii) epoching (−200 ms to +1000 ms relative to stimulus onset), (iii) baseline correction (−200 ms to 0 ms), and (iv) averaging of epochs per condition. Conditions were compared by pairs on each time-point and differences were considered to be significant if they

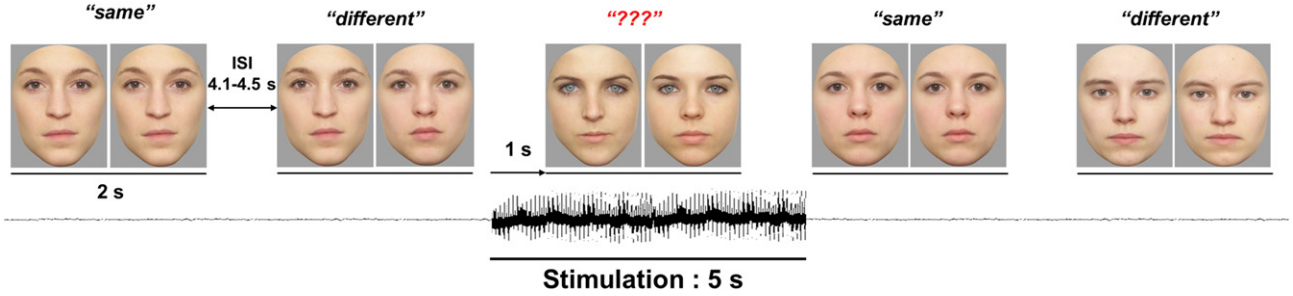

Fig. 2. Schematic representation of the individual face discrimination task during electrical intracerebral stimulation in the right inferior occipital gyrus. The electrical stimulation was performed randomly on one of five consecutive trials, always on a pair showing two different faces.

reached $p < 0.05$ for 10 consecutive time-points (10 ms). To compare ERPs that were shifted in time, a paired t-test ($p < 0.05$) was done on maximum amplitudes of single trials.

Gamma-ERSP analysis

Event-related spectral perturbations (ERSP) were computed using *Letswave* and MATLAB v7.9. Variation in signal amplitude as a function of time and frequency was estimated by a Morlet wavelet transform on each single trial from frequencies of 2 to 200 Hz in 120 steps (non-filtered data). The number of cycles (i.e., central frequency) of the wavelet was adapted as a function of frequency from 2 cycles at the lowest frequency to 10 cycles at the highest frequency. The wavelet transform was computed on each time-sample and the resulting amplitude envelope was downsampled by a factor of 10 (i.e., to a 102.4 Hz sampling rate). Amplitude was normalized across time and frequency to obtain the percentage of power change generated by the stimulus onset relative to the mean power in a pre-stimulus time-window (−600 ms to −300 ms relative to stimulus onset).

The amplitude difference between the gamma-band signal (30–100 Hz) generated by face and car stimuli was statistically assessed by running a permutation test at each time-sample of the response between −100 and 800 ms relative to stimulus onset. This frequency range for gamma was selected on the basis of the prior intracerebral studies (Engell and McCarthy, 2011). In short, the single-trial amplitudes obtained in the two conditions at a given time-point were randomly assigned in two bins, the number of trials in each bin being equal to the number of trials in each original condition. Next, the difference between the means of the two random bins was computed and stored. Because permutation shuffles the assignment of the conditions, the difference between the means of the two new bins reflects the difference between conditions under the null hypothesis. This process was performed 10,000 times to generate a distribution of differences at a $p < 0.001$ (two-tailed) and values that reached this threshold for at least 3 consecutive time-samples (i.e., 30 ms) were considered as significant.

Repetition suppression effects for individual faces measured with fast periodic visual stimulation

The main aspects of the procedure for this experiment have been previously described in two different studies comparing the presentation of trains of different faces to identical faces at a fixed frequency rate (Rossion and Boremanse, 2011; Rossion et al., 2012b). From a methodological perspective, this fast periodic visual stimulation (FPVS) approach – which leads to so-called steady-state visual evoked potentials (SSVEPs, Regan, 1966, 1989) – has multiple advantages: objectivity of definition and quantification of the response of interest, high signal-to-noise ratio (SNR), short time duration of the experiment, and recording of the response of interest during a simple incidental task (see Rossion, 2014 for a review), making it a tool of choice for the study of patients implanted with intracerebral electrodes. Here faces were presented at a 6 Hz rate because this frequency rate provides the largest repetition suppression effect on the right occipito-temporal scalp (Alonso-Prieto et al., 2013).

Stimuli

Eighteen full-front color pictures of unfamiliar faces (7° × 10° of visual angle for the base face size) equalized in luminance online by the stimulation software were used.

Procedure

In each condition, a face stimulus appeared and disappeared (sinusoidal contrast modulation) on the screen, at a stimulation rate of 6 faces/s (one face every 166.66 ms; Fig. 3; see Movie 1 for an example of a 6 Hz periodic stimulation of different faces). A trigger was sent to the parallel port of the EEG recording computer at each minimal level of visual stimulation (gray background) using a photodiode placed on the left upper corner of a laptop monitor. In the *identical face* condition, a randomly selected face picture was presented repeatedly during the whole stimulation duration (70 s). In the *different face* condition, the same face identity was presented for the first 15 s, and from then on the face identity changed with every cycle until the end of the sequence (Rossion et al., 2012b). In that condition, 18 individual faces of the same sex were used and presented in random order. The same face identity never appeared twice in a row, so that the face identity change rate was always 6 Hz. To minimize repetition suppression effects due to low-level cues, the face stimulus changed substantially in size with each presentation, i.e., at a rate of 6 Hz, in all conditions (random face size between 82% and 118% of base face size).

The patient performed 8 sequences of 70 s in total: 2 (identity change: identical or different faces) × 2 (orientation: upright/inverted) × 2 repetitions (sex: male or female faces). The whole experiment lasted about 10 min, including the pauses between the runs. The order of conditions was randomized. During each 70 s run, the patient was instructed to fixate on a small black cross located centrally on the face, slightly below the bridge of the nose. The fixation cross changed color (black to red) briefly (200 ms) 6 to 8 times during each run and the patient was instructed to report the color changes by pressing a response key.

SEEG analysis for periodic stimulation

All analyses were performed using Letswave (http://nocions.webnode.com/letswave/, Mouraux and Ianetti, 2008) and MATLAB v7.8 (The Mathworks, Inc.), according to the procedure described in Rossion et al. (2012b). Fifty seconds of stimulation (300 cycles at 6.0 Hz) from the 18th second onset point (i.e., 18 s onset to 67 s offset) were considered for analysis. Discrete Fourier Transform (DFT) was applied to the individual windows, and SEEG amplitude extracted at a high spectral resolution of 1/50 = 0.02 Hz. Frequency spectra of the two trials of each condition were averaged. Signal-to-noise ratio (SNR) was computed at each channel for all frequency bins between 0 and 100 Hz as the ratio of the amplitude at each frequency to the average amplitude of the 20 neighboring bins (e.g., Rossion et al., 2012b). Significant responses above noise level were defined by computing a Z-score using the mean and standard deviation of the 20 neighboring bins of the frequency of interest. Comparison between conditions was made separately for each orientation by computing Z-scores on the subtracted SEEG spectra (*different faces* − *identical faces*). A complementary analysis was performed by segmenting the SEEG windows in 13 pieces of 4 s (17 s to 69 s), which were Fourier Transformed (resolution 0.25 Hz). A paired t-test was then performed between the two conditions using 26 trials by condition.

Results

Functional location of intracerebral contacts

Contacts D5, D6 and D7 were located within a functionally face-selective area in the right inferior occipital gyrus (right OFA; Fig. 4). Lateral contacts of electrode L (L6 and L7) were adjacent to the right OFA. Contacts D5 and D7 were found face-selective in ERP and/or in gamma-ERSP. On contact D5, a P170 component and the gamma-ERSP were much larger for faces than for cars (normal pictures only, Fig. 5). Contact D7 was only face-selective in gamma-ERSP. The adjacent D6 was not face-selective (but located in the white matter, see Fig. 1).

Twenty other contacts in the right occipito-temporal cortex were also found to be face-selective in ERP and/or in gamma-ERSP. Eight contacts were found face-selective in both ERP and gamma-ERSP (D4, L3, L4, L5, F6, F7, F8, F9). The remaining 12 contacts (D3, D8, L1, L6, L7, L8, F1, F2, F3, F4, F10, F11) were only found face selective in gamma-ERSP. This is in line with a previously reported co-localization on the occipito-temporal cortical surface of electrode sites showing both ERP and gamma-ERSP face-selective responses and sites showing only

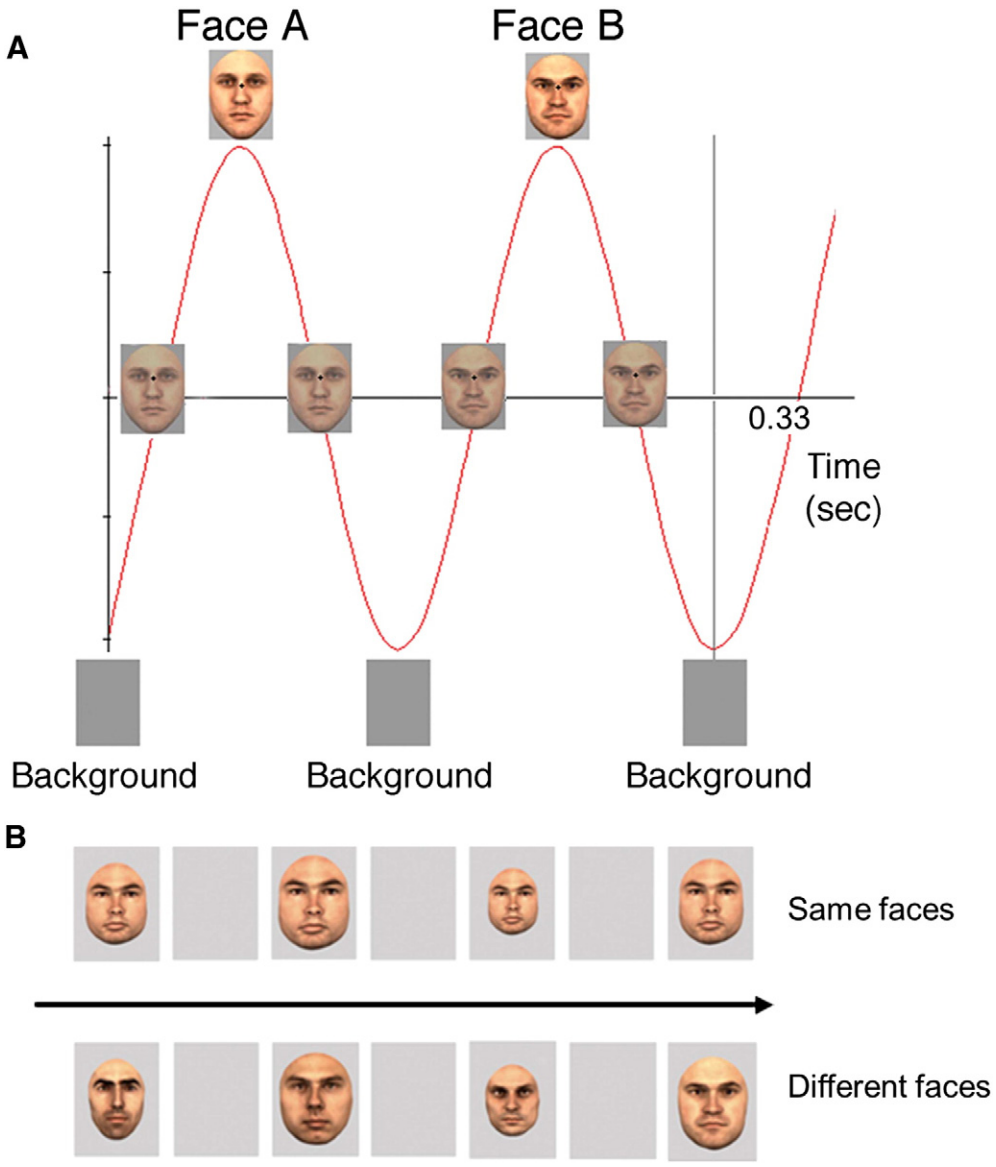

Fig. 3. A. Visual stimulation to measure an electrophysiological index of individual face discrimination. Full-front pictures of faces were presented at a periodic rate of 6 cycles/s (6 Hz, one face every 166 ms, here two cycles presented), following sinusoidal contrast stimulation (Rossion and Boremanse, 2011; see Movie 1). The beginning of the 70-s stimulation (420 cycles in total, here 2 cycles represented) was always the (gray) background. The lower contrast face stimulus in the midline, between the background and the full face stimulus, represents an intermediary stage of stimulation at the onset of the face stimulus. **B**. The two main conditions of the study, in which either the same face was repeated throughout the 70-s stimulation sequence (above) or different face identities were presented successively (below). Note that there were large changes of size between each face picture to minimize low-level adaptation effects. A fixation cross was also present on the top of the nose.

gamma-ERSP face-selective responses (Engel and McCarthy, 2011). Fig. 1 shows selectivity results across all intracerebral contacts in MRI axial slices. No amplitude differences were found between responses evoked by scrambled faces and scrambled cars on face-selective contacts in ERP or in gamma-ERSP.

Intracerebral electrical stimulation

Pre-experiment recognition task

Among the 15 sites tested with the recognition task (Table 1), the patient reported difficulties in recognizing famous faces during stimulation of 3 sites, all located in the right inferior occipital gyrus. When stimulating contacts located within the right OFA, the patient reported such difficulties for 4 out of 4 stimulations (D5–D6: 2 stimulations; D6–D7: 2 stimulations). When stimulating contacts adjacent to the right OFA, she also reported such subjective difficulties but with less reproducibility (L6–L7: 3 out of 5 stimulations). The patient reported these difficulties specifically for famous faces presented during the stimulation and never for faces presented without stimulation. These difficulties occurred only after stimulation onset and recovered immediately upon termination of the stimulation. The patient spontaneously reported: "*something disturbs the identification of an entity that is the face*", "*I did not process the face as a whole*", "*my brain had to process the different facial elements simultaneously*", "*my brain had to process several pieces of information simultaneously, the forehead, the chin, the eyes, the nose*". It is important to note that the patient was able to name all the famous faces (without and with stimulation) and she never reported distortions of faces during stimulation; she correctly recognized all the non-face images and she never reported these recognition difficulties when presented objects or visual scenes during stimulations (in total, her

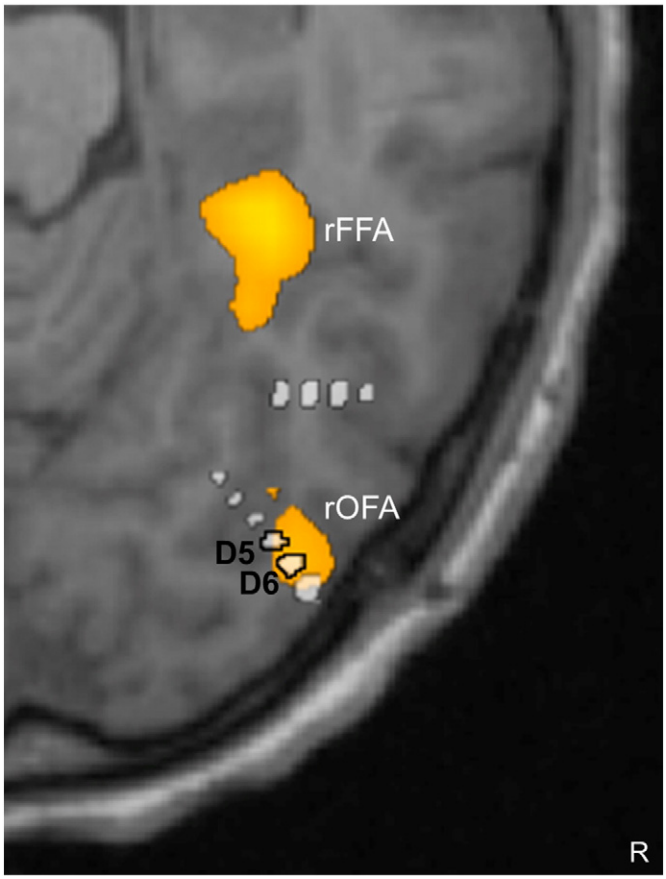

Fig. 4. Functional location of the 2 stimulated contacts D5-D6 inducing reproducible impairment of individual face discrimination (6 times). Contacts D5-D6 are both located within the right OFA. D7 is located also within this region also, just laterally to D6. The figure was obtained by fusing the functional MRI and the post-operative stereotactic CT-scan.

performance at the recognition task was at 100% for face and non-face stimuli, including the stimuli presented during stimulation).

Main experiment: individual face discrimination task

Without stimulation, the patient performed the individual discrimination task with an accuracy rate of 91% (49/54, 4 errors when faces were different). For comparison, a group of 11 age-, sex- and education level-matched controls performed the same task with an accuracy rate of 74%, +/− 8% (91% vs. 74%, $t = 1.858$, $p = 0.093$). In contrast, when stimulating the contacts D5–D6 located in the right OFA, the patient's correct response rate dropped to 0% (0/6) (for functional location of contacts D5–D6 see Fig. 4; for a video of stimulation see Movie 2). Specifically, although the morphed faces were different, the patient always responded "same". The patient stated: "*I saw the faces, I had a feeling of a strong resemblance*", "*for me, there were two identical faces*". She clearly stated that there were no visual distortions of the presented faces and that she was always aware that she was seeing faces: "*the faces are not distorted*", "*there was no deformation*", "*I knew it was a face*", "*the outlines are distinct, there is no blurring*", "*there was no disturbed arrangement of the facial elements*". Note that her score of 0/6 should not be compared to chance level but to her performance without stimulation, on the 'different' trials (23/27, 85.2%) ($p = 0.037$, Fisher's exact test). She was also incorrect for 2 out of 4 morphs presented when stimulating contacts L6–L7, adjacent to the right OFA. At contacts D6–D7, she responded correctly during the single stimulation tested (1/1). Stimulations at these sites (D5–D6, D6–D7 and L6–L7) never produced epileptic discharges. When present, afterdischarges were always limited to the immediate vicinity of the stimulated site.

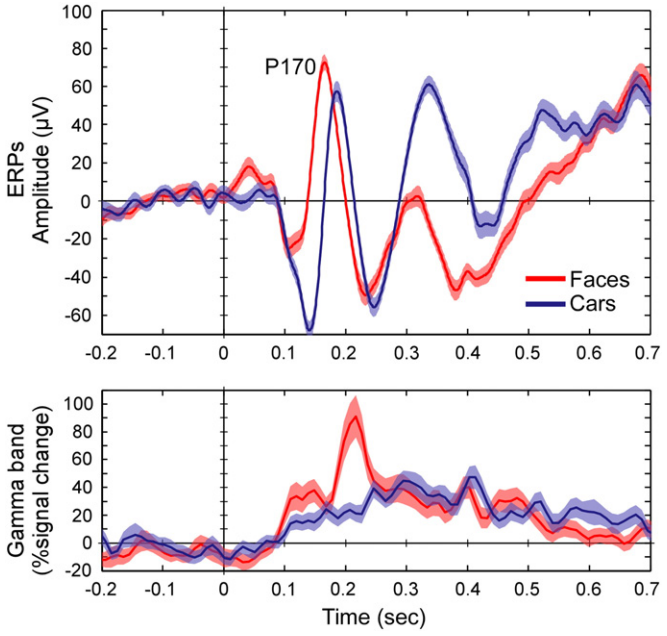

Fig. 5. Face-selectivity in ERP (above) and gamma-ERSP (below) of the stimulated contact D5. On average, the potential evoked by faces (i.e., P170, see Jonas et al., 2012) peaked earlier (167 ms) and had larger amplitude (75.3 μV) than the P170 evoked by cars (186 ms, 55.7 μV). At this contact, the P170 peak could be identified on single trials (after low-pass filtering at 20 Hz). The maximum amplitude was extracted automatically for each single trial between 140 and 200 ms for faces and 160 ms and 223 ms for cars. The P170 at contact D5 was significantly larger for pictures of faces than pictures of cars ($t = 2.021$; $p = 0.036$).

Repetition suppression effects for individual faces

Upright faces

For upright faces, a large response confined to the 6 Hz frequency bin and its harmonics (2 F = 12Hz, 3 F = 18 Hz, etc.) was observed on many contacts of electrodes D and L. Much weaker responses were observed on electrode F. There were large repetition suppression effects on electrode contact D5, whose stimulations evoked impairment in individual face discrimination (i.e., 6 Hz response 2 μV larger for different than same faces, $Z > 2.9$, $p < 0.05$, corrected for multiple tests on all electrodes, Fig. 6A). A t-test performed using the 26 segments of EEG data (see methods) showed the same results ($t_{25} = 31.34$, $p < 0.0001$ at channel D5). Fig. 6C shows the time–frequency analysis for the relevant contact D5. The response is centered on the 6 Hz stimulation band, showing an immediate rebound and then sustained activity when different face identities are presented, as compared to when the exact same face is presented until the end of the sequence. There were also statistically significant repetition suppression effects recorded on other electrode contacts located in the right inferior occipital gyrus and in the right posterior fusiform gyrus (D7, D8, L7, L8, F3, F8, see Fig. 7 for quantification of repetition suppression effects in each contact and Fig. 8 for anatomical locations of repetition suppression results). In Fig. 8, we can see clearly see that the largest effect for upright faces was located in the right inferior occipital cortex, in contacts located within or close to the right OFA (D5, D7, D8, L7, L8).

Inverted faces

Large 6 Hz-specific responses were also observed for inverted faces at the same contacts as for upright faces. Although the differences between conditions were much smaller than in the upright condition, the 6 Hz response was significantly larger for different than for same faces on contacts located in the right inferior occipital gyrus and in the right posterior fusiform gyrus (D7, D8, L7, L8, F6, F8, F9, $Z > 2.9$, $p < 0.05$, corrected for multiple comparisons, see Fig. 7 for quantification of repetition suppression effects on each contact). For contact D5,

the difference was strongly reduced as compared to the upright condition (0.99 μV vs. 2.03 μV; see Fig. 6B) and was not statistically significant in the inverted condition ($p > 0.05$). This reduction of repetition suppression effects for inverted faces is consistent with effects observed on the scalp with the same approach in normal participants (Rossion and Boremanse, 2011; Rossion et al., 2012b). More generally, inversion is a manipulation that preserves low-level features of the face but disrupts individual face discrimination performance (e.g., Yin, 1969; Freire et al., 2000; Rossion, 2008 for a review) and substantially reduces repetition suppression effects in face-selective areas (Gilaie-Dotan et al., 2010; Mazard et al., 2006; Yovel and Kanwisher, 2005). This effect is known to be highly specific to faces (i.e., non-face stimuli elicit either no inversion effect or an inversion effect of smaller magnitude than face stimuli, Yin, 1969; Rossion, 2008). Therefore, the lack of repetition suppression effect for inverted faces on contact D5 reinforces the fact that this contact was located in a face-selective region involved in individual face discrimination.

Upright vs. inverted faces

For all contacts, the repetition suppression effect for upright faces was subtracted out from the effect for inverted faces (i.e. repetition suppression index). This index reflects the specificity of repetition suppression to upright faces on each intracerebral contact. Of all recorded contacts, the largest repetition suppression index was observed on electrode contact D5 (1.24 μV, $Z = 5.24$, $p < 0.0001$; Fig. 7).

Discussion

In the present study, we had a unique opportunity to test the critical role of a face-selective region of the right inferior occipital cortex in individual face discrimination. We were able to test only a single case because the patient had a rare electrode implantation. Moreover, the patient performed extremely well at face recognition and individual face discrimination when she was not stimulated in this brain region. Electrically stimulating contacts within this region (contacts D5-D6) evoked a transient impairment at discriminating two simultaneously presented photographs of different faces. By means of fast periodic visual stimulation with unfamiliar faces, we found on the stimulated contact D5 the most specific face identity repetition suppression effects of all recorded contacts in the patient's brain. Altogether, these data provide converging evidence for a causal role of the right face-selective inferior occipital cortex in individual face discrimination.

The right OFA is critical for individual face discrimination behavior

Intracerebral electrical stimulation of a face-selective cortical area in a unique patient impaired individual discrimination of unfamiliar faces. This observation goes beyond our previous report of impairment in recognizing famous faces during a previous implantation in the same region (Jonas et al., 2012) and other electrical stimulation studies reporting impairment in face vs. no face categorization (Chong et al., 2013, see also Afraz et al., 2006 for modulation of face categorization by electrical stimulation of the monkey infero-temporal cortex), impairment in face naming (Allison et al., 1994; Puce et al., 1999) or distortions of the physician's face following electrical stimulation of other face-selective regions (Parvizi et al., 2012; Vignal et al., 2000). More related to our observations, Mundel et al. (2003) reported an epileptic patient who stated that "all faces look the same" following electrical brain stimulation of the right fusiform gyrus, suggesting impairment in individual face discrimination. However, the patient reported the same feeling during epileptic seizures, and individual face discrimination was not tested experimentally during electrical stimulation. Most importantly, relevant electrical stimulations were performed over a undefined brain lesion in the right fusiform gyrus.

Here, to our knowledge, we report the first case in which individual face discrimination was experimentally tested during electrical stimulation of the human brain. Indeed, here we were able to design a psychophysical task of matching similarly looking faces that specifically tested individual face discrimination. Moreover, since the faces were unfamiliar and were presented simultaneously on the screen, there were no memory processes involved during the individual face discrimination task. Hence, these findings indicate that the area targeted by the intracerebral stimulation is critical for the *perception* of the individuality of the face, independently of long-term memory representations.

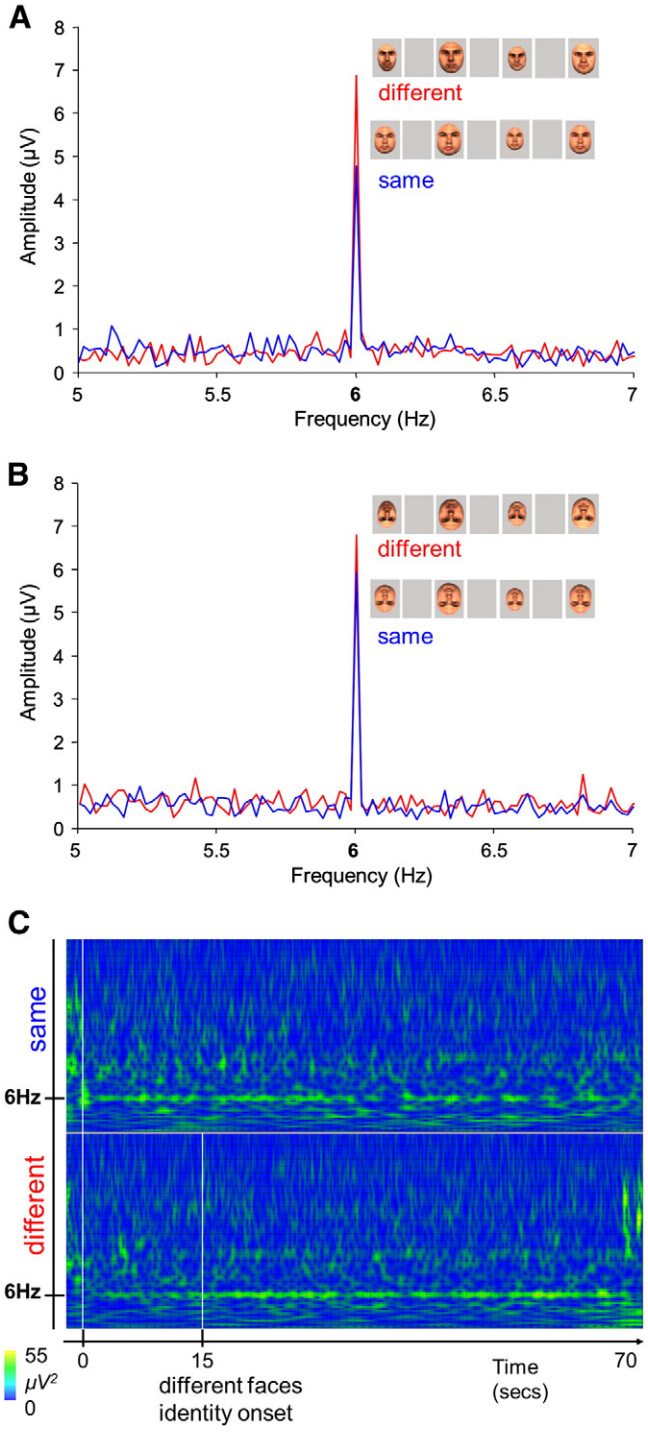

Fig. 6. Repetition suppression effect for individual faces on intracerebral contact D5 with fast periodic visual stimulation. **A.** For upright faces in the frequency domain. **B.** For inverted faces in the frequency domain. **C.** For upright faces in the time domain: time-frequency analysis (Morlet wavelet) for the relevant contact D5 between −1 and 70 s and between 0 and 30 Hz for same and different upright faces.

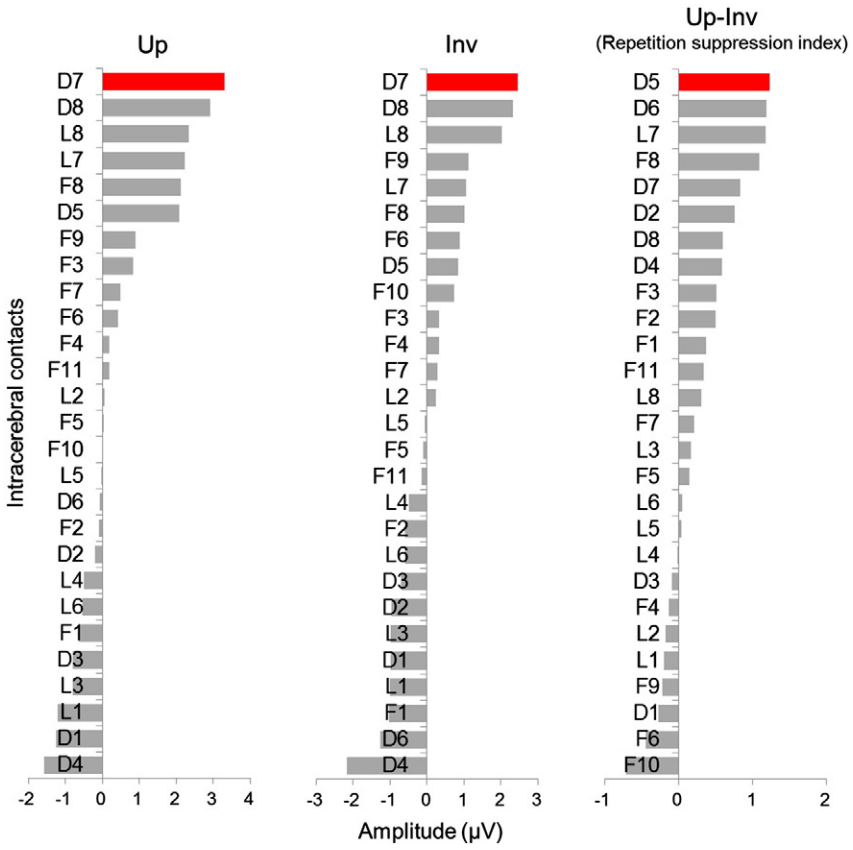

Fig. 7. Graphical representation of individual face repetition suppression effects obtained on each intracerebral contact (upright condition, inverted condition and repetition suppression index that is upright condition minus inverted condition). Of all contacts, the largest difference when comparing the magnitude of the effect between upright and inverted faces was observed on contact D5. It is important to note that there was also a large repetition suppression index on contact D6, but essentially related to a larger response for identical than for different faces in the inverted condition. Therefore, the high repetition suppression index found on D6 does not reflect a high sensitivity to individual faces, which is consistent with the absence of face-selective responses and repetition suppression effect for upright faces recorded on this contact and its anatomical location in the white matter.

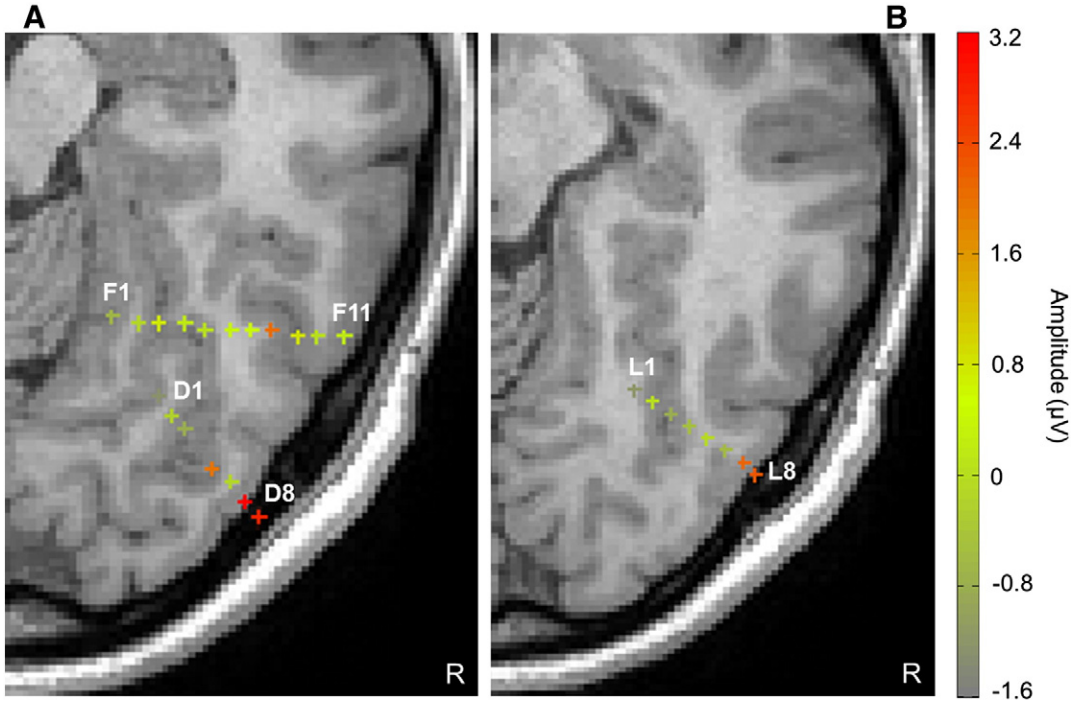

Fig. 8. Anatomical location of individual face repetition suppression effects for the upright condition on MRI axial slices. **A.** Electrodes D and F. **B.** Electrode L. Each contact is represented by a cross. The color of the cross indicates the magnitude of repetition suppression in the upright condition. Only the most medial and the most lateral contacts of each electrode are named. Electrode L is located slightly above electrodes F and D. Note that the largest repetition suppression is located in the lateral section of the right inferior occipital cortex. Contact D8 is the most lateral contact of electrode D and was not located inside the brain but sitting on the surface of the lateral occipital cortex.

It is very unlikely that other factors were involved in the impairment in individual face discrimination reported here: (i) low-level process: the patient clearly stated that there were no distortions of the face stimuli and the relevant electrical stimulations were done within a high-level visual area (i.e., OFA); (ii) habituation or simulation: the patient was not informed about the exact time and duration of electrical stimulation, which was performed randomly during one out of five consecutive individual face discrimination trials; (iii) neuropsychological deficit in face perception: without electrical stimulation, the patient's performance was similar to normal controls, and her performance at an extensive battery of neuropsychological tests of face perception indicates that she has no impairment at individualizing faces (Jonas et al., 2012). Hence, her failure to discriminate the individual faces in six out of six trials during electrical stimulation (a relatively high number of stimulations at the same location in a clinical setting) cannot be attributed to chance. Rather, the effect of focal electrical stimulation appears to disrupt the processing of visual information that is necessary to discriminate individual faces.

The relevant stimulation producing this transient inability in individual face discrimination was located in a face-selective cortical region, as determined both by electrophysiological (ERP, gamma synchronization) and hemodynamic responses (fMRI). This area corresponds to the most posterior face-selective area of the cortical face network, the so-called right OFA. Therefore, the effect of focal electrical stimulation provides original evidence for a causal link between a well-defined face-selective region (i.e., the right OFA) and behavioral individual face discrimination.

Although due to the constraints of the clinical setting we were not able to test stimuli other than faces in the individual discrimination task, the functional location of the stimulation (i.e., a cortical region identified as face-selective) and the much larger repetition suppression effects to upright faces as compared to inverted faces recorded at the stimulation site suggest that the impairment in individual face discrimination is limited to the category of faces. Moreover, the patient was also tested with a recognition task of face and non-face stimuli at 15 different anatomical sites and she reported recognition difficulties only for faces. These face recognition difficulties were observed specifically during stimulation of contacts located within or adjacent to the right OFA (D5, D6, D7, L6, L7), thus reinforcing the view that stimulation of this region impairs face-specific processes.

This observation of a critical role of the face-selective right occipito-temporal cortex in individual face discrimination is in agreement with lesion studies, the right occipital cortex being one of the most consistent sites of brain damage causing prosopagnosia (Bouvier and Engel, 2006). Interestingly, patients with prosopagnosia following lesions to the right inferior occipital cortex are impaired at individual face discrimination (e.g., Busigny et al., 2010b; Rossion et al., 2003) and may be impaired for faces only (Busigny et al., 2010a). Moreover, applying TMS on the scalp above the right OFA may specifically impair face discrimination in a delayed matching task (Pitcher et al., 2007; Pitcher et al., 2009; Solomon-Harris et al., 2013). However, an impairment of individual discrimination of faces with TMS is not always found (e.g. Pitcher et al., 2008) and this effect remains relatively small in magnitude, whether it is expressed in terms of a slowing down of the response or a small drop of accuracy rates. Here, during intracerebral stimulation of the right OFA, our patient was completely unable to discriminate individual faces. Moreover, while the localizing value of TMS is limited, the Stereo-EEG approach used here provides electrical stimulation contacts that are embedded into brain tissue, with the low voltage-electrical currents, causing local disruptive effects.

The functional value of repetition suppression effects during fast periodic visual stimulation

The effect of stimulation in the right face-selective occipito-temporal cortex is also consistent with fMRI studies showing repetition suppression effects for individual faces in this OFA region (e.g., Andrews and Ewbank, 2004; Davies-Thompson et al., 2009; Ewbank et al., 2013; Gauthier et al., 2000; Gilaie-Dotan and Malach, 2007; Grill-Spector and Malach, 2001; Schiltz et al., 2006). This stimulation result complements these observations by indicating that the right OFA is a critical node among the set of areas showing sensitivity to individual face information. More importantly, our observation shows that the right OFA carries crucial individual face information that is directly related to individual face discrimination behavior.

A recent study has reported electrophysiological face repetition suppression effects at multiple frequency rates (alpha, low and high gamma) for face-selective contacts over the ventral occipito-temporal cortex (Engell and McCarthy, 2014). Here, release from repetition suppression was evidenced intracerebrally by means of a fast periodic visual stimulation paradigm, providing a robust face identity repetition suppression effect at an experimentally defined stimulation frequency (Rossion and Boremanse, 2011; Rossion, 2014 for a review). The electrode contact D5, associated with the transient impairment in individual face discrimination, recorded the largest and most specific repetition suppression effect for individual faces (i.e., the largest difference when comparing the magnitude of the repetition suppression effect between upright and inverted faces among all contacts). This observation – which is consistent with the right occipito-temporal localization of this effect on the scalp (Rossion and Boremanse, 2011; Rossion et al., 2012b) – provides further evidence for the sensitivity of the right OFA to differences between individual faces. Moreover, the unique correlation between the repetition suppression effects and the behavioral impairment at individual face discrimination highlights the functional value of face adaptation/repetition suppression effects, at least when they are measured in electrophysiology with the fast periodic visual stimulation approach.

Given the fact that the most consistent effect of electrical stimulation and the largest repetition suppression effect were found on the same electrode site, our findings even suggest that crucial information for individual face discrimination may be encoded in brain regions showing the largest repetition suppression effect to individual faces. If this is the case, measuring objectively the magnitude of repetition suppression effects (i.e., at an experimentally-defined frequency rate) and with a high signal-to-noise ratio may be particularly important, suggesting that the fast periodic visual stimulation approach used here may be a tool of choice in the future to rapidly identify cortical nodes that are critical for individual face discrimination and other brain functions.

Conclusion

In summary, to our knowledge, this is the first report of transient impairment of individual discrimination of unfamiliar faces following intracerebral electrical stimulation. These findings point to the causal role of the right face-selective inferior occipital cortex in the perception of the individuality of the face, independently of long-term memory representations. These findings also support the functional relevance of repetition suppression/visual adaptation effects obtained with high-level visual stimuli by means of fast periodic visual stimulation, and provide evidence that these effects index the neural representation of the changed stimulus property.

Supplementary data to this article can be found online at http://dx.doi.org/10.1016/j.neuroimage.2014.06.017.

Acknowledgments

The authors would like to thank Meike Ramon and Joan Liu for the morph face stimuli, as well as Talia Retter for her careful comments on a previous version of the paper. Jacques Jonas and Bruno Rossion are supported by the Belgian National Fund for Scientific Research (Fonds de la Recherche Scientifique; FNRS). Corentin Jacques is supported by a postdoctoral grant from the Belgian Federal Government (BELSPO).

This work was supported by a grant from the European Research Council (ERC, facessvep 284025).

References

Afraz, S.R., Kiani, R., Esteky, H., 2006. Microstimulation of inferotemporal cortex influences face categorization. Nature 10 (442), 692–695.

Allison, T., McCarthy, G., Nobre, A., Puce, A., Belger, A., 1994. Human extrastriate visual cortex and the perception of faces, words, numbers, and colors. Cereb. Cortex 4, 544–554.

Alonso-Prieto, E., Belle, G.V., Liu-Shuang, J., Norcia, A.M., Rossion, B., 2013. The 6Hz fundamental stimulation frequency rate for individual face discrimination in the right occipito-temporal cortex. Neuropsychologia 51, 2863–2875.

Andrews, T.J., Ewbank, M.P., 2004. Distinct representations for facial identity and changeable aspects of faces in the human temporal lobe. Neuroimage 23, 905–913.

Barton, J.J., 2008. Structure and function in acquired prosopagnosia: Lessons from a series of 10 patients with brain damage. J. Neuropsychol. 2, 197–225.

Bouvier, S.E., Engel, S.A., 2006. Behavioral deficits and cortical damage loci in cerebral achromatopsia. Cereb. Cortex 16, 183–191.

Busigny, T., Joubert, S., Felician, O., Ceccaldi, M., Rossion, B., 2010a. Holistic perception of the individual face is specific and necessary: Evidence from an extensive case study of acquired prosopagnosia. Neuropsychologia 48, 4057–4092.

Busigny, T., Graf, M., Mayer, E., Rossion, B., 2010b. Acquired prosopagnosia as a face-specific disorder: Ruling out the general visual similarity account. Neuropsychologia 48, 2051–2067.

Calder, A.J., Young, A.W., 2005. Understanding the recognition of facial identity and facial expression. Nat. Rev. Neurosci. 6, 641–651.

Catenoix, H., Mauguière, F., Guénot, M., Ryvlin, P., Bissery, A., Sindou, M., Isnard, J., 2008. SEEG-guided thermocoagulations: A palliative treatment of nonoperable partial epilepsies. Neurology 71, 1719–1726.

Chong, S.C., Jo, S., Park, K.M., Joo, E.Y., Lee, M.J., Hong, S.C., Hong, S.B., 2013. Interaction between the electrical stimulation of a face-selective area and the perception of face stimuli. Neuroimage 77, 70–76.

Davies-Thompson, J., Gouws, A., Andrews, T.J., 2009. An image-dependent representation of familiar and unfamiliar faces in the human ventral stream. Neuropsychologia 47, 1627–1635.

DiCarlo, J.J., Cox, D.D., 2007. Untangling invariant object recognition. Trends Cogn. Sci. 11, 333–341.

Engell, A.D., McCarthy, G., 2011. The relationship of γ oscillations and face-specific ERPs recorded subdurally from occipitotemporal cortex. Cereb. Cortex 21, 1213–1221.

Engell, A.D., McCarthy, G., 2014. Repetition suppression of face-selective evoked and induced EEG recorded from human cortex. Hum. Brain Mapp. http://dx.doi.org/10.1002/hbm.22467.

Ewbank, M.P., Henson, R.N., Rowe, J.B., Stoyanova, R.S., Calder, A.J., 2013. Different neural mechanisms within occipitotemporal cortex underlie repetition suppression across same and different-size faces. Cereb. Cortex 23, 1073–1084.

Freire, A., Lee, K., Symons, L.A., 2000. The face-inversion effect as a deficit in the encoding of configural information: Direct evidence. Perception 29, 159–170.

Gauthier, I., Tarr, M.J., Moylan, J., Skudlarski, P., Gore, J.C., Anderson, A.W., 2000. The fusiform "face area" is part of a network that processes faces at the individual level. J. Cogn. Neurosci. 12, 495–504.

Gilaie-Dotan, S., Malach, R., 2007. Sub-exemplar shape tuning in human face-related areas. Cereb. Cortex 17, 325–338.

Gilaie-Dotan, S., Gelbard-Sagiv, H., Malach, R., 2010. Perceptual shape sensitivity to upright and inverted faces is reflected in neuronal adaptation. Neuroimage 50, 383–395.

Goesaert, E., Op de Beeck, H.P., 2013. Representations of facial identity information in the ventral visual stream investigated with multivoxel pattern analyses. J. Neurosci. 33, 8549–8558.

Grill-Spector, K., Malach, R., 2001. fMR-adaptation: A tool for studying the functional properties of human cortical neurons. Acta Psychol. (Amst.) 107, 293–321.

Grill-Spector, K., Henson, R., Martin, A., 2006. Repetition and the brain: Neural models of stimulus-specific effects. Trends Cogn. Sci. 10, 14–23.

Haxby, J.V., Hoffman, E.A., Gobbini, M.I., 2000. The distributed human neural system for face perception. Trends Cogn. Sci. 4, 223–233.

Jonas, J., Descoins, M., Koessler, L., Colnat-Coulbois, S., Sauvée, M., Guye, M., Vignal, J.P., Vespignani, H., Rossion, B., Maillard, L., 2012. Focal electrical intracerebral stimulation of a face-sensitive area causes transient prosopagnosia. Neuroscience 222, 281–288.

Kriegeskorte, N., Formisano, E., Sorger, B., Goebel, R., 2007. Individual faces elicit distinct response patterns in human anterior temporal cortex. Proc. Natl. Acad. Sci. U. S. A. 18 (104), 20600–20605.

Maillard, L., Koessler, L., Colnat-Coulbois, S., Vignal, J.P., Louis-Dorr, V., Marie, P.Y., Vespignani, H., 2009. Combined SEEG and source localisation study of temporal lobe schizencephaly and polymicrogyria. Clin. Neurophysiol. 120, 1628–1636.

Mazard, A., Schiltz, C., Rossion, B., 2006. Recovery from adaptation to facial identity is larger for upright than inverted faces in the human occipito-temporal cortex. Neuropsychologia 44, 912–922.

Mouraux, A., Lannetti, G.D., 2008. Across-trial averaging of event-related EEG responses and beyond. Magn. Reson. Imaging 26, 1041–1054.

Mundel, T., Milton, J.G., Dimitrov, A., Wilson, H.W., Pelizzari, C., Uftring, S., Torres, I., Erickson, R.K., Spire, J.P., Towle, V.L., 2003. Transient inability to distinguish between faces: Electrophysiologic studies. J. Clin. Neurophysiol. 20, 102–110.

Nestor, A., Plaut, D.C., Behrmann, M., 2011. Unraveling the distributed neural code of facial identity through spatiotemporal pattern analysis. Proc. Natl. Acad. Sci. U. S. A. 108, 9998–10003.

Parvizi, J., Jacques, C., Foster, B.L., Witthoft, N., Rangarajan, V., Weiner, K.S., Grill-Spector, K., 2012. Electrical stimulation of human fusiform face-selective regions distorts face perception. J. Neurosci. 32, 14915–14920.

Pitcher, D., Walsh, V., Yovel, G., Duchaine, B., 2007. TMS evidence for the involvement of the right occipital face area in early face processing. Curr. Biol. 17, 1568–1573.

Pitcher, D., Garrido, L., Walsh, V., Duchaine, B.C., 2008. Transcranial magnetic stimulation disrupts the perception and embodiment of facial expressions. J. Neurosci. 28, 8929–8933.

Pitcher, D., Charles, L., Devlin, J.T., Walsh, V., Duchaine, B., 2009. Triple dissociation of faces, bodies, and objects in extrastriate cortex. Curr. Biol. 19, 319–324.

Puce, A., Allison, T., McCarthy, G., 1999. Electrophysiological studies of human face perception. III: Effects of top-down processing on face-specific potentials. Cereb. Cortex 9, 445–458.

Regan, D., 1966. Some characteristics of average steady-state and transient responses evoked by modulated light. Electroencephalogr. Clin. Neurophysiol. 20, 238–248.

Regan, D., 1989. Human brain electrophysiology: Evoked potentials and evoked magnetic fields in science and medicine. Elsevier, New York.

Rossion, B., 2008. Picture-plane inversion leads to qualitative changes of face perception. Acta Psychol. (Amst.) 128, 274–289.

Rossion, B., 2014. Understanding individual face discrimination by means of fast periodic visual stimulation. Exp. Brain Res. 232, 1599–1621.

Rossion, B., Boremanse, A., 2011. Robust sensitivity to facial identity in the right human occipito-temporal cortex as revealed by steady-state visual-evoked potentials. J. Vis. 11 (2).

Rossion, B., Caharel, S., 2011. ERP evidence for the speed of face categorization in the human brain: Disentangling the contribution of low-level visual cues from face perception. Vis. Res. 51, 1297–1311.

Rossion, B., Caldara, R., Seghier, M., Schuller, A.M., Lazeyras, F., Mayer, E., 2003. A network of occipito-temporal face-sensitive areas besides the right middle fusiform gyrus is necessary for normal face processing. Brain 126, 2381–2395.

Rossion, B., Hanseeuw, B., Dricot, L., 2012a. Defining face perception areas in the human brain: A large-scale factorial fMRI face localizer analysis. Brain Cogn. 79, 138–157.

Rossion, B., Prieto, E.A., Boremanse, A., Kuefner, D., Van Belle, G., 2012b. A steady-state visual evoked potential approach to individual face perception: Effect of inversion, contrast-reversal and temporal dynamics. Neuroimage 63, 1585–1600.

Sack, A.T., Linden, D.E., 2003. Combining transcranial magnetic stimulation and functional imaging in cognitive brain research: Possibilities and limitations. Brain Res. Brain Res. Rev. 43, 41–56.

Schiltz, C., Sorger, B., Caldara, R., Ahmed, F., Mayer, E., Goebel, R., Rossion, B., 2006. Impaired face discrimination in acquired prosopagnosia is associated with abnormal response to individual faces in the right middle fusiform gyrus. Cereb. Cortex 16, 574–586.

Sergent, J., Signoret, J.L., 1992. Varieties of functional deficits in prosopagnosia. Cereb. Cortex 2, 375–388.

Sergent, J., Ohta, S., MacDonald, B., 1992. Functional neuroanatomy of face and object processing. A positron emission tomography study. Brain 115, 15–36.

Solomon-Harris, L.M., Mullin, C.R., Steeves, J.K., 2013. TMS to the "occipital face area" affects recognition but not categorization of faces. Brain Cogn. 83, 245–251.

Talairach, J., Bancaud, J., 1973. Stereotaxic approach to epilepsy: Methodology of anatomo-functional stereotactic investigations. Prog. Neurol. Surg. 5, 297–354.

Vignal, J.P., Chauvel, P., Halgren, E., 2000. Localised face processing by the human prefrontal cortex: Stimulation-evoked hallucinations of faces. Cogn. Neuropsychol. 17, 281–291.

Weiner, K.S., Grill-Spector, K., 2010. Sparsely-distributed organization of face and limb activations in human ventral temporal cortex. Neuroimage 52, 1559–1573.

Xu, X., Biederman, I., 2010. Loci of the release from fMRI adaptation for changes in facial expression, identity, and viewpoint. J. Vis. 10 (14).

Yin, R.K., 1969. Looking at upside-down faces. J. Exp. Psychol. 81, 141–145.

Yovel, G., Kanwisher, N., 2005. The neural basis of the behavioral face-inversion effect. Curr. Biol. 15, 2256–2262.

CORTEX 72 (2015) 140–155

Available online at www.sciencedirect.com

ScienceDirect

Journal homepage: www.elsevier.com/locate/cortex

Special issue: Research report

Beyond the core face-processing network: Intracerebral stimulation of a face-selective area in the right anterior fusiform gyrus elicits transient prosopagnosia

Jacques Jonas [a,b,c], *Bruno Rossion* [c,*], *Hélène Brissart* [a], *Solène Frismand* [a], *Corentin Jacques* [c], *Gabriela Hossu* [d], *Sophie Colnat-Coulbois* [e], *Hervé Vespignani* [a,b], *Jean-Pierre Vignal* [a,b] *and Louis Maillard* [a,b]

[a] *Service de Neurologie, Centre Hospitalier Universitaire de Nancy, Nancy, France*
[b] *UMR 7039, CNRS, Université de Lorraine, Nancy, France*
[c] *Université de Louvain, Louvain-La-Neuve, Belgium*
[d] *CIC-IT, Centre Hospitalier Universitaire de Nancy, Nancy, France*
[e] *Service de Neurochirurgie, Centre Hospitalier Universitaire de Nancy, Nancy, France*

ARTICLE INFO

Article history:
Received 8 November 2014
Reviewed 13 April 2015
Revised 2 May 2015
Accepted 19 May 2015
Published online 4 June 2015

Keywords:
Intracerebral recordings
Electrical brain stimulation
Prosopagnosia
Anterior fusiform gyrus
Fusiform face area

ABSTRACT

According to neuropsychological evidence, a distributed network of regions of the ventral visual pathway – from the lateral occipital cortex to the temporal pole – supports face recognition. However, functional magnetic resonance imaging (fMRI) studies have generally confined ventral face-selective areas to the posterior section of the occipito-temporal cortex, i.e., the inferior occipital gyrus occipital face area (OFA) and the posterior and middle fusiform gyrus fusiform face area (FFA). There is recent evidence that intracranial electrical stimulation of these areas in the right hemisphere elicits face matching and recognition impairments (i.e., prosopagnosia) as well as perceptual face distortions. Here we report a case of transient inability to recognize faces following electrical stimulation of the right anterior fusiform gyrus, in a region located anteriorly to the FFA. There was no perceptual face distortion reported during stimulation. Although no fMRI face-selective responses were found in this region due to a severe signal drop-out as in previous studies, intracerebral face-selective event-related potentials and gamma range electrophysiological responses were found at the critical site of stimulation. These results point to a causal role in face recognition of the right anterior fusiform gyrus and more generally of face-selective areas located beyond the "core" face-processing network in the right ventral temporal cortex. It also illustrates the diagnostic value of intracerebral electrophysiological recordings and stimulation in understanding the neural basis of face recognition and visual recognition in general.

* *Corresponding author*. University of Louvain (UCL), Psychological Sciences Research Institute and Institute of Neuroscience, 10, Place du Cardinal Mercier, 1348 Louvain-La-Neuve, Belgium.
E-mail address: bruno.rossion@uclouvain.be (B. Rossion).
http://dx.doi.org/10.1016/j.cortex.2015.05.026
0010-9452/

1. Introduction

The ability to recognize people by their face is an extremely important function of the human brain, critical for social interactions. The neural basis of this function has been defined by studies of patients with face recognition impairment following brain damage – prosopagnosia – (Bodamer, 1947), which point to a large territory of the ventral occipito-temporal cortex, from the lateral occipital cortex to the temporal pole, with a right hemisphere advantage (Barton, 2008; Busigny et al., 2014a; Hécaen & Angelergues, 1962; Meadows, 1974; Rossion et al., 2003a; Sergent & Signoret, 1992; see Rossion, 2014 for a review). Early neuroimaging studies using positron emission tomography (PET) as well as intracranial recordings by means of subdural grids of electrodes electrocorticography (ECOG) have also shown larger responses to faces than objects (i.e., "face-selective" responses) across the entire ventral occipito-temporal cortex, again with a right hemisphere advantage (Sergent, Ohta, & MacDonald, 1992 for PET; Allison, McCarthy, Nobre, Puce, & Belger, 1994 and Allison, Puce, Spencer, & McCarthy, 1999 for ECOG).

Subsequent studies using functional magnetic resonance imaging (fMRI) have generally confined face-selective areas to the posterior half of the ventral occipito-temporal cortex, namely in the inferior occipital gyrus [occipital face area (OFA), Gauthier et al., 2000] and in the posterior and middle fusiform gyrus [fusiform face area (FFA), Kanwisher, McDermott, & Chun, 1997; Puce, Allison, Gore, & McCarthy, 1995]. Together with a face-selective region in the posterior part of the superior temporal sulcus (pSTS), these areas have been defined as the "core" network for face perception (Atkinson & Adolphs, 2011; Calder & Young, 2005; Haxby, Hoffman, & Gobbini, 2000; Ishai, 2008; Rossion, 2008; Weiner & Grill-Spector, 2010). Moreover, transcranial magnetic stimulation (TMS) applied on the scalp, and intracranial electrical stimulation, have shown that areas of the core network play a causal role in face recognition (Pitcher, Walsh, Yovel, & Duchaine, 2007; Solomon-Harris, Mullin, & Steeves, 2013 for TMS studies of the OFA; Jonas et al., 2012, 2014; Parvizi et al., 2012 for intracranial electrical stimulation studies). Jonas et al. (2012) reported a case of transient prosopagnosia by electrically stimulating the right OFA of an epileptic patient implanted with depth electrodes. Parvizi et al. (2012) reported a distortion of a clinician's face during electrical stimulation of the cortical surface over the right FFA (see also Rangarajan et al., 2014).

Most recently, fMRI studies have also reported ventral face-selective regions anterior to the FFA, up to the temporal pole (e.g., Avidan et al., 2014; Nasr & Tootell, 2012; Rajimehr, Young, & Tootell, 2009; Rossion, Hanseeuw, & Dricot, 2012; Tsao, Moeller, & Freiwald, 2008; for a recent review, see Collins & Olson, 2014). Unfortunately, due to large hemodynamic signal drop-outs caused by magnetic susceptibility artifacts (Axelrod & Yovel, 2013; Ojemann et al., 1997), fMRI studies are limited in their understanding of the function(s) of the anterior ventral temporal face-selective areas, in particular in the anterior part of the fusiform gyrus (e.g., Fig. S7 in Rajimehr et al., 2009; Fig. S7 in Tsao et al., 2008). Moreover, unlike the OFA and pSTS, the function of these ventral regions cannot be disrupted by TMS during face recognition. Hence, aside from the association of lesions in the right anterior temporal lobe with acquired prosopagnosia (e.g., Busigny et al., 2014a) and reduced cortical volume of the anterior part of the fusiform gyrus in low performers at face recognition (i.e., "congenital prosopagnosia", Behrmann, Avidan, Gao, & Black, 2007), the causal role of anterior ventral temporal regions in this function remains largely unknown.

Here we report a novel case of transient prosopagnosia following electrical stimulation of a face-selective region of the right ventral temporal cortex located anteriorly to the FFA. As in previous studies of our group (Jonas et al., 2012, 2014), this epileptic patient (CD) was implanted with depth intracerebral electrodes [stereotactic electroencephalography (SEEG), Talairach & Bancaud, 1973; e.g., Barbeau et al., 2008; Halgren et al., 1994]. While performing electrical stimulation of the patient's right anterior fusiform gyrus (anterior FG), we observed her transient inability to recognize famous face photographs. Intracerebral electrophysiological face-selective responses were recorded at the critical site of stimulation. A subsequent fMRI examination showed that the critical stimulation site was located anteriorly to the right FFA, extending further the causal role of face-selective areas to anterior ventro-temporal regions beyond the core face-processing network.

2. Materials and methods

2.1. Case description

The patient was a 44-year-old woman (CD) who had medically intractable left temporal epilepsy related to a left temporal lobe schizencephaly. She never complained of face recognition difficulties in everyday life or during and after epileptic seizures.

She was right-handed as attested by the Edinburgh Handedness Inventory (Oldfield, 1971) and also by intracerebral electrical stimulations performed during the SEEG exploration (stimulations in the left FG elicited impairments in naming and reading, showing unambiguously the left hemispheric language dominance). The SEEG exploration took place in June 2011. SEEG exploration delineated the seizure onset zone in the left ventral temporal cortex. CD was contraindicated to conventional resection and she did not have surgery eventually. The face processing behavioral tests and the neuroimaging recordings took place in April and May 2014. CD gave written consent to participate in the experimental procedures, which were part of the clinical investigation.

2.2. Neuropsychological assessment

2.2.1. General assessment

Patient CD showed a general intelligence in the lower range (full-scale IQ of 70) with verbal-performance IQ discrepancy (performance score > verbal score). She was impaired in object naming and verbal fluency. This impairment in language functions is consistent with the localization of the brain lesion and the epileptic focus in the left temporal lobe. Importantly, CD showed normal basic visual perception attested by the

Visual Object and Space Perception Battery (VOSP). The results of this neuropsychological assessment are summarized in Table 1.

2.2.2. *Face perception and memory*

We conducted a series of stringent behavioral tests to assess CD's face/object perception and memory. Six control participants (age-, sex- and education level-matched controls, not matched in IQ) performed the same tests. To compare the results of CD to the control participants, we used the modified *t*-test of Crawford–Howell for single-case studies (Crawford & Howell, 1998) with a p value of <.05 considered as statistically significant. These tests included: (1) individual discrimination of unfamiliar categories: individual face matching (Benton Face Recognition Test: BFRT, Benton, Sivan, Hamsher, Varney, & Spreen, 1983) and individual face and car matching at upright and inverted orientations (experiment 22 in Busigny, Joubert, Felician, Ceccaldi, & Rossion, 2010); (2) visual memory: encoding followed by an old/new forced choice decision with faces (experiment 3 in Busigny et al., 2010) and on the same task with bird pictures, using the same parameters as for faces; (3) a famous face recognition test for French celebrities (cropped faces, CELEB test, Busigny et al., 2014b).

The results of these tests are shown in Table 2. Patient CD was in the normal range at individualizing unfamiliar faces. She was in the normal range at the BFRT and at matching upright and inverted faces. Her decrease of performance for inverted compared to upright faces (accuracy: 86.6% *vs* 72.2%; reaction times: 1553 msec *vs* 1869 msec) was also in the normal range ($t = .62$, $p = .56$ and $t = .99$, $p = .37$ respectively, revised standardized difference test, Crawford & Garthwaite, 2005). However, she scored below normal controls at the old/new test for faces and non-face objects (birds), although her performance at memorizing faces was well above chance level (73.3%). She was also below normal controls at recognizing famous faces [CELEB test, Face Recognition Index (FRI)] and at naming famous faces [CELEB test, Name Access Index (NAI)].

In summary, patient CD had no impairment at perceiving faces but she was below normal controls at memorizing unfamiliar faces, and at recognizing and naming famous faces. Such difficulties are often found in patients with temporal lobe epilepsy (Glosser, Salvucci, & Chiaravalloti, 2003). Nevertheless, we acknowledge that this is a factor to take into account for the experimentation (i.e., the identity of the famous faces selected) and the interpretation of the behavioral tests with faces performed during intracerebral stimulation (see Discussion section).

Table 1 – General neuropsychological assessment of patient CD.

	Score
IQ	
WAIS-R	
Verbal IQ	64
Performance IQ	80
Full-scale IQ	70
Memory	
Immediate memory/Working memory	
Forward span	5
Backward span	4
Grober & Buschke 16 items	
Encoding	16/16
Immediate free recall	9-9-12/16
Immediate total recall	15-16-16/16
Recognition	16
Delayed free recall	11/16
Delayed total recall	16/16
Basic visual perception	
Visual Object and Space Perception Battery (VOSP)	
Screening test	19/20
Incomplete letters (test 1)	20/20
Silhouettes (test 2)	20/30
Dot counting (test 5)	10/10
Position discrimination (test 6)	17/20
Number location (test 7)	10/10
Language	
Verbal fluency in 2 min	
Semantic (letter R)	20
Phonological ("fruit" category)	12[a]
Naming (DO 80)	65/80[a]
Reading words	20/20

[a] Indicates impaired scores.

2.3. *Stereotactic placement of intracerebral electrodes*

Intra-cerebral electrodes (Dixi Medical, Besançon, France) were stereotactically implanted in the patient's brain in order to delineate the seizure onset zone (Talairach & Bancaud, 1973). The sites of electrode implantation were determined based on non-invasive data collected during an earlier phase of the investigation. Each intracerebral electrode consists in a cylinder of .8 mm diameter and contains 5–18 contiguous contacts of 2 mm in length separated by 1.5 mm from edge to edge. A few days before surgery, a non-stereotactic T1 weighted MRI with gadolinium was carried out and imported into a computer-assisted software (iPlan Stereotaxy, Brainlab, Germany). Each electrode trajectory was then determined according to the investigation planning with careful avoidance of vascular structures. The day of surgery, after induction of general anesthesia, the stereotactic frame (Leksell G-frame, Elekta, Sweden) was positioned on the patient's head. A stereotactic CT-scan was then carried out and fused to the pre-operative non-stereotactic MRI. Stereotactic coordinates were then calculated for each trajectory. A post-operative non-stereotactic CT-scan was carried out and fused with a T1-weighted MRI to determine the exact position of each electrode.

Nine electrodes were placed in the left hemisphere targeting the occipito-temporal cortex. Two electrodes were also placed in the right hemisphere, targeting the right ventral occipito-temporal cortex. Electrode F (containing 12 contacts) explored the anterior FG and the adjacent occipito-temporal sulcus (OTS). The border between the anterior and posterior FG was defined as the most posterior temporal lobe slice where the hippocampus was visible (e.g., Onitsuka et al., 2003). Electrode O (containing 12 contacts) explored the ventral occipital cortex (inferior bank of the calcarine sulcus and inferior occipital gyrus).

Table 2 – Performances of CD and 6 control participants in neuropsychological tests on face/object perception and memory (Acc: accuracy; RT: reaction times in ms; BFRT: Benton Face Recognition Test; FRI: Face Recognition Index; NAI: Name Access Index).

		Patient CD	Normal controls ($n = 6$)	t-test (Crawford–Howell)
BFRT	Acc	40/54	45.4/54 ± 2.7	$t = 1.808$, $p = .065$
	RT	445[a]	254 ± 77.6	**$t = 2.278$, $p = .036$**
Face matching (upright and inverted)	Acc upright	86.1%	93.3% ± 5	$t = 1.326$, $p = .121$
	Acc inverted	72.2%	80% ± 10	$t = .716$, $p = .253$
	RT upright	1553	1292 ± 229	$t = 1.055$, $p = .17$
	RT inverted	1869	1496 ± 469	$t = .738$, $p = .247$
Car matching (upright and inverted)	Acc upright	94.4%	95% ± 3.6	$t = .144$, $p = .446$
	Acc inverted	86.1%[a]	95.6% ± 3.7	**$t = 2.365$, $p = .032$**
	RT upright	1528[a]	1086 ± 185	**$t = 2.212$, $p = .039$**
	RT inverted	1752[a]	1134 ± 234	**$t = 2.261$, $p = .037$**
Old/New face	Acc	73.3%[a]	90% ± 4.7	**$t = 3.276$, $p = .011$**
	RT	1624	1763 ± 513	$t = .250$, $p = .406$
Old/New bird	Acc	50%[a]	87.8% ± 8.4	**$t = 4.183$, $p = .004$**
	RT	2168	1742 ± 557	$t = .709$, $p = .255$
CELEB test	FRI	63.5[a]	90.8 ± 8.7	**$t = 2.909$, $p = .017$**
	NAI	53.1[a]	87.3 ± 10.4	**$t = 3.053$, $p = .014$**

[a] Indicates impaired scores compared to matched normal controls ($p < .05$).

2.4. *Intracerebral electrical stimulations*

Intracerebral electrical stimulations targeting the right ventral occipito-temporal cortex (contacts of electrodes F and O) were carried out while the patient performed famous face and object recognition tasks and a face versus object categorization task (Table 3). These stimulations were applied between two contiguous contacts along one common electrode and performed at 50 Hz during 5 sec or 10 sec at intensities ranging from .8 to 1.2 mA (usual stimulation settings in SEEG). CD was not aware of the stimulation onset and termination, the stimulation site and the nature of the impairments that could be potentially elicited.

Table 3 – Number of electrical stimulations performed at each stimulation site and type of task asked. The corresponding number of stimulations that evoked a transient impairment is indicated in brackets (aFG: anterior fusiform gyrus; CoS: collateral sulcus; CS: calcarine sulcus; IOG: inferior occipital gyrus; ITG: inferior temporal gyrus; ITS: inferior temporal sulcus; OTS: occipito-temporal sulcus; WM: white matter).

Stimulation site	Cognitive tasks		
	Famous face recognition	Object recognition	Face/object categorization
F1–F2 (CoS-aFG)	1 (0)		
F3–F4 (aFG)	5 (5)	2 (0)	3 (0)
F4–F5 (aFG-OTS)	2 (2)	1 (0)	
F5–F6 (OTS)	1 (1)		
F7–F8 (ITS)	1 (0)		
F8–F9 (ITG)	1 (0)		
O1–O2 (CS)	1 (0)		
O2–O3 (CS)	1 (0)		
O3–O4 (CS)	1 (0)		
O5–O6 (CS)	1 (0)		
O6–O7 (CS)	1 (0)		
O7–O8 (WM)	1 (0)		
O9–O10 (IOG)	1 (0)		

2.4.1. *Famous face and object recognition task*

Stimulations were carried out during recognition of sets of photographs of the same category presented one by one (famous faces with all external features or common objects). The patient had to name each photograph in turn. She had to recognize several photographs, before, during and after the stimulation (Fig. 1A, Table 4). For each set, the stimulation was triggered randomly during the presentation of one of the photographs. The stimulation was triggered manually, around .5–1 sec before the visual presentation and the current was delivered throughout the entire duration of the visual presentation. Because of a limited time of testing due to the clinical context, we first screened all the contacts located in the right hemisphere using one stimulation per site (electrodes F and O). Next, we studied more extensively the relevant contacts evoking face recognition impairment by performing additional electrical stimulations on these sites. Thirteen famous faces that CD easily recognized and named prior to the stimulation procedure were selected. The number of stimulations was well above the number of face photographs used, so that the same faces were repeated across stimulations. In total the patient was presented with 51 photographs of faces, 22 during electrical stimulation, 19 before and 10 after. CD was also presented with 16 different objects (no repetition), 6 during the time of the stimulation, 4 before and 6 after.

Immediately after 3 stimulations of one site in the anterior FG (contacts F3–F4), CD was asked to recall the faces that were presented during the stimulation procedure (recall task, Fig. 2B). She was presented again with the faces presented during the stimulation procedure along with distractors (for 2 stimulations) and was asked to indicate verbally which of these faces she saw a moment ago.

2.4.2. *Face/object categorization task*

During stimulations of one site in the right anterior FG (F3–F4, Table 3), CD was presented alternatively with photographs of faces and objects (the same as in the recognition task) and was

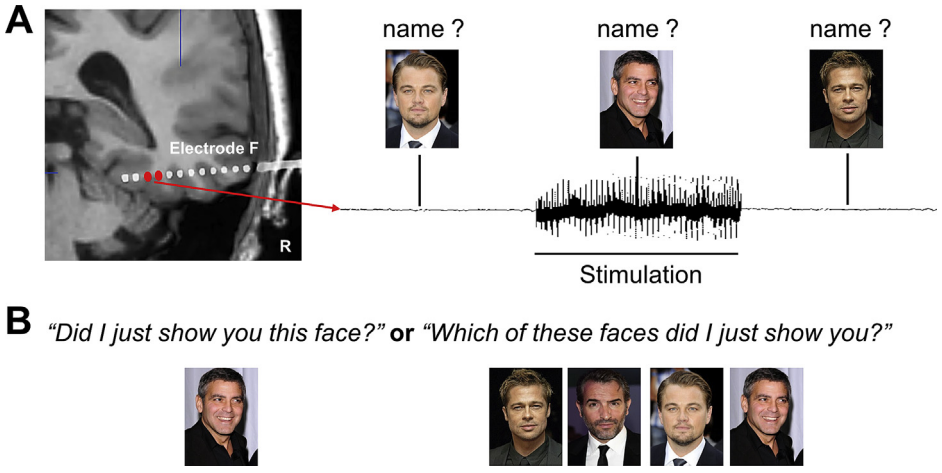

Fig. 1 – Schematic representation of the stimulation procedure for the famous face recognition task and the recall task. A. In the famous face recognition task, the patient CD had to recognize several photographs of famous faces before, during and after the electrical stimulation of 2 contiguous electrode contacts (here located in the anterior FG). She was presented mainly with famous faces of French politicians, actors, singers, etc. but famous faces of internationally renowned celebrities are showed here for illustration. B. When tested, after the stimulation procedure, CD was presented with the faces again as well as faces not presented during the stimulation (face distractors) and she was asked to indicate the faces that were presented before (recall task).

Table 4 – Details of electrical stimulation during famous face recognition: stimulation site, stimulation parameters (intensity, duration), performance (before, during and after stimulation) and transcripts of the patient responses during stimulation. The anatomical locations of the stimulation sites are indicated in Table 3.

Stimulation site	Stimulation parameters	Performance	Patient responses during stimulation
F1–F2	1 mA, 5sec	Before: 1/1 During: 1/1	Named the face
F3–F4	1 mA, 5sec	During: 0/1	Remained silent
F3–F4	1 mA, 5sec	During: 0/1	"Damn"
F3–F4	1 mA, 10sec	Before: 3/3 During: 0/1	"Damn" (see Video S3)
F3–F4	1 mA, 10sec	Before: 3/3 During: 0/1 After: 3/5	"Why am I blocked?" (see Video S2)
F3–F4	1 mA, 10sec	During: 0/1	"It's a man, he is smiling"
F4–F5	1 mA, 5sec	During: 0/1	"I'm blanking"
F4–F5	1 mA, 5sec	Before: 3/3 During: 0/1	"Damn" (see Video S1)
F5–F6	1 mA, 5sec	Before: 1/1 During: 0/1 After: 1/1	"Er"
F7–F8	1.2 mA, 5sec	During: 1/1	Named the face
F8–F9	1.2 mA, 5sec	During: 1/1	Named the face
O1–O2	1 mA, 5sec	During: 2/2 After: 4/4	Named the 2 faces
O2–O3	.8 mA, 5sec	During: 1/1	Named the face
O3–O4	.8 mA, 5sec	Before: 2/2 During: 2/2	Named the 2 faces
O4–O5	.8 mA, 5sec	Before: 1/1 During: 1/1	Named the face
O5–O6	.8 mA, 5sec	Before: 2/2 During: 1/1	Named the face
O6–O7	.8 mA, 5sec	Before: 1/1 During: 1/1	Named the face
O7–O8	.8 mA, 5sec	Before: 2/2 During: 2/2	Named the 2 faces
O9–O10	1.2 mA, 5sec	During: 1/1	Named the face

asked to tell whether the photograph represented a face or an object. In total, she was presented with 23 stimuli (11 faces, 12 objects) with 17 of these stimuli presented during the time of stimulation (9 faces, 8 objects) and 6 before or after stimulation (3 faces, 3 objects).

2.5. *Face-selectivity: intracerebral ERP and gamma activity*

2.5.1. *Procedure*

The material consisted of 60 grayscale pictures of faces and of 60 grayscale pictures of objects. All faces showed a frontal view with a neutral background and neutral or mildly positive expressions. The patient seated in a hospital bed facing a computer screen placed 70 cm from her face. Stimuli were presented on the center of the screen using Bq-Evoque v1.0.3 software (Micromed, Italy). Stimulus duration was 396 msec. Interstimulus interval was filled by a black screen and varied randomly between 2000 and 3000 msec. The task consisted of determining whether the presented stimulus was a face or an object (by pressing keyboard buttons). The patient performed 2 blocks of 120 trials (60 faces and 60 objects in each block, randomized). The signal was recorded at a 512 kHz sampling rate on a 128 channels amplifier (2 SD LTM 64 Headbox; Micromed, Italy). The reference electrode was an intracerebral contact located in the white matter (left parietal lobe).

2.5.2. *ERP analysis*

Off-line processing of intracerebral EEG was computed using Letswave 5 (http://nocions.webnode.com/letswave/) and MATLAB v7.9 (The Mathworks, Inc.). Epochs were created beginning 200 msec before stimulus onset and lasting until 1000 msec post-stimulus. A baseline correction was applied between −200 msec and 0 msec. Averaging was computed separately for faces and objects stimuli. Amplitude differences between faces and objects ERPs were assessed with a two-tailed *t*-test ($p < .01$, 10 consecutive milliseconds at least).

2.5.3. *Gamma-ERSP analysis*

Event-related spectral perturbations (ERSP) were computed using Letswave 5 and MATLAB v7.9. Variation in signal amplitude as a function of time and frequency was estimated by a Morlet wavelet transform on each single trial from frequencies of 1–160 Hz, in 160 steps. Analyses concentrated on the high frequency broadband range (gamma: 30–160 Hz; Lachaux et al., 2005; Parvizi et al., 2012; Sato et al., 2014; Vidal et al., 2010). Broadband gamma activity increase has been shown to be correlated with the local neuronal population spiking activity (Manning, Jacobs, Fried, & Kahana, 2009). The number of cycles (i.e., central frequency) of the wavelet was adapted as a function of frequency from 2 cycles at the lowest frequency to 10 cycles at the highest frequency. The wavelet transform was computed on each time-sample and the resulting amplitude envelope was downsampled by a factor of 4 (i.e., to a 128 Hz sampling rate). Amplitude was normalized across time and frequency to obtain the percentage of power change generated by the stimulus onset relative to the mean power in a pre-stimulus time-window (−700 msec to −300 msec relative to stimulus onset).

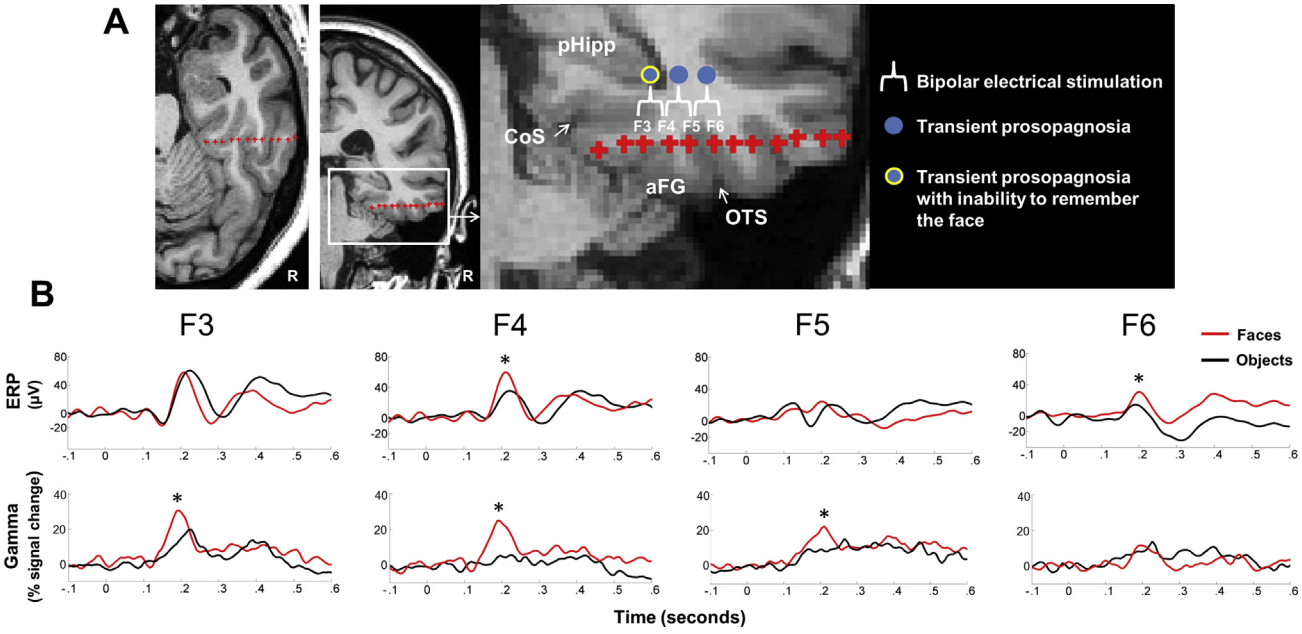

Fig. 2 – Anatomical and functional location of the stimulation sites inducing transient prosopagnosia: these sites were located in a face-selective region of the anterior FG. A. Anatomical location of electrode F (in red) and relevant contacts inducing transient prosopagnosia (F3, F4, F5, and F6). These contacts are located in the anterior FG (the posterior hippocampus, pHipp, is visible). B. Low- (ERP) and high-frequency (gamma: 30–160 Hz) electrophysiological responses to faces and objects recorded on these contacts. These contacts were face-selective in ERP and/or in gamma-ERSP. Abbreviations: aFG: anterior fusiform gyrus; OTS: occipito-temporal sulcus; CoS: collateral sulcus; pHipp: posterior hippocampus. *face-selective responses ($p < .01$).

The amplitude difference between the gamma-band signal (30–160 Hz) generated by face and object stimuli was statistically assessed by running a permutation test at each time-sample of the response between −300 and 700 msec relative to stimulus onset. In short, the single-trial amplitudes obtained in the two conditions at a given time-point were randomly assigned in two bins, the number of trials in each bin being equal to the number of trials in each original condition. Next, the difference between the means of the two random bins was computed and stored. Because permutation shuffles the assignment of the conditions, the difference between the means of the two new bins reflects the difference between conditions under the null hypothesis. This process was performed 5000 times to generate a distribution of differences at a $p < .01$ (two-tailed) and values that reached this threshold for at least 10 consecutive milliseconds were considered as significant.

2.6. *Face-selectivity: fMRI*

The comprehensive methods (stimuli, stimulation procedures) used for this fMRI localizer study were the same as those used in several previous studies (summarized in Rossion et al., 2012).

2.6.1. *Stimuli*

Four categories of stimuli were used: photographs of faces (F), cars (C), and their phase-scrambled versions: scrambled faces (SF) and scrambled cars (SC). The face condition consisted of 43 pictures of faces (22 females) cropped so that no external features (hair, etc.) were revealed. All faces were shown in frontal view (for all stimulus information, see Rossion & Caharel, 2011). They were inserted in a gray rectangle. Similarly, the car condition consisted of 43 pictures of different cars in a full-front view also embedded in a gray rectangle. The scrambled stimuli were made using a Fourier phase randomization procedure (FFT with phase replaced by phase of a uniform noise) that yields images preserving the low-level properties of the original image (i.e., luminance, contrast, spectral energy, etc.), while completely degrading any category-related information. Pictures of faces/cars and the phase scrambled face/car pictures subtended equal shape, size and contrast against background.

2.6.2. *Paradigm*

The patient performed 3 runs of 11 min duration each. In each run, there were 6 blocks of 18 sec duration for each of the 4 types of stimuli. Blocks were separated by a baseline condition (cross fixation) of 9 sec. In each block, 24 stimuli of the same condition were presented (750 msec per stimuli, no ISI) on a black background screen, with 2 or 3 consecutive repetitions of the exact same stimulus in each block (target trials in the one-back task). This gave a total amount of 144 stimuli per category per run. The stimuli and the fixation cross were presented centrally, but stimulus location varied randomly in x (6%) and in y (8%) direction at each presentation. This change in stimulus location was made so that specific elements of the non-scrambled face and car stimuli (e.g., the eyes or headlights) do not appear at the same location at each trial, as it would be the case for scrambled stimuli even without jittering position. The patient performed a one-back identity task (2 or 3 targets per block).

2.6.3. *Imaging acquisition parameters*

Functional MR images of brain activity were collected using a 3T head scanner (Signa HDXT, GE Medical Systems, Milwaukee, WI) at the University Hospital of Nancy with repeated single-shot echo-planar imaging: echo time (TE) = 33 msec, flip angle (FA) = 77°, matrix size = 64 × 64, field of view (FOV) = 192 mm, slice thickness = 3 mm, repetition time (TR) = 2250 msec, 36 slices. A high-resolution anatomical volume of the whole brain was acquired using a T1-weighted sequence (resolution: 1 × 1 × 1 mm).

2.6.4. *Data analysis*

The fMRI signal in the different conditions was compared using Brain Voyager QX (Version 2.8.0, Brain Innovation, Maastricht, The Netherlands). Preprocessing consisted of a linear trend removal for excluding scanner-related signal, a temporal high-pass filtering applied to remove temporal frequencies lower than three cycles per run, and a correction for small interscan head movements by a rigid body algorithm rotating and translating each functional volume in 3D space. Functional data were smoothed in the spatial domain (FWHM 4 mm, all three directions), and spatially aligned with the high-resolution anatomical volume which was previously aligned to the AC-PC plane (automatic co-registration in Brain Voyager QX, adjusted manually). Subsequently, the functional data were analyzed using one multiple regression model [General Linear Model (GLM)] consisting of predictors, which corresponded to the particular experimental conditions of each experiment. The predictor time courses used were computed on the basis of a linear model of the relation between neural activity and hemodynamic response, assuming a rectangular neural response during phases of visual stimulation.

The contrast of interest was the conjunction contrast [(F-C) and (F-SF)]. This contrast was aimed at isolating the regions responding more to faces than non-faces objects, and for which this difference could not be accounted for by low-level visual cues (Rossion et al., 2012). The statistical threshold was set at $p < .01$ (uncorrected), corresponding to t-values above 2.58. A relatively liberal statistical threshold was used because the goal of the fMRI examination was not to test the whole brain but to assess whether the face-selective regions overlapped with the stimulated electrodes.

2.6.5. *Intracerebral contact localization*

The high-resolution T1 (aligned to the AC-PC plane) was fused with the post-operative CT-scan. The electrode contact coordinates were automatically extracted (MRI coordinates in the individual anatomy centered on the AC-PC plane). These electrode contact coordinates were then rendered in Brain Voyager software. The anatomical locations of relevant fMRI activations and intracerebral contacts were therefore assessed in the individual anatomy. Anatomical and functional volumes were also spatially normalized (Talairach & Tournoux, 1988) but only to determine Talairach coordinates of fMRI activations and intracerebral contacts.

3. Results

3.1. Electrical stimulation of the anterior FG elicits transient prosopagnosia

Eight out of eight stimulations involving the right anterior FG and adjacent OTS induced a transient inability to recognize the face, i.e., transient prosopagnosia (stimulation of contacts F3–F4, F4–F5, F5–F6, Talairach coordinates: x: 29 to 45, y: −30, z: −18; see Fig. 2A for stimulation site location; see also Table 4). During the stimulation, the patient was unable to name or identify the famous faces presented (i.e., name or provide any semantic information about the person from his/her face). The patient stated: *"I didn't recognize him at first"*, *"I asked to myself, who is this person?"*, *"I'm not able to tell who this person is"* (see Videos S1, S2 and S3). Importantly, these stimulations never produced visual distortions of the face. When asked explicitly if the face was distorted, the patient responded: *"distorted? No, not at all"*, *"the face was not distorted"*. In most trials, the prosopagnosia stopped upon the termination of the stimulation (but see Video S2 for a persistent effect with 2 non-recognized faces just after the termination of the stimulation). In total, the patient did not recognize the 8 faces presented during stimulation of the right anterior FG (1 face per stimulation), and 2 faces presented immediately after 1 stimulation of contacts F3–F4 (performance during anterior FG stimulation: 0/8, 0%, see Table 4). In contrast, she immediately recognized and named the 41 remaining faces, either presented during stimulation of contacts outside the anterior FG (14 faces) or without stimulation (27 faces) (performance beside anterior FG stimulation: 41/43, 95.3%; see Table 4; performance during *vs* beside anterior FG stimulation: $p = .008$, Fisher's exact test). Stimulation of the right anterior FG did not evoke object recognition impairment (the 6 objects presented during the time of stimulation were correctly recognized, Table 3). Moreover, stimulations of contacts F3–F4 (right anterior FG) did not disrupt her face detection ability, since she was 100% correct at the face/object categorization task (23 stimuli in total, 17 during stimulation).

Supplementary video related to this article can be found at http://dx.doi.org/10.1016/j.cortex.2015.05.026.

When tested at the end of the stimulation procedure, CD was unable to remember specifically the non-recognized faces presented during the stimulation (3 stimulations of contacts F3–F4 in the right anterior FG, see Video S2 and S3). Across the 3 stimulations performed to test this point specifically, CD did not remember the 3 faces presented during stimulation (1 face per stimulation), but she correctly remembered 3 faces presented outside the stimulation and she correctly detected the 4 distractor faces. Therefore, in total, her accuracy rate at this task was 0% during stimulation (0/3) and 100% outside stimulation (7/7).

Stimulation of the right anterior FG never produced afterdischarges, epileptic spikes or epileptic seizures. Note also that the right anterior FG stimulation results were independent from the patient epilepsy: (i) contacts F3, F4, F5 and F6 never recorded epileptic spikes; (ii) the epileptic focus was found in the contralateral (left) hemisphere. Stimulation of contacts outside the right anterior FG did not produce any recognition impairment (contacts F1, F2, F7, F8, F9 of electrode F, contacts of electrode O; Tables 3 and 4).

3.2. Stimulation sites in the right anterior FG are located in a face-selective region

We tested the face-selectivity of each intracerebral contact by comparing electrophysiological responses to unknown faces and non-faces objects. Stimulated electrode contacts producing transient prosopagnosia (F3, F4, F5, F6) recorded larger responses to faces than non-face objects in ERP and/or in gamma-ERSP (ERP and gamma-ERSP: F4; ERP only: F6; gamma-ERSP only: F3 and F5, see Fig. 2B, see Engell & McCarthy, 2011 for a similar co-localization of these 3 types of responses in the human ventral temporal cortex). This shows that these contacts were located in a face-selective region of the anterior FG. On contacts F4 and F6, we recorded a positive face-selective ERP peaking at 200 msec after stimulus onset (Fig. 2B). On contacts F3, F4 and F5, we recorded significantly higher gamma band activity to faces compared to objects, starting from 100 msec and peaking at 200 msec after stimulus onset (Fig. 2B, see Supplementary Fig. S1 for time-frequency analyses). Contact F4, whose stimulation systematically evoked transient prosopagnosia (7 out of 7 stimulations) was the only face-selective contact both in ERPs and gamma-ERSP. Contacts of electrode F that were not associated with a face recognition impairment did not record face-selective responses (i.e., medial contacts F1 and F2 recorded larger responses for objects than for faces in both ERP and gamma-ERSP; lateral contacts F7, F8 and F9 did not record any visual responses). Contacts located in the right inferior occipital gyrus (O9, O10, O11) recorded face-selective ERPs but their stimulation did not produce face recognition impairment. However, this region was tested only once while presenting faces (1 stimulation on contacts O9–O10). In the left hemisphere, face-selective ERPs were observed in the FG (5 contacts: F′2, F′3, L′3, L′5, L′6) and in the inferior occipital gyrus (1 contact: O′8). These left face-selective contacts were not tested with faces during stimulation.

3.3. Stimulation sites are located anteriorly to the core face-processing network defined in fMRI

In fMRI, the conjunction contrast [(F-C) and (F-SF)] revealed typical face-selective activations of the core processing network (Figs. 3 and 4, Table 5). In the right hemisphere, we found the OFA in the inferior occipital gyrus, the pSTS the posterior section of the superior temporal sulcus and the FFA in the fusiform gyrus. Specifically, the right FFA was located in the posterior FG (posteriorly to the end of the hippocampus) in its lateral section (lateral FG, laterally to the mid-fusiform sulcus; Weiner & Grill-Spector, 2010; Weiner et al., 2014). We also found a face-selective activation in the left hemisphere (left FFA in the posterior FG). The left OFA was not found in fMRI but a face-selective ERP was found in the left inferior occipital gyrus. Taken together, all these left sided face-selective responses (left FFA in fMRI and intracranial face-selective ERPs in the left FG and left inferior occipital gyrus)

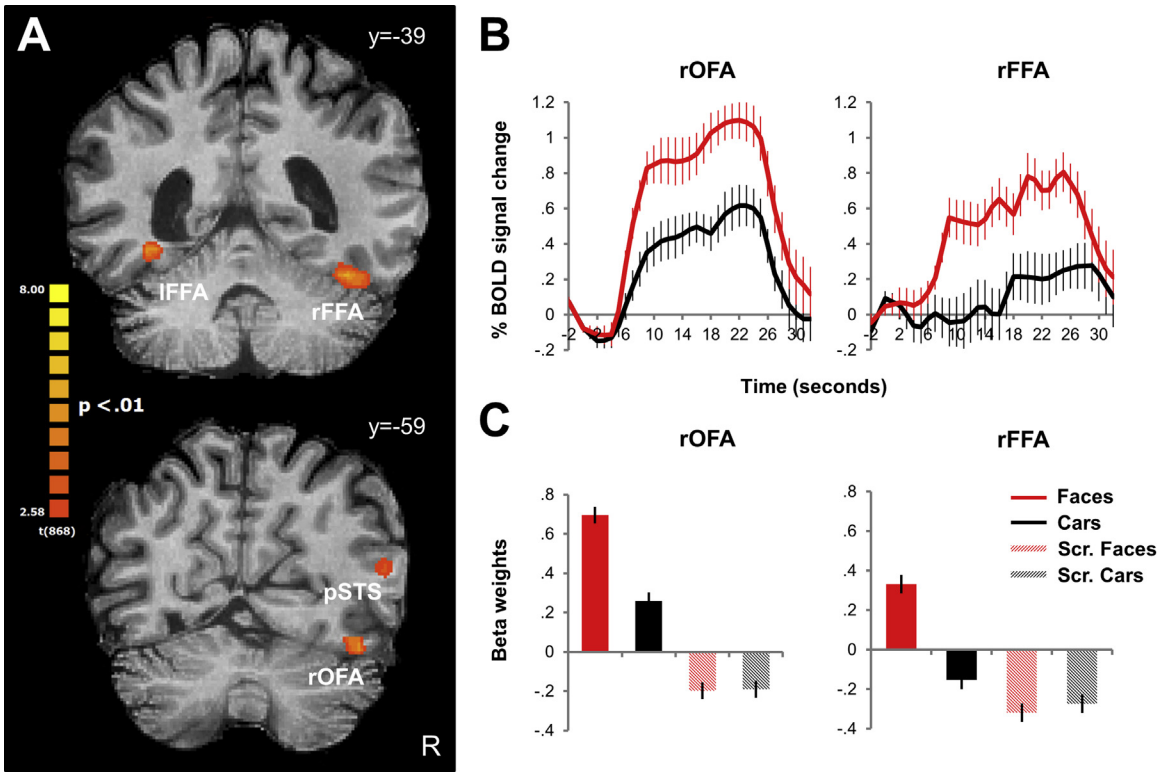

Fig. 3 – Patient CD shows a typical core face-processing network as revealed with fMRI. A. Face-selective areas of the core face-processing network on coronal slices [conjunction contrast (F-C) and (F-SF), $p < .01$ uncorrected]. B. BOLD time courses (right OFA and FFA). C. Beta weights (right OFA and FFA). Abbreviations: FFA: fusiform face area; OFA: occipital face area; pSTS: posterior superior temporal sulcus face-selective area. Vertical bars indicate standard errors.

suggest normal face processing functions in the left hemisphere, despite the patient's left temporal epilepsy.

Importantly, the electrode contacts whose stimulation led to transient prosopagnosia (F3, F4, F5 and F6) were located anteriorly to the right FFA (Fig. 4). More precisely, these contacts were located 8 mm forward of the anterior edge of the right FFA and 12 mm forward of the center of mass of the right FFA (*y* axis, native space). Although these contacts were located in a face-selective region, no face-selective activations overlapped the location of these contacts contrast [contrast (F-C) and (F-SF), $p < .01$ uncorrected, see Fig. 4]. No face-selective activations were found in 2-mm-diameter ROIs centered on

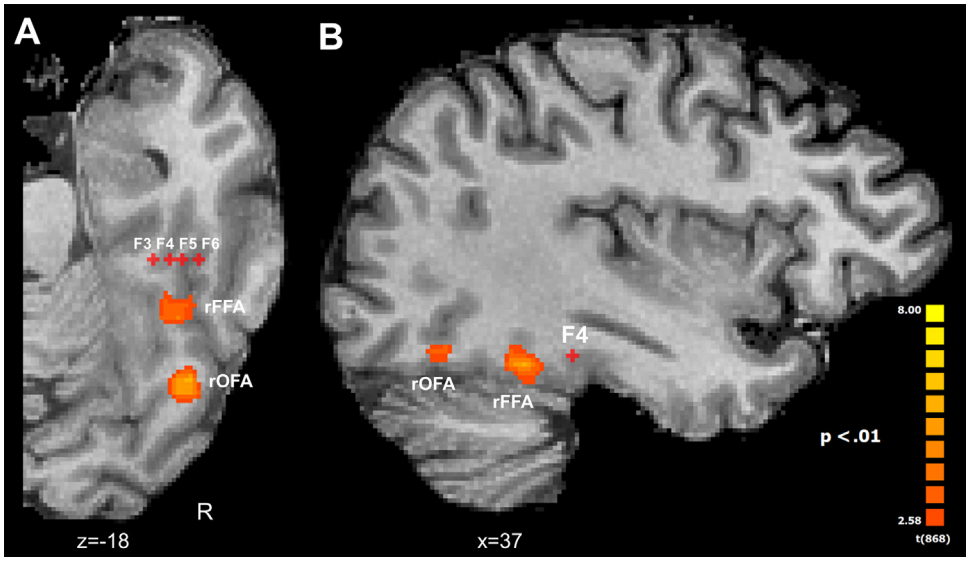

Fig. 4 – The critical stimulation sites eliciting transient prosopagnosia are located anteriorly to the core face processing network. A. Axial slice passing through electrode F contacts. B. Sagittal slice passing through contact F4.

Table 5 – Talairach coordinates (center of mass), mean *t* and *p* values of face-selective activations of the core processing network identified in fMRI (conjunction contrast F-C and F-SF, $p < .01$ uncorrected).

	Talairach coordinates			Cluster size (number of voxels)	Mean *t* value	Mean *p* value
	x	*y*	*z*			
Right OFA	37	−60	−23	322	3.67	.0019
Right pSTS	52	−47	8	2001	3.26	.0027
Right FFA	37	−39	−26	589	3.42	.0022
Left FFA	−36	−37	−15	408	3.46	.0022

the location of each of the intracerebral contacts F3, F4, F5 and F6 ($p > .05$ for all ROIs using a contrast F-C). Moreover, no significant activation overlapped these contacts, even when using an unspecific contrast [(F + C)−(SF + SC), $p < .01$ uncorrected].

It is well known that a strong MRI signal drop-out occurs in the antero-inferior temporal cortex (Axelrod & Yovel, 2013; Ojemann et al., 1997). This signal drop-out is caused by susceptibility artifacts related to the local anatomy (mainly the ear canals). This may explain why we did not find any fMRI face-selective activation in the right anterior FG. When displaying fMRI face-selective activations and relevant contacts on raw functional slices (e.g., Rajimehr et al., 2009; Tsao et al., 2008), we observed indeed that the stimulation sites (contacts F3, F4, F5 and F6) lie within a severe signal drop-out involving the antero-inferior temporal cortex (Fig. 5A). For instance, the MRI intensity was around 3000 (scanner units) in the right FFA while it was around 300 in the vicinity of contact F4. This signal drop-out specifically involved the anterior FG and inferior temporal gyrus and spared more medial structures as the parahippocampal gyrus and adjacent collateral sulcus (Fig. 5B, see also Rajimehr et al., 2009).

4. Discussion

We report a case of transient inability to recognize faces following electrical stimulation of a face-selective region in the right anterior FG. This observation provides original evidence that a face-selective region of the right ventral temporal cortex anterior to the FFA is critical for face recognition.

4.1. *Electrically stimulating the anterior FG induces transient prosopagnosia*

As mentioned in the introduction, in Humans, previous evidence for a causal role of brain regions in face recognition come from lesion studies, TMS and intracerebral electrical stimulation. In right-handed individuals, this evidence systematically concerns the right hemisphere (see Bukowski, Dricot, Hanseeuw, & Rossion, 2013 and Rossion, 2014 for discussion of this issue of lateralization). Although studies of acquired prosopagnosic patients provide invaluable sources of information regarding the neuro-functional aspects of face recognition (Rossion, 2014), these patients usually have large and variable lesions, preventing to draw firm conclusions about the necessity of a specific region such as the anterior FG for face recognition (Barton, 2008; Barton, Press, Keenan, & O'Connor, 2002; Bouvier & Engel, 2006; Busigny et al., 2010; Sergent & Signoret, 1992; Sorger, Goebel, Schiltz, & Rossion, 2007). Moreover, these lesion studies cannot determine if the site of the lesion was face-selective prior to brain damage. TMS cannot be applied to ventral occipito-temporal areas (e.g., in the FG), so that TMS-evoked impairments in face processing have been found only following stimulation of the lateral occipital cortex (right OFA, e.g., Pitcher et al., 2007; Solomon-Harris et al., 2013) or of the lateral temporal cortex (pSTS, e.g., Dzhelyova, Ellison, & Atkinson, 2011). Moreover, these significant TMS effects concern decreases of a few percent in accuracy rates and/or increase in RTs in face discrimination tasks, but no interruption of the ability to recognize faces. Finally, in previous studies, electrical stimulation of the cortical surface of the posterior and middle FG caused visual distortion of real faces (Parvizi et al., 2012; Rangarajan et al., 2014). However, these latter studies do not report face recognition impairments. Thus, to our knowledge, prior to the present study, the only instance of an impairment of face recognition following electrical stimulation is the case of KV reported by Jonas et al. (2012). When stimulating the right OFA, KV was transiently unable to recognize famous faces along with face distortions for some stimulations.

Here, stimulating the right anterior FG induced transient prosopagnosia (i.e., inability to recognize faces) without any face distortions (i.e., the patient denied any such distortions when she was asked specifically, Video S1). Electrical stimulation of the anterior FG affected face recognition without affecting face/object categorization ability (i.e., face detection), as also sometimes observed following electrical stimulation of the FG (Chong et al., 2013). Moreover, here, the patient was subsequently unable to remember the presented faces that she did not recognize, suggesting that these faces were not encoded. This latest observation show that the impairment reported here was related to visual encoding/recognition rather than an impairment in face–name association as previously reported (e.g., Allison et al., 1994). Taken together, these observations indicate that we transiently evoked a prosopagnosia as typically described in chronically brain damaged patients: inability to recognize and encode faces, absence of conscious distortion of the face percept, and, in most cases, intact face detection ability (Barton, 2008; Busigny et al., 2010, 2014a; Rossion, 2014; Rossion et al., 2003a; Sergent & Signoret, 1992).

Without electrical stimulation, CD was able to discriminate/match pictures of unfamiliar faces and showed a typical face inversion effect. This shows that her face perception ability was in the normal range. Admittedly, a potential limitation of the present report is that CD's ability to recognize famous faces as evaluated by neuropsychological tests was below normal controls (CELEB test; Busigny et al., 2014b). This is not surprising since patients with temporal lobe epilepsy usually score below normal controls at famous face recognition and naming tests (Glosser et al., 2003). Unfortunately, face perception/recognition ability (i.e., discrimination of unfamiliar faces, familiar face recognition) was not tested in intracranial electrical stimulation studies that reported face perceptual distortions (Parvizi et al., 2012; Rangarajan et al., 2014; Vignal, Chauvel, & Halgren, 2000) or face–name association impairments (Allison et al., 1994). Therefore, we argue

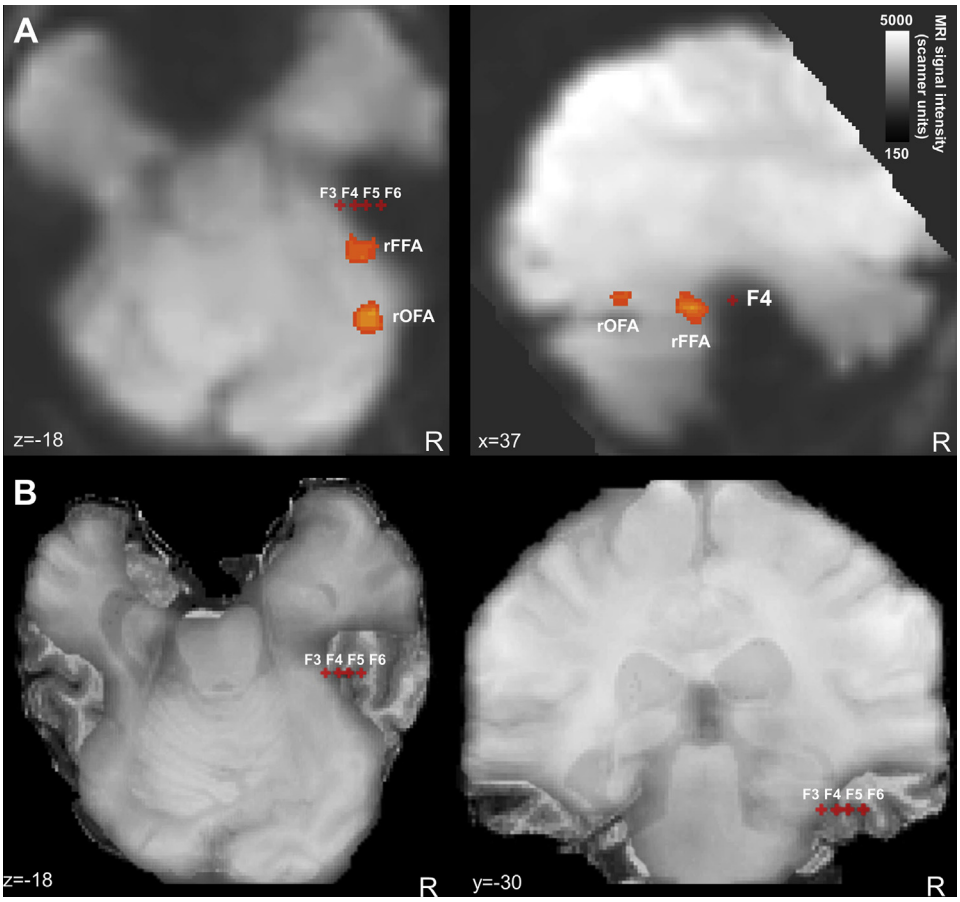

Fig. 5 – The critical stimulation sites are located in a MRI signal drop-out. A. Face-selective areas (rOFA and rFFA) and intracerebral contacts F3, F4, F5 and F6 are shown on raw functional slices (axial and sagittal slices). The MRI signal intensity shows a strong signal drop-out in the antero-inferior temporal cortex (in black), where these contacts are located. The right OFA and FFA are spared by this drop-out. B. Superimposition of raw functional and anatomical images (axial and coronal slices), showing that the signal drop-out specifically involved the anterior FG and the inferior temporal gyrus.

that the stringent neuropsychological evaluation performed here (as well as in Jonas et al., 2012) is a strength of the present study, and that such evaluations should be routinely performed in intracerebral stimulation studies. In this context, there are at least two arguments suggesting that CD's difficulties with face recognition outside of the stimulation cannot account for the transient prosopagnosia observed during intracerebral stimulation. First, the neuropsychological test assessing famous face recognition performance (CELEB) was quite difficult, using faces without external features and limited presentation times. In contrast, the faces shown during the stimulation had external features, and were presented until response. Second, beside anterior FG stimulation, CD's performance at recognizing famous faces with such pictures was almost perfect (41 out of 43 famous faces, 95.3%), while she was completely unable to recognize any of the famous faces during anterior FG stimulation (0/8, 0%).

4.2. *Specificity and nature of the functional impairment*

Even though we did not test famous non-face objects (such as famous places, Jonas et al., 2012), several considerations suggest that CD's recognition impairment was specific to faces. Firstly, the anatomical location of the stimulation sites was relatively distant from medial temporal structures (hippocampus, rhinal cortex), involved in recognition memory and long-term memory representations. Secondly, the patient was not impaired at recognizing common non-face objects when stimulating the anterior FG. Thirdly, the stimulation sites were located in a face-selective cortical region, as shown by the intracerebral face-selective responses in ERP and in the gamma band recorded within this region. Moreover, as responses recorded in the gamma band typically reflect local cortical activity (Crone, Miglioretti, Gordon, & Lesser, 1998; Manning et al., 2009; Miller et al., 2007), this shows that face-selective responses were generated by a local face-selective region of the right anterior fusiform gyrus.

Given the reported absence of face distortion, it may be tempting to interpret CD's deficit as a form of "associative prosopagnosia", namely an impairment of face recognition despite an intact percept (Davies-Thompson, Pancaroglu, & Barton, 2014; De Renzi, 1986; Gainotti & Marra, 2011; McNeil & Warrington, 1991; Sergent & Signoret, 1992), and to contrast it with the kind of "apperceptive prosopagnosia"

evoked by stimulating the OFA (Jonas et al., 2012, 2014) and FFA (Parvizi et al., 2012; Rangarajan et al., 2014). However, the distinction between perception and memory impairments in neuropsychological patients with (prosop)agnosia (or in congenital/developmental forms of prosopagnosia) is not clear-cut (Farah, 1990; Rossion, 2014). That is, so-called pure associative cases of prosopagnosia usually perform below normal range at matching different pictures of unfamiliar faces or use extremely slow and painstaking strategies (e.g., Davidoff & Landis, 1990; Delvenne, Seron, Coyette, & Rossion, 2004; Farah, 1990; Levine & Calvanio, 1989), even when brain damage is restricted to anterior regions (e.g., Busigny et al., 2014a). Hence, given that CD was not tested with simultaneous matching of unfamiliar face pictures, there is no objective evidence that her percept was intact, and thus one should remain cautious in interpreting CD's transient impairment as reflecting a form of associative prosopagnosia.

4.3. *The anterior FG: an undefined face-selective region*

The critical stimulation site in the anterior FG was located anteriorly to the right FFA individually identified in CD's brain. This right FFA was localized in the posterior and middle FG (Talairach y axis: −39), a localization fully consistent with the typical localization of the right FFA (Talairach y axis around −40/−70; e.g., Fox, Iaria, & Barton, 2009; Kanwisher et al., 1997; Rossion et al., 2012). Moreover, the stimulation site was located anteriorly to the most anterior FFA cluster when the FFA is separated into 2 clusters along the FG, as in some recent studies (e.g., "mFus-faces/FFA-2", Weiner & Grill-Spector, 2010; Weiner et al., 2014). Indeed, this most anterior FFA cluster is located in the middle FG at the level of the mid-fusiform sulcus (Weiner et al., 2014), whereas our stimulation site was located in the anterior FG, where the mid-fusiform sulcus is not visible (Fig. 3A). However, it is important to note that the critical stimulation site was located posteriorly to most anterior fMRI face-selective activations found in the ventral temporal lobe, these activations being generally found in the anterior segment of the collateral sulcus (Talairach y axis around 0/−10; Avidan et al., 2014; Axelrod & Yovel, 2013; Nasr & Tootell, 2012; Pinsk et al., 2009; Pyles, Verstynen, Schneider, & Tarr, 2013; Rajimehr et al., 2009; Rossion et al., 2012; Tsao et al., 2008).

In sum, our critical stimulation site was located anteriorly to the FFA but posteriorly to the most anterior face-selective activations in the ventral temporal lobe. In fMRI, these "intermediate" ventral temporal face-selective activations have been reported specifically in the anterior FG in a handful of studies (Talairach y axis around −30; Axelrod & Yovel, 2013; Nasr & Tootell, 2012; Pyles et al., 2013; Rossion et al., 2012). However, anterior FG face-selective activations were rarely reported and were not consistently found in individual subjects in these studies due to a hemodynamic signal drop-out created by magnetic susceptibility artifacts (Axelrod & Yovel, 2013; Ojemann et al., 1997; Rajimehr et al., 2009; Tsao et al., 2008). Consistently with these observations, we were unable to find fMRI face-selective activations overlapping the relevant stimulation sites due to a severe signal drop-out affecting specifically the anterior FG, even though we recorded local ERP and gamma face-selective responses showing the face-selectivity of this region. This hemodynamic signal drop-out in fMRI may also explain why little is known about the role of anterior FG face-selective region in face processing (beyond PET studies, see below). In this context, our study illustrates the value of both intracerebral recordings, revealing highly significant local ERPs and gamma band face-selective responses here in the anterior FG, and electrical stimulation for better understanding face-selective regions anterior to the FFA and thus the function of the whole cortical face network.

Although intracerebral electrical stimulations are focal (thanks to low intensity stimulations of small contacts directly embedded into the gray matter), the stimulation signal may propagate to other connected face-selective areas throughout white matter tracts (Gomez et al., 2015; Gschwind, Pourtois, Schwartz, Van De Ville, & Vuilleumier, 2012; Pyles, et al., 2013).[1] In monkeys, microstimulation of face-selective patches has been shown to produce activation in other face patches (Moeller, Freiwald, & Tsao, 2008). However, the specific connectivity of the face-selective anterior FG region remains unknown so that the propagation of the stimulation signal is difficult to estimate (Gschwind et al., 2012; Pyles, et al., 2013). One potential reason for this lack of knowledge is that fMRI-tractography studies have so far failed to localize this face-selective region in a sufficient number of participants. For instance, one study identified face-selective activations in the anterior FG in 2 subjects only, so that the specific connectivity of this region was not examined further (Pyles, et al., 2013).

4.4. *What is the role of the right anterior FG in face processing?*

Using famous faces, we showed that the right anterior FG is critical for familiar face recognition. This suggests that the anterior FG plays a role in person identification and memory. This hypothesis is consistent with fMRI and brain lesions studies showing that anterior temporal lobe may play a role in face individualization and semantic knowledge about people (e.g., Busigny et al., 2014a; Joubert et al., 2006; Kriegeskorte, Formisano, Sorger, & Goebel, 2007; Nestor, Plaut, & Behrmann, 2011; Sergent et al., 1992; Von Der Heide, Skipper, & Olson, 2013; for reviews see Collins & Olson, 2014; Gainotti, 2007; Gobbini & Haxby, 2007; Olson, Plotzker, & Ezzyat, 2007). However, these studies rarely investigated the role of the anterior FG specifically. As discussed above, fMRI studies rarely reported activation in this region since fMRI signal is notoriously weak in the anterior FG. Brain lesions studies have concentrated on anterior temporal lobe damaged patients following stroke, trauma, neurodegenerative disorder (such as fronto-temporal dementia) or cortical resection. These lesions were usually large or undefined, extending from

[1] It is very unlikely that our stimulation effects were solely related to the stimulation of white matter tracts connected with more posterior face-selective areas, for several reasons: (i) the stimulated contacts were located in the gray matter; (ii) stimulation of adjacent contacts in the white matter did not evoke any recognition impairment (e.g., contact F7); (iii) the stimulation sites were located in a face-selective cortical area; (iv) only contacts showing face-selective responses were associated with face recognition impairment.

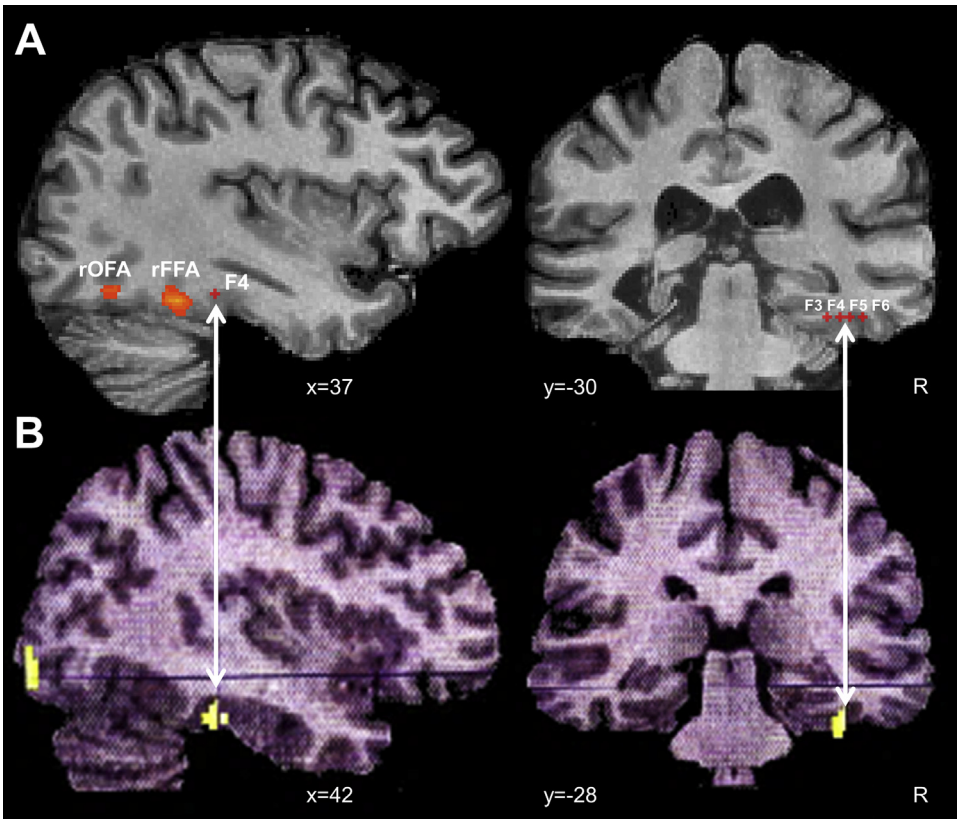

Fig. 6 – The critical stimulation sites overlap the location of PET activations for familiar faces (Rossion et al., 2001). Comparison of the locations of the stimulated region in the present study (A.) and the differential activation for familiar and unfamiliar faces in the PET study of Rossion et al. (2001) (B.), in sagittal and coronal slices. The right anterior FG PET activation displayed below (Talairach coordinates: *x*: 42, *y*: −28, *z*: −24) was anterior to the localized right FFA (*x*: 38, *y*: −44, *z*: −28; Rossion et al., 2003b).

the middle ventral temporal cortex to the temporal pole, and thus not specific to the anterior FG.

Overall, our findings regarding the critical function of the right anterior FG relate better to two independent, and rather unusual, observations. First, two early studies using PET, in which there is no issue of signal drop-out to consider in these regions, identified the right anterior FG in a contrast between familiar and unfamiliar faces (Rossion, Schiltz, Robaye, Pirenne, & Crommelinck, 2001; Wiser et al., 2000). In the first of these studies, the right anterior FG signaled a clear-cut (i.e., categorical) difference between familiar and unfamiliar faces in an orthogonal task (Rossion et al., 2001). The localization of the focus of activation strikingly corresponds to the site of stimulation evoking prosopagnosia here (Fig. 6), and was clearly distinct from the right FFA as defined independently in the same group of subjects (Rossion, Schiltz, & Crommelinck, 2003b). Second, a study investigating the anatomical structure of the fusiform gyrus in congenital prosopagnosic patients reported specifically a volume reduction of the anterior FG in these patients compared to normal controls (Behrmann, et al., 2007). Moreover, this volumetric reduction of the anterior FG was correlated with participants' behavioral decrement in famous face recognition. Taken together, these studies and the present original report point to the right anterior FG as a critical node for distinguishing familiar and unfamiliar faces and thus recognizing familiar faces.

5. Conclusion

To our knowledge, this is the first report of transient impairment of familiar face recognition with no evidence of perceptual face distortion, and following electrical stimulation a face-selective region anterior to the middle fusiform gyrus. These findings point to the causal role in face recognition of the right anterior fusiform gyrus and more generally of face-selective regions located beyond the OFA and FFA, i.e., anteriorly to the so-called “core” cortical network for face processing in humans.

Acknowledgments

We thank the patient CD for taking part in the study. JJ and BR are supported by the Belgian National Foundation for Scientific Research (FNRS), and CJ is supported by the Belgian Federal Science Policy Office (BELSPO). This work was partly

supported by an ERC grant (facessvep 284025) and a FRSM 3.4601.12 grant.

Supplementary data

Supplementary data related to this article can be found at http://dx.doi.org/10.1016/j.cortex.2015.05.026.

REFERENCES

Allison, T., McCarthy, G., Nobre, A., Puce, A., & Belger, A. (1994). Human extrastriate visual cortex and the perception of faces, words, numbers, and colors. *Cerebral Cortex, 4*, 544–554.

Allison, T., Puce, A., Spencer, D. D., & McCarthy, G. (1999). Electrophysiological studies of human face perception. I: potentials generated in occipitotemporal cortex by face and non-face stimuli. *Cerebral Cortex, 9*, 415–430.

Atkinson, A. P., & Adolphs, R. (2011). The neuropsychology of face perception: beyond simple dissociations and functional selectivity. *Philosophical Transactions of the Royal Society of London B: Biological Sciences, 366*, 1726–1738.

Avidan, G., Tanzer, M., Hadj-Bouziane, F., Liu, N., Ungerleider, L. G., & Behrmann, M. (2014). Selective dissociation between core and extended regions of the face processing network in congenital prosopagnosia. *Cerebral Cortex, 24*, 1565–1578.

Axelrod, V., & Yovel, G. (2013). The challenge of localizing the anterior temporal face area: a possible solution. *NeuroImage, 81*, 371–380.

Barbeau, E. J., Taylor, M. J., Regis, J., Marquis, P., Chauvel, P., & Liégeois-Chauvel, C. (2008). Spatio temporal dynamics of face recognition. *Cerebral Cortex, 18*, 997–1009.

Barton, J. J. (2008). Structure and function in acquired prosopagnosia: lessons from a series of 10 patients with brain damage. *Journal of Neuropsychology, 2*, 197–225.

Barton, J. J., Press, D. Z., Keenan, J. P., & O'Connor, M. (2002). Lesions of the fusiform face area impair perception of facial configuration in prosopagnosia. *Neurology, 58*, 71–78.

Behrmann, M., Avidan, G., Gao, F., & Black, S. (2007). Structural imaging reveals anatomical alterations in inferotemporal cortex in congenital prosopagnosia. *Cerebral Cortex, 17*, 2354–2363.

Benton, A. L., Sivan, A. B., Hamsher, K., Varney, N. R., & Spreen, O. (1983). *Benton facial recognition: Stimulus and multiple choice pictures*. Lutz: Psychological Assessment Resources Inc.

Bodamer, J. (1947). Die Prosop-Agnosie. *Archiv für Psychiatrie und Nervenkrankheiten, vereinigt mit Zeitschrift für die gesamte Neurologie und Psychiatrie, 118*, 6–53.

Bouvier, S. E., & Engel, S. A. (2006). Behavioral deficits and cortical damage loci in cerebral achromatopsia. *Cerebral Cortex, 16*, 183–191.

Bukowski, H., Dricot, L., Hanseeuw, B., & Rossion, B. (2013). Cerebral lateralization of face-sensitive areas in left-handers: only the FFA does not get in right. *Cortex, 49*, 2853–2859.

Busigny, T., Joubert, S., Felician, O., Ceccaldi, M., & Rossion, B. (2010). Holistic perception of the individual face is specific and necessary: evidence from an extensive case study of acquired prosopagnosia. *Neuropsychologia, 48*, 4057–4092.

Busigny, T., Prairial, C., Nootens, J., Kindt, V., Engels, S., Verplancke, S., et al. (2014b). CELEB : a neuropsychological tool for famous face recognition and proper name production. *Revue de Neuropsychologie, 6*, 69–81.

Busigny, T., Van Belle, G., Jemel, B., Hosein, A., Joubert, S., & Rossion, B. (2014a). Face-specific impairment in holistic perception following focal lesion of the right anterior temporal lobe. *Neuropsychologia, 56*, 312–333.

Calder, A. J., & Young, A. W. (2005). Understanding the recognition of facial identity and facial expression. *Nature Reviews Neuroscience, 6*, 641–651.

Chong, S. C., Jo, S., Park, K. M., Joo, E. Y., Lee, M. J., Hong, S. C., et al. (2013). Interaction between the electrical stimulation of a face-selective area and the perception of face stimuli. *NeuroImage, 77*, 70–76.

Collins, J. A., & Olson, I. R. (2014). Beyond the FFA: the role of the ventral anterior temporal lobes in face processing. *Neuropsychologia, 61*, 65–79.

Crawford, J. R., & Garthwaite, P. H. (2005). Testing for suspected impairments and dissociations in single-case studies in neuropsychology: evaluation of alternatives using Monte Carlo simulations and revised tests for dissociations. *Neuropsychology, 19*, 318–331.

Crawford, J. R., & Howell, D. C. (1998). Comparing an individual's test score against norms derived from small samples. *The Clinical Neuropsychologist, 12*, 482–486.

Crone, N. E., Miglioretti, D. L., Gordon, B., & Lesser, R. P. (1998). Functional mapping of human sensorimotor cortex with electrocorticographic spectral analysis. II. Event-related synchronization in the gamma band. *Brain, 121*, 2301–2315.

Davidoff, J., & Landis, T. (1990). Recognition of unfamiliar faces in prosopagnosia. *Neuropsychologia, 28*, 1143–1161.

Davies-Thompson, J., Pancaroglu, R., & Barton, J. (2014). Acquired prosopagnosia: structural basis and processing impairments. *Frontiers in Bioscience, 6*, 159–174.

De Renzi, E. (1986). Current issues on prosopagnosia. In H. D. Ellis, M. A. Jeeves, F. Newcombe, & A. Young (Eds.), *Aspects of face processing* (pp. 243–252). Dordrecht, Netherlands: Martinus Nijhoff.

Delvenne, J. F., Seron, X., Coyette, F., & Rossion, B. (2004). Evidence for perceptual deficits in associative visual (prosop) agnosia: a single-case study. *Neuropsychologia, 42*, 597–612.

Dzhelyova, M. P., Ellison, A., & Atkinson, A. P. (2011). Event-related repetitive TMS reveals distinct, critical roles for right OFA and bilateral posterior STS in judging the sex and trustworthiness of faces. *Journal of Cognitive Neuroscience, 23*, 2782–2796.

Engell, A. D., & McCarthy, G. (2011). The relationship of γ oscillations and face-specific ERPs recorded subdurally from occipitotemporal cortex. *Cerebral Cortex, 21*, 1213–1221.

Farah, M. J. (1990). *Visual agnosia: Disorders of object recognition and what they tell us about normal vision*. Cambridge, MA: MIT Press.

Fox, C. J., Iaria, G., & Barton, J. J. (2009). Defining the face processing network: optimization of the functional localizer in fMRI. *Human Brain Mapping, 30*, 1637–1651.

Gainotti, G. (2007). Different patterns of famous people recognition disorders in patients with right and left anterior temporal lesions: a systematic review. *Neuropsychologia, 45*, 1591–1607.

Gainotti, G., & Marra, C. (2011). Differential contribution of right and left temporo-occipital and anterior temporal lesions to face recognition disorders. *Frontiers in Human Neuroscience, 5*, 55.

Gauthier, I., Tarr, M. J., Moylan, J., Skudlarski, P., Gore, J. C., & Anderson, A. W. (2000). The fusiform "face area" is part of a network that processes faces at the individual level. *Journal of Cognitive Neuroscience, 12*, 495–504.

Glosser, G., Salvucci, A. E., & Chiaravalloti, N. D. (2003). Naming and recognizing famous faces in temporal lobe epilepsy. *Neurology, 61*, 81–86.

Gobbini, M. I., & Haxby, J. V. (2007). Neural systems for recognition of familiar faces. *Neuropsychologia, 45*, 32–41.

Gomez, J., Pestilli, F., Witthoft, N., Golarai, G., Liberman, A., Poltoratski, S., et al. (2015). Functionally defined white matter

reveals segregated pathways in human ventral temporal cortex associated with category-specific processing. *Neuron, 85*, 216–227.
Gschwind, M., Pourtois, G., Schwartz, S., Van De Ville, D., & Vuilleumier, P. (2012). White-matter connectivity between face-responsive regions in the human brain. *Cerebral Cortex, 22*, 1564–1576.
Halgren, E., Baudena, P., Heit, G., Clarke, J. M., Marinkovic, K., & Clarke, M. (1994). Spatio-temporal stages in face and word processing. I. Depth-recorded potentials in the human occipital, temporal and parietal lobes. *Journal of Physiology – Paris, 88*, 1–50.
Haxby, J. V., Hoffman, E. A., & Gobbini, M. I. (2000). The distributed human neural system for face perception. *Trends in Cognitive Science, 4*, 223–233.
Hécaen, H., & Angelergues, R. (1962). Agnosia for faces (prosopagnosia). *Archives of Neurology, 7*, 92–100.
Ishai, A. (2008). Let's face it: it's a cortical network. *NeuroImage, 40*, 415–419.
Jonas, J., Descoins, M., Koessler, L., Colnat-Coulbois, S., Sauvée, M., Guye, M., et al. (2012). Focal electrical intracerebral stimulation of a face-sensitive area causes transient prosopagnosia. *Neuroscience, 222*, 281–288.
Jonas, J., Rossion, B., Krieg, J., Koessler, L., Colnat-Coulbois, S., Vespignani, H., et al. (2014). Intracerebral electrical stimulation of a face-selective area in the right inferior occipital cortex impairs individual face discrimination. *NeuroImage, 99*, 487–497.
Joubert, S., Felician, O., Barbeau, E., Ranjeva, J. P., Christophe, M., Didic, M., et al. (2006). The right temporal lobe variant of frontotemporal dementia: cognitive and neuroanatomical profile of three patients. *Journal of Neurology, 253*, 1447–1458.
Kanwisher, N., McDermott, J., & Chun, M. M. (1997). The fusiform face area: a module in human extrastriate cortex specialized for face perception. *The Journal of Neuroscience, 17*, 4302–4311.
Kriegeskorte, N., Formisano, E., Sorger, B., & Goebel, R. (2007). Individual faces elicit distinct response patterns in human anterior temporal cortex. *Proceedings of the National Academy of Sciences of the United States of America, 104*, 20600–20605.
Lachaux, J. P., George, N., Tallon-Baudry, C., Martinerie, J., Hugueville, L., Minotti, L., et al. (2005). The many faces of the gamma band response to complex visual stimuli. *NeuroImage, 25*, 491–501.
Levine, D. N., & Calvanio, R. (1989). Prosopagnosia: a defect in visual configural processing. *Brain and Cognition, 10*, 149–170.
Manning, J. R., Jacobs, J., Fried, I., & Kahana, M. J. (2009). Broadband shifts in local field potential power spectra are correlated with single-neuron spiking in humans. *The Journal of Neuroscience, 29*, 13613–13620.
McNeil, J. E., & Warrington, E. K. (1991). Prosopagnosia: a reclassification. *The Quarterly Journal of Experimental Psychology, 43*, 267–287.
Meadows, J. C. (1974). The anatomical basis of prosopagnosia. *Journal of Neurology, Neurosurgery and Psychiatry, 37*, 489–501.
Miller, K. J., Leuthardt, E. C., Schalk, G., Rao, R. P., Anderson, N. R., Moran, D. W., et al. (2007). Spectral changes in cortical surface potentials during motor movement. *The Journal of Neuroscience, 27*, 2424–2432.
Moeller, S., Freiwald, W. A., & Tsao, D. Y. (2008). Patches with links: a unified system for processing faces in the macaque temporal lobe. *Science, 320*, 1355–1359.
Nasr, S., & Tootell, R. B. (2012). Role of fusiform and anterior temporal cortical areas in facial recognition. *NeuroImage, 63*, 1743–1753.
Nestor, A., Plaut, D. C., & Behrmann, M. (2011). Unraveling the distributed neural code of facial identity through spatiotemporal pattern analysis. *Proceedings of the National Academy of Sciences of the United States of America, 108*, 9998–10003.
Ojemann, J., Akbudak, E., Snyder, A., McKinstry, R., Raichle, M., & Conturo, T. (1997). Anatomic localization and quantitative analysis of gradient refocused echo-planar fMRI susceptibility artifacts. *NeuroImage, 6*, 156–167.
Oldfield, R. C. (1971). The assessment and analysis of handedness: the Edinburgh inventory. *Neuropsychologia, 9*, 97–113.
Olson, I. R., Plotzker, A., & Ezzyat, Y. (2007). The Enigmatic temporal pole: a review of findings on social and emotional processing. *Brain, 130*, 1718–1731.
Onitsuka, T., Shenton, M. E., Kasai, K., Nestor, P. G., Toner, S. K., Kikinis, R., et al. (2003). Fusiform gyrus volume reduction and facial recognition in chronic schizophrenia. *Archives of General Psychiatry, 60*, 349–355.
Parvizi, J., Jacques, C., Foster, B. L., Witthoft, N., Rangarajan, V., Weiner, K. S., et al. (2012). Electrical stimulation of human fusiform face-selective regions distorts face perception. *The Journal of Neuroscience, 32*, 14915–14920.
Pinsk, M. A., Arcaro, M., Weiner, K. S., Kalkus, J. F., Inati, S. J., Gross, C. G., et al. (2009). Neural representations of faces and body parts in macaque and human cortex: a comparative FMRI study. *Journal of Neurophysiology, 101*, 2581–2600.
Pitcher, D., Walsh, V., Yovel, G., & Duchaine, B. (2007). TMS evidence for the involvement of the right occipital face area in early face processing. *Current Biology, 17*, 1568–1573.
Puce, A., Allison, T., Gore, J. C., & McCarthy, G. (1995). Face-sensitive regions in human extrastriate cortex studied by functional MRI. *Journal of Neurophysiology, 74*, 1192–1199.
Pyles, J. A., Verstynen, T. D., Schneider, W., & Tarr, M. J. (2013). Explicating the face perception network with white matter connectivity. *PLoS One, 8*, e61611.
Rajimehr, R., Young, J. C., & Tootell, R. B. (2009). An anterior temporal face patch in human cortex, predicted by macaque maps. *Proceedings of the National Academy of Sciences of the United States of America, 106*, 1995–2000.
Rangarajan, V., Hermes, D., Foster, B. L., Weiner, K. S., Jacques, C., Grill-Spector, K., et al. (2014). Electrical stimulation of the left and right human fusiform gyrus causes different effects in conscious face perception. *The Journal of Neuroscience, 34*, 12828–12836.
Rossion, B. (2008). Constraining the cortical face network by neuroimaging studies of acquired prosopagnosia. *NeuroImage, 40*, 423–426.
Rossion, B. (2014). Understanding face perception by means of prosopagnosia and neuroimaging. *Frontiers in Bioscience, 6*, 258–307.
Rossion, B., & Caharel, S. (2011). ERP evidence for the speed of face categorization in the human brain: disentangling the contribution of low-level visual cues from face perception. *Vision Research, 51*, 1297–1311.
Rossion, B., Caldara, R., Seghier, M., Schuller, A. M., Lazeyras, F., & Mayer, E. (2003a). A network of occipito-temporal face-sensitive areas besides the right middle fusiform gyrus is necessary for normal face processing. *Brain, 126*, 2381–2395.
Rossion, B., Hanseeuw, B., & Dricot, L. (2012). Defining face perception areas in the human brain: a large-scale factorial fMRI face localizer analysis. *Brain and Cognition, 79*, 138–157.
Rossion, B., Schiltz, C., & Crommelinck, M. (2003b). The functionally defined right occipital and fusiform "face areas" discriminate novel from visually familiar faces. *NeuroImage, 19*, 877–883.
Rossion, B., Schiltz, C., Robaye, L., Pirenne, D., & Crommelinck, M. (2001). How does the brain discriminate familiar and unfamiliar faces?: a PET study of face categorical perception. *Journal of Cognitive Neuroscience, 13*, 1019–1034.
Sato, W., Kochiyama, T., Uono, S., Matsuda, K., Usui, K., Inoue, Y., et al. (2014). Rapid, high-frequency, and theta-coupled gamma

oscillations in the inferior occipital gyrus during face processing. *Cortex, 60*, 52–68.
Sergent, J., Ohta, S., & MacDonald, B. (1992). Functional neuroanatomy of face and object processing. A positron emission tomography study. *Brain, 115*, 15–36.
Sergent, J., & Signoret, J. L. (1992). Varieties of functional deficits in prosopagnosia. *Cerebral Cortex, 2*, 375–388.
Solomon-Harris, L. M., Mullin, C. R., & Steeves, J. K. (2013). TMS to the "occipital face area" affects recognition but not categorization of faces. *Brain and Cognition, 83*, 245–251.
Sorger, B., Goebel, R., Schiltz, C., & Rossion, B. (2007). Understanding the functional neuroanatomy of acquired prosopagnosia. *NeuroImage, 35*, 836–852.
Talairach, J., & Bancaud, J. (1973). Stereotaxic approach to epilepsy: methodology of anatomo-functional stereotactic investigations. *Progress in Neurological Surgery, 5*, 297–354.
Talairach, J., & Tournoux, P. (1988). *Coplanar stereotaxic atlas of the human brain: 3-dimensional proportional system: An approach to cerebral imaging*. Stuttgart: Thieme.
Tsao, D. Y., Moeller, S., & Freiwald, W. A. (2008). Comparing face patch systems in macaques and humans. *Proceedings of the National Academy of Sciences of the United States of America, 105*, 19514–19519.
Vidal, J. R., Ossandón, T., Jerbi, K., Dalal, S. S., Minotti, L., Ryvlin, P., et al. (2010). Category-specific visual responses: an intracranial study comparing gamma, beta, alpha, and ERP response selectivity. *Frontiers in Human Neuroscience, 4*, 195.
Vignal, J. P., Chauvel, P., & Halgren, E. (2000). Localised face processing by the human prefrontal cortex: stimulation-evoked hallucinations of faces. *Cognitive Neuropsychology, 17*, 281–291.
Von Der Heide, R. J., Skipper, L. M., & Olson, I. R. (2013). Anterior temporal face patches: a meta-analysis and empirical study. *Frontiers in Human Neuroscience, 7*, 17.
Weiner, K. S., Golarai, G., Caspers, J., Chuapoco, M. R., Mohlberg, H., Zilles, K., et al. (2014). The mid-fusiform sulcus: a landmark identifying both cytoarchitectonic and functional divisions of human ventral temporal cortex. *NeuroImage, 84*, 453–465.
Weiner, K. S., & Grill-Spector, K. (2010). Sparsely-distributed organization of face and limb activations in human ventral temporal cortex. *NeuroImage, 52*, 1559–1573.
Wiser, A. K., Andreasen, N., O'Leary, D. S., Crespo-Facorro, B., Boles-Ponto, L. L., Watkins, G. L., et al. (2000). Novel vs. well-learned memory for faces: a positron emission tomography study. *Journal of Cognitive Neuroscience, 12*, 255–266.

Systems/Circuits

The Face-Processing Network Is Resilient to Focal Resection of Human Visual Cortex

Kevin S. Weiner,[1] Jacques Jonas,[2,3,4] Jesse Gomez,[5] Louis Maillard,[2,4] Hélène Brissart,[2] Gabriela Hossu,[6] Corentin Jacques,[3] David Loftus,[7] Sophie Colnat-Coulbois,[2] Anthony Stigliani,[1] Michael A. Barnett,[1] Kalanit Grill-Spector,[1,5]* and Bruno Rossion[3]*

[1]Department of Psychology, Stanford University, Stanford, California 94305, [2]Department of Neurology and Neurosurgery, University Hospital of Nancy, 54000 Nancy, France, [3]Psychological Science Research Institute and Institute of Neuroscience, University of Louvain, 1348 Louvain-la-Neuve, Belgium, [4]CRAN, UMR 7039, CNRS and University of Lorraine, 54000 Nancy, France, [5]Neurosciences Institute, Stanford University, Stanford, California 94305, [6]Clinical Investigation Centre Innovative Technology, University Hospital of Nancy, 54000 Nancy, France, and [7]Department of Psychology, Pomona College, Claremont, California 91711

Human face perception requires a network of brain regions distributed throughout the occipital and temporal lobes with a right hemisphere advantage. Present theories consider this network as either a processing hierarchy beginning with the inferior occipital gyrus (occipital face area; IOG-faces/OFA) or a multiple-route network with nonhierarchical components. The former predicts that removing IOG-faces/OFA will detrimentally affect downstream stages, whereas the latter does not. We tested this prediction in a human patient (Patient S.P.) requiring removal of the right inferior occipital cortex, including IOG-faces/OFA. We acquired multiple fMRI measurements in Patient S.P. before and after a preplanned surgery and multiple measurements in typical controls, enabling both within-subject/across-session comparisons (Patient S.P. before resection vs Patient S.P. after resection) and between-subject/across-session comparisons (Patient S.P. vs controls). We found that the spatial topology and selectivity of downstream ipsilateral face-selective regions were stable 1 and 8 month(s) after surgery. Additionally, the reliability of distributed patterns of face selectivity in Patient S.P. before versus after resection was not different from across-session reliability in controls. Nevertheless, postoperatively, representations of visual space were typical in dorsal face-selective regions but atypical in ventral face-selective regions and V1 of the resected hemisphere. Diffusion weighted imaging in Patient S.P. and controls identifies white matter tracts connecting retinotopic areas to downstream face-selective regions, which may contribute to the stable and plastic features of the face network in Patient S.P. after surgery. Together, our results support a multiple-route network of face processing with nonhierarchical components and shed light on stable and plastic features of high-level visual cortex following focal brain damage.

Key words: **brain lesion; cortical plasticity; face perception; fusiform face area; hierarchical networks; occipital face area**

Significance Statement

Brain networks consist of interconnected functional regions commonly organized in processing hierarchies. Prevailing theories predict that damage to the input of the hierarchy will detrimentally affect later stages. We tested this prediction with multiple brain measurements in a rare human patient requiring surgical removal of the putative input to a network processing faces. Surprisingly, the spatial topology and selectivity of downstream face-selective regions are stable after surgery. Nevertheless, representations of visual space were typical in dorsal face-selective regions but atypical in ventral face-selective regions and V1. White matter connections from outside the face network may support these stable and plastic features. As processing hierarchies are ubiquitous in biological and nonbiological systems, our results have pervasive implications for understanding the construction of resilient networks.

Introduction

Visual recognition requires a series of processing stages along the ventral visual pathway of the human brain ascending from primary visual cortex to occipitotemporal cortex (Ungerleider and Mishkin, 1982; Felleman and Van Essen, 1991; Kravitz et al., 2013). Understanding the structural-functional organization of this pathway is a major neuroscientific goal. Human face perception is of unique interest to achieve this goal because faces are the most socially meaningful stimuli in our environment; and as such, face perception recruits a series of cortical regions responding more strongly to faces than nonfaces extending from lateral occipital cortex to ventral aspects of the temporal lobe, with a

right hemisphere dominance (Sergent et al., 1992; Puce et al., 1995; Haxby et al., 2000; Fox et al., 2008; Rossion, 2008; Pitcher et al., 2011a; Zhen et al., 2013; Duchaine and Yovel, 2015). A subset of these regions composes the "core" face network (Haxby et al., 2000): the inferior occipital gyrus/occipital face area (IOG-faces/OFA) (Gauthier et al., 2000; Weiner and Grill-Spector, 2010), the fusiform gyrus (FG)/fusiform face area (FFA) (Kanwisher et al., 1997), which can be divided into separate regions on the posterior and mid-fusiform gyrus (Pinsk et al., 2009; Weiner and Grill-Spector, 2010), and regions along the superior temporal sulcus (STS) (Puce et al., 1998; Pinsk et al., 2009; Pitcher et al., 2011b). The prevailing neurofunctional model of face perception (Haxby et al., 2000; Fairhall and Ishai, 2007) proposes that this "core" face network is organized hierarchically, which suggests that neural computations in regions of the face network follow and depend on computations performed by what is considered the input of the entire network: IOG-faces/OFA.

However, the hierarchical model of the face network has been questioned by studies showing face-selective responses within the FG and STS, even in the absence of face-selective responses in the IOG, both in participants with unilateral or bilateral lesions to the IOG (Rossion et al., 2003; Steeves et al., 2006) and healthy participants (Rossion et al., 2011; Pitcher et al., 2014). These findings have inspired alternative nonhierarchical models of the face network (Rossion, 2008; Atkinson and Adolphs, 2011; Pitcher et al., 2011a; Duchaine and Yovel, 2015; Yang et al., 2016), suggesting that information can reach more anterior regions of the face network without the IOG. Although fMRI studies in patients with long-term brain damage provide causal support for these nonhierarchical proposals, functional measurements in these patients are conducted years after the damage has occurred, with no baseline measurement before the lesion. Consequently, a putative normative state of the functional region or network of interest before damage is assumed rather than known. Further, it is impossible to know whether any reorganization has occurred during the prolonged time interval between the damage and eventual measurement. An appealing alternative to directly test hierarchical and nonhierarchical models of the face network is a functional neuroanatomical investigation of the face network before and after surgical removal of the right IOG. However, this approach is largely impossible in humans due to the rarity of fMRI measurements before a preplanned surgery (Gaillard et al., 2006).

Here, we present a unique case in which a patient (Patient S.P.) required focal resection of the right IOG, including IOG-faces/OFA. We examined the functional organization of the cortical face network before and after removal of the right IOG using numerous methods: (1) multiple sessions of fMRI, (2) intracerebral electrophysiology (iEEG), (3) neuropsychological testing, and (4) diffusion weighted imaging (DWI) with tractography.

Received Dec. 16, 2015; revised June 21, 2016; accepted June 22, 2016.

Author contributions: K.S.W., J.J., L.M., K.G.-S., and B.R. designed research; K.S.W., J.J., L.M., H.B., G.H., C.J., A.S., M.A.B., K.G.-S., and B.R. performed research; K.S.W., J.J., J.G., C.J., S.C.-C., A.S., M.A.B., K.G.-S., and B.R. contributed unpublished reagents/analytic tools; K.S.W., J.J., J.G., C.J., D.L., A.S., M.A.B., K.G.-S., and B.R. analyzed data; K.S.W., J.J., K.G.-S., and B.R. wrote the paper.

This work was supported by National Institutes of Health 1R01 EY 02391501A1 to K.G.-S., ERC Grant facessvep 284025 to B.R., the Belgian National Fund for Scientific Research, and Belgian Science Policy Office.

The authors declare no competing financial interests.

*K.G.-S. and B.R. contributed equally to this study.

Correspondence should be addressed to Dr. Kevin S. Weiner, Department of Psychology, Stanford University, Stanford, CA 94305. E-mail: kweiner@stanford.edu.

DOI:10.1523/JNEUROSCI.4509-15.2016

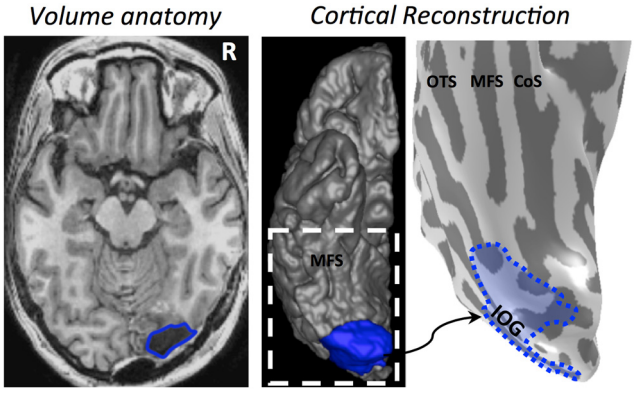

Figure 1. Reconstructing the resection. The resection (blue) included the IOG and surrounding cortex. After aligning the preoperative and postoperative anatomies, we projected the resected tissue onto the presurgical anatomy. All analyses were done on the pre-resection anatomy. Left, Axial slice of the post-resection T1. Middle, Reconstruction of the postoperative cortical surface and resected tissue (blue). White dotted line indicates the zoomed portion in the rightmost image. Right, Inflated preoperative cortical surface with the aligned resected cortex shaded in blue. CoS, Collateral sulcus; MFS, mid-fusiform sulcus; OTS, occipitotemporal sulcus.

This combinatorial approach directly examines how physically removing the putative input to a cortical hierarchy in the living human brain affects the neurofunctional organization of downstream regions compared with the original state of the network, as well as presents a unique opportunity to causally test the hierarchical and nonhierarchical models of the face network. The former predicts a detrimental effect of resection on downstream face-selective regions, whereas the latter predicts resiliency of downstream face-selective responses despite the removal of right IOG-faces/OFA.

Materials and Methods

Patient S.P.

Patient S.P. is a 36-year-old right-handed woman who had refractory epilepsy related to a right benign dysembryoplastic neuroepithelial tumor. The tumor involved the right occipital pole and extended to the infracalcarine region. Patient S.P. is a high-functioning patient: (1) before resection, she had an IQ of 98, her visual field was normal, and her scores on the Visual Object and Space Perception battery assessing basic visual functions (Warrington and James, 1991) were maximal for all 8 subtests; (2) she works as a pharmacist and has a high level of education (baccalauréat + 6 in France, totaling 18 years of studies since she was 6 years old); and (3) as far as we know, she has a typical social life, interacting with her family, colleagues, and friends.

The iEEG delineated the seizure onset zone within the tissue related to the tumor. The epileptic onset zone did not involve IOG-faces/OFA. Anatomically, surgical resection involved the tumor zone and surrounding cortex, including the IOG, posterior FG, and portions of the lateral occipitotemporal cortex (Fig. 1). Two years after the operation, the patient remains seizure-free. Written consent was obtained from Patient S.P., and the procedures were approved by the local ethical committee of the University Hospital of Nancy for clinical protocols.

fMRI

fMRI data acquisition

Exclusive to our case, we acquired multiple fMRI sessions before and after resection to distinguish the effect of resection from session-to-session variability. Patient S.P. participated in five fMRI sessions (S1, S2, S3, S4, and S5) on different days. S1 and S2 were presurgical. S3, S4, and S5 were postsurgical. S1 and S2 were 30 and 4 d before surgery, respectively. S3, S4, and S5 were 30 d, 8 months, and 18 months after surgery, respectively. In S1, S2, S3, and S4, Patient S.P. participated in multiple runs of a block design experiment designed to measure responses to different visual categories. In S1, Patient S.P. also participated in a stan-

dard retinotopic mapping experiment, as well as an event-related experiment using images of faces, cars, and their phase-scrambled counterparts. In S5, Patient S.P. participated in an experiment during which images of faces, limbs, and houses appeared at fixation or 3° to the right or left of fixation (3 position experiment).

All functional and anatomical imaging sessions were performed on the same 3 Tesla GE scanner (Signa HDXT, GE Medical Systems) at the University Hospital of Nancy (Nancy, France) using an 8-channel head coil. In S1, we acquired 38 slices at a resolution of 3.75 × 3.75 × 3.5 mm using a standard EPI sequence (FOV = 240 mm, TE = 35 ms, TR = 2000 ms, flip angle = 90°). In S2-S5, we acquired 36 slices at a resolution of 3 × 3 × 3 mm using a standard EPI sequence (FOV = 192 mm, TE = 33 ms, TR = 2000 ms, flip angle = 77°). In S2-S5, inplane anatomicals were also acquired with the same slice prescription as the functionals using a T1-weighted SPGR pulse sequence (FOV = 192 mm, TE = minimum, flip angle = 25°). In all sessions, high-resolution anatomical volumes of the whole brain were acquired using a T1-weighted SPGR pulse sequence (resolution: 1 × 1 × 1 mm), which was used to create reconstructions of the cortical surface.

fMRI experiments

Localizer, block experiment. Patient S.P. participated in 3 runs of this experiment in S1, 2 runs in S2, and 2 runs in two of the postsurgical scanning sessions (S3, S4). During the fMRI scan, she viewed images of faces, limbs, places, objects, and phase-scrambled images. Exemplars appeared in variable viewing conditions and were not repeated across runs. Each run was 288 s long, consisted of randomized 12 s blocks of each condition (3 per condition), and contained 8 blank blocks. Each run began and ended with 12 s of blank. Patient S.P. performed a 1-back task as in our prior experiments (Weiner and Grill-Spector, 2010, 2011, 2013; Weiner et al., 2014).

Localizer, event-related experiment. Patient S.P. participated in 3 runs of this experiment in presurgical S1. Images of faces, cars, and phase-scrambled images were presented for 2.25 s, followed by a 7.75–11.25 s blank interval. Each run lasted 504 s, during which 11 images of each type (44 in total) were presented. Images were not repeated within or across runs.

Traveling wave retinotopy experiment. Patient S.P. participated in standard retinotopic mapping (Engel et al., 1997) in S1. While fixating, she participated in 2 runs during which she viewed rotating black-and-white checkerboard wedges or expanding checkerboard rings. Patient S.P. was instructed to fixate on a central cross and respond by button press when the fixation cross changed colors.

Three position experiment. During S5, Patient S.P. participated in an experiment designed to measure fMRI responses to contralateral and ipsilateral stimuli. During fMRI, images of faces, houses, and limbs appeared in three positions: (1) at fixation, (2) 3° of visual angle to the left of fixation, and (3) 3° of visual angle to the right of fixation. Exemplars appeared in variable viewing conditions within 4 s blocks for 3 runs. Each run was 200 s long, consisted of randomized blocks of each condition (4 per condition), and contained 12 blank blocks. Each run also began and ended with 4 s of a blank screen. Patient S.P. was instructed to fixate on a central cross and respond by button press when the fixation changed color.

fMRI data analysis

Data were analyzed with MATLAB (The MathWorks) using the mrVista toolbox (http://white.stanford.edu/software). Presurgical and postsurgical T1 scans were aligned to the AC-PC plane. Automated (Dale et al., 1999) (FreeSurfer: http://surfer.nmr.mgh.harvard.edu) and manual (ITK-SNAP: http://www.itksnap.org/pmwiki/pmwiki.php) segmentation tools were used to segment gray and white matter, from which we reconstructed the cortical surface (Wandell et al., 2000). For visualization, data were projected to the presurgical anatomy after aligning presurgical and postsurgical volumes and determining resection boundaries from postsurgical scans (Fig. 1). Functional data of each session were motion corrected and temporally high-pass filtered with 1/20 Hz cutoff and converted to percentage signal change. Response amplitudes were estimated using a GLM applied to the time-series of each voxel using as predictors the experimental conditions convolved with the hemodynamic impulse response function used in SPM. Data were not spatially smoothed. A GLM was also used to generate *t* maps of selectivity showing significantly higher responses to one condition versus others.

Definition of face-selective regions of interest (ROIs). Four face-selective clusters were defined in the right hemisphere of Patient S.P. from the localizer experiment from 1 run in S1 with a contrast of faces > limbs, places, and objects ($t > 3$, voxel level) as in our prior studies (Weiner and Grill-Spector, 2010, 2013): (1) posterior fusiform (pFus)-faces/FFA-1, (2) IOG-faces/OFA, (3) posterior superior temporal sulcus (pSTS)-faces, and (4) mid superior temporal sulcus (mSTS)-faces. In the left hemisphere, we were able to identify mFus-faces/FFA-2, pFus-faces/FFA-1, and pSTS-faces in all sessions, but not the left IOG-faces/OFA in any session. We compared the localization of these activations before and after resection. Data from right hemisphere are presented in Figures 3–5, and 7, and data from the left hemisphere in Figures 6 and 7.

We were able to identify two additional regions in the right hemisphere in a subset of the sessions. Specifically, we were able to identify mFus-faces/FFA-2 (Weiner and Grill-Spector, 2010) only in one of the pre-resection sessions (Fig. 4). To test whether this was a measurability problem due to the ear canal artifact, we measured the time course signal-to-noise ratio (tSNR) in each run. A tSNR threshold of 35 is necessary to measure a statistically meaningful result given our resolution, magnetic strength, and scan duration (Murphy et al., 2007). However, in 3 of the 4 independent pre-resection runs in mFus-faces, tSNR was not significantly higher than the required tSNR for measurability (all p values >0.29). This is not specific to Patient S.P. as we have previously shown that MR artifacts induced by the ear canal can affect the measurability and tSNR of mFus-faces/FFA-2 (Weiner and Grill-Spector, 2013). Because mFus-faces/FFA-2 is unstable before resection, we do not include this region in our subsequent analyses. It is also important to reiterate that we can identify this region in Patient S.P. in the left hemisphere; this is because MR artifacts are not subject-specific, but hemisphere-specific, and can differentially affect the measurability of the same region across hemispheres (Weiner and Grill-Spector, 2013). Indeed, in Patient S.P., whereas the tSNR is low in right mFus-faces/FFA-2 across sessions as reported above, it is stable and >35 across sessions in left mFus-faces/FFA-2 (pre-resection tSNR mean ± SD: 102 ± 59; post-resection tSNR: 105 ± 28; these values are not significantly different, $p = 0.93$, paired t test).

We were also able to identify an additional region on the inferior occipital sulcus (IOS) in both pre-resection sessions (see Fig. 4). However, this region is typically not included in neurocognitive models of face perception as it does not respond specifically to faces but responds to animate stimuli more generally, as well as overlaps with nearby body-selective regions (Weiner and Grill-Spector, 2013). Indeed, responses to faces and bodies within the IOS were not significantly different in Patient S.P. (before resection, $p = 0.60$) or in a group of typical controls ($N = 10$, $p = 0.70$; see fMRI and diffusion weighted imaging in control subjects).

Mean response amplitudes and selectivity. Analyses of mean response amplitudes and selectivity were conducted on data that were independent from those used to define the ROIs. For the former, we first calculated mean response amplitudes estimated from GLM betas in each voxel and then averaged these responses across voxels in each ROI. For the latter, we first calculated face selectivity within each voxel as faces > other stimuli and then calculated the mean selectivity across voxels of each ROI within each run of the experimental session (see Figs. 3, 4, 6). Importantly, all analyses within right pFus-faces excluded resected portions to assure that comparisons before and after resection included the same voxels.

Reliability of face selectivity across voxels. To examine the reliability of face selectivity across voxels, we calculated the distributed face selectivity in each ROI for each run and then calculated the correlation (r) between distributed face selectivity of the ROI across sessions. We calculated these values three different ways in Patient S.P.: (1) between experimental runs across pre-resection sessions (see Fig. 5, red); (2) between experimental runs across post-resection sessions (see Fig. 5, black); and (3) between experimental runs across pre-resection and post-resection sessions (see

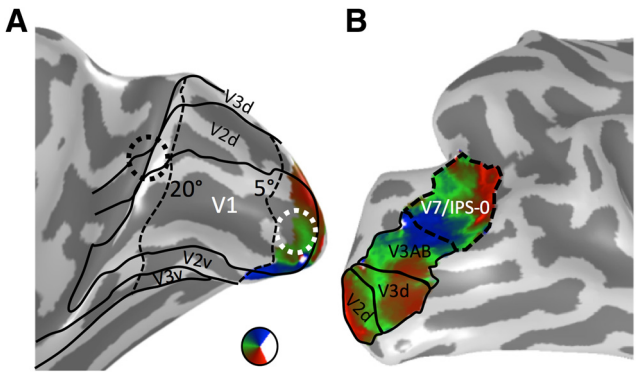

Figure 2. Retinotopic ROIs. ***A***, The polar angle map of V1 on the medial inflated cortical surface of Patient S.P. before resection. Our fMRI scanning setup allowed us to map eccentricities out to 5°. Representations of the far periphery (>20°) were defined from the cortical sheet using recently published tools (Benson et al., 2014). We defined two ROIs for white matter tracking: the central 5° of V1 (white circle) and eccentricities outside the postsurgery scotoma (beyond 20°, black circle). ***B***, Polar angle maps from V2d to V7/IPS-0 on the lateral inflated cortical surface of Patient S.P. before resection. V7/IPS-0 (dashed line) was used for identifying potential vertical white matter tracts reaching pFus-faces.

Fig. 5, blue). We calculated these reliability metrics for right pFus-faces, pSTS-faces, and mSTS-faces.

Definition of retinotopic ROIs. We delineated retinotopic visual areas V1-V7/IPS-0 from the traveling wave retinotopic experiment conducted before resection in S1 (Fig. 2). Because of limitations of the scanner setup, we could only map visual field representations within the central 5°. V1 was used for examining visual field representations in the three position experiment, and to define ROIs for DWI tracking of white matter tracts between early visual cortex to downstream face-selective regions. V7/IPS-0 ROI was defined for white matter tracking of vertical tracts to the fusiform. Additionally, we used cortex-based alignment techniques to align templates of early visual regions V1-V3 (Benson et al., 2012, 2014) to Patient S.P.'s cortical surface to delineate the entire eccentricity representation of these regions (Fig. 2*A*).

Visual field preference (3 position experiment). Within V1, pFus-faces, mSTS-faces, and pSTS-faces, we calculated the visual field preference in response to stimuli presented in the right and left visual field in each voxel by calculating the *t* value comparing responses to stimuli in the left versus right visual field collapsed across categories. Negative numbers indicate preference for the left visual field (expected for right hemisphere ROIs), and positive numbers indicate preference for the right visual field (expected for left hemisphere ROIs). We report the distribution of these visual field preferences across all voxels of an ROI separately for the right, resected hemisphere and the left, nonresected hemisphere. We assessed differences in visual field preferences in the left versus right ROIs using a Kolmogorov–Smirnov test.

DWI

Data acquisition. We acquired DWI in S1, S3, and S4 using a diffusion-weighted, single-shot echo-planar imaging sequence: presurgery/postsurgery S1 and S3 parameters: 25 diffusion directions, b = 1000 s/mm^2, resolution of 2 × 2 × 2 mm; postsurgery S4 parameters: 64 diffusion directions, b = 2000 s/mm^2, resolution 2 × 2 × 2.6 mm.

Data analysis. Eddy-current distortions and subject motion were corrected and removed using a constrained 14-parameter nonlinear coregistration method according to the eddy-current distortions created by the specific phase-encoded direction of the acquired data. Diffusion-weighted images were registered to the non–diffusion-weighted (b0) image using a two-stage coarse-to-fine approach to maximize mutual information. The b0 image was aligned to the T1 image with a rigid body algorithm. All processing was performed using Stanford University's open-source mrDiffusion package (http://white.stanford.edu/software).

We performed whole-brain white matter tractography using MRtrix software (Tournier et al., 2007, 2012). Each white matter voxel was used as a seed of origin for fiber tracking, and a constrained-spherical deconvolution (as in Gomez et al., 2015) model of diffusion was fit at every voxel within white matter. Fibers were traced within a white matter mask using the probabilistic tractography implementation within MRtrix using 600,000 seedpoints and a maximum harmonic envelope of 4 was used to model crossing fibers.

Candidate white matter bundles were extracted by intersecting the optimized connectome with volume ROIs. ROIs were constructed by dilating each functional ROI in each subject's native brain space, with a 3-voxel smoothing kernel to encompass the neighboring white matter voxels. Candidate pathways interconnecting two ROIs were extracted from the whole brain connectome through Boolean 'AND' operations.

Examining white matter tracts between early visual areas and face-selective regions. Recent results show that face-selective regions on the IOG and STS are structurally connected to the calcarine sulcus via longitudinal white matter tracts (Gschwind et al., 2012). However, it is likely that these tracts originate separately from the foveal and peripheral representations of early visual areas. Indeed, nonhuman primates have anatomical connections from the periphery of V1/V2 to the periphery of MT (Desimone and Ungerleider, 1986). It is feasible that STS face-selective regions may be structurally connected to the periphery of early visual areas as these regions are adjacent to the periphery of MT in humans (Weiner and Grill-Spector, 2013). Thus, we examined both sets of longitudinal white matter tracts connecting (1) an ROI within the central 5° of V1 (Fig. 2*A*) and ventral face-selective regions (IOG-faces and pFus-faces, respectively) and (2) an ROI overlapping eccentricities >20° of early visual areas (Fig. 2*A*) and STS face-selective regions (pSTS-faces and mSTS-faces). For tracking, we refer to these ROIs as V1/V2 because growing these ROIs as spheres into white matter likely encroached into portions of V2.

Recent results also show that the posterior fusiform is connected to dorsal retinotopic regions via vertical white matter tracts (Kim et al., 2006; Takemura et al., 2016). As the latter study revealed that these tracts are part of the vertical occipital fasciculus (VOF) (Yeatman et al., 2014; Takemura et al., 2016; Weiner et al., 2016) and connect hV4 ventrally to retinotopic maps dorsally extending to V7/IPS-0, we also examined whether portions of the VOF connect V7/IPS-0 (Fig. 2*B*) to pFus-faces. The VOF was defined by including all fibers terminating in posterior aspects of ventral occipitotemporal cortex with a vertical to horizontal length ratio of ≥1.3 (Yeatman et al., 2014).

Mapping fiber endpoints to the resected volume. It is difficult to acquire DWI data following stroke or cortical damage due to artifacts in the diffusion signal as a result of increased diffusivity surrounding the damage (Pasternak et al., 2009). Consistent with these prior reports, the resected tissue generated significant artifacts in and around the resection, which prevented us from being able to accurately track longitudinal fiber tracts to the FG in post-resection scans S3 and S4. Despite these difficulties, to gain clarity regarding how connectivity of the face network is affected by the loss of connections associated with IOG-faces/OFA, we mapped the pre-resection cortical endpoints of the tracts from early visual cortex to either IOG-faces/OFA or pFus-faces/FFA-1 to the post-resection volume (see Fig. 8). In contrast to the artifacts affecting ventral longitudinal tracts, the resection did not affect DWI signals in dorsal longitudinal tracts or vertical tracts in Patient S.P. (see Figs. 9, 10).

iEEG

IEEG recording was performed to identify the epileptogenic zone, using intracerebral electrodes (stereo-EEG) (Bancaud and Talairach, 1973). The iEEG was performed once, 6 months before resection. Electrode implantation sites were chosen according to noninvasive data collected during the earlier phase of the investigation to localize and delineate the zone of epileptic seizure onset and early propagation. Nine electrodes were placed in the right hemisphere targeting the hippocampus, the rhinal cortex, the ventral occipitotemporal cortex (lingual gyrus, collateral sulcus, fusiform gyrus, and occipitotemporal sulcus), the occipital pole, the calcarine sulcus, and the occipitoparietal junction. One electrode was placed in the left hemisphere, in the middle ventral temporal region. Postimplant CT images were aligned to the preoperative MRI anatomical brain volume (Hermes et al., 2010). Electrodes were visualized on the subject's own

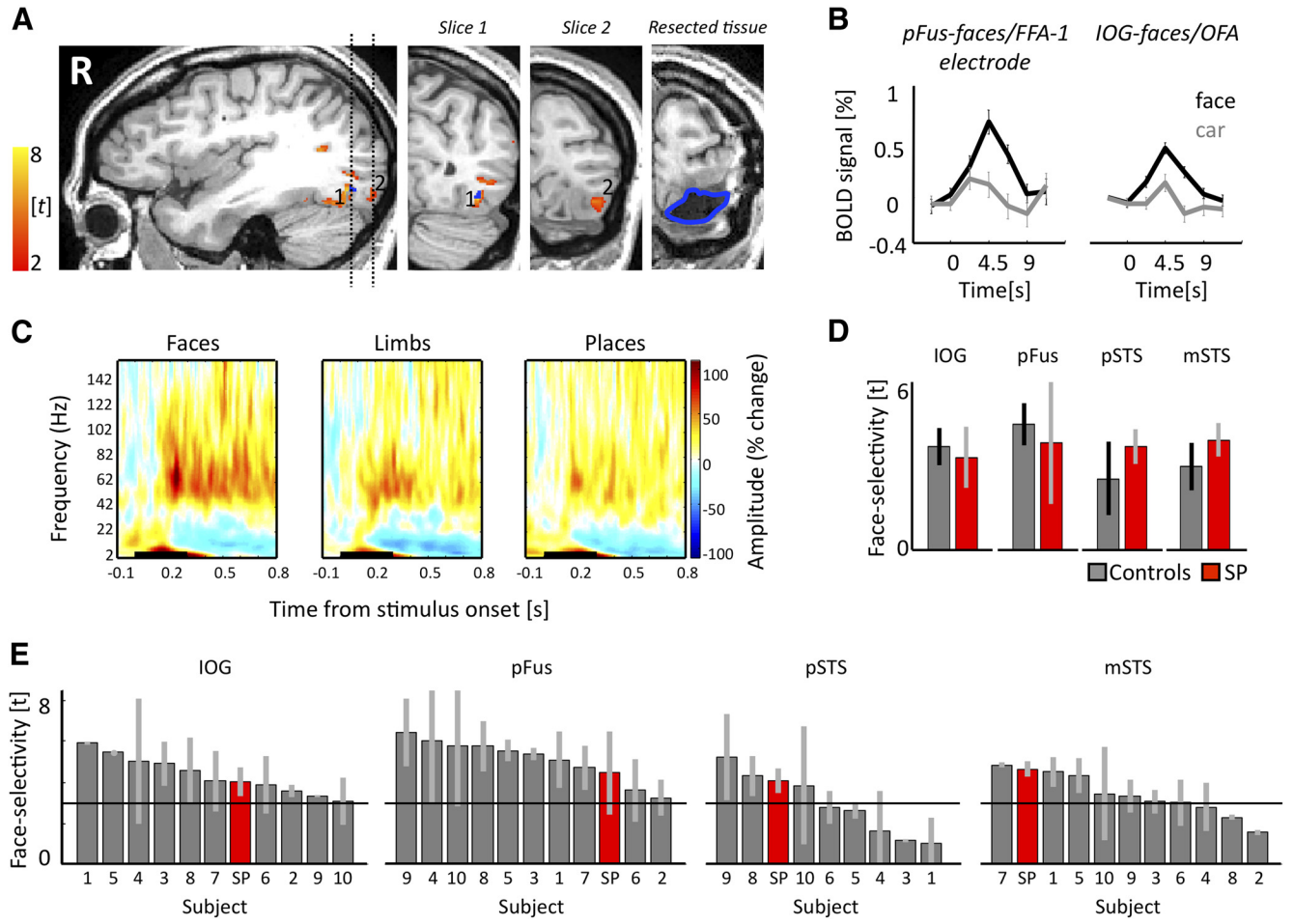

Figure 3. The face network is typical before surgery. ***A***, Regions illustrating face-selective responses ($t > 3$) before surgery. Blue represents intracerebral electrode within pFus-faces/FFA-1. Dotted lines indicate location of the two coronal slices shown on the right two panels. 1, pFus-faces/FFA-1; 2, IOG-faces/OFA. Blue outline indicates resected tissue on post-resection anatomy in similar position as slice at left. ***B***, fMRI response under electrode and from IOG-faces/OFA from an independent experiment. Error bars indicate SEM across runs. ***C***, Time-frequency responses of pFus-faces/FFA-1 electrode. Signal amplitude (% change from baseline) is averaged across trials and category. Black line indicates stimulus ON window (300 ms). High-frequency broadband responses showed significantly higher ($p < 0.005$) power to faces compared with limbs or places 150 ms after stimulus onset. ***D***, Mean face selectivity in controls (gray) and Patient S.P. (red) in the IOG ($N = 10$), pFus ($N = 10$), pSTS ($N = 8$), and mSTS ($N = 10$). Error bars for controls indicate mean and SD between runs averaged across subjects. Error bars for Patient S.P. indicate SD across 4 independent pre-resection runs. ***E***, Mean and SD of face selectivity in individual controls (gray) and Patient S.P. (red) in the IOG ($N = 10$), pFus ($N = 10$), pSTS ($N = 8$), and mSTS ($N = 10$). Each bar indicates data from one participant. The *x*-axis is ranked in a descending order to indicate where Patient S.P. falls in the distribution of typical participants. Error bars indicate SD between runs. Solid black line indicates the statistical threshold ($t > 3$) used to define each region from independent data.

brain volume and reconstructed 3D cortical surface allowing for accurate anatomical localization of electrodes (Fig. 3).

Category iEEG experiment. Patient S.P. viewed 50 black-and-white pictures of faces, body parts, places, and phase-scrambled faces in the hospital room at a distance of 70 cm from a computer monitor. In each trial, a stimulus was displayed at the center of the monitor for 300 ms, followed by an average intertrial interval of 1750 ms (1450–2050 ms). The patient fixated on a central cross and pressed a key when a face image was presented upside-down (9% of trials). Patient S.P. performed 4 blocks of 77 trials with conditions randomized within each block.

Data acquisition and analysis. The iEEG signal was recorded at 512 kHz using a 128-channel amplifier (2 SD LTM 64 Headbox; Micromed) relative to a prefrontal scalp reference electrode. Continuous EEG data were notch-filtered to remove line noise (50 Hz and harmonics) and segmented in −1.8 to 1.8 s epochs centered on the onset of each trial. Noisy trials in which signal amplitude in a −0.6 to 0.4 s time-window was >3.3 or <3.3 times the across-trial SD were discarded. The signal at each electrode was then rereferenced to the average of all intracranial electrodes. Variations in signal amplitude as a function of time and frequency were estimated using a Morlet wavelet approach as in prior studies (Jacques et al., 2016). Face selectivity was tested by comparing the response amplitude in the high-frequency broadband range (40–100 Hz) elicited by face images compared with place and body part images. Statistical significance was calculated using permutation tests at each time sample of the response between −0.1 and 0.8 s relative to stimulus onset. This process was performed 10,000 times to generate a distribution. Differences at a $p < 0.01$ (two-tailed) that lasted for at least 4 consecutive time samples were considered significant.

Neuropsychological assessment

We conducted a stringent battery of behavioral tests on subject Patient S.P. before (11 months) and after (1 month) cortical resection to assess her general cognitive function, basic visual perception, as well as face and object perception and recognition. These tests included full-scale IQ testing (WAIS-IV), basic visual perception testing (Visual Object and Space Perception battery), and visual field tests. We also implemented a face/no face categorization test with Mooney faces during which participants categorized upright or inverted two-toned black-and-white face profiles as a face or not a face (Busigny et al., 2010). Finally, we implemented five tests of face individuation as follows: (1) The classical neuropsychological Benton Face Recognition Test. Subjects were required to match a face among distractor faces varying in viewpoint and lighting (in this test, all faces are shown simultaneously) (Benton et al., 1983). (2) An old/new face recognition test (Busigny et al., 2010). Subjects viewed a series of face

images during a study phase; and then during a test phase, they were presented with new and old images and were asked to respond whether each image was old or new. (3) The Cambridge Face Memory Test (Duchaine and Nakayama, 2006). Subjects first studied 6 faces. Then, in 72 trials, subjects were asked to identify which of three faces was one that they had previously studied. Throughout the experiment, trials became increasingly harder as faces were shown in new views, illuminations, and with added noise. (4) Face matching across viewpoints (Busigny et al., 2010). Subjects were shown a frontal face on the top of the screen and two three-quarter views of faces below. They were then asked to indicate which of the two three-quarter probes on the bottom were the same as the frontal view on top. (5) Delayed face matching of upright and inverted faces (Busigny et al., 2010).

It should be noted that, when asked specifically about her face recognition abilities a few months before the operation (at the time of the SEEG implantation), Patient S.P. acknowledged that she "had never been very good at recognizing people from their face." We should, however, remain cautious with such statements, given that there is little relationship between subjective reports of face recognition abilities and behavioral measures of face matching and face memory, such as the Cambridge Face Memory Test (Palermo et al., 2016). Five control female participants (age, sex, and education level matched) also participated in two behavioral sessions taken 12 months apart to assess any variations in test-retest performance on these behavioral tests. The modified *t* test of Crawford-Howell for single-case studies (Crawford and Howell, 1998) was used to compare the results of Patient S.P. and controls. Five typical control female subjects 31–40 years of age (mean age 35 ± 4.6 years) participated in behavioral testing S1. Four of these subjects (mean age 36 ± 5.5 years) participated in a second behavioral testing session a year later.

fMRI and DWI in control subjects

Subjects. Ten adults (19–45 years old; 3 females; all right-handed) were recruited to serve as controls for the selectivity and reliability analyses. All participants were scanned at Stanford University and gave their written informed consent. Procedures were approved by the Stanford Internal Review Board on Human Subjects Research.

Scanning. Subjects were scanned on a 3T GE scanner at the Center for Neurobiological Imaging at Stanford University.

Anatomical brain volumes. A high-resolution anatomical volume of the whole brain was acquired with a T1-weighted BRAVO pulse sequence (TR = 450 ms, flip angle = 12°, 1 NEX, FOV = 240 mm, resolution: 1.0 mm isotropic).

fMRI. Because the comparisons of Patient S.P.'s brain responses were conducted across sessions, all individuals participated in two fMRI scanning sessions. Participants were scanned using a T2* sequence (TE = 30 ms, TR = 2000 ms, flip angle = 77°, bandwidth = 128 kHz, resolution: 2.4 mm isotropic voxels, 34 slices, FOV = 192 mm).

Functional localizer. Participants viewed a block design experiment consisting of images of faces and nonface categories presented at 1 Hz. The nonface categories were as follows: places (houses/corridors), bodies, limbs, characters (pseudowords/numbers), and objects (cars/guitars). Participants were instructed to respond by button press when a phase-scrambled image appeared (Stigliani et al., 2015). Subjects participated in 2 runs in S1 and 2 runs in S2 using different stimuli.

fMRI data analysis. Data were analyzed with the same pipeline as described for Patient S.P.

ROI definition and mean selectivity measurements. IOG-faces (10 of 10 participants), pFus-faces (10 of 10 participants), pSTS-faces (8 of 10 participants), and mSTS-faces (10 of 10 participants) were defined as in Patient S.P. (threshold of $t > 3$, voxel level) and in our prior experiments (Weiner et al., 2010; Stigliani et al., 2015) using both anatomical and functional criteria for the mean selectivity analyses. Each ROI was defined in S1, and mean selectivity was calculated for runs 1 and 2 in S2 (Fig. 3*E*; error bars indicate SDs between runs 1 and 2). It is important to underscore that only the categories overlapping with Patient S.P.'s experiment (faces, limbs, objects, and houses) were used to calculate selectivity.

ROI definition and reliability measurements. Because we only had 4 runs for each control subject (2 runs in S1 and 2 runs in S2), and to ensure that all data were independent, we defined ROIs from run 1 in S1 and calculated the reliability of face selectivity between run 2 in S1 and (1) run 1 in S2 and (2) run 2 in S2. This resulted in two measurements per subject. Because ROIs were now defined with only 1 run of data, mSTS-faces were only identifiable in 8 of 10 subjects. Reliability was calculated in the same way as in Patient S.P. as described above.

DWI. Because we identify a new pathway connecting V7/IPS-0 to pFus-faces/FFA-1 in Patient S.P., we sought to validate this pathway in control participants. Five (24–45 years old; 2 female; all right-handed) of our typical controls participated in 2 runs of a diffusion-weighted dual-spin echo sequence (60 slices, TE = 96.8 ms, TR = 8000 ms, 96 diffusion directions, b = 2000 s/mm^2, voxel size = 2 × 2 × 2 mm). Ten non–diffusion-weighted images were collected at the beginning of each scan.

DWI data analysis. Preprocessing was done as described above, and MRtrix probabilistic tractography was run using a harmonic envelope of 8 on the first diffusion dataset (as in Gomez et al., 2015). We statistically validated these new fibers connecting V7/IPS-0 and pFus-faces using LiFE (Pestilli et al., 2014). d' values >4 indicate statistically significant tracts, and the average of these tracts across subjects was 31.52 ± 4.13 (SD across subjects; see Fig. 10).

Results

Before surgery, Patient S.P.'s face network is not significantly different than control participants

Preoperatively, Patient S.P.'s face-selective regions are located on the IOG (IOG-faces/OFA), lateral FG (pFus-faces/FFA-1 and mFus-faces/FFA-2), as well as the posterior and main branches of the STS (pSTS-faces and, mSTS-faces, respectively; Figs. 3, 4), which is consistent with measurements of the face network in typical subjects (Weiner and Grill-Spector, 2013; Weiner et al., 2014). Independent measurements with event-related fMRI (Fig. 3*B*) and iEEG (Fig. 3*C*) show that the selectivity of these regions is also characteristic, manifesting as higher responses to faces than nonfaces ($p < 0.01$). IEEG recordings in pFus-faces/FFA-1 further showed characteristic latencies of this selectivity emerging at ~150 ms after stimulus onset (Allison et al., 1994; Parvizi et al., 2012).

To examine the typicality of Patient S.P.'s face network before resection with respect to face selectivity, we compared Patient S.P.'s face-selective regions with those of 10 healthy control participants. Independent analyses of mean selectivity in right hemisphere face-selective regions show that selectivity of Patient S.P.'s face network was not different from the mean selectivity in controls (modified *t* test of Crawford-Howell for single-case studies: all *t* values <1.9; all *p* values >0.10; Fig. 3*D*) or from selectivity in individual subjects (Fig. 3*E*). Additionally, comparison of the variability in measurements of selectivity across runs was also not different across Patient S.P. and controls in any of the face-selective regions (modified *t* test of Crawford-Howell for single-case studies comparing the differences between runs 1 and 2 in Patient S.P. and controls: all *t* values <0.72; all *p* values >0.50; Fig. 3*E*). It is important to underscore that, because of independent analyses, selectivity can be below the threshold used to define the voxels of the ROI (Fig. 3*E*, dotted line). This occurs in both Patient S.P. and controls, indicating that fluctuations of selectivity across runs occur whether the individual is a patient or not. Together, these pre-resection measurements validate that, at least as far as category selectivity is concerned, the cortical layout, response characteristics, selectivity, and run-to-run variability of Patient S.P.'s face network before resection are not significantly different from healthy controls.

Behavioral performance is stable before and after surgery

Behaviorally, before surgery, Patient S.P. was in the normal range for categorizing two-tone images as either faces or nonfaces

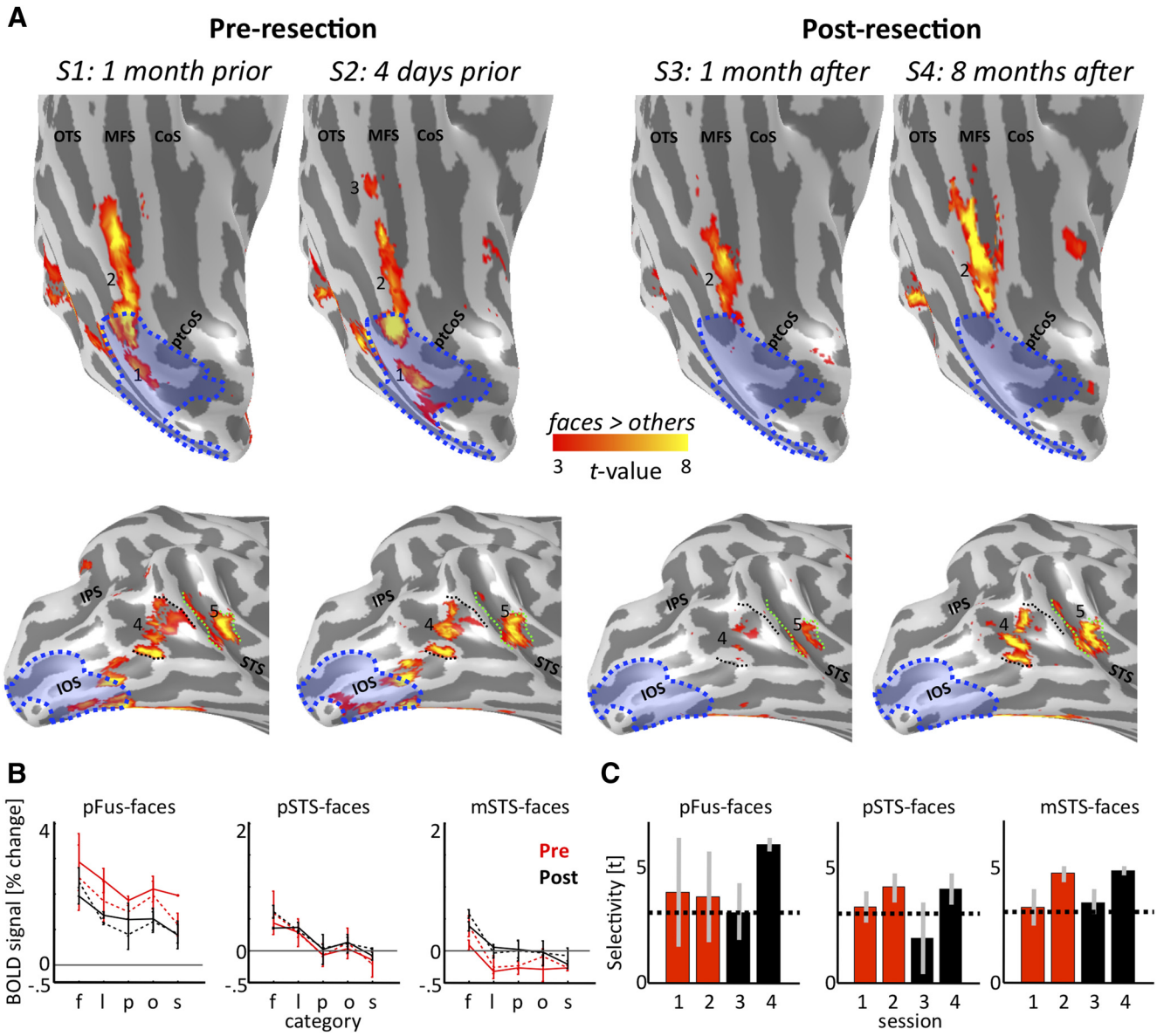

Figure 4. The face network is stable after resection. ***A***, The face network before and after resection on the inflated cortical reconstruction of the right hemisphere of Patient S.P. before resection. 1, IOG-faces/OFA; 2, pFus-faces/FFA-1; 3, mFus-faces/FFA-2; 4, pSTS-faces; 5, mSTS-faces. IOG-faces/OFA (1) and the posterior portion of pFus-faces/FFA-1 (2) have been resected. Blue shading represents resected cortex. Black represents superior and inferior extent of pSTS-faces in S1. Green represents posterior and anterior extent of mSTS-faces in S1. The unnumbered region on the lateral surface overlapping the IOS was also partially resected, but this region is not typically included in models of the face network because it exhibits comparable selectivity with other animate stimuli (see Materials and Methods). ***B***, Mean fMRI response amplitude (% change) as a function of category in face-selective regions before (red) and after (black) resection. Error bars indicate SDs across runs in each session. S1, S3, Solid. S2, S4, Dotted. f, Faces; l, limbs; p, places; o, objects; s, scrambled. Conditions are ordered by rank. ***C***, Face selectivity as a function of session. Error bars indicate mean selectivity across voxels of independently defined ROIs for run 1 and run 2 in each session. Error bars indicate SDs across runs in each session. Dotted line indicates the statistical threshold ($t > 3$) used to define each region from independent data. CoS, Collateral sulcus; IOS, inferior occipital sulcus; IPS, intraparietal sulcus; MFS, mid-fusiform sulcus; OTS, occipitotemporal sulcus; ptCoS, posterior transverse collateral sulcus.

(Mooney faces, Patient S.P.: 86.3%; age- and gender-matched controls: 90.3 ± 5%, no significant difference, $t = 0.677$, $p = 0.54$). Patient S.P. was also in the normal range on the old/new face recognition test (Patient S.P.: 90%; controls: 94 ± 3%, $t = 1.299$, $p = 0.132$). Although she performed well above chance level, she was impaired relative to controls on behavioral tasks requiring unfamiliar face individuation (Table 1). However, as illustrated in case studies in patients with long-term brain damage (Schiltz et al., 2006; Steeves et al., 2009), behavioral impairments in face individuation do not impede the ability to measure face-selective responses (i.e., faces > nonfaces) in high-level visual cortex. Thus, before surgery, Patient S.P. displayed an intact face network and abilities within the normal range for both remembering faces and categorizing faces from other stimuli.

After resection, Patient S.P. remained in the normal performance range for categorizing two-tone images as either faces or nonfaces (Mooney faces, Patient S.P.: 84.4%, no significant difference from age- and gender-matched controls: 92.8 ± 5%, $t = 1.439$, $p = 0.123$; Table 1). It is important to highlight that this is a difficult task and subjects cannot rely on local, low-level features to perform well. For example, a visual agnosic patient, such as Patient D.F., is at chance at this task, even when she can discern a face from an object in other formats (Steeves et al., 2006). Finally, Patient S.P. was not our worst subject, as one of our typical con-

Table 1. Behavioral performance of Patient S.P. and age- and gender-matched control participants

	Before operation	After operation (1 month)	Control participants	Control participants (1 year after)
Categorize upright/inverted Mooney faces	86.3%	84.4%	90.3% (±5.4)	92.8% (±5.2)
Old/new face memory test	90%	93.3%	94% (±2.8)	95% (±4.3)
Benton Face Recognition Test	35/54**	40/54**	44.6/54 (±3.6)	47.2/54 (±3.3)
Cambridge Face Memory Test	41/72**	40/72**	59.2/72 (±8.6)	59.2/72 (±10.4)
Face matching across viewpoints	65%*	64%*	82.2% (±7.0)	87% (±6.2)
Face matching				
Upright	80.6%*	80.6%*	95.5% (±1.5)	96.5% (±4.2)
Inverted	75%	77.8%	80.5% (±10.4)	75% (±8.2)
Age (yr)	36	36	35 ± 5	36 ± 5

*Impaired scores compared with normal controls ($p < 0.05$).

**Impaired scores according to Benton Face Recognition Test and Cambridge Face Memory Test scales.

trols scored less than Patient S.P. in this task. Given the present tests before and after resection, we believe an accurate interpretation of these results is that Patient S.P.'s ability to categorize a face as a face is intact.

Additionally, Patient S.P.'s IQ remained in the normal range (score: 101), and her score at all 8 tests of the Visual Object and Space Perception battery remained at ceiling. Patient S.P.'s ability to individuate faces was still below controls in several tasks but did not worsen following surgery, and her performance on the old/new face recognition memory task remained in the typical range (Patient S.P.: 93.3%; controls: 95 ± 4%, no significant difference, $t = 0.353$, $p = 0.374$; Table 1). Together, Patient S.P.'s behavioral performance in all of the face tasks was stable after compared with before surgery despite having a left hemianopic central scotoma after surgery.

The cortical layout of the face network is stable after resection of IOG-faces/OFA and the posterior portion of pFus-faces/FFA-1

The resection included the right IOG and portions of surrounding gyri, sulci, and white matter (Figs. 1, 3, 4). We aligned data from all fMRI sessions to the presurgical anatomy after defining the locus of the resected tissue (Figs. 1, 4). This approach revealed that all of IOG-faces and the posterior 23.3% of pFus-faces were surgically removed.

Surprisingly, after resection, the cortical topology and extent of pFus-faces in ventral temporal cortex (VTC) remained stable. Even the posterior portion of pFus-faces, which abutted the resection, was similar to its presurgery location. Regions along the STS displayed more variability after resection than regions in VTC (Fig. 4*A*, bottom). For example, 1 month after surgery, pSTS-faces and mSTS-faces were less activated than before surgery. However, 8 months after surgery, both regions were activated to a similar extent before surgery.

In contrast to the general stability of pFus-faces, pSTS-faces, and mSTS-faces in the resected hemisphere, we observed instabilities in the localization of mFus-faces/FFA-2 before resection and in a region on the IOS after resection. The instability of mFus-faces across sessions is likely driven by low tSNR from the ear canal artifact and not by the surgery, as the tSNR in mFus-faces before resection was lower than the minimum for reliable measurements (see Materials and Methods). Before resection, the IOS responded similarly to faces and bodies (no significant difference, $p = 0.60$) and was significantly modulated by visual stimuli (variance of the time-series explained by the GLM is 59.1 ± 8.9%). The surgery resected 26.9% of the IOS. Consequently, the variance of the IOS time-series explained by the GLM dropped close to zero (5.4 ± 2.0%) after resection, which was significantly ($p < 0.008$) lower than before surgery. This indicates that, after the resection, this region is not significantly modulated by visual stimuli modeled by the GLM. However, because the IOS is not included in traditional neurocognitive models of face perception and is also not strictly face-selective in either Patient S.P. or controls (see Materials and Methods), we focus the remainder of our analyses on pFus-faces, pSTS-faces, and mSTS-faces.

In addition to qualitatively examining the cortical topology of right pFus-faces, pSTS-faces, and mSTS-faces, we also quantitatively compared the mean response amplitudes and face selectivity within each region before and after resection. These analyses revealed that the resection differentially affected the mean BOLD response across face-selective regions. In pFus-faces, overall response amplitudes were lower after than before resection, whereas in mSTS-faces, the opposite was true; meanwhile in pSTS-faces, there was no substantial change in the overall signal level (Fig. 4*B*). Indeed, a three-way ANOVA with factors region (right pFus-faces/mSTS-faces/pSTS-faces), category, and resection (before resection/after resection) yielded a region × resection interaction ($F_{(2,90)} = 34.3$, $p < 10^{-3}$). Importantly, the

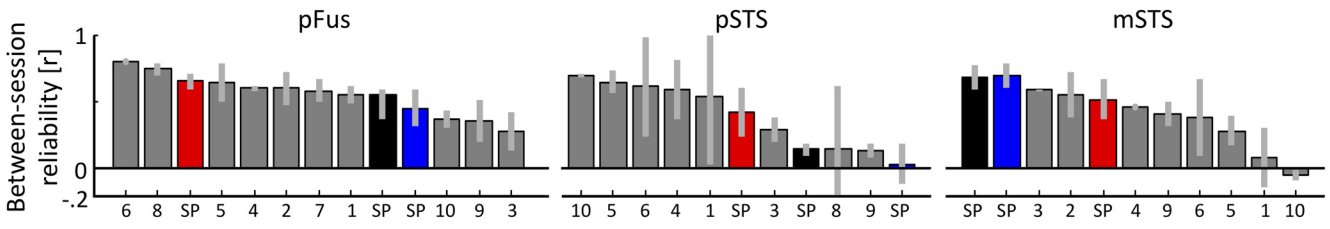

Figure 5. The reliability of distributed patterns of face selectivity in Patient S.P. is not significantly different than controls. Each bar represents data from a single subject and reflects the correlation between the distributed face selectivity in individual voxels across runs from two different sessions. Gray represents controls. Red represents Patient S.P. before resection. Black represents Patient S.P. after resection. Blue represents correlation between pre-resection and post-resection distributed face selectivity in Patient S.P. The *x*-axis is ranked in a descending order to indicate where Patient S.P. falls in the distribution of typical participants.

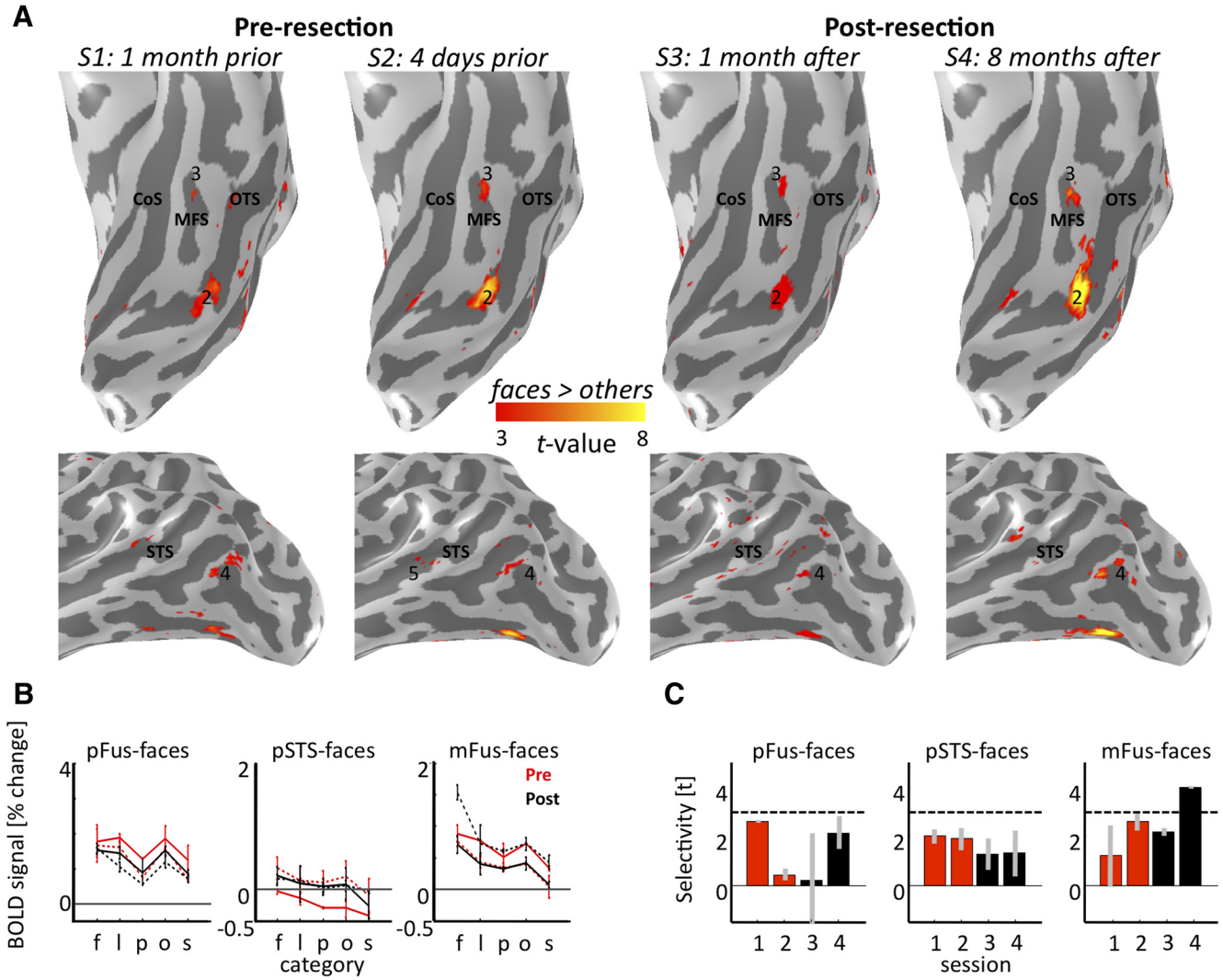

Figure 6. Weak face selectivity in the left hemisphere of Patient S.P. ***A***, Face-selective network in VTC (top) and LOTC (bottom) before resection and after resection projected to the inflated cortical reconstruction of the left hemisphere of Patient S.P. 2, pFus-faces/FFA-1; 3, mFus-faces/FFA-2; 4, pSTS-faces; 5, mSTS-faces. Left IOG-faces/OFA (1) could not be identified in any session, whereas left mSTS-faces (5) could only be identified in S2. CoS, Collateral sulcus; MFS, mid-fusiform sulcus; OTS, occipitotemporal sulcus. ***B***, ***C***, Same layout as Figure 4, but for face-selective regions in the left hemisphere. Red represents before surgery. Black represents after surgery. S1, S3, Solid. S2, S4, Dotted. f, Faces; l, limbs; p, places; o, objects; s, scrambled. Regions in the left hemisphere have lower face selectivity than the right hemisphere (Fig. 4).

resection only affected the overall magnitude of the signal but did not change the profile of response within each region (no region × category × resection interaction: $F_{(8,90)} = 0.27, p = 0.98$). Specifically, each ROI showed the same ranking of responses across categories of stimuli before compared with after resection.

Likewise, we find that all face-selective regions maintain significant face selectivity after the resection despite fluctuations in the magnitude of selectivity (Fig. 4*C*). A two-way ANOVA with factors region (right pFus-faces/pSTS-faces/mSTS-faces) and session (1/2/3/4) revealed a main effect of session ($F_{(3,12)} = 3.77, p < 0.04$). However, there were no significant differences in the level of selectivity after compared with before the resection (two-way ANOVA with factors of region (pFus-faces/pSTS-faces/mSTS-faces) and resection (before/after), no effect of resection, $F_{(1,18)} = .01, p = 0.9$). Importantly, after resection, both the mean selectivity (all t values <1.96; all p values >0.08) of each face-selective region in Patient S.P. and the fluctuations in selectivity between runs within each session (all t values <1.18; all p values >0.27) were not different than controls. These results indicate that, although there are fluctuations in the selectivity value across sessions (Fig. 4*C*), these fluctuations are comparable before and after resection, are comparable with controls (Fig. 3*E*), and are not due to a general increase or decrease in selectivity after surgery.

The present analyses underscore the importance of acquiring multiple functional measurements before and after resection. For example, in pSTS-faces and mSTS-faces, S1 (pre) and S3 (post) have comparable selectivity values, as do S2 (pre) and S4 (post; Fig. 4*C*). However, if we had only acquired a single session before and a single session after surgery, we would have arrived at different conclusions based on the particular combination of the subset of sessions we may have obtained. For instance, had we only acquired S1 and S4, we would have concluded that the resection increases selectivity. In contrast, had we only acquired S2 and S3, we would have arrived at an opposite conclusion: that the resection decreases selectivity. However, both of these conclusions are inaccurate. Instead, our data show that there are fluctuations in selectivity across sessions regardless of the resection.

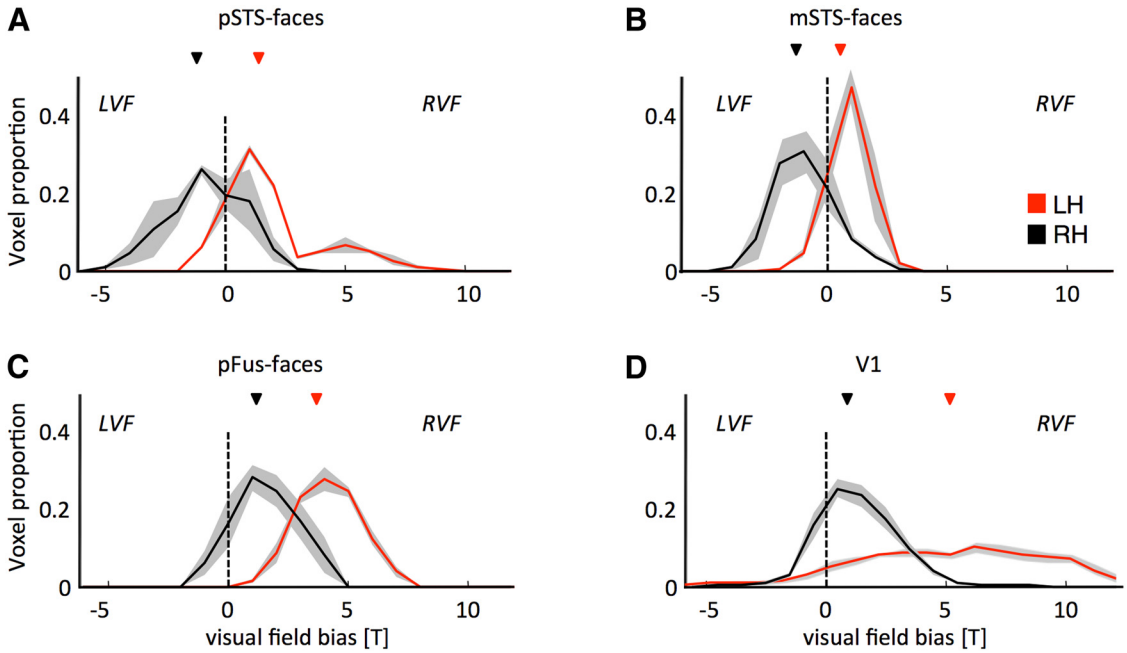

Figure 7. Typical contralateral bias in the superior temporal sulcus, but atypical ipsilateral bias in the fusiform gyrus and V1, after removal of IOG-faces/OFA. Histograms represent the proportion of voxels biased to the right visual field (positive *t* value) or the left visual field (negative *t* value) for functional ROIs in the right (black) and left (red) hemispheres. pSTS-faces and mSTS-faces in the resected hemisphere have the typical contralateral bias displayed by visual areas, whereas pFus-faces and V1 in the resected hemisphere have an unexpected ipsilateral bias. ***A***, pSTS-faces. ***B***, mSTS-faces. ***C***, pFus-faces. ***D***, V1. LH, Left hemisphere; LVF, left visual field; RH, right hemisphere; RVF, right visual field. Light gray shading represents SE across voxels.

The resection differentially affects the distributed pattern of face selectivity within regions of the face network surviving the resection

To complement our mean signal and mean selectivity analyses and to further quantify the stable and plastic features of pFus-faces, pSTS-faces, and mSTS-faces, we calculated the between-session reliability of distributed face selectivity across voxels within each face-selective region (see Materials and Methods). Before resection, the distributed patterns of face selectivity within right pFus ($r = 0.65 \pm 0.06$), pSTS ($r = 0.42 \pm 0.19$), and mSTS ($r = 0.51 \pm 0.15$) were positively correlated between each pair of experimental runs taken between pre-resection sessions (all p values $<10^{-4}$; Fig. 5, red). After resection, the reliability of distributed face selectivity across voxels was also positively correlated across experimental runs between sessions in pFus ($r = 0.45 \pm 0.11, p < 0.04$) and mSTS ($r = 0.70 \pm 0.09, p < 0.006$), but not in pSTS ($r = 0.14 \pm 0.05, p = 0.08$; Fig. 5, black). A two-way ANOVA with region and resection as factors revealed a main effect of region ($F_{(2,18)} = 17.1, p < 10^{-4}$), a borderline effect of resection ($F_{(1,18)} = 4.2, p = 0.06$), and a significant region × resection interaction ($F_{(2,18)} = 8.6, p < 0.002$). Thus, the resection differentially affected the distributed pattern of face selectivity within regions of the face network surviving the surgery.

While these analyses separately assess the stability of distributed face selectivity patterns before versus after resection, they do not directly quantify the relationship between face selectivity patterns before resection to after resection. To do so, we calculated the correlation among distributed patterns of face selectivity before resection compared with after resection. This analysis revealed two main findings. First, the distributed patterns of face selectivity were positively correlated between pre-resection and post-resection sessions in pFus ($r = 0.48 \pm 0.14$) and mSTS ($r = 0.68 \pm 0.10$; all p values $<10^{-4}$; Fig. 5, blue). In contrast, only 5 of 16 pre-resection and post-resection pairs had a positively correlated relationship in pSTS, and the average ($r = 0.03 \pm 0.15$) was not significantly different from zero ($t_{(15)} = 0.2, p = 0.85$). This decorrelated relationship can be interpreted as a change in the distributed pattern of face selectivity across voxels within pSTS-faces preoperatively and postoperatively. Second, the correlations between distributed face selectivity patterns pre-resection and post-resection sessions in Patient S.P. (Fig. 5, blue) were not significantly different from controls (Fig. 5, light gray) in pFus (all t values < 0.57, all p values >0.58), and mSTS (all t values <1.5; all p values >0.17). Even in pSTS, where we find a decorrelated relationship in distributed face selectivity between pre-resection and post-resection experimental runs, this difference was not significant compared with controls, as two of our controls also had nonreproducible distributed face selectivity across sessions (all t values <1.7, all p values >0.13).

These findings emphasize the value of pre-resection and post-resection assessments within the same patient in combination with benchmarks relative to controls. For example, if we only had post-resection measurements in Patient S.P., as is common in cases with patients that have long-term brain damage, we would have concluded that the reliability of face selectivity within pSTS-faces is within the range of controls. Although that is accurate, the incorporation of pre-resection measurements enable us to conclude that the distributed pattern of face selectivity in Patient S.P. is different after compared with before surgery within pSTS-faces, but not in other regions of the face network. These conclusions would not be possible without (1) multiple pre-resection and post-resection measurements in Patient S.P., (2) multiple scales of analysis (e.g., analyses of mean selectivity as well as distributed patterns across voxels), and (3) analogous measurements in multiple sessions in typical controls.

Examining the role of the left hemisphere in the post-resection stability of the face network

Our neuroimaging data indicate that the cortical layout and selectivity of the right hemispheric face network remained largely

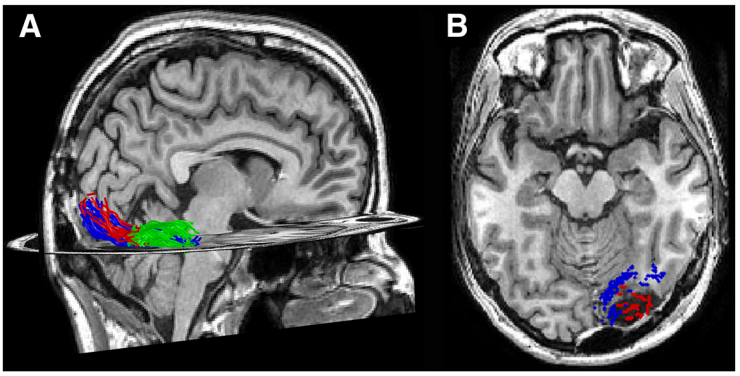

Figure 8. White matter tracts connecting early visual cortex to IOG-faces, but not pFus-faces, were likely resected. ***A***, Pre-resection measurement of white matter tracts connecting the central 5° of V1/V2 and pFus-faces/FFA-1 (blue) and IOG-faces/OFA (red), respectively, projected to the post-resection T1. White matter tracts connecting IOG-faces/OFA and pFus-faces/FFA-1 (green) are also depicted. ***B***, Axial slice illustrating endpoints of fascicles from the central 5° of V1/V2 to pFus-faces/FFA-1 (blue) and IOG-faces/OFA (red) projected onto the post-resection T1. The former largely run a more medial route, whereas the latter terminate directly into the resection.

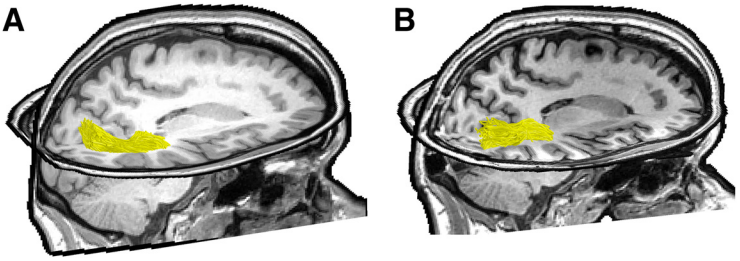

Figure 9. White matter fascicles extending from the periphery of early visual cortex likely contribute to the stability of STS face-selective regions postoperatively. White matter tracts (gold) connecting the far periphery (>20°) of V1/V2 and pSTS and mSTS face-selective regions, respectively, in the resected hemisphere. ***A***, Before surgery. ***B***, After surgery. To display the tracts clearly, functional regions are not shown.

stable following removal of the right IOG. Although this finding is consistent with predictions from a multiple route network with nonhierarchical components, it is also possible that this resiliency may be achieved via inputs from face-selective regions in the intact, left hemisphere. However, several pieces of evidence suggest that the resiliency of the right hemispheric face network is not driven by inputs from the left face network. First, it is unlikely that inputs from left IOG-faces support the stability of right pFus-faces because we were unable to identify IOG-faces in the left hemisphere in any session (Fig. 6*A*) and left IOG-faces is also not always detected in typical individuals (Zhen et al., 2015). Second, face selectivity in the left hemisphere (Fig. 6*C*) is consistently weaker than in the right hemisphere both before and after resection (three-way ANOVA with factors region, hemisphere, and resection yielded a main effect of hemisphere: $F_{(1,24)} = 19.9$, $p < 10^{-3}$, and no interactions: all F values <1.8; all p values >0.19). These findings are consistent with the literature showing a larger spatial extent, selectivity, and response amplitude to faces in the right compared with the left hemisphere (Sergent et al., 1992; Kanwisher et al., 1997; Rossion et al., 2012; Zhen et al., 2015).

To directly examine the role of the left hemisphere, we conducted an experiment in which the position of visual images from different categories was presented at the center, right, or left of fixation (see Materials and Methods). A characteristic feature of visual areas, including high-level visual regions (Hemond et al., 2007; Kay et al., 2015), is a contralateral preference for visual stimuli: that is, stronger neural responses to stimuli presented in the right visual field compared with stimuli presented in the left visual field in the left hemisphere and vice versa in the right hemisphere; this experiment directly tests the role of the left hemisphere in supporting the stability of the right hemispheric face-selective regions after resection. Based on prior evidence (Felleman and Van Essen, 1991), a contralateral preference in face-selective regions within the resected hemisphere likely reflects signals propagated through within-hemisphere connections. On the contrary, an ipsilateral preference would suggest that inputs from the left hemisphere affect responses in the resected hemisphere.

As expected, in the unresected, left hemisphere, face-selective regions showed a contralateral preference for stimuli in the right visual field. In the resected, right hemisphere, pSTS-faces and mSTS-faces also showed the characteristic contralateral preference for stimuli in the left visual field (Fig. 7*A*,*B*). However, even though the visual field preference in right pFus-faces is significantly different from left pFus-faces ($p < 10^{-3}$), it exhibited an ipsilateral, not a contralateral, preference (Fig. 7*C*). Although this suggests that inputs from the left hemisphere contribute to the stability of right pFus-faces, this reduced contralateral preference is already present in the central 5° of right V1 (Fig. 7*D*). Thus, the ipsilateral bias in pFus-faces in the right hemisphere likely originates in the central 5° of V1 of the right hemisphere (consistent with the postoperative central hemianopic scotoma), which then communicates signals downstream to right pFus-faces.

Together, these results show that: (1) the resiliency of the right hemispheric face network is likely not driven by inputs from the left face network; (2) the left hemisphere may play a role for the stability of right pFus-faces, but these signals may be communicated directly from right V1 to downstream right pFus-faces; and (3) the contributions of the left hemisphere cannot explain the entire resiliency of the face network because the face-selective regions of the STS maintain a contralateral bias after resection.

Longitudinal and vertical white matter tracts provide an anatomical infrastructure connecting early visual areas to FG and STS face-selective regions independent of IOG-faces/OFA

If the post-resection resiliency of the right hemisphere is largely not driven by inputs from the left hemisphere, are there white matter connections in the right hemisphere that enable signals to reach downstream face-selective regions? Prior studies have identified white matter tracts connecting early visual areas to downstream face-selective regions. For example, Gschwind et al. (2012) have identified separate longitudinal tracts from the calcarine sulcus to face-selective regions on the FG and STS, respectively. Additionally, Kim et al. (2006) have identified vertical tracts connecting dorsal retinotopic areas to face-selective regions on the FG. Thus, it seems plausible that these white matter tracts from outside the face network could provide an anatomical infrastructure supporting both the stable (e.g., face selectivity) and plastic (e.g., representation of visual

space in right pFus-faces) features of the face network following resection of IOG-faces/OFA. To test this hypothesis, we used DWI and tractography in Patient S.P. before and after resection (see Materials and Methods). DWI after resection enables testing whether these tracts are preserved postoperatively.

Supporting this hypothesis of bypass routes, we find evidence for both longitudinal and vertical tracts connecting early visual areas to downstream face-selective regions independent of IOG-faces. Before resection, we identified separate longitudinal white matter tracts connecting the central 5° of V1/V2 to IOG-faces/OFA (Fig. 8*A*, red) and to pFus-faces-FFA-1 (Fig. 8*A*, blue) in Patient S.P., which are consistent with prior research in typical subjects (Gschwind et al., 2012; Pyles et al., 2013). However, after resection, we could not measure these ventral longitudinal tracts in Patient S.P. due to diffusivity artifacts produced by the resection (see Materials and Methods). Nevertheless, to gain insight into what pathways might exist after resection, we projected the cortical endpoints of these pre-resection white matter tracts to the post-resection anatomy. This approach reveals that the tracts between early visual cortex and IOG-faces/OFA (red) terminate in the resected tissue and are likely to have been included in the resection. Comparatively, a majority of the tracts from early visual cortex to pFus-faces/FFA-1 (blue) terminate medially in the posterior FG largely outside the resected tissue (Fig. 8*B*). Thus, it is likely that these tracts exist after resection and contribute to the resiliency of pFus-faces/FFA-1 after resection.

To test whether there are white matter connections from early visual cortex to STS regions, we seeded an ROI in the far periphery (>20°) of V1/V2, which is outside the scotoma, and examined whether there are connections to STS regions. This analysis identified a set of longitudinal white matter tracts connecting the periphery of early visual cortex and STS face-selective regions both before and after resection (Fig. 9). These tracts may contribute to the preserved contralateral bias in STS regions after resection, as contralateral information originating in the periphery of early visual areas may be communicated through these preserved tracts to STS regions. Identifying white matter tracts connecting the periphery of V1/V2 to STS regions is consistent with evidence of anatomical connections from the periphery of V1/V2 to the periphery of MT in nonhuman primates (Desimone and Ungerleider, 1986). These connections have been postulated to convey signals about dynamic facial motion to the pSTS (O'Toole et al., 2002; Pitcher et al., 2014; Bernstein and Yovel, 2015), as pSTS abuts the peripheral representation of MT in humans (Amano et al., 2009; Weiner and Grill-Spector, 2013).

It is also possible that additional pathways within the right hemisphere provide inputs to STS face-selective regions via MT. These tracts may include within-hemisphere connections from mid-brain structures to MT bypassing V1, such as white matter tracts connecting the lateral geniculate nucleus (Ajina et al., 2015) and the superior colliculus (Ajina et al., 2015) to MT, as well as tracts connecting the pulvinar and MT (Warner et al., 2010). However, due to the artifacts in the postsurgical diffusion scan, we were unable to measure these tracts in Patient S.P.'s brain.

In addition to longitudinal tracts, we were also able to identify vertical tracts connecting dorsal retinotopic areas to ventral face-selective regions. Specifically, the VOF is a recently rediscovered major white matter pathway connecting dorsal and ventral components of the occipital lobe (Yeatman et al., 2014; Takemura et al., 2016; Weiner et al., 2016). We first identified the VOF in Patient S.P. and controls (Fig. 10; see Materials and Methods). Importantly, a subcomponent of the VOF connects V7/IPS-0 dorsally to pFus-faces/FFA-1 ventrally in Patient S.P. and controls (Fig. 10, cyan). This subcomponent of the VOF is identifiable in Patient S.P. both before resection (Fig. 10, cyan) and after resection (Fig. 10, purple).

These longitudinal and vertical tracts that are intact in Patient S.P. after surgery provide an anatomical infrastructure for signals to reach downstream face-selective regions on the FG and STS independent of IOG-faces/OFA. Although these tracts provide alternate routes of information flow to downstream face-selective regions, the face network may not always use bypass routes for normative function, which is a hypothesis that can be tested in future research.

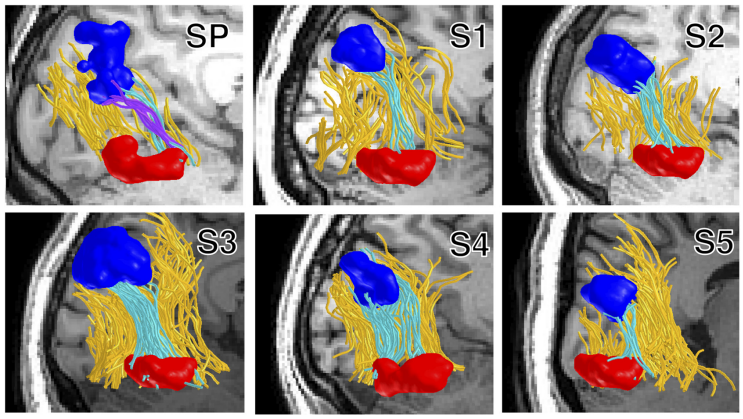

Figure 10. A subcomponent of the VOF connects pFus-faces ventrally to V7/IPS-0 dorsally. VOF fibers (yellow) interconnect pFus-faces (red) and retinotopic area V7/IPS-0 (dark blue). Fibers of the VOF terminating in both pFus-faces and V7/IPS-0 are colored in cyan (presurgery data in Patient S.P.) and in controls (S1–S5). In Patient S.P., vertical fibers observed after surgery interconnecting V7/IPS-0 and pFus-faces are shown in purple.

Discussion

We examined the structure and function of the face network in a rare patient before and after removal of right IOG-faces/OFA, which is considered the critical input of the face network according to prevailing models of neural face processing. We found that downstream face-selective regions surviving the resection are largely resilient after surgery, which is consistent with proposals of a multiple route face network with nonhierarchical components (Rossion, 2008; Atkinson and Adolphs, 2011; Pitcher et al., 2011a; Duchaine and Yovel, 2015).

Non strict hierarchical components of the face network enable efficiency and resiliency

Our results indicate that face-selective neural responses in downstream regions are preserved in patient Patient S.P. as early as 1 month following the removal of right IOG-faces/OFA. These results specify that, even though regions within the face network are functionally (Fairhall and Ishai, 2007; Turk-Browne et al., 2010; Zhu et al., 2011; Lohse et al., 2016) and structurally interconnected (Fairhall and Ishai, 2007; Turk-Browne et al., 2010; Zhu et al., 2011; Gschwind et al., 2012; Pyles et al., 2013; Tavor et al., 2014), the network itself is not arranged in a strict hierarchy where information is always systematically transmitted in a serial manner from IOG-faces/OFA to subsequent processing stages.

These findings serve as causal evidence that a multiple route network with nonhierarchical components supports face processing (Rossion, 2008; Atkinson and Adolphs, 2011; Pitcher et al., 2011a; Duchaine and Yovel, 2015). Additionally, our DWI measurements show that there are multiple white matter connections from retinotopic regions to the face network (Figs. 8–10), which not only validate recent models (Rossion, 2008; Atkinson and Adolphs, 2011; Pitcher et al., 2011a; Duchaine and Yovel, 2015), but also provide evidence explaining how within hemisphere connections may provide inputs to downstream face-selective regions in the absence of IOG-faces/OFA.

We propose that these additional routes may serve two functions. First, they may increase the efficiency of typically functioning networks by allowing nonserial processing. For example, they may serve as reentrant connections enabling coarse-to-fine processing (Rossion et al., 2003; Rossion, 2008; Goffaux et al., 2011; Jiang et al., 2011), reverse hierarchical processing (Mumford, 1992; Bullier, 2001; Ahissar and Hochstein, 2004), or recurrent processing (Kravitz et al., 2013). Second, they may provide resiliency to the face network by preserving global network functionality following focal network damage. While these white matter tracts verify multiple routes of information from retinotopic areas to downstream face-selective regions, future studies are necessary to clarify their role for normative face processing in typical participants. For example, longitudinal connections may serve to segregate dynamic and static face processing in the lateral and ventral streams, respectively, whereas vertical connections may serve to integrate these two types of information. Further, our findings do not imply that face processing is always nonserial or that there are no hierarchical components in the face network (Kay et al., 2015). Future studies in typical subjects and patients will shed further light on functional processes that are hierarchical and those that are not.

Methodological advancements: the necessity for multiple sessions and metrics

A unique aspect of our study is that we acquired multiple functional measurements before and after focal resection of human visual cortex. The importance of this approach is that it allows distinguishing meaningful functional changes due to reorganization after surgery from changes that occur due to session-to-session variability. Because pre-resection and post-resection measurements quantify changes between sessions, it is important for future cases to quantify the stability of functional measurements (1) with multiple metrics (mean and voxel level), (2) relative to typical subjects, and (3) across sessions. This suggested approach is not only relevant for cases involving cortical resection or lobectomies, but also any studies that track brain function across an intervention (Op de Beeck et al., 2006) or longitudinal development (Golarai et al., 2007; Scherf et al., 2007) as the session to session variability may outweigh the manipulation itself.

Multiple factors likely contribute to cortical resiliency

Cortical systems illustrate both stable and plastic features following damage or surgery (Wandell and Smirnakis, 2009). If and how cortex recovers from damage or surgery is linked to the extent of the damage itself. Indeed, research in nonhuman primates reveals that neural responses in inferotemporal cortex can be stable following focal resection but detrimentally affected when extensive amounts of early and intermediate ventral visual areas are removed (Bertini et al., 2004; Buffalo et al., 2005; Kravitz et al., 2013). As such, the extent of the damage directly influences resiliency (or lack thereof) of cortical networks, as well as behavior. For example, it may seem surprising that removal of IOG-faces/OFA and the posterior portion of pFus-faces/FFA-1 did not further impair Patient S.P.'s behavioral performance on face individualization tasks as predicted by prior research in humans (Rossion et al., 2003; Bouvier and Engel, 2006; Pitcher et al., 2007; Jonas et al., 2012). However, the present results of stability are less surprising in the context of prior studies in nonhuman primates showing small performance decrements, after (1) removing an entire face patch (little to no impairment) (Heywood and Cowey, 1992), (2) focally deactivating face patches (2%–5%) (Afraz et al., 2015), or (3) removing entire gyri (~10%–15%) (Weiskrantz and Saunders, 1984; Buckley et al., 1997). We speculate that the combination of being seizure-free and the striking stability of the rest of the face network after resection likely contributed to the fact that Patient S.P.'s behavioral performance did not worsen after removal of IOG-faces/OFA and posterior portion of pFus-faces/FFA-1.

Nevertheless, we cannot rule out the possibility that other, more difficult, face tasks may have revealed a further impairment in Patient S.P. after resection or that additional neural changes may have occurred within smaller temporal or spatial scales than those presently measured. At least two alternatives are possible: (1) short-term changes may occur immediately (e.g., seconds to hours) following resection after which the organization recovers within days or weeks; or (2) brain changes may occur at the submillimeter level, and cannot be detected with fMRI measurements at the millimeter and centimeter scale. Future studies will test these alternatives and further uncover the different spatial and temporal scales of cortical resiliency following focal damage.

Confronting limitations in neuroimaging case studies

We acknowledge that our case has two main limitations. Before surgery, Patient S.P. had (1) chronic seizures, and (2) aspects of her individual face discrimination were below normal, but above chance. These two limitations raise the question whether Patient S.P.'s brain was impaired before surgery. To address these limitations, we compared her face network before surgery with healthy controls. Our data show that the presurgery localization, selectivity, and variability of her face network and, the IOG in particular, were not different from these control participants. Nonetheless, it is possible that our experimental manipulations and metrics were not sensitive enough and that more sensitive manipulations, such as fMRI adaptation (Grill-Spector and Malach, 2001; Schiltz et al., 2006; Fox et al., 2013), may have identified subtle changes in her face network. An alternative possibility is that her behavioral impairment is due to brain changes outside the "core" face network as has been observed in developmental/congenital prosopagnosics (Behrmann et al., 2007; Avidan and Behrmann, 2009; Garrido et al., 2009). Critically, we prioritized test-retest reliability across sessions before surgery rather than conducting additional measurements to establish a between-session baseline relative to which we could determine the effects of surgery on cortical responses.

Despite these limitations, we believe that our case provides important causal evidence for a multiple route face network with nonhierarchical components. As there is only one other documented case with pre-resection and post-resection neuroimaging measurements (Gaillard et al., 2006), the present gold standard of causal tests in the field is neuropsychological case studies of patients with long-term brain damage. While these cases provide invaluable insights into the causal effects of cortical damage to perception, there are also limitations to these studies. For example, the brain damage in tested patients is often large and nonspe-

cific and can encompass both hemispheres, the timescale from damage to measurement is long (on the order of years), and finally, each case only has a functional measurement after, but not before, damage has occurred. Because of these limitations, it is unknown exactly which aspects of the brain and behavior were typical before the damage (Marotta et al., 2001; Rossion et al., 2003; Schiltz et al., 2006; Steeves et al., 2006; Sorger et al., 2007; Rossion, 2008; Fox et al., 2011, 2013; Konen et al., 2011; Yang et al., 2016). Nevertheless, despite the different approaches between the present case and these prior cases in patients with long-term brain damage, it is reassuring that the results converge toward consistent conclusions of a multiple route hierarchy of cortical face processing supporting face perception.

In conclusion, our unique data provide causal insight into the construction of functional networks in the human brain and provide empirical support for recent neurocognitive models proposing a multiple route cortical network with nonhierarchical components underlying face processing.

References

Afraz A, Boyden ES, DiCarlo JJ (2015) Optogenetic and pharmacological suppression of spatial clusters of face neurons reveal their causal role in face gender discrimination. Proc Natl Acad Sci U S A 112:6730–6735. CrossRef Medline

Ahissar M, Hochstein S (2004) The reverse hierarchy theory of visual perceptual learning. Trends Cogn Sci 8:457–464. CrossRef Medline

Ajina S, Pestilli F, Rokem A, Kennard C, Bridge H (2015) Human blindsight is mediated by an intact geniculo-extrastriate pathway. Elife 4:piiee08935. CrossRef Medline

Allison T, McCarthy G, Nobre A, Puce A, Belger A (1994) Human extrastriate visual cortex and the perception of faces, words, numbers, and colors. Cereb Cortex 4:544–554. CrossRef Medline

Amano K, Wandell BA, Dumoulin SO (2009) Visual field maps, population receptive field sizes, and visual field coverage in the human MT$^+$ complex. J Neurophysiol 102:2704–2718. CrossRef Medline

Atkinson AP, Adolphs R (2011) The neuropsychology of face perception: beyond simple dissociations and functional selectivity. Philos Trans R Soc Lond B Biol Sci 366:1726–1738. CrossRef Medline

Avidan G, Behrmann M (2009) Functional MRI reveals compromised neural integrity of the face processing network in congenital prosopagnosia. Curr Biol 19:1146–1150. CrossRef Medline

Bancaud J, Talairach J (1973) [Methodology of stereo EEG exploration and surgical intervention in epilepsy]. Rev Otoneuroophtalmol 45:315–328. Medline

Behrmann M, Avidan G, Gao F, Black S (2007) Structural imaging reveals anatomical alterations in inferotemporal cortex in congenital prosopagnosia. Cereb Cortex 17:2354–2363. CrossRef Medline

Benson NC, Butt OH, Datta R, Radoeva PD, Brainard DH, Aguirre GK (2012) The retinotopic organization of striate cortex is well predicted by surface topology. Curr Biol 22:2081–2085. CrossRef Medline

Benson NC, Butt OH, Brainard DH, Aguirre GK (2014) Correction of distortion in flattened representations of the cortical surface allows prediction of V1–V3 functional organization from anatomy. PLoS Comput Biol 10: e1003538. CrossRef Medline

Benton AL, Sivan AB, Hamsher K, Varney NR, Spreen O (1983) Benton facial recognition: stimulus and multiple choice pictures. Lutz, FL: Psychological Assessment Resources.

Bernstein M, Yovel G (2015) Two neural pathways of face processing: a critical evaluation of current models. Neurosci Biobehav Rev 55:536–546. CrossRef Medline

Bertini G, Buffalo EA, De Weerd P, Desimone R, Ungerleider LG (2004) Visual responses to targets and distracters by inferior temporal neurons after lesions of extrastriate areas V4 and TEO. Neuroreport 15:1611–1615. CrossRef Medline

Bouvier SE, Engel SA (2006) Behavioral deficits and cortical damage loci in cerebral achromatopsia. Cereb Cortex 16:183–191. CrossRef Medline

Buckley MJ, Gaffan D, Murray EA (1997) Functional double dissociation between two inferior temporal cortical areas: perirhinal cortex versus middle temporal gyrus. J Neurophysiol 77:587–598. Medline

Buffalo EA, Bertini G, Ungerleider LG, Desimone R (2005) Impaired filtering of distracter stimuli by TE neurons following V4 and TEO lesions in macaques. Cereb Cortex 15:141–151. CrossRef Medline

Bullier J (2001) Integrated model of visual processing. Brain Res Brain Res Rev 36:96–107. CrossRef Medline

Busigny T, Joubert S, Felician O, Ceccaldi M, Rossion B (2010) Holistic perception of the individual face is specific and necessary: evidence from an extensive case study of acquired prosopagnosia. Neuropsychologia 48:4057–4092. CrossRef Medline

Crawford JR, Howell DC (1998) Comparing an individual's test score against norms derived from small samples. Clin Neuropsychol 12: 482–486. CrossRef

Dale AM, Fischl B, Sereno MI (1999) Cortical surface-based analysis: I. Segmentation and surface reconstruction. Neuroimage 9:179–194. CrossRef Medline

Desimone R, Ungerleider LG (1986) Multiple visual areas in the caudal superior temporal sulcus of the macaque. J Comp Neurol 248:164–189. CrossRef Medline

Duchaine B, Nakayama K (2006) The Cambridge Face Memory Test: results for neurologically intact individuals and an investigation of its validity using inverted face stimuli and prosopagnosic participants. Neuropsychologia 44:576–585. CrossRef Medline

Duchaine B, Yovel G (2015) A revised neural framework for face processing. Annu Rev Vis Sci 1:393–416. CrossRef

Engel SA, Glover GH, Wandell BA (1997) Retinotopic organization in human visual cortex and the spatial precision of functional MRI. Cereb Cortex 7:181–192. CrossRef Medline

Fairhall SL, Ishai A (2007) Effective connectivity within the distributed cortical network for face perception. Cereb Cortex 17:2400–2406. CrossRef Medline

Felleman DJ, Van Essen DC (1991) Distributed hierarchical processing in the primate cerebral cortex. Cereb Cortex 1:1–47. CrossRef Medline

Fox CJ, Iaria G, Barton JJ (2008) Disconnection in prosopagnosia and face processing. Cortex 44:996–1009. CrossRef Medline

Fox CJ, Hanif HM, Iaria G, Duchaine BC, Barton JJ (2011) Perceptual and anatomic patterns of selective deficits in facial identity and expression processing. Neuropsychologia 49:3188–3200. CrossRef Medline

Fox CJ, Iaria G, Duchaine BC, Barton JJ (2013) Residual fMRI sensitivity for identity changes in acquired prosopagnosia. Front Psychol 4:756. CrossRef Medline

Gaillard R, Naccache L, Pinel P, Clémenceau S, Volle E, Hasboun D, Dupont S, Baulac M, Dehaene S, Adam C, Cohen L (2006) Direct intracranial, FMRI, and lesion evidence for the causal role of left inferotemporal cortex in reading. Neuron 50:191–204. CrossRef Medline

Garrido L, Furl N, Draganski B, Weiskopf N, Stevens J, Tan GC, Driver J, Dolan RJ, Duchaine B (2009) Voxel-based morphometry reveals reduced grey matter volume in the temporal cortex of developmental prosopagnosics. Brain 132:3443–3455. CrossRef Medline

Gauthier I, Skudlarski P, Gore JC, Anderson AW (2000) Expertise for cars and birds recruits brain areas involved in face recognition. Nat Neurosci 3:191–197. CrossRef Medline

Goffaux V, Peters J, Haubrechts J, Schiltz C, Jansma B, Goebel R (2011) From coarse to fine? Spatial and temporal dynamics of cortical face processing. Cereb Cortex 21:467–476. CrossRef Medline

Golarai G, Ghahremani DG, Whitfield-Gabrieli S, Reiss A, Eberhardt JL, Gabrieli JD, Grill-Spector K (2007) Differential development of high-level visual cortex correlates with category-specific recognition memory. Nat Neurosci 10:512–522. CrossRef Medline

Gomez J, Pestilli F, Witthoft N, Golarai G, Liberman A, Poltoratski S, Yoon J, Grill-Spector K (2015) Functionally defined white matter reveals segregated pathways in human ventral temporal cortex associated with category-specific processing. Neuron 85:216–227. CrossRef Medline

Grill-Spector K, Malach R (2001) fMR-adaptation: a tool for studying the functional properties of human cortical neurons. Acta Psychol (Amst) 107:293–321. CrossRef Medline

Gschwind M, Pourtois G, Schwartz S, Van De Ville D, Vuilleumier P (2012) White matter connectivity between face-responsive regions in the human brain. Cereb Cortex 22:1564–1576. CrossRef Medline

Haxby JV, Hoffman EA, Gobbini MI (2000) The distributed human neural system for face perception. Trends Cogn Sci 4:223–233. CrossRef Medline

Hemond CC, Kanwisher NG, Op de Beeck HP (2007) A preference for contralateral stimuli in human object- and face-selective cortex. PLoS One 2:e574. CrossRef Medline

Hermes D, Miller KJ, Noordmans HJ, Vansteensel MJ, Ramsey NF (2010) Automated electrocorticographic electrode localization on individually rendered brain surfaces. J Neurosci Methods 185:293–298. CrossRef Medline

Heywood CA, Cowey A (1992) The role of the 'face-cell' area in the discrimination and recognition of faces by monkeys. Philos Trans R Soc Lond B Biol Sci 335:31–37; discussion 37–38. CrossRef Medline

Jacques C, Witthoft N, Weiner KS, Foster BL, Rangarajan V, Hermes D, Miller KJ, Parvizi J, Grill-Spector K (2016) Corresponding ECoG and fMRI category-selective signals in human ventral temporal cortex. Neuropsychologia 83:14–28. CrossRef Medline

Jiang F, Dricot L, Weber J, Righi G, Tarr MJ, Goebel R, Rossion B (2011) Face categorization in visual scenes may start in a higher order area of the right fusiform gyrus: evidence from dynamic visual stimulation in neuroimaging. J Neurophysiol 106:2720–2736. CrossRef Medline

Jonas J, Descoins M, Koessler L, Colnat-Coulbois S, Sauvée M, Guye M, Vignal JP, Vespignani H, Rossion B, Maillard L (2012) Focal electrical intracerebral stimulation of a face-sensitive area causes transient prosopagnosia. Neuroscience 222:281–288. CrossRef Medline

Kanwisher N, McDermott J, Chun MM (1997) The fusiform face area: a module in human extrastriate cortex specialized for face perception. J Neurosci 17:4302–4311. Medline

Kay KN, Weiner KS, Grill-Spector K (2015) Attention reduces spatial uncertainty in human ventral temporal cortex. Curr Biol 25:595–600. CrossRef Medline

Kim M, Ducros M, Carlson T, Ronen I, He S, Ugurbil K, Kim DS (2006) Anatomical correlates of the functional organization in the human occipitotemporal cortex. Magn Reson Imaging 24:583–590. CrossRef Medline

Konen CS, Behrmann M, Nishimura M, Kastner S (2011) The functional neuroanatomy of object agnosia: a case study. Neuron 71:49–60. CrossRef Medline

Kravitz DJ, Saleem KS, Baker CI, Ungerleider LG, Mishkin M (2013) The ventral visual pathway: an expanded neural framework for the processing of object quality. Trends Cogn Sci 17:26–49. CrossRef Medline

Lohse M, Garrido L, Driver J, Dolan RJ, Duchaine BC, Furl N (2016) Effective connectivity from early visual cortex to posterior occipitotemporal face areas supports face selectivity and predicts developmental prosopagnosia. J Neurosci 36:3821–3828. CrossRef Medline

Marotta JJ, Genovese CR, Behrmann M (2001) A functional MRI study of face recognition in patients with prosopagnosia. Neuroreport 12:1581–1587. CrossRef Medline

Mumford D (1992) On the computational architecture of the neocortex: II. The role of cortico-cortical loops. Biol Cybern 66:241–251. CrossRef Medline

Murphy K, Bodurka J, Bandettini PA (2007) How long to scan? The relationship between fMRI temporal signal to noise ratio and necessary scan duration. Neuroimage 34:565–574. CrossRef Medline

Op de Beeck HP, Baker CI, DiCarlo JJ, Kanwisher NG (2006) Discrimination training alters object representations in human extrastriate cortex. J Neurosci 26:13025–13036. CrossRef Medline

O'Toole AJ, Roark DA, Abdi H (2002) Recognizing moving faces: a psychological and neural synthesis. Trends Cogn Sci 6:261–266. CrossRef Medline

Palermo R, Rossion B, Rhodes G, Laguesse R, Tez T, Hall B, Albonico A, Malaspina M, Daini R, Irons J, Al-Janabi S, Taylor LC, Rivolta D, McKone E (2016) Do people have insight into their face recognition abilities? Q J Exp Psychol (Hove) 23:1–16. CrossRef Medline

Parvizi J, Jacques C, Foster BL, Withoft N, Rangarajan V, Weiner KS, Grill-Spector K (2012) Electrical stimulation of human fusiform face-selective regions distorts face perception. J Neurosci 32:14915–14920. CrossRef Medline

Pasternak O, Sochen N, Gur Y, Intrator N, Assaf Y (2009) Free water elimination and mapping from diffusion MRI. Magn Reson Med 62:717–730. CrossRef Medline

Pestilli F, Yeatman JD, Rokem A, Kay KN, Wandell BA (2014) Evaluation and statistical inference for human connectomes. Nat Methods 11:1058–1063. CrossRef Medline

Pinsk MA, Arcaro M, Weiner KS, Kalkus JF, Inati SJ, Gross CG, Kastner S (2009) Neural representations of faces and body parts in macaque and human cortex: a comparative FMRI study. J Neurophysiol 101:2581–2600. CrossRef Medline

Pitcher D, Walsh V, Yovel G, Duchaine B (2007) TMS evidence for the involvement of the right occipital face area in early face processing. Curr Biol 17:1568–1573. CrossRef Medline

Pitcher D, Walsh V, Duchaine B (2011a) The role of the occipital face area in the cortical face perception network. Exp Brain Res 209:481–493. CrossRef Medline

Pitcher D, Dilks DD, Saxe RR, Triantafyllou C, Kanwisher N (2011b) Differential selectivity for dynamic versus static information in face-selective cortical regions. Neuroimage 56:2356–2363. CrossRef Medline

Pitcher D, Duchaine B, Walsh V (2014) Combined TMS and FMRI reveal dissociable cortical pathways for dynamic and static face perception. Curr Biol 24:2066–2070. CrossRef Medline

Puce A, Allison T, Gore JC, McCarthy G (1995) Face-sensitive regions in human extrastriate cortex studied by functional MRI. J Neurophysiol 74:1192–1199. Medline

Puce A, Allison T, Bentin S, Gore JC, McCarthy G (1998) Temporal cortex activation in humans viewing eye and mouth movements. J Neurosci 18:2188–2199. Medline

Pyles JA, Verstynen TD, Schneider W, Tarr MJ (2013) Explicating the face perception network with white matter connectivity. PLoS One 8:e61611. CrossRef Medline

Rossion B (2008) Constraining the cortical face network by neuroimaging studies of acquired prosopagnosia. Neuroimage 40:423–426. CrossRef Medline

Rossion B, Caldara R, Seghier M, Schuller AM, Lazeyras F, Mayer E (2003) A network of occipito-temporal face-sensitive areas besides the right middle fusiform gyrus is necessary for normal face processing. Brain 126:2381–2395. CrossRef Medline

Rossion B, Dricot L, Goebel R, Busigny T (2011) Holistic face categorization in higher order visual areas of the normal and prosopagnosic brain: toward a non-hierarchical view of face perception. Front Hum Neurosci 4:225. CrossRef Medline

Rossion B, Hanseeuw B, Dricot L (2012) Defining face perception areas in the human brain: a large-scale factorial fMRI face localizer analysis. Brain Cogn 79:138–157. CrossRef Medline

Scherf KS, Behrmann M, Humphreys K, Luna B (2007) Visual category selectivity for faces, places and objects emerges along different developmental trajectories. Dev Sci 10:F15–F30. CrossRef Medline

Schiltz C, Sorger B, Caldara R, Ahmed F, Mayer E, Goebel R, Rossion B (2006) Impaired face discrimination in acquired prosopagnosia is associated with abnormal response to individual faces in the right middle fusiform gyrus. Cereb Cortex 16:574–586. CrossRef Medline

Sergent J, Ohta S, MacDonald B (1992) Functional neuroanatomy of face and object processing: a positron emission tomography study. Brain 115:15–36. CrossRef Medline

Sorger B, Goebel R, Schiltz C, Rossion B (2007) Understanding the functional neuroanatomy of acquired prosopagnosia. Neuroimage 35:836–852. CrossRef Medline

Steeves JK, Culham JC, Duchaine BC, Pratesi CC, Valyear KF, Schindler I, Humphrey GK, Milner AD, Goodale MA (2006) The fusiform face area is not sufficient for face recognition: evidence from a patient with dense prosopagnosia and no occipital face area. Neuropsychologia 44:594–609. CrossRef Medline

Steeves J, Dricot L, Goltz HC, Sorger B, Peters J, Milner AD, Goodale MA, Goebel R, Rossion B (2009) Abnormal face identity coding in the middle fusiform gyrus of two brain-damaged prosopagnosic patients. Neuropsychologia 47:2584–2592. CrossRef Medline

Stigliani A, Weiner KS, Grill-Spector K (2015) Temporal processing capacity in high-level visual cortex is domain-specific. J Neurosci 35:12412–12424. CrossRef Medline

Takemura H, Rokem A, Winawer J, Yeatman JD, Wandell BA, Pestilli F (2016) A major human white matter pathway between dorsal and ventral visual cortex. Cereb Cortex 26:2205–2214. CrossRef Medline

Tavor I, Yablonski M, Mezer A, Rom S, Assaf Y, Yovel G (2014) Separate parts of occipito-temporal white matter fibers are associated with recognition of faces and places. Neuroimage 86:123–130. CrossRef Medline

Tournier JD, Calamante F, Connelly A (2007) Robust determination of the fibre orientation distribution in diffusion MRI: non-negativity constrained super-resolved spherical deconvolution. Neuroimage 35:1459–1472. CrossRef Medline

Tournier JD, Calamante F, Connelly A (2012) MRtrix: diffusion tractography in crossing fibre regions. Int J Imaging Syst Technol 22:53–66. CrossRef

Turk-Browne NB, Norman-Haignere SV, McCarthy G (2010) Face-specific resting functional connectivity between the fusiform gyrus and posterior superior temporal sulcus. Front Hum Neurosci 4:176. CrossRef Medline

Ungerleider LG, Mishkin M (1982) Two cortical visual systems. In: Analysis of visual behavior (Ingle DJ, Goodale MA, Mansfield RJW, eds), pp 549–586. Cambridge, MA: Massachusetts Institute of Technology.

Wandell BA, Smirnakis SM (2009) Plasticity and stability of visual field maps in adult primary visual cortex. Nat Rev Neurosci 10:873–884. CrossRef Medline

Wandell BA, Chial S, Backus BT (2000) Visualization and measurement of the cortical surface. J Cogn Neurosci 12:739–752. CrossRef Medline

Warner CE, Goldshmit Y, Bourne JA (2010) Retinal afferents synapse with relay cells targeting the middle temporal area in the pulvinar and lateral geniculate nuclei. Front Neuroanat 4:8. CrossRef Medline

Warrington EK, James M (1991) The Visual Object and Space Perception Battery. Bury St Edmunds, England: Thames Valley Test.

Weiner KS, Grill-Spector K (2010) Sparsely-distributed organization of face and limb activations in human ventral temporal cortex. Neuroimage 52: 1559–1573. CrossRef Medline

Weiner KS, Grill-Spector K (2011) Not one extrastriate body area: using anatomical landmarks, hMT$^+$, and visual field maps to parcellate limb-selective activations in human lateral occipitotemporal cortex. Neuroimage 56:2183–2199. CrossRef Medline

Weiner KS, Grill-Spector K (2013) Neural representations of faces and limbs neighbor in human high-level visual cortex: evidence for a new organization principle. Psychol Res 77:74–97. CrossRef Medline

Weiner KS, Golarai G, Caspers J, Chuapoco MR, Mohlberg H, Zilles K, Amunts K, Grill-Spector K (2014) The mid-fusiform sulcus: a landmark identifying both cytoarchitectonic and functional divisions of human ventral temporal cortex. Neuroimage 84:453–465. CrossRef Medline

Weiner KS, Yeatman JD, Wandell BA (2016) The posterior arcuate fasciculus and the vertical occipital fasciculus. Cortex. Advance online publication. Retrieved Mar. 31, 2016. doi: 10.1016/j.cortex.2016.03.012. CrossRef Medline

Weiskrantz L, Saunders RC (1984) Impairments of visual object transforms in monkeys. Brain 107:1033–1072. CrossRef Medline

Yang H, Susilo T, Duchaine B (2016) The anterior temporal face area contains invariant representations of face identity that can persist despite the loss of right FFA and OFA. Cereb Cortex 26:1096–1107. CrossRef Medline

Yeatman JD, Weiner KS, Pestilli F, Rokem A, Mezer A, Wandell BA (2014) The vertical occipital fasciculus: a century of controversy resolved by in vivo measurements. Proc Natl Acad Sci U S A 111:E5214–E5223. CrossRef Medline

Zhen Z, Fang H, Liu J (2013) The hierarchical brain network for face recognition. PLoS One 8:e59886. CrossRef Medline

Zhen Z, Yang Z, Huang L, Kong XZ, Wang X, Dang X, Huang Y, Song Y, Liu J (2015) Quantifying interindividual variability and asymmetry of face-selective regions: a probabilistic functional atlas. Neuroimage 113:13–25. CrossRef Medline

Zhu Q, Zhang J, Luo YL, Dilks DD, Liu J (2011) Resting-state neural activity across face-selective cortical regions is behaviorally relevant. J Neurosci 31:10323–10330. CrossRef Medline

A face-selective ventral occipito-temporal map of the human brain with intracerebral potentials

Jacques Jonas[a,b,c,1], Corentin Jacques[a,1], Joan Liu-Shuang[a], Hélène Brissart[b], Sophie Colnat-Coulbois[d], Louis Maillard[b,c], and Bruno Rossion[a,2]

[a]Psychological Sciences Research Institute and Institute of Neuroscience, University of Louvain, B-1348 Louvain-La-Neuve, Belgium; [b]Neurology Unit, University Hospital of Nancy, F-54000 Nancy, France; [c]Centre de Recherche en Automatique de Nancy, UMR 7039, CNRS and University of Lorraine, F-54500 Vandœuvre-lès-Nancy, France; and [d]Neurosurgery Unit, University Hospital of Nancy, F-54000 Nancy, France

Edited by Aina Puce, Indiana University, Bloomington, IN, and accepted by Editorial Board Member Randolph Blake May 6, 2016 (received for review November 26, 2015)

Human neuroimaging studies have identified a network of distinct face-selective regions in the ventral occipito-temporal cortex (VOTC), with a right hemispheric dominance. To date, there is no evidence for this hemispheric and regional specialization with direct measures of brain activity. To address this gap in knowledge, we recorded local neurophysiological activity from 1,678 contact electrodes implanted in the VOTC of a large group of epileptic patients ($n = 28$). They were presented with natural images of objects at a rapid fixed rate (six images per second: 6 Hz), with faces interleaved as every fifth stimulus (i.e., 1.2 Hz). High signal-to-noise ratio face-selective responses were objectively (i.e., exactly at the face stimulation frequency) identified and quantified throughout the whole VOTC. Face-selective responses were widely distributed across the whole VOTC, but also spatially clustered in specific regions. Among these regions, the lateral section of the right middle fusiform gyrus showed the largest face-selective response by far, offering, to our knowledge, the first supporting evidence of two decades of neuroimaging observations with direct neural measures. In addition, three distinct regions with a high proportion of face-selective responses were disclosed in the right ventral anterior temporal lobe, a region that is undersampled in neuroimaging because of magnetic susceptibility artifacts. A high proportion of contacts responding only to faces (i.e., "face-exclusive" responses) were found in these regions, suggesting that they contain populations of neurons involved in dedicated face-processing functions. Overall, these observations provide a comprehensive mapping of visual category selectivity in the whole human VOTC with direct neural measures.

face perception | intracerebral recordings | fast periodic visual stimulation | face selectivity | fusiform gyrus

A brief glance at a face provides a wealth of information about a person's identity, emotional state, sex, age, attractiveness, and other important cues for social communication. Hence, being able to identify a face as a face and distinguish it from multiple variable nonface objects (i.e., face categorization) is a prerequisite for understanding all face-perception functions. The functional definition of brain regions supporting face categorization in humans has been investigated extensively as a primary research goal, and these findings may serve as a rich model for understanding perceptual categorization and brain organization in general.

Postmortem brain autopsies and structural imaging of individuals with face-recognition impairment after brain damage (i.e., prosopagnosia) (1, 2) point to a large territory of the human ventral occipito-temporal cortex (VOTC), from the occipital pole to the temporal pole, with a right hemispheric advantage, as the neural basis of face categorization (refs. 3–7; for recent reviews, see refs. 8 and 9). In the normal human brain, functional neuroimaging has been the primary method for investigating the neural basis of face categorization, first with positron emission tomography (PET) (10) and then with functional MRI (fMRI) (11, 12). Collectively, these studies have reported larger brain responses to face images than other visual objects in clusters, patches, or functional regions of a few cubic millimeters within the human VOTC (e.g., refs. 10–16). The clusters consistently reported across studies are localized in the lateral part of the middle/posterior fusiform gyrus [fusiform face area (FFA)] (12) and in the lateral part of the inferior occipital gyrus [occipital face area (OFA)] (17), as well as in the posterior superior temporal sulcus, a region that may be involved in more general and dynamic social communication functions (18). In right-handed individuals at least, these face-selective regions are typically larger in the right than the left hemisphere (14, 19). More recently, some fMRI studies have defined two face-selective regions in the lateral part of the middle/posterior fusiform gyrus (FFA1 and FFA2) (15) and one in the anterior temporal lobe (fATL) (14, 20–23).

Each of these regions is thought to have a definite function, or computational role, as a node in a vast network of face-selective areas (8, 13). However, fMRI provides only a hemodynamic (i.e., indirect) measure of neural activity, suffering from wide variations in signal-to-noise ratio (SNR) across brain regions, which has important consequences. For instance, the heterogeneous magnetic susceptibility of the local anatomy causes a strong signal dropout in the anterior VOTC (22, 24) so that fMRI studies may fail to report genuine face-selective responses in this region (25), and category selectivity in general is often limited to the posterior section of the VOTC (15). Moreover, smaller, scattered, face-selective responses in the VOTC may be entirely missed by

Significance

Understanding the neural basis of face perception, arguably the most important visual function for human social ecology, is of the utmost importance. With an original fast periodic visual stimulation approach, we provide a comprehensive quantification of selective brain responses to faces throughout the ventral visual stream with direct recordings in the gray matter. Selective responses to faces are distributed in the whole ventral occipito-temporal cortex, with a right hemispheric and regional specialization supporting two decades of indirect recordings of human brain activity in neuroimaging. We also disclose three distinct face-selective regions in the anterior temporal lobe, an undersampled region in neuroimaging, and reveal exclusive responses to faces at the neural population level in these regions.

Author contributions: J.J., C.J., and B.R. designed research; J.J., C.J., J.L.-S., H.B., and S.C.-C. performed research; C.J. contributed new reagents/analytic tools; J.J. and C.J. analyzed data; and J.J., C.J., J.L.-S., L.M., and B.R. wrote the paper.

The authors declare no conflict of interest.

This article is a PNAS Direct Submission. A.P. is a Guest Editor invited by the Editorial Board.

Data deposition: The intracranial electroencephalographic data have been deposited in the Dryad Digital Repository, datadryad.org (doi: 10.5061/dryad.5f9v7).

[1]J.J. and C.J. contributed equally to this work.

[2]To whom correspondence should be addressed. Email: bruno.rossion@uclouvain.be.

This article contains supporting information online at www.pnas.org/lookup/suppl/doi:10.1073/pnas.1522033113/-/DCSupplemental.

fMRI studies that identify only sufficiently large clusters of activation near blood vessels. More generally, these variations in SNR make it impossible for neuroimaging studies to identify, quantify, and thus compare face-selective responses across the whole human VOTC.

To date, the only alternative approach to clarify this issue is afforded by field potentials recorded in awake patients implanted with intracranial electrodes along the ventral and lateral occipitotemporal cortex (26, 27). These relatively rare (i.e., compared with neuroimaging) intracranial electroencephalographic (iEEG) recordings offer a unique opportunity to measure direct local neural activity with a very high SNR. iEEG studies comparing faces and nonface objects have recorded face-selective responses in widely distributed regions of the VOTC and made a number of important observations for understanding the neural basis of face categorization (26–34). However, even when large samples of participants are tested, face-selective responses are broadly distributed in the VOTC, without evidence of a clustered organization as found in fMRI (27, 30, 34). Thus, even though a good correlation between fMRI and iEEG face-selective responses has been shown in specific cortical regions of a few participants (35–39), the dominant role of the posterior fusiform gyrus (FG) and inferior occipital gyrus (IOG), and of the right hemisphere, in face categorization, has never been validated by direct measures of neural activity. More generally, although iEEG recordings do not suffer from regional variations in SNR, direct neural face-selective responses have not been localized, quantified, and compared across anatomical regions of the human VOTC.

Up to now, beyond the intrinsic difficulty of such studies and the limited availability of implanted patients, the major obstacle against a cartography of face selectivity at a large anatomical field of view in the VOTC has been the lack of objectivity in the definition of iEEG face-selective responses. For instance, increases of neural activity to faces compared with nonface objects can be found at various time scales, both in low-frequency responses time-locked and phase-locked to the stimulus [i.e., event-related potentials (ERPs), such as the N200/N170 component (27, 31, 36, 40)] and in non-phase-locked high-frequency electrophysiological activity [high-frequency broadband, i.e., gamma activity (29, 30, 33–35, 40)]. In the latter case, relevant frequency bands vary substantially across recording sites, individual brains, and time windows, making it virtually impossible to objectively define, quantify, and compare face-selective responses across different brain regions.

A potential powerful approach to overcome this problem is to stimulate the human brain at a fast fixed frequency rate for a prolonged time, a rather old stimulation method (41) best known for the type of electrophysiological responses that it generates, the "steady-state visual evoked potentials", on the scalp (42). The main advantages of this approach are its extremely high SNR, providing significant responses in a few minutes of stimulation or less, and its objectivity: The neural response of interest concentrates in the EEG exactly and exclusively at the known frequency rate of stimulation and its harmonics (42, 43). To our knowledge, the application of this approach in intracerebral recordings is rare (37, 44) and has not been used to address the issue of category selectivity.

Here, we use this fast periodic visual stimulation (FPVS) approach to report a comprehensive definition and quantification of face-selective responses across the VOTC in a large group of participants (n = 28) implanted with intracerebral electrodes. Using a paradigm recently validated in human adults (45) and infants (46), participants were shown sequences (70 s) of widely variable natural images of multiple object categories presented at a rapid periodic rate of six images per second (6 Hz). Images of faces were presented as every fifth image (Fig. 1 *A* and *B*). In this design, the common neural response to faces and nonface objects projects to the 6-Hz base rate. However, if faces elicit a differential neural response compared with all other categories, it will appear exactly at the experimentally defined frequency (i.e., 6 Hz/5 = 1.2 Hz). Thus, irrespective of the presence and magnitude of a 6-Hz response, a response at 1.2 Hz indicates category selectivity for faces, or face selectivity. This face-selective response can be objectively defined (i.e., at a known stimulation frequency) without subtraction across conditions (45) and quantified within anatomical regions throughout the whole VOTC, providing a cartography of category (face) selectivity in the human brain.

Results

A total of 192 electrode arrays, each containing 5–18 contiguous recording contacts, were implanted in the VOTC of 28 participants (44 individual hemispheres). These electrodes contained 1,678 individual recording contacts in the gray matter (left hemisphere, 988; right hemisphere, 690) (see Fig. 1*C* for typical electrode trajectories). In the frequency domain, responses occurring at 6 Hz and harmonics reflect the common response to faces and nonface stimuli (i.e., general visual response) whereas responses at 1.2 Hz and harmonics (2.4 Hz, 3.6 Hz, etc.) reflect face-selective responses (Fig. 1*A*) (45). A contact was considered as face-selective if a significant response was found at one or more of the first four face stimulation frequency harmonics.

Despite the brief recording time (two or four sequences of 70 s), high SNR face-selective responses were recorded in the VOTC exactly at 1.2 Hz and harmonics (see Fig. 2*A* for an example of

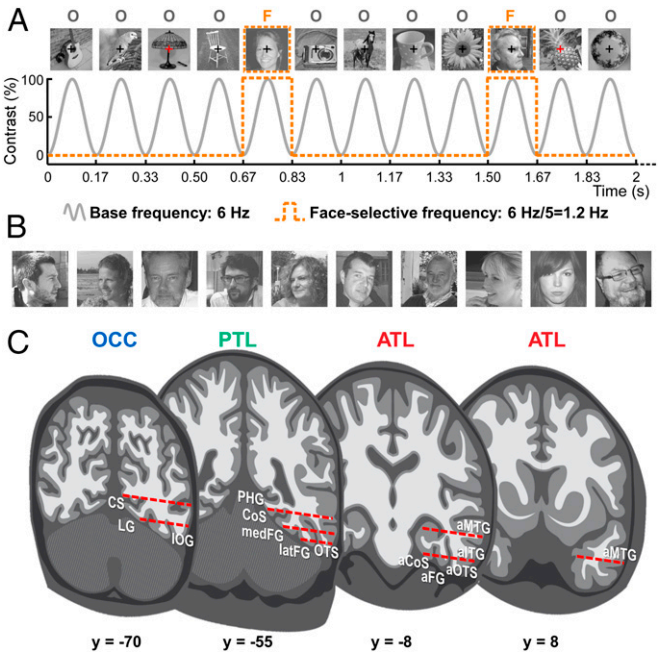

Fig. 1. FPVS and SEEG methods. (*A*) The FPVS paradigm. Images of objects were presented by sinusoidal contrast modulation at a rate of six stimuli per second (6 Hz). In the periodic condition shown here, a different face image was presented every five stimuli (i.e., appearing at the frequency of 6/5 = 1.2 Hz). (*B*) Representative examples of natural face images used in the study (actual images not shown for copyright reasons). Faces were embedded in their natural backgrounds and varied in size, viewpoint, and lighting conditions (50 face exemplars were used in total). (*C*) Schematic representation of the typical trajectories of depth electrodes (SEEG) implanted in the right VOTC. Intracerebral electrodes consist of 8–15 contiguous recording contacts spread along the electrode length, along the medio-lateral axis. Typical trajectories of electrodes are represented as arrays of red rectangles on schematic coronal slices (with Talairach *y* coordinates indicated below slices). Electrodes penetrate both gyral and sulcal cortical tissues. a, anterior; CS, calcarine sulcus; lat, lateral; LG, lingual gyrus; med, medial; PHG, parahippocampal gyrus.

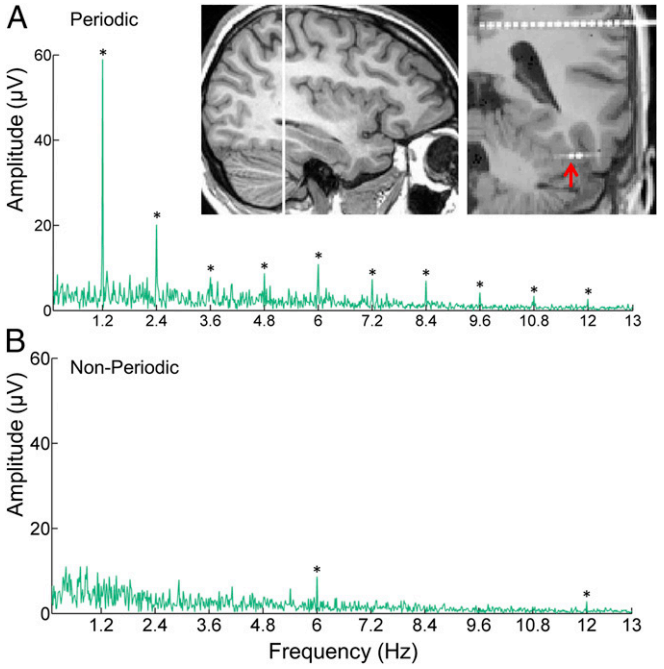

Fig. 2. Objective and high-SNR intracerebral responses in the VOTC. iEEG frequency-domain responses recorded at an individual recording contact (raw FFT amplitude) located in the right latFG (participant 14) are shown. The location of the recording contact (indicated by a red arrow) is shown using a postoperative CT coregistered to a preoperative MRI. (*A*) In the periodic condition, significant face-selective responses exactly at the face-selective frequency (1.2 Hz) and harmonics (up to 10.8 Hz) were observed. Note the high SNR of these responses (i.e., high amplitude at the specific frequency compared with the neighboring frequency bins), despite the brief recording time (two sequences of 70 s here). (*B*) In the nonperiodic condition, no face-selective responses were observed. In both conditions, general visual responses occurring exactly at the base frequency (6 Hz) and harmonics were recorded, with comparable amplitudes and SNR across conditions. *$z > 3.1$; $P < 0.001$.

recording in the right FG). In a nonperiodic condition (where the exact same stimuli were shown in random order, with no face periodicity), there were no contacts with significant responses at 1.2 Hz and harmonics (Fig. 2*B*), even though the 6-Hz general visual response was comparable to that observed in the periodic condition.

Spatial Distribution of Face-Selective Responses in the VOTC. Across the VOTC, we found a high proportion of face-selective contacts (33.1%; 555 of 1,678), with no difference between the left and right hemispheres (left: 313 of 988, 31.7%; right: 242 of 690, 35.1%; $P = 0.146$, Pearson's χ^2 test). These contacts were found in many regions of the occipital and temporal lobes and were widely distributed along the VOTC (Fig. 3*A*; see also Fig. S1*A* for the spatial relationship with contacts showing only a significant general visual response). The anatomical location of each face-selective contact was determined in the individual anatomy by using a topographic parcellation of the VOTC based on predefined well-established anatomical landmarks [Fig. S2; see also Fig. S1*B* for the spatial distribution of face-selective contacts in the Montreal Neurological Institute (MNI) space labeled according to their location in the individual anatomy]. Then, contacts were grouped by anatomical region of interest across all participants (Fig. 4). Table 1 shows the number of contacts in each of these regions (individual brains were not normalized, but see Table S1 for the coordinates of these regions in the MNI and Talairach spaces).

Fig. 4 displays the averaged iEEG frequency spectra in each region of the right hemisphere (see Fig. S3 for the left hemisphere). In the occipital lobe (OCC), face-selective responses were recorded in the IOG and in a large portion of the ventral and medial occipital cortex. Responses in the ventro-medial occipital cortex were distributed over multiple anatomical regions and were generally small relative to large general visual responses. Therefore, for sake of simplicity, these responses were grouped into the same region of interest [ventromedial occipital (VMO), comprising the occipital part of the CoS, the lingual gyrus, the calcarine sulcus, the cuneus, and the occipital pole].

In the posterior temporal lobe (PTL), face-selective responses were mainly recorded in the middle FG. The middle FG is divided longitudinally by the midfusiform sulcus in its medial and lateral sections (15). We recorded face-selective responses in the medial FG and adjacent CoS (medFG) and in the lateral FG and adjacent occipito-temporal sulcus (latFG). Face-selective responses

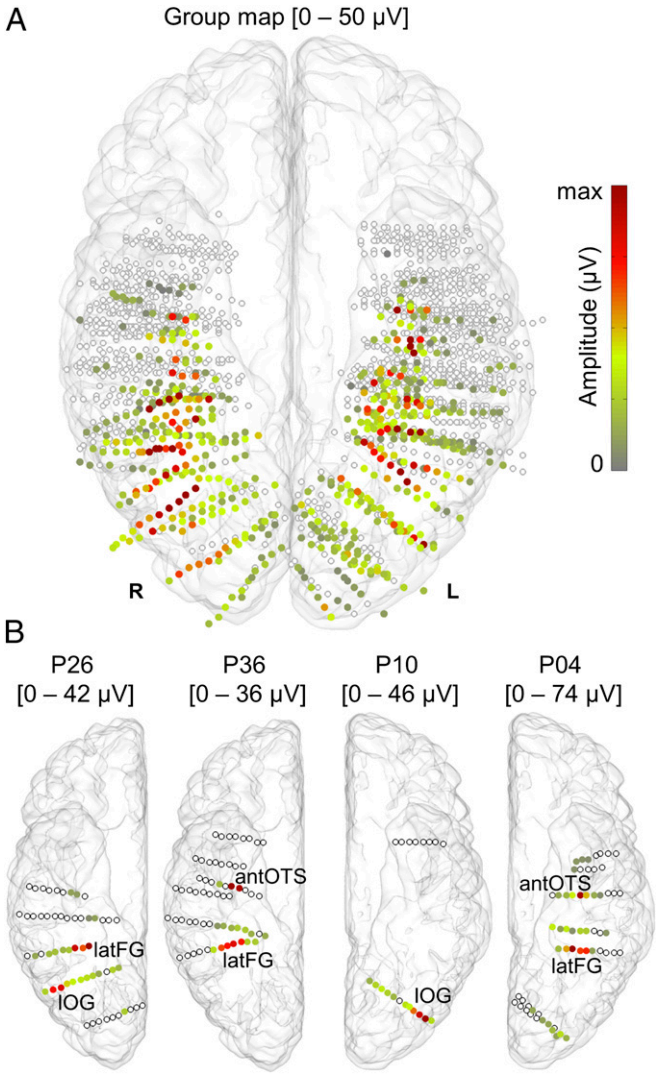

Fig. 3. Spatial distribution of face-selective contacts in the MNI space (ventral view). (*A*) Map of all 1,678 VOTC recording contacts across the 28 individual brains displayed in the MNI space using a transparent reconstructed cortical surface of the Colin27 brain. Each circle represents a single contact. Colored circles correspond to face-selective contacts color-coded according to their face-selective response amplitude. White-filled circles correspond to contacts that are not face-selective. For visualization purposes, individual contacts are displayed larger than their actual size (2 mm in length). (*B*) Examples of four individual participant hemispheres. Anatomical labels of the face-selective clusters in each participant are derived from the individual native anatomy.

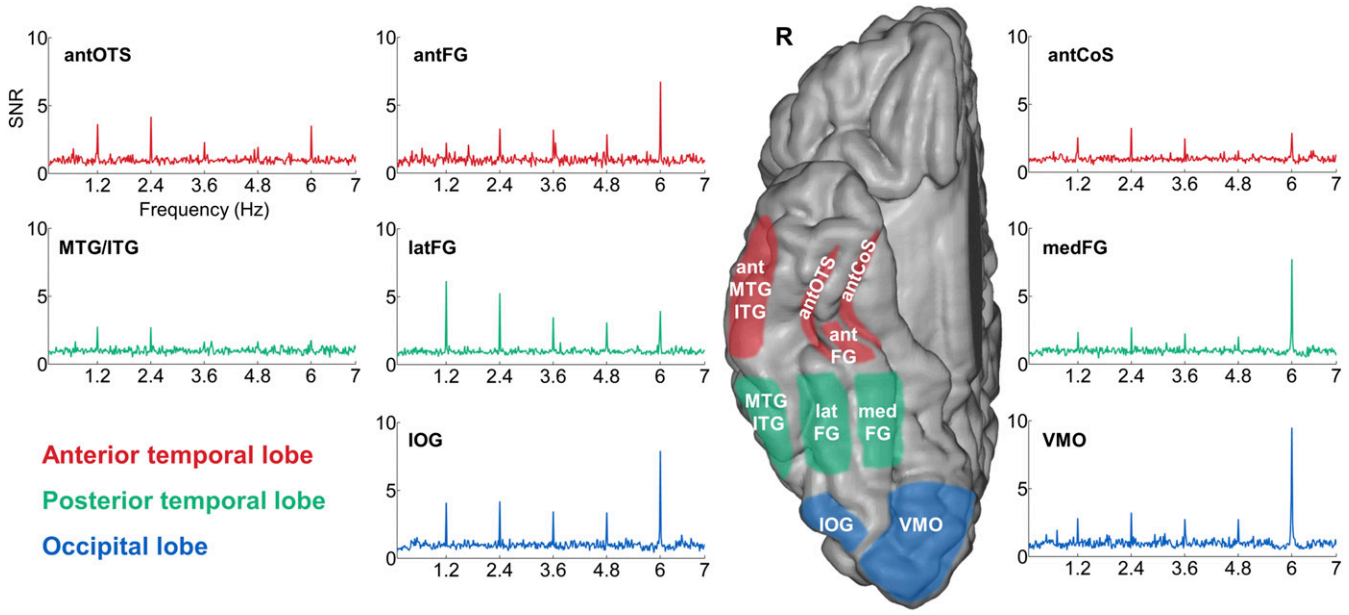

Fig. 4. Face-selective responses in distinct anatomical VOTC regions. iEEG SNR frequency spectra in each region of the right hemisphere averaged across all face-selective contacts located in the same region. SNR is computed by comparing amplitude at the frequency bin of interest to amplitude at neighboring bins (i.e., SNR = 1, no signal above noise level). The schematic locations of each region are shown on a reconstructed cortical surface of the Colin27 brain. For simplicity, regions are depicted over the cortical surface although responses were recorded within the cortex. Note the particularly large (i.e., high SNR) face-selective response recorded in the latFG and to a lesser extent in the IOG compared with other regions. Although face-selective contacts were found in the right antMTG/ITG (Fig. 8*A*), no clear responses were visible on the averaged spectrum, which is therefore not shown. Note that we did not record in the most posterior (in the OCC) and anterior parts of the FG.

were also recorded more laterally in the inferior temporal gyri (ITG) and middle temporal gyri (MTG).

In the anterior temporal lobe (ATL), face-selective responses were mainly recorded in the ventral ATL in three distinct regions: (*i*) along the anterior segment of the collateral sulcus (antCoS); (*ii*) along the anterior segment of the occipito-temporal sulcus [antOTS; located laterally to the CoS (47)]; and (*iii*) in the anterior FG [antFG; located between the antCoS and the antOTS, anteriorly to the posterior tip of the hippocampus (HIP) (25, 48)]. Fig. 5 displays typical recordings from the ventral ATL, as well as their precise anatomical locations in a single participant (P16). Face-selective responses were also recorded more laterally in the anterior part of the MTG and ITG (antMTG/ITG).

In summary, we recorded high-SNR face-selective responses in many regions of the VOTC, extending from the occipital pole to the ATL. These face-selective responses were particularly large in the latFG and IOG (Fig. 4). The general visual responses at 6 Hz were predominant in the OCC, medFG, and antFG.

Quantification of Face-Selective Response Amplitudes. To quantify and compare response amplitudes across regions, we summed the baseline-subtracted amplitudes over harmonics for each face-selective contact, separately for the face-selective responses (sum of the 12 first face-selective frequency harmonics, excluding the 5th and 10th harmonics that coincided with the base frequency) and for the general visual responses (sum over the first four base frequency harmonics). We averaged across contacts to obtain the mean response amplitude for each type of response and region.

Across all regions, the largest face-selective response, by far, was recorded in the right latFG (Fig. 6). This right latFG response was significantly larger than in all other regions taken independently ($P < 0.05$, two-tailed permutation test) (*SI Text*), except for the right antFG, which had the second largest response together with the right IOG (Fig. 6 and Table S2). Strikingly, the mean Talairach coordinates of the face-selective responses found in the right latFG ($x = 41$, $y = -45$, $z = -16$) (Table 2) and in the right IOG ($x = 43$, $y = -71$, $z = -7$) match the coordinates of face-selective clusters found with fMRI in these regions [right FFA and right OFA, respectively; e.g., ref. 14; right FFA average Talairach coordinates in a study with a large sample of participants: $x = 38$, $y = -43$, and $z = -17$ (14)]. The largest general visual responses were recorded in the OCC (VMO and IOG), in the medFG and in the antFG, whereas the smallest responses were recorded in the MTG/ITG and in the ATL (antCoS, antOTS, and antMTG/ITG) (Fig. 6). Note that the results of the quantification analysis were independent of the number of harmonics included in the analysis (Fig. S4*A*).

Although the proportion of face-selective contacts did not differ between right and left latFG (left: 30 of 36, 83.3%; right: 33 of 35, 94.3%; $P = 0.144$, Pearson's χ^2 test), there was a significantly

Table 1. Number of contacts showing face-selective responses in each anatomical region

Regions	Left hemisphere	Right hemisphere	Total
VMO	89 (7)	50 (5)	139 (11)
IOG	26 (6)	36 (6)	62 (11)
Subtotal OCC	115 (7)	86 (6)	201 (12)
medFG	40 (11)	30 (8)	70 (17)
latFG	30 (11)	33 (8)	63 (17)
MTG/ITG	30 (7)	25 (8)	55 (13)
Subtotal PTL	109 (13)	96 (11)	188 (21)
antCoS	33 (11)	23 (9)	56 (18)
antFG	10 (4)	11 (4)	21 (7)
antOTS	35 (12)	17 (5)	52 (15)
antMTG/ITG	20 (7)	17 (8)	37 (12)
Subtotal ATL	107 (16)	79 (15)	166 (23)
Total	313 (21)	242 (17)	555 (28)

The corresponding number of participants in which these face-selective contacts were found is indicated in parentheses.

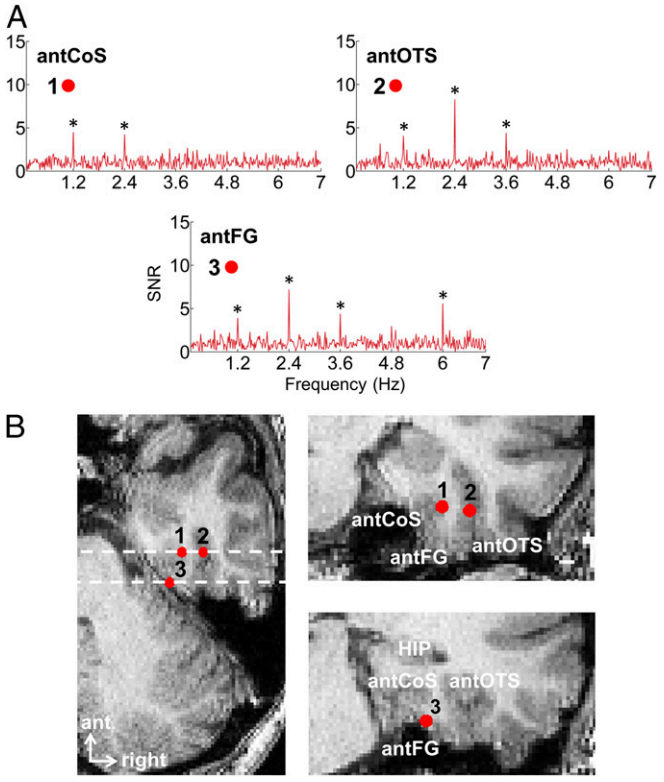

Fig. 5. Example of face-selective responses in three distinct anatomical regions of ventral ATL. (*A*) Face-selective responses recorded from the right antCoS, antOTS, and antFG in a single brain (participant 16). Note that in the antCoS and antOTS, no general visual responses were recorded at 6 Hz and harmonics (face-exclusive responses; see also Fig. 8*A*). *$z > 3.1$; $P < 0.001$. (*B*) Anatomical locations of corresponding recording contacts on MRI slices. Contacts are shown as red dots on axial (*Left*) and coronal (*Right*) slices. Electrode contacts 1, 2, and 3 are respectively located in the antCoS, antOTS, and antFG. The antFG is located between the antCoS and antOTS, at a level where the HIP is visible on a coronal slice.

larger face-selective response in the right latFG (mean difference: 26.03 μV) (Fig. 6; see Table 2 for results of the permutation tests). However, the general visual response did not differ between these two regions (Fig. 6 and Table 2). The IOG also showed a nonsignificant trend toward a larger face-selective response in the right hemisphere (Fig. 6 and Table 2).

In the ventral ATL, the face-selective response was larger in the antFG than in its adjacent sulci (antOTS and antCoS) in the right hemisphere only ($P < 0.05$). The general visual response was also larger in the antFG than in the antOTS and antCoS in both hemispheres ($P < 0.05$).

Because of the very high frequency resolution, the analysis used here is highly resistant to (intracerebral) artifacts (mainly epileptic spikes), which are more broadly distributed across the frequency spectrum than the specific frequencies of visual stimulation (37, 42). Nevertheless, to test for the robustness of the results, we performed the same quantification analysis after artifact rejection (*SI Text*). This complementary analysis yielded virtually identical results to those without artifact rejection (Fig. S5).

Clustered Spatial Organization of Face Selectivity in VOTC. Face-selective responses were widely distributed across the VOTC, with the largest responses found in specific anatomical regions of the right hemisphere. Because of the high spatial resolution of the SEEG approach (in the present study, the intercontact center-to-center spacing is 3.5 mm, whereas it is 5–10 mm in recent electrocorticography or ECoG studies) (e.g., refs. 35 and 49), we were also able to explore the spatial organization of face-selective responses at a finer scale within the different face-selective regions.

To do so, we first visualized face selectivity at single contacts within individual brains (see Fig. 3*B* for examples of four individual brains). We observed that face-selective contacts along an electrode (i.e., array of recording contacts mainly in the medio-lateral axis) tend to be spatially contiguous. This finding was reflected in the mean number of contiguous face-selective contacts (OCC, 4.3 ± 3.6 contacts; PTL, 4.9 ± 3.5; ATL, 2.6 ± 1.9; both hemispheres grouped) and in the mean distances between face-selective contacts (OCC, 5.1 ± 3.2 mm; PTL, 4.1 ± 0.9; ATL, 5.5 ± 4.2) which were significantly different from when randomly shuffling the contact location ($P < 0.01$ for all comparisons) (*SI Text*).

We also observed that, among face-selective contacts, the contacts with the largest face-selective amplitude tended to be spatially contiguous. This finding is exemplified in Fig. 3*B*, where the largest face-selective responses were grouped in specific regions (latFG, antOTS, and IOG). Highly face-selective contacts were defined for each electrode separately as contacts with a distinctively high amplitude (i.e., amplitude >3 SDs from the amplitude of the lowest contacts) (*SI Text*). The proportion of electrodes containing highly face-selective contacts was maximal in the antCoS, antFG, antOTS, medFG, latFG, and IOG, while being smaller in the VMO or equal to zero in the remaining regions (Fig. 7*A*; both hemispheres grouped). Among these electrodes, the mean distance between these contacts was significantly smaller than when randomly shuffling their positions on the electrodes (Fig. 7*B* and *SI Text*), showing that highly face-selective contacts tended to spatially cluster.

To further visualize and examine the spatial clustering of highly face-selective responses in each anatomical region, we quantified the spatial variation of face-selective response amplitude across the length of each electrode (*SI Text*). The profiles displayed in

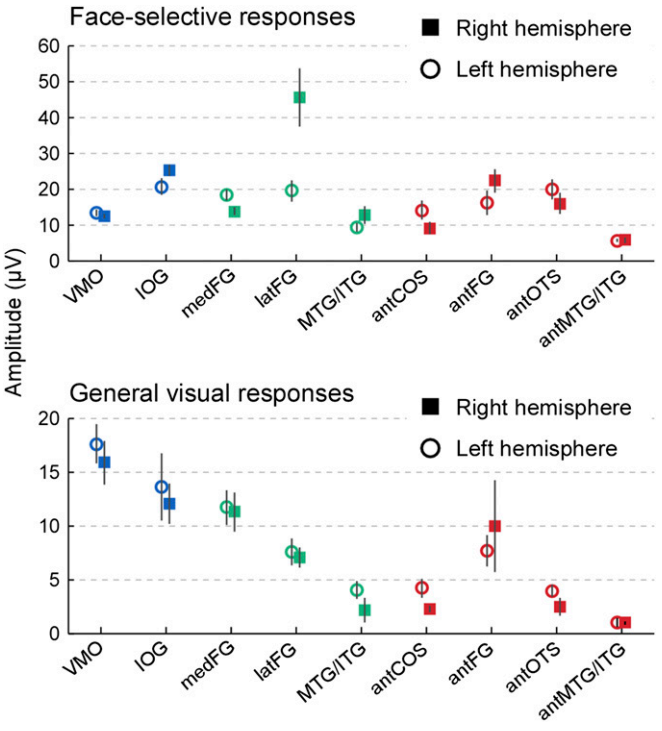

Fig. 6. Quantification of the response amplitudes in each region. Face-selective (*Upper*) and general visual (*Lower*) responses were quantified in each region as the average of the response amplitudes across contacts. The average across contacts for each region is shown separately for the left and right hemispheres. Error bars represent the SEM across contacts.

Table 2. Statistical comparisons between right and left hemisphere homologous regions using a permutation test

Regions	Face-selective response		General visual response	
	Mean difference R-L (μV)	*P* value	Mean difference R-L (μV)	*P* value
VMO	−0.93	0.526	−1.71	0.542
IOG	4.49	0.112	−1.56	0.657
medFG	−4.68*	0.020	−0.43	0.840
latFG	26.03*	0.001	−0.53	0.723
MTG/ITG	3.41	0.205	−1.83	0.187
antCoS	−4.93	0.165	−1.96	0.097
antFG	6.15	0.219	2.34	0.628
antOTS	−3.90	0.400	−1.49	0.165
antMTG/ITG	0.12	0.904	−0.05	0.914

See *SI Text* for details. L, left; R, right. *$P < 0.05$.

Fig. 7*C* represent the mean variation of face-selective response amplitude as a function of the distance from the maximum amplitude in each region (averaging both sides around the maximum and pooling across hemispheres to increase the number of data points). In most regions (except in MTG/ITG and antMTG/ITG), the second or third largest responses were contiguous to the maximum and significantly above the amplitude expected by chance if the contacts were randomly located (i.e., 95% confident interval) (Fig. 7*C*, gray area). This finding indicates that the largest face-selective responses tend to cluster in specific regions.

Face-Exclusive Responses. Strikingly, some individual recording contacts in the VOTC exhibited exclusive responses to faces—i.e., significant face-selective responses without any general visual response (for examples, see Fig. 8*A*). There were few face-exclusive responses in the occipital cortex (15, mainly in the IOG), 38 in the PTL (mainly in the MTG/ITG and in the latFG), and 58 in the ATL (mainly in the antOTS, antCoS, and antMTG/ITG). The proportion of face-exclusive contacts (with respect to all face-selective contacts) increased from posterior to anterior regions (Fig. 8*B*) and was maximal in the right ATL (30 of 68; 44.1%). In the ATL only, the proportion of face-exclusive contacts was significantly higher in the right than in the left hemisphere (44.1% vs. 28.6% respectively; $P = 0.039$, Pearson's χ^2 test).

To rule out the possibility that the higher proportion of face-exclusive responses in the ATL was merely due to this region's inability to generate responses at a fast rate (i.e., 6-Hz base rate), 11 of the participants performed a control experiment in which the exact same stimuli were presented at a slower base frequency rate (1.5 Hz) (*SI Text*). The reduction of general visual responses from posterior to anterior regions was similar whether we used 1.5 or 6 Hz as the base stimulation frequency (Fig. S4*B*). Moreover, the disappearance of the general visual responses on some contacts was not due to a global amplitude reduction, which would have affected first the general visual response because it is lower than face-selective response to begin with ("floor effect"). Indeed, we observed a similar reduction of general visual responses from posterior to anterior regions when general responses were extracted from groups of contacts with similar mean face-selective response amplitudes across regions (Fig. S4*C*).

Summary. In quantifying face selectivity across the whole human VOTC with intracerebral recordings and a high-sensitivity stimulation approach in a large group of individual brains, we made a number of key observations regarding the neural basis of face categorization. First, in line with human intracranial recording studies, we reported face-selective responses across all of the VOTC. Second, we validated two decades of functional neuroimaging findings with a direct measure of neural activity: Among all VOTC regions, the right latFG, corresponding to the right FFA, shows the largest face-selective response, followed by the right IOG (OFA). Third, we found different spatial organizations of face-selective responses across regions, with the key regions (i.e., IOG, latFG, and ATL regions) showing a clustered organization of highly face-selective responses. Fourth, we identified three regions exhibiting face-selective responses in the ventral ATL, specifically the antCoS, the antFG, and the antOTS. Finally, we report a number of face-exclusive responses at the population level, with these responses increasing along a posterior to anterior axis in the VOTC to reach almost 50% in the right ATL.

Discussion

Wide Distribution of Face-Selective Responses Across the VOTC. Besides the dominant latFG and IOG, face-selective responses were found in regions that are not, or are rarely, identified as face-selective in fMRI: the VMO, the medFG, the MTG/ITG, and in a large portion of the ventral ATL. These results are in line with

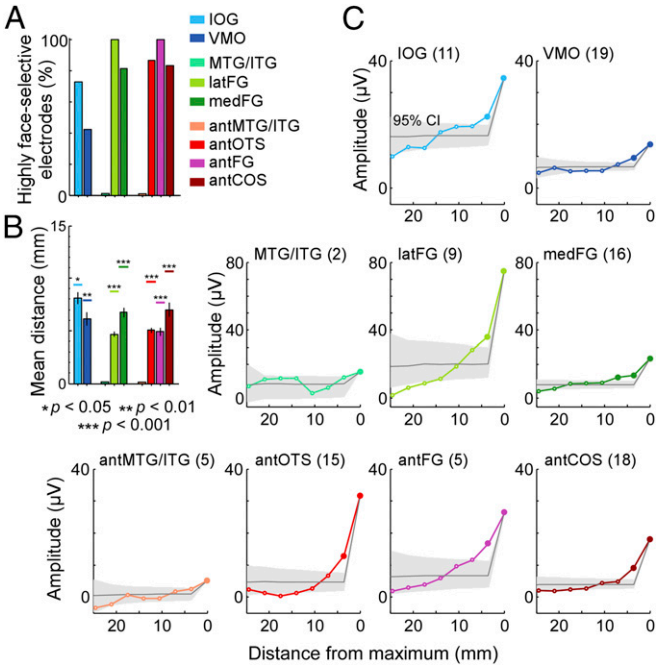

Fig. 7. Clustered organization of face selectivity within each region. (*A*) Proportion of electrodes showing highly face-selective contacts in each region. (*B*) Mean distance between highly face-selective contacts in electrodes highlighted in *A*. Error bars represent the SEM. These distances were significantly smaller than when randomly shuffling the locations of contacts on the electrodes (95% lower confidence interval indicated by horizontal lines). (*C*) Spatial variation of face-selective response amplitude in each region. All electrodes containing at least one face-selective contact were identified and pooled across hemispheres. The number of electrodes included in the analysis for each region is indicated in parentheses. Next, electrodes were spatially centered with respect to the contact recording the largest face-selective response. Each electrode was then folded around the maximum by averaging responses from equidistant contacts on both sides of the maximum. Face-selective responses measured at corresponding contacts across electrodes were then averaged by region. The resulting profiles represent the mean variation of face-selective response amplitude as a function of the distance from the maximum (maximum located at 0 mm). To statistically assess the clustering of highly face-selective responses in each region, these profiles were compared with a random distribution of profiles generated by repeatedly performing the exact same analysis after randomly shuffling the location of contacts in each electrode (i.e., both original and random profiles were spatially centered on the largest face-selective response). Shaded gray areas and thin gray lines, respectively, represent the 95% confidence interval and the mean of these random distributions. Face-selective responses above or equal to the 95% confidence interval are shown as larger filled markers.

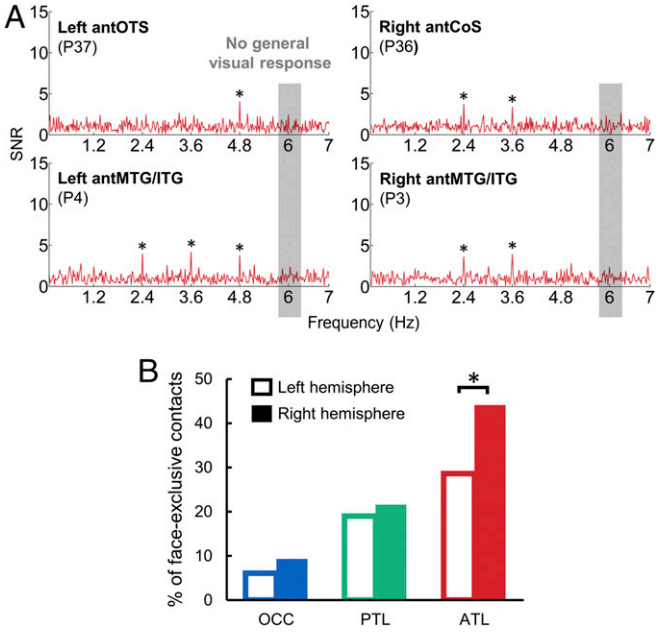

Fig. 8. Face-exclusive responses. (*A*) Examples of recordings in single participants in right and left ATL regions. *$z > 3.1$; $P < 0.001$. (*B*) Proportion of face-exclusive contacts. The proportion of face-exclusive contacts (with respect to all face-selective contacts) is displayed for the three main regions (OCC, PTL, and ATL). *$P < 0.05$ (Pearson's χ^2 test).

previous iEEG observations of widely distributed face-selective responses in the VOTC (27, 30, 33–35, 50). However, face-selective responses are even more extensively distributed here than previously observed, in particular compared with the seminal study of Allison et al. (27), using grids of electrodes on the cortical surface (ECoG). Moreover, our proportion of VOTC face-selective responses is larger than in previous studies. For example, whereas Allison et al. (27) reported 121 face-selective responses in 98 participants (N200: 82 responses, P350: 39 responses), we disclosed 555 face-selective responses in 28 participants.

Importantly, our wide distribution and high proportion of face-selective responses cannot reflect low-level visual differences between faces and nonface objects, not only because all images were equalized for mean pixel luminance and contrast. Most critically, the numerous natural images of face and object vary widely in lighting, contrast, size, viewpoint, etc. Thus, low-level cues do not vary systematically at the specific periodic rate of faces (1.2 Hz), eliminating the putative contribution of these cues to the measured face-selective response (45). Hence, face-selective responses in this stimulation mode disappear when images are phase-scrambled, preserving low-level visual cues (i.e., power spectrum; refs. 45 and 46). Moreover, with this approach, both generalization (across widely variable face exemplars) and discrimination (from widely variable nonface objects) are mandatory to elicit face-selective responses. Generalization is necessary because categorizing only a subset of the face stimuli as faces would break the 1.2-Hz periodicity. Discrimination of faces from each of the other object categories, not only from an average of their response as in a standard fMRI localizer (e.g., refs. 12, 16, and 51), is also necessary here. Indeed, if one of the nonface categories elicits the same response as faces, the 1.2-Hz periodicity will be disrupted. Finally, high selectivity to faces is ensured by using 14 nonface categories, a larger number than in previous studies, with a majority of studies comparing faces to a single nonface category (houses or cars typically; e.g., ref. 14; see also ref. 27 for 4–6 nonface categories in iEEG). Despite this control, and even though there is no other visual category than faces eliciting such a large specific response at the population level with such a right hemisphere advantage in the human brain, we cannot formally exclude the possibility that yet another visual category would also elicit category-specific 1.2-Hz responses in the VOTC if presented every fifth stimuli in our rapid visual stimulation sequence. Such a comparison of different category-selective response maps could be directly performed in future studies with the present FPVS approach.

Here we argue that two key aspects of the present study may account for the particularly large proportion and wide spatial distribution of face-selective responses identified. First, unlike ECoG (27), stereotactic electroencephalography (SEEG) records within cortical sulci, in which a substantial proportion of face-selective responses were found (i.e., CoS and OTS in the PTL and antCoS and antOTS in the ventral ATL). Second, we used a FPVS approach providing: (*i*) an objective criterion to identify even small neural responses above noise level in the frequency domain and (*ii*) an extremely high SNR compared with standard stimulation approaches (42, 43, 45). In summary, our results support the view that neural populations widely distributed across the human VOTC, rather than a few localized functional regions only as found in neuroimaging studies, generate robust selective responses to faces.

Regional Peaks of Face Selectivity. Although the right latFG shows the largest and most consistent face-selective response in human neuroimaging (e.g., refs. 8 and 12–14), previous iEEG studies did not identify this region as showing the largest face-selective response in the VOTC, because face-selective responses were not compared across regions (30, 34), the issue of FG lateralization was not addressed (35), or face-selective responses in the FG were not lateralized [ERPs (27); broadband gamma activity (40)]. Here, of all anatomically defined VOTC regions, the largest face-selective iEEG response was found in the lateral section of the right middle FG (latFG; Talairach coordinates: $x = 41, y = -45, z = -16$), which corresponds to the right FFA (10, 12). This observation therefore validates with a direct measure of neural activity the predominant face-selective activation in the right latFG found in human neuroimaging (i.e., the FFA) (12).

The larger face-selective response in the right than in the left latFG may be at least partly due to the spatial organization of face-selective neuronal populations. To record large face-selective responses on some contacts in the right latFG as here, a large number of face-selective neurons should be densely grouped nearby the recording contacts. Although we were not able to compare right and left latFG with our clustering analysis because of a low statistical power (6 and 3 electrodes peaking in right and left latFG, respectively), this hypothesis is supported by the dense clustered organization of highly face-selective responses found in the latFG when both hemispheres were grouped. In addition, although face-selective responses were also recorded in the medFG here, they were substantially smaller in amplitude than in the latFG. This observation supports the recently discovered cytoarchitectonic and fMRI-based functional mediolateral division of the FG (52).

The right hemispheric dominance of our electrophysiological measures is in line with the well-established dominance of this hemisphere in face perception as evidenced by divided visual field presentation (53), neuroimaging (e.g., refs. 10, 12, and 14) and scalp EEG (54), including studies performed with the same paradigm as used here (45, 46). Most importantly, our results agree with the localization of brain damage in patients with acquired prosopagnosia, whose lesions are either bilateral or localized unilaterally in the right hemisphere (refs. 2–7, except in a few left-handed patients: for review, see ref. 9), as well as with the right dominance of the lateral section of the middle FG in producing conscious distortions of a perceived face (38, 40).

Importantly, prosopagnosia can also be due to lesions of the right IOG (refs. 4 and 51; see also ref. 55 for face-processing

impairment due to transcranial magnetic stimulation over this region), as well as of the right ATL (56). In line with evidence from these lesion studies, here, the second largest face-selective responses were found in the right IOG and antFG, two regions in which highly face-selective responses were also clustered. The right IOG corresponds to the cortical territory where the OFA is typically located (16, 17, 51), so that our observations again validate the findings of neuroimaging studies of face perception. The right antFG is part of the ventral ATL, whose role in face perception is currently the focus of intense research (ref. 25; for review, see ref. 57) and which will be discussed next.

A Set of Face-Selective Regions in the ATL. Although the fMRI signal in the ventral ATL is absent or very weak, previous iEEG studies have found widely distributed face-selective responses in this region, yet without providing precise anatomical information (i.e., ref. 32). Here, we took advantage of the high spatial resolution of depth electrodes and their specific recordings of both gyri and sulci to clarify the locations of face-selective responses in the ventral ATL. We found a wide distribution of face-selective responses in the ventral ATL (antCoS, antFG, and antOTS) in specific and reproducible anatomical locations across individual participants. In these regions, we also found clusters of highly face-selective responses, even if their mean amplitude was not among the largest (except in the right antFG). This result is probably because our anatomical regions of interest were larger in size than the corresponding clusters.

Face selectivity in the antCoS is in line with the finding of face-selective responses in the anterior segment of the CoS bilaterally in a few relatively recent fMRI studies (14, 20–23, 58). Moreover, we found face-selective responses in the antOTS, which is a major VOTC sulcus, located laterally to the antCoS (47). Although the antOTS was never explicitly mentioned as a face-selective area in fMRI, visual analysis of individual data from these studies suggests that some anterior face-selective activations fall into the antOTS, and not into the antCoS as described (20, 22, 23). Our finding is also in agreement with ECoG studies reporting face-selective responses close to the antCoS and antOTS (27, 50). Given that antCoS and antOTS correspond to different cytoarchitectonic structures [perirhinal cortex and temporal isocortex, respectively (59)], these two regions may be functionally distinct and may support different face-selective neural processes.

The antFG is located anteriorly to the posterior FG and the typical location of the FFA (25, 48, 60). Unfortunately, because of magnetic susceptibility artifacts, fMRI signal recorded from this antFG region is absent or very weak (20–25). As a result, only a handful of fMRI studies reported face-selective activations in the antFG, and little is known about the role of this region in face processing (refs. 21, 23, and 58; but see ref. 61 for categorical differences between unfamiliar and familiar faces in the right antFG using PET). A recent iEEG study using depth electrodes recorded electrophysiological face-selective responses directly from the right antFG in a single participant (25). Electrically stimulating these intracerebral sites evoked transient prosopagnosia, pointing to a causal role of the right antFG in face recognition. Identifying clear iEEG face-selective responses specifically in this region in several individual brains here further supports its prominent role in human face recognition.

Accumulating data with the present approach over very large samples of individual brains, as well as refined anatomical definitions of the regions of interest (for example, based on cyto- or receptor-architectonics) (e.g., ref. 52) should progressively clarify the relative functional importance of these ATL regions in face categorization.

Face-Exclusive Responses Predominant in the Right ATL. Previous human iEEG studies recorded large responses to faces with weak responses to nonface stimuli over the VOTC (27, 50). Here, thanks to a clear definition of signal and noise provided by the fast periodic stimulation and the frequency domain analysis (43), we were able to objectively assess the absence of response (i.e., no signal above noise) to nonface objects at face-selective contacts. We found numerous face-selective responses in the absence of a general visual response. Such EEG spectra have not been found on the human scalp (45). Because intracerebral contacts pool the activity of hundreds of thousands of neurons, this finding reveals the presence of exclusive responses to faces at a macroscopic level of cortical organization (i.e., cell population level). Exclusive responses to the category of faces have been found in single neurons in the monkey superior temporal sulcus (62, 63), and there is evidence that these neurons are grouped in cortical columns or larger clusters (64) so that face-selective areas identified in fMRI in monkeys contain an extremely large proportion of neurons responding exclusively to faces (64). Here, to our knowledge, we report the first evidence of face-exclusive responses at a cell-population level in humans.

The right ATL recorded the highest proportion of face-exclusive responses, suggesting that it is involved in the highest stages of face processing. Compared with face processes that require information about the context (e.g., face detection among visual scenes or other objects), processing faces independently from the context (i.e., nonface categories) may be particularly useful for processes that are known to be specific to faces (e.g., encoding and retrieval of information specific to an individual face, holistic processing of individual exemplars, sex, age, expression, social judgments, etc.). This suggestion is consistent with fMRI and brain lesions studies showing that right ATL may play a role in face individualization and semantic knowledge about people (10, 56, 65, 66).

Conclusions

Thanks to intracerebral recordings performed in a large human population and a fast periodic presentation of objects and faces, objective face-selective responses were defined and quantified by anatomical regions along the whole VOTC. Our findings reconcile two main views of the large-scale functional organization of face selectivity in the VOTC: on the one hand, the partial and clustered organization identified by fMRI studies and, on the other hand, the widely distributed, scattered face-selective responses found by iEEG studies. Although face-selective populations of neurons are present across the whole VOTC, they are more densely distributed in specific regions, such as the right latFG, which are typically identified in fMRI and may be the most critical regions for this function. Even though the frequency-tagging approach used here essentially concentrated on quantitative differences between regions, it also revealed a qualitative difference at a finer-scale level, with an increasing proportion of electrode contacts showing exclusive response to faces as one progresses from posterior to anterior VOTC regions, particularly in the right hemisphere. Taking advantage of this objective and sensitive approach, future studies with higher recording samples in each region may be able to extract significant information from the patterns of face-selective harmonic responses in amplitude and phase (i.e., the shape of the output function) in various VOTC regions, and make further progress in our understanding of the spatiotemporal dynamics of face categorization in the human brain.

Materials and Methods

Participants. The study included 28 right-handed participants (15 females, mean age: 30.5 ±4.4 y) undergoing clinical intracerebral evaluation with depth electrodes [SEEG (67)] for refractory partial epilepsy. Participants were studied in the Epilepsy Unit of the University Hospital of Nancy between December 2012 and March 2015. Participants were included in the study if they had at least one intracerebral electrode implanted in the temporal or occipital lobe and if they were right-handed (as assessed by the Edinburgh Handedness Inventory). They all gave written consent to participate to the

study, which was part of a protocol approved by the human investigation committee of the University Hospital of Nancy. All but two participants performed the Benton Face Recognition Test (68) before the SEEG exploration, with an average score of 41.8 ± 4.4 (20 participants above a score of 39 of 54, indicating normal performances in matching individual faces, and 6 participants below 39 of 54, indicating mild impairment).

Intracerebral Electrode Implantation and Recording. Intracerebral electrodes were stereotactically implanted within the participants' brains to delineate their seizure onset zone. Each intracerebral electrode consisted of a cylinder of 0.8 mm diameter and contained 8–15 independent recording contacts of 2 mm in length separated by 1.5 mm from edge to edge and by 3.5 mm center-to-center (for details about the electrode implantation procedure, see ref. 25). Typical trajectories of depth electrodes implanted in the temporal and occipital lobes are shown in Fig. 1*C*. Intracerebral EEG was recorded at a 512-Hz sampling rate with a 256-channel amplifier with either a midline prefrontal scalp electrode (FPz, in 21 participants) or an intracerebral contact in the white matter serving as reference electrode (in 7 participants).

FPVS Paradigm.

Stimuli. A total of 200 grayscale natural images of various nonface objects (from 14 nonface categories: cats, dogs, horses, birds, flowers, fruits, vegetables, houseplants, phones, chairs, cameras, dishes, guitars, and lamps) and 50 grayscale natural images of faces were used, and were the same as in a recent study (45) [see Fig. 1*B* for examples of various face exemplars (stimuli available at dx.doi.org/10.5061/dryad.5f9v7) and Fig. S6 for mean images for each category]. Each image contained an unsegmented object or face near the center that differed in terms of size, viewpoint, lighting conditions, and background. Images were equalized for mean pixel luminance and contrast.

Procedure. Participants viewed continuous sequences with highly variable natural images of objects presented at a rate of 6 Hz through sinusoidal contrast modulation (Fig. 1*A*). A sequence lasted 70 s, including 66 s of stimulation at full contrast flanked by 2 s of fade-in and fade-out, where contrast gradually increased or decreased, respectively. The long sequence duration produces a high-frequency resolution (sequences of 63 s long were taken into account in the analysis, yielding a frequency resolution of 1/63 = 0.016 Hz) that allows isolating the response of interest into a narrow frequency bin, which greatly enhanced its SNR (42, 43). The experiment consisted of two types of sequences: (*i*) periodic and (*ii*) nonperiodic. In the main condition (i.e., periodic), highly variable natural images of faces were presented periodically as every fifth image (i.e., at 1.2 Hz = 6/5 Hz), with all images being randomly selected from their respective categories (Fig. 1*A*; see also Movie S1 for an example of visual stimulation in the periodic condition). In the control condition (i.e., nonperiodic), the exact same stimuli were shown in random order so that there was no face periodic input at 1.2 Hz. Participants were unaware of the periodicity of the faces in the periodic condition. Each participant was presented with at least two sequences of the periodic condition and one sequence of the nonperiodic condition, in pseudorandom order (~5 min of experiment, including short breaks). The experiment was repeated a second time for 12 of 28 participants. No participant had seizures in the 2 h preceding FPVS recordings. During the sequences, participants were instructed to fixate on a small black cross which was presented continuously at the center of the stimuli and to detect brief (500 ms) color changes (black to red) of this fixation cross.

Intracerebral EEG Analysis.

Frequency domain processing. Segments of iEEG corresponding to stimulation sequences were extracted (74-s segments, −2 to +72 s). In our main analyses, no artifact rejection was performed because intracerebral artifacts (mainly epileptic spikes, but also electro-oculographic and electro-myographic activity because we used a prefrontal scalp electrode as reference electrode for most of the participants) are more broadly distributed across the frequency spectrum than the frequencies of interest (i.e., 1.2 and 6 Hz and their respective harmonics). The 74-s data segments were cropped to contain an integer number of 1.2-Hz cycles beginning 2 s after the onset of the sequence (right at the end of the fade-in period) until ~65 s, before stimulus fade-out (75 face cycles ~ 63 s). Sequences were averaged in the time domain, separately for each condition and each participant. Subsequently, a fast Fourier transform (FFT) was applied to these averaged segments, and amplitude spectra were extracted for all contacts.

Face-selective responses. The FPVS approach used here allows for identifying and separating two distinct types of responses (45): (*i*) a general visual response occurring at the base stimulation frequency (6 Hz) and its harmonics, as well as (*ii*) a face-selective response at 1.2 Hz and its harmonics. Face-selective responses significantly above noise level at the face stimulation frequency (1.2 Hz) and its harmonics (2.4, 3.6 Hz, etc.) were determined by transforming the frequency spectra to *z* scores (45, 69). The *z* scores were computed as the difference between amplitude at each frequency bin and the mean amplitude of the corresponding 48 surrounding bins (25 bins on each side, i.e., 50 bins, but excluding the 2 bins directly adjacent to the bin of interest, i.e., 48 bins) divided by the SD of amplitudes in the corresponding 48 surrounding bins. A contact was considered as face-selective if a *z* score was >3.1 (i.e., $P < 0.001$, one-tailed: signal > noise) for at least one of the first four face-selective frequency harmonics in the periodic condition (1.2, 2.4, 3.6, or 4.8 Hz; we considered it unlikely that face-selective responses would manifest only at harmonics above the 6-Hz base frequency).

Quantification of responses amplitude. Baseline-corrected amplitudes were computed as the difference between the amplitude at each frequency bin and the average of 48 corresponding surrounding bins (25 bins on each side, i.e., 50 bins, but excluding the 2 bins directly adjacent to the bin of interest, i.e., 48 bins) (e.g., ref. 70). The face-selective and general visual responses were then quantified at each face-selective contact as the sum of the baseline-subtracted amplitude across harmonics (70, 71). The range over which face and base frequency harmonics were summed was constrained by the highest significant harmonic across participants (*z* score > 3.1; $P < 0.001$). Across all participants, no significant face-selective response was found above the 14th harmonic (i.e., 16.8 Hz), and no significant base frequency responses was found above the 4th harmonic (i.e., 24 Hz). Face-selective responses were therefore quantified as the sum of the baseline-subtracted amplitudes at the face-selective frequency harmonics from the 1st until the 14th (1.2 until 16.8 Hz), excluding the 5th and 10th harmonics (6 and 12 Hz) that coincided with the base frequency. General visual responses were similarly quantified by summing the amplitudes from the 1st until the 4th base frequency harmonics (6 until 24 Hz). Thus, for each face-selective contact, we obtained two amplitude values that respectively represented the overall face-selective response and the overall general visual response. SNR spectra were also calculated as the ratio between the amplitude at each frequency bin and the average of the corresponding 48 surrounding bins for display purposes and comparison across studies.

Contact Localization in the Individual Anatomy. Rather than normalizing individual brains by linear transformation, which blurs the individuality of functional organization, we subdivided individual brains in anatomical regions of interest using individual anatomical landmarks (i.e., gyri and sulci) (Fig. S2). Individual face-selective contacts were then localized according to this anatomical subdivision and grouped by anatomical location across all participants. We used a topographic parcellation of the VOTC close to that proposed by Kim et al. (48). Major VOTC sulci served as medio-lateral landmarks (CoS and OTS), and coronal reference planes containing given landmarks served as postero-anterior landmarks (Fig. S2). A coronal plane including the anterior tip of the parieto-occipital sulcus served as the border of the occipital and temporal lobes. A coronal plane including the posterior tip of the HIP served as the border of PTL and ATL. In a separate analysis, anatomical MRIs were also spatially normalized to determine Talairach and MNI coordinates of intracerebral contacts.

ACKNOWLEDGMENTS. We thank the participants for their involvement in the study; Ernest Galbrun for helping coregistering brain images; and Talia Retter and two anonymous reviewers for their comments on a previous version of the manuscript. J.J., J.L.-S., and B.R. are supported by the Belgian National Fund for Scientific Research (FNRS) and C.J. is supported by the Belgian Federal Government (BELSPO, return grant 2012). This work was supported by European Research Council Grant facessvep 284025.

1. Bodamer J (1947) Die Prosop-agnosie; die Agnosie des Physiognomieerkennens. *Arch Psychiatr Nervenkr Z Gesamte Neurol Psychiatr* 118(1-2):6–53.
2. Quaglino A, Borelli GB, Della Sala S, Young AW (2003) Quaglino's 1867 case of prosopagnosia. *Cortex* 39(3):533–540.
3. Barton JJ (2008) Structure and function in acquired prosopagnosia: Lessons from a series of 10 patients with brain damage. *J Neuropsychol* 2(Pt 1):197–225.
4. Bouvier SE, Engel SA (2006) Behavioral deficits and cortical damage loci in cerebral achromatopsia. *Cereb Cortex* 16(2):183–191.
5. De Renzi E, Perani D, Carlesimo GA, Silveri MC, Fazio F (1994) Prosopagnosia can be associated with damage confined to the right hemisphere—an MRI and PET study and a review of the literature. *Neuropsychologia* 32(8):893–902.
6. Hécaen H, Angelergues R (1962) Agnosia for faces (prosopagnosia). *Arch Neurol* 7:92–100.
7. Meadows JC (1974) The anatomical basis of prosopagnosia. *J Neurol Neurosurg Psychiatry* 37(5):489–501.
8. Duchaine B, Yovel G (2015) A revised neural framework for face processing. *Annu Rev Vis Sci* 1:393–416.

9. Rossion B (2014) Understanding face perception by means of prosopagnosia and neuroimaging. *Front Biosci (Elite Ed)* 6:258–307.
10. Sergent J, Ohta S, MacDonald B (1992) Functional neuroanatomy of face and object processing. A positron emission tomography study. *Brain* 115(Pt 1):15–36.
11. Puce A, Allison T, Gore JC, McCarthy G (1995) Face-sensitive regions in human extrastriate cortex studied by functional MRI. *J Neurophysiol* 74(3):1192–1199.
12. Kanwisher N, McDermott J, Chun MM (1997) The fusiform face area: A module in human extrastriate cortex specialized for face perception. *J Neurosci* 17(11):4302–4311.
13. Haxby JV, Hoffman EA, Gobbini MI (2000) The distributed human neural system for face perception. *Trends Cogn Sci* 4(6):223–233.
14. Rossion B, Hanseeuw B, Dricot L (2012) Defining face perception areas in the human brain: A large-scale factorial fMRI face localizer analysis. *Brain Cogn* 79(2):138–157.
15. Weiner KS, Grill-Spector K (2010) Sparsely-distributed organization of face and limb activations in human ventral temporal cortex. *Neuroimage* 52(4):1559–1573.
16. Zhen Z, et al. (2015) Quantifying interindividual variability and asymmetry of face-selective regions: A probabilistic functional atlas. *Neuroimage* 113:13–25.
17. Gauthier I, et al. (2000) The fusiform "face area" is part of a network that processes faces at the individual level. *J Cogn Neurosci* 12(3):495–504.
18. Puce A, Allison T, Bentin S, Gore JC, McCarthy G (1998) Temporal cortex activation in humans viewing eye and mouth movements. *J Neurosci* 18(6):2188–2199.
19. Bukowski H, Dricot L, Hanseeuw B, Rossion B (2013) Cerebral lateralization of face-sensitive areas in left-handers: Only the FFA does not get it right. *Cortex* 49(9): 2583–2589.
20. Tsao DY, Moeller S, Freiwald WA (2008) Comparing face patch systems in macaques and humans. *Proc Natl Acad Sci USA* 105(49):19514–19519.
21. Rajimehr R, Young JC, Tootell RB (2009) An anterior temporal face patch in human cortex, predicted by macaque maps. *Proc Natl Acad Sci USA* 106(6):1995–2000.
22. Axelrod V, Yovel G (2013) The challenge of localizing the anterior temporal face area: A possible solution. *Neuroimage* 81:371–380.
23. Nasr S, Tootell RB (2012) Role of fusiform and anterior temporal cortical areas in facial recognition. *Neuroimage* 63(3):1743–1753.
24. Ojemann JG, et al. (1997) Anatomic localization and quantitative analysis of gradient refocused echo-planar fMRI susceptibility artifacts. *Neuroimage* 6(3):156–167.
25. Jonas J, et al. (2015) Beyond the core face-processing network: Intracerebral stimulation of a face-selective area in the right anterior fusiform gyrus elicits transient prosopagnosia. *Cortex* 72:140–155.
26. Halgren E, et al. (1994) Spatio-temporal stages in face and word processing. I. Depth-recorded potentials in the human occipital, temporal and parietal lobes [corrected]. *J Physiol Paris* 88(1):1–50; erratum in *J Physiol Paris* 1994; 88(2): following 151.
27. Allison T, Puce A, Spencer DD, McCarthy G (1999) Electrophysiological studies of human face perception. I: Potentials generated in occipitotemporal cortex by face and non-face stimuli. *Cereb Cortex* 9(5):415–430.
28. Barbeau EJ, et al. (2008) Spatio temporal dynamics of face recognition. *Cereb Cortex* 18(5):997–1009.
29. Davidesco I, et al. (2014) Exemplar selectivity reflects perceptual similarities in the human fusiform cortex. *Cereb Cortex* 24(7):1879–1893.
30. Engell AD, McCarthy G (2011) The relationship of γ oscillations and face-specific ERPs recorded subdurally from occipitotemporal cortex. *Cereb Cortex* 21(5):1213–1221.
31. Liu H, Agam Y, Madsen JR, Kreiman G (2009) Timing, timing, timing: Fast decoding of object information from intracranial field potentials in human visual cortex. *Neuron* 62(2):281–290.
32. Puce A, Allison T, McCarthy G (1999) Electrophysiological studies of human face perception. III: Effects of top-down processing on face-specific potentials. *Cereb Cortex* 9(5): 445–458.
33. Sato W, et al. (2014) Rapid, high-frequency, and theta-coupled gamma oscillations in the inferior occipital gyrus during face processing. *Cortex* 60:52–68.
34. Vidal JR, et al. (2010) Category-specific visual responses: An intracranial study comparing gamma, beta, alpha, and ERP response selectivity. *Front Hum Neurosci* 4:195.
35. Jacques C, et al. (2016) Corresponding ECoG and fMRI category-selective signals in human ventral temporal cortex. *Neuropsychologia* 83:14–28.
36. Jonas J, et al. (2012) Focal electrical intracerebral stimulation of a face-sensitive area causes transient prosopagnosia. *Neuroscience* 222:281–288.
37. Jonas J, et al. (2014) Intracerebral electrical stimulation of a face-selective area in the right inferior occipital cortex impairs individual face discrimination. *Neuroimage* 99: 487–497.
38. Parvizi J, et al. (2012) Electrical stimulation of human fusiform face-selective regions distorts face perception. *J Neurosci* 32(43):14915–14920.
39. Puce A, Allison T, Spencer SS, Spencer DD, McCarthy G (1997) Comparison of cortical activation evoked by faces measured by intracranial field potentials and functional MRI: Two case studies. *Hum Brain Mapp* 5(4):298–305.
40. Rangarajan V, et al. (2014) Electrical stimulation of the left and right human fusiform gyrus causes different effects in conscious face perception. *J Neurosci* 34(38):12828–12836.
41. Adrian ED, Matthews BH (1934) The Berger rhythm: Potential changes from the occipital lobes in man. *Brain* 4(57):355–385.
42. Regan D (1989) *Human Brain Electrophysiology: Evoked Potentials and Evoked Magnetic Fields in Science and Medicine* (Elsevier, New York).
43. Norcia AM, Appelbaum LG, Ales JM, Cottereau BR, Rossion B (2015) The steady-state visual evoked potential in vision research: A review. *J Vis* 15(6):4.
44. Winawer J, et al. (2013) Asynchronous broadband signals are the principal source of the BOLD response in human visual cortex. *Curr Biol* 23(13):1145–1153.
45. Rossion B, Torfs K, Jacques C, Liu-Shuang J (2015) Fast periodic presentation of natural images reveals a robust face-selective electrophysiological response in the human brain. *J Vis* 15(1):18.
46. de Heering A, Rossion B (2015) Rapid categorization of natural face images in the infant right hemisphere. *eLife* 4:e06564.
47. Huntgeburth SC, Petrides M (2012) Morphological patterns of the collateral sulcus in the human brain. *Eur J Neurosci* 35(8):1295–1311.
48. Kim JJ, et al. (2000) An MRI-based parcellation method for the temporal lobe. *Neuroimage* 11(4):271–288.
49. Matsuo T, et al. (2015) Alternating zones selective to faces and written words in the human ventral occipitotemporal cortex. *Cereb Cortex* 25(5):1265–1277.
50. Tanji K, Iwasaki M, Nakasato N, Suzuki K (2012) Face specific broadband electrocorticographic spectral power change in the rhinal cortex. *Neurosci Lett* 515(1):66–70.
51. Rossion B, et al. (2003) A network of occipito-temporal face-sensitive areas besides the right middle fusiform gyrus is necessary for normal face processing. *Brain* 126(Pt 11):2381–2395.
52. Weiner KS, Zilles K (2016) The anatomical and functional specialization of the fusiform gyrus. *Neuropsychologia* 83:48–62.
53. Hillger LA, Koenig O (1991) Separable mechanisms in face processing: Evidence from hemispheric specialization. *J Cogn Neurosci* 3(1):42–58.
54. Rossion B, Joyce CA, Cottrell GW, Tarr MJ (2003) Early lateralization and orientation tuning for face, word, and object processing in the visual cortex. *Neuroimage* 20(3): 1609–1624.
55. Pitcher D, Walsh V, Yovel G, Duchaine B (2007) TMS evidence for the involvement of the right occipital face area in early face processing. *Curr Biol* 17(18):1568–1573.
56. Busigny T, et al. (2014) Face-specific impairment in holistic perception following focal lesion of the right anterior temporal lobe. *Neuropsychologia* 56:312–333.
57. Collins JA, Olson IR (2014) Beyond the FFA: The role of the ventral anterior temporal lobes in face processing. *Neuropsychologia* 61:65–79.
58. Pyles JA, Verstynen TD, Schneider W, Tarr MJ (2013) Explicating the face perception network with white matter connectivity. *PLoS One* 8(4):e61611.
59. Braak H, Braak E (1985) On areas of transition between entorhinal allocortex and temporal isocortex in the human brain. Normal morphology and lamina-specific pathology in Alzheimer's disease. *Acta Neuropathol* 68(4):325–332.
60. Onitsuka T, et al. (2003) Fusiform gyrus volume reduction and facial recognition in chronic schizophrenia. *Arch Gen Psychiatry* 60(4):349–355.
61. Rossion B, Schiltz C, Robaye L, Pirenne D, Crommelinck M (2001) How does the brain discriminate familiar and unfamiliar faces?: A PET study of face categorical perception. *J Cogn Neurosci* 13(7):1019–1034.
62. Gross CG, Rocha-Miranda CE, Bender DB (1972) Visual properties of neurons in inferotemporal cortex of the macaque. *J Neurophysiol* 35(1):96–111.
63. Desimone R (1991) Face-selective cells in the temporal cortex of monkeys. *J Cogn Neurosci* 3(1):1–8.
64. Tsao DY, Freiwald WA, Tootell RB, Livingstone MS (2006) A cortical region consisting entirely of face-selective cells. *Science* 311(5761):670–674.
65. Nestor A, Plaut DC, Behrmann M (2011) Unraveling the distributed neural code of facial identity through spatiotemporal pattern analysis. *Proc Natl Acad Sci USA* 108(24):9998–10003.
66. Gainotti G (2007) Different patterns of famous people recognition disorders in patients with right and left anterior temporal lesions: A systematic review. *Neuropsychologia* 45(8):1591–1607.
67. Talairach J, Bancaud J (1973) Stereotaxic approach to epilepsy: Methodology of anatomo-functional stereotactic investigations. *Prog Neurol Surg* 5:297–354.
68. Benton AL, Sivan AB, Hamsher K, Varney NR, Spreen O (1983) *Benton Facial Recognition: Stimulus and Multiple Choice Pictures* (Psychological Assessment Resources, Lutz, FL).
69. Liu-Shuang J, Norcia AM, Rossion B (2014) An objective index of individual face discrimination in the right occipito-temporal cortex by means of fast periodic oddball stimulation. *Neuropsychologia* 52:57–72.
70. Dzhelyova M, Rossion B (2014) Supra-additive contribution of shape and surface information to individual face discrimination as revealed by fast periodic visual stimulation. *J Vis* 14(14):15.
71. Appelbaum LG, Wade AR, Vildavski VY, Pettet MW, Norcia AM (2006) Cue-invariant networks for figure and background processing in human visual cortex. *J Neurosci* 26(45):11695–11708.

Supporting Information

Jonas et al. 10.1073/pnas.1522033113

SI Text

Statistical Comparison Between Regions. Amplitudes of general visual and face-selective responses were statistically compared across pairs of regions containing groups of face-selective contacts by using a permutation test. Specifically, the signal amplitudes measured at all recording contacts in two given regions were randomly assigned in two bins, with the number of contacts in each bin being equal to the number of contacts in each region. Next, the difference between the means of the two random bins was computed and stored. Because permutation shuffles the region label of each contact, the difference between the means of the two new bins reflects the difference between regions under the null hypothesis (i.e., that the contacts in the two regions are drawn from the same population). This process was repeated 20,000 times to obtain a distribution of differences across regions expected under the null hypothesis. A two-tailed P value was computed as the fraction of the permutation distribution that was either smaller or larger than the observed mean difference between compared regions (depending on the sign of this difference). The minimal attainable P value was constrained by the number of permutations performed (i.e., here, minimal P value = 2/20,000 = 0.0001).

Complementary Analysis with Artifact Rejection. In addition to the analyses reported in the main text, an amplitude quantification analysis after a step of SEEG artifact rejection was performed. For each patient's data, the following steps were performed: the 63-s sequences were segmented in epochs of duration of one cycle of 1.2 Hz (i.e., 833 ms); epochs from separate sequences were pooled together; epochs in which signal amplitude at any time point was above or below 4.5 times the across-epoch SD were rejected (the mean percentage of rejected epochs across participants was 28.8% ± 12.5%); remaining epochs were averaged together; and a FFT was performed on these averaged epochs (frequency resolution of 1.2 Hz). The face-selective and general visual responses at the face-selective contacts identified by our main analysis were quantified by using the same methodology.

Clustered Spatial Organization in Face-Selective Regions. The spatial organization of face-selective responses was explored at a finer scale within the different face-selective regions.

Clustering of face-selective contacts. The tendency of face-selective contacts to be spatially contiguous with each other was determined by measuring for each main region (*i*) the mean distance between face-selective contacts and (*ii*) the mean number of face-selective contacts spatially grouped together (i.e., immediately adjacent to each other). Given that recording contacts are regularly spaced apart on electrodes (i.e., arrays of 8–15 recording contacts), this analysis was performed at the level of individual electrodes in each participant's native anatomy. For each participant, we first selected all VOTC electrodes that contained at least one face-selective contact. Each selected electrode was labeled according to the main region where it was located (OCC, PTL, or ATL). Next, the following steps were performed: (*i*) in each electrode, the number of face-selective contacts contiguously located and the distance between adjacent face-selective contacts were computed and stored; and (*ii*) these values were averaged across participants/electrodes for each main region. The spatial contiguity and mean distances across face-selective contacts were statistically tested by running a randomization test. Specifically, distributions of contiguity and mean distances expected by chance were built by repeating steps (*i*) and (*ii*) 2,000 times after randomly shuffling the location of all contacts from each electrode at each iteration. The significance of the original contiguity and distances were determined by comparing them to the random distribution.

Clustering of highly face-selective contacts. The tendency of the contacts showing the largest face-selective amplitude to be spatially contiguous was also tested. Highly face-selective contacts were defined at the level of single electrodes, as contacts with a distinctively high amplitude relative to the distribution of amplitudes in the electrode. Highly face-selective contacts were identified as contacts with an amplitude >3 SDs from the mean amplitude of the 75% of the contacts with the lowest amplitude. Each electrode was labeled according to the anatomical location of its most face-selective contact (i.e., contact showing the largest face-selective response amplitude). The clustering of highly face-selective contacts in each anatomical region was examined by first determining the proportion of electrodes containing highly face-selective contacts. Among these electrodes, the mean distances between highly face-selective contacts were measured and statistically tested by using a randomization test similar to that described above.

The spatial clustering of face selectivity was further examined in each anatomical region. To do so, the spatial variation of face-selective response amplitude across the length of each electrode (an electrode is an array of recording contacts) was quantified in the following way: (*i*) All VOTC electrodes with at least one face-selective recording contact were selected; (*ii*) the amplitude of the face-selective response at all contacts (face selective or not) of the selected electrodes (i.e., 8–15 contacts separated by 3.5 mm center-to-center, per electrode) was measured; (*iii*) each electrode was labeled according to the anatomical location of its most face-selective contact; (*iv*) all electrodes were spatially aligned with respect to the location of the contact with maximal face-selective response amplitude; (*v*) electrodes were pooled by regions across the left and right hemispheres (to increase the number of data points); (*vi*) each electrode was "folded" around the maximum by averaging amplitude values from equidistant contacts on both sides of the maximum; and (*vii*) the resulting face-selective profiles for each region were averaged. The averaged profiles represent the mean variation of face-selective response amplitude as a function of the distance from the maximum. To statistically assess the clustering of highly face-selective responses in each region, a randomization analysis was used. Specifically, the original averaged face-selectivity profiles was compared with a random distribution of profiles generated by repeating steps (*iv*) to (*vii*) 2,000 times, randomly shuffling the location of contacts separately in each electrode, at each iteration. This process allowed generating for each region a confidence interval for the average profile expected by chance if the contacts were randomly located. Because we centered each electrode relative to the maximum face-selective amplitude both for the original and the random contact locations, both types of profiles exhibit a maximum of equal amplitude. However, if the largest face-selective responses tend to spatially cluster in a given region (and therefore tend to be contiguous to the maximum), the responses around the maximum should be significantly above the profiles computed after randomly shuffling contacts location.

Control Experiment at 1.5-Hz Stimulation Rate. To ensure that the pattern of variation of the general visual responses across regions was independent from the stimulation rate (6 Hz), the amplitude of general visual responses was measured in an additional control experiment performed in 11 of our participants. They performed the exact same experiment but with a lower base frequency rate (base frequency, 1.5 Hz; face-selective frequency, 1.5/5 = 0.3 Hz;

three to six sequences of 70 s per participant). General visual responses at 1.5 Hz were quantified at each face-selective contact (defined using the 6-Hz experiment) as the sum of the baseline-corrected amplitude across harmonics (up to the highest significant harmonic across patients, i.e., 24 Hz for the 6-Hz experiment and up to 13.5 Hz for the 1.5-Hz experiment).

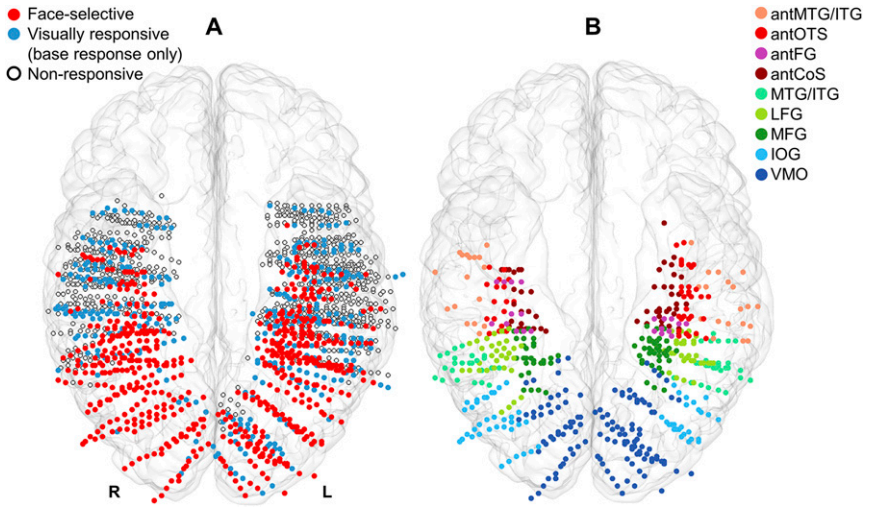

Fig. S1. Spatial distribution of face-selective, visually responsive, and nonresponsive contacts in the MNI space (ventral view). (*A*) Map of all 1,678 VOTC recording contacts across the group of 28 participants displayed in the MNI space using a transparent reconstructed cortical surface of the Colin27 brain. Each circle represents a single contact. Face-selective contacts (red) are represented along with contacts visually responsive to the base frequency but not face-selective (blue) and nonresponsive contacts (white, no face-selective or general visual responses recorded). The number of recorded contacts was higher in the left than in the right hemisphere (988 vs. 690). (*B*) Face-selective contacts in the MNI space colored according to their anatomical label in the individual anatomy.

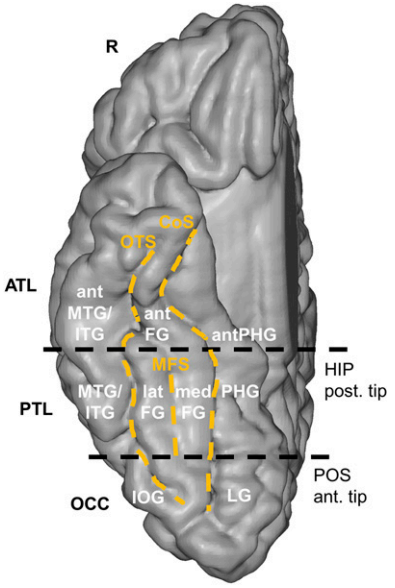

Fig. S2. Schematic representation of the parcellation scheme used to determine the anatomical label of each face-selective contact. Anatomical regions were defined in each individual hemisphere according to major anatomical landmarks. The ventral temporal sulci [CoS, OTS, and midfusiform sulcus (MFS)] serve as medial/lateral borders of regions, whereas two coronal reference planes containing anatomical landmarks [posterior tip of the HIP and anterior tip of the parieto-occipital sulcus (POS)] serve as an anterior/posterior boundary for each region. The anatomical location of each face-selective contact was determined in the individual brain according to this anatomical subdivision and contacts were grouped by anatomical location across all participants. The schematic locations of these anatomical structures are shown on a reconstructed cortical surface of the Colin27 brain.

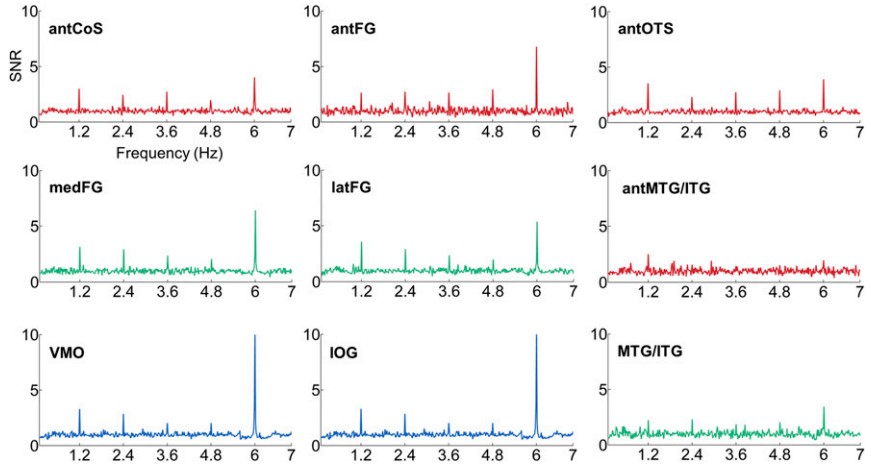

Fig. S3. Averaged iEEG frequency spectra in each region of the left hemisphere. IEEG frequency spectra in each region of the left hemisphere averaged across all face-selective contacts located in the same region are shown.

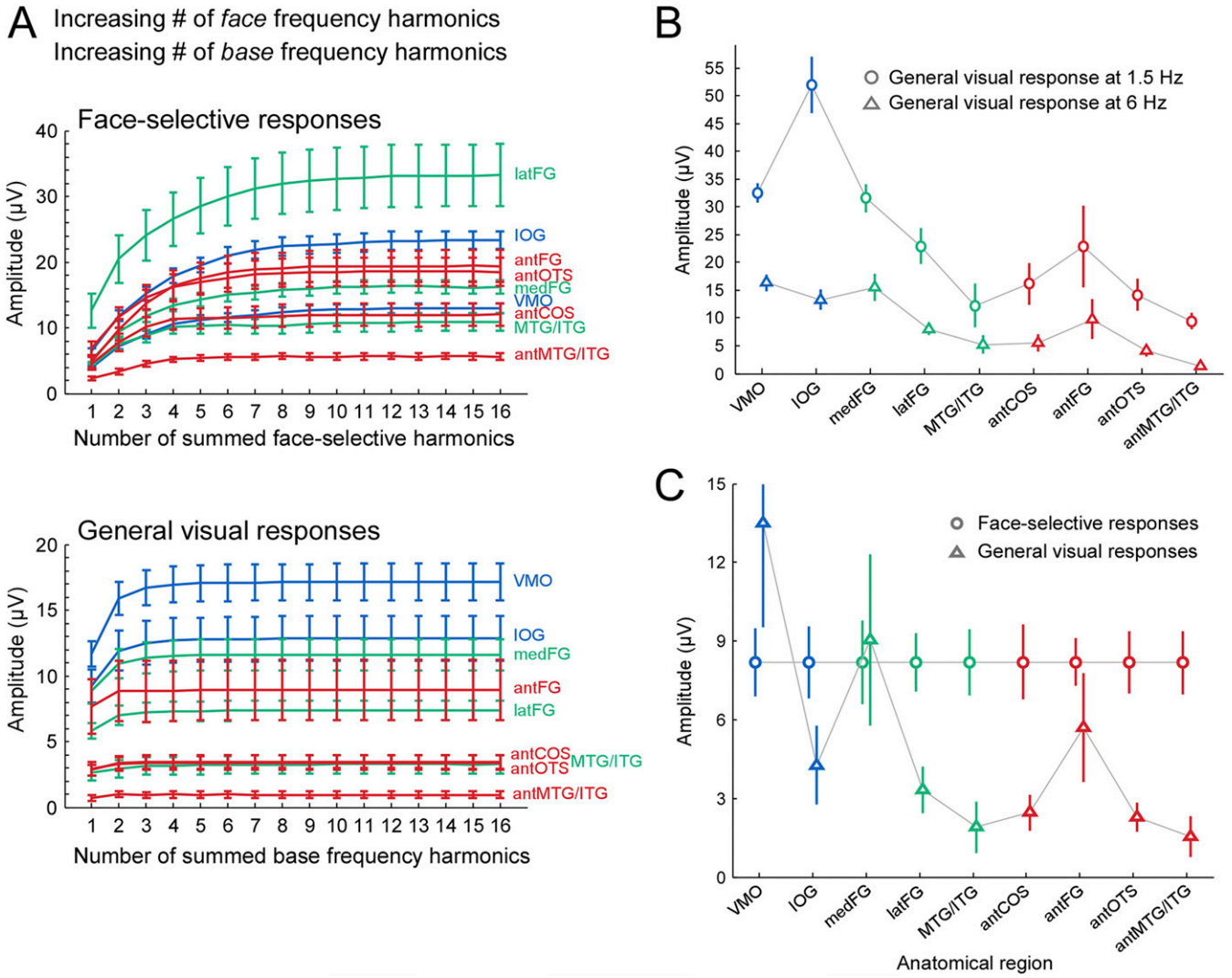

Fig. S4. Control analyses and experiments. (*A*) The pattern of response amplitudes is independent from the number of harmonics included in the quantification. Although the number of harmonics included to quantify the responses was objectively defined (from the first until the highest significant harmonic across participants), the pattern of results is stable whatever the number of harmonics included in the analyses. Here face-selective responses (*Upper*) and general visual responses (*Lower*) are quantified as a function of the number of harmonics included in the analyses. Data are represented as the mean across contacts for each VOTC region (SEMs across contacts are represented as error bars). Differences between regions already emerge from the first harmonics and remain stable regardless of the number of face or base frequency harmonics used in the analyses. (*B*) The decrease of the general visual response in anterior regions does not result from an inability of these anterior regions to generate a response at 6 Hz. The figure compares the mean baseline-subtracted amplitude of general visual responses in the 1.5-Hz experiment (control experiment) to the general visual responses in the 6-Hz experiment (main experiment) in the 11 patients who performed both experiments. The same pattern of response amplitude in the 6- and 1.5-Hz base rate experiments are found, with a decrease of amplitudes from posterior to anterior regions. (*C*) The decrease of the general visual response in anterior regions is not due to a global response amplitude reduction. The mean baseline-subtracted amplitude of the general visual responses is compared across regions for groups of contacts showing similar mean face-selective response amplitudes. To do so, the following analysis was performed: (*i*) contacts from left and right regions were grouped together; (*ii*) in each region, contacts for which the face-selective response amplitude was located between 0 and 15 μV were selected (based on the range of the response of the least responsive region: antMTG/ITG): the minimum number of contacts within this amplitude range across regions was 7 in antFG; (*iii*) for each region a combination of 7 contacts (by randomly sampling from the pool of contacts in the range of 0–15 μV) for which the mean amplitude was the closest to the mean amplitude of the region with the least number of contacts (i.e., antFG: 7 contacts) was searched for; and (*iv*) the mean general visual response amplitude at corresponding contacts was extracted. A similar reduction of general visual responses from posterior to anterior regions as for the main analysis with all of the contacts was observed.

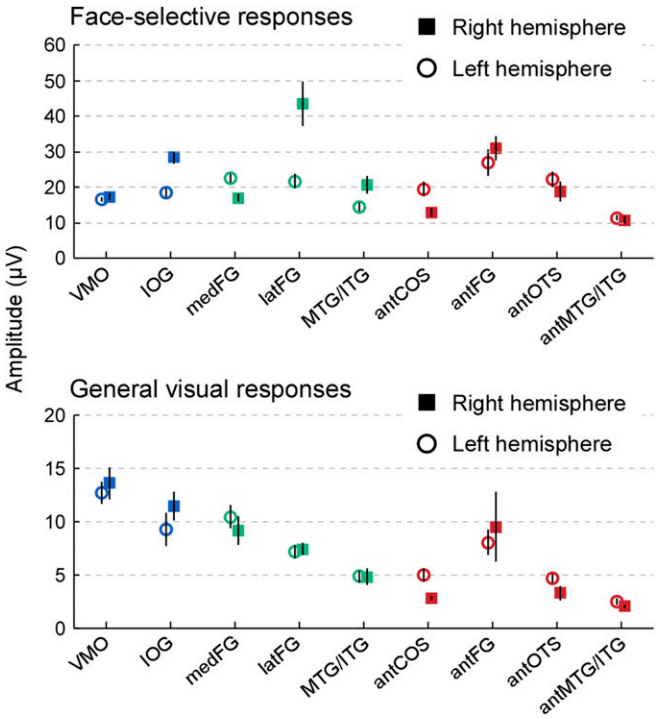

Fig. S5. Quantification of mean face-selective and general visual responses in each region after artifact rejection. The average across contacts for each region is shown separately for the left and right hemispheres. Error bars represent the SEM across contacts. For the artifact rejection procedure, see *SI Text*.

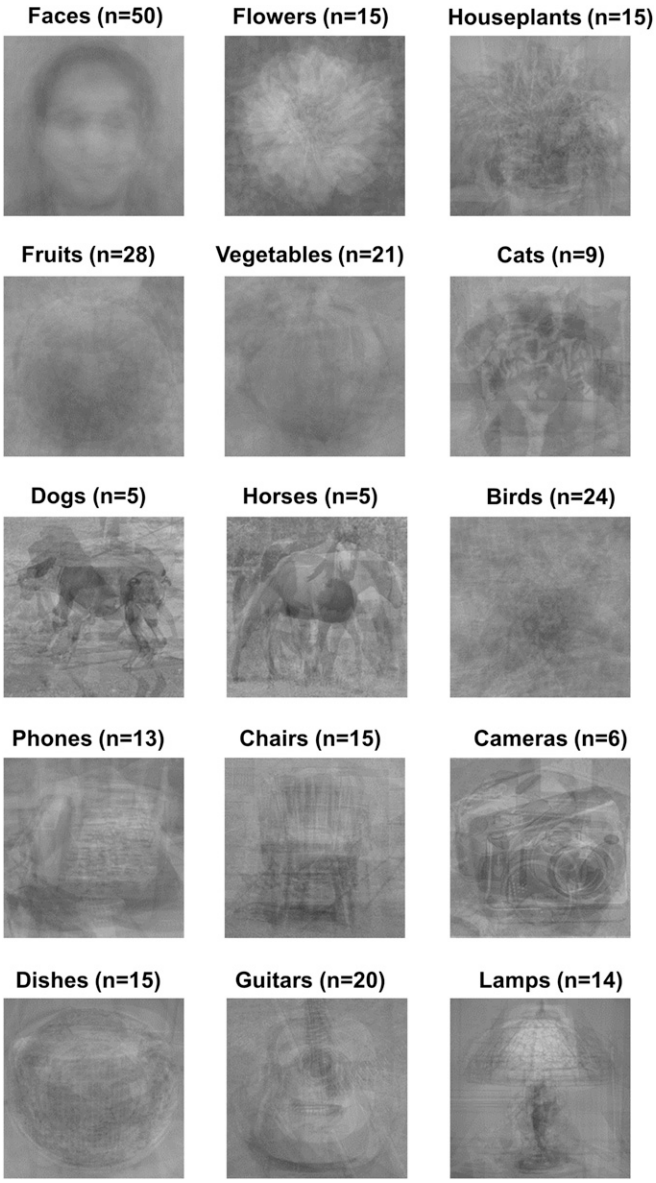

Fig. S6. Average across images in each category (faces and 14 categories including cats, dogs, horses, birds, flowers, fruits, vegetables, houseplants, phones, chairs, cameras, dishes, guitars, and lamps). *n* indicates the number of images for each category in our set of stimuli.

Table S1. Talairach and MNI coordinates of each region

	Left			Right		
Regions	*x*	*y*	*z*	*x*	*y*	*z*
Talairach						
VMO	−16 ± 9	−80 ± 12	3 ± 13	18 ± 7	−75 ± 12	1 ± 7
lOG	−37 ± 6	−74 ± 6	−8 ± 6	43 ± 9	−71 ± 8	−7 ±10
medFG	−24 ± 4	−44 ± 6	−11 ± 4	28 ± 5	−46 ± 6	−10 ± 6
latFG	−38 ± 6	−46 ± 5	−12 ± 4	41 ± 6	−45 ± 7	−16 ± 6
MTG/ITG	−48 ± 6	−50 ± 7	−9 ± 8	55 ± 7	−48 ± 4	−9 ± 9
antCoS	−29 ± 5	−23 ± 10	−17 ± 6	32 ± 6	−23 ± 9	−15 ± 7
antFG	−28 ± 3	−31 ± 5	−18 ± 1	35 ± 6	−24 ± 8	−23 ± 4
antOTS	−38 ± 3	−23 ± 11	−20 ± 5	40 ± 4	−21 ± 9	−20 ± 7
antMTG/ITG	−55 ± 9	−26 ± 12	−15 ± 5	55 ± 5	−16 ± 11	−16 ± 4
MNI						
VMO	−15 ± 8	−80 ± 12	2 ± 12	17 ± 7	−77 ± 13	1 ± 7
lOG	−36 ± 6	−75 ± 6	−7 ± 6	42 ± 9	−75 ± 9	−7 ± 9
medFG	−24 ± 4	−46 ± 6	−11 ± 4	26 ± 5	−49 ± 7	−9 ± 5
latFG	−36 ± 5	−48 ± 5	−12 ± 3	41 ± 6	−49 ± 9	−16 ± 5
MTG/ITG	−48 ± 7	−53 ± 6	−9 ± 7	53 ± 7	−52 ± 5	−9 ± 9
antCoS	−28 ± 4	−25 ± 10	−16 ± 6	31 ± 5	−27 ± 10	−15 ± 6
antFG	−28 ± 4	−36 ± 3	−17 ± 1	35 ± 5	−29 ± 9	−21 ± 4
antOTS	−37 ± 3	−25 ± 11	−20 ± 5	40 ± 3	−26 ± 9	−20 ± 6
antMTG/ITG	−52 ± 8	−27 ± 11	−14 ± 5	52 ± 6	−19 ± 13	−16 ± 4

Values are mean coordinates of face-selective contacts ± SD.

Table S2. Regions of interest ranked from the highest to the lowest face-selective response amplitude, and the corresponding general visual response amplitude

Regions	Hemisphere	Mean face-selective response (μV)	Mean general visual response (μV)
LFG	Right	45.47 ± 8.0	7.02 ± 0.9
lOG	Right	25.11 ± 1.6	12.03 ± 1.9
antFG	Right	22.28 ± 3.3	9.99 ± 4.3
lOG	Left	20.62 ± 2.3	13.59 ± 3.1
antOTS	Left	19.80 ± 2.9	3.93 ± 0.6
latFG	Left	19.44 ± 3.0	7.55 ± 1.2
medFG	Left	18.30 ± 1.5	11.69 ± 1.6
antFG	Left	16.13 ± 3.4	7.65 ± 1.4
antOTS	Right	15.90 ± 3.0	2.44 ± 0.8
antCoS	Left	13.97 ± 2.6	4.19 ± 0.9
medFG	Right	13.63 ± 1.1	11.26 ± 1.8
VMO	Left	13.27 ± 1.0	17.58 ± 1.8
MTG/ITG	Right	12.62 ± 2.5	2.16 ± 1.1
VMO	Right	12.34 ± 0.8	15.86 ± 2.0
MTG/ITG	Left	9.20 ± 1.2	3.99 ± 0.8
antCoS	Right	9.04 ± 1.6	2.23 ± 0.3
antMTG/ITG	Right	5.74 ± 0.8	0.94 ± 0.2
antMTG/ITG	Left	5.62 ± 0.6	0.99 ± 0.4

Values are means ± SE.

Movie S1. Sample movie of the fast periodic sequence.

Movie S1

Brain and Language 175 (2017) 71–76

Contents lists available at ScienceDirect

Brain and Language

journal homepage: www.elsevier.com/locate/b&l

Short communication

Intracerebral stimulation of left and right ventral temporal cortex during object naming

Line Bédos Ulvin[a,*], Jacques Jonas[b,c], Hélène Brissart[b], Sophie Colnat-Coulbois[d], Anne Thiriaux[a], Jean-Pierre Vignal[b,c], Louis Maillard[b,c]

[a] Service de Neurologie, Centre Hospitalier Universitaire de Reims, Reims, France
[b] Service de Neurologie, Centre Hospitalier Universitaire de Nancy, Nancy, France
[c] CRAN, UMR 7039, CNRS et Université de Lorraine, Nancy, France
[d] Service de Neurochirurgie, Centre Hospitalier Universitaire de Nancy, Nancy, France

ARTICLE INFO

Keywords:
Language
Naming
Language lateralization
Electrical brain stimulation
Basal temporal language area
SEEG

ABSTRACT

While object naming is traditionally considered as a left hemisphere function, neuroimaging studies have reported activations related to naming in the ventral temporal cortex (VTC) bilaterally. Our aim was to use intracerebral electrical stimulation to specifically compare left and right VTC in naming. In twenty-three epileptic patients tested for visual object naming during stimulation, the proportion of naming impairments was significantly higher in the left than in the right VTC (31.3% vs 13.6%). The highest proportions of positive naming sites were found in the left fusiform gyrus and occipito-temporal sulcus (47.5% and 31.8%). For 17 positive left naming sites, an additional semantic picture matching was carried out, always successfully performed. Our results showed the enhanced role of the left compared to the right VTC in naming and suggest that it may be involved in lexical retrieval rather than in semantic processing.

1. Introduction

The ability to name surrounding visual objects is a complex language function depending on a series of stages of mental processing. Naming visual objects requires the recognition of the visual stimulus, the access to the meaning of the object in the semantic system, the retrieval of the lexical representation, the access to its phonological word form in the lexical system and finally the planning of the motor programs that drive articulation (Caramazza, 1997; Dell, Schwartz, Martin, Saffran, & Gagnon, 1997; Levelt, Roelofs, & Meyer, 1999).

The identification of cortical regions dedicated to specific language functions has a long and well documented history (Broca, 1861). A number of previous studies of object naming in neurological patients have provided key insights into the neural basis involved in naming (Baldo, Arevalo, Patterson, & Dronkers, 2013; Brambati et al., 2006; Damasio, Grabowski, Tranel, Hichwa, & Damasio, 1996; Davies et al., 1998; DeLeon et al., 2007; Drane et al., 2008; Hamamé, Alario, Llorens, Liégeois-Chauvel, & Trébuchon-Da Fonseca, 2014; Hillis et al., 2006; Llorens et al., 2016; Trébuchon-Da Fonseca et al., 2009). They have reported the implications of various brain regions in the left hemisphere, in the temporal lobe (lateral, anterior and basal temporal cortices, hippocampus), in the frontal lobe (Broca's area) and in the parietal lobe (inferior parietal lobule). Neuroimaging studies (PET and fMRI) performed in normal subjects have contrasted object naming to various baseline tasks to highlight object naming related areas (Price, Devlin, Moore, Morton, & Laird, 2005). They have found activations in similar regions, that is in the anterior temporal lobe, ventral temporal cortex, lateral occipito-temporal cortex, hippocampus, inferior frontal gyrus and angular gyrus (Bookheimer et al., 1997; Damasio et al., 1996; De Zubicaray, Fraser, Ramajoo, & McMahon, 2017; Hamberger, Habeck, Pantazatos, Williams, & Hirsch, 2014; Hocking, McMahon, & de Zubicaray, 2009; Kiyosawa et al., 1996; Martin, Wiggs, Ungerleider, & Haxby, 1996; Moore & Price, 1999; Murtha, Chertkow, Beauregard, & Evans, 1999; Price et al., 2005; Tomaszewki Farias, Harrington, Broomand, & Seyal, 2005; Van Turennout, Ellmore, & Martin, 2000).

Direct electrical brain stimulation studies performed in epileptic patients have shown the critical role in naming of the above mentioned regions (for a review, see Hamberger, 2007). Electrical stimulation of these regions evoked naming deficits (anomia or paraphasia). Importantly, electrical stimulation studies have highlighted the critical role of the left ventral temporal cortex in object naming. Indeed,

* Corresponding author at: Klinisk nevrofysiologisk laboratorium, Nevrologisk avdeling, Oslo universitetssykehus Ullevål, Kirkeveien 166, 0450 Oslo, Norway.
E-mail addresses: linbed@ous-hf.no (L. Bédos Ulvin), j.jonas@chru-nancy.fr (J. Jonas), h.brissart@chru-nancy.fr (H. Brissart), s.coulbois@chru-nancy.fr (S. Colnat-Coulbois), athiriaux@chu-reims.fr (A. Thiriaux), jp.vignal@chru-nancy.fr (J.-P. Vignal), l.maillard@chru-nancy.fr (L. Maillard).

http://dx.doi.org/10.1016/j.bandl.2017.09.003
Received 2 January 2017; Received in revised form 6 September 2017; Accepted 18 September 2017

electrical cortical stimulation of the left ventral temporal cortex (VTC, comprising the inferior temporal gyrus, fusiform gyrus and parahippocampal gyrus) has consistently elicited visual naming impairments, along with deficits in other language functions in the visual (reading, reading comprehension) and auditory realms (auditory comprehension, repetition, and naming). (Bookheimer et al., 1997; Burnstine et al., 1990; Krauss et al., 1996; Lüders et al., 1991; Malow et al., 1996; Mani et al., 2008). This region has been named the Basal Temporal Language Area (BTLA, Lüders et al., 1991).

Although naming is generally considered as a left hemisphere function, the respective roles of the left and right VTC in naming remain unclear. Numerous neuroimaging studies have reported similar activations in terms of size, size effect and location in both left and right VTC (Garn, Allen, & Larsen, 2009; Hamberger et al., 2014; Kemeny et al., 2006; Kiyosawa et al., 1996; Martin et al., 1996; Murtha et al., 1999; Tomaszewki Farias et al., 2005; Van Turennout et al., 2000). Based on a meta-analysis of 18 object naming neuroimaging studies, Price et al. (2005) found bilateral VTC activations. Therefore, a critical question remains to be addressed: what is the functional relevance of the right VTC in naming?

Electrical brain stimulation studies offer the advantage of identifying critical regions for a function and appear to be well suited to disentangle the respective critical role of the left and right VTC cortex in naming. However, previous electrical brain stimulation studies focused only on the role of the left VTC (they only stimulated the left VTC) and therefore have not addressed this issue of hemispheric lateralization (Bookheimer et al., 1997; Burnstine et al., 1990; Krauss et al., 1996; Malow et al., 1996; Mani et al., 2008).

The aim of this study was to use intracerebral electrical stimulation to compare the critical role of left and right VTC in naming. Importantly, while previous electrical stimulation studies have relied on subdural electrodes applied on the cortical surface, our approach relies on intracerebral recordings with depth electrodes (Stereo-electroencephalography: SEEG). In contrast to subdural electrodes, SEEG offer several advantages (Jonas et al., 2014): the specific stimulation of sulci, the focal effect of intra-cerebral stimulation and most importantly bilateral explorations providing the evaluation of the respective roles of left and right VTC in individual patients.

2. Materials and methods

2.1. Patients

The study included 23 consecutive patients undergoing intracerebral evaluation (SEEG) for refractory partial epilepsy in the Department of Neurology at the University Hospital of Nancy between 2007 and 2013 (Supplementary Table 1). The inclusion criteria were the presence of intracerebral electrodes in the VTC. The patients were 13 women and 10 men (mean age: 33 years ± 10). Eighteen were right-handed and 5 were left-handed, as assessed by Edinburgh Handedness Inventory. Six had right hemispheric epilepsy, 16 had left hemispheric epilepsy and 1 had bilateral epilepsy. To lateralize language functions, we analyzed the presence or absence of language disturbance during the ictal and post-ictal periods, and during electrical stimulation of the VTC (Supplementary Table 1). Twenty patients showed a left dominance for language and 1 patient a right dominance. The lateralization of language functions remained ambiguous for 2 patients. All patients gave their informed and written consent to participate to the study which was a part of their routine pre-surgical SEEG investigations.

2.2. Stereotactic placement of intracerebral electrodes

Intracerebral electrodes (Dixi Medical, Besançon, France) were stereotactically implanted in the patients' temporal regions in order to localize the epileptogenic zone and to determine the post-surgical neuropsychological outcome (Talairach & Bancaud, 1973). Each intracerebral electrode consisted of a cylinder of 0.8 mm diameter and contained 8–15 independent recording contacts of 2 mm in length separated by 1.5 mm from edge to edge (for details about the electrode implantation procedure, see Jonas et al., 2015). The anatomical location of each electrode contact was determined in the individual anatomy by co-registering the pre-operative structural MRI with CT images collected after the electrode implantation. A total of 860 intracerebral contacts were implanted in the VTC across the 23 patients (390 in the right hemisphere and 470 in the left).

2.3. Intracerebral stimulations and visual object naming task

Bipolar stimulations were applied between 2 contiguous contacts to localize the epileptogenic zone and to map functionally relevant areas (50 Hz, 5–10 s, 0.5–2 mA, according to clinical criteria). Functional mapping of language functions was assessed using a visual object naming task. Patients were shown sets of drawing pictures (black and white) representing living or manufactured objects presented one by one in a random order. The patients had to name each image. For each set, the patient had to name approximately 10 images, before, during and after the stimulation. One to 4 consecutive images were shown during the stimulation (depending on the stimulation duration and the delay of answer of the patient). A positive naming site was defined as two contiguous contacts whose electrical stimulation elicited a naming impairment (anomia or paraphasia, that is verbal output but with inability to name the displayed object accurately). Sites were considered to be positive if a clear naming impairment was elicited during stimulation relative to patient's baseline performance (Koubeissi et al., 2012), that is relative to the performance for images presented just before and after the stimulation. All stimulations were performed at least two hours after the last seizure to exclude any potential bias related to enduring post-ictal aphasia. None of the analyzed stimulations elicited a seizure.

2.4. Intracerebral stimulations and semantic task

For some positive naming sites, an additional semantic picture matching task that did not require naming was performed during electrical stimulation (picture version of the Pyramids and Palm Trees Test, PPTT, Howard & Patterson, 1992). Patients were asked to match a target image with one of 2 other images presented at the same time (one semantically-related image and one distractor). They were asked to point the semantically-related image with their fingers. For each individual stimulation site, we used the same stimulation parameters (duration, intensity) for the object naming and semantic tasks.

2.5. Contact localization in the individual anatomy and in Talairach space

We localized each stimulated contact in the individual anatomy (i.e., individual gyri and sulci) based on the co-registered pre-implantation cerebral MRI and post-implantation CT scan. Therefore, each contact was assigned one of the following basal temporal structures of the individual anatomy: parahippocampal gyrus (PHG), fusiform gyrus (FG), occipito-temporal sulcus (OTS) and inferior temporal gyrus (ITG). For each structure, we computed the percentage of positive naming positive sites that is the number of positive naming sites divided by the total number of stimulated sites, multiplied by 100 (Jonas et al., 2014).

3. Results

Among 290 stimulated sites in 23 patients, we found 83 positive naming sites in 21 patients. Seventy-seven were found in the left hemisphere in 19 patients and 6 in the right hemisphere in 2 patients (Fig. 1A, Table 1, see Supplementary Table 1 for individual results). Among the 83 positive naming sites, 75 elicited complete anomia

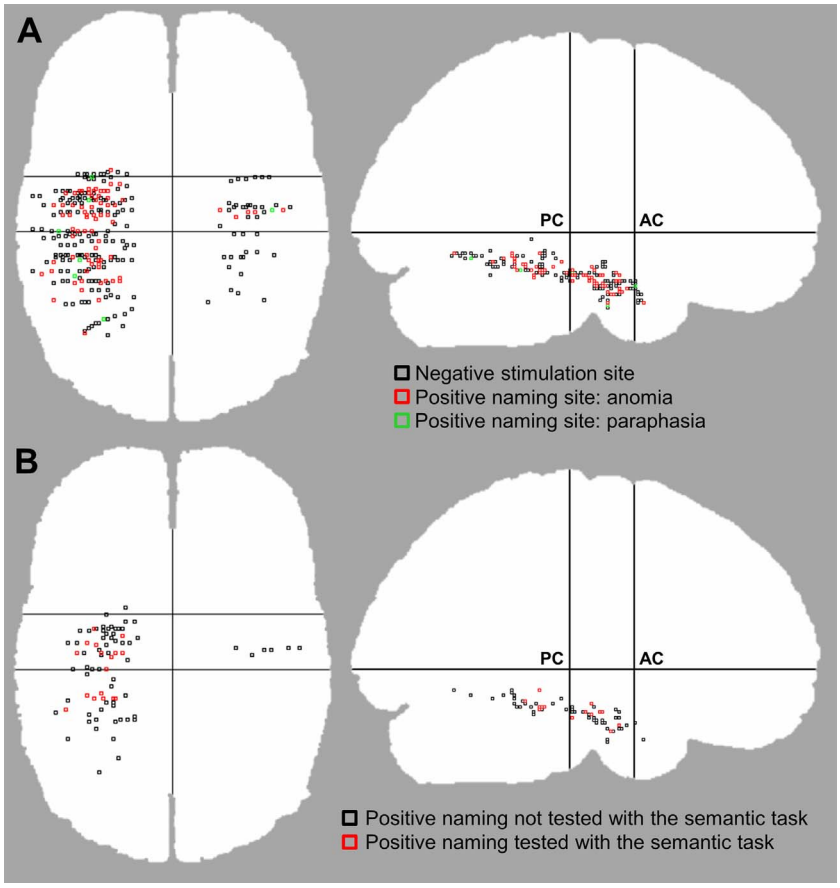

Fig. 1. Spatial distribution of the stimulated sites in the Talairach space (sagittal and axial views). Each square represents a single intracerebral contact. (A) Spatial distribution of negative and positive sites for the naming task (eliciting anomias or paraphasias). (B) Spatial distribution of tested and non-tested naming sites for the semantic task (the semantic task was always successfully performed). AC: anterior commissure; PC: posterior commissure.

(90.4%) and 8 elicited paraphasias (9.6%, replacement of one word by another phonologically-related word or by a non-related word). No semantic paraphasias were observed. Naming impairments were evoked when stimulating left VTC structures (PHG, OTS, FG, ITG) but also when stimulating the same regions in the right hemisphere (Table 1). In the left hemisphere, the positive naming sites were widely distributed over the VTC, from the ventral occipito-temporal junction to the anterior VTC (Fig. 1A).

The proportion of naming sites was higher in the left than in the right hemisphere (Table 1, 31.3% vs 13.6%, Chi^2 test, $p = 0.017$). The intensity of stimulations did not account for this result because mean intensity of stimulations was higher in the right than in the left hemisphere (all stimulations: 1.31 mA ± 0.2 vs. 1.18 mA ± 0.24, $t = 3.44$, $p < 0.001$; positive stimulations only: 1.47 mA ± 0.04 vs. 1.15 mA ± 0.2, $t = 3.83$, $p < 0.001$). The highest and the second highest proportion of naming sites were found in the left FG and OTS, respectively (47.5% and 31.8%, Table 1, Fig. 2). A direct statistical comparison between left and right proportions in each anatomical structure was not possible given the low number of stimulation sites in each right structure (Table 1).

Stimulation sites were unilateral in 15 patients (13 in the left and 2 in the right) and bilateral in 8 (Supplementary Table 1). In these patients with bilateral stimulations, positive naming sites were only evoked in one hemisphere, showing a strictly unilateral representation of naming functions in the VTC. Critical regions for naming in the VTC were strictly left lateralized in 7 (7/8) and right lateralized in 1 patient (1/8). It is important to note that this latter patient (patient 5) mostly accounted for the right positive naming sites reported here. Five out of the 6 right positive naming sites reported in this study were found in this patient. In this same patient, none of the 25 left stimulation sites were positive and no ictal and post-ictal aphasia was observed during her left temporal seizures, strongly supporting a right lateralization of language functions (Supplementary Table 1).

For 17 positive left naming sites in 7 patients (16 anomia sites and 1

Table 1
Number of stimulated sites, number and percentage of positive naming sites for the visual object naming task (and the corresponding number of anomias and paraphasias) in each anatomical structure. The number of sites tested with the semantic task is also indicated (task only performed in the left hemisphere). The corresponding number of subjects is indicated in parentheses (PHG: parahippocampal gyrus, FG: fusiform gyrus, OTS: occipito-temporal sulcus, ITG: inferior temporal gyrus).

	Left hemisphere						Right hemisphere				
	Nb. of stimulated sites	Nb. of positive sites	Proportion	Nb. of anomias	Nb. of paraphasias	Nb. of sites tested with the semantic task	Nb. of stimulated sites	Nb. of positive sites	Proportion	Nb. of anomias	Nb. of paraphasias
PHG	53 (18)	11 (5)	20.7%	11 (5)	0	0	17 (7)	3 (1)	17.6%	3 (1)	0
FG	80 (18)	38 (18)	47.5%	36 (17)	2 (2)	11 (5)	17 (8)	1 (1)	5.9%	1 (1)	0
OTS	22 (12)	7 (5)	31.8%	5 (4)	2 (2)	2 (1)	4 (3)	1 (1)	25%	0	1 (1)
ITG	91 (15)	21 (12)	23.1%	18 (9)	3 (3)	4 (3)	6 (4)	1 (1)	16.7%	1 (1)	0
Total	246 (21)	77 (19)	31.3%	70 (19)	7 (6)	17 (7)	44 (10)	6 (2)	13.6%	5 (2)	1 (1)

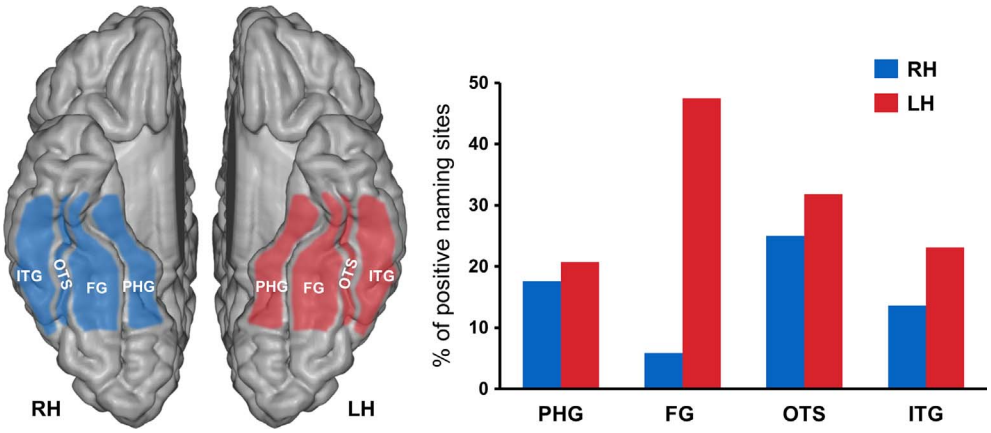

Fig. 2. Percentage of positive naming sites in each left and right anatomical structure (PHG: parahippocampal gyrus, FG: fusiform gyrus, OTS: occipito-temporal sulcus, ITG: inferior temporal gyrus).

paraphasia site), an additional semantic picture matching task that did not require naming was performed during electrical stimulation. Patients were asked to match a target image with one of 2 other images presented at the same time (one semantically-related image and one distractor). The same intensity was used for both naming and semantic matching tasks at a given stimulation site. This task was always successfully performed (no semantic impairment elicited at positive naming sites) even in the left anterior VTC, i.e. the ventral part of the anterior temporal lobe (see the spatial distribution of the tested sites in Fig. 1B).

4. Discussion

In this intracerebral study, we electrically stimulated both the right and left VTC during visual object naming and found a significantly higher proportion of critical naming sites in the left than in the right VTC. All the patients with bilateral stimulations showed a strict lateralization of naming functions: left in 7 out of 8 and right in the remaining case. We found some naming sites in the right VTC and with a high proportion for some regions (e.g., right OTS). However, this observation should be taken with caution because it was mostly accounted by one patient with a right lateralization of language functions. Accordingly, these results showed: (1) at an individual level, that critical regions for naming in the VTC are strictly left lateralized in most patients of this sample and (2) at a broader level, the enhanced role of the left compared to the right VTC in naming. Our results therefore suggest that naming functions in the VTC are strictly lateralized to one single hemisphere (mostly the left) and that the right VTC may not play a critical role in naming unless naming functions are fully shifted to the right VTC in some healthy subjects or degraded following damage to the left hemisphere (compensatory role; Riès, Dronkers, & Knight, 2016).

These findings contrast with the strong and bilateral VTC activations for naming in neuroimaging studies. Activations observed in functional imaging may highlight both critical (left) and non-critical (right) regions whereas electrical stimulations only highlight critical (left) regions. An alternative hypothesis is that, while there is strong evidence that processes directly related to language are left lateralized, processes related to object recognition and semantic processing may be more bilateral (e.g., Lambon Ralph, Pobric, & Jefferies, 2009; Maillard et al., 2011; Nobre, Allison, & McCarthy, 1994; Sharp, Scott, & Wise, 2004). Object recognition and semantic processing related to naming may evoke bilateral VTC activations in neuroimaging studies, overlapping left lateralized language activations like lexical retrieval and phonological processes.

Picture naming is a complex cognitive process resulting from multiple steps including object recognition, semantic processing, lexical retrieval, and finally word articulation (Caramazza, 1997; Dell et al., 1997; Levelt et al., 1999). Theoretically, transient naming impairments observed during electrical stimulation could result from the disturbance of any of these processes. However, the pattern of elicited paraphasias (phonetically related words and non-related words, but no semantic paraphasias), and the fact that when tested, we did not evoke any semantic impairment, even when stimulating the left anterior VTC, indicate that semantic processing was not impaired (Caramazza & Hillis, 1990). This is consistent with previous VTC stimulation studies which reported the so called “tip-of-the-tongue” states during object naming (Lüders et al., 1991). Patients were not able to name objects but were still able to define its function or to imitate the action related to the object, showing that object recognition and conceptual knowledge of the objects were preserved. This is also consistent with neurological studies showing that pure anomia, defined as a lack of word retrieval despite preserved semantic processing, is observed in patients with lesions or dysfunction of the left fusiform gyrus (Cloutman et al., 2009; DeLeon et al., 2007; Raymer et al., 1997; Trébuchon-Da Fonseca et al., 2009). Taken all together, these observations strongly suggest that the observed naming impairments during electrical stimulation of the left basal temporal cortex more likely concern subsequent processes as the lexical retrieval, the access to the phonological form or the phonological buffer.

The BTLA was firstly delineated in the left fusiform gyrus (Lüders et al., 1991) and was subsequently extended to the left inferior temporal gyrus and the left parahippocampal gyrus (Burnstine et al., 1990; Schäffler, Lüders, Morris, & Wyllie, 1994; Schäffler, Lüders, & Beck, 1996). Based on the proportion of naming sites per structure, we found in the left hemisphere that the FG was the most critical region for visual object naming, followed by the OTS, lateral to the FG (the opposite pattern was found in the right VTC, however the small number of stimulations in the right hemisphere prevented us from drawing any conclusions about this result). The importance of the OTS extends the conclusions of previous electrical stimulation studies that all used subdural electrodes placed over the cortical surface (Bookheimer et al., 1997; Burnstine et al., 1990; Krauss et al., 1996; Lüders et al., 1991; Malow et al., 1996; Mani et al., 2008; Schäffler, Lüders, & Beck, 1996). Cytoarchitectonic studies have shown that the FG and part of the OTS belong to the same cytoarchitectonic area (Lorenz et al., 2017). Taken together, these results suggest that the left FG and OTS are located in the same functional area involved in naming, as it is the case for visual face processing in the right VTC (the Fusiform Face Area encompasses both FG and OTS, Jonas et al., 2016; Weiner & Grill-Spector, 2010). More generally, the functional and anatomical relationships between naming and visual processes in the VTC are little understood. On one hand, the FG and the OTS are the most important structures of the BTLA, a modality-independent area (visual and auditory) involved in naming (Lüders et al., 1991; Mani et al., 2008; Schäffler et al., 1994; Schäffler et al., 1996). On the other hand, the FG and the OTS are

critical structures of the visual ventral pathway involved in object categorization and identification specifically in the visual modality (Grill-Spector & Weiner, 2014). This proximity with an object identification system (the visual ventral pathway) is specific to the BTLA in comparison to other brain regions involved in naming. Future studies are needed to determine the relationship between these two processes and this may help to better understand the role of the VTC and its subregions in naming.

Statement of significance to the neurobiology of language

The article addresses the question of a hemispheric lateralization of naming and aims to identify the critical regions in the ventral temporal cortex involved in this important language function. The results highlight the importance of the left ventral temporal cortex, and suggest that it may be critical for lexical retrieval rather than for semantic processing.

Acknowledgements

This research did not receive any specific grant from funding agencies in the public, commercial, or not-for-profit sectors. All authors declare that they have no conflict of interest. We thank the two anonymous reviewers for their comments on a previous version of the manuscript.

Appendix A. Supplementary materials

Supplementary data associated with this article can be found, in the online version, at http://dx.doi.org/10.1016/j.bandl.2017.09.003.

References

Baldo, J. V., Arevalo, A., Patterson, J. P., & Dronkers, N. F. (2013). Grey and white matter correlates of picture naming: Evidence from a voxel-based lesion analysis of the Boston Naming Test. *Cortex, 49*(3), 658–667.

Bookheimer, S. Y., Zeffiro, T. A., Blaxton, T., Malow, B. A., Gaillard, W. D., Sato, S., ... Theodore, W. H. (1997). A direct comparison of PET activation and electrocortical stimulation mapping for language localization. *Neurology, 48*(4), 1056–1065.

Brambati, S. M., Myers, D., Wilson, A., Rankin, K. P., Allison, S. C., Rosen, H. J., ... M.L., Gorno-Tempini (2006). The anatomy of category-specific object naming in neurodegenerative diseases. *Journal of Cognitive Neuroscience, 18*(10), 1644–1653.

Broca, P. (1861). Remarques sur le siège de la faculté du langage articulé; suivies d'une observation d'aphémie (perte de la parole). *Bulletins de la Société anatomique de Paris, 36*, 330–357.

Burnstine, T. H., Lesser, R. P., Hart, J., Jr., Uematsu, S., Zinreich, S. J., Krauss, G. L., ... Gordon, B. (1990). Characterization of the basal temporal language area in patients with left temporal lobe epilepsy. *Neurology, 40*(6), 966–970.

Caramazza, A. (1997). How many levels of processing are there in lexical access? *Cognitive Neuropsychology, 14*, 177–208.

Caramazza, A., & Hillis, A. E. (1990). Where do semantic errors come from? *Cortex, 26*(1), 95–122.

Cloutman, L., Gottesman, R., Chaudry, P., Davis, C., Kleinman, J. T., Pawlak, M., ... Hillis, A. E. (2009). Where (in the brain) do semantic errors come from? *Cortex, 45*(5), 641–649.

Damasio, H., Grabowski, T. J., Tranel, D., Hichwa, R. D., & Damasio, A. R. (1996). A neural basis for lexical retrieval. *Nature, 380*(6574), 499–505.

Davies, K. G., Bell, B. D., Bush, A. J., Hermann, B. P., Dohan, F. C., Jr., & Jaap, A. S. (1998). Naming decline after left anterior temporal lobectomy correlates with pathological status of resected hippocampus. *Epilepsia, 39*(4), 407–419.

De Zubicaray, G., Fraser, D., Ramajoo, K., & McMahon, K. (2017). Interference from related actions in spoken word production: Behavioural and fMRI evidence. *Neuropsychologia, 96*, 78–88.

DeLeon, J., Gottesman, R. F., Kleinman, J. T., Newhart, M., Davis, C., Heidler-Gary, J., ... Hillis, A. E. (2007). Neural regions essential for distinct cognitive processes underlying picture naming. *Brain, 130*(Pt 5), 1408–1422.

Dell, G. S., Schwartz, M. F., Martin, N., Saffran, E. M., & Gagnon, D. A. (1997). Lexical access in aphasic and nonaphasic speakers. *Psychological Review, 104*(4), 801–838.

Drane, D. L., Ojemann, G. A., Aylward, E., Ojemann, J. G., Johnson, L. C., Silbergeld, D. L., ... Tranel, D. (2008). Category-specific naming and recognition deficits in temporal lobe epilepsy surgical patients. *Neuropsychologia, 46*(5), 1242–1255.

Garn, C. L., Allen, M. D., & Larsen, J. D. (2009). An fMRI study of sex differences in brain activation during object naming. *Cortex, 45*(5), 610–618.

Grill-Spector, K., & Weiner, K. S. (2014). The functional architecture of the ventral temporal cortex and its role in categorization. *Nature Reviews Neuroscience, 15*(8), 536–548.

Hamamé, C. M., Alario, F. X., Llorens, A., Liégeois-Chauvel, C., & Trébuchon-Da Fonseca, A. (2014). High frequency gamma activity in the left hippocampus predicts visual object naming performance. *Brain and Language, 135*, 104–114.

Hamberger, M. J. (2007). Cortical language mapping in epilepsy: A critical review. *Neuropsychology Review, 17*(4), 477–489.

Hamberger, M. J., Habeck, C. G., Pantazatos, S. P., Williams, A. C., & Hirsch, J. (2014). Shared space, separate processes: Neural activation patterns for auditory description and visual object naming in healthy adults. *Human Brain Mapping, 35*(6), 2507–2520.

Hillis, A. E., Kleinman, J. T., Newhart, M., Heidler-Gary, J., Gottesman, R., Barker, P. B., ... Chaudhry, P. (2006). Restoring cerebral blood flow reveals neural regions critical for naming. *Journal of Neuroscience, 26*(31), 8069–8073.

Hocking, J., McMahon, K. L., & de Zubicaray, G. I. (2009). Semantic context and visual feature effects in object naming: An fMRI study using arterial spin labeling. *Journal of Cognitive Neuroscience, 21*(8), 1571–1583.

Howard, D., & Patterson, K. (1992). The pyramids and palm trees test. *A test of semantic access from words and pictures*. Bury St. Edmunds: Thames Valley Company.

Jonas, J., Frismand, S., Vignal, J. P., Colnat-Coulbois, S., Koessler, L., Vespignani, H., ... Maillard, L. (2014). Right hemispheric dominance of visual phenomena evoked by intracerebral stimulation of the human visual cortex. *Human Brain Mapping, 35*(7), 3360–3371.

Jonas, J., Jacques, C., Liu-Shuang, J., Brissart, H., Colnat-Coulbois, S., Maillard, L., & Rossion, B. (2016). A face-selective ventral occipito-temporal map of the human brain with intracerebral potentials. *Proceedings of the National Academy of the Science U S A, 113*(28), E4088–E4097.

Jonas, J., Rossion, B., Brissart, H., Frismand, S., Jacques, C., Hossu, G., ... Maillard, L. (2015). Beyond the core face-processing network: Intracerebral stimulation of a face-selective area in the right anterior fusiform gyrus elicits transient prosopagnosia. *Cortex, 72*, 140–155.

Kemeny, S., Xu, J., Park, G. H., Hosey, L. A., Wettig, C. M., & Braun, A. R. (2006). Temporal dissociation of early lexical access and articulation using a delayed naming task–an FMRI study. *Cerebral Cortex, 16*(4), 587–595.

Kiyosawa, M., Inoue, C., Kawasaki, T., Tokoro, T., Ishii, K., Ohyama, M., ... Soma, Y. (1996). Functional neuroanatomy of visual object naming: A PET study. *Graefes Archive for Clinical and Experimental Ophthalmology, 234*(2), 110–115.

Koubeissi, M. Z., Lesser, R. P., Sinai, A., Gaillard, W. D., Franaszczuk, P. J., & Crone, N. E. (2012). Connectivity between perisylvian and bilateral basal temporal cortices. *Cerebral Cortex, 22*(4), 918–925.

Krauss, G. L., Fisher, R., Plate, C., Hart, J., Uematsu, S., Gordon, B., & Lesser, R. P. (1996). Cognitive effects of resecting basal temporal language areas. *Epilepsia, 37*(5), 476–483.

Lambon Ralph, M. A., Pobric, G., & Jefferies, E. (2009). Conceptual knowledge is underpinned by the temporal pole bilaterally: Convergent evidence from rTMS. *Cerebral Cortex, 19*(4), 832–838.

Levelt, W. J., Roelofs, A., & Meyer, A. S. (1999). A theory of lexical access in speech production. *Behavioral and Brain Sciences, 22*(1), 1–38.

Llorens, A., Dubarry, A. S., Trébuchon, A., Chauvel, P., Alario, F. X., & Liégeois-Chauvel, C. (2016). Contextual modulation of hippocampal activity during picture naming. *Brain and Language, 159*, 92–101.

Lorenz, S., Weiner, K. S., Caspers, J., Mohlberg, H., Schleicher, A., Bludau, S., ... Amunts, K. (2017). Two New Cytoarchitectonic Areas on the Human Mid-Fusiform Gyrus. *Cerebral Cortex, 27*(1), 373–385.

Lüders, H., Lesser, R. P., Hahn, J., Dinner, D. S., Morris, H. H., Wyllie, E., & Godoy, J. (1991). Basal temporal language area. *Brain, 114*(Pt 2), 743–754.

Maillard, L., Barbeau, E. J., Baumann, C., Koessler, L., Benar, C., Chauvel, P., & Liegeois-Chauvel, C. (2011). From perception to recognition memory: Time course and lateralization of neural substrates of word and abstract picture processing. *Journal of Cognitive Neuroscience, 23*(4), 782–800.

Malow, B. A., Blaxton, T. A., Sato, S., Bookheimer, S. Y., Kufta, C. V., Figlozzi, C. M., & Theodore, W. H. (1996). Cortical stimulation elicits regional distinctions in auditory and visual naming. *Epilepsia, 37*(3), 245–252.

Mani, J., Diehl, B., Piao, Z., Schuele, S. S., Lapresto, E., Liu, P., ... Lüders, H. O. (2008). Evidence for a basal temporal visual language center: Cortical stimulation producing pure alexia. *Neurology, 71*(20), 1621–1627.

Martin, A., Wiggs, C. L., Ungerleider, L. G., & Haxby, J. V. (1996). Neural correlates of category-specific knowledge. *Nature, 379*(6566), 649–652.

Moore, C. J., & Price, C. J. (1999). Three distinct ventral occipitotemporal regions for reading and object naming. *Neuroimage, 10*(2), 181–192.

Murtha, S., Chertkow, H., Beauregard, M., & Evans, A. (1999). The neural substrate of picture naming. *Journal of Cognitive Neuroscience, 11*(4), 399–423.

Nobre, A. C., Allison, T., & McCarthy, G. (1994). Word recognition in the human inferior temporal lobe. *Nature, 372*(6503), 260–263.

Price, C. J., Devlin, J. T., Moore, C. J., Morton, C., & Laird, A. R. (2005). Meta-analyses of object naming: Effect of baseline. *Human Brain Mapping, 25*(1), 70–82.

Raymer, A. M., Foundas, A. L., Maher, L. M., Greenwald, M. L., Morris, M., Rothi, L. J., & Heilman, K. M. (1997). Cognitive neuropsychological analysis and neuroanatomic correlates in a case of acute anomia. *Brain & Language, 58*(1), 137–156.

Riès, S. K., Dronkers, N. F., & Knight, R. T. (2016). Choosing words: Left hemisphere, right hemisphere, or both? Perspective on the lateralization of word retrieval. *Annals of the New York Academy of Sciences, 1369*(1), 111–131.

Schäffler, L., Lüders, H. O., & Beck, G. J. (1996). Quantitative comparison of language deficits produced by extraoperative electrical stimulation of Broca's, Wernicke's, and basal temporal language areas. *Epilepsia, 37*(5), 463–475.

Schäffler, L., Lüders, H. O., Morris, H. H., & Wyllie, E. (1994). Anatomic distribution of cortical language sites in the basal temporal language area in patients with left temporal lobe epilepsy. *Epilepsia, 35*(3), 525–528.

Sharp, D. J., Scott, S. K., & Wise, R. J. (2004). Retrieving meaning after temporal lobe infarction: The role of the basal language area. *Annals of Neurology, 56*(6), 836–846.
Talairach, J., & Bancaud, J. (1973). Methodology of stereo EEG exploration and surgical intervention in epilepsy. *Revue d'oto-neuro-ophtalmologie, 45*(4), 315–328.
Tomaszewki Farias, S., Harrington, G., Broomand, C., & Seyal, M. (2005). Differences in functional MR imaging activation patterns associated with confrontation naming and responsive naming. *AJNR. American Journal of Neuroradiology, 26*(10), 2492–2499.
Trébuchon-Da Fonseca, A., Guedj, E., Alario, F. X., Laguitton, V., Mundler, O., Chauvel, P., & Liegeois-Chauvel, C. (2009). Brain regions underlying word finding difficulties in temporal lobe epilepsy. *Brain, 132*(Pt 10), 2772–2784.
Van Turennout, M., Ellmore, T., & Martin, A. (2000). Long-lasting cortical plasticity in the object naming system. *Nature Neuroscience, 3*(12), 1329–1334.
Weiner, K. S., & Grill-Spector, K. (2010). Sparsely-distributed organization of face and limb activations in human ventral temporal cortex. *Neuroimage, 52*(4), 1559–1573.

Selective visual representation of letters and words in the left ventral occipito-temporal cortex with intracerebral recordings

Aliette Lochy[a,b,c,1], Corentin Jacques[a,b,d,1], Louis Maillard[e,f], Sophie Colnat-Coulbois[g], Bruno Rossion[a,b,e,f,2], and Jacques Jonas[a,b,e,f]

[a]Psychological Sciences Research Institute, UCLouvain, B-1348 Louvain-La-Neuve, Belgium; [b]Institute of Neuroscience, UCLouvain, B-1348 Louvain-La-Neuve, Belgium; [c]Cognitive Science and Assessment Institute, Education, Culture, Cognition, and Society Research Unit, Université du Luxembourg, L-4366 Esch-sur-Alzette, Luxembourg; [d]Center for Developmental Psychiatry, Department of Neuroscience, KU Leuven, B-3000 Leuven, Belgium; [e]Université de Lorraine, CNRS, CRAN, F-54000 Nancy, France; [f]Université de Lorraine, CHRU-Nancy, Service de Neurologie, F-54000 Nancy, France; and [g]Université de Lorraine, CHRU-Nancy, Service de Neurochirurgie, F-54000 Nancy, France

Edited by Brian A. Wandell, Stanford University, Stanford, CA, and approved June 25, 2018 (received for review November 3, 2017)

We report a comprehensive cartography of selective responses to visual letters and words in the human ventral occipito-temporal cortex (VOTC) with direct neural recordings, clarifying key aspects of the neural basis of reading. Intracerebral recordings were performed in a large group of patients ($n = 37$) presented with visual words inserted periodically in rapid sequences of pseudofonts, nonwords, or pseudowords, enabling classification of responses at three levels of word processing: letter, prelexical, and lexical. While letter-selective responses are found in much of the VOTC, with a higher proportion in left posterior regions, prelexical/lexical responses are confined to the middle and anterior sections of the left fusiform gyrus. This region overlaps with and extends more anteriorly than the visual word form area typically identified with functional magnetic resonance imaging. In this region, prelexical responses provide evidence for populations of neurons sensitive to the statistical regularity of letter combinations independently of lexical responses to familiar words. Despite extensive sampling in anterior ventral temporal regions, there is no hierarchical organization between prelexical and lexical responses in the left fusiform gyrus. Overall, distinct word processing levels depend on neural populations that are spatially intermingled rather than organized according to a strict postero-anterior hierarchy in the left VOTC.

word reading | lexical representation | intracerebral recordings | SEEG | fusiform gyrus

The ability to read relies on the rapid mapping of perceived visual letters and their combinations (i.e., visual word forms) to phonology and meaning. The central role of the left ventral occipito-temporal cortex (VOTC) in processing letter strings, initially suggested by pure alexia in lesion studies (1–3), is now widely accepted (4–6). However, within this region, the precise organization for processing letters and their combination remains largely unknown. Here, we report a comprehensive functional mapping of the VOTC for selective responses to visual letter strings and words with intracerebral recordings in a large population of individual human brains. Objective identification and quantification of VOTC activity during rapid discrimination of words from pseudofonts, nonwords, or pseudowords (Fig. 1) shed light on key issues regarding the neural basis of visual letter and word processing.

A first outstanding issue is whether there is a hierarchy of increasingly complex linguistic processes along the postero-anterior axis in VOTC (7). According to this view, bilateral early visual cortices, V1 to V4, or even MT (8), extract oriented bars, local letter features, and case-specific letter shapes (9), which are then recombined into increasingly abstract letter string representations up to the middle section of the left lateral fusiform gyrus [the visual word form area (VWFA)] (3, 7). This view is supported by functional magnetic resonance imaging (fMRI) evidence: in posterior VOTC, the fMRI signal does not differ for various categories of wordlike stimuli (pseudofonts, consonant strings, pseudowords), while in the (more anterior) VWFA, the fMRI signal is larger for words and pseudowords than for less wordlike stimuli (10). However, opposite results have been reported, with larger fMRI activity for less wordlike stimuli in the VWFA (11, 12). Moreover, the location of the brain region showing greater selectivity for letter strings as opposed to non-letters varies from the VWFA site ($y \simeq -54$ in Talairach coordinates) to more anterior VOTC regions ($y \simeq -42$) (13, 14) (for a recent metaanalysis, see ref. 15), depending on the contrasted material (checkerboards, pseudofonts, or symbols), the task, as well as the stimulus presentation time.

In general, whether the functional organization of the VOTC obeys a hierarchy of increasingly complex representations from individual letters to words (10), and if so up to which region, has proved difficult to resolve not only due to methodological differences between studies but moreover because the fMRI signal-to-noise ratio (SNR) is not equivalent across the VOTC, with large magnetic susceptibility artifacts in its anterior portion (4). In this context, a complementary approach to increase understanding of the function of the VOTC in reading, which is not affected by such artifacts, is to record electrical field potentials in awake patients implanted with intracranial electrodes. While

Significance

The left ventral occipito-temporal cortex (VOTC) is a critical part of the reading circuitry. We made measurements with intracerebral electrodes in 37 participants to understand whether this region contains functionally separated brain loci for processing letters and words. Letter-selective responses are found in much of VOTC. Responses to word forms are absent in posterior VOTC but are present and intermingled with letter-specific responses in left anterior VOTC. The results are inconsistent with a hierarchical model in which posterior regions uniquely perform letter identification functions and increasingly anterior regions perform increasingly complex linguistic functions.

Author contributions: A.L., C.J., B.R., and J.J. designed research; A.L., C.J., S.C.-C., and J.J. performed research; A.L., C.J., and J.J. analyzed data; and A.L., C.J., L.M., B.R., and J.J. wrote the paper.

The authors declare no conflict of interest.

This article is a PNAS Direct Submission.

Data deposition: The raw electrophysiological data used for analyses in this paper, along with the xyz coordinates for the position of the electrodes, and the stimuli used have been deposited in the Dryad Digital Repository (doi:10.5061/dryad.6s39h64).

[1]A.L. and C.J. contributed equally to this work.

[2]To whom correspondence should be addressed. Email: bruno.rossion@univ-lorraine.fr.

This article contains supporting information online at www.pnas.org/lookup/suppl/doi:10.1073/pnas.1718987115/-/DCSupplemental.

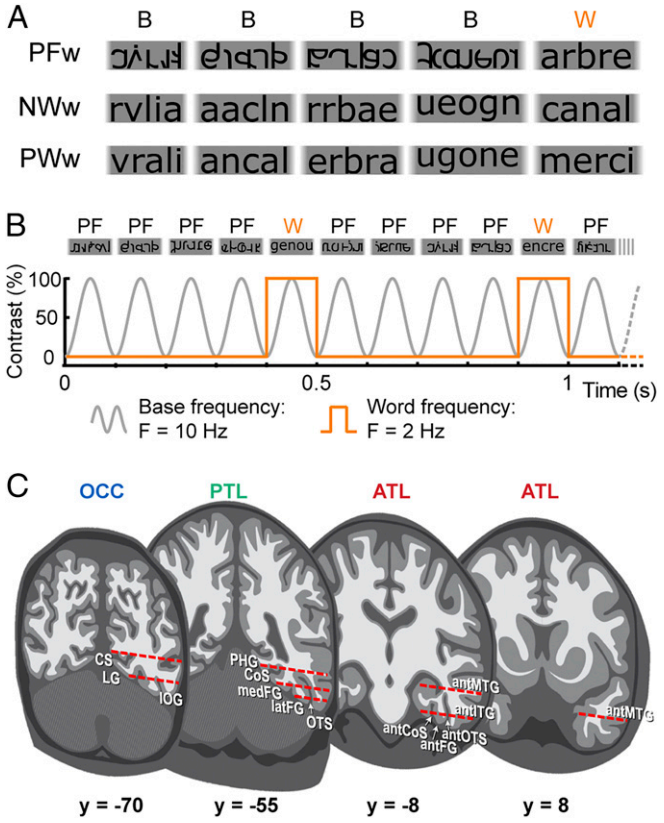

Fig. 1. Fast periodic visual stimulation (FPVS) and SEEG methods. (*A*) Experimental conditions and example stimuli. Words (w) are inserted within three different types of base stimuli (B), that is, in three conditions: words in pseudofonts (PFw), in nonwords (NWw), and in pseudowords (PWw). (*B*) FPVS paradigm. Sequences of PW, NW, and PF are presented at a rate of 10 Hz through sinusoidal contrast modulation with words inserted every fifth item, at 2 Hz, that is, 10 Hz/5 (the PFw condition is represented here). (*C*) Schematic coronal representation of the typical trajectories of depth electrodes implanted in the VOTC. Electrodes consist of 8–15 contiguous recording contacts (red rectangles) spread along the electrode length, along the mediolateral axis. Acronyms: ant, anterior; ATL, anterior temporal lobe; CoS, collateral sulcus; CS, calcarine sulcus; FG, fusiform gyrus; IOG, inferior occipital gyrus; ITG, inferior temporal gyrus; lat, lateral; LG, lingual gyrus; med, medial; MTG, middle temporal gyrus; OCC, occipital lobe; OTS, occipito-temporal sulcus; PHG, parahippocampal gyrus; PTL, posterior temporal lobe.

fMRI measurements typically reflect a general elevation of neural activity only partly due to stimulus-locked responses, intracranial recordings may isolate stimulus-locked responses (16). A seminal study using subdural grids of electrodes [electrocorticography (ECoG)] reported that various letter strings (words, pseudowords, or nonwords) generate an equivalent intracranial response (N200) over the posterior fusiform gyrus, while selectivity to words interpreted in terms of semantic processing was found only in more anterior sections of the VOTC (17). More recently, letter-selective responses (consonant strings > pseudofonts) were found in a more posterior region of the left fusiform gyrus than word-selective responses (words > consonant strings) (18). These observations support a hierarchy of word form processing in the VOTC. However, these recent recordings were performed in targeted VOTC subregions, such that a comprehensive mapping and quantification across the whole VOTC for selective responses to letter strings and words aiming at thoroughly evaluating its hierarchical organization, is currently lacking. Moreover, in these studies, the use of ECoG, which is restricted to the gyral surface, may have underestimated responses arising from sulci. The success of a comprehensive mapping for letter and word processing may thus be enhanced by evenly measuring responses from both gyri and sulci with depth intracerebral electrodes, and by a relatively large recording sample (see ref. 19).

A second outstanding issue regarding the neural basis of letter and word processing is whether the VOTC, in particular the VWFA, is sensitive to whole-word form (i.e., lexical) representations of written strings or is only tuned to prelexical factors characterizing letter strings (e.g., orthographic structure, such as frequently co-occurring letters in a given orthography). This issue is usually operationalized by testing for differential representation of visual real words (lexical items) and pseudowords (orthographically and phonologically plausible sequences of letters) in the VWFA. Here again, previous studies yielded conflicting findings. On the one hand, most fMRI studies did not report differential responses to words vs. pseudowords in this region (10, 20, 21), supporting a prelexical representation level in the VWFA (3, 7, 22). On the other hand, larger responses have been found in this region for pseudowords vs. words (23–26), and for nonfrequent vs. frequent words (27); these observations being interpreted in terms of neural sensitivity to whole-word forms, thus lexical representation. fMR-adaptation paradigms have also shown that the decrease of the response due to pseudoword repetition depends on the number of repeated letters, with a single letter identity change in words resulting in full release from adaptation (24, 25), hence supporting whole-word form coding. Finally, recent intracranial electrophysiology findings suggest that words and pseudowords recruit identical populations of neurons in the VWFA but at different timescales (28). However, the stimuli compared in that study differed only by prelexical factors (number of common letters or bigram frequency). Moreover, since depth recording in three individual brains was limited to the left VWFA only, whether differential responses to words and pseudowords extend to other VOTC regions remains unknown.

Here, we clarify these issues by providing a comprehensive functional mapping of the VOTC for selective responses to visual letter strings at the level of letter recognition, prelexical, or lexical processing. We report data of 37 patients (60 hemispheres) implanted in the VOTC with multiple intracerebral electrodes, each comprising 8–15 recording contacts (2,172 recording contacts in the gray matter) during stereoencephalography (SEEG) (Fig. 1*C*). In our paradigm, validated in scalp EEG studies (29, 30), visual words appear periodically among different stimuli presented at 10 Hz and varying in wordlikeness (Fig. 1 *A* and *B*): (*i*) pseudofonts (PF; Movie S1), (*ii*) letter strings that form orthographically implausible words [nonwords (NW; Movie S2)], or (*iii*) letter strings that form orthographically plausible words [pseudowords (PW; Movie S3)].

We classified each intracerebral recording contact based on the pattern of present (+) or absent (−) significant responses in these three conditions. Three response patterns have a clear theoretical interpretation, reflecting increasingly complex linguistic processing levels. First, contacts with a significant response only to words among PF but not among NW or PW (+PFw, −NWw, −PWw) reflect a letter-selective neural response. Second, discrimination of words from PF and NW but not from PW (+PFw, +NWw, −PWw) reflects a prelexical level of processing. Finally, discrimination of words in all three conditions (+PFw, +NWw, +PWw) reflects a lexical processing level. We focus on these three response patterns and refer to these responses as "word discrimination responses" in the manuscript. Importantly, wordlike stimuli (PF, NW, PW) are presented at a rapid rate of 10 Hz in different 70-s streams, with words inserted every five items (i.e., every 500 ms or 2 Hz; Fig. 1 *A* and *B*; Movies S1–S3). In these conditions, briefly presented words (100-ms stimulus onset asynchrony) are forward- and backward-masked by wordlike stimuli, and word discrimination neural responses can be objectively identified and quantified in the intracerebral EEG spectrum at 2 Hz and harmonics (see refs. 19 and 31 for this frequency-tagging approach in intracerebral SEEG mapping). Moreover, the rapid presentation rates and low attentional-demand tasks reduce the involvement of higher level (semantic) processes (10).

A strict hierarchical view of letter string representation in the VOTC predicts a posterior-to-anterior hierarchy of responsive contacts following the three levels of word discrimination tested. Moreover, if the VWFA responds only to statistical mappings of recurring letters and not to whole-word forms (3, 10), words should not be discriminated from PW in this region but rather in the ventral anterior temporal lobe, extensively sampled here. However, if the VWFA is tuned to whole-word forms (25), contacts reflecting lexical discrimination should be found in this region, with a potential intraregion hierarchical organization (i.e., prelexical posterior to lexical anterior contacts).

Results

Despite the brief recording time (two to six sequences of 70 s per condition), high SNR word discrimination responses were identified in the VOTC exactly at the word presentation frequency (2 Hz) and its harmonics following fast Fourier transform (FFT) (Fig. 2*A*) of SEEG data. Significant word discrimination responses were determined based on a combination of the first four harmonics (i.e., 2, 4, 6, and 8 Hz; Fig. 2*B*) and a *z*-score transform ($z > 3.1$, $P < 0.001$; Fig. 2*C*).

Broad Distribution of Word Discrimination Responses Along the Left VOTC. Across the VOTC, we found 212 significant word discrimination contacts in 27 participants, that is, 9.8% of all recorded contacts. Note that word discrimination contacts can be letter selective (+PF, −NW, −PW), prelexical (+PF, +NW, −PW), or lexical (+PF, +NW, +PW). Every word discrimination contact was labeled according to the individual anatomy (Table 1 and Fig. 3*A*), using a topographic parcellation of the VOTC (*SI Appendix*, Fig. S1; see ref. 32). Word discrimination contacts were distributed broadly across the VOTC with two prominent features: (*i*) these contacts were much more numerous in the left hemisphere; and (*ii*) their density was highest around the left fusiform region (Fig. 3*A* and *SI Appendix*, Fig. S1). In addition, anterior temporal lobe (ATL) word discrimination contacts were mostly restricted to its posterior part, close to the junction with the posterior temporal lobe (PTL) (Fig. 3*A*).

Overall, the proportion of word discrimination contacts relative to all recorded contacts (i.e., responsive and unresponsive) was much higher in the left than in the right hemisphere (left: 169/1,326, 12.7%; right: 43/846, 5.1%; two-tailed permutation test, $p < 0.0001$). To estimate and visualize the prominence of word discrimination contacts at a more local level over the group of participants, we computed maps of the proportion of word discrimination contacts relative to all recorded contacts (Fig. 3*B*). In the left hemisphere, the proportion of word discrimination contacts was significantly above zero ($P < 0.01$) in the ventro-medial occipital cortex (VMO) and all along the left fusiform gyrus and adjacent sulci (from the posterior fusiform gyrus close to the occipital lobe to the anterior fusiform gyrus). We found a similar pattern of results when considering the local proportions of individual brains showing word discrimination contacts (*SI Appendix*, Fig. S2). In the right hemisphere, the proportion of contacts was also significantly above zero along the fusiform gyrus with a maximum in the posterior lateral fusiform gyrus (latFG) (Fig. 3*B*). Nevertheless, the proportion of word discrimination contacts was significantly higher in the left hemisphere in part of the VMO and along the fusiform gyrus (Fig. 3*C*).

Spatial Dissociation Between Letter and Word Processing Levels. Fig. 4 illustrates the classification of letter-selective (+PFw, −NWw, −PWw), prelexical (+PFw, +NWw, −PWw), and lexical (+PFw, +NWw, +PWw) word discrimination contacts with the data of a few individual participants (*SI Appendix*, Fig. S3). The respective number of contacts at each level of discrimination is shown in Table 2. The other classes of response patterns, that is, significant responses in at least one condition but without an unambiguous a priori theoretical interpretation (e.g., −PFw, +NWw, +PWw, exhibiting a discrimination response for words presented among the most but not the least wordlike conditions; *SI Appendix*, Table S1), were not considered in the main analysis.

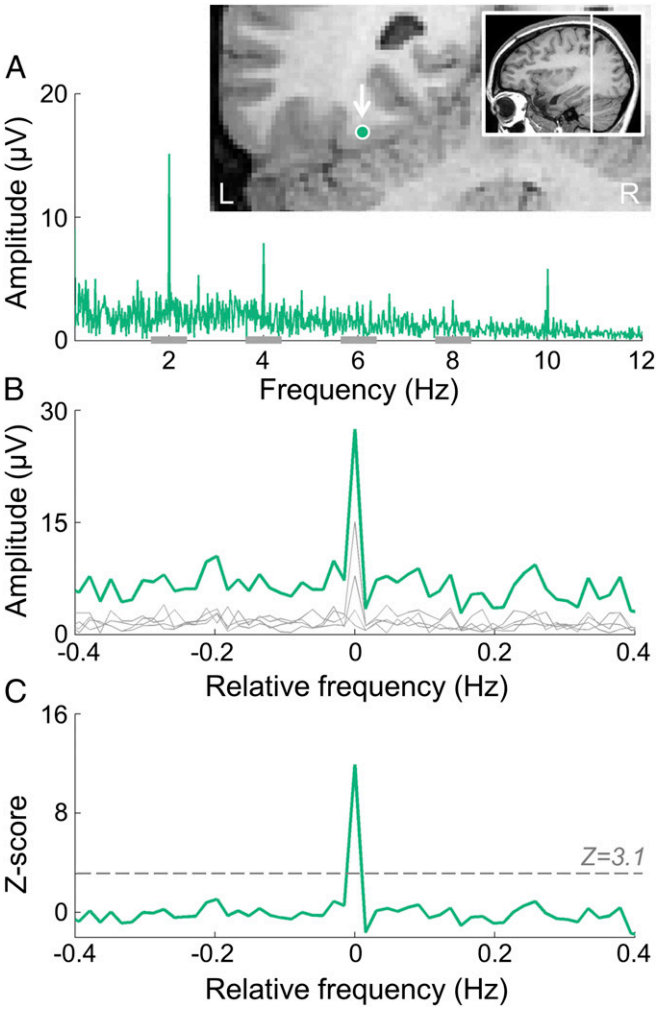

Fig. 2. Objective and high-SNR intracerebral word discrimination responses recorded in the VOTC. (*A*) SEEG frequency-domain responses recorded at an individual recording contact in the PFw condition. The displayed contact was the 10th best of this type, with an average response amplitude of 21 μV, while the best contact had a response amplitude of 86.8 μV. The anatomical location of the contact (in the left latFG, white arrow) is shown in a coronal MRI slice. Word discrimination responses are observed at the exact word stimulation frequency and harmonics (mainly at 2 and 4 Hz). (*B*) Significant word discrimination responses were determined by first segmenting the FFT spectrum into four segments centered at the frequency of word stimulation and its harmonics up to 8 Hz (i.e., 2, 4, 6, and 8 Hz). Individual FFT segments are shown in gray (see horizontal gray bars on the *X* axis in *A*, representing the length of each FFT segment). The four segments, containing both the signal and the surrounding noise, were then summed (green line). The 0 mark corresponds to the word stimulation frequency. (*C*) *Z*-score transformation of the summed FFT spectrum for statistical purpose. The *Z* score at the word stimulation frequency exceeds 3.1 ($P < 0.001$), indicating that this contact shows a significant word discrimination response.

This led to the exclusion of 16.2% of the contacts. Although interpretation of these responses is not straightforward, these contacts may reflect subtle lexical and prelexical processes (*Discussion*). Therefore, we performed the same analyses as presented here, including these contacts, yielding virtually identical findings (*SI Appendix*, Fig. S4).

The spatial organization of the three types of word discrimination contacts across all individual brains is displayed in Fig. 5*A*. Letter-selective contacts were the most frequent and were widely distributed across all individually defined anatomical VOTC regions [VMO, inferior occipital gyrus (IOG), medial fusiform

Table 1. Number of contacts and corresponding number of participants (in parentheses) showing word discrimination responses in each anatomical region

Regions	Left	Right	Both hemispheres
VMO	21 (4)	1 (1)	22 (4)
IOG	13 (4)	6 (2)	19 (6)
Total OCC	34 (5)	7 (3)	41 (9)
MedFG	21 (12)	2 (1)	23 (13)
LatFG	34 (10)	8 (3)	42 (12)
MTG/ITG	19 (7)	1 (1)	20 (8)
Total PTL	74 (14)	11 (4)	85 (17)
AntCOS	23 (12)	8 (4)	31 (13)
AntFG	10 (6)	2 (2)	12 (8)
AntOTS	25 (11)	7 (3)	32 (14)
AntMTG/ITG	3 (1)	8 (4)	11 (5)
Total ATL	61 (17)	25 (8)	86 (20)
Total VOTC	169 (17)	43 (11)	212 (27)

gyrus (medFG), latFG, middle temporal gyrus and inferior temporal gyrus (MTG/ITG), anterior collateral sulcus (antCoS), anterior fusiform gyrus (antFG), anterior occipito-temporal sulcus (antOTS), antMTG/ITG, bilaterally]. Despite this wide distribution, the proportion of letter-selective contacts was maximal in posterior regions (occipital lobe and posterior part of the fusiform gyrus; Fig. 6*A*) and progressively decreased along the anterior axis of the VOTC (Fig. 6*B*).

We found fewer contacts supporting the existence of prelexical (+PFw, +NWw, −PWw) and lexical (+PFw, +NWw, +PWw) visual word representations in the VOTC. Strikingly, these contacts were almost all located along the left fusiform gyrus and adjacent sulci (medFG, latFG, antCoS, antFG, and antOTS; Fig. 5*A* for group visualization). Hence, the proportion of prelexical and lexical contacts was above zero in a restricted middle and anterior area of the left fusiform gyrus and adjacent sulci, defined as midFG (Fig. 6*A*). This proportion was maximal at a postero-anterior location where the proportion of letter contacts was reduced by half compared with its maximum in the posterior region (Fig. 6*B*). The same observation was made considering the proportion of participants showing word discrimination contacts (*SI Appendix*, Fig. S2).

The spatial distribution of the different types of contacts therefore reveals a spatial dissociation between letter-selective and prelexical/lexical processing levels (Fig. 5*A*) in the left hemisphere: while letter-selective contacts are distributed from posterior to anterior VOTC, with a peak in posterior VOTC, prelexical and lexical contacts are confined to the middle and anterior left fusiform gyrus. This observation is also valid in individual participants (Fig. 5*B*) and does not depend on statistical thresholds used to classify word discrimination contacts (*SI Appendix*, Fig. S5).

Lexical Responses in the Left Fusiform Gyrus. A major finding here is the recording of lexical responses in the VOTC, that is, words discriminated even from the most wordlike stimuli, that is, PW (see Fig. 4 and *SI Appendix*, Fig. S3 for individual participants' lexical responses). In total, we found 18 left hemisphere lexical contacts in nine participants, specifically located along the fusiform

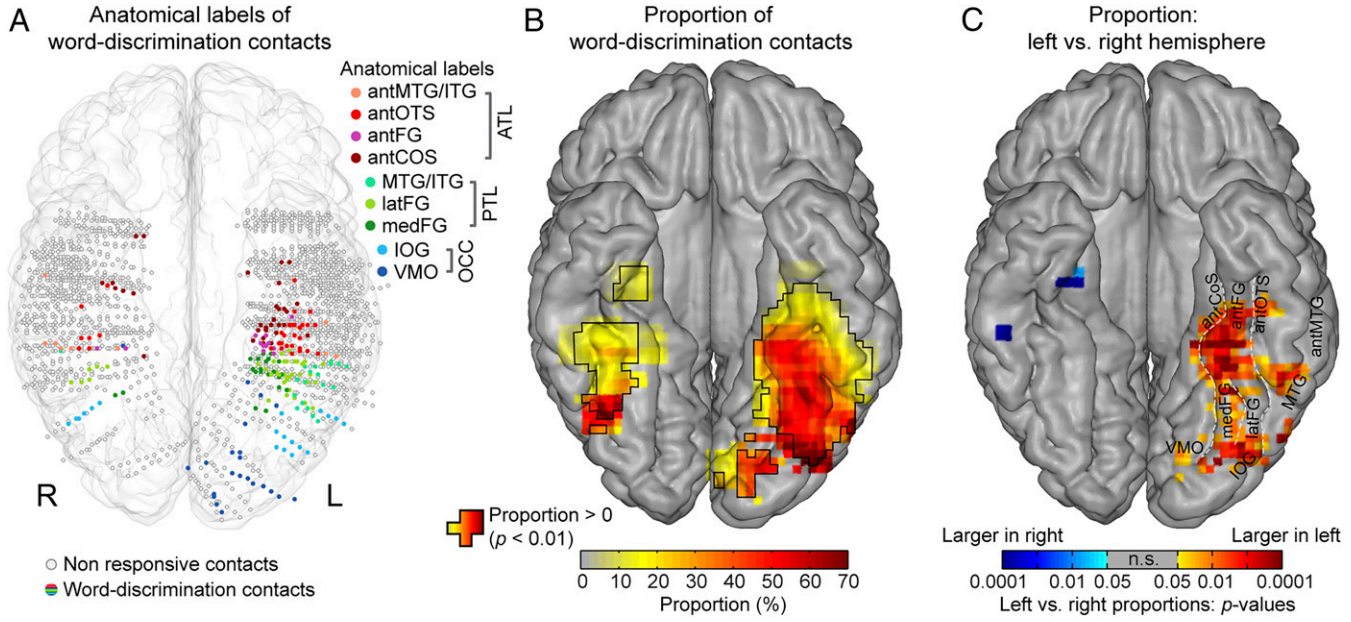

Fig. 3. Spatial distribution of word discrimination contacts in the MNI space (ventral view). (*A*) Map of all 2,156 VOTC recording contacts across the 37 individual brains displayed in the MNI space using a transparent reconstructed cortical surface of the Colin27 brain. Each circle represents a single contact. Color-filled circles correspond to word discrimination contacts colored according to their anatomical location in the original individual anatomy. White-filled circles correspond to contacts on which no word discrimination responses were recorded. For visualization purposes, individual contacts are displayed larger than their actual size (2 mm in length). Acronyms: antCoS, anterior collateral sulcus; antFG, anterior fusiform gyrus (located between the antCoS and the antOTS); antMTG/ITG, anterior middle and inferior temporal gyri; antOTS, anterior occipito-temporal sulcus; ATL, ventral anterior temporal lobe; IOG, inferior occipital gyrus; latFG, lateral fusiform gyrus and occipito-temporal sulcus; medFG, medial fusiform gyrus and collateral sulcus; MTG/ITG, the inferior and middle temporal gyri; OCC, occipital lobe; PTL, posterior temporal lobe; VMO, ventro-medial occipital cortex. (*B*) Map of the local proportion of word discrimination contacts relative to recorded contacts across VOTC, displayed on the cortical surface. Local proportions were computed in 15 × 15 voxels (for *X* and *Y* dimensions, respectively) using contacts collapsed over the *Z* dimension (superior–inferior) for better visualization. For the sake of replicability, only voxels containing significant responses from at least two individual brains were considered. Black contours outline proportions significantly above zero. (*C*) Statistical comparison of local proportions of word discrimination contacts across hemispheres. Proportions (as displayed in *B*) at corresponding voxels in the left and right hemisphere were statistically compared using permutation tests. *P* values associated with a significantly ($P < 0.05$) larger proportion in the left/right hemisphere are displayed using warm/cool colors over the left/right hemisphere.

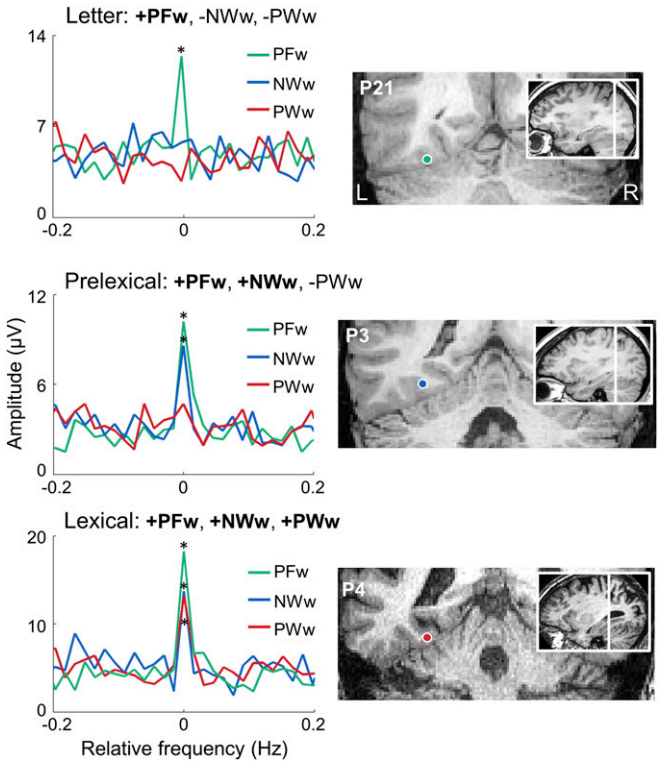

Fig. 4. Classification of word discrimination contacts in three processing levels: example in individual participants (P21, P3, and P4). Example of summed segmented FFT spectra for the three conditions recorded in three contacts (shown on coronal MRI slices). The three rows illustrate how hierarchical word processing levels are defined in each contact by the pattern of responses across conditions. Top row: a letter-selective contact significant only in the PFw condition; middle row: a prelexical contact significant in PFw and NWw conditions; bottom row: a lexical contact significant in all three conditions. The asterisk (*) indicates statistically significant responses ($Z > 3.1$, $P < 0.001$).

gyrus and adjacent sulci (i.e., left midFG), plus a single contact in the right hemisphere in a 10th participant (Table 2). In the left midFG, the proportion of participants with electrodes implanted in this region who showed lexical responses reached up to 50% (*SI Appendix*, Fig. S2). Fig. 7 displays SEEG frequency spectra averaged across the 18 left lexical contacts for each condition. High SNR word discrimination responses are visible in each condition, even in the most wordlike (PWw), in both original and summed-harmonic spectra.

Next, we tested whether lexical responses truly reflect a qualitatively unique level of word discrimination, or if SEEG responses at these contacts is generally larger. To test this, we quantified the response amplitude for each condition and each type of contact (Fig. 8*A*) and compared conditions across prelexical and lexical contacts types. If the difference between prelexical and lexical contacts reflects a general amplitude increase, there should be a significant difference in amplitude in all conditions between these types of contacts (note that the amplitude increase in the PWw condition between prelexical and lexical contacts is expected and noninformative, given that significance of response in this condition served to differentiate prelexical and lexical contacts). We found a highly significant interaction between Condition (PFw, NWw; i.e., excluding the PWw condition) and Contact Type [prelexical, lexical; two-way mixed-model ANOVA: $F_{(1,40)} = 8.14$, $P = 0.007$]. For the PFw condition, response amplitude was significantly larger in lexical (15.4 ± 8 μV) compared with prelexical (10.0 ± 4.3 μV) contacts ($P < 0.005$, permutation test), but this was not the case for NWw condition (lexical, 6.7 ± 2.8 μV; prelexical, 6.6 ± 3.1 μV; $P = 0.89$). Both the interaction and the lack of amplitude increase in the NWw condition indicate that the difference between prelexical and lexical contacts does not merely result from a general amplitude increase in all conditions. Rather, prelexical and lexical contacts appear to reflect functionally different word discrimination processes.

This conclusion is further supported by evaluating the relationship between the amplitudes in the PWw and the NWw conditions, separately for prelexical and lexical contacts (Fig. 8*B*). While there is a strong common source of variability in amplitude for both types of contacts (Pearson's $r = 0.52$; Fig. 8*B*), there is an additional source of variability separating lexical from prelexical contacts (i.e., the regression lines fitted to the two groups of contacts are separate and parallel). Hence, principal-component analysis reveals that lexical and prelexical contacts are significantly different along the second principal component ($P = 0.001$), which aligns well with the PWw axis of amplitude variation (i.e., roughly orthogonal to the regression lines in Fig. 8*B*).

Finally, given that NW and PW differ on a number of prelexical variables (bigram frequency, syllabic and consonant–vowel structure, etc.), the observation that in lexical contacts the response amplitude in the NWw condition is not significantly larger than in PWw (0.78-μV difference; 6.7 ± 2.8 vs. 5.9 ± 2.2 μV for NWw and PWw, respectively; $P < 0.07$, permutation test) implies that prelexical processes mostly do not contribute to the responses recorded in the PWw condition on lexical contacts.

No Hierarchical Organization Between Prelexical and Lexical Contacts. Prelexical and lexical responses appear intermingled in the same region in the left fusiform gyrus, at coordinates encompassing the VWFA as identified in fMRI, but also more anteriorly (up to $y = -25$; Fig. 6*B*). There was no statistical difference in the anterior–posterior axis of group average Talairach coordinates between prelexical and lexical contacts (mean ± SD: $y = -37.1 \pm 14.8$ vs. -40.8 ± 11.2; two-tailed permutation test: $P = 0.37$, uncorrected), going against a hierarchical organization at this level. Moreover, no differences were found in the other spatial dimensions ($x = -34.7 \pm 7$ vs. -31.9 ± 5.1, $P = 0.18$; $z = -13.7 \pm 5.5$ vs. -14.9 ± 5.5, $P = 0.45$). In an additional control analysis, we selected only participants who had both prelexical and lexical contacts in the left hemisphere ($n = 5$) and compared the mean coordinates of prelexical contacts to the mean coordinates of lexical contacts within participant. We found no significant difference along any dimensions (x: prelexical minus lexical = -3.5 ± 5.4, $P = 0.25$; y: 11.2 ± 21.5, $P = 0.38$; z: -3.5 ± 8.6, $P = 0.94$). As in previous analyses, this spatial organization was independent of the exact definition of conditions (*SI Appendix*, Fig. S4) and statistical threshold (*SI Appendix*, Fig. S5).

Discussion

By coupling a fast periodic visual stimulation paradigm identifying selective responses objectively (i.e., at a predefined frequency) with intracerebral recordings in a large number of individual brains, our study provides original evidence regarding the functional organization of the human VOTC for reading. Word discrimination responses were measured between words (w) and three types of stimuli: (*i*) pseudofonts (PFw); (*ii*) letter strings that form implausible words, referred to as nonwords (NWw); and (*iii*) letter strings that are plausible words, referred to as pseudowords (PWw). We classified the response from each contact based on the presence (+) or absence (−) of a significant

Table 2. Number of contacts and corresponding number of participants (in parentheses) as a function of word discrimination level

Word discrimination level	Left	Right	Total
Letter	127 (20)	31 (10)	158 (24)
Prelexical	24 (12)	11 (4)	35 (16)
Lexical	18 (9)	1 (1)	19 (10)

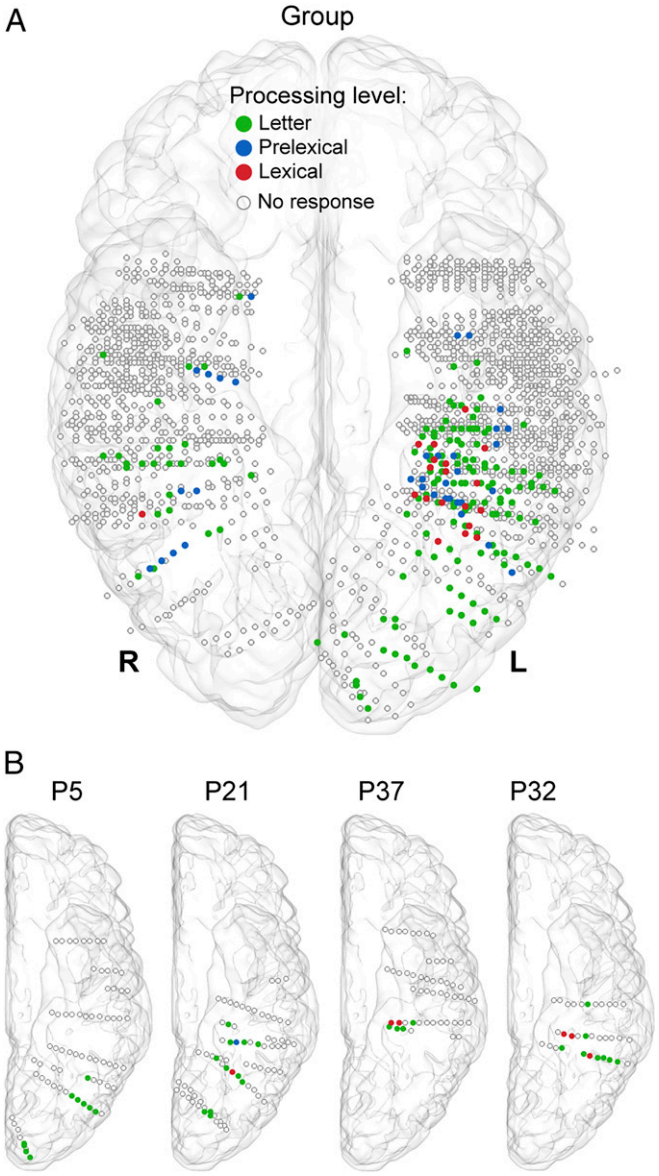

Fig. 5. Spatial organization across the three processing levels. (*A*) Map of all VOTC recording contacts across the 37 patients displayed in the MNI space. Each circle represents a single contact. White-filled circles correspond to contacts at which no word discrimination responses were recorded. Each color-filled circle corresponds to a word discrimination contact colored according to its level of processing. (*B*) Recorded contacts and word discrimination contacts in the left hemisphere of four example individual participants, displayed in MNI space over the Colin27 brain. For visualization purposes in both *A* and *B*, individual contacts are displayed larger than their actual size (2 mm in length).

response to these three types of contrasts: letter-selective (+PFw, −NWw, −PWw), prelexical (+PFw, +NWw, −PWw), and lexical (+PFw, +NWw, +PWw). We found a wide spatial distribution of letter-selective contacts over the VOTC in the left hemisphere. The left midFG, corresponding roughly to the VWFA, emerged from this analysis by the presence of intermingled significant prelexical and lexical contacts, which were found only in the anterior VOTC region. These findings have important implications for understanding the neural basis of reading.

Left Posterior Selectivity to Letters. The large coverage of the bilateral VOTC with intracerebral electrodes reveals widely distributed selective responses to letter strings in the left hemisphere (Figs. 3, 5, and 6). However, the proportion of letter-selective responses with respect to the number of recorded contacts clearly indicates the dominance of a left posterior region, the inferior occipital gyrus, in selective letter representation (Fig. 6). This finding contrasts with studies in which pseudofonts generate as much activation as letter strings in these posterior regions (e.g., ref. 10). In the RH, there were only few, scattered, responses in the midFG, with no response in posterior regions. Although sampling was limited in the right posterior cortex, these observations suggest an early (i.e., in terms of visual hierarchy) left-lateralized selective tuning to letters in the occipital cortex (18) rather than a posterior bilateral representation (7).

In the left hemisphere, there was a postero-anterior hierarchy between letter-selective and (pre)lexical responses. This is congruent with fMRI measures, in which posterior regions selective to letter shapes (i.e., words among pseudofonts) do not respond to words among alphabetic characters (7, 10). The maximal local proportion of letter-selective responses has been shown in the left IOG, in a region corresponding to a previously located "letter area" (18). In that study, participants had to perform a semantic task potentially triggering a shallower processing of nonmeaningful pseudofonts compared with letter strings. In contrast, in our study, there was no explicit reading task to extract the meaning of the presented strings. Hence, we provide original evidence that letter selectivity is triggered automatically in this left posterior region, even when letters appear for a brief time—less than 100 ms—among pseudofonts.

Our finding of a letter-selective brain region indicates that letters are processed specifically, independently of words, in the

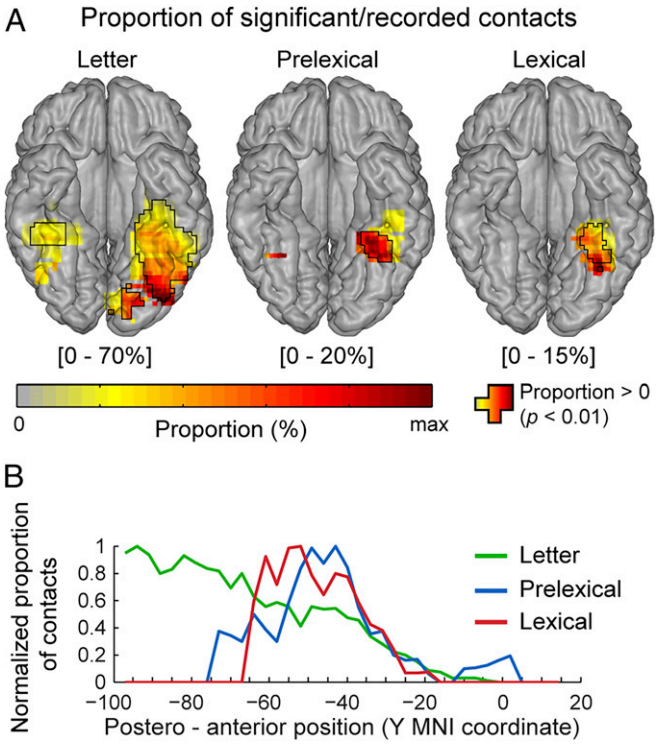

Fig. 6. Spatial dissociation between word processing levels. (*A*) VOTC maps of the local proportion of significant contacts over recorded contacts shown in MNI space for each word processing level. The color scale was adjusted for each map (see scaling values between brackets below each map). Black contours outline proportions significantly above zero. Note that, for letter contacts, the proportion is smaller in the midFG region than in posterior VOTC regions due to the far greater number of recorded (nonsignificant) contacts in the midFG. (*B*) The proportion of significant contacts relative to the number of recorded contacts (normalized between 0 and 1) is shown for each word processing level as a function of the position along the *Y* (posterior–anterior) dimension in the left hemisphere. See also *SI Appendix*, Fig. S2.

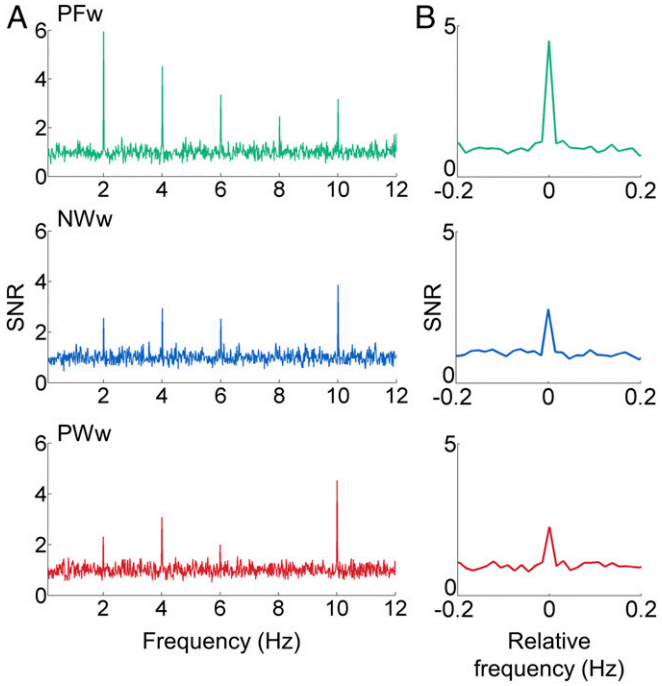

Fig. 7. SEEG lexical responses over the left hemisphere. (*A*) SNR frequency spectra recorded over the 18 lexical contacts in the left hemisphere for the PFw (top row), NWw (middle row), and PWw (bottom row) conditions. Raw FFT spectra were first averaged across the 18 lexical contacts separately for each condition and then transformed to SNR (as the ratio of the amplitude at the frequency bin of interest to the averaged amplitudes at neighboring bins). (*B*) Data from *A* replotted as summed-harmonic segmented FFT spectra (summed FFT spectra were averaged across the 18 lexical contacts separately for each condition and then transformed to SNR).

cortical hierarchy of reading. During reading acquisition, letters are first learned in isolation, that is, as single symbols representing specific phonemes, leading to an early left hemispheric lateralization in their cortical representation (30). Letters may be combined into syllables, morphemes, and words, and new combinations of letters may be encountered throughout the lifetime as new words. The independent representation of letters from words is supported by neuropsychological case studies of pure alexia, where patients cannot read words "at a glance" but can still recognize and name letters one by one (33, 34).

Another finding of the current study is that letter-selective responses were found up to the middle and even anterior FG, with a progressive decrease in proportion, not magnitude, of responses along the posterior–anterior axis (Fig. 6). This suggests that, while letters are selectively coded in the left posterior VOTC, this process extends in a distributed network of regions and overlaps with higher-level processes in anterior VOTC. This is consistent with the greater selectivity for words vs. pseudofonts even in anterior ventrotemporal regions in fMRI (e.g., refs. 10 and 13). Such larger responses to words (vs. pseudofonts) in these anterior regions have been interpreted as showing higher selectivity for increasingly large segments of letter strings (7, 10), or as reflecting phonological or semantic feedback (32, 35). Here, our data reveal letter selectivity even in anterior regions of the VOTC: on the very same contacts, words may not be distinguished from other alphabetic strings.

Identification of the Visual Word Form Area in Intracerebral Recordings. In our cartography of the VOTC, the left midFG showed the largest letter-selective response in amplitude across all significant contacts (*SI Appendix*, Table S2) and, most importantly, showed significant responses to words among other alphabetic strings (nonwords or pseudowords). This region corresponds relatively well to the VWFA as found in fMRI. While previous intracranial studies did not identify this region (17), or targeted directly and solely the midFG (28), it emerges here from our sampling of the whole VOTC with direct intracerebral recordings. While the range of coordinates of the region found here overlaps with the VWFA, the average coordinate is slightly anterior ($y \simeq -40$) to the VWFA as typically defined in fMRI (e.g., $y \simeq -54$ in ref. 3), with individual electrode contacts up to $y = -25$ here (Fig. 6*B*). As presented in the Introduction, this difference may be due to difficulties in recording the anterior section of the VOTC in fMRI due to large magnetic susceptibility artifacts (4). This observation further illustrates the additive value of human brain mapping with intracerebral recordings, in particular with a large sample of participants, a wide spatial coverage, and objective quantification of significant responses as afforded by EEG frequency tagging (31).

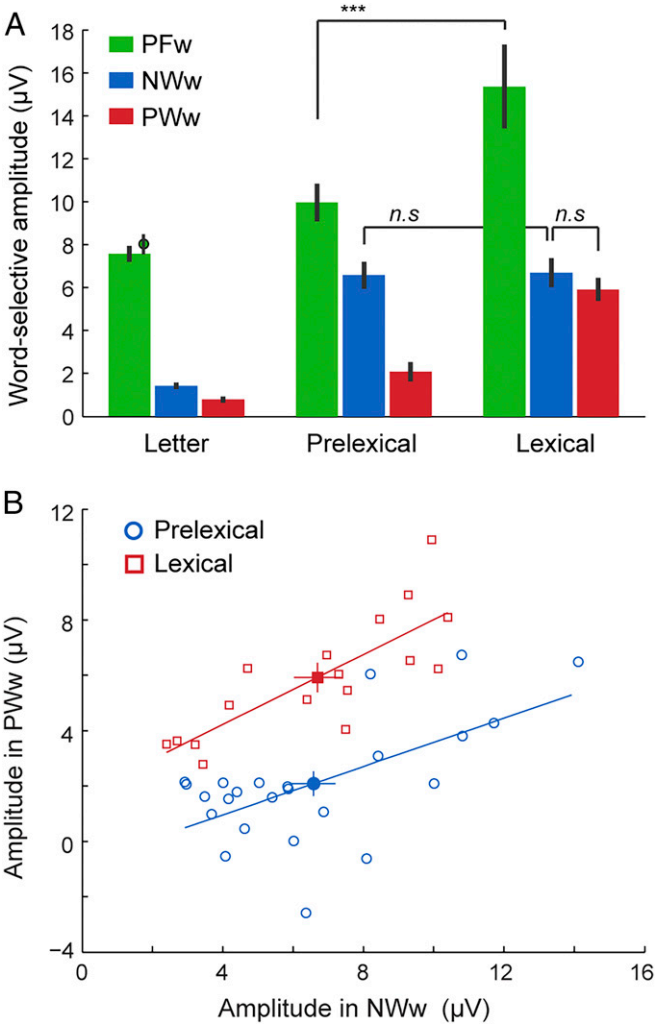

Fig. 8. Amplitude quantification across conditions and processing levels. (*A*) Response amplitudes were quantified as the average of the amplitudes across recording contacts, separately for each processing level (letter, prelexical, and lexical) and each condition (PFw, NWw, and PWw). The additional data point over the left-most column represents the averaged response amplitude over contacts located in the same anatomical regions as the prelexical and lexical contacts (latFG, medFG, antFG, antOTS, and antCoS). (*B*) Relationship between the amplitude in the PWw and the NWw conditions, separately for the prelexical and the lexical recording contacts. Each white-filled point is a single contact, and the mean across contacts is shown as filled markers. Lines represent the least-square linear fit computed separately for prelexical and lexical contacts. Error bars are the SEM.

An Objective Lexical Representation in the Left midFG. First, we found strong evidence for neuronal populations in the left midFG sensitive to familiar, known words, supporting visual lexical representations of written words. Whether the VWFA, and the VOTC in general, hold visual lexical representations is the matter of a long-standing debate in the scientific reading community. On the one hand, the VWFA is thought to compute abstract but prelexical representations (3, 7); on the other hand, it is thought to be tuned for whole-word forms and to discriminate words differing only by one letter (24, 25, 28). The present observations provide original and direct evidence supporting the latter view. Second, despite a wide sampling of the VOTC, including the most anterior ventral temporal regions, significant lexical responses were found almost exclusively in the left midFG (i.e., including the location of the VWFA), highlighting the fundamental role of this local region in reading. Note that this conclusion also holds even when lowering the statistic threshold (*SI Appendix*, Fig. S5) and when including response patterns that do not obey our strict criterion of significance for the three contrasts (*SI Appendix*, Fig. S4). Indeed, a number of additional contacts show responses to words only when presented among letter strings but not among pseudofonts (*SI Appendix*, Table S1). These contacts could potentially reflect more subtle processes, for example, selectivity to word forms only in the context of letters, that is, when a baseline level of activity is sufficiently high.

Both the large number of highly variable word and pseudoword stimuli used in the present study, and the strict control of stimuli in which pseudowords shared the same letters as words in a rearranged order (*Materials and Methods* and ref. 29) rule out an account of lexical responses in the midFG in terms of mere physical differences between words and pseudowords. This is supported by the lack of lexical responses in posterior visual regions sampled in this study. Moreover, although words and pseudowords differed in bigram frequency (*Materials and Methods*), and this factor can modulate VWFA activity in fMRI (36), lexical responses in this paradigm are unlikely to be related to this, for several reasons. First, in scalp EEG, the robust selective response over the left occipito-temporal cortex for words inserted in pseudowords is not reduced when bigram frequency is equated (29). Moreover, directly contrasting pseudowords differing significantly in bigram frequency does not lead to any EEG activity (29). Obviously, this does not completely rule out putative effects of bigram frequency inside the brain that would not be captured on the scalp. In this context, however, there is evidence that lexical contacts in the present intracerebral study do not show a modulation of the response according to bigram frequency. Specifically, while the difference in bigram frequency with words is much higher for NW (7,387 ± 3,291) than PW (2979 ± 4014), NWw responses are not significantly larger than PWw responses in lexical contacts (Fig. 8*A*). Finally, a complementary analysis (*SI Appendix*, Fig. S6) shows that the modulation of bigram frequency in different PWw sequences does not correlate with the response amplitude in these sequences.

Given the high stimulus presentation rate (10 Hz) as well as the forward and backward masking provided by the stimuli in the sequence (Fig. 1), we would like to argue that word selectivity effects found here likely reflect neural coding for visual word forms rather than integration of an abstract visual form with higher-order factors stemming from putative feedback from anterior language areas (32, 37). Supporting this view, we found no evidence of representations of letters and words anteriorly to the midFG in the left VOTC, contrary to intracranial findings with a slower stimulus presentation rate, revealing late semantic effects (17). Future studies could examine this issue further by defining the timing of lexical effects in the VOTC. This investigation is possible with the approach used here (e.g., see ref. 38) but requires inserting more stimuli between word items, reducing SNR as word repetition decreases in a given sequence length.

Interestingly, the contacts classified as lexical discriminate words from nonwords and pseudowords with a similar range of response amplitudes (Fig. 8). This result argues against additive processing stages (i.e., prelexical then lexical) at different time points, or parametrically modulated sensitivity to orthographic structure. Indeed, both of these modes of processing would have generated larger responses to words in the NWw than in the PWw condition in lexical contacts. Rather, in these left midFG populations of neurons classified as lexical, whole-word recognition is relatively independent of the letter strings' plausibility context.

Since responses to words among nonwords (NWw) are not larger in lexical than prelexical contacts, these contacts do not differ only quantitatively, that is, by a generally larger response in lexical contacts. However, the larger response to words among pseudofonts on these lexical contacts suggests that neuronal populations tuned to lexical representations could be less activated by nonletters. These representations could therefore reflect a recognition pattern within an orthographic memory system (26) or a storage of whole-word forms, that is, a lexicon (24, 25, 39). Such a unique visual coding of individual words, allowing fast recognition processes, is necessary for fluent reading. This is consistent with neuropsychological studies showing that lesions in the left midFG cause deficits in word reading, leading to slow and effortful letter-by-letter reading (2, 34, 40, 41).

Nonhierarchical Spatial Prelexical and Lexical Representations. Finally, a crucial finding of our intracerebral recording study is that different levels of word processing appear intermingled in the same region of the midFG: besides the lexical responses identified, some contacts responded to words among orthographically implausible nonwords (i.e., prelexical response) and not to words among pseudowords, without a clear spatial hierarchy between the two types of contacts (Fig. 5). This finding—which also holds when lowering the statistic threshold (*SI Appendix*, Fig. S5) and when including contacts that do not conform to the three strict combinations of conditions to define the three processing levels (*SI Appendix*, Fig. S4)—does not support the proposal of strict successive stages for the coding of letters, bigrams, and quadrigrams at specific positions along the y axis [$y = -64$, -56, and -48 respectively; LCD model (7)]. Indeed, according to this view, lexical contacts should have been located, on average, more anteriorly than prelexical contacts. Also, many contacts with the largest responses in the NWw condition did not discriminate words among pseudowords, ruling out a simple explanation in terms of magnitude of response (Fig. 8). Rather, responses to words at a prelexical level only may be considered as indirect evidence for responses to pseudowords: populations of neurons that are sensitive to the plausibility or statistical regularity of letter combinations rather than to letter strings previously encountered, that is, whole-word forms.

Both the spatial organization of prelexical and lexical contacts and the absence of additivity of responses in lexical contacts strongly suggest that prelexical processes and lexical processes are functionally separated (Fig. 8*B*) rather than constituting ordered additive, spatially hierarchical, stages in visual word recognition. Hence, within the midFG region, distinct neuronal populations compute different levels of representation of words: a letter-selective representation coding for abstract letters; a coarse word representation sensitive to visual characteristics such as plausibility of letter combinations; and a precise, fine-grained representation where neurons have become tuned to previously encountered words. This finding was afforded by our approach of intracerebral recordings where each electrode contact records electrophysiological responses from a limited neuronal population, compared with commonly used fMRI analyses where spatial smoothing and region-of-interest approach average responses originating potentially from different neuronal populations.

In summary, our large-scale intracerebral recording study with fast periodic visual stimulation clarifies the neural basis of reading by revealing (*i*) a spatial dissociation in the left VOTC between a posterior IOG/FG letter-selective representation, and a representation for words, at prelexical and lexical levels, confined to the middle and anterior section of the left fusiform gyrus; (*ii*) true lexical responses, that is, fine-tuning to real words, in a region extending more anteriorly than the visual word form area typically

identified with fMRI; (*iii*) prelexical responses suggesting sensitivity to the statistical regularity of letter combinations only; and (*iv*) a lack of spatial organization between qualitatively distinct prelexical and lexical responses in the left fusiform gyrus.

Materials and Methods

Participants. The study included 37 native French-speaker participants (20 females; mean age, 33 ± 8.4 y; 35 right-handed) undergoing clinical intracerebral evaluation with depth electrodes (SEEG) (42) for refractory partial epilepsy, studied in the Epilepsy Unit of the University Hospital of Nancy between September 2013 and June 2016. Participants with at least one intracerebral electrode implanted in the VOTC were included in the study (Fig. 1*C*). They gave written consent to participate to the study, which was approved by the Ethics Committee of the University Hospital of Nancy.

Intracerebral Electrode Implantation and Recording. Intracerebral electrodes were stereotactically implanted within the participants' brains for clinical purposes, that is, to delineate their seizure onset zones (43). Each 0.8-mm diameter intracerebral electrode contains 8–15 independent recording contacts of 2 mm in length separated by 1.5 mm from edge to edge (for details about the electrode implantation procedure, see ref. 44). Intracerebral EEG was sampled at a 512 Hz and referenced to either a midline prefrontal scalp electrode (FPz, in 32 participants) or an intracerebral contact in the white matter (in five participants).

Fast Periodic Visual Stimulation Paradigm. The paradigm was previously validated in a scalp EEG study (29).

Stimuli. Stimuli were words, pseudowords, nonwords, and pseudofonts (30 of each type), all composed of five elements (letters or pseudofonts) (Fig. 1*A*). French words were selected from the Lexique 3.55 database (45) with the following criteria: they were frequent common nouns (84.99 per million) in singular form, with limited orthographic neighbors (average, 1.9; range from 0 to 4), no foreign language origin, and no accents. PW and NW were built on an item-by-item basis by rearranging the letters of the words [e.g., from the word "avril" ("April") were built the PW "vrali" and the NW "rvlia"]. PF items were also built on an item-by-item basis: letters from words were vertically flipped, segmented, and segments were rearranged into five pseudoletters with the same overall size as the original word. Each word thus had a corresponding PW, NW, and PF containing the exact same amount of black-on-white contrast, so that all conditions were similar in terms of lower-level visual properties. Bigram frequencies were calculated with Wordgen (46) and are reported as summated type bigram frequencies (from the French CELEX database). As in Lochy et al. (29), bigram frequencies differed between words (mean ± SD: 12,038 ± 3,715) and nonwords [4,650 ± 2,803; $t_{(29)} = 10.665$, $P < 0.0001$] as well as between words and pseudowords [9,059 ± 4,293; $t_{(29)} = 4.485$, $P < 0.0001$]. This was done intentionally to respect natural differences in bigram frequencies. Importantly, however, differences in bigram frequency alone do not contribute to selective responses to words recorded in this paradigm since (*i*) these responses are also found for words among pseudowords equated in bigram frequency and (*ii*) no response emerges when two sets of PWs differing in bigram frequency are contrasted [experiment 2; Lochy et al. (29)]. Stimuli were presented in Verdana font, with the size ranging from 4.8 to 7.7 (width) and 1.15 to 2 (height) degrees of visual angle.

Procedure. Participants viewed continuous sequences of visual stimuli (PW, NW, or PF) presented periodically at a rate of 10 Hz through sinusoidal contrast modulation (from 0 to 100% in 50 ms, then back to 0% in 50 ms) with words inserted as every fifth item, so that the word presentation frequency was 2 Hz (10 Hz/5) (Fig. 1*B* and Movies S1–S3). A sequence started by a fixation cross displayed for 2–5 s, followed by 70 s of visual stimulation: 66 s of stimulation at full contrast flanked by 2 s of fade-in and fade-out, wherein contrast gradually increased or decreased, respectively. Randomly selected words were inserted in three different sequences of base stimuli (PF, NW, or PW) resulting in three conditions (Fig. 1*A*): words embedded in PW (PWw; Movie S3), in NW (NWw; Movie S2), and in PF (PFw; Movie S1). Each condition was repeated two times, resulting in six sequences for a total of ∼10 min of testing time, including short breaks. The experiment was repeated a second time for 13 participants and a third time for 3 participants, depending on their availability. Participants were not informed about the periodicity of the words and were unaware of the objectives of the study. No participant had seizures in the 2 h preceding the recordings. During the sequences, participants were instructed to fixate a small blue cross (15 pix) presented continuously at the center of the stimuli, and to detect and respond to (by key press) brief (200-ms) nonperiodic color changes (blue to red, six times per sequence) of this fixation cross.

Intracerebral EEG Analysis. Intracerebral EEG analysis largely followed a procedure of a recently reported group study on the neural basis of selective face perception (31).

Frequency domain processing. Segments of SEEG corresponding to stimulation sequences were extracted, starting 2 s after the onset of the sequence (i.e., after the fade-in period) until ∼68 s (before stimulus fade-out) so as to contain an integer number of 2-Hz cycles (∼66 s). No artifact rejection was performed because intracerebral artifacts (mainly epileptic spikes, but also electro-oculographic and electro-myographic activity, since we used a prefrontal scalp electrode as reference electrode for most of the participants) are more broadly distributed across the frequency spectrum than the frequencies of interest (i.e., 2 Hz, 10 Hz, and their respective harmonics). Sequences were averaged in the time domain separately for each condition and each participant, and amplitude spectrum was computed for each contact using FFT.

Word discrimination responses. Word discrimination responses significantly above noise level at the word stimulation frequency (2 Hz) and its harmonics were determined in each condition as follows: (*i*) the FFT spectrum was cut into segments centered at the word response frequency and the four first harmonics, that is, 2, 4, 6, and 8 Hz (10 Hz corresponds to the base visual stimulation frequency and was not included in the analyses; no word discrimination responses were found above 10 Hz), and surrounded by 25 neighboring bins on each side (Fig. 2*A*); (*ii*) the amplitude values of these four FFT segments were summed (Fig. 2*B*); (*iii*) the summed FFT spectrum was transformed into a *Z* score (Fig. 2*C*). *Z* scores were computed as the difference between the amplitude at the word frequency bin and the mean amplitude of 48 surrounding bins (25 bins on each side, excluding the 2 bins directly adjacent to the bin of interest, i.e., 48 bins) divided by the SD of amplitudes in the corresponding 48 surrounding bins. A contact was considered as showing a word discrimination response in a given condition if the *Z* score at the frequency bin of word stimulation exceeded 3.1 (i.e., $P < 0.001$, one-tailed: signal > noise).

Levels of word discrimination contacts. Based on the pattern of word discrimination responses across the three conditions (i.e., significant or not), we labeled each contact according to three hierarchical levels of word discrimination: (*i*) contacts showing a significant word discrimination response only when presented among pseudofonts, that is, not in the NWw and PWw conditions, were defined as letter selective (+PFw, −NWw, and −PWw); (*ii*) contacts showing significant responses in the PFw and NWw conditions but not in the PWw condition were defined as prelexical (+PFw, +NWw, and −PWw); and (*iii*) contacts showing significant responses in the three conditions (PFw, NWw, and PWw) were defined as lexical (+PFw, +NWw, and +PWw). These three types of contacts are referred to as word discrimination contacts. Contacts that displayed a significant response in at least one condition but that did not conform to any of these three combinations of conditions (e.g., exhibiting a significant response in PWw and NWw conditions but not in more basic PFw condition) were excluded from the main analyses (*SI Appendix*, Fig. S4 and Table S1). Note that the three word processing levels result from combining an increasing number of significant conditions (1–3), resulting in a stricter statistical criterion (thus a different likelihood of false positives) across the three levels. Because these conditions are not statistically independent, one cannot solve this issue by simply adapting the statistical threshold according to the number of tests performed. This issue is not present when including all contacts responding to at least one condition and labeling these contacts according to a single test (*SI Appendix*, *Supplemental Analysis* and Fig. S4).

Quantification of response amplitude. Baseline-corrected amplitudes were computed as the difference between the amplitude at each frequency bin and the average of 48 surrounding bins (i.e., 50 bins, excluding the 2 bins directly adjacent to the bin of interest, i.e., 48 bins). Word discrimination responses were quantified as the sum of the baseline-subtracted amplitudes at the word frequency from the first until the fourth harmonic (2 Hz until 8 Hz) (38), and averaged for each condition and contact type. We removed a single outlier lexical contact in which the response amplitude in each condition was more than 3 SDs away from the mean. SNR spectra were also calculated as the ratio between the amplitude at each frequency bin and the average of the corresponding 48 surrounding bins for display purposes and comparison across studies.

Contact Localization in the Individual Anatomy. The exact position of each contact in the individual anatomy was determined by fusing the postoperative CT scan with a T1-weighted MRI. Contacts inside the gray matter were anatomically labeled in the individual anatomy using the same topographic VOTC parcellation as in ref. 32 (*SI Appendix*, Fig. S1), based on anatomical landmarks. Major VOTC sulci (collateral sulcus and occipito-temporal sulcus) served as medio-lateral divisions. Postero-anterior divisions were the anterior tip of the parieto-occipital sulcus for the border between occipital and temporal lobes, and the posterior tip of the hippocampus for the border between PTL and ATL.

Group Visualization and Proportion Analyses in MNI Space. In a separate analysis, anatomical MRIs were spatially normalized to determine Talairach and MNI coordinates of intracerebral contacts. MNI coordinates of the intracerebral contacts were used to perform group analyses and visualization. Using MNI transformed coordinates, we computed the local proportion of word discrimination intracerebral contacts across the VOTC. Local proportion of contacts was computed in volumes (i.e., "voxels") of size $15 \times 15 \times 100$ mm (for the *X*, left–right; *Y*, posterior–anterior; and *Z*, inferior–superior dimensions, respectively) by steps of $3 \times 3 \times 100$ mm over the whole VOTC. A large voxel size in the *Z* dimension was used as a way to collapse across contacts along the inferior–superior dimension.

For each voxel, we extracted the following information across all participants in our sample: (*i*) the number of recorded contacts located within the voxel; (*ii*) the number of contacts showing a significant response for each level of word discrimination; (*iii*) the number of participants having at least one contact recorded in the voxel; and (*iv*) the number of participants having at least one contact showing a significant word discrimination response. From these values, for each voxel and each level of word discrimination, we computed the proportion of significant contacts/participants over recorded contacts/participants (proportions are crucial here since sampling differs across regions). To ensure reliability and reproducibility, we only considered voxels in which at least two participants showed significant responses. Then, for each voxel, we determined whether the proportion of significant contacts was significantly above zero using a bootstrap procedure in the following way: (*i*) sampling contacts from the voxel (the same number as the number of recorded contacts in the voxel) with replacement; (*ii*) determining the proportion of significant contacts for this bootstrap sample and storing this value; (*iii*) repeating steps *i* and *ii* 5,000 times to generate a distribution of bootstrap proportions and to estimate the *P* value as the fraction of bootstrap proportions equal to zero. In addition, we also statistically compared proportions of word discrimination contacts across corresponding voxels of the left vs. right hemisphere using permutation tests with 20,000 permutations.

We also visualized the variations in the proportions of contacts in each word processing level as a function of the posterior–anterior axis (*Y* dimension) in the left hemisphere. Proportions were computed along the *Y* dimension (MNI coordinates) using a running average procedure (in segments of 15 mm by steps of 3 mm) by collapsing contacts across the *X* (lateral–medial) and *Z* (inferior–superior) dimensions. The resulting proportion profiles were normalized between 0 and 1.

ACKNOWLEDGMENTS. We thank the participants for their involvement in the study, and Talia Retter for careful editing of a previous version of the manuscript. This work was supported by European Research Council Grant facessvep 284025 and Belgian Science Policy Office Grant PAI/33.

1. Dejerine J (1892) Contribution à l'étude anatomo-pathologique et clinique des différentes variétés de cécité verbale. *Mémoires la Société Biol* 4:61–90.
2. Damasio AR, Damasio H (1983) The anatomic basis of pure alexia. *Neurology* 33: 1573–1583.
3. Cohen L, et al. (2002) Language-specific tuning of visual cortex? Functional properties of the visual word form area. *Brain* 125:1054–1069.
4. Wandell BA (2011) The neurobiological basis of seeing words. *Ann N Y Acad Sci* 1224:63–80.
5. Taylor JSH, Rastle K, Davis MH (2013) Can cognitive models explain brain activation during word and pseudoword reading? A meta-analysis of 36 neuroimaging studies. *Psychol Bull* 139:766–791.
6. Schuster S, Hawelka S, Richlan F, Ludersdorfer P, Hutzler F (2015) Eyes on words: A fixation-related fMRI study of the left occipito-temporal cortex during self-paced silent reading of words and pseudowords. *Sci Rep* 5:12686.
7. Dehaene S, Cohen L, Sigman M, Vinckier F (2005) The neural code for written words: A proposal. *Trends Cogn Sci* 9:335–341.
8. Rauschecker AM, et al. (2011) Visual feature-tolerance in the reading network. *Neuron* 71:941–953.
9. Szwed M, et al. (2011) Specialization for written words over objects in the visual cortex. *Neuroimage* 56:330–344.
10. Vinckier F, et al. (2007) Hierarchical coding of letter strings in the ventral stream: Dissecting the inner organization of the visual word-form system. *Neuron* 55:143–156.
11. Vogel AC, Petersen SE, Schlaggar BL (2012) The left occipitotemporal cortex does not show preferential activity for words. *Cereb Cortex* 22:2715–2732.
12. Tagamets M-A, Novick JM, Chalmers ML, Friedman RB (2000) A parametric approach to orthographic processing in the brain: An fMRI study. *J Cogn Neurosci* 12:281–297.
13. Olulade OA, Flowers DL, Napoliello EM, Eden GF (2013) Developmental differences for word processing in the ventral stream. *Brain Lang* 125:134–145.
14. Turkeltaub PE, Gareau L, Flowers DL, Zeffiro TA, Eden GF (2003) Development of neural mechanisms for reading. *Nat Neurosci* 6:767–773.
15. Martin A, Schurz M, Kronbichler M, Richlan F (2015) Reading in the brain of children and adults: A meta-analysis of 40 functional magnetic resonance imaging studies. *Hum Brain Mapp* 36:1963–1981.
16. Hermes D, Nguyen M, Winawer J (2017) Neuronal synchrony and the relation between the blood-oxygen-level dependent response and the local field potential. *PLoS Biol* 15:e2001461.
17. Nobre AC, Allison T, McCarthy G (1994) Word recognition in the human inferior temporal lobe. *Nature* 372:260–263.
18. Thesen T, et al. (2012) Sequential then interactive processing of letters and words in the left fusiform gyrus. *Nat Commun* 3:1284.
19. Rossion B, Jacques C, Jonas J (February 26, 2018) Mapping face categorization in the human ventral occipitotemporal cortex with direct neural intracranial recordings. *Ann N Y Acad Sci*, 10.1111/nyas.13596.
20. Gaillard R, et al. (2006) Direct intracranial, FMRI, and lesion evidence for the causal role of left inferotemporal cortex in reading. *Neuron* 50:191–204.
21. McCandliss BD, Cohen L, Dehaene S (2003) The visual word form area: Expertise for reading in the fusiform gyrus. *Trends Cogn Sci* 7:293–299.
22. Dehaene S, Cohen L (2011) The unique role of the visual word form area in reading. *Trends Cogn Sci* 15:254–262.
23. Bruno JL, Zumberge A, Manis FR, Lu Z-L, Goldman JG (2008) Sensitivity to orthographic familiarity in the occipito-temporal region. *Neuroimage* 39:1988–2001.
24. Glezer LS, Jiang X, Riesenhuber M (2009) Evidence for highly selective neuronal tuning to whole words in the "visual word form area." *Neuron* 62:199–204.
25. Glezer LS, Kim J, Rule J, Jiang X, Riesenhuber M (2015) Adding words to the brain's visual dictionary: Novel word learning selectively sharpens orthographic representations in the VWFA. *J Neurosci* 35:4965–4972.
26. Baeck A, Kravitz D, Baker C, Op de Beeck HP (2015) Influence of lexical status and orthographic similarity on the multi-voxel response of the visual word form area. *Neuroimage* 111:321–328.
27. Kronbichler M, et al. (2004) The visual word form area and the frequency with which words are encountered: Evidence from a parametric fMRI study. *Neuroimage* 21:946–953.
28. Hirshorn EA, et al. (2016) Decoding and disrupting left midfusiform gyrus activity during word reading. *Proc Natl Acad Sci USA* 113:8162–8167.
29. Lochy A, Van Belle G, Rossion B (2015) A robust index of lexical representation in the left occipito-temporal cortex as evidenced by EEG responses to fast periodic visual stimulation. *Neuropsychologia* 66:18–31.
30. Lochy A, Van Reybroeck M, Rossion B (2016) Left cortical specialization for visual letter strings predicts rudimentary knowledge of letter-sound association in preschoolers. *Proc Natl Acad Sci USA* 113:8544–8549.
31. Jonas J, et al. (2016) A face-selective ventral occipito-temporal map of the human brain with intracerebral potentials. *Proc Natl Acad Sci USA* 113:E4088–E4097.
32. Price CJ, Devlin JT (2011) The interactive account of ventral occipitotemporal contributions to reading. *Trends Cogn Sci* 15:246–253.
33. Habekost T, Petersen A, Behrmann M, Starrfelt R (2014) From word superiority to word inferiority: Visual processing of letters and words in pure alexia. *Cognit Neuropsychol* 31:413–436.
34. Leff AP, et al. (2001) The functional anatomy of single-word reading in patients with hemianopic and pure alexia. *Brain* 124:510–521.
35. Kherif F, Josse G, Price CJ (2011) Automatic top-down processing explains common left occipito-temporal responses to visual words and objects. *Cereb Cortex* 21: 103–114.
36. Binder JR, Medler DA, Westbury CF, Liebenthal E, Buchanan L (2006) Tuning of the human left fusiform gyrus to sublexical orthographic structure. *Neuroimage* 33:739–748.
37. Price CJ, Devlin JT (2003) The myth of the visual word form area. *Neuroimage* 19:473–481.
38. Retter TL, Rossion B (2016) Uncovering the neural magnitude and spatio-temporal dynamics of natural image categorization in a fast visual stream. *Neuropsychologia* 91:9–28.
39. Wimmer H, Ludersdorfer P, Richlan F, Kronbichler M (2016) Visual experience shapes orthographic representations in the visual word form area. *Psychol Sci* 27:1240–1248.
40. Beversdorf DQ, Ratcliffe NR, Rhodes CH, Reeves AG (1997) Pure alexia: Clinical-pathologic evidence for a lateralized visual language association cortex. *Clin Neuropathol* 16:328–331.
41. Seghier ML, et al. (2012) Reading without the left ventral occipito-temporal cortex. *Neuropsychologia* 50:3621–3635.
42. Talairach J, Bancaud J (1973) Stereotaxic approach to epilepsy. Methodology of anatomo-functional stereotaxic investigations. *Prog Neurol Surg* 5:297–354.
43. Salado AL, et al. (2018) sEEG is a safe procedure for a comprehensive anatomic exploration of the insula: A retrospective study of 108 procedures representing 254 transopercular insular electrodes. *Oper Neurosurg (Hagerstown)* 14:1–8.
44. Jonas J, et al. (2015) Beyond the core face-processing network: Intracerebral stimulation of a face-selective area in the right anterior fusiform gyrus elicits transient prosopagnosia. *Cortex* 72:140–155.
45. New B, Pallier C, Ferrand L, Matos R (2001) Une base de données lexicales du français contemporain sur internet: Lexique™. *Annee Psychol* 101:447–462.
46. Duyck W, Desmet T, Verbeke LPC, Brysbaert M (2004) WordGen: A tool for word selection and nonword generation in Dutch, English, German, and French. *Behav Res Methods Instrum Comput* 36:488–499.

CORTEX 99 (2018) 296–310

Available online at www.sciencedirect.com

ScienceDirect

Journal homepage: www.elsevier.com/locate/cortex

Research report

A face identity hallucination (palinopsia) generated by intracerebral stimulation of the face-selective right lateral fusiform cortex

Jacques Jonas [a,b,c], *Hélène Brissart* [a], *Gabriela Hossu* [d], *Sophie Colnat-Coulbois* [e], *Jean-Pierre Vignal* [a], *Bruno Rossion* [a,c,*] and *Louis Maillard* [a,b]

[a] *Service de Neurologie, Centre Hospitalier Universitaire de Nancy, Nancy, France*
[b] *CRAN, UMR 7039, CNRS et Université de Lorraine, Vandoeuvre-lès-Nancy, France*
[c] *Institut de recherche en sciences psychologiques, Université Catholique de Louvain, Louvain-La-Neuve, Belgium*
[d] *CIC-IT, Centre Hospitalier Universitaire de Nancy, Nancy, France*
[e] *Service de Neurochirurgie, Centre Hospitalier Universitaire de Nancy, Nancy, France*

ARTICLE INFO

Article history:
Received 29 May 2017
Reviewed 17 August 2017
Revised 27 September 2017
Accepted 29 November 2017
Action editor Holger Wiese
Published online 9 December 2017

Keywords:
SEEG
Electrical brain stimulation
Palinopsia
Face perception
Fusiform face area

ABSTRACT

We report the case of a patient (MB, young female human subject) who systematically experienced confusion between perceived facial identities specifically when electrically stimulated inside the lateral section of the right fusiform gyrus. In the presence of a face stimulus (an experimenter or a photograph), intracerebral electrical stimulation in this region generated a perceptual hallucination of an individual facial part integrated within the whole perceived face, i.e., facial palinopsia. In the presence of a distracting stimulus (visual scene or object picture), the patient also experienced an individual face percept superimposed on the non-face stimulus. The stimulation site evoking this category-selective transient palinopsia was localized in a region showing highly selective responses to faces both with functional magnetic resonance imaging ("Fusiform Face Area", "FFA") and intracerebral electrophysiological recordings during fast periodic visual stimulation (FPVS). Importantly, the largest electrophysiological response to fast periodic changes of facial identity was also found at this location. Altogether, these observations suggest that the face-selective right lateral fusiform gyrus plays a role in generating vivid percepts of individual faces, supporting the active role of this region in individual face representation.

* *Corresponding author*. Université Catholique de Louvain (UCL) 10, Place du Cardinal Mercier, B-1348 Louvain-La-Neuve, Belgium.
E-mail address: bruno.rossion@uclouvain.be (B. Rossion).

https://doi.org/10.1016/j.cortex.2017.11.022
0010-9452/

1. Introduction

Individual face recognition plays a critical role in human social interactions. Studies of patients showing individual face recognition impairment after brain damage (i.e., prosopagnosia, following Bodamer, 1947; see Della Sala & Young, 2003 for an early report by Quaglino and Borelli in 1867) have long suggested that this brain function is supported by a large territory of the human ventral occipito-temporal cortex (VOTC), from the occipital pole to the temporal pole, with a right hemispheric advantage (Barton, 2008; Hécaen & Angelergues, 1962; Meadows, 1974; Rossion, 2014; Sergent & Signoret, 1992).

Within this cortical territory, the lateral section of the right posterior/middle fusiform gyrus (latFG) may be particularly important, as this region shows the largest selective response to faces both in neuroimaging ("Fusiform Face Area", "FFA", e.g., fMRI: Puce, Allison, Gore, & McCarthy, 1995; Kanwisher, McDermott, & Chun, 1997; Kanwisher, 2017; PET: Sergent, Ohta, & MacDonald, 1992; Rossion et al., 2000) and intracerebral recordings (Jonas et al., 2016). Recent studies have shown that electrical intracranial stimulation over the right – but not the left – latFG may elicit transient impairment in face perception, with patients reporting a selective distortion of the visual face input (i.e., distortion of people's faces in the room: "prosopometamorphopsia", Parvizi et al., 2012; Rangarajan et al., 2014). However, patients with prosopometamorphopsia, often a transient phenomenon observed shortly after brain damage (e.g., Bodamer, 1947: case 3/patient B), do not present with major difficulties in individual face recognition, in spite of their perceptual distortions (Bodamer, 1947; Hwang et al., 2012; Hécaen & Angelergues, 1962; Nass, Sinha, & Solomon, 1985; Trojano, Conson, Salzano, Manzo, & Grossi, 2009). Although stimulation of the right latFG inducing prosopometamorphopsia offers a causal link between face perception and this area, impairment in individual face recognition, which characterizes patients with prosopagnosia (Hécaen & Angelergues, 1962; Rossion, 2014; Sergent & Signoret, 1992), has so far not been observed following electrical stimulation of this region.

Here, we report a rare case of confusion of facial identity following focal electrical stimulation directly in the grey matter of the right latFG, without any face distortion. When stimulated only in this region, the patient (MB) systematically reported visual hallucinations characterized by the recurrence of individual facial parts (facial palinopsia, Critchley, 1951) integrated within the whole perceived face (a person in the room, or a photograph). Importantly, the electrode contact evoking this category-selective transient palinopsia was localized in a region showing highly selective responses to faces both with functional magnetic resonance imaging and with intracerebral recordings, as well as sensitivity to individual face discrimination with intracerebral recordings. These observations show that a local face-selective region of the right latFG can generate a vivid hallucination of an individual face, highlighting the active role of this region in individual face representation.

2. Materials and methods

2.1. Case description and neuropsychological assessment

The subject is a 30-year-old woman (MB) with refractory focal epilepsy. Intracerebral stereo-electroencephalography (SEEG) delineated her epileptogenic zone in the right lateral occipito-parietal junction (posterior parietal cortex and superior occipital gyrus). The patient was right-handed as attested by the Edinburgh Handedness Inventory (Oldfield, 1971). At the time of the SEEG exploration, her treatment included eslicarbazepine acetate and lacosamide. She was never treated with topiramate, which has been found to be related to generate palinopsia in some cases (Gersztenkorn & Lee, 2015). The fMRI experiment and the FPVS recordings were approved by the local ethical committee, for which she gave a written consent. She also gave a specific and written consent for using the video material.

MB showed a general intelligence level in the normal range (full-scale IQ of 97). Neuropsychological evaluations revealed normal performance on memory (Taylor Complex Figure, Selective Reminding Test), language (DO80 naming test) and basic visual perception (Visual Object and Space Perception battery, VOSP) functions. The patient never complained of individual face recognition difficulties in everyday life, nor during or after epileptic seizures. Before intracerebral implantation, we conducted an extensive series of behavioral tests to assess MB's face/object perception and memory. Ten control participants (age-, sex- and education level-matched controls) performed the same tests. To compare the results of MB to the control participants, we used the modified *t*-test of Crawford–Howell for single-case studies (Crawford & Howell, 1998) with a p value of $<.05$ considered as statistically significant. These tests included: (1) face/no face categorization test (Mooney faces, experiment 16 in Busigny, Joubert, Felician, Ceccaldi, & Rossion, 2010); (2) tests of face individuation including the Benton Face Recognition Test (BFRT, Benton, Sivan, Hamsher, Varney, & Spreen, 1983), the Cambridge Face Memory Test (CFMT, Duchaine & Nakayama, 2006), an individual face- and car-matching at upright and inverted orientations (experiment 4 in Busigny & Rossion, 2010), as well as an individual matching task of faces presented in different viewpoints (experiment 22 in Busigny et al., 2010); (3) tests of visual memory including an old/new face task (encoding phase followed by an old/new forced choice decision with faces, experiment 3 in Busigny et al., 2010) and an old/new bird task (same task with bird pictures, using the same parameters as for faces); (4) a famous face recognition test (CELEB test, Busigny et al., 2014).

The results of these tests are shown in Table 1. MB performed in the normal range compared to matched normal controls for nearly all tests, either in accuracy or in response times, except that she was significantly slower at a visual memory test with faces and birds (old/new face and old/new bird tests, see Table 1), a slowing down that is often found in epileptic patients under medication. Her decrease of performance for inverted compared to upright faces was also in the

Table 1 – Performance of patient MB and 10 control participants in neuropsychological tests of face/object perception and memory.

		Subject MB	Controls ($n = 10$)	t-test (Crawford–Howell)
Mooney faces	Acc	97.5%	92.1 ± 3.2	$t = 1.61$, $p = .07$
	RT	1708	1243 ± 635	$t = .7$, $p = .25$
BFRT	Acc	44/54	44.9 ± 2.5	$t = -.34$, $p = .37$
	RT	456	315 ± 158	$t = .85$, $p = .21$
CFMT	Acc	52/72	53.6 ± 7.6	$t = -.2$, $p = .42$
Face matching (different viewpoints)	Acc	86%	81.90 ± 8.16	$t = .48$, $p = .32$
	RT	4518	2761 ± 975	$t = 1.72$, $p = .6$
Face matching (upright and inverted)	Acc upright	97.2%	93 ± 4.9	$t = .81$, $p = .22$
	inverted	77.8%	79.4 ± 7.8	$t = -.2$, $p = .42$
	RT upright	1791	1712 ± 658	$t = .11$, $p = .46$
	inverted	2334	1979 ± 624	$t = .39$, $p = .35$
Car matching (upright and inverted)	Acc upright	100%	96.7 ± 9.6	$t = .33$, $p = .37$
	inverted	100%	94.2 ± 11.1	$t = .5$, $p = .31$
	RT upright	1485	1712 ± 658	$t = -.33$, $p = .37$
	inverted	1601	1979 ± 624	$t = -.58$, $p = .29$
Old/New face	Acc	96.7%	94 ± 3.1	$t = .83$, $p = .21$
	RT	3859*	1959 ± 820	$t = 2.21$, $p = .03$
Old/New bird	Acc	83.3	84 ± 7.3	$t = -.09$, $p = .46$
	RT	4279*	2227 ± 900	$t = 2.17$, $p = .03$
CELEB test	FRI	82	86.9 ± 13	$t = -.36$, $p = .36$
	NAI	95.1	90.7 ± 12	$t = .35$, $p = .37$

Acc: accuracy; RT: reaction time in ms; BFRT: Benton Face Recognition Test; CFMT: Cambridge Face Memory Test; FRI: Face Recognition Index; NAI: Name Access Index.
*Indicates lower performance compared to matched normal controls ($p < .05$).

normal range in accuracy and response times ($t = .68$, $p = .51$ and $t = .73$, $p = .48$ respectively, revised standardized difference test, Crawford & Garthwaite, 2005). Taken together, these results show that MB has normal face perception and memory abilities.

2.2. *Stereotactic placement of intracerebral electrodes*

Intracerebral electrodes (Dixi Medical, Besançon, France) were stereotactically implanted in the patient's brain in order to delineate the seizure onset zone (SEEG, Talairach & Bancaud, 1973; Cardinale et al., 2013; Salado et al., 2018). The sites of electrode implantation were determined based on non-invasive data collected during an earlier phase of the investigation. Each intracerebral electrode consists of a cylinder of .8 mm diameter and contains 8–15 contiguous contacts of 2 mm in length separated by 1.5 mm from edge to edge. A few days before surgery, a non-stereotactic T1 weighted MRI with gadolinium was carried out and imported into a computer-assisted software (Iplanstereotaxy, Brainlab, Germany). Each electrode trajectory was then determined according to the investigation planning with careful avoidance of vascular structures. The day of surgery, after induction of general anesthesia, the stereotactic frame (Leksell G-frame, Elekta, Sweden) was positioned on the patient's head. A stereotactic CT-scan was then carried out and fused to the pre-operative non stereotactic MRI. Stereotactic coordinates were then calculated for each trajectory. A post-operative non-stereotactic CT-scan was carried out and fused with a T1-weighted MRI to determine the exact position of each electrode.

The SEEG exploration took place in April 2014. Anatomical locations of intracerebral electrodes were determined to target the most potential epileptogenic zone (right parietal cortex), to monitor the extent of epileptic seizures and to map functional regions next to the epileptic network (i.e., not all electrodes are implanted in regions that are thought to be the source of the seizures). Eleven electrodes were implanted in the right hemisphere targeting the occipito-parieto-temporal cortex and the hippocampus (Fig. 1A). In total, these electrodes contained 138 individual recording contacts. Electrode F (containing 10 contacts, F1 to F10) was located in the right ventral temporal cortex, targeting specifically the latFG, the occipito-temporal sulcus and the inferior temporal gyrus (Fig. 1B). No electrodes were placed in the left hemisphere.

The SEEG signal was recorded at a 512 kHz sampling rate on a 256-channel amplifier (4 SD LTM 64 Headbox, Micromed, Italy). The reference electrode during data acquisition was a midline prefrontal scalp electrode (FPz).

2.3. *Intracerebral electrical stimulations*

2.3.1. *General procedure*

Electrical intracerebral stimulation of the right occipito-parieto-temporal cortex and hippocampus was carried out while the patient performed active recognition or passive viewing of visual objects (photographs of famous faces, famous scenes, common objects, unknown faces or real faces, Table 2). These stimulations were applied between two contiguous contacts on the same electrode and performed at 50 Hz during 5 s at low intensities ranging from 1 to 1.6 mA (i.e., usual stimulation settings in SEEG). MB was not aware of the stimulation onset and termination, the stimulation site and the nature of the effects that could be potentially elicited. In total, 59 electrical stimulations were performed (Table 2). Authors JJ, JPV, LM and BR were present during electrical stimulations, which were video recorded.

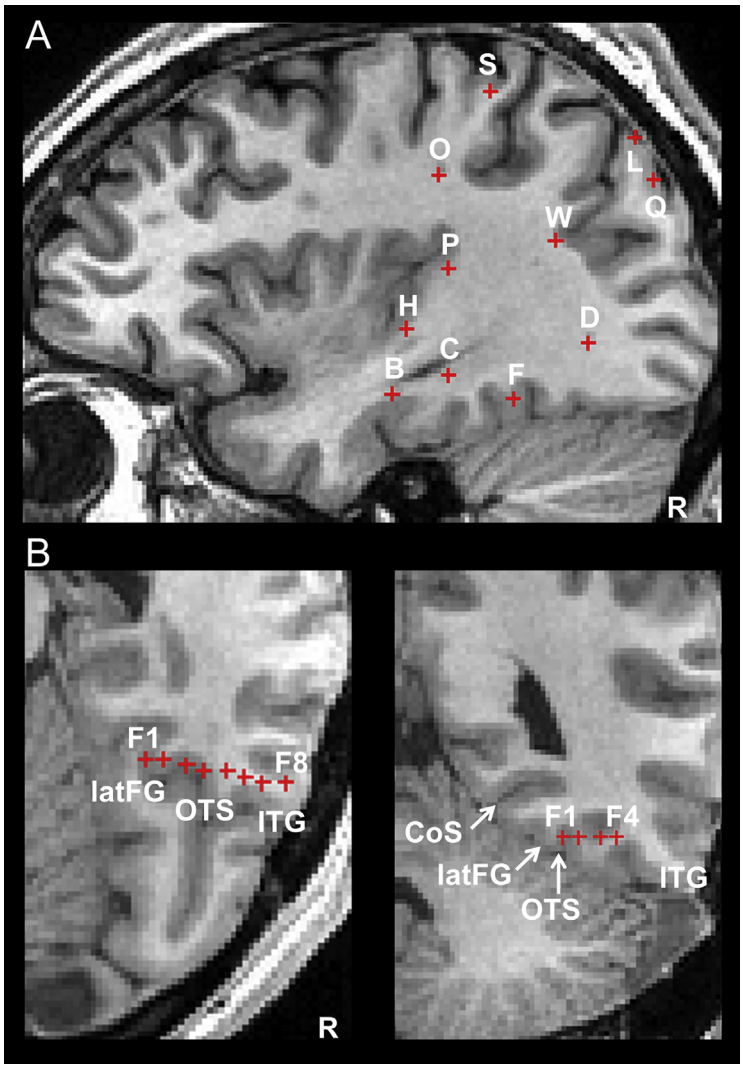

Fig. 1 – Locations of intracerebral electrodes implanted in subject MB's brain. Each electrode is an array of individual recording contacts. Here, each contact is represented by a red cross. A. Locations of all electrodes on a sagittal slice. Since electrodes are usually implanted perpendicularly to the skull, only one contact per electrode is visible on a sagittal slice. B. Location of electrode F in the ventral temporal cortex on axial and coronal slices. CoS: collateral sulcus; ITG: inferior temporal gyrus; latFG: lateral fusiform gyrus; OTS: occipito-temporal sulcus.

2.3.2. *Active recognition*

Thirty stimulations were carried out during the recognition of sets of photographs of the same category presented one by one (famous faces without external features, common objects or famous scenes). MB had to name each photograph in turn. For each set, the stimulation was triggered randomly during the presentation of 1 or 2 successive photographs. We only used photographs that were easily recognized by MB before the stimulation procedure.

2.3.3. *Passive viewing*

Twenty-nine stimulations were carried out while MB was asked to passively watch photographs of unknown faces, common objects, or real faces of people in the room. MB was instructed to describe any perceptual changes she experienced. For each stimulation, only a single visual object image was shown, and the stimulation was triggered manually several seconds after the patient started to look at the stimulus.

2.4. *Face-selectivity: fMRI*

The comprehensive methods (stimuli, stimulation procedures) used for this fMRI study were the same as those used in several previous studies (combined in a large-scale analysis in Rossion, Hanseeuw, & Dricot, 2012). The fMRI experiment took place in September 2014 that is 5 months later than the SEEG exploration.

2.4.1. *Stimuli*

Four categories of stimuli were used: photographs of faces (F), cars (C), and their phase-scrambled versions: scrambled faces

Table 2 – Number of electrical stimulations performed and type of task required.

	Active recognition			Passive viewing		
	Famous faces	Famous scenes	Common objects	Unknown faces	Common objects	Real faces
Contacts F1–F2 (latFG, OTS)	3	1	1	1	1	2
Ventral temporal cortex except contacts F1–F2 (OTS, CoS)	3		1			2
Lateral temporal cortex (ITG, MTG, STG)	4		2		1	2
Occipital cortex (IOG, lateral occipital cortex, cuneus, LG)	3	1			4	3
Parietal cortex (lateral parietal cortex, precuneus)	4	2	3		2	11
Hippocampus			2			
Total	17	4	9	1	8	20

CoS: collateral sulcus; IOG: inferior occipital gyrus; ITG: inferior temporal gyrus; latFG: lateral fusiform gyrus; LG: lingual gyrus; MTG: middle temporal gyrus; OTS: occipito-temporal sulcus; STG: superior temporal gyrus.

(SF) and scrambled cars (SC). The face condition consisted of 43 pictures of faces (22 females) cropped so that no external features (hair, etc.) were revealed. All faces were shown in frontal view (for all stimulus information, see Rossion & Caharel, 2011). They were inserted in a grey rectangular background. Similarly, the car condition consisted of 43 pictures of different cars in a full-front view also embedded in a gray background. The scrambled stimuli were made using a Fourier phase randomization procedure (FFT with phase replaced by the phase of a uniform noise) that yields images preserving the low-level properties of the original image (i.e., luminance, contrast, spectral energy, etc.), while completely degrading any category-related information. Pictures of faces/cars and the phase scrambled face/car pictures subtended equal shape, size and contrast against the background.

2.4.2. *Paradigm*

MB performed 4 runs of 11 min duration each. In each run, there were 6 blocks of 18 sec duration for each of the 4 types of stimuli. Blocks were separated by a baseline condition (cross fixation) of 9 sec. In each block, 24 stimuli of the same condition were presented (750 ms per stimuli, no ISI) on a black background screen, with 2 or 3 consecutive repetitions of the exact same stimulus in each block (target trials in the one-back task). This gave a total amount of 144 stimuli per category per run. The stimuli and the fixation cross were presented centrally, but stimulus location varied randomly in x (6%) and in y (8%) directions at each presentation. This change in stimulus location was made so that specific elements of the non-scrambled face and car stimuli (e.g., the eyes or headlights) do not appear at the same location at each trial, as it would be the case for scrambled stimuli even without jittering position. The patient performed a one-back identity task (2 or 3 targets per block).

2.4.3. *Imaging acquisition parameters*

Functional MR images of brain activity were collected using a 3T head scanner (Signa HDxt, GE Medical Systems, Milwaukee, WI) at the University Hospital of Nancy with repeated single-shot echo-planar imaging: echo time (TE) = 33 ms, flip angle (FA) = 77°, matrix size = 64 × 64, field of view (FOV) = 192 mm, slice thickness = 3 mm, repetition time (TR) = 2250 ms, 36 slices. A high-resolution anatomical volume of the whole brain was acquired using a T1-weighted sequence (resolution: 1 × 1 × 1 mm).

2.4.4. *Data analysis*

The fMRI signal in the different conditions was compared using BrainVoyager QX (Version 2.8.0, Brain Innovation, Maastricht, The Netherlands). Preprocessing consisted of a linear trend removal for excluding scanner-related signal, a temporal high-pass filtering applied to remove temporal frequencies lower than three cycles per run, and a correction for small interscan head movements by a rigid body algorithm rotating and translating each functional volume in 3D space. Functional data (unsmoothed) were spatially aligned with the high-resolution anatomical volume which was previously aligned to the AC-PC plane (automatic co-registration in BrainVoyager QX, adjusted manually). Subsequently, the functional data were analyzed using a multiple regression model (General Linear Model; GLM) consisting of predictors, which corresponded to the particular experimental conditions of each experiment. The predictor time courses used were computed on the basis of a linear model of the relation between neural activity and hemodynamic response, assuming a rectangular neural response during phases of visual stimulation.

The contrast of interest was the conjunction contrast [(F-C) and (F-SF)]. This contrast was aimed at isolating the regions responding more to faces than non-faces objects, and for which this difference could not be accounted for by low-level visual cues (Rossion et al., 2012). A conservative statistical threshold (Bonferroni-corrected, $p < .05$) was used to define face-sensitive areas corresponding to t-values above 4.93.

2.4.5. *Intracerebral contact localization*

The high-resolution T1 (aligned to the AC-PC plane) was fused with the post-operative CT-scan. The electrode contact coordinates were automatically extracted (MRI coordinates in the individual anatomy centered on the AC-PC plane). These electrode contact coordinates were then rendered in Brain Voyager software. The anatomical locations of relevant fMRI activations and intracerebral contacts were therefore assessed in the individual anatomy. Anatomical and functional volumes were also spatially normalized in the Talairach space, but only to determine Talairach coordinates of fMRI activations and intracerebral contacts.

2.5. Face-selectivity: intracerebral responses

We used a "frequency-tagging" or fast periodic visual stimulation (FPVS) approach with natural images to identify and to quantify intracerebral face-selective responses. This paradigm has been validated in several studies (Retter & Rossion, 2016; Rossion, Torfs, Jacques, & Liu-Shuang, 2015; de Heering & Rossion, 2015) and consists of presenting widely variable face stimuli at regular intervals, here, as every 5 stimuli, in a fast periodic train of variable non-face object images (usually 6 Hz) (Fig. 2). Frequency domain representation of the EEG recorded during stimulation separates common responses to faces and objects at 6 Hz and its harmonics from face-selective responses occurring at 6 Hz/5, 1.2 Hz and its harmonics. The technique is highly sensitive and largely free of low-level visual confounds (Rossion et al., 2015), making it ideal for intracerebral recordings. The comprehensive methods used here (stimuli, stimulation procedures) were the same as in a recently reported intracerebral group study (Jonas et al., 2016).

2.5.1. Stimuli

Two hundred grayscale natural images of various non-face objects (from 14 non-face categories: cats, dogs, horses, birds, flowers, fruits, vegetables, houseplants, phones, chairs, cameras, dishes, guitars, lamps) and 50 grayscale natural images of faces were used (see Fig. 2A for examples of stimuli, which are available here: http://face-categorization-lab.webnode.com/resources/natural-face-stimuli/). Each image contained an unsegmented object or face near the center which differed in terms of size, viewpoint, lighting conditions and background. Images were equalized for mean pixel luminance and contrast.

2.5.2. Experimental procedure

MB viewed 2 continuous sequences with highly variable natural images of objects presented at a fast rate of 6 Hz, with faces presented periodically as every 5th image (i.e., at 1.2 Hz = 6 Hz/5, see Fig. 2A, see also Video 1 for an example of visual stimulation). All images were randomly selected from their respective categories. A sequence lasted 70 sec: 66 sec of stimulation at full-contrast flanked by 2 sec of fade-in and fade-out, where contrast gradually increased or decreased, respectively (total duration of the experiment: 2 × 70 sec = 2 min 20 sec). During the sequences, MB was instructed to fixate a small black cross which was presented continuously at the center of the stimuli and to detect brief (500 ms) color-changes (black to red) of this fixation-cross.

Supplementary video related to this article can be found at https://doi.org/10.1016/j.cortex.2017.11.022.

2.5.3. Frequency domain processing

Segments of SEEG corresponding to stimulation sequences were extracted (74-s segments, −2 sec to +72 sec). The 74 sec data segments were cropped to contain an integer number of 1.2 Hz cycles beginning 2 sec after the onset of the sequence (right at the end of the fade-in period) until approximately 65 sec, before stimulus fade-out (75 face cycles ≈ 63 sec). The 2 sequences were averaged in the time domain. Subsequently, a Fast Fourier Transform (FFT) was applied to these averaged segments and amplitude spectra were extracted for all contacts.

2.5.4. Face-selective responses

The FPVS approach used here allows identification and separation of two distinct types of responses (Jonas et al., 2016; Rossion et al., 2015): (1) a *general visual response* occurring at the base stimulation frequency (6 Hz) and its harmonics, as well as (2) a *face-selective response* at 1.2 Hz and its harmonics. Face-selective responses significantly above noise level at the face stimulation frequency (1.2 Hz) and its harmonics (2.4, 3.6 Hz, etc.) were determined by transforming the frequency spectra to Z-scores. The Z-scores were computed as the difference between amplitude at each frequency bin and the mean amplitude of the corresponding 48 surrounding bins (up to 25 bins on each side, i.e., 50 bins, but excluding the 2 bins directly adjacent to the bin of interest, i.e., 48 bins) divided by the standard deviation of amplitudes in the corresponding 48 surrounding bins. A contact was considered to be face-selective if a Z-score exceeded 3.1 (i.e., $p < .001$ one-tailed: signal > noise) for at least one of the first 4 face-selective frequency harmonics (1.2, 2.4, 3.6 or 4.8 Hz; Jonas et al., 2016).

2.5.5. Quantification of responses amplitude

Baseline-corrected amplitudes were computed as the difference between the amplitude at each frequency bin and the average of 48 corresponding surrounding bins (up to 25 bins on each side, i.e., 50 bins, but excluding the 2 bins directly adjacent to the bin of interest, i.e., 48 bins). The face-selective responses were then quantified at each face-selective contact as the sum of the baseline-subtracted amplitude across harmonics (Retter & Rossion, 2016). The range over which face and base frequency harmonics were summed was constrained by the highest significant harmonic (Z-score>3.1, $p < .001$). In MB study, as in a previous intracerebral study of 28 subjects (Jonas et al., 2016), no significant face-selective responses were found above the 14th harmonic (i.e., 16.8 Hz). Face-selective responses were therefore quantified as the sum of the baseline-subtracted amplitudes at the face-selective frequency harmonics from the 1st until the 14th (1.2 Hz until 16.8 Hz), excluding the 5th and 10th harmonics (6 Hz and 12 Hz) that coincided with the base frequency. Signal-to-noise ratio (SNR) spectra were also calculated as the ratio between the amplitude at each frequency bin and the average of the corresponding 48 surrounding bins for display purposes and comparison across studies.

2.6. Visual discrimination of individual faces: intracerebral responses

We also tested MB with a FPVS experiment providing high SNR and behavior-free measures of the brain's discriminative response to individual faces (Liu-Shuang, Norcia, & Rossion, 2014; Liu-Shuang, Torfs, & Rossion, 2016). MB viewed sequences with a randomly selected face identity presented at a fast rate of 6 Hz, with changes of stimulus size at every cycle and, critically, different face identities inserted every 5th

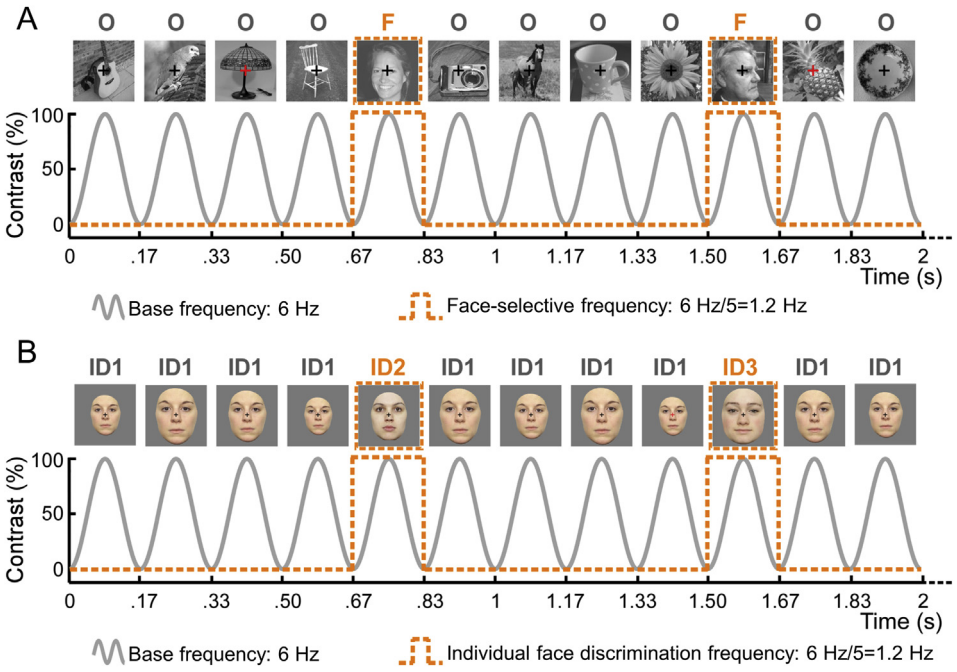

Fig. 2 – FPVS paradigms. A. Paradigm used to define face-selective neural activity (from Rossion et al., 2015). Natural object images are presented by sinusoidal contrast modulation at a rate of 6 stimuli per second (6 Hz). A different face image appears every 5 stimuli (i.e., 6 Hz/5 = 1.2 Hz). In these conditions, a significant electrophysiological response at 1.2 Hz and harmonics reflects a differential, i.e., selective, periodic response to faces (Jonas et al., 2016; Rossion et al., 2015; de Heering & Rossion, 2015). B. Paradigm measuring sensitivity to individual faces (from Liu-Shuang et al., 2014). Images of a randomly selected face identity are presented by sinusoidal contrast modulation at a rate of 6 Hz (ID1). Different face identities (ID2, ID3, etc.) appear every 5th stimulus. Hence, face identity changes occurred at a rate of 6Hz/5 = 1.2Hz. Responses at this frequency and harmonics reflect individual face discrimination responses (Liu-Shuang et al., 2014, 2016).

image (identity change frequency = 1.2 Hz, i.e., 6 Hz/5). In the frequency domain, responses at 1.2 Hz and harmonics (2.4 Hz, 3.6 Hz, etc.) reflect high-level individual face discrimination responses (i.e., abolished by inversion and contrast reversal of faces, Liu-Shuang et al., 2014; and in acquired prosopagnosia; Liu-Shuang et al., 2016). The stimuli and experimental procedures are almost identical to the use of this paradigm on the scalp in these latter studies but the methods are also detailed here for the first report of its application inside the brain.

2.6.1. *Stimuli*

Full-front colored photographs of 25 male and 25 female faces with a neutral expression, taken under standardized conditions with respect to lighting, background, and distance from the camera were used (Fig. 2B for examples of faces). External features such as hair and ears were cropped out and the isolated faces were put against a neutral grey background. Final images were resized to a height of 250 pixels (width: 186 ± 11 pixels).

2.6.2. *Experimental procedure*

MB viewed 2 continuous sequences of faces presented at a rate of 6 Hz (1 sequence with male faces and 1 with female faces). A sequence lasted 65 sec: 60 sec of stimulation at full-contrast ending with 5 sec of fade-out, where contrast gradually decreased (total duration of the experiment: 2 × 65 sec = 2 min 10 sec). In every sequence, the base face was a randomly selected face identity (within the 25 faces of one gender set) repeating throughout the sequence (e.g., identity 1, ID1). At fixed intervals of every 5th base face, a different facial identity (selected from the 25 remaining faces) was presented (ID2, ID3, ID4, etc.). Thus, a trial sequence contained face changes at a frequency of 6 Hz/5, i.e, 1.2 Hz (ID1–ID1-ID1-ID1-ID2-ID1-ID1-ID1-ID1-ID3-ID1-ID1-ID1-ID1-ID4, etc., see Fig. 2B, see also Video 2). As a result, EEG amplitude at this frequency (1.2 Hz) and its harmonics (2.4 Hz, 3.6 Hz, etc.) was used as an index of the visual system's discrimination of individual faces. To avoid confounding changes in face identity with changes with local pixel intensity changes (e.g., blue eyes *vs.* brown eyes), face size varied randomly between 74% and 120% in 2% steps at every 6 Hz stimulation cycle so that the low-level features of the faces did not overlap (see Dzhelyova & Rossion, 2014). During the sequences, MB fixated a small black cross presented continuously at the center of the stimuli and had to detect brief (500 ms) color-changes of this fixation-cross (black to red).

Supplementary video related to this article can be found at https://doi.org/10.1016/j.cortex.2017.11.022.

2.6.3. *Frequency domain processing*

Segments of SEEG corresponding to stimulation sequences were extracted (69-s segments, −2 sec to +67 sec). The 69 sec data segments were cropped to contain an integer number of 1.2 Hz cycles beginning 2 s after the onset of the sequence until approximately 60 s, before stimulus fade-out (69 identity

change cycles ≈ 58 sec). The 2 sequences were averaged in the time domain. Subsequently, FFT was applied to these averaged segments and amplitude spectra were extracted for all contacts.

2.6.4. *Individual face discrimination responses*

The FPVS approach used here allows identifying and separating two distinct types of responses: (1) a *base response* occurring at the base stimulation frequency (6 Hz) and its harmonics, as well as (2) an *individual face discrimination response* at 1.2 Hz and its harmonics. Individual face discrimination responses significantly above noise level at the face identity change frequency (1.2 Hz) and its harmonics (2.4, 3.6 Hz, etc.) were determined by transforming the frequency spectrums to Z-scores (difference between amplitude at each frequency bin and the mean amplitude of the corresponding 48 surrounding bins). Similarly to the FPVS paradigm with faces inserted among objects, a contact was considered as showing individual face discrimination responses if a Z-score exceeded 3.1 (i.e., $p < .001$ one-tailed: signal > noise) for at least one of the first 4 identity change frequency harmonics (1.2, 2.4, 3.6 or 4.8 Hz).

2.6.5. *Quantification of response amplitude*

We quantified the individual face discrimination responses the same way as for the face-selective responses, except that we summed across the first 4 harmonics (in subject MB's brain, no significant responses were found above the 4th harmonic, i.e., 4.8 Hz). Individual face discrimination responses were therefore quantified as the sum of the baseline-corrected amplitudes at the identity change frequency harmonics from the 1st until the 4th (1.2 Hz until 4.8 Hz) (Liu-Shuang et al., 2016).

3. Results

3.1. *Two intracerebral contacts within the face-selective right latFG*

The fMRI face-localizer experiment identified typical face-selective activations of the "core" face network (right and left OFA, FFA, and posterior STS) and of the "extended" face network (right anterior temporal lobe) (Fig. 3, Table 3). Contacts F1–F2 implanted in the latFG and in the adjacent occipito-temporal sulcus (Talairach coordinates: x: 34 to 37, y: −40, z: −17) were located within the right FFA (Figs. 3 and 4A). FMRI activity in a 2-mm-radius ROI centered on the location of contacts was face-selective specifically for contacts F1 and F2 but not for adjacent contacts F3 and F4 (Fig. 4B).

On contacts F1 and F2 in the right FFA, we recorded large face-selective responses occurring exactly at 1.2 Hz and harmonics (Fig. 4C). Significant face-selective responses were also found on 14 other contacts: contacts F3 and F4 located in the right occipito-temporal sulcus (Fig. 4A), 2 contacts in the right middle temporal gyrus (lateral contacts of electrodes F), 4 contacts in the right inferior occipital gyrus (lateral contacts of electrode D), 2 contacts in the right anterior part of the collateral sulcus (electrode C) and 4 contacts in the ventral and medial part of the right occipital cortex (electrodes D and Q).

We quantified the overall face-selective response amplitude on each contact (138 contacts in total) by summing the baseline-subtracted amplitudes over face-selective harmonics (sum of the 12 first face-selective frequency harmonics). Strikingly, contact F1 in the right FFA recorded the largest face-selective response amplitude among the 138 recording contacts implanted in MB's brain (Fig. 5A), followed by a series of contacts located adjacent to the FFA (F3), within the FFA (F2) and in the right inferior occipital gyrus (D9, D10, D11 and D12).

Taken together, fMRI and intracerebral responses recorded during FPVS showed that 2 contacts (F1 and F2) were located within a face-selective region in the right latFG, and that of all contacts, F1 showed the largest face-selective response amplitude.

3.2. *Stimulating the right latFG induces individual facial hallucinations (palinopsia) without distortions*

Low intensity stimulations (1.2 mA) involving contacts F1–F2 located in the right latFG (Fig. 4A) evoked hallucinations of individual face parts. In the famous face recognition task in which 2 faces were successively presented during the time of the stimulation, MB reported seeing facial elements of the first famous face appropriately incorporated into the second famous face (stimulations 1 and 2). MB stated for stimulation 1: "*the photograph of Sarkozy* [former French president, first presented face during stimulation] *was transposed onto the other face* [second presented face during stimulation]". Similarly, MB reported for stimulation 2: "*I saw these eyes* [indicating the first presented face during stimulation] *with this mouth and this mole* [indicating the second face during stimulation]" (see Video 3).

Supplementary video related to this article can be found at https://doi.org/10.1016/j.cortex.2017.11.022.

During stimulation of the same F1–F2 contacts, when MB was asked to passively look at a single face (a real face or a photograph of an unknown face), she reported hallucinations of individual facial elements incorporated appropriately into the face being perceived (stimulations 3, 4, 5 and 6). When MB was looking at the doctor's face, she stated: "*I saw you with eyes and ears which were not yours*", "*the ears were not yours, they were those of somebody else*" (stimulation 3, see Video 4). Stimulating these contacts when MB looked at a photograph of an unknown face, she stated: "*the eyes changed, the pupil took another form that is familiar to me*" (stimulation 6). MB reported that these facial parts were familiar to her but without being able to retrieve where and when she had already seen these features. She stated for example: "*they were not your eyes, they were the eyes of someone I had already seen, maybe coming from the images you showed me earlier*" (stimulation 3, see Video 4), "*It is something familiar but I can't put a name on it; it is like when you meet someone you have already seen but without being able to retrieve his name*" (stimulation 6). Although MB was unable to remember whose face these features belonged to, these facial elements were always linked to individual familiar identities. Interestingly, the change in the percept concerned only part of the face, with some facial elements remaining intact. When asked if the nose changed, MB answered: "*no*" (stimulation 3); when asked if the eyes, the ears, the mouth, the hair changed,

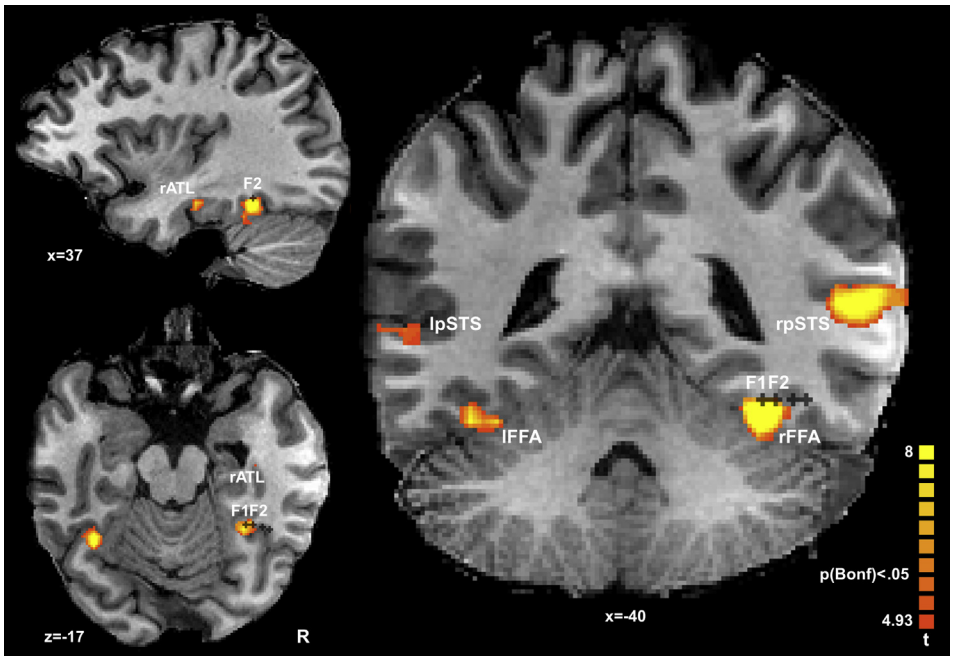

Fig. 3 – Two contacts F1 and F2 are located within the face-selective right latFG ("FFA") defined in fMRI. FMRI revealed typical face-selective activations (conjunction contrast F-C and F-SF, $p < .05$ Bonferroni-corrected): bilateral FFA, bilateral pSTS-faces, right ATL-faces and bilateral OFA (not shown here but see Table 3). Two contacts of electrode F (F1 and F2) were located within the right latFG-faces. Acronyms: ATL: anterior temporal lobe; FFA: fusiform face area; pSTS: posterior superior temporal sulcus.

Table 3 – Talairach coordinates (center of mass), size, mean t and *p* values of face-selective areas identified in fMRI (Conjunction contrast F-C and F-SF, p < .05 Bonferroni-corrected).

	Talairach coordinates			Cluster size (number of voxels)	Mean t value	Mean *p* value
	x	y	z			
Right ATL-faces	32	−19	−22	90	5.82	$<10^{-6}$
Right FFA	28	−46	−23	688	8.04	$<10^{-7}$
Left FFA	−42	−53	−23	687	8.88	$<10^{-7}$
Right OFA	50	−61	0	636	8.14	$<10^{-7}$
Left OFA	−46	−64	5	588	6.85	$<10^{-7}$
Right pSTS	51	−44	6	652	7.22	$<10^{-7}$
Left pSTS	−61	−43	0	214	5.68	$<10^{-6}$

ATL: anterior temporal lobe; FFA: fusiform face area; OFA: occipital face area; pSTS: posterior superior temporal sulcus.

she answered: "*no, only the nose*" (stimulation 5). MB also spontaneously stated: "*only the eyes changed, the rest of the face did not change*" (stimulation 6).

Supplementary video related to this article can be found at https://doi.org/10.1016/j.cortex.2017.11.022.

Importantly, MB never reported any facial distortions and reproducibly stated that the facial structure was preserved ("*it was a normal face*" she said; when asked if the face was distorted, MB answered without hesitation: "*no*"). Once MB said "*your face was distorted*", but it was a way to explain that the face changed because of the hallucinatory facial elements (stimulation 3, Video 4). Moreover, MB was always able to recognize the faces during the stimulation.

For the stimulations with non-face stimuli (active recognition of famous scenes and passive viewing of common objects), MB also reported individual face hallucinations (stimulations 7 and 8). During stimulation 7, MB was presented with famous scenes and asked to recognize them. MB reported seeing a pair of eyes looking at her, superimposed on the scene (Mont Saint-Michel in France, see Video 5). She stated: "*I saw the eyes that I saw earlier*", "*they were not in place of something, they were superimposed on the scene*". When asked where these eyes came from, she said: "*I don't know which face but it was a face that I saw recently*". During stimulation 8, MB was presented with a photograph of a car and was asked to passively look at it. She reported seeing a whole face in the rear-view mirror. She stated: "*A face put itself in the rear-view mirror*", "*It was something familiar*". A third stimulation with active recognition of common object did not evoke any visual effect (stimulation 9). MB never reported palinopsia of face hallucinations during her epileptic seizures and the

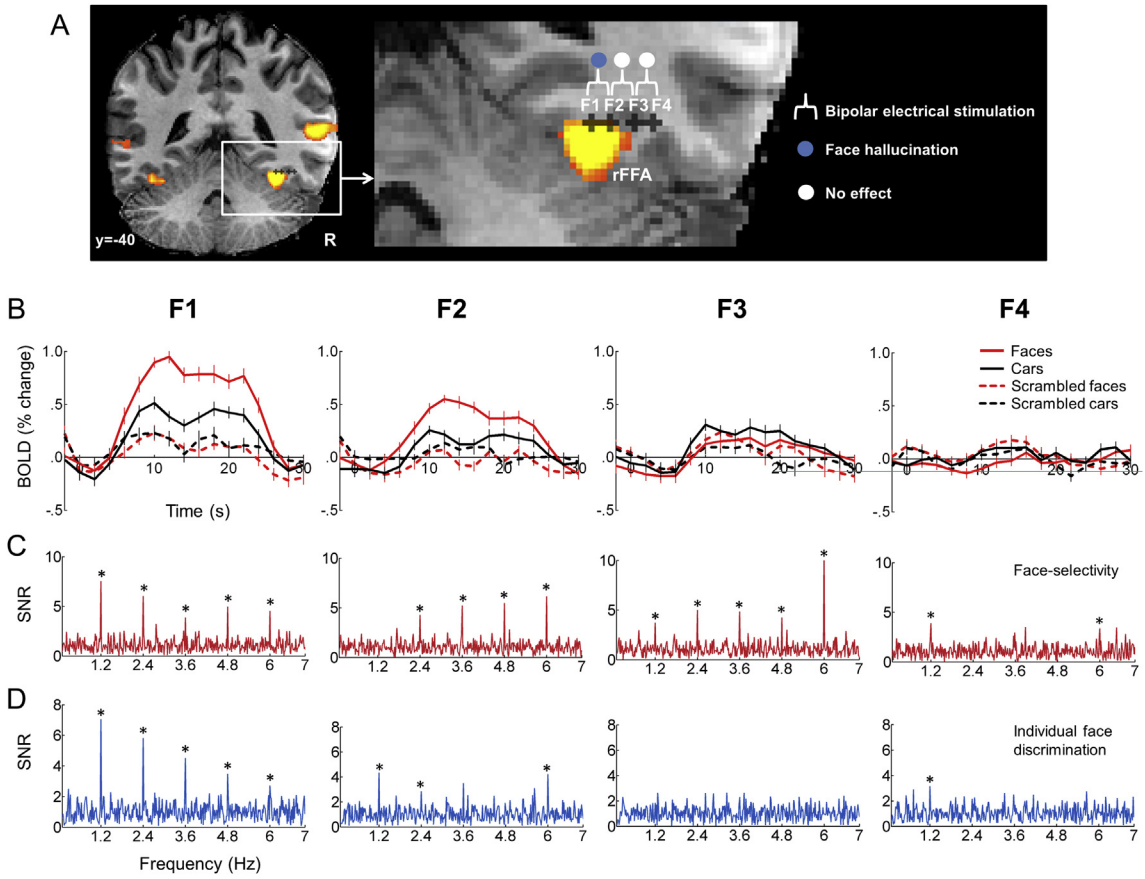

Fig. 4 – FMRI and electrophysiological measurements on contacts within and outside the right FFA. A. Locations of contacts F1, F2, F3 and F4. F1 and F2 were located within the right FFA while F3 and F4 were located just next to the FFA in the right OTS. Electrical stimulation of contacts F1 and F2 elicited individual face hallucinations. B. BOLD time courses recorded during the face-localizer fMRI experiment and extracted from a 2-mm-radius ROI centered on the location of contacts F1, F2, F3 and F4. C. Intracerebral responses recorded during the FPVS paradigm measuring face-selective activity. Significant face-selective responses occurring exactly at the face stimulation frequency (1.2 Hz and harmonics: 2.4, 3.6 and 4.8 Hz) were recorded on these 4 contacts with a maximum amplitude on contact F1 (see Fig. 5A). D. Intracerebral responses recorded during the individual face discrimination paradigm. Significant individual face discrimination responses exactly at the identity change frequency rate (1.2 Hz and harmonics) were recorded with a maximum amplitude at contact F1 (see Fig. 5B). *Indicates statistically significant responses ($Z > 3.1$, $p < .001$).

stimulations of the right latFG never produced epileptic seizures. None of the stimulations performed outside the face-selective right latFG (50 stimulations in total) evoked similar effects or visual recognition impairments.

Supplementary video related to this article can be found at https://doi.org/10.1016/j.cortex.2017.11.022.

3.3. *The stimulated region is sensitive to individual face identity*

With FPVS, we recorded large individual face discrimination responses occurring exactly at 1.2 Hz and harmonics at contact F1 (Fig. 4D). We also recorded clear, albeit smaller, responses on contact F2. Ten contacts also recorded individual discrimination responses, mainly in the right inferior occipital gyrus (D7, D8, D9, D10 and D11). We quantified the individual face discrimination responses on each contact by summing the baseline-subtracted amplitudes over harmonics (sum of the 4 first harmonics). Contact F1 recorded, by far, the largest response amplitude (Fig. 5B), followed by contact F2 and contacts in the right inferior occipital gyrus (D7, D8, D9, D10 and D11).

4. Discussion

We report a case of individual facial hallucination following the stimulation of the face-selective cortex of the right latFG. Two main characteristics make the reported hallucinations particularly original: (1) hallucinated face parts were linked to individual identities (i.e., to famous faces during the recognition task and to personally familiar faces during the passive face viewing task); (2) in the presence of a face stimulus,

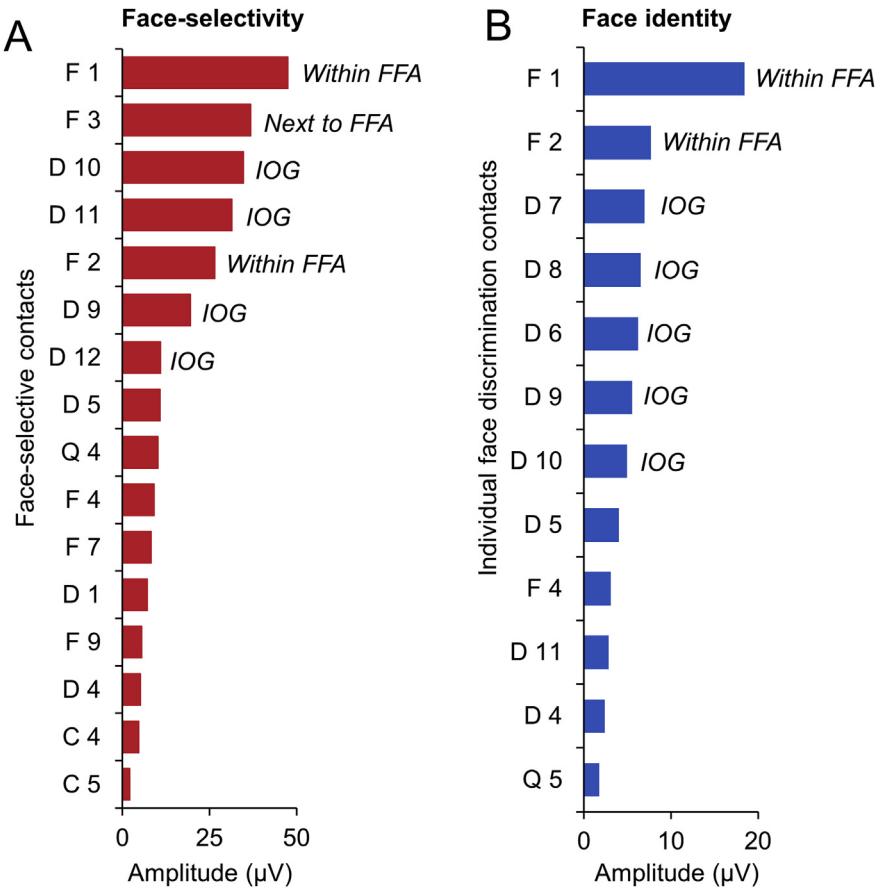

Fig. 5 – Quantification of the intracerebral response amplitude obtained with FPVS. A. Face-localizer FPVS paradigm. Among the 16 significant face-selective contacts, F1 located in the right FFA recorded the largest face-selective response amplitude. B. Face identity FPVS paradigm. Among the 12 significant individual face discrimination contacts, F1 located in the right FFA recorded the largest response amplitude. FFA: fusiform face area; IOG: inferior occipital gyrus.

hallucinated face parts were appropriately integrated within the perceived face. Thus, MB experienced confusion of facial identity perception by mixing different face parts coming from different identities in a coherent whole face. Moreover, these hallucinations were specific to the category of faces, as only face hallucinations were reported (regardless of the presence of face or non-face stimuli). Thanks to fast periodic visual stimulation, we also observed clear face-selective and individual face discrimination neural responses in the regions explored with intracerebral electrodes, with a peak of activation for both functions corresponding exactly to the electrode contact leading to the perceptual hallucination (Fig. 5).

Puce, Allison, and McCarthy (1999) reported facial hallucinations by stimulating the face-selective cortex of the VOTC (isolated eyes, single or multiple faces). However, there was no report that these hallucinations belonged to particular individuals and patients were not looking at faces during stimulation. Moreover, these hallucinations followed stimulation of distributed sites along the postero–anterior axis of the VOTC. In contrast, MB hallucinations here followed the stimulation of a specific region, not only highly selective to faces as defined in fMRI and SEEG, but also coding for differences between individual faces.

In two studies (Parvizi et al., 2012; Rangarajan et al., 2014), patients looking at faces during stimulation of the face-selective cortex in the right latFG reported "prosopometamorphopsia" (Bodamer, 1947; Brust & Behrens, 1977; Ebata, Ogawa, Tanaka, Mizuno, & Yoshida, 1991; Hwang et al., 2012; Hécaen & Angelergues, 1962; Miwa & Kondo, 2007; Mooney, Carey, Ryan, & Bofin, 1965; Trojano et al., 2009). Specifically, patients self-reported distortions of the perceived faces, involving the whole face or face parts (e.g., subject statements in Parvizi et al., 2012: "*Your face metamorphosed … your nose got saggy and went to the left*"; in Rangarajan et al. (2014)'s study, subject S3: "*Her nose looked different, larger*"; subject S4: "*Chin looks a little droopy*"; subject S5: "*It was almost like you were a cat*"). These reports are typical of prosopometamorphopsia, a condition in which faces may appear distorted, torn, warped, disfigured, or cartoonized, with, for example, face parts bulging, shrinking, dropping or floating. However, there is no hallucination or confusion between individual faces in such cases. The patient tested in Parvizi et al. (2012) stated that "*You almost look like somebody I've seen before, but somebody different*", however, he also described severe distortions of the face ("*your nose got saggy and went to the left*", "*it's almost like the shape of your face, your features drooped*"), making unlikely that this

transformed face corresponds to an existing individual. Moreover, subsequent observations described in Rangarajan et al. (2014) only mentioned prosopometamorphopsia. In contrast, the present case MB never reported face distortions, and clearly stated that these hallucinations formed "*a normal face*". In addition, brain-damaged patients experiencing prosopometamorphopsia are usually still able to recognize individual faces (Bodamer, 1947; Hécaen & Angelergues, 1962), which is in line with patients' reports during stimulation (Parvizi et al., 2012; Rangarajan et al., 2014). Finally, here, we were able for the first time to link an hallucination of confusion between individual faces with a face-selective electrophysiological marker of individual face discrimination, in a patient who is unimpaired at this function as established with neuropsychological tests (see below).

A potential reason for the lack of individual face recognition impairment or hallucination following intracranial electrical stimulation of the right latFG in previous studies may be the size of the cortical region concerned. That is, electrical stimulation of the right latFG generating transient prosopometamorphopsia has been applied in previous studies through subdural electrodes posed on the cortical surface ("Electrocorticography", ECoG), which are relatively large in size and distant from one another (i.e., electrodes of 2.3 mm in diameter with 5–10 mm inter-electrode spacing) and using high current intensities (2–8 mA). This approach may interfere with face perception in a non-specific manner (i.e., global distortion of the face) and contrasts with focal and low intensity electrical stimulation directly in the grey matter, as applied here with depth electrodes (SEEG) with which specific processes could be disturbed (i.e., face identity). Interestingly, in previous SEEG studies, focal intracerebral stimulation applied to other face-selective regions such as the right inferior occipital gyrus or the right anterior fusiform gyrus has sometimes elicited a transient impairment in individual face recognition (as observed in famous face recognition or face identity matching tasks), most often without face distortion (Jonas et al., 2012, 2014, 2015). However, we should make it clear from our experience that the observation of such phenomena following focal intracerebral stimulation within the latFG remains rare. A major limiting factor is obviously the positioning of the electrodes inside the brain, which follows strict clinical guidelines, and will often fall partly or completely outside of the critical cortical nodes for face perception. Hence, here the patient experienced recurrent face hallucinations following stimulation of a single electrode contact, while neighboring electrode contacts failed to elicit any effect (see also Jonas et al., 2012 for electrical stimulation at the edge of the right latFG/FFA without any effect on face perception).

MB's visual experience corresponds to "palinopsia", a condition in which there is persistence or recurrence of a visual image after the exciting object stimulus has been removed (Bender, Feldman, & Sobin, 1968; Critchley, 1951; Gersztenkorn & Lee, 2015). Some types of palinopsia share a few characteristics with MB's reports: recurrence of face images ("facial palinopsia", all stimulations), recurrence appropriately integrated into the scene being perceived (all stimulations except number 7), recurrence of an object superimposed into comparable objects ("categorical incorporation", e.g., eyes into a face, all stimulations with a face stimulus), recurrence after a short interval after exposure ("immediate form", stimulations 1 and 2) and recurrence associated with a sense of familiarity, without being able to recall where or when the object has been seen before (stimulations 3 to 8) (Critchley, 1951; Kinsbourne & Warrington, 1963; Bender et al., 1968; Jacobs, Feldman, & Bender, 1972; Meadows & Munro, 1977; for a review see; Gersztenkorn & Lee, 2015). For example, Meadows and Munro (1977) reported the famous case of a woman who, following a stroke of the right lingual and fusiform gyri, noticed that a Santa Claus beard became superimposed appropriately upon the faces of people at a Christmas party. Michel and Troost (1980) described two patients, who after a stroke of the right occipital lobe, reported that each person they saw had the face of someone they just had seen on television. Palinopsia including face hallucinations is usually reported following various lesions of the right occipito-temporo-parietal cortex and is usually associated with the recurrence of other object categories (Bender et al., 1968; Kupersmith, Berenstein, Nelson, ApSimon, & Setton, 1999; Maillot, Belin, Perrier, & Larmande, 1993; Meadows & Munro, 1977; Michel & Troost, 1980). Our study shows that palinopsia restricted to faces can be evoked by stimulating a specific face-selective region of the right temporal lobe. The physiopathology of this type of palinopsia (i.e., hallucinatory palinopsia) is assumed to be related to an activation of images encoded in visual memory (Gersztenkorn & Lee, 2015). Stimulation of the right face-selective latFG may have released visual representations of individual faces encoded in this region.

Here electrophysiological face-selective responses were recorded using a fast periodic visual stimulation approach providing objective, high SNR and quantifiable responses (e.g., Retter & Rossion, 2016; Rossion et al., 2015) which are particularly relevant for intracerebral recordings (e.g., Jonas et al., 2016). Among all the brain regions explored with intracerebral electrodes, the largest face-selective response was found at the eloquent stimulation site. Moreover, we were also able to obtain intracerebral individual face discrimination responses with a sensitive FPVS paradigm validated in scalp EEG studies (Liu-Shuang et al., 2014, 2016) and again, the largest individual face discrimination response was observed at the eloquent stimulation site (Fig. 5). To our knowledge, this is the first evidence of a high-level (i.e., not image-based) individual face discrimination response obtained inside key category-selective regions of the human right cortical face network with direct recordings of neural activity.

Altogether, the generation of vivid hallucinations of individual faces with electrical stimulation and the recording of large individual face discrimination responses with FPVS point to the face-selective region in the right latFG as playing an active role in individual face representation. Note that despite the effect being only observed on a single focal electrode contact, we cannot rule out a spread of the stimulation current to other connected face-selective regions, so that the facial palinopsia reported here may in fact be related to a co-activation of multiple areas of the cortical face network. However, even in this case, the present observations suggest at least that the face-selective right latFG is a necessary node within this network to generate a vivid percept of an individual face. This conclusion, obviously, rests on the ability of the patient to individualize faces, which was ensured here

through stringent neuropsychological evaluation before the SEEG recoding and stimulation. Moreover, the patient's epileptogenic zone was located in the right lateral occipito-parietal junction (posterior parietal cortex and superior occipital gyrus), i.e., outside of the cortical face network including the eloquent site of perceptual hallucination. The observation of sensitivity to individual faces in the right latFG, including causal evidence through intracerebral stimulation, is largely in agreement with findings of fMRI-adaptation studies, which have reported decreases to individual (unfamiliar) face repetition particularly in the face-selective cortex of the fusiform gyrus (e.g., Davies-Thompson, Gouws, & Andrews, 2009; Ewbank, Henson, Rowe, Stoyanova, & Calder, 2013; Gauthier et al., 2000; Hermann et al., 2017; Schiltz et al., 2006; Xu & Biederman, 2010), with some studies showing a right hemispheric predominance of this effect (e.g., Gilaie-Dotan & Malach, 2007; Mazard, Schiltz, & Rossion, 2006; Winston, Henson, Fine-Goulden, & Dolan, 2004). In addition, the disturbance reported by the patient here may be tentatively associated with a holistic/configural process defined as the integration of multiple facial elements into a single representation of the whole face (e.g., Rossion, 2013; Tanaka & Farah, 1993). Indeed, hallucinated facial elements were appropriately incorporated within the face being perceived into a coherent face whole. Therefore, and although this is based on a subjective report of a single case, our observations suggest a role of the right latFG in holistic/configural perception, a fundamental process for individual face recognition (Rossion, 2013; Schiltz & Rossion, 2006) according to which there is no decomposition of the face representation in isolated parts in the cortical face network. Moreover, our observations point to a large overlap between regions involved in categorization of a face as a face and individualization of that face (Figs. 4 and 5). Altogether, these observations are compatible with accumulation of evidence in the same cortical face network, with an initially coarse representation allowing generic face categorization (i.e., faces *vs.* objects) being progressively refined, again without part decomposition, into a detailed representation supporting the individualization of the face percept (Rossion, 2014).

The co-localization between fMRI and intracranial electrophysiological responses is essential for electrical brain stimulation studies since it provides converging evidence of the functional specificity of the stimulated region. A spatial overlap between fMRI and electrophysiological face-selective responses has been shown in the latFG using transient stimuli (Jacques et al., 2016; Parvizi et al., 2012; Puce, Allison, Spencer, Spencer, & McCarthy, 1997). Thanks to the FPVS approach here, we were not only able to show this co-localization, but also to quantify intracerebral responses and to rank brain regions according to their level of face-selectivity, this following a very short experiment time (e.g., 2 min here). One major problem in human electrical brain stimulation studies is the time constraint due to the clinical settings. In this context, FPVS appears to provide quick and reliable detection of the most important brain regions for a function, in order to primarily target them with electrical stimulation. This makes FPVS a tool of choice for subsequent electrical brain studies.

5. Conclusion

By stimulating the right latFG face-selective cortex in subject MB, we evoked vivid percepts of individual faces. Along with intracerebral electrophysiological recordings during FPVS showing that this region is highly sensitive to individual faces, these results point to the active role of this region in individual face representation.

Acknowledgments

We thank subject MB for her involvement in the study. We thank Joan Liu-Shuang for the FPVS individual face identity paradigm and Talia Retter for editing the manuscript. JJ and BR are supported by the Belgian National Fund for Scientific Research (FNRS). This work was supported by a European Research Council Grant (facessvep 284025).

REFERENCES

Barton, J. J. (2008). Structure and function in acquired prosopagnosia: Lessons from a series of 10 patients with brain damage. *Journal of Neuropsychology, 2*, 197–225.

Bender, M. B., Feldman, M., & Sobin, A. J. (1968). Palinopsia. *Brain, 91*, 321–338.

Benton, A. L., Sivan, A. B., Hamsher, K., Varney, N. R., & Spreen, O. (1983). *Benton facial recognition: Stimulus and multiple choice pictures*. Lutz, FL: Psychological Assessment Resources Inc.

Bodamer, J. (1947). Die Prosop-agnosie; die Agnosie des Physiognomieerkennens. *Archiv für Psychiatrie und Nervenkrankheiten, 118*, 6–53.

Brust, J. C., & Behrens, M. M. (1977). "Release hallucinations" as the major symptom of posterior cerebral artery occlusion: A report of 2 cases. *Annals of Neurology, 2*, 432–436.

Busigny, T., Joubert, S., Felician, O., Ceccaldi, M., & Rossion, B. (2010). Holistic perception of the individual face is specific and necessary: Evidence from an extensive case study of acquired prosopagnosia. *Neuropsychologia, 48*, 4057–4092.

Busigny, T., Prairial, C., Nootens, J., Kindt, V., Engels, S., Verplancke, S., et al. (2014). Celeb : Une batterie d'évaluation de la reconnaissance des visages célèbres et de l'accès aux noms propres. *Revue de Neuropsychologie, 6*, 69–81.

Busigny, T., & Rossion, B. (2010). Acquired prosopagnosia abolishes the face inversion effect. *Cortex, 46*, 965–981.

Cardinale, F., Cossu, M., Castana, L., Casaceli, G., Schiariti, M. P., Miserocchi, A., et al. (2013). Stereoelectroencephalography: Surgical methodology, safety, and stereotactic application accuracy in 500 procedures. *Neurosurgery, 72*, 353–366.

Crawford, J. R., & Garthwaite, P. H. (2005). Testing for suspected impairments and dissociations in single-case studies in neuropsychology: Evaluation of alternatives using monte carlo simulations and revised tests for dissociations. *Neuropsychology, 19*, 318–331.

Crawford, J. R., & Howell, D. C. (1998). Comparing an individual's test score against norms derived from small samples. *The Clinical Neuropsychologist, 12*, 482–486.

Critchley, M. (1951). Types of visual perseveration: "paliopsia" and "illusory visual spread". *Brain, 74*, 267–299.

Davies-Thompson, J., Gouws, A., & Andrews, T. J. (2009). An image-dependent representation of familiar and unfamiliar

faces in the human ventral stream. *Neuropsychologia, 47*, 1627–1635.
Della Sala, S., & Young, A. W. (2003). Quaglino's 1867 case of prosopagnosia. *Cortex, 39*, 533–540.
Duchaine, B., & Nakayama, K. (2006). The Cambridge face memory test: Results for neurologically intact individuals and an investigation of its validity using inverted face stimuli and prosopagnosic participants. *Neuropsychologia, 44*, 576–585.
Dzhelyova, M., & Rossion, B. (2014). The effect of parametric stimulus size variation on individual face discrimination indexed by fast periodic visual stimulation. *BMC Neuroscience, 15*(1), 87.
Ebata, S., Ogawa, M., Tanaka, Y., Mizuno, Y., & Yoshida, M. (1991). Apparent reduction in the size of one side of the face associated with a small retrosplenial haemorrhage. *Journal of Neurology, Neurosurgery & Psychiatry, 54*, 68–70.
Ewbank, M. P., Henson, R. N., Rowe, J. B., Stoyanova, R. S., & Calder, A. J. (2013). Different neural mechanisms within occipitotemporal cortex underlie repetition suppression across same and different-size faces. *Cerebral Cortex, 23*, 1073–1084.
Gauthier, I., Tarr, M. J., Moylan, J., Skudlarski, P., Gore, J. C., & Anderson, A. W. (2000). The fusiform "face area" is part of a network that processes faces at the individual level. *Journal of Cognitive Neuroscience, 12*, 495–504.
Gersztenkorn, D., & Lee, A. G. (2015). Palinopsia revamped: A systematic review of the literature. *Survey of Ophthalmology, 60*, 1–35.
Gilaie-Dotan, S., & Malach, R. (2007). Sub-exemplar shape tuning in human face-related areas. *Cerebral Cortex, 17*, 325–338.
Hécaen, H., & Angelergues, R. (1962). Agnosia for faces (prosopagnosia). *Archives of Neurology, 7*, 92–100.
de Heering, A., & Rossion, B. (2015). Rapid categorization of natural face images in the infant right hemisphere. *Elife, 2*(4), e06564.
Hermann, P., Grotheer, M., Kovács, G., & Vidnyánszky, Z. (2017). The relationship between repetition suppression and face perception. *Brain Imaging and Behavior, 7*, 1018–1028.
Hwang, J. Y., Ha, S. W., Cho, E. K., Han, J. H., Lee, S. H., Lee, S. Y., et al. (2012). A case of prosopometamorphopsia restricted to the nose and mouth with right medial Temporooccipital lobe Infarction that included the fusiform face area. *Journal of Clinical Neurology, 8*, 311–313.
Jacobs, L., Feldman, M., & Bender, M. B. (1972). The persistence of visual or auditory percepts as symptoms of irritative lesions of the cerebrum of man. *Zeitschrift für Neurologie, 203*, 211–218.
Jacques, C., Witthoft, N., Weiner, K. S., Foster, B. L., Rangarajan, V., Hermes, D., et al. (2016). Corresponding ECoG and fMRI category-selective signals in human ventral temporal cortex. *Neuropsychologia, 83*, 14–28.
Jonas, J., Descoins, M., Koessler, L., Colnat-Coulbois, S., Sauvée, M., Guye, M., et al. (2012). Focal electrical intracerebral stimulation of a face-sensitive area causes transient prosopagnosia. *Neuroscience, 222*, 281–288.
Jonas, J., Jacques, C., Liu-Shuang, J., Brissart, H., Colnat-Coulbois, S., Maillard, L., et al. (2016). A face-selective ventral occipito-temporal map of the human brain with intracerebral potentials. *Proceedings of the National Academy of Sciences USA, 113*, E4088–E4097.
Jonas, J., Rossion, B., Brissart, H., Frismand, S., Jacques, C., Hossu, G., et al. (2015). Beyond the core face-processing network: Intracerebral stimulation of a face-selective area in the right anterior fusiform gyrus elicits transient prosopagnosia. *Cortex, 72*, 140–155.
Jonas, J., Rossion, B., Krieg, J., Koessler, L., Colnat-Coulbois, S., Vespignani, H., et al. (2014). Intracerebral electrical stimulation of a face-selective area in the right inferior occipital cortex impairs individual face discrimination. *Neuroimage, 99*, 487–497.
Kanwisher, N. (2017). The Quest for the FFA and Where It Led. *Journal of Neuroscience, 37*, 1056–1061.
Kanwisher, N., McDermott, J., & Chun, M. M. (1997). The fusiform face area: A module in human extrastriate cortex specialized for face perception. *Journal of Neuroscience, 17*, 4302–4311.
Kinsbourne, M., & Warrington, E. K. (1963). A study of visual perservation. *Journal of Neurology, Neurosurgery & Psychiatry, 26*, 468–475.
Kupersmith, M. J., Berenstein, A., Nelson, P. K., ApSimon, H. T., & Setton, A. (1999). Visual symptoms with dural arteriovenous malformations draining into occipital veins. *Neurology, 52*, 156–162.
Liu-Shuang, J., Norcia, A. M., & Rossion, B. (2014). An objective index of individual face discrimination in the right occipito-temporal cortex by means of fast periodic oddball stimulation. *Neuropsychologia, 52*, 57–72.
Liu-Shuang, J., Torfs, K., & Rossion, B. (2016). An objective electrophysiological marker of face individualisation impairment in acquired prosopagnosia with fast periodic visual stimulation. *Neuropsychologia, 83*, 100–113.
Maillot, F., Belin, C., Perrier, D., & Larmande, P. (1993). Visual perseveration and palinopsia: A visual memory disorder? *Revue Neurologique, 149*, 794–796.
Mazard, A., Schiltz, C., & Rossion, B. (2006). Recovery from adaptation to facial identity is larger for upright than inverted faces in the human occipito-temporal cortex. *Neuropsychologia, 44*, 912–922.
Meadows, J. C. (1974). The anatomical basis of prosopagnosia. *Journal of Neurology, Neurosurgery & Psychiatry, 37*, 489–501.
Meadows, J. C., & Munro, S. S. (1977). Palinopsia. *Journal of Neurology, Neurosurgery & Psychiatry, 40*, 5–8.
Michel, E. M., & Troost, B. T. (1980). Palinopsia: Cerebral localization with computed tomography. *Neurology, 30*, 887–889.
Miwa, H., & Kondo, T. (2007). Metamorphopsia restricted to the right side of the face associated with a right temporal lobe lesion. *Journal of Neurology, 254*, 1765–1767.
Mooney, A. J., Carey, P., Ryan, M., & Bofin, P. (1965). Parasagittal parieto-occipital meningioma with visual hallucinations. *American Journal of Ophthalmology, 59*, 197–205.
Nass, R., Sinha, S., & Solomon, G. (1985). Epileptic facial metamorphopsia. *Brain & Development, 7*, 50–52.
Oldfield, R. C. (1971). The assessment and analysis of handedness: The Edinburgh inventory. *Neuropsychologia, 9*, 97–113.
Parvizi, J., Jacques, C., Foster, B. L., Witthoft, N., Rangarajan, V., Weiner, K. S., et al. (2012). Electrical stimulation of human fusiform face-selective regions distorts face perception. *Journal of Neuroscience, 32*, 14915–14920.
Puce, A., Allison, T., Gore, J. C., & McCarthy, G. (1995). Face-sensitive regions in human extrastriate cortex studied by functional MRI. *Journal of Neurophysiology, 74*, 1192–1199.
Puce, A., Allison, T., & McCarthy, G. (1999). Electrophysiological studies of human face perception.III: Effects of top-down processing on face-specific potentials. *Cerebral Cortex, 9*, 445–458.
Puce, A., Allison, T., Spencer, S. S., Spencer, D. D., & McCarthy, G. (1997). Comparison of cortical activation evoked by faces measured by intracranial field potentials and functional MRI: Two case studies. *Human Brain Mapping, 5*, 298–305.
Rangarajan, V., Hermes, D., Foster, B. L., Weiner, K. S., Jacques, C., Grill-Spector, K., et al. (2014). Electrical stimulation of the left and right human fusiform gyrus causes different effects in conscious face perception. *Journal of Neuroscience, 34*, 12828–12836.
Retter, T. L., & Rossion, B. (2016). Uncovering the neural magnitude and spatio-temporal dynamics of natural image categorization in a fast visual stream. *Neuropsychologia, 91*, 9–28.

Rossion, B. (2013). The composite face illusion: A whole window into our understanding of holistic face perception. *Visual Cognition, 21*, 139–253.
Rossion, B. (2014). Understanding face perception by means of prosopagnosia and neuroimaging. *Frontiers in Bioscience (Elite Ed), 6*, 258–307.
Rossion, B., & Caharel, S. (2011). ERP evidence for the speed of face categorization in the human brain: Disentangling the contribution of low-level visual cues from face perception. *Vision Research, 51*, 1297–1311.
Rossion, B., Dricot, L., Devolder, A., Bodart, J. M., Crommelinck, M., De Gelder, B., et al. (2000). Hemispheric asymmetries for whole-based and part-based face processing in the human fusiform gyrus. *Journal of cognitive neuroscience, 12*, 793–802.
Rossion, B., Hanseeuw, B., & Dricot, L. (2012). Defining face perception areas in the human brain: A large-scale factorial fMRI face localizer analysis. *Brain and Cognition, 79*, 138–157.
Rossion, B., Torfs, K., Jacques, C., & Liu-Shuang, J. (2015). Fast periodic presentation of natural images reveals a robust face-selective electrophysiological response in the human brain. *Journal of Vision, 15*, 15.1.18.
Salado, A. L., Koessler, L., De Mijolla, G., Schmitt, E., Vignal, J. P., Civit, T., et al. (2018). sEEG is a safe procedure for a comprehensive anatomical exploration of the insula in drug resistant epilepsy: A retrospective study of 108 procedures representing 254 transopercular insular electrodes. *Operative Neurosurgery, 14*, 1–14.
Schiltz, C., & Rossion, B. (2006). Faces are represented holistically in the human occipito-temporal cortex. *Neuroimage, 32*, 1385–1394.
Schiltz, C., Sorger, B., Caldara, R., Ahmed, F., Mayer, E., Goebel, R., et al. (2006). Impaired face discrimination in acquired prosopagnosia is associated with abnormal response to individual faces in the right middle fusiform gyrus. *Cerebral Cortex, 16*, 574–586.
Sergent, J., Ohta, S., & MacDonald, B. (1992). Functional neuroanatomy of face and object processing. A positron emission tomography study. *Brain, 115*, 15–36.
Sergent, J., & Signoret, J. L. (1992). Varieties of functional deficits in prosopagnosia. *Cerebral Cortex, 2*, 375–388.
Talairach, J., & Bancaud, J. (1973). Stereotaxic approach to epilepsy: Methodology of anatomo-functional stereotactic investigations. *Progress in Neurological Surgery, 5*, 297–354.
Tanaka, J. W., & Farah, M. J. (1993). Parts and wholes in face recognition. *The Quarterly Journal of Experimental Psychology, 46*, 225–245.
Trojano, L., Conson, M., Salzano, S., Manzo, V., & Grossi, D. (2009). Unilateral left prosopometamorphopsia: A neuropsychological case study. *Neuropsychologia, 47*, 942–948.
Winston, J. S., Henson, R. N., Fine-Goulden, M. R., & Dolan, R. J. (2004). fMRI-adaptation reveals dissociable neural representations of identity and expression in face perception. *Journal of Neurophysiology, 92*, 1830–1839.
Xu, X., & Biederman, I. (2010). Loci of the release from fMRI adaptation for changes in facial expression, identity, and viewpoint. *Journal of Vision, 10*(14).

ANNALS OF THE NEW YORK ACADEMY OF SCIENCES
Special Issue: *The Year in Cognitive Neuroscience*
REVIEW

Mapping face categorization in the human ventral occipitotemporal cortex with direct neural intracranial recordings

Bruno Rossion,[1,2,3] Corentin Jacques,[1,4] and Jacques Jonas[1,2,3]

[1]Psychological Sciences Research Institute, Institute of Neuroscience, University of Louvain (UCLouvain), Louvain-la-Neuve, Belgium. [2]Service de Neurologie, Centre Hospitalier Régional Universitaire (CHRU) de Nancy, Nancy, France. [3]CRAN, UMR 7039, CNRS et Université de Lorraine, Nancy, France. [4]Research Group Psychiatry, Department of Neuroscience, University of Leuven, Leuven, Belgium

Address for correspondence: Bruno Rossion, Institute of Research in Psychology (IPSY), Institute of Neuroscience (IoNS), University of Louvain (UCLouvain), 10 Place du Cardinal Mercier, Louvain-la-Neuve 1348, Belgium.
bruno.rossion@uclouvain.be

The neural basis of face categorization has been widely investigated with functional magnetic resonance imaging (fMRI), identifying a set of face-selective local regions in the ventral occipitotemporal cortex (VOTC). However, indirect recording of neural activity with fMRI is associated with large fluctuations of signal across regions, often underestimating face-selective responses in the anterior VOTC. While direct recording of neural activity with subdural grids of electrodes (electrocorticography, ECoG) or depth electrodes (stereotactic electroencephalography, SEEG) offers a unique opportunity to fill this gap in knowledge, these studies rather reveal widely distributed face-selective responses. Moreover, intracranial recordings are complicated by interindividual variability in neuroanatomy, ambiguity in definition, and quantification of responses of interest, as well as limited access to sulci with ECoG. Here, we propose to combine SEEG in large samples of individuals with fast periodic visual stimulation to objectively define, quantify, and characterize face categorization across the whole VOTC. This approach reconciles the wide distribution of neural face categorization responses with their (right) hemispheric and regional specialization, and reveals several face-selective regions in anterior VOTC sulci. We outline the challenges of this research program to understand the neural basis of face categorization and high-level visual recognition in general.

Keywords: face categorization; human brain; intracerebral; SEEG; fast periodic visual stimulation

Introduction

Recognizing individual people by their face and decoding, for example, their emotional expression and gender from facial signals is critical for social interactions. These functions rely first and foremost on the brain's ability to categorize faces as faces, that is, to discriminate faces from other visual signals such as nonface objects in the environment and to generalize this discrimination across widely variable exemplars of faces. The neural basis of face processing has been intensively investigated for three decades with functional neuroimaging, first with positron emission tomography[1] and then with functional magnetic resonance imaging (fMRI[2]). FMRI studies, in particular, have defined a set of regions in the ventral occipitotemporal cortex (VOTC) of the typical human adult brain responding significantly more to pictures of faces than nonface objects even when no explicit categorization task is required. These *face-selective* regions are thought to form the core of the human cortical network to process faces.[3–6] While fMRI has been the dominant player to map face-selective regions, other neuroscientific methodologies have been used. For instance, constraints from lesion studies, that is, neurological patients suffering from the loss of ability to recognize individual faces (prosopagnosia[7]), have helped better understand the functional organization of this VOTC network.[3,8]

doi: 10.1111/nyas.13596

Among the various methods available to probe the human cortical face network, the recording of direct neural activity from intracranial electrodes implanted in epileptic patients is a long-standing technique,[9,10] which has been increasingly used in recent years. Here, we provide a critical and constructive review of the contribution of this approach to our understanding of the categorization of faces in the human VOTC. We begin by outlining the limitations of fMRI to derive a comprehensive face-selective map of the VOTC, calling for complementary direct measurements of neural activity in this region. Next, we remind the reader of the two different types of intracranial approaches and briefly summarize the findings of the studies using these approaches to understand the neural basis of face categorization. We then outline some difficulties encountered by these studies, which make their findings sometimes inconsistent with each other and with fMRI findings. Finally, on the basis of a recent large-scale intracranial study, we outline a research program to map face categorization processes in the whole VOTC on the basis of the following principles: (1) test large samples of patients in intracranial electroencephalography (iEEG) while (2) preserving individual anatomy information, and (3) rely on fast periodic visual stimulation (FPVS) to (4) objectively (i.e., a priori) define and quantify highly sensitive responses in a frequency-domain representation with minimal computational procedures.

Local fluctuations in fMRI signal strength and the lack of anterior VOTC activation

FMRI provides a sluggish and indirect (i.e., hemodynamic) measure of neural activity. For this reason, researchers often emphasize its low temporal resolution as a weakness, since fMRI provides little information about the temporal unfolding of face processes in different regions of the cortical face network. Nevertheless, time-resolved fMRI may provide information about the *relative* timing of face-selective activation in the VOTC,[11–14] supporting findings from lesion studies[15–17] and diffusion tensor imaging[17] for a nonhierarchical organization of this network.[8] In fact, at the current state of knowledge, we view the main limitation of an indirect measure of brain activity with fMRI for our object of study as being elsewhere: although reliable and meaningful fMRI measurements are made in parts of the brain that can be measured, the signal-to-noise ratio (SNR) of the neural activity recorded (i.e., the hemodynamic blood oxygenation-level dependent, BOLD, contrast) suffers from local signal variations caused by heterogeneous magnetic susceptibility of the local anatomy.[18] For this reason, the relative magnitude of the face-selective neural response cannot be fairly compared across various VOTC regions, and some of these regions (e.g., the fusiform face area, "FFA"[19,20]) may be attributed a dominant role possibly because they are relatively well spared from magnetic susceptibility artifacts.

Most importantly for our purpose, the anterior section of the VOTC is affected by a large susceptibility artifact arising from the ear canals.[18,21,22] Therefore, with conventional fMRI sequences, reliable BOLD activation is difficult to measure in this region. Several fMRI studies have located this artifact, which primarily affects the anterior half of the VOTC, between the anterior tip of the middle fusiform gyrus and the temporal pole[23–26] (Fig. 1). Consequently, fMRI studies may fail to disclose, or may underestimate, genuine face-selective responses in the anterior half of the VOTC. Most notably, face-selective activations anterior to the lateral section of the middle fusiform gyrus (i.e., the localization of the FFA) are rarely reported (Fig. 1A). Since most fMRI studies of face perception only report measures of face-selectivity in the posterior half of the VOTC, where the occipital face area (OFA) and FFA lie, the map that emerges from this research is often limited anteriorly to the middle fusiform gyrus (Fig. 1B). Hence, between 1990 and 2016, this map might have evolved from a "big blob to sharp and crisp spots" thanks to fMRI, as noted in a recent review,[20] but it did not extend anteriorly (Fig. 1C; see also Ref. 4).

Importantly, while there is growing evidence for anterior VOTC fMRI face-selective activations, in particular when using coronal slices[22] or optimized sequences for anterior temporal lobe (ATL) coverage,[27,28] these activations remain inconsistent across studies, relatively small in volume and found only in a fraction of individual brains tested (e.g., half of the subjects in Refs. 23 and 29). Most importantly, they are mostly found very anteriorly, that is, close to the temporal pole.[22,23,29–33] Thus, despite the optimization of scanning parameters, there is a gap in fMRI maps between the FFA and anterior face-selective activations close to or in the temporal pole (see the gap in Fig. 1A; see also Ref. 34 for a

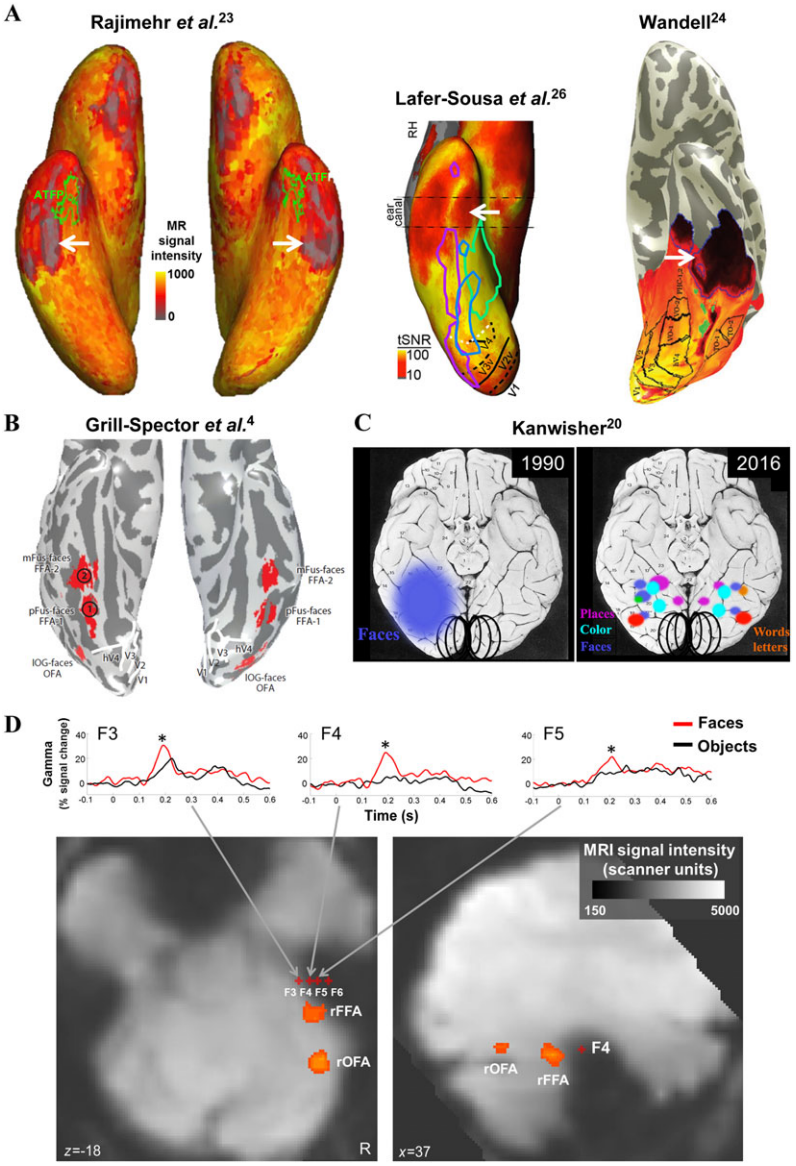

Figure 1. Magnetic susceptibility artifact due to the ear canal (or anterior VOTC signal dropout) in fMRI and its consequences on the current picture of fMRI neural basis of face categorization. (A) These examples show the BOLD signal level on ventral views of the inflated cortical surface. The anterior VOTC signal dropout is indicated by a white arrow (gray or black zone in Rajimehr *et al.*[23] and Wandell;[24] red zone in Lafer-Sousa *et al.*[26]). In these regions, BOLD measurements are not reliable. In Lafer-Sousa *et al.*,[26] the face-selective activations are indicated by purple outlines: note that face-selective activations are found all along the VOTC except in the region of the signal dropout. (B) Topological organization of the face-selective activations in the VOTC (in red) in one of the most recent reviews on the functional architecture of face perception in the VOTC.[4] Note that there are no activations anteriorly to the middle fusiform gyrus (FFA, spot indicated by "2" in the figure). (C) Schematic representation (from Ref. 20) of the progress made in the understanding of functional architecture of the VOTC between 1990 (birth of fMRI) and 2016. Although the posterior VOTC is refined, little or no progress appears to have been made in mapping and understanding anterior VOTC regions. (D) Genuine face-selective responses in the right anterior fusiform gyrus as found by intracranial recordings (top row: electrodes F3, F4, and F5) are not observed in fMRI because of the signal dropout caused by the ear canal (bottom row: fMRI face-selective areas and intracranial electrodes are shown on raw axial (left) and sagittal (right) functional slices; from Ref. 25). *Face-selective responses ($P < 0.01$). Note that this region, in the heart of the artifact, was not covered in an fMRI study using coronal slices to improve signal detection of face-selective activations in the anterior VOTC.[22]

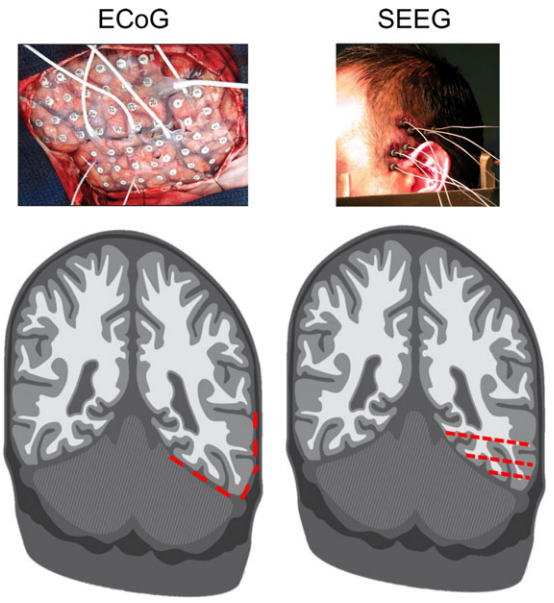

Figure 2. Intracranial (iEEG) recording techniques: ECoG and SEEG. Above, pictures of the surgical procedure involved in placing the intracranial electrodes. In ECoG, part of the skull is removed to apply electrodes onto the cortical surface (here, grids of electrodes). In SEEG, small holes are drilled in the skull to implant thin depth electrodes. Below, schematic coronal representation of intracranial electrodes in contact with the middle fusiform gyrus. The electrodes are represented in red.

meta-analysis and empirical study of anterior temporal face patches, figs. 2 and 3 of that paper).

Evidence for face-selective responses with intracranial EEG recordings

To date, the only alternative approach to provide a more comprehensive map of face-selectivity in humans is afforded by electrophysiological recordings in awake patients implanted with intracranial electrodes along the VOTC as part of their presurgical evaluation for drug-resistant focal epilepsy. These relatively rare—compared with neuroimaging—iEEG recordings allow millisecond resolution measurements of electrical fields directly associated with local neural activity. Crucially, these measurements have a high and stable SNR across VOTC regions, from the occipital pole to the temporal pole. In practice, there are two possible surgical techniques for intracranial electrode placement (Fig. 2). On the one hand, electrocorticography (ECoG[35]) consists of applying electrodes onto the cortical surface after removing part of the skull (i.e., subdural electrodes). Subdural electrodes have a circular shape and are spatially arranged as grids or strips with typically 5–10 mm interelectrode spacing. On the other hand, stereotactic electroencephalography (SEEG[36]) consists of inserting depth electrodes within the brain, from the cortical surface to the medial cortex (i.e., *intracerebral* electrodes). The *intracerebral* electrodes are thin cylinders (e.g., 0.8 mm diameter[37]) typically containing 8–15 contiguous individual recording sites (or contacts) separated by an insulating material. From the point of view of fundamental research, both techniques have their own advantages. For example, while ECoG has the advantage of offering an extensive superficial spatial coverage, SEEG provides recordings directly inside the gray matter, allowing the specific exploration of cortical sulci and medial structures (e.g., amygdala and hippocampus). It is important to note that in both techniques, electrodes target the putative epileptogenic zone but also the surrounding normal cortex in order to assess the limits of surgical resection.

The first recordings of face-evoked potentials in the human VOTC were reported in the 1990s by Allison and colleagues[9] at Yale using ECoG and Halgren and colleagues[10] working in Paris and Rennes with SEEG. Allison *et al.*[9] recorded a negative potential larger for pictures of faces than objects, the N200, over the posterior and anterior sections of the fusiform gyrus, and the inferior occipital gyrus (IOG). This work provided the impetus for the subsequent recording of the face-selective N170 over the human scalp of typical individuals with the same paradigm and stimuli.[38] Subsequently, the Yale research team published three seminal papers, reporting ECoG recordings performed in 98 patients over the ventral and lateral occipitotemporal cortex.[39–41] Face-selective N200s were recorded over the fusiform gyrus (as in Allison *et al.*,[9] Fig. 3A) and a later additional face-selective potential (AP350) located anteriorly to the N200 in the ATL (Fig. 3A). More precisely, this AP350 potential was located over the anterior fusiform gyrus, the anterior inferior temporal gyrus, and the temporal pole, with a right hemispheric dominance.

Using SEEG, Halgren *et al.*[10] recorded a complex triphasic potential (N130-P180-N240) evoked by faces in the fusiform gyrus (the P180 potentially being the positive counterpart of the N200 inside the brain). They also recorded various types of

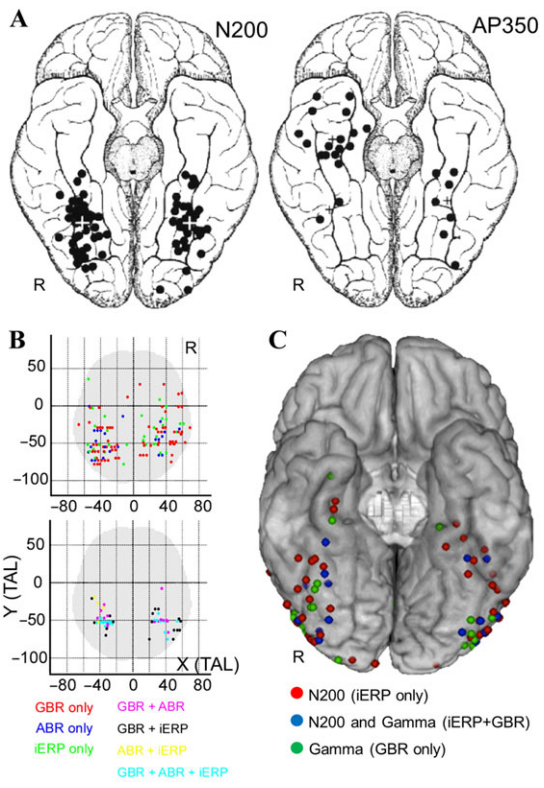

Figure 3. Spatial distribution of face-selective responses in the VOTC with iEEG. (A) Face-selective ERPs (N200 and AP350) reported in Allison *et al.*[39] (B) Face-selective responses found in Vidal *et al.*,[46] plotted in the Talairach space. Each dot represents a face-selective electrode. Electrodes are colored according to the frequency band where face-selective responses were found (GBR: gamma; ABR: alpha/beta; and iERP: event-related potentials). Note that some contacts shown here are in fact located in frontal and parietal lobes, and not in the VOTC (sagittal views not shown). (C) Face-selective responses found in Engell and McCarthy,[60] plotted in the MNI (Montreal Neurological Institute) system. Face-selective electrodes are colored according to the frequency band where face-selective responses were found.

potentials evoked by faces (varying in latency and polarity) in widespread regions of the temporal lobe (lingual gyrus, superior and middle temporal gyri, temporal pole, hippocampus, and amygdala). However, this SEEG study did not measure face-selective responses by comparing evoked responses to faces and meaningful nonface object stimuli (see also Ref. 42).

More recent studies of groups of patients of various sizes have made several important contributions for the understanding of the spatial functional organization of face-selectivity. These studies showed the predominance of face-selective responses in the lateral over the medial fusiform gyrus,[43,44] clarified the spatial relationship between face-selective and nonface category-selective responses in VOTC,[43–46] investigated the temporal dynamics of face-selective responses,[47,48] explored face-selectivity in specific VOTC regions (IOG,[49] fusiform gyrus,[50] and ventral ATL[51]), simultaneously recorded and functionally related face-selective intracranial and scalp event-related potentials (ERPs) (i.e., N200s and N170s[45]), showed the complementarity of ERPs and high-frequency broadband (HFB) activity in decoding face versus house responses,[52] or yet showed a correspondence between local iEEG and fMRI face-selective responses in posterior VOTC.[43,53,54]

The challenge of VOTC mapping with intracranial EEG recordings

Despite their interest, it is fair to say that human iEEG studies identifying face-selective cortical responses, or using face stimuli in general, have so far failed to provide a coherent map of the VOTC at a large spatial scale. Moreover, they have been largely unable to offer consistent and complementary information to fMRI studies regarding exact localization and spatial organization of face-selective responses in the VOTC. As a result, they have had little impact so far on neurofunctional models of face processing.[3,5] Let us provide three examples to support these claims.

First, larger face-selective responses are usually found in the right as compared with the left fusiform gyrus in neuroimaging[1,19,33,55] in line with brain lesion studies that have long showed a clear right hemispheric predominance of the posterior VOTC for individual face recognition (i.e., in causing prosopagnosia[8,56–58]). However, surprisingly, iEEG studies have been unable to show this right hemispheric predominance in terms of signal amplitude in the posterior VOTC, either with ERPs[39,45] or in HFB.[59]

Second, since the early work of Allison *et al.*[39] (Fig. 3A), very few iEEG studies have reported face-selective responses in the anterior VOTC.[51] This could be partly due to the dominant use of ECoG, which may be less sensitive to detect anterior VOTC face-selective responses located primarily in sulci. Perhaps for this reason, and despite good coverage of anterior VOTC regions in temporal epilepsy investigations (anterior temporal epilepsy is the most frequently investigated epilepsy

in epilepsy surgery), most iEEG studies focus on posterior VOTC[43,44,50] activity. This is unfortunate since the anterior VOTC lies precisely in the heart of the fMRI magnetic susceptibility artifact as shown earlier (Fig. 1). A recent iEEG case study showed that the anterior VOTC, in particular in between the middle fusiform gyrus and the temporal pole, may contain critical face-selective responses[25] (Fig. 1).

Third and more generally, apart from the local correspondence between iEEG and fMRI face-selective responses in the posterior VOTC,[43,53] the large-scale clustered organization of face-selective activity depicted in fMRI studies is difficult to reconcile with the mosaic distribution of face-selective responses as found with iEEG (i.e., contrast Figs. 1B and 3). Are these differences merely due to the comparison of individual maps in fMRI to group maps in iEEG, or to other trivial differences in data visualization such as comparing maps averaged across subjects in fMRI (e.g., Ref. 33) versus maps showing the superposition of all significant electrodes across subjects in iEEG (e.g., Ref. 39)? Is there truly a clustered organization of face-selective neural responses in the VOTC or are those clusters emerging in fMRI maps because they are based on a lower SNR measurement with a conservative statistical threshold? And, if clusters or peaks of activity can be found in iEEG across the whole VOTC, do they correspond to the typical locations found in fMRI (i.e., denser concentration of face-selective responses in the lateral section of the middle fusiform gyrus, FFA, or the lateral IOG, OFA)? The difficulty in addressing these issues with current sources of evidence appears to be due to a number of factors.

First, there is undoubtedly an issue of spatial sampling, with iEEG recordings remaining relatively rare despite a growing interest in the scientific community, and the localization of electrodes being determined by clinical purposes. Unlike the seminal studies cited above,[9,10,39] most studies rely on relatively small samples (e.g., $N < 10$) of individual brains and often target specific regions[48–51,59] rather than the whole VOTC.

Second, most studies with a large sample of participants (e.g., >10) combine data at the group level by normalizing individual brains into a common space (MNI or Talairach space), known to blur the individuality of functional organization (e.g., Refs. 46, 50, and 60; Fig. 3B and C). Few studies take advantage of the high anatomical resolution of iEEG studies to locate electrodes in the individual anatomy in order to group electrodes across patients (e.g., Refs. 42–44 and 47). The seminal studies of Allison and colleagues[39–41] used a combination of these approaches. Electrode locations were determined and plotted in Talairach space for the antero-posterior (y) axis and according to their gyri and sulci position as determined in individual anatomy for the mediolateral (x) and inferosuperior (y) axes.

The importance of the individual anatomy has been illustrated by fMRI studies showing that, despite the anatomical interindividual variability, some anatomical landmarks in the visual cortex can predict the location of functional visual areas (e.g., the mid-fusiform sulcus predicts the location of the face-selective activations in the fusiform gyrus;[61] the posterior transverse collateral sulcus predicts the VO1/hV4 boundary;[62] and the posterior inferior temporal sulcus predicts the location of hMT+[63]). However, grouping electrodes according to their location in individual anatomical structures across patients and across a large cortical surface (e.g., the whole VOTC) involves solving many issues such as the interindividual variability of anatomical structures, the variable ways to anatomically subdivide the brain, and the scale at which to perform this subdivision.

A third factor relates to the intracranial recording method (Fig. 2). On the one hand, ECoG allows covering an extended cortical territory but electrodes are restricted (and therefore most sensitive) to the gyral surface, further away from (and therefore less sensitive to) sulcal activity. On the other hand, SEEG covers less space on the external and gyral cortical surface but offers the opportunity to penetrate sulci and explore medial structures. In addition, ECoG and SEEG recording units have different positions relative to the cortex, which can affect the type and origin of electrophysiological signal measured.[64] Specifically, ECoG electrodes are always over the most superficial layer of the cortex, while SEEG electrodes are mostly located within the cortical sheet or at the surface of the gray/white boundary.

Fourth, the iEEG electrophysiological signal is multidimensional, varying both in time and frequency. With respect to the temporal dimension, face-selectivity can be complex to apprehend and describe, as it varies across time both within and across VOTC subregions. For instance, as

indicated above, face-selective responses are measured before 200 ms in the posterior VOTC,[39,43,47,48] and after 300 ms in anterior VOTC.[39,51] With respect to the frequency dimension, iEEG studies report increased neural activity to pictures of faces compared with nonface objects mainly in two distinct types of neural activity: (1) low-frequency responses time-locked and phase-locked to the stimulus (i.e., ERPs, such as the N200/N170 component)[9,39,45–47] and (2) high-frequency electrophysiological activity (HFB) which is often nonphase locked to the stimulus.[43,44,46,49,51,59,60,65,66] Both high- and low-frequency face-selective responses have been mainly measured in the posterior VOTC (Fig. 3). However, iEEG studies comparing these types of responses reported distinct, although overlapping spatial maps of face-selectivity[46,60] (Fig. 3B and C) and further discrepancies are found when activities in an "intermediate" frequency band are considered[46] (alpha/beta activity, from 8 to 24 Hz; see Fig. 3B). Altogether, these observations have led some authors to suggest that face-selective responses occurring in different frequency bands reflect separate, perhaps complementary processes of the face processing system,[52,60] in line with observations indicating that different frequencies reflect partly independent neural processes.[67–71] Yet, discrepancies between the spatial distributions of face-selectivity across frequency bands may also be partly due to methodological parameters. For instance, face-selective ERPs and HFB signals have sometimes been measured using different time-windows (e.g., amplitude of N200 component in ERPs versus area under the curve in a 200–600 ms time-window for HFB[60]), showing that more objective criteria for defining and quantifying face-selective responses would be welcome.

Finally, the control stimuli/categories used to define face-selective responses vary enormously across studies. In many studies, responses to faces are compared with responses to one or a few object categories without ensuring that the discrimination response is not related to confounding stimulus properties, such as differences in amplitude spectrum.[72] Most studies use 1–4 control categories, which may be too few to ensure that the face-selective response (or absence of) is generalizable.[43,45,49,51] In addition, the nonface stimuli compared with pictures of faces may be meaningless,[42] presented against a different background compared wtih faces (e.g., uniform versus cluttered background, segmented versus embedded in a visual scene;[39] difference in background luminance[48]), or have other systematic low-level differences compared with face images (e.g., face versus houses in Ref. 45). As an example of potential stimulus confound, in the studies of Allison and colleagues,[9,39] the control stimuli (cars especially) did not elicit any N200 deflection at many electrode sites, which therefore appeared as producing face-exclusive responses at the population level. However, the exact same stimuli did not evoke N170 responses on the scalp either,[38] despite the fact that the scalp N170 is typically evoked by pictures of nonface objects (in particular for cars).[73,74]

In the next section, we describe a research program that addresses these challenges specifically, in order to build an extensive cartography of the human VOTC with iEEG recordings.

A research program combining FPVS and individual anatomical localization in SEEG

Two approaches are combined in this research program. First, iEEG recordings are performed during FPVS. Second, SEEG electrodes implanted across large groups of patients are localized in individual brains using an anatomical framework across the whole VOTC. For the sake of simplicity, we will refer to this combination as the FPVS-SEEG approach.

Fast periodic visual stimulation to define face-selectivity

Face-selective neural responses are measured by presenting natural images of objects at a fast rate of six images by second (Fig. 4A, movie 1; from Ref. 75). The stimulation runs continuously for about 1 min, and the subject does not explicitly categorize the images, simply maintaining fixation on a central cross and detecting its 6–8 times random changes of color. A Fourier transform of the whole minute of (S)EEG recording reveals peaks of neural activity in the amplitude spectrum, exactly at the stimulation frequency F, that is, 6 Hz, and its harmonics (2F = 12 Hz, etc.; Fig. 4B). With this paradigm, such frequency-tagged responses are readily (i.e., with minimal computational steps) identified both on the scalp[75–77] and inside the human brain.[78]

The property of the human brain to synchronize its activity to a flickering light is a fairly old observation in scalp EEG[79] (see Ref. 80 for an early

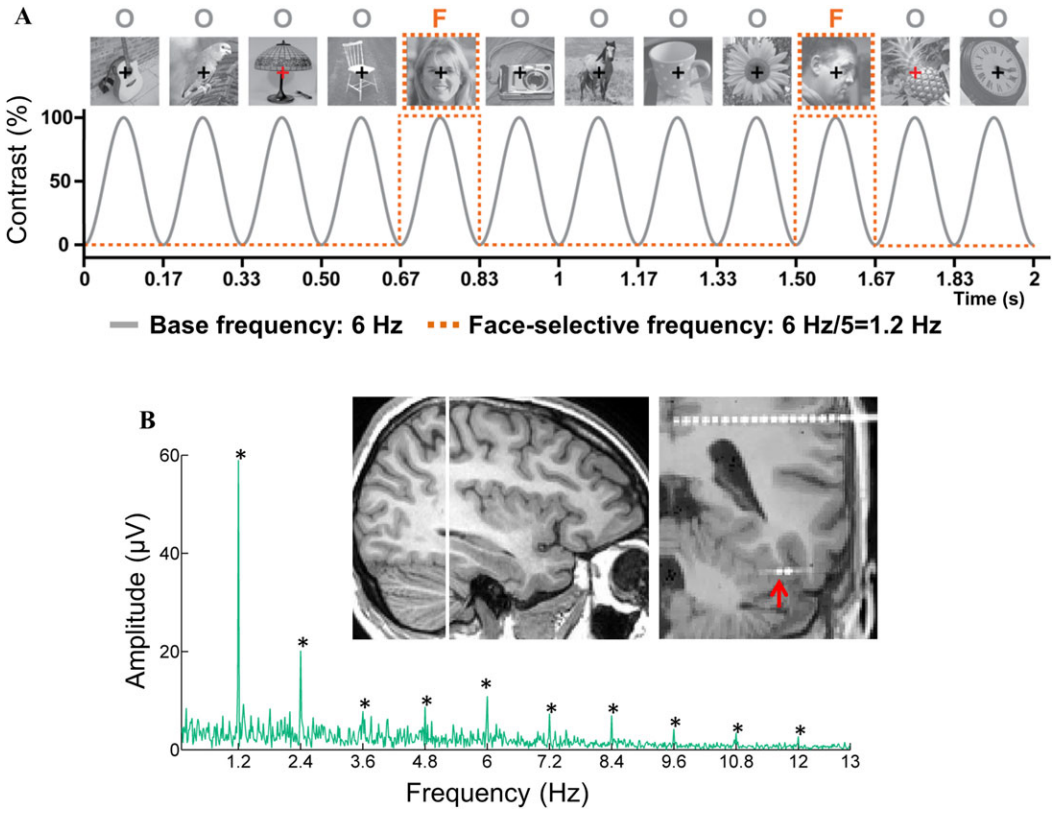

Figure 4. Experimental FPVS paradigm and example of a face-selective response recorded on a single electrode contact in the fusiform gyrus (from Ref. 78). (A) The FPVS paradigm. Images of objects are presented by sinusoidal contrast modulation at a rate of six stimuli per second (6 Hz), with a different face image presented every five stimuli (i.e., appearing at the frequency of 6 Hz/5 = 1.2 Hz). (B) Objective and high SNR intracerebral responses in the VOTC of a single individual brain. IEEG frequency-domain responses recorded at an individual recording contact (raw FFT amplitude) located in the right latFG are shown. The location of the recording contact (indicated by a red arrow) is shown using a postoperative CT coregistered to a preoperative MRI. Significant face-selective responses exactly at the face-selective frequency (1.2 Hz) and harmonics (up to 10.8 Hz) are observed. *Statistically significant responses ($Z > 3.1$, $P < 0.001$).

use of the approach in intracranial recordings). Regan[81] used a Fourier analyzer to show that EEG responses recorded in these conditions at various frequency rates could be expressed in the frequency domain as narrow peaks of activity exactly at the frequency of stimulation with extremely high SNR (see Refs. 82 and 83 for reviews). Here, the original and critical aspect of the approach is to present *variable* complex stimuli at each stimulation cycle. Moreover, a second frequency of interest is generated by inserting pictures of faces—also widely variable and nonsegmented from their natural background (Fig. 4A)—every five stimuli. Hence, an EEG response at 6 Hz/5, that is, 1.2 Hz, reflects a selective (i.e., differential) response to faces, which translates as a 1.2 Hz peak of activity in the frequency spectrum, with corresponding harmonics (2.4 Hz, etc.; Fig. 4B). Crucially, a population of neurons responding identically to faces and nonface objects will be reflected in the common 6 Hz response, and not in the 1.2 Hz response. Hence, a response at 1.2 Hz and its harmonics (excluding 6 Hz) does not only reflect a face-evoked response, but also directly a *face-selective* response.[75,84]

This relatively simple approach has many strengths, making it a unique tool for understanding face categorization in the human brain, particularly with iEEG.

First, it is associated with an extremely *high SNR*, providing significant responses even on the scalp

within a few minutes of recording.[45,76,84] This high SNR is mainly due to the very high frequency resolution obtained by analyzing a single long sequence of stimulation (e.g., 0.016 Hz, i.e., 1/60 s). Thanks to this high frequency resolution, while the SEEG noise is distributed across many frequency bins, the signal of interest projects to a single tiny bin (i.e., of 0.016 Hz) associated with very little noise.[82] This offers considerable advantages over other stimulation approaches using slow rate transient nonperiodic events. In particular for iEEG, this approach can be highly resistant to epileptic spikes, which are very large deflections (several hundreds of μV), sometimes occurring repeatedly throughout the recordings.[85] These spikes increase the general noise level, and in the case of a transient stimulation paradigm can lead to the rejection of a large number of trials containing epileptic spikes, therefore resulting in a reduced amount of reliable data or in the increase in the experiment duration. In a group study detailed below,[78] it can be shown that the results are virtually identical with or without an artifact rejection step (i.e., epileptic spikes rejection). Obviously, this high SNR affords short recording sessions, which is particularly important in iEEG studies with epileptic patients in a clinical setting.

Second, this paradigm provides a *valid* measure of face categorization. That is, instead of measuring the response to one type of stimulus and another type of stimulus separately, it aims at measuring the *process* of face categorization, which involves direct *discrimination* (between faces and nonface objects), and *generalization* of this discrimination across widely variable images. Indeed, a significant face-selective response in this paradigm emerges only if there is a response at most face stimuli, thus ensuring generalization across a widely variable set of images. For instance, a population of neurons responding only to full front faces would respond only once in the short example of 2 s illustrated in Figure 4A, and thus not contribute to a 1.2 Hz response. Moreover, faces need to elicit a differential brain response to the various object categories presented in the sequence, and not just one type of object. For instance, a population of neurons responding selectively to living things will fire four times over 2 s as shown in the example provided in Figure 2, breaking the periodicity. Hence, the paradigm does not merely measure an average response to faces as compared with an average response across the nonface object categories. Thanks to the same periodicity constraints, the face-selective response is not contaminated by low-level visual cues that would have to be systematically, that is, periodically, associated with faces and never or rarely associated with nonfaces to generate a low-level 1.2 Hz response. Therefore, the approach provides control by variability rather than by elimination/homogenization. This has been shown in scalp EEG studies, showing that phase-scrambling of the stimuli eliminates face-selective occipito-temporal responses.[75] Of course, this is only true if a wide variety of images belonging to different categories are used (see fig. 1 in Rossion *et al.*[75] and stimuli available here: http://face-categorization-lab.webnode.com/resources/natural-face-stimuli/).

Finally, the response of interest can be identified in the frequency domain objectively, that is, exactly at the frequency of stimulation determined a priori by the experimenter.[82] Quantification is performed by summing the harmonics related to the frequency of interest, corrected for noise level by subtracting the activity in the neighboring frequency bins.[84] This leads to a relatively straightforward and replicable data analysis procedure that provides a common systematic metric to estimate face-selectivity across brain regions, studies, and methodologies (i.e., ECoG and SEEG). Note that with this frequency-domain representation, face-selectivity here is not restricted to a *larger* response to faces than objects but to a systematically *distinct* neural response to faces. Indeed, a population of neurons responding significantly *less* to faces than to all other object categories, hence providing a strong signal to the brain that a face is present in the visual environment, will lead to a 1.2 Hz face-selective response in this paradigm. Moreover, a population of neurons responding with the same magnitude overall to faces and objects, but systematically earlier or later, or with a different shape of response, to faces than all other images should also lead to a 1.2 Hz response in this paradigm. Hence, the frequency-domain representation captures a full selective response to faces, making no assumption as to the form and properties of the face-selective response.

SEEG and electrode location in the individual anatomy

The problem of spatial localization of responses is addressed by labeling each individual recording

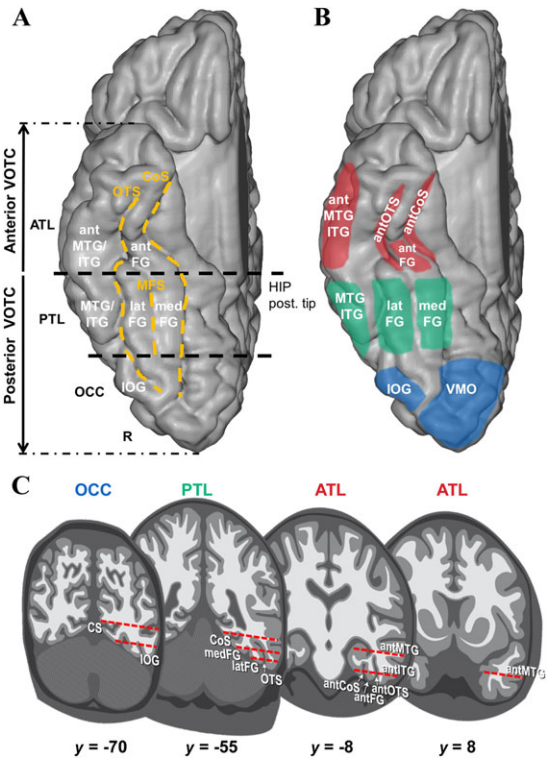

Figure 5. Individual anatomical localization of SEEG electrodes. (A) Example of a VOTC parcellation used in Jonas *et al.*[78] Major VOTC sulci served as mediolateral landmarks (CoS and OTS), and coronal reference planes containing given landmarks served as posteroanterior landmarks. A coronal plane including the anterior tip of the parieto-occipital sulcus served as the border of the occipital and temporal lobes. A coronal plane including the posterior tip of the hippocampus served as the border between PTL and ATL, and between posterior and anterior VOTC. (B) Anatomical regions that were found face selective in Jonas *et al.*[78] are highlighted in color. (C) Schematic representation of the typical trajectories of depth electrodes (SEEG) implanted in the right VOTC. Typical trajectories of electrodes are represented as arrays of red rectangles on schematic coronal slices (with Talairach *y* coordinates indicated below slices). ATL, anterior temporal lobe; PTL, posterior temporal lobe; OCC, occipital lobe; CoS, collateral sulcus; CS, calcarine sulcus; FG, fusiform gyrus; HIP, hippocampus; IOG, inferior occipital gyrus; ITG, inferior temporal gyrus; MFS, mid-fusiform sulcus; MTG, middle temporal gyrus; OTS, occipitotemporal sulcus; VMO, ventromedial occipital cortex; a, anterior; lat, lateral; med, medial.

site (contact) in the individual brain anatomy, as in previous studies.[42–44,47] The whole VOTC is subdivided in a relatively fine grid pattern,[86] with each anatomical subdivision defined by medio-lateral and posteroanterior landmarks (Fig. 5A). Using a fine anatomical subdivision allows to apprehend anatomy at multiple spatial scales by grouping anatomical partitions that show similar response properties. Importantly, the anatomical subdivision should be as much as possible independent from the interindividual variability in brain anatomy and in expertise of the experimenters in analyzing a brain MRI. Therefore, major anatomical landmarks that can be easily identified in each individual brain and by each experimenter are used. Note that an automated anatomical parcellation procedure[87] (e.g., see Refs. 44, 47, and 88) is not used, for two reasons: first, the anatomical scale at which current automatic parcellation is performed is too coarse, particularly in the anteroposterior axis; second, even when performing automated parcellation, careful verification of the parcellation is needed to avoid labeling errors.

A comprehensive definition of face-selective activity in the human VOTC

Using this approach, a first definition and quantification of face-selective responses across the whole VOTC was reported in a large group of participants ($N = 28$) implanted with SEEG.[78] Patients were selected on the basis of the presence of at least one implanted electrode in the VOTC (Fig. 5C). In the context of the present review, we summarize and illustrate the methodology and the main observations of that study, before discussing its implications in the context of a general research program.

A wide distribution of responses

Despite a brief recording time (2–4 sequences of 70 s) for each individual, face-selective responses are found in the VOTC exactly at 1.2 Hz and harmonics (see Fig. 4B for an example of recording on a face-selective contact). From a total of 1678 individual recording contacts in the gray matter of the VOTC across 28 individual brains, there were a large number of face-selective contacts (555 contacts, or 33%). These contacts were widely distributed over the VOTC, from the occipital lobe (OCC) to the ATL (see Figs. 5B, 6A, and B in the individual anatomy and Fig. 7A in the MNI space). Thus, the spatial analysis reveals a wide distribution of face-selective responses across the VOTC, in line with previous iEEG studies.[39,46] In the OCC, face-selective responses were recorded in the IOG and in a large portion of the ventral and medial occipital cortex (Figs. 5B and 7A, middle panel). In

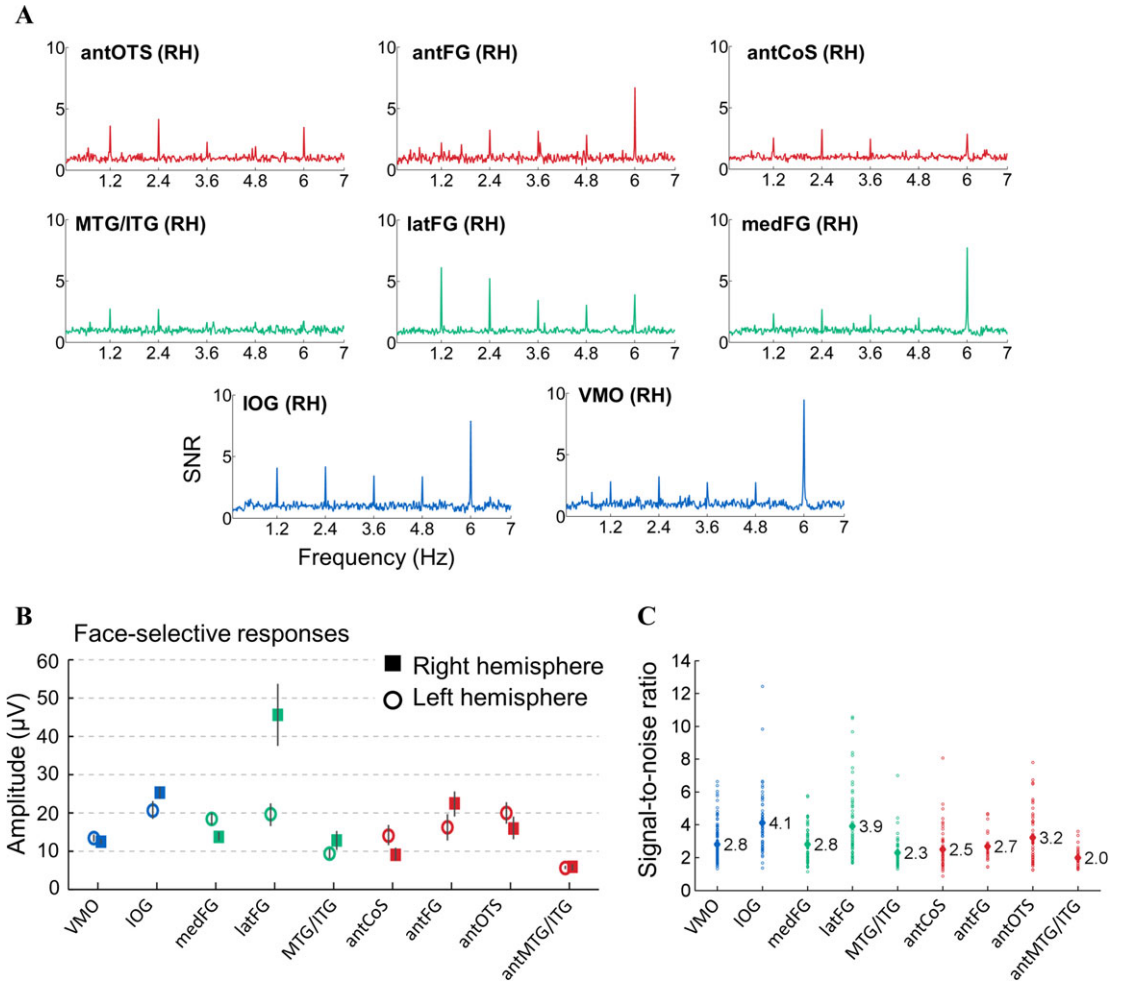

Figure 6. Face-selective responses grouped according to the individual anatomy (from Ref. 78). (A) IEEG frequency spectra in selected regions of the right VOTC averaged across all face-selective contacts located in the same region. (B) Quantification of the face-selective response amplitude in the individual anatomy. Face-selective contacts were grouped by anatomical region-of-interest across all participants and the face-selective amplitude was averaged across contacts to obtain the mean response amplitude for each region separately for the left and right hemisphere (note that this result was independent from the number of harmonics taken into account). The schematic locations of each region are shown in Figure 5B. (C) Signal-to-noise ratio (SNR) of face-selective responses in each anatomical region. Open circles display SNR for individual recording contacts and filled diamonds show the average SNR across contacts (see exact value on the right of each diamond). SNR was quantified over the first four harmonics of the face-selective frequency as follows: for each contact (1) the FFT spectrum was cut into segments centered at the face frequency (1.2 Hz) and the first four harmonics (1.2 to 4.8 Hz) and surrounded by 25 neighboring bins on each side; (2) the amplitude values of the four FFT segments were summed; and (3) the summed FFT spectrum was transformed into SNR. SNRs were computed as the ratio of the amplitude at the face frequency bin to the mean amplitude of 48 surrounding bins (25 bins on each side, excluding the two bins directly adjacent to the bin of interest).

the posterior temporal lobe, face-selective responses were recorded in the posterior fusiform gyrus, in its medial (medFG) and lateral (latFG) sections. In the ATL, face-selective responses were mainly recorded in the ventral ATL in three distinct regions: (1) along the anterior segment of the collateral sulcus or rhinal sulcus (antCoS), (2) along the anterior segment of the occipitotemporal sulcus (antOTS, located laterally to the CoS), and (3) in the anterior fusiform gyrus (antFG, located between the antCoS and antOTS, anteriorly to the posterior tip of the hippocampus). In all these regions, the mean SNR

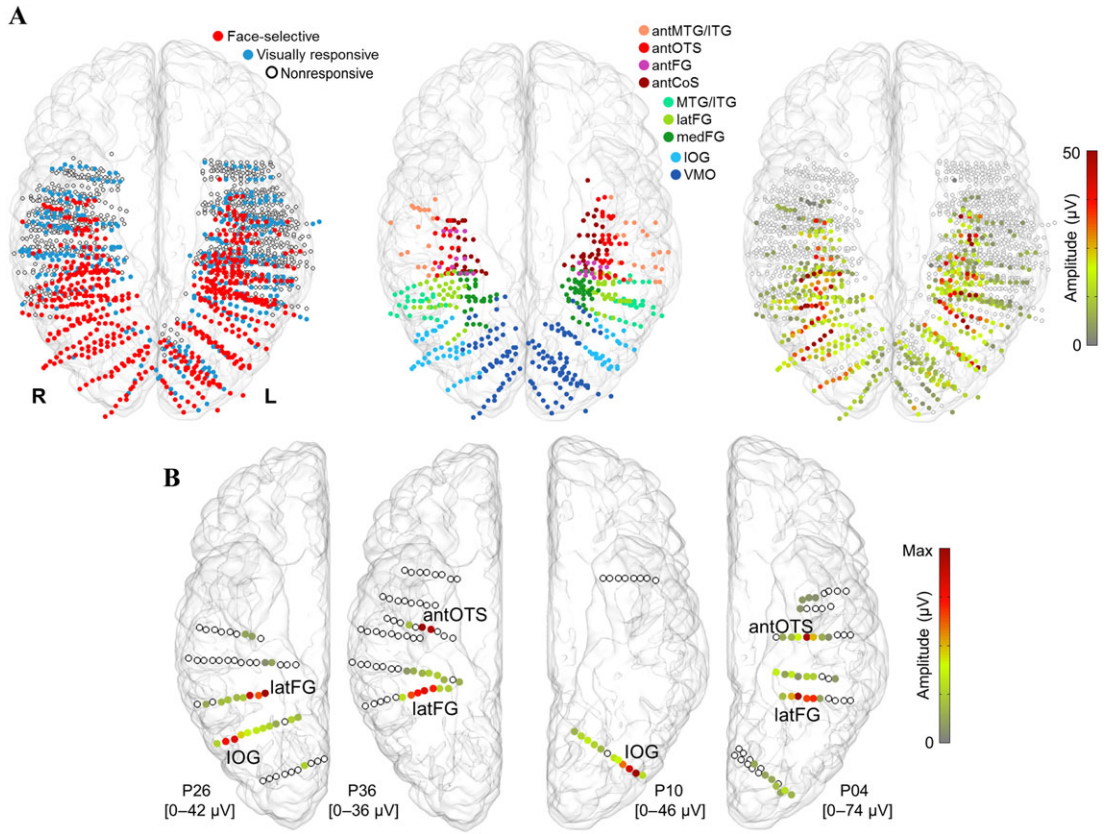

Figure 7. Spatial distribution of face-selective response across participants and in individual brains (from Ref. 78). (A) Maps of recording contacts across the group of 28 participants displayed in the MNI space using a transparent reconstructed cortical surface of the Colin27 brain. Each circle represents a single contact. Left panel: spatial distribution of face-selective, visually responsive (responsive to the base frequency but not face-selective) and nonresponsive contacts. Middle panel: face-selective contacts are colored according to their anatomical label in the individual anatomy. Note that the location of antFG contacts is blurred in the MNI space, mainly because of their proximity with the latFG, antOTS, and antCoS. Right panel: face-selective contacts are colored according to their face-selective response amplitude (white-filled circles correspond to contacts that are not face selective). (B) Examples of four individual participant hemispheres. Face-selective contacts are colored according to their face-selective response amplitude. Contacts are displayed in the MNI space, but anatomical labels of the face-selective clusters are derived from the individual native anatomy.

across contacts obtained with FPVS is very high, that is, between 2 in the antMTG and 4 in the IOG (i.e., 100–300% of signal increase; Fig. 6C).

Regional peaks of face-selectivity

To quantify face-selectivity, amplitudes are summed over harmonics for each face-selective contact,[84] and amplitude is averaged across contacts for each region. A key observation is that, across all regions, the largest face-selective response is, by far, recorded in the middle section of the right latFG (Fig. 6B). This observation therefore validates, with a direct measure of neural activity, the predominant face-selective activation in the right middle latFG found in human neuroimaging for more than two decades (i.e., the "FFA"[19]). Moreover, this finding illustrates the importance of localizing contacts in the individual anatomy. Although grouping contacts and their corresponding amplitude values in common space (MNI) showed that face-selective responses were widely distributed and more frequent in the posterior VOTC, the specific predominance of the right latFG is not readily apparent with this display (Fig. 7A, right panel). In contrast, this dominance is clear when grouping contacts according to the individual anatomy (Fig. 6B).

Distributed versus clustered spatial organization of face-selectivity

Importantly, the dominance of the face-selective response in the right middle latFG emerges by considering a relatively large group of patients and a division in relatively large anatomical regions (Fig. 5A). Hence, at a group level, the spatial resolution is relatively coarse and is inherently limited by the anatomical definition of the regions. However, at the individual level, while the sampling is limited in coverage, the spatial resolution is much higher (i.e., an intercontact center-to-center spacing is 3.5 mm with these SEEG electrodes), which affords exploring the spatial organization of face-selective responses at a finer scale within each face-selective region. Quantifying the spatial variation of face-selective response amplitude across the length of each electrode reveals that the second and third largest face-selective contacts are often contiguous to the highest face-selective contact along the same electrode (Fig. 7B), indicating a local clustering of strong face-selectivity. This observation shows that there is not a single definition of spatial resolution in iEEG. Rather, spatial resolution depends on the grouping across individuals and the type of analysis and inference that one aims to make.

Overall, this approach to iEEG and its findings reconcile—at least partly—two main views of the large-scale functional organization of face selectivity in the VOTC: on the one hand, the clustered organization identified by fMRI studies in individual participants[19,21,33,55] (Fig. 1B) and on the other hand, the widely distributed face-selective responses found with iEEG studies[39,46,60] (Fig. 3). Although face-selective populations of neurons are present across the whole VOTC, they are more densely distributed in specific regions such as the right latFG.

A set of three face-selective regions in the anterior VOTC

Critically for the issue raised at the beginning of the review, there is a wide distribution of face-selective responses in the anterior section of the VOTC in specific and reproducible anatomical locations across individual participants: in the antCoS, antOTS, and antFG (Figs. 5B and 6A, for an example of face-selective response in the anterior VOTC in a single participant, see Fig. 8). Such wide distribution in the anterior VOTC goes well beyond what was found previously in fMRI. Because of the susceptibility artifact around the ear canal, fMRI studies reported small and inconsistent face-selective activation in the anterior VOTC and, if it were the case, only in the antCoS, very anteriorly.[22,23,29–33] Moreover, as also mentioned above, few iEEG studies reported face-selective responses in the anterior VOTC. Three key aspects may account for the observation of face-selective responses in the ventral ATL with the FPVS-EEG approach:[78] (1) the recording within cortical sulci in SEEG, in which a substantial proportion of ventral ATL face-selective responses were found (antCoS and antOTS), (2) the particularly high SNR of the technique, and (3) the objective criterion to identify even small neural peaks above noise level in the frequency domain.

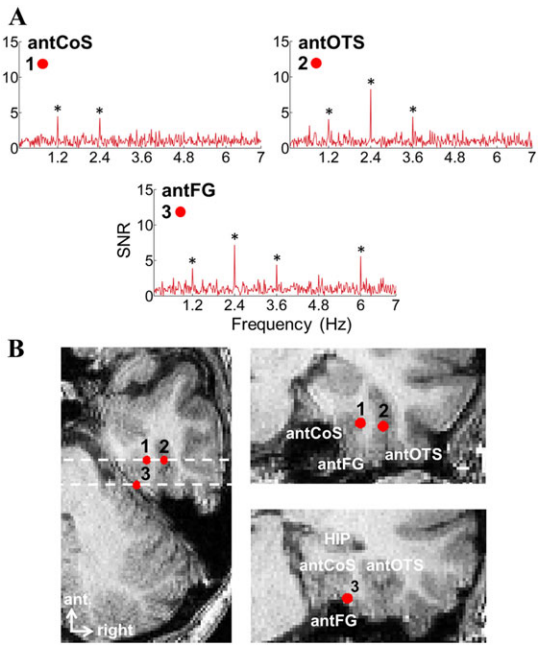

Figure 8. Example of face-selective responses in three distinct anatomical regions of the ventral ATL (from Ref. 78). (A) Face-selective responses recorded from the right antCoS, antOTS, and antFG in a single brain. Note that in the examples shown here for the antCoS and antOTS, no general visual responses were recorded at 6 Hz and harmonics ("face-exclusive" responses). *Statistically significant responses ($Z > 3.1$, $P < 0.001$). (B) Anatomical locations of corresponding recording contacts on MRI slices. Contacts are shown as red dots on axial (left panel) and coronal (right panel) slices. Electrode contacts 1, 2, and 3 are, respectively, located in the antCoS, antOTS, and antFG. The antFG is located between the antCoS and antOTS, at a level where the hippocampus (HIP) is visible on a coronal slice.

A particularly interesting face-selective region is the antFG, located between the antCoS and antOTS,

just anterior to the middle FG (Talairach *y* axis around –30). As illustrated in Figure 1, this region is primarily affected by the fMRI signal dropout and, as a result, has been identified as being face selective only in a handful of fMRI studies.[31–33] SEEG face-selective responses in the right antFG had been previously identified with a conventional approach in a single patient (Fig. 1C), who showed transient prosopagnosia when electrically stimulated in this region.[25] The pattern of responses recorded in the right antFG differs from responses recorded in adjacent regions, such as the right latFG (higher face-selective response) located posteriorly, the antCoS and antOTS (i.e., smaller face-selective response and smaller general visual response at 6 Hz). This suggests that the specific anatomical region of the right antFG is functionally different from adjacent regions (latFG, antCoS, and antOTS). This anatomofunctional specificity of the right antFG has been highlighted thanks to the use of an individual anatomy approach and would have been blurred using a brain normalization approach (Fig. 7A).

Face-exclusive responses at the population level

The careful reader will not have missed two example SEEG spectra in Figure 8 in the antCoS and antOTS showing *exclusive* responses to faces, that is, significant face-selective responses without any 6 Hz general visual response. Such face-exclusive responses are found in increasing proportions from posterior to anterior regions, being maximal in the right ATL,[78] and are also observed in a control experiment with a much lower base rate frequency (1.5 Hz) to rule out a simple low-pass filter effect. Importantly, such EEG spectra have not been found on the human scalp,[75] ruling out an inadequacy of nonface stimuli to evoke population responses as discussed above for the N200/N170.[9,38,39]

Since intracerebral contacts pool the activity of hundreds of thousands of neurons, this finding reveals the presence of exclusive responses to faces at a macroscopic level of cortical organization (i.e., cell population level) for the first time in humans. These responses, which were in highest proportion in the anterior section of the VOTC, may reflect the processing of faces independently from the context (i.e., nonface categories), which could be particularly useful for certain processes that are known to be specific to faces (e.g., encoding and retrieval of information specific to an individual face, holistic processing of individual exemplars, sex, age, expression, social judgments, etc.). An alternative account for these neural responses frequency-locked exclusively to the face stimuli is that they reflect a general response to the only category that is presented periodically in the stimulation sequence, that is, faces in the paradigm[78] (Fig. 4). Indeed, scalp EEG experiments have shown that selective responses to other categories such as houses and limbs inserted periodically in such object sequences can also lead to significant category-selective responses.[43] However, such responses are of much smaller amplitude and are associated with a distinct spatial topography than face-selective responses.[43] Moreover, the face-selective response observed on the scalp is identical whether faces appear periodically or not.[89] Future iEEG studies could build upon such paradigms to assess the exclusivity of the responses to faces particularly in the right VATL (ventral anterior temporal lobe).

Summary and challenges ahead in iEEG mapping of face and visual categorization

Summary and implications for models of face-selectivity

In this review, we presented an approach that overcomes many of the difficulties of iEEG studies to map category-selective responses in the human brain, using faces as a model and recording across the whole VOTC. Thanks to the combination of FPVS, which provides highly sensitive, objective, and quantifiable responses in the frequency domain, with SEEG allowing to record both from gyri and inside sulci of nonnormalized individual brains, we describe a first extensive cartography of face-selectivity in the human VOTC. Besides supporting the wide distribution of face-selective responses across the VOTC, this approach reveals (1) a strong right lateralization of the middle portion of the lateral fusiform gyrus in iEEG; (2) the dominance of this region—corresponding to the so-called FFA in neuroimaging—over all other VOTC regions in relation to the magnitude of the face-selective response; (3) clear face-selective responses in the anterior VOTC, mainly in sulci (antCoS and antOTS); and (4) the presence of exclusive responses to faces in a large proportion of electrode contacts in anterior VOTC regions.

These observations should constrain neurofunctional reviews and models of face processing, which generally fail to incorporate hemispheric specialization, as well as several face-selective/exclusive regions in the VATL[3,5] between the midfusiform gyrus ("FFA") and face-selective clusters in the temporal pole.[4] They also raise novel questions of interest such as whether face-selective or face-exclusive responses functionally differ with respect to sensitivity to other face categorizations (e.g., face identity), and also whether face-selective responses observed outside of the dominant clustered regions are associated with different functional processes.

Importantly, the FPVS-SEEG approach presented here can be used in future studies to measure finer grained face categorization processes, such as individual face discrimination,[90] or the discrimination of various facial expressions,[91] as demonstrated with scalp EEG. Selective responses to other visual categories such as letters and words could also be investigated with the same approach.[92]

Validity of the epileptic brain model, limitations, and the need for large samples

Since iEEG recordings are performed in patients with drug-resistant epilepsy, the validity of this approach to provide a model of the normal functional organization of face-selectivity can be questioned. In this respect, there are a number of methodological issues that need to be considered (e.g., exclude recordings in lesions, artifact rejection if necessary, and selection of patients based on minimal neuropsychological criteria). However, beyond these issues, the neural organization of these patients with long-term drug-resistant epilepsy appears to offer a highly valid model of the typical organization of the human brain. For instance, iEEG and scalp EEG recordings in typical adults show a similar face-selective ERP component in occipito-temporal regions (i.e., N170/N200, iEEG;[37,39,45,47,49] scalp EEG[38,93,94]). Moreover, patients explored with iEEG have so far showed typical fMRI face-selective activations.[17,25,37,43,53] The largest face-selective response in regions identified with fMRI in typical brains (e.g., the right latFG) also provides strong support for the validity of iEEG recordings in the epileptic brain.

One of the limitations of the FPVS-SEEG approach for a large-scale mapping of brain functions is dictated by the sparse-sampling problem, that is, the variable and limited electrode coverage in any given individual participant.[44,88] To deal with such constrain, a large sample of participants is needed to obtain a reliable and global view of the VOTC. For example, while the right IOG is rarely explored in iEEG, this region showed one of the highest face-selective responses in our study,[78] consistent with fMRI observations in typical brains. However, despite a trend for right hemispheric lateralization, there was no significant effect in this region, unlike the clear right lateralization observed in fMRI[33] and the dominant role of the right over the left IOG in causing permanent[95] or transient[37,96–98] individual face recognition impairments. This suggests either a genuine difference between signals collected with different modalities and paradigms or a limitation of the current iEEG approach to capture this lateralization factor in this region. One limitation is undoubtedly related to the large variability between individual patients and recording contacts in terms of response amplitude so that a large sample size is necessary to ensure reproducibility of the findings. In addition, providing that a sufficiently large number of recording contacts across patients are localized in the gray matter of different regions, the *proportion* of significant electrode contacts in a given anatomically defined VOTC region could also serve as complementary information to the average response amplitude.

A large sample of participants also provide the opportunity to refine and fine-tune anatomical subdivisions, as each subdivision will contain a sufficient number of recording contacts to measure reproducible responses. For instance, in the described study,[78] the large sample of participants allowed to split the anterior fusiform gyrus from adjacent sulci. Moreover, thanks to large samples, future iEEG studies might be able to use VOTC cytoarchitectonic divisions that might more closely match functional organization of the cortex than divisions on the basis of macroanatomic landmarks.[60,99,100]

What are the other limitations of the approach? Currently, there is a lack of information about the frequency ranges of stimulation that are associated with the most sensitive and specific responses. The paradigm presented in Figure 4 and used in the described study[78] relies on a 6 Hz stimulation rate, which provides similar responses on the scalp as 12–12.5 Hz rates.[84,89] However, higher

frequency rates may be associated with lower face-selective responses, owing to the limited presentation and duration of (masked) faces. Further validating work is certainly required with scalp EEG to define frequency-tuning functions for various face categorizations.[101]

Timing and high-frequency activity

Besides its high spatial resolution, iEEG also provides a high temporal resolution, which has not been exploited so far in the research program presented here. Several iEEG studies explored the timing of face-selectivity in specific VOTC regions (e.g., the fusiform gyrus[43,48]) but few studies recorded in large samples to understand the temporal dynamics of face-selectivity across the whole VOTC.[39] Future iEEG studies will be needed to understand the timing of face-selectivity in the anterior VOTC. In this respect, even though the quantification and detection of significant responses is performed in the frequency domain to reduce complexity, the FPVS approach can also be used to address questions about the precise timing of neural events. This can be done either by using phase information[102] or by simply averaging epochs of EEG segmented around the events of interest, as performed in the traditional ERP approach but after filtering out the carrier frequency (e.g., 6 Hz[75,76]). With this approach, EEG recorded on the scalp with FPVS leads to complex face-selective responses at multiple time windows between 100 and 600 ms, which are associated with distinct scalp topographies.[75,76,84] Applying the FPVS time-domain analysis to iEEG recordings should help isolating the specific generators of each of these face-selective components recorded on the scalp, and recover precious information to understand the time-course of face categorization processes in the human brain.

Finally, one aspect not addressed yet with FPVS-EEG as presented here is the distinction between low (e.g., ERPs) and high (e.g., HFB) iEEG frequencies.[52,60,69] As explained above, typical iEEG studies in this field tend to concentrate on one or the other, and when both types of activities are analyzed, they have been difficult to reconcile, probably in part due to different analysis parameters[50,60] (but see Ref. 52 for evidence of complementary information to discriminate faces from houses provided by ERPs and HFB). With the approach presented here, the key principle is to frequency-tag the stimulus, that is, project brain activity to a specific frequency, known in advance, and measure a response of interest only at that known frequency. Scalp studies indicate that this approach is very efficient at capturing all of the responses of interest: even if it varies in shape and time, the specific response to faces is periodically locked to the onset of faces, so that all of it is captured in the compact frequency-domain representation. Moreover, response properties of high-frequency activity can also be measured with this approach, by computing the amplitude envelope of the high-frequency signal across time and by performing Fourier analyses.[103] This may offer a potentially powerful approach not only to identify high-frequency activity tagged to the stimuli of interest—here faces inserted among objects—but also to objectively relate or dissociate low- and high-frequency activities related to face categorization or other visual function.

Electrical stimulation to determine critical face-selective regions

iEEG offers the opportunity to electrically stimulate specific face-selective regions in the VOTC, in order to evaluate their causal role in face categorization. Early ECoG studies of Allison and colleagues[9] reported a temporary inability to name photographs of famous faces following electrical stimulation in face-selective (N200) VOTC sites. However, the ability to provide semantic information about the face and the dominance of effects in the left as compared with the right VOTC rather pointed to naming deficits.[104,105] Puce *et al.*[41] described facial hallucinations (isolated eyes, single or multiple faces), without looking at faces, following stimulation of distributed face-selective sites along the posteroanterior axis of the VOTC. More recent ECoG studies have focused on the latFG, reporting facial perceptual distortions in the right but not in the left hemisphere,[59,106] or deficits in face categorization.[107,108]

In SEEG, the spatial coverage of electrodes in the VOTC is more limited in a single patient and the effects of stimulation on face perception have been described less frequently. However, electrical stimulation can be applied directly in the gray matter, allowing for more focal stimulation at lower amplitudes, potentially leading to an increase in specificity of the effect. An early study[109] reported a distortion of faces presented in front of the patient,

following stimulation in the right ventrolateral prefrontal cortex. More recently, Jonas *et al.*[37] reported a case of transient prosopagnosia, that is, a patient who had normal individual face recognition abilities outside of stimulation but suddenly failed to recognize pictures of famous faces following intracerebral stimulation. The site of interest in the right IOG was face selective as determined both with iEEG and fMRI recordings, and the patient was still able to recognize objects during stimulation of the same site. A second SEEG recording in the same area of the same patient led to an impairment in discriminating simultaneously presented pictures of unfamiliar individual faces,[96] ruling out a naming impairment. Electrical stimulation of the right antFG, in the heart of the fMRI susceptibility artifact, also caused prosopagnosia in another patient[25] (Fig. 1C).

In general, iEEG stimulation studies interfering with face perception showed that these effects are confined to face-selective electrodes, and that the amplitude of iEEG responses to faces—which must be related to the density of neuronal populations responding to faces—is positively correlated with the amount of facial perception disturbance[59,108] or face identity disturbance (Ref. 96 with an FPVS approach). Collectively, these observations show that these regions play a critical role in face perception, although it is difficult to relate specific regions to the disturbance of specific face processing subfunctions at this stage. From a practical standpoint, they indicate that iEEG studies should target (i.e., electrically stimulate) regions showing the highest face-selective or face-identity sensitive responses in order to test for their causal role. In this context, and in keeping with the general theme of the review, FPVS-SEEG, with short experiments (i.e., few minutes), straightforward first pass signal analyses (Fourier transform without artifact rejection) and high SNR objective responses also appear advantageous to quickly detect the most important brain regions to target with electrical stimulation.[96]

Acknowledgment

B.R. and J.J. are supported by the Belgian National Fund for Scientific Research (F.R.S.-FNRS).

Competing interests

The authors declare no competing interests.

References

1. Sergent, J., S. Ohta & B. Macdonald. 1992. Functional neuroanatomy of face and object processing—a positron emission tomography study. *Brain* **115:** 15–36.
2. Puce, A., T. Allison, J.C. Gore, *et al.* 1995. Face-sensitive regions in human extrastriate cortex studied by functional MRI. *J. Neurophysiol.* **74:** 1192–1199.
3. Duchaine, B. & G. Yovel. 2015. A revised neural framework for face processing. *Annu. Rev. Vis. Sci.* **1:** 393–416.
4. Grill-Spector, K., K.S. Weiner, K.N. Kay & J. Gomez. 2017. The functional neuroanatomy of human face perception. *Annu. Rev. Vis. Sci.* **3:** 167–196.
5. Haxby, J.V., E.A. Hoffman & M.I. Gobbini. 2000. The distributed human neural system for face perception. *Trends Cogn. Sci.* **4:** 223–233.
6. Rossion, B. 2015. Face perception. In *Brain Mapping: An Encyclopedic Reference*, Vol. 2. A. Toga, Ed.: 515–522. Academic Press, Elsevier.
7. Bodamer, J. 1947. Die-Prosop-agnosie. *Arch. Psychiatr. Nervenkrankh* **179:** 6–54.
8. Rossion, B. 2008. Constraining the cortical face network by neuroimaging studies of acquired prosopagnosia. *Neuroimage* **40:** 423–426.
9. Allison, T., G. McCarthy, A. Nobre, *et al.* 1994. Human extrastriate visual cortex and the perception of faces, words, numbers, and colors. *Cereb. Cortex* **4:** 544–554.
10. Halgren, E., P. Baudena, G. Heit, *et al.* 1994. Spatio-temporal stages in face and word processing. I. Depth-recorded potentials in the human occipital, temporal and parietal lobes. *J. Physiol.* **88:** 1–50.
11. Goffaux, V., J. Peters, J. Haubrechts, *et al.* 2011. From coarse to fine? Spatial and temporal dynamics of cortical face processing. *Cereb. Cortex* **21:** 467–476.
12. Jiang, F., L. Dricot, J. Weber, *et al.* 2011. Face categorization in visual scenes may start in a higher order area of the right fusiform gyrus: evidence from dynamic visual stimulation in neuroimaging. *J. Neurophysiol.* **106:** 2720–2736.
13. Jiang, F., J.B. Badler, G. Righi, *et al.* 2015. Category search speeds up face-selective fMRI responses in a non-hierarchical cortical face network. *Cortex* **66:** 69–80.
14. Gentile, F., J. Ales & B. Rossion. 2017. Being BOLD: the neural dynamics of face perception. *Hum. Brain Mapp.* **38:** 120–139.
15. Rossion, B., R. Caldara, M. Seghier, *et al.* 2003. A network of occipito-temporal face-sensitive areas besides the right middle fusiform gyrus is necessary for normal face processing. *Brain* **126:** 2381–2395.
16. Steeves, J.K., J.C. Culham, B.C. Duchaine, *et al.* 2006. The fusiform face area is not sufficient for face recognition: evidence from a patient with dense prosopagnosia and no occipital face area. *Neuropsychologia* **44:** 594–609.
17. Weiner, K.S., J. Jonas, J. Gomez, *et al.* 2016. The face-processing network is resilient to focal resection of human visual cortex. *J. Neurosci.* **36:** 8425–8440.
18. Ojemann, J.G., E. Akbudak, A.Z. Snyder, *et al.* 1997. Anatomic localization and quantitative analysis of gradient refocused echo-planar fMRI susceptibility artifacts. *Neuroimage* **6:** 156–167.

19. Kanwisher, N., J. McDermott & M.M. Chun. 1997. The fusiform face area: a module in human extrastriate cortex specialized for face perception. *J. Neurosci.* **17:** 4302–4311.
20. Kanwisher, N. 2017. The quest for the FFA and where it led. *J. Neurosci.* **37:** 1056–1061.
21. Weiner, K.S. & K. Grill-Spector. 2010. Sparsely-distributed organization of face and limb activations in human ventral temporal cortex. *Neuroimage* **52:** 1559–1573.
22. Axelrod, V. & G. Yovel. 2013. The challenge of localizing the anterior temporal face area: a possible solution. *Neuroimage* **81:** 371–380.
23. Rajimehr, R., J.C. Young & R.B.H. Tootell. 2009. An anterior temporal face patch in human cortex, predicted by macaque maps. *Proc. Natl. Acad. Sci. USA* **106:** 1995–2000.
24. Wandell, B.A. 2011. The neurobiological basis of seeing words. *Ann. N.Y. Acad. Sci.* **1224:** 63–80.
25. Jonas, J., B. Rossion, H. Brissart, *et al.* 2015. Beyond the core face-processing network: intracerebral stimulation of a face-selective area in the right anterior fusiform gyrus elicits transient prosopagnosia. *Cortex* **72:** 140–155.
26. Lafer-Sousa, R., B.R. Conway & N.G. Kanwisher. 2016. Color-biased regions of the ventral visual pathway lie between face- and place-selective regions in humans, as in macaques. *J. Neurosci.* **36:** 1682–1697.
27. Ross, L.A. & I.R. Olson. 2012. What's unique about unique entities? An fMRI investigation of the semantics of famous faces and landmarks. *Cereb. Cortex* **22:** 2005–2015.
28. Collins, J.A., J.E. Koski & I.R. Olson. 2016. More than meets the eye: the merging of perceptual and conceptual knowledge in the anterior temporal face area. *Front. Hum. Neurosci.* **10:** 189.
29. Pinsk, M.A., M. Arcaro, K.S. Weiner, *et al.* 2009. Neural representations of faces and body parts in macaque and human cortex: a comparative FMRI study. *J. Neurophysiol.* **101:** 2581–2600.
30. Avidan, G., M. Tanzer, F. Hadj-Bouziane, *et al.* 2014. Selective dissociation between core and extended regions of the face processing network in congenital prosopagnosia. *Cereb. Cortex* **24:** 1565–1578.
31. Nasr, S. & R.B.H. Tootell. 2012. Role of fusiform and anterior temporal cortical areas in facial recognition. *Neuroimage* **63:** 1743–1753.
32. Pyles, J.A., T.D. Verstynen, W. Schneider, *et al.* 2013. Explicating the face perception network with white matter connectivity. *PLoS One* **8:** e61611.
33. Rossion, B., B. Hanseeuw & L. Dricot. 2012. Defining face perception areas in the human brain: a large-scale factorial fMRI face localizer analysis. *Brain Cogn.* **79:** 138–157.
34. Von Der Heide, R.J., L.M. Skipper & I.R. Olson. 2013. Anterior temporal face patches: a meta-analysis and empirical study. *Front. Hum. Neurosci.* **7:** 17.
35. Wyler, A.R., G.A. Ojemann, E. Lettich, *et al.* 1984. Subdural strip electrodes for localizing epileptogenic foci. *J. Neurosurg.* **60:** 1195–1200.
36. Talairach, J. & J. Bancaud. 1973. Stereotaxic approach to epilepsy. Methodology of anatomo-functional stereotaxic investigations. *Prog. Neurol. Surg.* **5:** 297–354.
37. Jonas, J., M. Descoins, L. Koessler, *et al.* 2012. Focal electrical intracerebral stimulation of a face-sensitive area causes transient prosopagnosia. *Neuroscience* **222:** 281–288.
38. Bentin, S., G. McCarthy, E. Perez, *et al.* 1996. Electrophysiological studies of face perception in humans. *J. Cogn. Neurosci.* **8:** 551–565.
39. Allison, T., A. Puce, D. Spencer, *et al.* 1999. Electrophysiological studies of human face perception. I: potential generated in occiptotemporal cortex by face and non-face stimuli. *Cereb. Cortex* **9:** 415–430.
40. McCarthy, G., A. Puce, A. Belger, *et al.* 1999. Electrophysiological studies of human face perception. II: response properties of face-specific potentials generated in occipitotemporal cortex. *Cereb. Cortex* **9:** 431–444.
41. Puce, A., T. Allison & G. McCarthy. 1999. Electrophysiological studies of human face perception. III: effects of top-down processing on face-specific potentials. *Cereb. Cortex* **9:** 445–458.
42. Barbeau, E.J., M.J. Taylor, J. Regis, *et al.* 2008. Spatio temporal dynamics of face recognition. *Cereb. Cortex* **18:** 997–1009.
43. Jacques, C., N. Witthoft, K.S. Weiner, *et al.* 2016. Corresponding ECoG and fMRI category-selective signals in human ventral temporal cortex. *Neuropsychologia* **83:** 14–28.
44. Kadipasaoglu, C.M., C.R. Conner, M.L. Whaley, *et al.* 2016. Category-selectivity in human visual cortex follows cortical topology: a grouped icEEG study. *PLoS One* **11:** e0157109.
45. Rosburg, T., E. Ludowig, M. Dümpelmann, *et al.* 2010. The effect of face inversion on intracranial and scalp recordings of event-related potentials. *Psychophysiology* **47:** 147–157.
46. Vidal, J.R., T. Ossandón, K. Jerbi, *et al.* 2010. Category-specific visual responses: an intracranial study comparing gamma, beta, alpha, and ERP response selectivity. *Front. Hum. Neurosci.* **4:** 195.
47. Liu, H., Y. Agam, J.R. Madsen, *et al.* 2009. Timing, timing, timing: fast decoding of object information from intracranial field potentials in human visual cortex. *Neuron* **62:** 281–290.
48. Ghuman, A.S., N.M. Brunet, Y. Li, *et al.* 2014. Dynamic encoding of face information in the human fusiform gyrus. *Nat. Commun.* **5:** 1–10.
49. Sato, W., T. Kochiyama, S. Uono, *et al.* 2014. Rapid, high-frequency, and theta-coupled gamma oscillations in the inferior occipital gyrus during face processing. *Cortex* **60:** 52–68.
50. Engell, A.D. & G. McCarthy. 2014. Face, eye, and body selective responses in fusiform gyrus and adjacent cortex: an intracranial EEG study. *Front. Hum. Neurosci.* **8:** 642.
51. Tanji, K., M. Iwasaki, N. Nakasato, *et al.* 2012. Face specific broadband electrocorticographic spectral power change in the rhinal cortex. *Neurosci. Lett.* **515:** 66–70.
52. Miller, K.J., G. Schalk, D. Hermes, *et al.* 2016. Spontaneous decoding of the timing and content of human object perception from cortical surface recordings reveals complementary information in the event-related potential and broadband spectral change. *PLoS Comput. Biol.* **12:** 1–20.
53. Puce, A., T. Allison, S.S. Spencer, *et al.* 1997. Comparison of cortical activation evoked by faces measured by intracranial field potentials and functional MRI: two case studies. *Hum. Brain Mapp.* **305:** 298–305.

54. Privman, E., Y. Nir, U. Kramer, *et al.* 2007. Enhanced category tuning revealed by intracranial electroencephalograms in high-order human visual areas. *J. Neurosci.* **27:** 6234–6342.
55. Zhen, Z., Z. Yang, L. Huang, *et al.* 2015. Quantifying interindividual variability and asymmetry of face-selective regions: a probabilistic functional atlas. *Neuroimage* **113:** 13–25.
56. Rossion, B. 2014. Understanding face perception by means of prosopagnosia and neuroimaging. *Front. Biosci.* **6:** 258–307.
57. Meadows, J.C. 1974. The anatomical basis of prosopagnosia. *J. Neurol. Neurosurg. Psychiatry* **37:** 489–501.
58. Hécaen, H. & R. Angelergues. 1962. Agnosia for faces (prosopagnosia). *Arch. Neurol.* **7:** 92–100.
59. Rangarajan, V., D. Hermes, B.L. Foster, *et al.* 2014. Electrical stimulation of the left and right human fusiform gyrus causes different effects in conscious face perception. *J. Neurosci.* **34:** 12828–12836.
60. Engell, A.D. & G. McCarthy. 2011. The relationship of gamma oscillations and face-specific ERPs recorded subdurally from occipitotemporal cortex. *Cereb. Cortex* **21:** 1213–1221.
61. Weiner, K.S., G. Golarai, J. Caspers, *et al.* 2014. The mid-fusiform sulcus: a landmark identifying both cytoarchitectonic and functional divisions of human ventral temporal cortex. *Neuroimage* **84:** 453–465.
62. Witthoft, N., M. Nguyen, G. Golarai, *et al.* 2014. Where is human V4? Predicting the location of hV4 and VO1 from cortical folding. *Cereb. Cortex* **24:** 2401–2408.
63. Dumoulin, S.O., R.G. Bittar, N.J. Kabani, *et al.* 2000. A new anatomical landmark for reliable identification of human area V5/MT: a quantitative analysis of sulcal patterning. *Cereb. Cortex* **10:** 454–463.
64. Buzsáki, G., C.A. Anastassiou & C. Koch. 2012. The origin of extracellular fields and currents—EEG, ECoG, LFP and spikes. *Nat. Rev. Neurosci.* **13:** 407–420.
65. Davidesco, I., E. Zion-Golumbic, S. Bickel, *et al.* 2014. Exemplar selectivity reflects perceptual similarities in the human fusiform cortex. *Cereb. Cortex* **24:** 1879–1893.
66. Fisch, L., E. Privman, M. Ramot, *et al.* 2009. Neural "ignition": enhanced activation linked to perceptual awareness in human ventral stream visual cortex. *Neuron* **64:** 562–574.
67. Miller, K.J., L.B. Sorensen, J.G. Ojemann, *et al.* 2009. Power-law scaling in the brain surface electric potential. *PLoS Comput. Biol.* **5:** e1000609.
68. Manning, J.R., J. Jacobs, I. Fried, *et al.* 2009. Broadband shifts in local field potential power spectra are correlated with single-neuron spiking in humans. *J. Neurosci.* **29:** 13613–13620.
69. Winawer, J., K.N. Kay, B.L. Foster, *et al.* 2013. Asynchronous broadband signals are the principal source of the BOLD response in human visual cortex. *Curr. Biol.* **23:** 1145–1153.
70. Podvalny, E., N. Noy, M. Harel, *et al.* 2015. A unifying principle underlying the extracellular field potential spectral responses in the human cortex. *J. Neurophysiol.* **114:** 505–519.
71. Schroeder, C.E. & P. Lakatos. 2009. Low-frequency neuronal oscillations as instruments of sensory selection. *Trends Neurosci.* **32:** 9–18.
72. Crouzet, S.M. & S.J. Thorpe. 2011. Low-level cues and ultra-fast face detection. *Front. Psychol.* **2:** 342.
73. Rossion, B. & S. Caharel. 2011. ERP evidence for the speed of face categorization in the human brain: disentangling the contribution of low-level visual cues from face perception. *Vision Res.* **51:** 1297–1311.
74. Rossion, B. & C. Jacques. 2008. Does physical interstimulus variance account for early electrophysiological face sensitive responses in the human brain? Ten lessons on the N170. *Neuroimage* **39:** 1959–1979.
75. Rossion, B., K. Torfs, C. Jacques & J. Liu-Shuang. 2015. Fast periodic presentation of natural images reveals a robust face-selective electrophysiological response in the human brain. *J. Vis.* **15:** 18.
76. Jacques, C., T.L. Retter & B. Rossion. 2016. A single glance at natural face images generate larger and qualitatively different category-selective spatio-temporal signatures than other ecologically-relevant categories in the human brain. *Neuroimage* **137:** 21–33.
77. Liu-Shuang, J., K. Torfs & B. Rossion. 2016. An objective electrophysiological marker of face individualisation impairment in acquired prosopagnosia with fast periodic visual stimulation. *Neuropsychologia* **83:** 100–113.
78. Jonas, J., C. Jacques, J. Liu-shuang, *et al.* 2016. A face-selective ventral occipito-temporal map of the human brain with intracerebral potentials. *Proc. Natl. Acad. Sci. USA* **113:** E4088–E4097. https://doi.org/10.1073/pnas.1522033113.
79. Adrian, E. & B. Matthews. 1934. The Berger rhythm: potential changes from the occipital lobes in man. *Brain* **57:** 355–385.
80. Kamp, A., C.W. Sem Jacobsen, W. Storm Van Leeuwen, *et al.* 1960. Cortical responses to modulated light in the human subject. *Acta Physiol. Scand.* **48:** 1–12.
81. Regan, D. 1966. Some characteristics of average steady-state and transient responses evoked by modulated light. *Electroencephalogr. Clin. Neurophysiol.* **20:** 238–248.
82. Regan, D. 1989. *Human Brain Electrophysiology: Evoked Potentials and Evoked Magnetic Fields in Science and Medicine.* New York: Elsevier.
83. Norcia, A.M., L.G. Appelbaum, J.M. Ales, *et al.* 2015. The steady-state visual evoked potential in vision research: a review. *J. Vis.* **15:** 4.
84. Retter, T.L. & B. Rossion. 2016. Uncovering the neural magnitude and spatio-temporal dynamics of natural image categorization in a fast visual stream. *Neuropsychologia* **91:** 9–28.
85. Maillard, L., L. Koessler, S. Colnat-Coulbois, *et al.* 2009. Combined SEEG and source localisation study of temporal lobe schizencephaly and polymicrogyria. *Clin. Neurophysiol.* **120:** 1628–1636.
86. Kim, J.-J., B. Crespo-Facorro, N.C. Andreasen, *et al.* 2000. An MRI-based parcellation method for the temporal lobe. *Neuroimage* **11:** 271–288.
87. Dale, A.M., B. Fischl & M.I. Sereno. 1999. Cortical surface-based analysis. I. Segmentation and surface reconstruction. *Neuroimage* **194:** 179–194.
88. Kadipasaoglu, C.M., K. Forseth, M. Whaley, *et al.* 2015. Development of grouped icEEG for the study of cognitive processing. *Front. Psychol.* **6:** 1008.

89. Quek, G.L. & B. Rossion. 2017. Category-selective human brain processes elicited in fast periodic visual stimulation streams are immune to temporal predictability. *Neuropsychologia* **104:** 182–200.
90. Liu-Shuang, J., A.M. Norcia & B. Rossion. 2014. An objective index of individual face discrimination in the right occipito-temporal cortex by means of fast periodic oddball stimulation. *Neuropsychologia* **52:** 57–72.
91. Dzhelyova, M., C. Jacques & B. Rossion. 2017. At a single glance: fast periodic visual stimulation uncovers the spatio-temporal dynamics of brief facial expression changes in the human brain. *Cereb. Cortex* **27:** 4106–4123.
92. Lochy, A., G. Van Belle & B. Rossion. 2015. A robust index of lexical representation in the left occipito-temporal cortex as evidenced by EEG responses to fast periodic visual stimulation. *Neuropsychologia* **66:** 18–31.
93. Itier, R.J. & M.J. Taylor. 2004. N170 or N1? Spatiotemporal differences between object and face processing using ERPs. *Cereb. Cortex* **14:** 132–142.
94. Rossion, B., I. Gauthier, M.J. Tarr, *et al.* 2000. The N170 occipito-temporal component is delayed and enhanced to inverted faces but not to inverted objects: an electrophysiological account of face-specific processes in the human brain. *Neuroreport* **11:** 69–74.
95. Bouvier, S.E. & S.A. Engel. 2006. Behavioral deficits and cortical damage loci in cerebral achromatopsia. *Cereb. Cortex* **16:** 183–191.
96. Jonas, J., B. Rossion, J. Krieg, *et al.* 2014. Intracerebral electrical stimulation of a face-selective area in the right inferior occipital cortex impairs individual face discrimination. *Neuroimage* **99:** 487–497.
97. Pitcher, D., V. Walsh, G. Yovel, *et al.* 2007. TMS evidence for the involvement of the right occipital face area in early face processing. *Curr. Biol.* **17:** 1568–1573.
98. Ambrus, G.G., F. Windel, A.M. Burton, *et al.* 2017. Causal evidence of the involvement of the right occipital face area in face-identity acquisition. *Neuroimage* **148:** 212–218.
99. Rosenke, M., K.S. Weiner, M.A. Barnett, *et al.* 2017. A cross-validated cytoarchitectonic atlas of the human ventral visual stream. *Neuroimage.* https://doi.org/10.1016/j.neuroimage.2017.02.040.
100. Lorenz, S., K.S. Weiner, J. Caspers, *et al.* 2017. Two new cytoarchitectonic areas on the human mid-fusiform gyrus. *Cereb. Cortex* **27:** 373–385.
101. Alonso-Prieto, E., G. Van Belle, J. Liu-Shuang, *et al.* 2013. The 6 Hz fundamental stimulation frequency rate for individual face discrimination in the right occipito-temporal cortex. *Neuropsychologia* **51:** 2863–2875.
102. Rossion, B., E.A. Prieto, A. Boremanse, *et al.* 2012. A steady-state visual evoked potential approach to individual face perception: effect of inversion, contrast-reversal and temporal dynamics. *Neuroimage* **63:** 1585–1600.
103. Nozaradan, S., A. Mouraux, J. Jonas, *et al.* 2017. Intracerebral evidence of rhythm transform in the human auditory cortex. *Brain Struct. Funct.* **222:** 2389–2404.
104. Damasio, H., T.J. Grabowski, D. Tranel, *et al.* 1996. A neural basis for lexical retrieval. *Nature* **380:** 499–505.
105. Bedos Ulvin, L., J. Jonas, H. Brissart, *et al.* 2017. Intracerebral stimulation of left and right ventral temporal cortex during object naming. *Brain Lang.* **175:** 71–76.
106. Parvizi, J., C. Jacques, B.L. Foster, *et al.* 2012. Electrical stimulation of human fusiform face-selective regions distorts face perception. *J. Neurosci.* **32:** 14915–14920.
107. Keller, C.J., I. Davidesco, P. Megevand, *et al.* 2017. Tuning face perception with electrical stimulation of the fusiform gyrus. *Hum. Brain Mapp.* **38:** 2830–2842.
108. Chong, S.C., S. Jo, K.M. Park, *et al.* 2013. Interaction between the electrical stimulation of a face-selective area and the perception of face stimuli. *Neuroimage* **77:** 70–76.
109. Vignal, J.P., P. Chauvel & E. Halgren. 2000. Localised face processing by the human prefrontal cortex: stimulation-evoked hallucinations of faces. *Cogn. Neuropsychol.* **17:** 281–291.

Received: 4 May 2018 | Revised and accepted: 22 October 2018

DOI: 10.1002/hbm.24455

WILEY

RESEARCH ARTICLE

The inferior occipital gyrus is a major cortical source of the face-evoked N170: Evidence from simultaneous scalp and intracerebral human recordings

Corentin Jacques[1,2] | Jacques Jonas[3,4] | Louis Maillard[3,4] | Sophie Colnat-Coulbois[3,5] | Laurent Koessler[3,4] | Bruno Rossion[1,3,4]

[1]Psychological Science Research Institute, Institute of Neuroscience, Université Catholique de Louvain, Louvain-la-Neuve, Belgium

[2]Department of Neuroscience, KU Leuven, Center for Developmental Psychiatry, Leuven, Belgium

[3]Université de Lorraine, CNRS, CRAN, F-54000 Nancy, France

[4]Université de Lorraine, CHRU-Nancy, Service de Neurologie, F-54000 Nancy, France

[5]Université de Lorraine, CHRU-Nancy, Service de Neurochirurgie, F-54000 Nancy, France

Correspondence
Bruno Rossion, CRAN, UMR 7039, CNRS - Université de Lorraine, Pavillon Krug (1er étage - entrée CC-1), Hôpital Central, CHRU Nancy - Centre Hospitalier Universitaire de Nancy, 29 Avenue du Maréchal de Lattre de Tassigny, 54000 Nancy, France
Email: bruno.rossion@univ-lorraine.fr

Funding information
Fédération Wallonie-Bruxelles, Grant/Award Number: ARC 13/18-053; Fonds de la Recherche scientifique, Grant/Award Number: PDR T.0207.16; Louvain Foundation

Abstract

The sudden onset of a face image leads to a prominent face-selective response in human scalp electroencephalographic (EEG) recordings, peaking 170 ms after stimulus onset at occipito–temporal (OT) scalp sites: the N170 (or M170 in magnetoencephalography). According to a widely held view, the main cortical source of the N170 lies in the fusiform gyrus (FG), whereas the posteriorly located inferior occipital gyrus (IOG) would rather generate earlier face-selective responses. Here, we report neural responses to upright and inverted faces recorded in a unique patient using multicontact intracerebral electrodes implanted in the right IOG and in the OT sulcus above the right lateral FG (LFG). Simultaneous EEG recordings on the scalp identified the N170 over the right OT scalp region. The latency and amplitude of this scalp N170 were correlated at the single-trial level with the N170 recorded in the lateral IOG, close to the scalp lateral occipital surface. In addition, a positive component maximal around the latency of the N170 (a P170) was prominent above the internal LFG, whereas this region typically generates an N170 (or "N200") over its external/ventral surface. This suggests that electrophysiological responses in the LFG manifest as an equivalent dipole oriented mostly along the vertical axis with likely minimal projection to the lateral OT scalp region. Altogether, these observations provide evidence that the IOG is a major cortical generator of the face-selective scalp N170, qualifying the potential contribution of the FG and questioning a strict serial spatiotemporal organization of the human cortical face network.

1 | INTRODUCTION

The human face is a highly complex, familiar, and socially critical stimulus in our visual environment. For these reasons, understanding the spatiotemporal organization of face processing in the human brain is a primary goal of cognitive neuroscience research. The neural basis of face processing has been intensively investigated for three decades with functional neuroimaging, first with positron emission tomography (Sergent, Ohta, & Macdonald, 1992) then with functional magnetic resonance imaging (fMRI; Puce, Allison, Gore, & McCarthy, 1995). The advent of fMRI, in particular, has allowed defining a set of regions in the occipito-temporal (OT) cortex of the typical human adult brain that respond significantly more to pictures of faces than nonface objects. The most prominent and consistent of these face-selective regions have been identified in the lateral section of the middle fusiform gyrus (LFG, the functional area being termed the "fusiform face area" [FFA]; Kanwisher, McDermott, & Chun, 1997), the inferior occipital gyrus (IOG) on the lateral section of the occipital cortex ("occipital face area" [OFA], Gauthier et al., 2000), as well as the posterior superior temporal sulcus (pSTS; Puce, Allison, Bentin, Gore, & McCarthy, 1998). These regions are typically defined as forming the core of a distributed cortical face network in the human brain (Calder & Young, 2005; Duchaine & Yovel, 2015; Grill-Spector, Weiner, Kay, & Gomez, 2017; Haxby, Hoffman, & Gobbini, 2000 for reviews; see, e.g., Gao, Gentile, & Rossion, 2018; Rossion, Hanseeuw, & Dricot, 2012; Zhen et al., 2015 for extensive fMRI investigations of the human cortical face network). However, as fMRI provides a slow and indirect (i.e., hemodynamic) measure of neural

Laurent Koessler and Bruno Rossion contributed equally to this work.

activity, the temporal organization of this network (i.e., when are these brain regions activated, for how long, etc.) remains largely elusive.

To provide complementary high temporal resolution information (at the expense of spatial precision), electrical potentials elicited by the sudden onset of face stimuli have also been recorded for decades from the human scalp with electroencephalography (EEG) (since Srebro, 1985). While early studies with few scalp electrodes emphasized a face-selective component recorded on the vertex (Cz electrode) at around 160–170 ms following the onset of a face stimulus (the vertex positive potential [VPP]; Botzel & Grusser, 1989; Jeffreys, 1989 for a review, see Jeffreys, 1996), the vast majority of EEG studies has focused on a prominent negative deflection peaking at the same latency over OT sites: the N170 (Bentin, McCarthy, Perez, Puce, & Allison, 1996; see also Botzel, Schulze, & Stodieck, 1995; George, Evans, Fiori, Davidoff, & Renault, 1996 for early studies; Rossion, 2014; Rossion & Jacques, 2011 for reviews). Studies using magnetoencephalography (MEG) have also recorded a similar "M170" component (e.g., Halgren, Raij, Marinkovic, Jousmaki, & Hari, 2000; Itier, Herdman, George, Cheyne, & Taylor, 2006; Liu, Higuchi, Marantz, & Kanwisher, 2000) which presents similar response properties as the N170, in particular a larger amplitude for faces than non-face object categories (Bentin et al., 1996; Ganis, Smith, & Schendan, 2012; Gao et al., 2013; Itier & Taylor, 2004; Rossion et al., 2000; Rossion & Jacques, 2008; Rousselet, Husk, Bennett, & Sekuler, 2008) and a substantial increase of both amplitude and latency to face stimuli presented upside down (Eimer, 2000; Itier et al., 2006; Itier & Taylor, 2004; Jacques & Rossion, 2007; Jacques, Schiltz, & Goffaux, 2014; Rossion et al., 1999; Rousselet, Mace, & Fabre-Thorpe, 2004; Sadeh & Yovel, 2010; see Rossion & Jacques, 2011 for review).

In order to characterize the spatiotemporal dynamics of face processing in the human brain, a number of authors have attempted to relate the face-evoked N170/M170 measured on the scalp to face-selective OT cortical regions defined in neuroimaging studies. Since the fusiform gyrus (FG) was the first region systematically associated with face-selective processing in neuroimaging studies (Kanwisher et al., 1997; Puce et al., 1995; Sergent et al., 1992), but also based on other sources of evidence (see below), the vast majority of studies consider that the N170/M170 primarily originates from the FG (see also the review of Yovel, 2016). Empirically, a first piece of evidence comes from early intracranial recording studies using electrocorticography (ECoG) in human epileptic patients, which reported a N170-like component (termed the N200) over the FG and inferior temporal gyrus, but not over the lateral IOG (Allison et al., 1994; see also Allison, Puce, Spencer, McCarthy, & Belger, 1999; McCarthy, Puce, Belger, & Allison, 1999; Puce, Allison, & McCarthy, 1999 for extensive reports). This work in fact provided the impetus for the subsequent recording of the face-selective N170 over the human scalp of typical individuals with the same paradigm and stimuli (Bentin et al., 1996). Second, a number of studies using various source localization approaches have emphasized the contribution of the posterior/middle FG (e.g., Botzel et al., 1995; Deffke et al., 2007; Gao et al., 2013; Halgren et al., 2000; Hoshiyama, Kakigi, Watanabe, & Miki, 2003; Mnatsakanian & Tarkka, 2004; Pizzagalli et al., 2002; Rossion, Joyce, Cottrell, & Tarr, 2003; Shibata et al., 2002; Swithenby et al., 1998; Tanskanen, Nasanen, Montez, Paallysaho, & Hari, 2005; Watanabe, Kakigi, & Puce, 2003) or even of the anterior FG (Herrmann, Ehlis, Muehlberger, & Fallgatter, 2005) as neural sources of the N170/M170 and its increased amplitude to faces. Third, some studies have reported significant correlations between face-selective fMRI activity in the FG (i.e., FFA) and the amplitude of the N170 when manipulating noise levels applied to the face stimuli (Horovitz, Rossion, Skudlarski, & Gore, 2004). In the same vein, a simultaneous EEG–fMRI study found a significant correlation between the magnitude of face selectivity measured in ERPs at the peak of the 170 ms and in fMRI in the FG (Sadeh, Podlipsky, Zhdanov, & Yovel, 2010).

In the latter study (Sadeh et al., 2010), the authors also emphasized the lack of significant correlation between the electrophysiological face-selectivity index at 170 ms and fMRI face-selective activity in the IOG (i.e., OFA). In fact, this most posterior cortical face-selective region, usually located in the lateral section of the IOG, is rarely considered as a potential source of the face-evoked N170/M170 in source localization studies (e.g., Henson, Mouchlianitis, & Friston, 2009; Itier et al., 2006). Rather, based on the timing of effects of transcranial magnetic stimulation (TMS) on face processing tasks as well as correlations of fMRI and scalp EEG face-selective responses, it has been proposed that face-selective activity in the IOG peaks and is correlated with scalp EEG at an earlier latency, that is, at around 80–120 ms, during the time window of the P1 component preceding the N170 (Pitcher, Garrido, Walsh, & Duchaine, 2008; Pitcher, Walsh, Yovel, & Duchaine, 2007; Sadeh et al., 2010). According to this serial/hierarchical spatiotemporal view, face-selective responses would initially peak at around 100 ms (i.e., at the level of the P1/M1 component) in the IOG—possibly involved in extracting specific face parts (eyes, nose, mouth, etc.)—and feeding later into the FG where face-selectivity peaking at around 170 ms would reflect a holistic/configural representation of faces (Duchaine & Yovel, 2015; Pitcher, Walsh, & Duchaine, 2011; Yovel, 2016).

So far, this serial/hierarchical view of category-selective face processing has been challenged only by indirect evidence. First, time-resolved fMRI in the healthy brain indicates that the initial activation to slowly revealed faces emerges initially in the FG rather than in the IOG (Gentile, Ales, & Rossion, 2017; Jiang et al., 2011; Jiang, Badler, Righi, & Rossion, 2015). Second, EEG recordings in individuals with lesions of various face-selective OT cortical regions (OFA, FFA, or pSTS) suggest that multiple face-selective regions are likely involved in generating the scalp N170 (Dalrymple et al., 2011; Prieto, Caharel, Henson, & Rossion, 2011). Third, given the anatomical location of the FG with the majority of its cortical surface facing toward the inferior part of the head (Figure 1), the contribution of face-selective responses in this region to the scalp N170 recorded over the lateral OT scalp regions should be questioned. This geometrical incompatibility was in fact noted by Bentin et al. (1996) in their seminal study. Bentin et al. (1996) speculatively attributed the source of the N170 to the OT sulcus (OTS), pointing toward the lateral surface of the brain and scalp (see fig. 8 in Bentin et al., 1996). More recently, Rosburg et al. (2010) performed simultaneous intracranial and scalp recordings of ERPs to upright and inverted faces, using inversion as a functional marker of the N170. As amplitude and latency increase with inversion were revealed for the intracranial N170 recorded in the lateral IOG

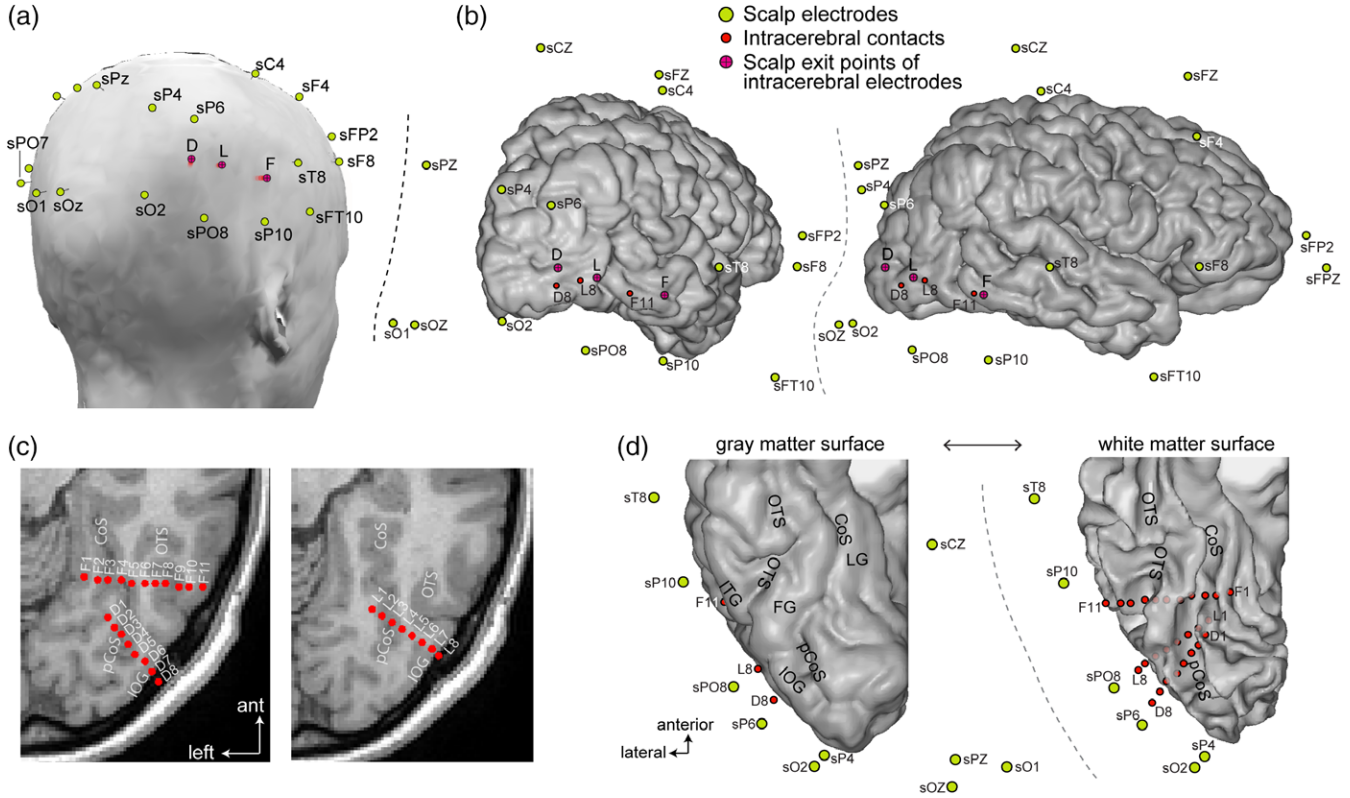

FIGURE 1 Simultaneous recording of scalp and intracerebral EEG. (a) Scalp view from the posterior right hemisphere showing the position of the scalp recording electrodes (shown in green) and the location on the scalp of the exit point of the three intracerebral electrodes (D, L, and F, shown as red dots). (b) Three/quarter posterior and profile views of three-dimensional (3D) reconstruction of the patient's right hemisphere cortical surface, showing the locations of the intracerebral electrodes (in red, only the most external contacts D8, L8, and F11 appear on the cortical surface) and the locations of the scalp electrodes (green). (c) Axial views of the posterior half of the right hemisphere of the patient, showing the locations of intracerebral contacts in the right OT cortex. Electrode L was slightly superior to D and F electrodes. (d) 3D ventral views of the posterior half of the right hemisphere of the patient, showing the anatomical location of the intracerebral contacts and scalp electrodes. The plots show the gray matter cortical surface (left) and the corresponding white matter surface (right). As intracerebral contacts penetrate the brain tissue, contacts are only visible when stripping away the gray matter and keeping only white matter surface (left). Abbreviations: FG = fusiform gyrus; IOG = inferior occipital gyrus; LG = lingual gyrus; OTS = occipito-temporal sulcus; (p)CoS = (posterior) collateral sulcus [Color figure can be viewed at wileyonlinelibrary.com]

but not in the FG, the authors concluded that the lateral IOG contributes primarily to the face inversion effect (FIE) observed in scalp recordings. Unfortunately, the use of few (n = 6) electrodes and a reference over the mastoid (i.e., close to OT regions) prevented from a direct investigation of the scalp N170 over OT regions in that study. Moreover, that study—similarly to the studies of Allison et al. (1994, 1999)—was performed with grids of electrodes applied on the cortical surface (ECoG) rather than with multicontact electrodes inserted directly in the brain volume (stereotactic EEG [SEEG], Talairach & Bancaud, 1973). Hence, Rosburg et al. (2010) observed only negative components intracranially, which were difficult to relate to the positivity that they observed simultaneously on the vertex, the VPP.

Here, we present a detailed report of a patient with rare SEEG recording of face-evoked responses inside both the IOG and LFG of the right hemisphere, together with simultaneous scalp EEG recording using multiple electrodes placed over the whole scalp, including the OT region. We examined the contribution of the IOG and LFG to the N170 measured on the scalp over OT regions. We asked the following questions: (a) can we find an intracerebral N170 response in the lateral IOG with similar response properties as the N170 measured on the scalp OT region in the same patient? (b) are the SEEG responses in the IOG and the LFG correlated with the scalp OT N170? and (c) does the topology of electrophysiological responses and the cortical geometry of the FG region support a contribution of this region to the scalp OT N170? Addressing these issues should also shed light on the above-described serial/hierarchical spatiotemporal framework of the human cortical face network.

2 | METHODS

2.1 | Case description

KV is a right-handed female suffering from refractory occipital epilepsy related to a focal cortical dysplasia involving the right lingual gyrus (LG) and posterior collateral sulcus (pCoS). Her case was previously reported as evidence of a transient inability to recognize famous faces (Jonas et al., 2012), following intracerebral electrical stimulation of the face-selective region of the right IOG (OFA). That study was performed during a first SEEG implantation in 2010 to delineate the source and extent of the patient's epileptic seizures. During a second implantation

performed in 2011 with fewer intracerebral electrodes targeting the focal cortical dysplasia and surrounding cortical areas for therapeutic purposes, OFA stimulation caused a transient impairment at discriminating pictures of unfamiliar individual faces (Jonas et al., 2014). The present data set was also collected during this second implantation. The patient was 32 years old at the time of this second implantation.

The patient has never reported face recognition difficulties and has preserved memory and preserved visual perception (including faces and objects), as shown by stringent neuropsychological evaluations (Jonas et al., 2012). These electrophysiological investigations were part of the presurgical functional mapping of the patient. She gave written informed consent for these data to be used for research purpose according to the rules of the ethical committee of the Nancy University Hospital.

2.2 | Simultaneous intracerebral–scalp EEG recordings

The patient underwent simultaneous intracerebral (SEEG) and scalp EEG recordings. The colocations of these electrodes are shown in Figure 1. Besides the relatively dense spatial coverage of scalp electrodes for such a study (e.g., compared to six electrodes in Rosburg et al., 2010), the right OT cortex was well sampled with both intracerebral and surface electrodes.

2.2.1 | Intracerebral electrodes

The patient was stereotactically implanted with three multicontact intracerebral electrodes targeting the right ventral OT cortex, according to a well-defined and previously described procedure (Jonas et al., 2014; Salado et al., 2018). Each intracerebral electrode consisted of a cylinder of 0.8 mm diameter and contained 8–11 independent recording contacts of 2 mm in length separated by 1.5 mm from edge to edge and by 3.5 mm center to center. Electrode D (8 recording contacts, D1–D8) targeted the right ventral occipital cortex, from the lateral part of the IOG to the pCoS. Electrode F (11 contacts, F1–11) was located more anteriorly in the ventral OT junction, from the right inferior temporal gyrus to the LG, passing above the posterior FG. Electrode L (eight contacts, L1–L8) was located between electrodes D and F, also in the right occipital cortex but slightly above these electrodes. All intracerebral recording contacts were in direct contact with the gray matter, either located completely within the gray matter (e.g., contact L7 in the lateral IOG, Figure 1c,d) or in contact with both the white and the gray matter (e.g., contacts L5, F6, and F7). Note that, this kind of electrode implantation is rare in clinical practice, where most epileptic patients are implanted with more anterior electrodes to sample the temporal lobe.

2.2.2 | Scalp electrodes

Simultaneous scalp EEG recordings were acquired with 28 Ag/AgCl electrodes of 10 mm diameter placed according to the 10–20 system (Figure 1, see Koessler et al., 2015; Seeck et al., 2017) using sterile procedures, with a particular spatial coverage of bilateral OT regions. Here, they are referred to with the prefix "s" for scalp (e.g., sPO8 for PO8). Some of the posterior electrodes were slightly displaced relative to the 10–20 positions to keep them away from the penetrating point of the intracerebral electrodes (Figure 1). Scalp electrode positions were determined using a three-dimensional digitizer system (3SPACE and FASTRAK; Polhemus, Colchester, VT). Note that the signal from electrode sP8 was not usable because of excessive noise and the impossibility to safely replace it during the long-term monitoring. However, electrodes sPO8, sP10, sO2, and sPO6 allowed a good coverage over the right OT cortex.

2.2.3 | Recordings

Simultaneous SEEG–scalp EEG signals were recorded at a 1,024 Hz sampling rate with a 128 channel amplifier (SD LTM 128 Headbox; Micromed, Mogliano Veneto, Italy). The reference electrode was a prefrontal midline surface electrode (FPz). The recording of the experiment reported here was performed 2 days after the scalp electrode placement.

2.3 | Stimuli and procedure

The methods used here (stimuli, procedure) were the same as in a previous scalp EEG study (Prieto et al., 2011). Stimuli were 30 photographs of front view, upright, unfamiliar faces with neutral expression (15 females). They were cropped to remove external features (hair and ears) and shown without glasses, facial hair, or makeup. Faces were equalized for global luminance. They were displayed at approximately $3^\circ \times 4^\circ$ of visual angle. An additional set of 30 stimuli was created by vertically flipping the 30 face images (inverted faces). We chose to compare the response to upright faces to the exact same stimuli upside down because inverted faces offer the best control for low-level visual properties (as compared to other nonface object categories). Moreover, inversion leads to clear and undisputed increases of amplitude and latency of the N170 (e.g., Eimer, 2000; Rossion et al., 1999; see Rossion & Jacques, 2011 for review).

Upright and inverted faces were presented in a random order using E-prime 2. In each trial, a fixation point displayed at the center of the screen for 100 ms, followed approximately 300 ms (randomized between 200 and 400 ms) later by the presentation of a face (upright or inverted) stimulus during 300 ms. The offset of this stimulus was followed by an intertrial interval of about 1,700 ms (1,600–1,800 ms). Patient KV had to press one response key on a computer keyboard if the stimulus was upright and another key on the stimulus was inverted. She was asked to maintain eye gaze fixation to the center of the screen and to respond as accurately and as fast as possible. KV performed 90 trials per condition in one session (30 stimuli in each set repeated three times each; 180 trials in total).

2.4 | Data processing and analyses

2.4.1 | EEG preprocessing

All analyses were performed using Letswave 5 (Mouraux & Iannetti, 2008) and MATLAB v7.8 (The MathWorks Inc., Natick, MA). Continuous EEG data were epoched in segments centered on stimulus onset (−1 to 1 s). Epochs were then DC corrected and low-pass filtered at 25 Hz (zero-phase shift Butterworth filter, order 4). Noisy epochs, epochs containing blink artifacts or large epileptic spikes—in which signal amplitude at any point in the time window from −0.2 to 0.6 s was above or below 5.5 times the *SD* computed across all trials for

each time sample—were discarded. If the rejection threshold was exceeded at one channel, then the epoch was rejected for all (i.e., scalp and intracranial) channels. This led to the rejection of 18% of the epochs. Additional expert visual inspection for potential remaining small epileptic spikes in the window of interest did not lead to further epoch rejection. Epochs were then baseline corrected by subtracting the amplitude in the 0.1 s prestimulus time window, and then averaged.

2.4.2 | N170/P170 analyses

N170/P170 peak was measured on intracerebral contacts and scalp electrodes with an identifiable ERP component within a time window of 140–200 ms (165–225 ms for SEEG contact F8, see below). The amplitude of the peak at each channel was quantified as the mean signal amplitude within a ±10 ms time window centered on the peak latency. The peak was identified automatically as the local minimum/maximum within a time window of 140–200 ms (165–225 ms for SEEG contact F8). Statistical comparisons between the N170 measured in the upright face versus inverted face condition were performed at each channel. We used a permutation test for the N170 amplitude (e.g., Jacques et al., 2014; Rousselet et al., 2008), by comparing the actual amplitude difference to a distribution of differences under the null hypothesis obtained by randomly shuffling the condition label for each trial (before computing the difference) 10,000 times. To statistically assess the latency inversion effect, we used a jackknife procedure (Miller, Patterson, & Ulrich, 1998) in which the *SD* of the single-trial latency is estimated (and corrected by multiplying the jackknife *SD* by the number of epochs minus one) separately for each condition, by systematically leaving-out one trial at a time before computing the ERP average and measuring the peak latency. The mean latency and *SD* for each condition was used to compute a *t* test. For the latency comparison, we upsampled single-trial data by a factor of 10 (i.e., to 10,240 Hz using cubic interpolation) to avoid always obtaining the same peak latency for all jackknife samples. For intracerebral contacts where the effect of inversion (amplitude and latency) was tested (N = 23), we used a Bonferroni correction to account for multiple comparisons.

2.4.3 | Correlation between intracerebral and scalp EEG signals in the N170 time window

We examined the relationship between the N170 peak latency and amplitude in intracerebral relative to scalp EEG recordings using a correlation approach, in the following way: (a) a subsample of 15 trials (out of 74 in the upright face condition) was randomly selected (without replacement); (b) these trials were averaged for each channel (an average over a subset of trials was used because the N170 could not be identified in single trials on scalp electrodes); (c) in the resulting averaged EEG segment, for each channel, the peak was identified as the local minimum or maximum amplitude in a 140–200 ms (165–225 ms for SEEG contact F8) time window (when no local maximum/minimum was present the derivative was computed, and the point closest to zero was considered as the peak) and the peak amplitude and latency values were stored; (d) steps a to c were repeated 5,000 times to obtain a distribution of amplitudes and latencies measured at all channels in corresponding subsets of 15 trials, and (e) the resulting 5,000 amplitude and latency data points for each channel were used to quantify the relationship (using Pearson's coefficients) across all pairs of channels, respectively, for the amplitude and the latency of the N/P170. Correlation coefficients were tested against chance level using a permutation test, repeating steps a to e (see above) 4,000 times, shuffling the order of trials at each permutation so that correlations across channels were measured between unmatched subsets of trials. At each of the 4,000 permutation cycles, we stored the maximum Pearson's coefficient across all intracerebral–scalp EEG pairs of channels to generate a permutation distribution (i.e., distribution of coefficients obtained by chance) which corrects for multiple comparisons (Nichols & Holmes, 2001). For each pair of channel, the actual Pearson's coefficient was then compared to the permutation distribution to derive a p value. Only significant correlations ($p < .05$, i.e., corrected for multiple comparisons) observed in at least two neighboring scalp electrodes (i.e., within a radius of 5 cm from each other) were considered.

3 | RESULTS

3.1 | Patient KV shows typical FIE on the scalp-N170 component

The visual presentation of upright face images elicited robust biphasic ERP responses over the patient's scalp during the first 200 ms following stimulus onset (Figure 2a). The shape, latency, and scalp distribution of these early ERP responses were similar to that observed in typical adult participants during foveal stimulation (Bentin et al., 1996; Eimer, 2000; Ganis et al., 2012; Itier & Taylor, 2004; Jacques et al., 2014; Rossion & Jacques, 2011; Rousselet et al., 2004, 2008). A first positive deflection peaking over broad bilateral OT regions at about 110–120 ms (P100) was followed by a negative deflection (N170) maximal over bilateral OT regions (Figure 2b) at about 160–170 ms (162 and 167 ms on sPO8 and sO2, respectively, for the right hemisphere; 169 and 176 ms on sPO7 and sO1, respectively, for the left hemisphere).

Notably, the N170 was strongly increased both in amplitude and latency in response to images of inverted faces (Figure 2), which is the typical signature of the FIE on the scalp-recorded N170 component as revealed by numerous EEG studies in healthy adults (Itier et al., 2006; Itier & Taylor, 2004; Jacques et al., 2014; Jacques & Rossion, 2007; Rossion et al., 1999, 2000; Rousselet et al., 2004). Over right OT channel sPO8, the peak amplitude of the N170 was 3.4 μV larger in response to inverted (−6.3 ± 9 μV) compared to upright faces (−2.9 ± 7.6 μV). The amplitude increase following face inversion was largest at right OT channels (Figure 2b). Testing 12 individual posterior scalp electrodes revealed a significant amplitude increase with inversion at four OT channels in the right hemisphere (sO2, sPO8, sP10, and sP6, *ps*' = 0.0077–0.032, one-tailed permutation test, uncorrected) and one OT channel in the left hemisphere (PO7, p = .042). When averaging across four OT channels, the amplitude increase was significant in the right hemisphere (3.01 μV, p = .014) but not in the left hemisphere (1.2 μV, p = .18). Similarly, the N170 peak latency at right OT channel

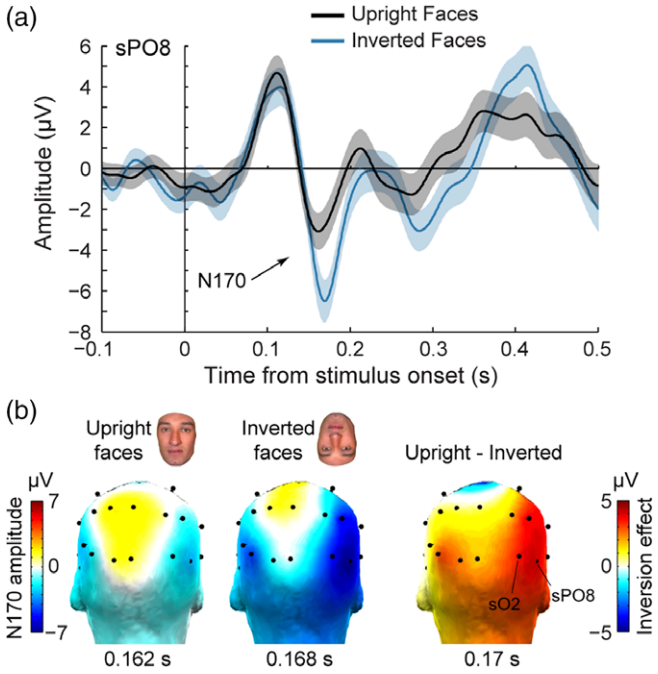

FIGURE 2 Scalp response to upright and inverted faces in patient KV. (a) Averaged ERP responses to upright and inverted faces at a single right hemispheric occipito-temporal (OT) scalp electrode (sPO8) in patient KV (see scalp location in panel B). Shaded regions are *SE* across trials. The large N170 component, peaking at around 170 ms, is increased in amplitude and latency for inverted faces compared to upright faces. (b) Patient KV's scalp topographical distribution of the N170 peak for upright faces (left), inverted faces (middle), and the difference between upright and inverted face conditions (right). Topographical maps are displayed from the back of the head at the latency of the peak component or peak difference (latency indicated below each map). These scalp topographies show typical N170 and N170 inversion effect of posterior OT regions, with a right hemispheric dominance [Color figure can be viewed at wileyonlinelibrary.com]

sPO8 was 7 ms later to inverted (170 ms) compared to upright (163 ms) faces. The latency increase following face inversion was significant at five right OT channels (sO2, sPO8, sP10, sP6, sT8, *p*s' = 0.019–0.0006 uncorrected, latency IE range: 6–11 ms) and one left OT channel (sPO7, $p = .007$, latency IE: 5 ms). Together, these observations indicate that patient KV's electrophysiological response to faces over OT scalp regions are typical compared to normal healthy adults.

3.2 | Corresponding N170 properties between right OT scalp region and lateral inferior occipital cortex

ERP responses to face images were also observed in intracerebral recordings, in most recording contacts in the ventral and lateral sections of the OT and posterior temporal cortex (Figure 3). We specifically focused on the contacts exhibiting a prototypical biphasic response during the first 200 ms following stimulus onset and resembling responses measured on the scalp. These biphasic responses consisted in either a P100–N170 sequence of ERP components or its polarity reversal N100–P170, and were observed in all contacts of electrodes D and L (occipital cortex: LG, pCoS, and IOG) and in 5 out of 11 contacts of electrode F (contacts F1, F2, and F5 in the lingual gyrus and the CoS, contacts F6 and F7 above the FG). All contacts with a N170 or P170 showed a robust FIE manifested as an increase in the amplitude and/or the latency of the N170/P170 component in response to inverted compared to upright faces (Figure 4). Across these contacts, the mean amplitude increase (±std across contacts) due to face inversion was 31 ± 14.2 μV, with a range of 11.5–58.8 μV (Figure 4a). The amplitude increase was significant ($p < .05$ Bonferroni corrected) at all contacts except F6 and F7. Across contacts, the mean latency increase for inverted faces was 6 ± 2.1 ms, with a range of 1.7–10.9 ms (Figure 4b). The latency increase was significant ($p < .05$ Bonferroni corrected) at all contacts except D1 and F1 (although the latency increase was significant on D1 if uncorrected: latency increase = 6.1 ms, $p = .008$ uncorrected). In addition to these SEEG contacts, we also considered contacts F8 and F9 located in the OTS (Figure 1c,d). These contacts did not display an early biphasic electrophysiological response, but showed a negative component around the time window of the N170 (Figure 3a), although with a slightly delayed peak latency as compared to lateral contacts of the L and D electrodes (198 ms in F8 and 182 ms in F9 in response to upright faces, Figure 4b). Amplitudes at these contacts were not significantly different for upright relative to inverted faces ($p = .3$ uncorrected, Figure 4a), but there was a significant latency increase with inversion in F8 ($p < .0001$, Bonferroni corrected), not F9 ($p = .9$ uncorrected, Figure 4b).

Importantly, specifically over the most external contacts of the D and L electrodes (D7-8 and L7-8) in the external surface of the lateral section of the IOG, responses to upright and to inverted faces were remarkably similar to responses measured over nearby scalp right OT channels (sPO8, sO2, sP10, and sP6). Indeed, the morphology, polarity, and latency of the negative component measured in lateral IOG match the polarity and latency of the N170 measured on scalp right OT channels both for upright and inverted faces (Figures 3 and 4). First, only D7-8 and L7-8 showed a polarity of the ERP components matching the polarity measured on the scalp (i.e., P1–N170, Figure 3a,b). The negative polarity "N170" was specifically recorded on these contacts. Moving toward more medial/deep intracerebral contacts in the posterior CoS (L1–L6 and D1–D6), there was a sudden shift in the polarity of both the P100 and N170 so that the P100 becomes an N100 and the N170 becomes a P170 (Figure 3a,b). This shift occurred between contacts D7 and D6, and L7 and L6, that is within the lateral part of the right IOG, with D7/L7 located close to the superficial layer of the cortex and D6/L6 in contact with the deeper part of the lateral IOG close to the posterior CoS. The polarity shift is best illustrated when visualizing the ERP waveforms as in the upper row of Figure 3a (e.g., contacts L8 and L6) or when visualizing the amplitude of the N170/P170 as colored dots as in Figure 3b (color changes from blue to red between contacts D7/L7 and D6/L6). A P170 of similar latency was also measured in contacts of electrode F located in the OTS, above the LFG (F6, F7, Figures 3b,c and 4b). Second, the latency of the scalp N170 to upright faces in right OT regions was very similar to that measured in lateral IOG (Figures 3c and 4b). Collapsing across face orientation, the mean N170 latency was 166 ± 4 ms for right OT scalp regions and 162 ± 5 ms for lateral IOG contacts (average of D7-8 and L7-8). In contrast, the P170

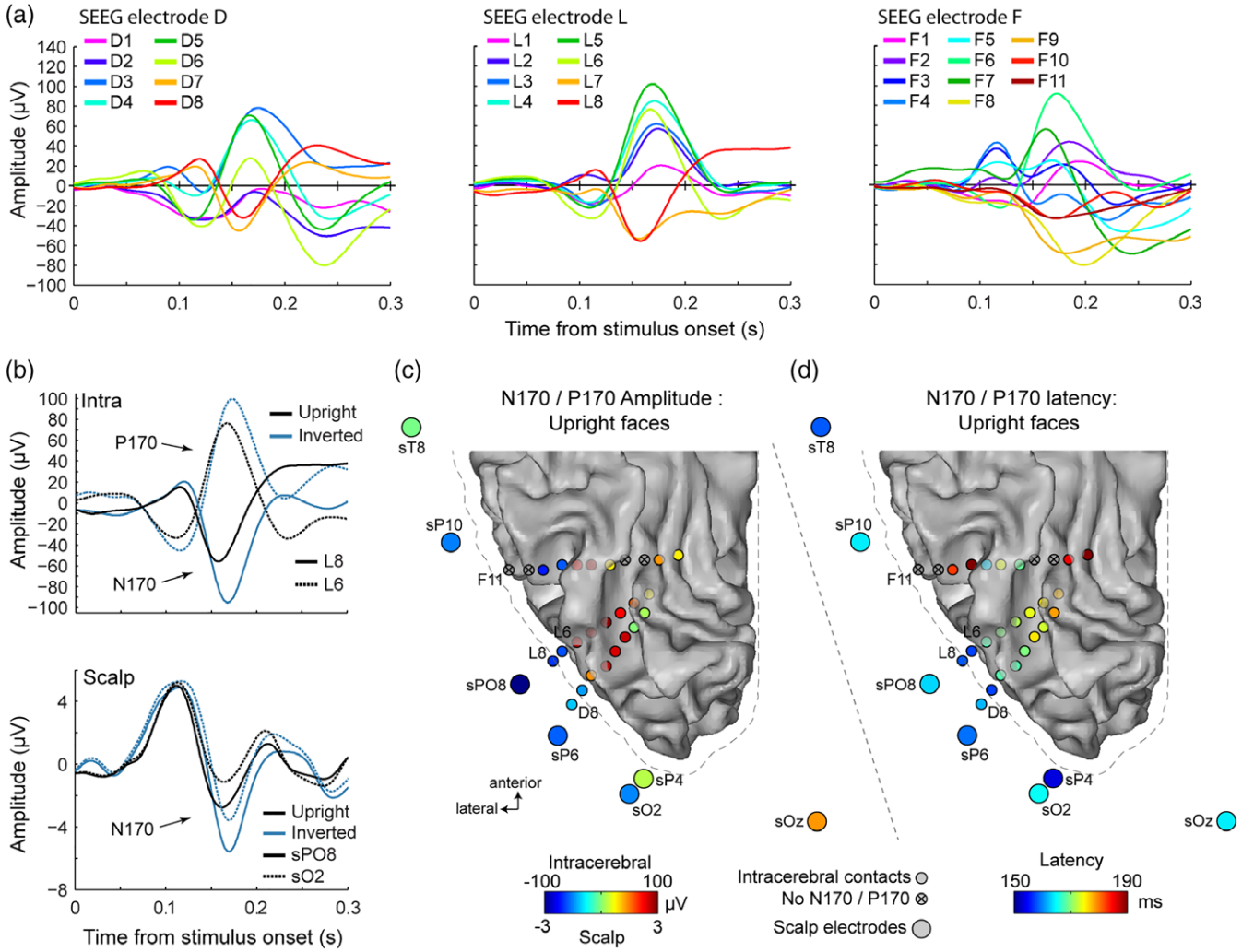

FIGURE 3 Intracerebral and scalp N170/P170 response to faces. (a) Averaged ERP responses to upright faces recorded at all 27 intracerebral recording contacts. Waveforms are displayed superimposed separately for the three multicontact electrodes (D, L, and F). (b) Top: averaged ERP responses to upright and inverted faces at two intracerebral contacts of electrodes L in the superficial part of the lateral inferior occipital gyrus (IOG) (L8) and in the deeper part of the lateral IOG close to the posterior collateral sulcus (L6). See panel B for their location. ERPs at these two contacts manifest an opposite polarity such that an N170 is measured in L8 and a P170 is measured in L6. Bottom: ERPs at two right occipito-temporal scalp electrodes near the intracerebral contacts shown above. Note the scale difference between intracerebral and scalp responses but the similarity in N170 latency. (c) Ventral view of the posterior half of the patient KV's right hemisphere (white matter surface with the gray matter surface shown as a dotted gray outline) together with intracerebral contacts (small circles) and selected surrounding scalp electrodes (large circles). The closest scalp electrodes to intracerebral contacts D8 and L8 were sPO8, sO2, sP10, and sP6 (Euclidian distance to D8 = 27, 26, 51, and 32 mm, respectively; Euclidian distance to L8 = 28, 35, 45, and 33, respectively). Channels are colored as a function of the amplitude of the N170/P170 for upright faces, measured as the mean amplitude in a ±10 ms around the peak. Note the difference in the color scale used for scalp and intracerebral data. (d) Same convention as for panel B but representing the N170/P170 latency for upright faces [Color figure can be viewed at wileyonlinelibrary.com]

recorded more medially (L1–L6 and D1–D6) peaked later overall (174 ± 5 ms) and progressively increased from more lateral to more medial contacts (Figure 4b). This latency difference between the N170 measured in the lateral IOG (D/L7-8) and adjacent more medial contacts (e.g., D/L5-6) suggests that the neural sources of the N170 measured in lateral IOG and P170 measured more medially might be, at least partly, different.

In summary, the similarity in polarity, latency, and inversion effect between the N170 measured on the scalp right OT regions and the N170 recorded on intracerebral lateral D and L contacts suggests that these scalp N170s arise from underlying neural sources in lateral IOG.

3.3 | Direct correlations of N170 latency and amplitude between scalp and intracerebral recordings

To more formally and directly determine the contribution of intracerebral sources to the N170 measured on the scalp, we quantified the correspondence of the N170 latency and amplitude between scalp and intracerebral recordings using a correlation approach.

First, we correlated the EEG peak *amplitude* during the N/P170 time window (i.e., 140–200 ms) across intracerebral contacts and scalp electrodes (Figure 5a). These analyses confirmed our hypothesis that N170 measured at OT scalp electrodes mainly arises from regions in lateral IOG. The highest and most consistent scalp-intracerebral correlations of EEG amplitude in the N170 window occurred between

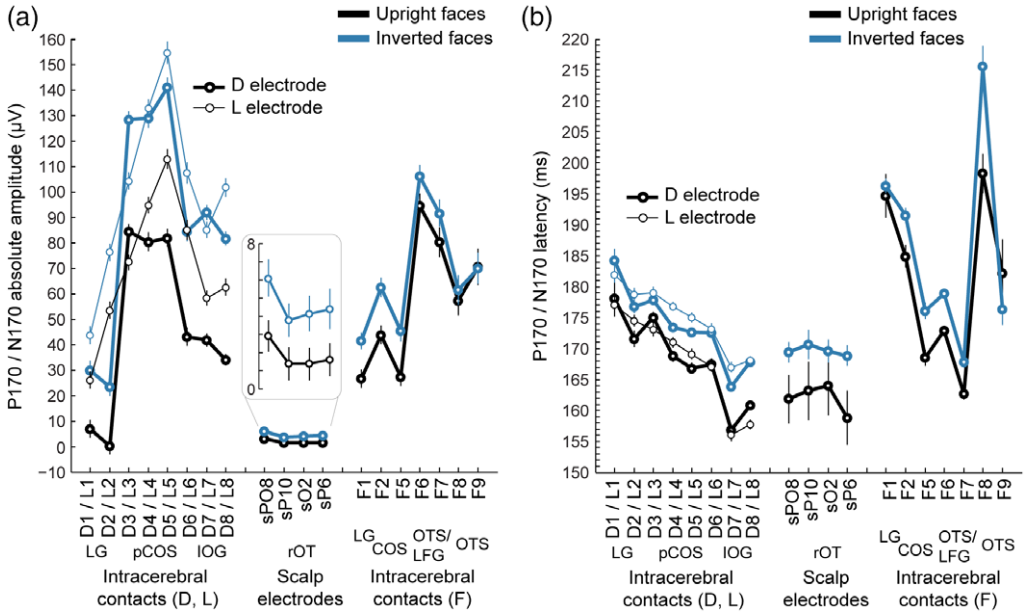

FIGURE 4 Intracerebral and scalp N170 amplitude and latency to upright and inverted faces. (a) The plot shows the absolute value of the peak amplitude of the N170/P170 measured at intracerebral contacts and right occipito-temporal scalp electrodes in response to upright and inverted faces. Error bars are *SE* of the mean. Amplitude at scalp OT channels is also displayed on a secondary scale in the square inset. (b) Same as for panel a but showing N170/P170 peak latency [Color figure can be viewed at wileyonlinelibrary.com]

intracerebral contacts in the lateral IOG (contacts D7-8, L7-8) and scalp electrodes distributed over bilateral OT and posterior parietal regions. Statistics indicate that the N170 amplitude measured at these four intracerebral contacts was significantly ($p < .05$, corrected for multiple comparison) correlated with a broad group of 11 scalp electrodes (mean Pearson's coefficient across 11 electrodes = 0.53 $\pm$ 0.05, range: 0.43–0.64, Figure 5b) for contacts D7-D8, and a group of five scalp electrodes (mean Pearson's coefficient across electrodes = 0.45 $\pm$ 0.03, range: 0.42–0.50, Figure 5b) for contacts L7-L8. When including the five common right OT scalp electrodes (sO2, sP4, sOZ, sP6, and sPO8) across D7-8 and L7-8, correlations were significantly ($t(4) = 15.401$, $p < .001$) higher with intracerebral contacts D7-8 ($r = 0.58 \pm 0.03$) than with contacts L7-8 ($r = 0.45 \pm 0.03$). Across the four intracerebral contacts (i.e., D7-8 and L7-8), correlations were also strongest with right posterior OT scalp regions (sP6, sPO8, sO2, sOZ, and sP4; mean Pearson's *r* coefficient = 0.52 $\pm$ 0.08, Figure 5) and were significantly stronger in scalp channels in the right OT (sP6, sPO8, s02, sP10, and sP4; mean $r = 0.5 \pm 0.09$) compared to left OT (sP5, sPO7, s01, sP9, and sP3; mean $r = 0.38 \pm 0.12$; $t(8) = 2.27$, $p = .027$, one-tailed). Significant correlations of left OT sites with right OT SEEG contacts mostly likely reflect an indirect correlation between the right and left hemispheres, in line with findings of interhemispheric connectivity of OT regions during face processing (Yang, Qiu, & Schouten, 2015). In the present study, these interhemispheric correlations are likely related to the commonality of input, early visual processing stages, and current state of the system when the image appears on the screen. In addition, correlations of 14 bilateral posterior scalp electrodes with intracerebral contacts D7-8 or L7-8 were significantly stronger than with directly adjacent contacts D6 (mean $r = 0.22$; D6 vs. D7-8: $t(13) = 10.2$, $p < .0001$) and L6 (mean $r = 0.13$; L6 vs. L7-8: $t(13) = 8.5$, $p < .0001$). Moreover, and in line with these latter observations, the correlations of N/P170 amplitude between lateral contacts D7-8 and L7-8, as well as between medial contacts D5-6 and L5-6 were much higher (mean r for D7-8/L7-8 = 0.92, mean *r* for D5-6/L5-6 = 0.93) than correlations between lateral and medial contacts (D6-D7: $r = 0.19$; L6-L7: $r = 0.13$). This suggests that the neural sources generating the N170 and P170 in lateral IOG and adjacent posterior CoS (D5 and L5) are mostly independent.

Second, we correlated the EEG peak *latency* during the N/P170 time window across intracerebral and scalp electrodes (Figure 6a). This analysis confirmed that the lateral IOG is a prominent neural source of the N170 measured at right OT scalp electrodes. We observed a specific pattern of positive correlations between contacts D7-8, L7-8, and OT scalp electrodes with a strong right hemispheric dominance. Statistics indicated that N170 peak latency at these four intracerebral contacts were significantly correlated with a cluster of 3 to 6 scalp right OT electrodes (Figure 6b, mean Pearson's coefficient across electrodes = 0.39 $\pm$ 0.04, range: 0.30–0.49). Across 6 right OT scalp electrodes (sP6, sPO8, s02, sOz, sP10, and sP4), Pearson's coefficients were slightly larger for contacts D7-8 (mean *r* across contacts = 0.39; range = 0.3–0.49) than for contacts L7-8 (mean $r = 0.33$; range: 0.25–0.41). In contrast, correlations of the same scalp electrodes with directly adjacent intracerebral contacts D5-6 and L5-6 in the deep part of the IOG and the posterior CoS were around zero (mean $r = 0.02 \pm 0.04$; range: −0.11 to 0.04).

For these contacts in the lateral IOG (i.e., D7-8 and L7-8), correlation coefficients between N170 peak latency were strongest at scalp electrodes in right OT, closest to the location of the corresponding intracerebral contacts (sPO8, sP6, sO2, sP4, sOz, and sP10). Moreover, for all four intracerebral contacts, correlations with posterior scalp electrodes were significantly stronger in the right hemisphere (mean *r* across 4 contacts/6 electrodes = 0.35) compared to the left hemisphere (mean $r = 0.10$; $ps < 0.001$).

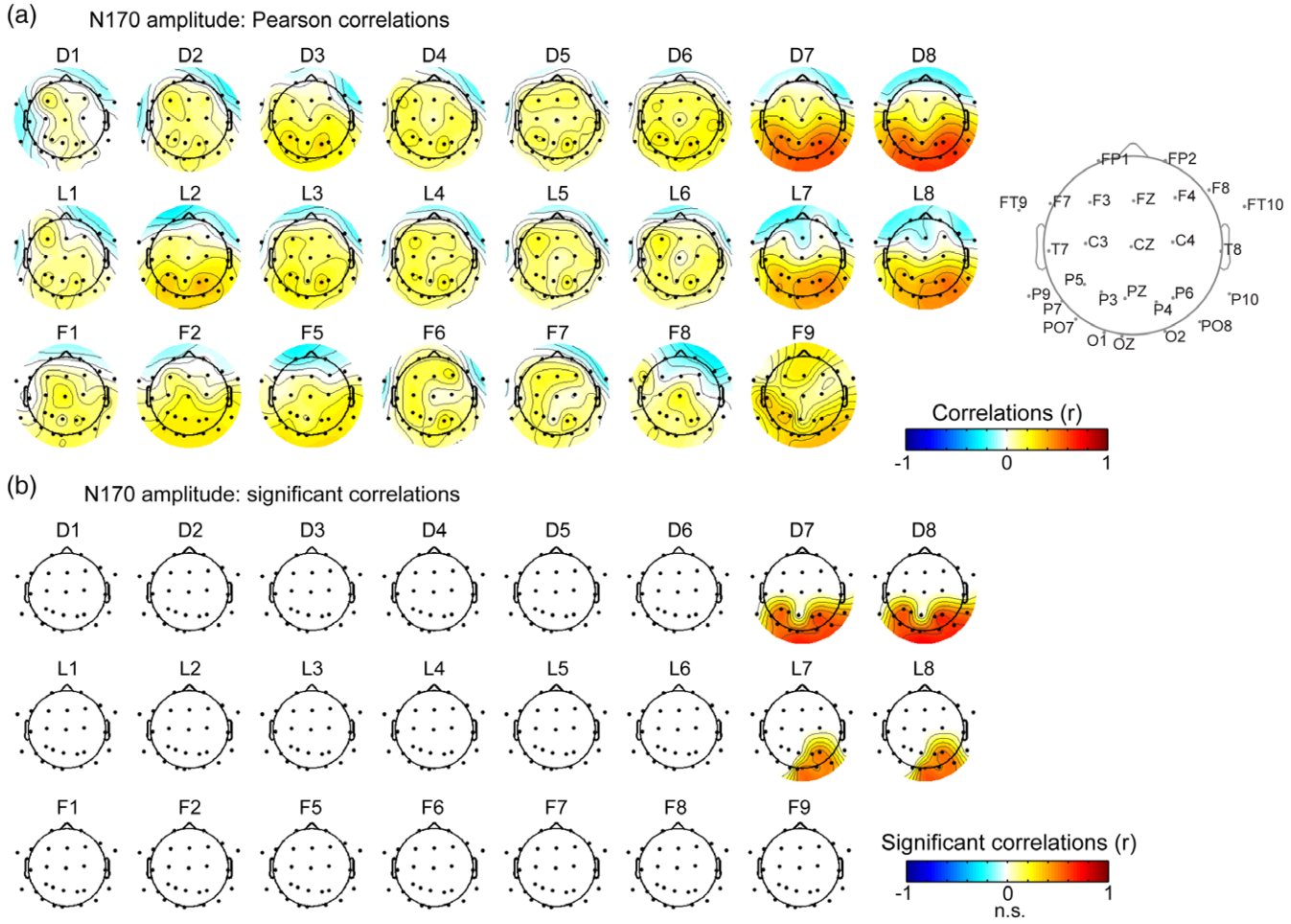

FIGURE 5 Correlations between intracerebral and scalp N170 amplitude to upright faces. (a) Scalp topographical maps (view from above the head) of the unthresholded Pearson correlation coefficients between the peak amplitude in the N170 time window measured at each intracerebral contact and each scalp electrode. Each map represents the correlations of one intracerebral contact with all scalp electrodes. Different intracerebral electrodes (D, L, and F) are shown in rows, and adjacent recording contacts are shown in columns (see Figure 1 for anatomical location of the contacts). Scalp electrodes' labels are shown on the right schematic head plot ("s" in front of the label is omitted for readability). (b) Topographical maps showing only significant correlation coefficients ($p < .05$, corrected for multiple comparisons). White indicates no significant correlation [Color figure can be viewed at wileyonlinelibrary.com]

These N170 latency analyses also revealed that while latency correlations between lateral contacts D7-8 and L7-8, as well as between medial contacts D5-6 and L5-6 were high (mean *r* for D7-8/L7-8 = 0.88, mean *r* for D5-6/L5-6 = 0.92), the N170 latencies were weakly correlated between lateral and medial contacts (D6-D7: $r = 0.3$; L6-L7: $r = 0.16$). Together with the similar observation made for the N/P170 amplitude, these observations support the view that although the N170 measured at the most lateral contacts in IOG (D7-8 and L7-8) and the P170 measured in adjacent contacts have very similar latencies (161 and 170 ms for N170 and P170, respectively, Figure 4), these components reflect the activity of separate neural sources. These analyses suggest again that only the most lateral source(s) (D7-8 and L7-8) contribute to the N170 measured on the scalp.

3.4 | Potential contribution of the LFG to OT scalp N170

The present data set shows that the right lateral IOG largely contributes to the N170 recorded on the scalp. We next examined whether the current data support an additional contribution of the LFG to the scalp OT N170. In KV, two contacts of intracerebral electrode F (F6 and F7) were located just 8 mm above the inferior surface of the LFG (Figure 7). Importantly, these two contacts exhibited a positive component peaking during the N170 time window ("P170"), and which latency was significantly increased by face inversion.

Our data suggest that in the current patient, the LFG does not contribute or contributes minimally to the OT scalp N170. First, we observed no specific correlation between the P170 (latency or amplitude) measured at F6 or F7 and the N170 measured on the scalp OT regions. Second, we rule out that the electrical field generating this P170 is parallel to the main axis of the F electrode (i.e., with a medio-lateral orientation pointing to the lateral OT scalp region) for two reasons: (a) a P170 or N170 of similar morphology as in F6-F7 was not measured at adjacent sites in the OTS (F8-9: negative component of longer duration and later latency) and CoS (F4-5: different morphologies), and (b) there was no significant correlation between N170 latency measured in contacts F6-F7 and adjacent contacts F5 and F8 (mean *r* across pairs of electrodes = -0.1 ± 0.14). This indicates that responses measured in contacts F6-F7 do not arise from an equivalent dipole oriented roughly parallel to the F electrode. Rather, we

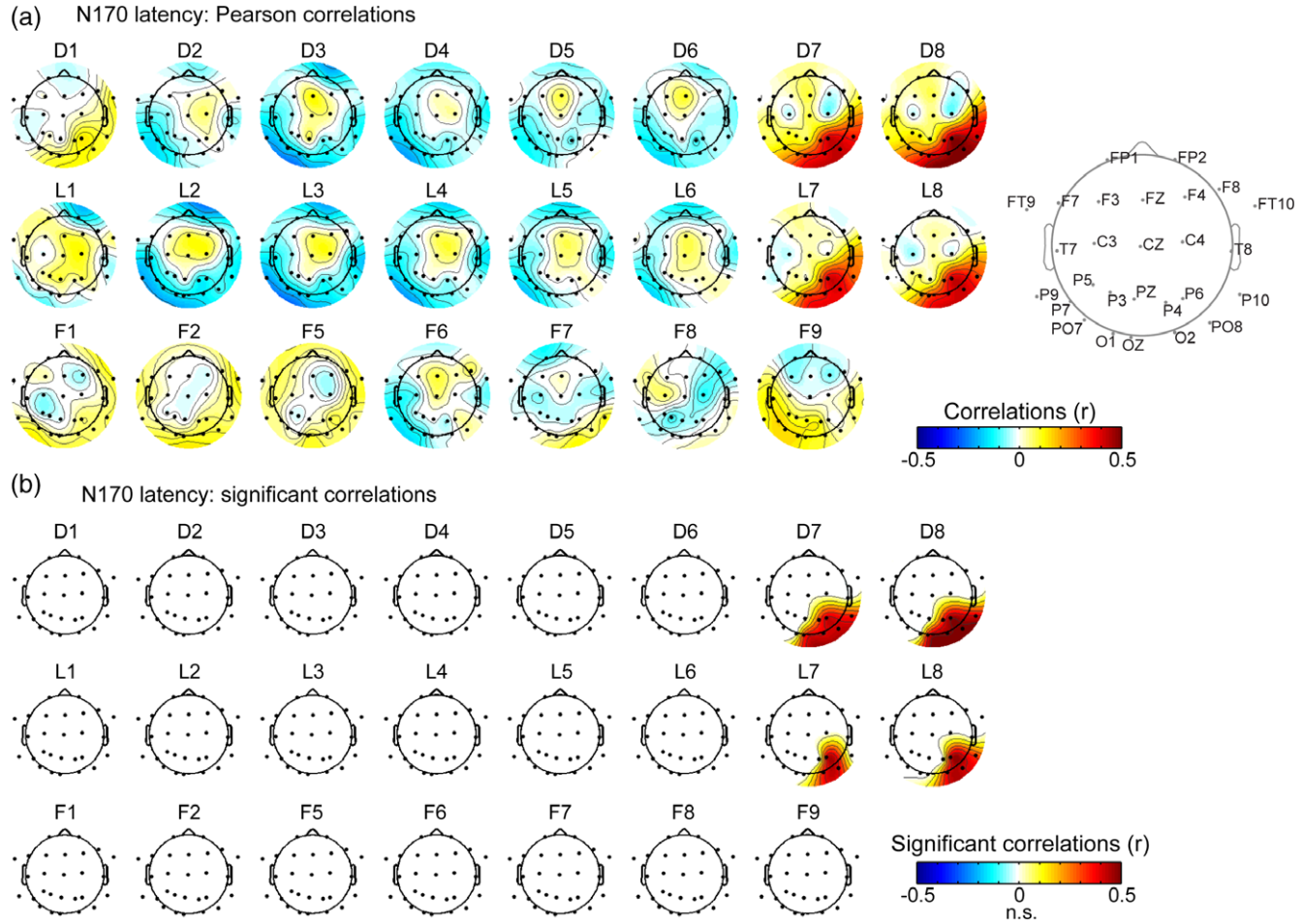

FIGURE 6 Correlations between intracerebral and scalp N170 latency to upright faces. (a) Scalp topographical maps (view from above the head) of the unthresholded Pearson correlation coefficients between the peak latency in the N170 time window measured at each intracerebral contact and each scalp electrode. Each map represents the correlations of one intracerebral contact with all scalp electrodes. Different intracerebral electrodes (D, L, and F) are shown in rows, and adjacent recording contacts are shown in columns (see Figure 1 for anatomical location of the contacts). Scalp electrodes' labels are shown on the right schematic head plot ("s" in front of the label is omitted for readability). (b) Topographical maps showing only significant correlation coefficients ($p < .05$, corrected for multiple comparisons). White indicates no significant correlation [Color figure can be viewed at wileyonlinelibrary.com]

hypothesize that the P170 measured in these contacts is generated from an equivalent dipole in the LFG located just below and oriented along a roughly vertical axis, pointing toward the bottom of the head and not toward the scalp lateral surface.

4 | DISCUSSION

4.1 | Summary and generalizability of our observations

The unique data set reported here points to the lateral section of the right IOG as a major cortical source of the scalp N170, a component evoked by the sudden onset of face stimuli and which has been described in hundreds of studies to characterize the functional properties of human face perception (Rossion & Jacques, 2011 for review) as well as its impairment in various neurological and psychiatric diseases (Feuerriegel, Churches, Hofmann, & Keage, 2015 for review). This conclusion is based on three key observations. First, the large N170 component elicited on recording contacts lying at the cortical surface of the lateral IOG (D8 and L8) or inside the IOG gray matter (D7 and L7) (Figure 1), 3–4 cm away from scalp electrodes over the OT regions where the largest N170 is recorded in the patient and in typical healthy individuals. Second, the functional properties of this intracerebral component, that is, its characteristic negative polarity and peak latency at 170 ms, as well as its large and specific increase in both amplitude and latency for inverted faces, a consistent marker of N170 face specificity reported in tens of scalp recording studies as cited above, as well as in a previous intracranial study (Rosburg et al., 2010). This observation directly contradicts the view that upright and inverted faces are represented in a similar manner in face-selective regions in the IOG (Pitcher et al., 2011; Yovel, 2016). Third, thanks to the original simultaneous scalp recording with a (good) coverage over OT regions, the observation of a striking similarity between the intracerebral and scalp N170s in terms of mean latency and sensitivity to face inversion, as well as across-trial correlations of amplitude and latency.

These observations were possible thanks to a rare case of simultaneous intracerebral–scalp EEG recording where we had both a simultaneous coverage of the lateral IOG and the LFG and a relatively

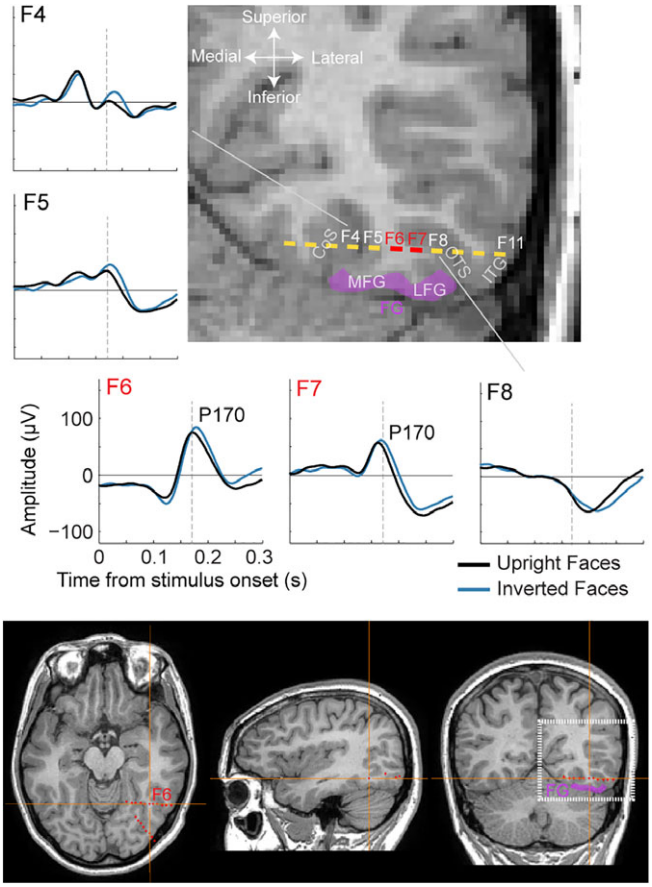

FIGURE 7 A P170 measured above the lateral fusiform gyrus (FG). (a) Averaged ERP responses to upright and inverted faces in five intracerebral contacts of the F electrode (F4–F8), passing from the collateral sulcus to the OTS above the FG. The anatomical location of the contacts from the F electrodes is shown on a coronal slide. Contacts F6 and F7 (highlighted in red), which are at the border of the OTS 8 mm above the inferior surface of the lateral FG show a prominent P170 component. The FG is highlighted in purple color. (b) Location of the F6 intracerebral contact relative to the patient's brain and head (see Figure 1 for additional anatomical details) [Color figure can be viewed at wileyonlinelibrary.com]

dense and even coverage of bilateral OT scalp regions. This scalp coverage over the OT region has been demonstrated to orthogonally project to the IOG (Koessler et al., 2009).

This data set is rare for several reasons. First, simultaneous IOG and LFG electrode implantation are rare, given that occipital lobe epilepsies are a very rare form of drug-refractory focal epilepsies. Second, simultaneous intracerebral and scalp recordings with sufficient scalp coverage are even scarcer because of fear of secondary infection. Third, compared to SEEG used here, ECoG—which has been the more widely used surgical method to record human intracranial electrophysiology—is suboptimal for simultaneous scalp–intracranial recordings. Indeed, the extensive craniotomies involved for placing ECoG grids/strips generally prevent from using high-density recordings and create large discontinuities in the skull which are known to distort the EEG signal on the scalp (e.g., Flemming et al., 2005). Such difficulties are minimized with SEEG (e.g., Dubarry et al., 2014).

Although the observations reported here are described in a single case patient with refractory epilepsy, we argue that they can be generalized to other (healthy) adult brains. Indeed, this patient appears to have a typically (i.e., similar to healthy normal adults) functioning face-selective brain network, as demonstrated by the following observations: this patient has: (a) a typical cortical face network as defined in fMRI (Jonas et al., 2012, 2014), (b) a large and typical scalp N170 with a right hemispheric dominance, (c) a typical N170 FIE (Figure 2), and (d) fully preserved face recognition skills as revealed with neuropsychological tests (see Jonas et al., 2012). Finally, electrical stimulation of the OFA in the right IOG of this patient impaired her ability to recognize familiar famous faces (Jonas et al., 2012) or to discriminate individual unfamiliar faces (Jonas et al., 2014), in line with the observation that acquired prosopagnosia is most frequently associated with brain lesions to this region (Bouvier & Engel, 2006) and can result from focal lesions to this region (Rossion et al., 2003). Yet, additional simultaneous EEG–SEEG measurements in other patients in similar experimental setups and a wide range of cortical geometry and spatial sampling of cortical activity are needed to ensure full generalizability of our observations.

4.2 | The right IOG is a major cortical source of the scalp N170

Overall, this data set provides direct evidence against the claim that only the P1, not the N170 evoked by faces is generated in the right IOG, and that the N170 would rather originate from the middle FG (Duchaine & Yovel, 2015; Pitcher et al., 2011; Sadeh et al., 2010; Yovel, 2016). As noted in Section 1, this serial/hierarchical view for the spatiotemporal organization of the cortical face network is based on the following observations: (a) correlational measures performed between (face-selective) responses on the OT scalp in EEG and in the IOG and FG in fMRI (Horovitz et al., 2004; Sadeh et al., 2010), (b) the early latency of TMS effects applied to the IOG on face processing (Pitcher et al., 2008, 2007), as well as (c) source localization of the N170/M170 mostly in the FG (Deffke et al., 2007; Halgren et al., 2000; Henson et al., 2009; Herrmann et al., 2005; Hoshiyama et al., 2003; Itier et al., 2006; Mnatsakanian & Tarkka, 2004; Pizzagalli et al., 2002; Rossion, Joyce, et al., 2003; Shibata et al., 2002; Watanabe et al., 2003).

Why do our observations fail to align with these previous findings? First, Sadeh et al. (2010) report that the magnitude of fMRI face selectivity in the IOG correlates with OT region EEG face selectivity only during the P1 time window (being significant in a single time-bin at 112 ms after stimulus onset), while fMRI face selectivity in the FG correlates with EEG responses only during the N170 time window (160–180 ms after stimulus onset). One key aspect that may have contributed to differences in findings between Sadeh et al. (2010) and the present study is that Sadeh et al. correlated EEG to fMRI using a metric of face selectivity computed for each subject while we directly correlated the absolute amplitude/latency of the N170. The correlation approach in the present study (i.e., using variability in trials measured simultaneously across channels) prevents from using such a metric (e.g., an index of face inversion) as responses to upright and inverted faces were measured in separate trials. Interestingly, a more recent attempt to correlate simultaneously recorded EEG and fMRI during face processing using raw amplitude rather than face selectivity also failed to find a strong relationship between the amplitude of the

BOLD signal in the FFA and the amplitude of the scalp N170 (Nguyen & Cunnington, 2014). In addition, Sadeh et al. (2010) prevented from having deviant face-selectivity index (i.e., outside [−1 1] range) due to the N170 being sometimes of opposite sign in response to face and nonface stimuli, by subtracting a constant value to the whole sample of N170 amplitude. This procedure can potentially have a strong impact on the face-selectivity index (especially for small N170 amplitudes), and resulting correlation values with small number of data points are unwarranted. Another important difference is that in Sadeh et al. (2010), correlations were performed using across-subjects variability (N = 10), while our study relies on within-subject across-trial variability of the N170 latency and amplitude, a more direct way of assessing the correspondence across these measurements. Finally, Sadeh et al. (2010) investigate the relationship between IOG and scalp-level responses using two very different signals (EEG vs. fMRI) with very different temporal properties, while the present study measured electrophysiological signals of the same nature on the scalp and inside the brain.

A second line of evidence for the serial/hierarchical view of face processing comes from observations that TMS double pulses directed to the OFA impairs performance in different face processing tasks only when these pulses are sent at 60 and 100 ms after face onset, but not when pulses are sent at 20 and 60 ms or 100 and 140 ms (Pitcher et al., 2008, 2007). The authors interpreted these observations as evidence that the OFA processes face information in the time window of the P1 component (typically 80–120 ms), thus before the N170 component. However, the pattern of performance modulation as a function of time in these studies strongly suggest that: (a) the first pulse at 60 ms is insufficient to significantly disrupt face processing (because it is not disrupted in the 20–60 ms pulse condition), and (b) it is the second TMS pulse (sent at 100 ms), adding up to the first pulse, that effectively generates the behavioral impairment. This indicates that the critical time window for disrupting face processes in the OFA is 100–140 ms, when the N170 rises, rather than strictly in the P1 time window. Such an interpretation would in fact be compatible with the current finding that a major source of the scalp N170 lies in the lateral IOG. In addition, this interpretation would also be compatible with the current finding that the N170 in the IOG and P170 above the LFG have very similar latencies (i.e., 160–170 ms, Figure 4), in line with the finding of simultaneous (or even earlier) face-selective response onsets in the FFA compared to the OFA with time-resolved fMRI (Gentile et al., 2017; Jiang et al., 2011, 2015).

Finally, the majority of electromagnetic source imaging studies of scalp EEG or MEG activity report main sources of the N170/M170 around the posterior to anterior FG (Deffke et al., 2007; Henson et al., 2009; Herrmann et al., 2005; Itier et al., 2006; Mnatsakanian & Tarkka, 2004; Rossion, Joyce, et al., 2003; Shibata et al., 2002; Watanabe et al., 2003), although some report main or additional sources in the IOG (Henson et al., 2009; Itier et al., 2006; Rossion, Joyce, et al., 2003) or the posterior STS (Itier & Taylor, 2004; Watanabe et al., 2003). However, the ill-posed nature of the inverse problem and the diversity in source imaging algorithms (see Grech et al., 2008 for a review) make it difficult to draw firm conclusions about the relative involvement of the IOG and FG regions (which are spatially close to each other and are likely to have correlated responses) in generating the scalp N170. Interestingly, numerous intracranial electrophysiological studies have reported face-selective negativities around 170–200 ms (N170 or N200, Allison et al., 1994, 1999; Davidesco et al., 2014; Miller, Schalk, Hermes, Ojemann, & Rao, 2016; Privman et al., 2007; Puce et al., 1999; Rangarajan et al., 2014; Rosburg et al., 2010) from posterior to anterior sections of the FG. However, none of these studies has reported scalp EEG data in order to establish a contribution of these intracranial FG responses to the scalp N170 (but see Rosburg et al., 2010 for simultaneous recording of FG and vertex scalp location). Our current findings of a major contribution of the lateral IOG in generating the scalp N170 are therefore not incompatible with the recording of large N170/N200 responses in the FG. Our findings are, however, directly in line with the few reports of N170 responses in the lateral IOG (Rosburg et al., 2010; Sato et al., 2014), as well as with the observation of a robust increase in the N170 amplitude and latency for inverted relative to upright faces in this region (Rosburg et al., 2010).

We acknowledge that our claim of the IOG as a major source for the scalp N170 seems incompatible with the finding of a preserved face-selective scalp N170 despite completely missing right IOG face-selective region in the brain-lesioned prosopagnosic patient PS (Prieto et al., 2011). However, it is fair to say that, contrary to the current case (Figure 2), PS's N170 showed both an abnormal scalp topography (which is found also for other face-selective responses and is likely to be related to the lesion in PS's skull over the right OT region; see Liu-Shuang, Torfs, & Rossion, 2016; Sorger, Goebel, Schiltz, & Rossion, 2007) and a reduced face-selectivity, suggesting that the IOG is still critical in generating a "normal" N170, in line with the current findings and with other sources of evidence in brain damaged prosopagnosic patients (Dalrymple et al., 2011). Moreover, since the N170 amplitude varies substantially across individuals, one cannot exclude that patient PS's N170 was much larger before her brain damage.

4.3 | Potential contribution of the LFG to the OT scalp N170

Given that we report data from a single patient implanted only with three intracerebral electrode arrays, our finding of the lateral IOG as a major source of the scalp N170 does not rule out the contribution of other cortical sources, including potential sources in or around the LFG. Indeed, it is clear that robust face-selective responses are generated in the LFG, as indicated both with fMRI (e.g., Gao et al., 2018; Kanwisher et al., 1997; Rossion et al., 2012; Weiner & Grill-Spector, 2010) and intracranial electrophysiology (Allison et al., 1994, 1999; Davidesco et al., 2014; Jacques et al., 2016; Jonas et al., 2016; Miller, Hermes, Pestilli, Wig, & Ojemann, 2017; Privman et al., 2007; Rangarajan et al., 2014). Moreover, these electrophysiological face-selective responses often occur between 100 and 200 ms following stimulus onset, with clear peaks at about 160–170 ms. Here, we would like to discuss some of the conditions that determine the potential contribution of the LFG to the scalp OT N170. In light of these, we argue that, in the current patient, the contribution of the LFG is likely minimal.

First, if the LFG strongly contributed to the scalp OT N170, we should have observed a correlation between the P170 amplitude (negative correlation) or latency (positive correlation) measured at F6 or

F7 and the N170 measured on the scalp OT regions. However, we did not observe such correlations. It is fair to say here that the spatial sampling of the LFG in this patient was far from complete. However, although it is possible that our sparse intracerebral sampling of the LFG may have missed the bulk of the face-selective responses in this region, we still measured a clear P170 component with an effect of face inversion at F6 and F7. Moreover, even though, the location of the LFG contacts may not have been optimal and the distance of these contacts from scalp OT electrodes is larger than with contacts in the IOG—likely weakening putative correlations—, we still may have expected a weak correlation between LFG and scalp OT channels.

Second, one should consider the local geometry of the cortical folding in this area, as this determines the orientation of the electrical fields generated in this region relative to the scalp surface. The LFG has the majority of its external cortical surface pointing toward the inferior part of the head (or toward more medial aspects of the head due to the cerebellum under it). In line with Bentin et al.'s (1996) original proposal, we argue that the electrical field (dipole) generating the N200–N170 component on the ventral surface of the LFG is oriented roughly vertically (i.e., perpendicular to the inferior cortical surface), with the negative pole pointing toward the bottom of the head (or the center of the neck when the LFG surface is slightly oblique), which is geometrically incompatible with a strong contribution of the LFG to the OT scalp N170. This hypothesis is supported by current and previous intracranial EEG studies: while SEEG studies using similar intracerebral electrodes as electrode F here, passing over or slightly above the internal/superior surface of the FG, consistently report a positive component (P170, Barbeau et al., 2008; Halgren et al., 1994), ECoG studies with electrodes placed over the external/inferior surface of the FG consistently report a negative component (N170 or N200, e.g., Allison et al., 1994, 1999; Miller et al., 2016; Rangarajan et al., 2014; Rosburg et al., 2010). In the current patient, the finding of a P170 sensitive to face inversion in contacts above the LFG provides original supports for this hypothesis by refuting the possibility that the P170 in LFG contacts is generated by a mediolateral dipole pointing to the lateral OT scalp surface. Indeed, the ERP response in contacts located just medially (in CoS) and laterally (in OTS and ITG) to FG contacts do no exhibit a component with a similar morphology or latency (Figures 3a and 7), suggesting that the P170 in LFG contacts is not generated by a dipole oriented along the mediolateral axis.

Although the argument about cortical geometry of the LFG makes it unlikely for this region to be a major contributor to the scalp OT N170, it does not completely rule out a potential contribution of the medial banks of the mid-fusiform sulcus (MFS) or the OTS around the FG region to the scalp N170. In most individuals, including patient KV of the present study, the FG is subdivided into a medial and lateral section by a small sulcus located along the posterior–anterior axis: the MFS (Weiner et al., 2014). While the (small) cortical surface of the medial bank of the MFS does point toward the lateral scalp OT region, its contribution to the face-sensitive N170 is unlikely. Indeed, the medial and lateral banks of the MFS are part of two distinct cytoarchitectonic structures (FG3 and FG4, respectively, Lorenz et al., 2017), with face-selective responses in the LFG being largely confined to the lateral bank of the MFS. In addition, potential neural sources located in the OTS, laterally to the FG, and generating a horizontal or oblique electrical field, may very well contribute to the N170 measured on OT scalp electrodes (Bentin et al., 1996). Indeed, fMRI face-selective activation in the LFG frequently spreads to the medial bank of the OTS (e.g., Gao et al., 2018; Weiner & Grill-Spector, 2010; Zhen et al., 2015). However, the large difference in peak latency between the scalp N170 (around 160 ms) and the negativity measured in the OTS (F8-F9: 180–200 ms), as well as the absence of a scalp-like N170 component in contacts lateral to the OTS (F10-F11) in the current patient do not bring support for such a contribution.

In the present study, we provide clear evidence for a major contribution of the IOG to the scalp OT N170. However, establishing the nature of the contribution of the FG region to this ERP component needs further exploration. As indicated earlier, we report the data from a single patient with a single intracerebral multicontact electrode passing over the FG, which may have missed other neural sources in the FG. To complement our findings, one approach would be to take advantage of the methodological tools developed here, where future studies would combine high-density scalp recordings and intracerebral recordings at different OT locations in larger groups of patients. A complementary approach would be to rely on forward source modeling, combining detailed modeling of the individual cortical geometry and head, with simulating the activation of distinct face-selective regions in the OT cortex (see Ales, Yates, & Norcia, 2010 for primary visual cortex simulations).

As a final note, while the FG may only minimally contribute to the OT scalp N170, this region may contribute to the face-sensitive VPP measured over the vertex, located above the FG, at the same time window as the N170, the two components sharing functional properties (Jeffreys, 1989, 1996; Joyce & Rossion, 2005). Unfortunately, here, we found no significant correlation between the P170 measured in contacts F6 and F7 and the signal at central scalp electrodes (e.g., Cz, Fz, Figures 5 and 6). However, these scalp electrodes are relatively far from the FG and signal quality at these channels was rather poor. Further studies investigating scalp to intracerebral relationship are needed to determine whether the FG distinctively contributes to the VPP, or if this component which shares functional properties with the N170 despite reduced sensitivity, emerges essentially at this location due to the use of reference electrodes near the OT regions (earlobes or mastoids, see Joyce & Rossion, 2005).

ACKNOWLEDGMENTS

This work was supported by the Belgian Fonds de la Recherche Scientifique (FNRS –PDR T.0207.16), Fédération Wallonie-Bruxelles under Grant No. ARC 13/18–053, and the Louvain Foundation.

ORCID

Corentin Jacques https://orcid.org/0000-0001-8917-4346
Bruno Rossion https://orcid.org/0000-0002-1845-3935

REFERENCES

Ales, J. M., Yates, J. L., & Norcia, A. M. (2010). V1 is not uniquely identified by polarity reversals of responses to upper and lower visual field

stimuli. *NeuroImage*, *52*, 1401–1409. https://doi.org/10.1016/j.neuroimage.2010.05.016

Allison, T., Ginter, H., McCarthy, G., Nobre, A. C., Puce, A., Luby, M., & Spencer, D. D. (1994). Face recognition in human extrastriate cortex. *Journal of Neurophysiology*, *71*, 821–825.

Allison, T., Puce, A., Spencer, D. D., McCarthy, G., & Belger, A. (1999). Electrophysiological studies of human face perception. I: Potential generated in occiptotemporal cortex by face and non-face stimuli. *Cerebral Cortex*, *9*, 415–430.

Barbeau, E. J., Taylor, M. J., Regis, J., Marquis, P., Chauvel, P., & Liégeois-Chauvel, C. (2008). Spatio temporal dynamics of face recognition. *Cerebral Cortex*, *18*, 997–1009. https://doi.org/10.1093/cercor/bhm140

Bentin, S., McCarthy, G., Perez, E., Puce, A., & Allison, T. (1996). Electrophysiological studies of face perception in humans. *Journal of Cognitive Neuroscience*, *8*, 551–565.

Botzel, K., & Grusser, O. J. (1989). Electric brain potentials-evoked by pictures of faces and non-faces – A search for face-specific EEG-potentials. *Experimental Brain Research*, *77*, 349–360.

Botzel, K., Schulze, S., & Stodieck, S. R. G. (1995). Scalp topography and analysis of intracranial sources of face-evoked potentials. *Experimental Brain Research*, *104*, 135–143.

Bouvier, S. E., & Engel, S. A. (2006). Behavioral deficits and cortical damage loci in cerebral achromatopsia. *Cerebral Cortex*, *16*, 183–191.

Calder, A. J., & Young, A. W. (2005). Understanding the recognition of facial identity and facial expression. *Nature Reviews Neuroscience*, *6*, 641–651.

Dalrymple, K. A., Oruç, I., Duchaine, B., Pancaroglu, R., Fox, C. J., Iaria, G., … Barton, J. J. (2011). The anatomic basis of the right face-selective N170 in acquired prosopagnosia: A combined ERP/fMRI study. *Neuropsychologia*, *49*, 2553–2563. https://doi.org/10.1016/j.neuropsychologia.2011.05.003

Davidesco, I., Zion-Golumbic, E., Bickel, S., Harel, M., Groppe, D. M., Keller, C. J., … Malach, R. (2014). Exemplar selectivity reflects perceptual similarities in the human fusiform cortex. *Cerebral Cortex*, *24*, 1879–1893. https://doi.org/10.1093/cercor/bht038

Deffke, I., Sander, T., Heidenreich, J., Sommer, W., Curio, G., Trahms, L., & Lueschow, A. (2007). MEG/EEG sources of the 170-ms response to faces are co-localized in the fusiform gyrus. *NeuroImage*, *35*, 1495–1501.

Dubarry, A., Badier, J., Fonseca, A. T., Gavaret, M., Carron, R., Bartolomei, F., … Bénar, C. G. (2014). Simultaneous recording of MEG, EEG and intracerebral EEG during visual stimulation: From feasibility to single-trial analysis. *NeuroImage*, *99*, 548–558. https://doi.org/10.1016/j.neuroimage.2014.05.055

Duchaine, B., & Yovel, G. (2015). A revised neural framework for face processing. *Annual Review of Vision Science*, *1*, 393–416. https://doi.org/10.1146/annurev-vision-082114-035518

Eimer, M. (2000). Effects of face inversion on the structural encoding and recognition of faces – Evidence from event-related brain potentials. *Cognitive Brain Research*, *10*, 145–158.

Feuerriegel, D., Churches, O., Hofmann, J., & Keage, H. A. D. (2015). The N170 and face perception in psychiatric and neurological disorders: A systematic review. *Clinical Neurophysiology*, *126*, 1141–1158. https://doi.org/10.1016/j.clinph.2014.09.015

Flemming, L., Wang, Y., Caprihan, A., Eiselt, M., Haueisen, J., & Okada, Y. (2005). Evaluation of the distortion of EEG signals caused by a hole in the skull mimicking the fontanel in the skull of human neonates. *Clinical Neurophysiology*, *116*, 1141–1152. https://doi.org/10.1016/j.clinph.2005.01.007

Ganis, G., Smith, D., & Schendan, H. E. (2012). The N170, not the P1, indexes the earliest time for categorical perception of faces, regardless of interstimulus variance. *NeuroImage*, *62*, 1563–1574. https://doi.org/10.1016/j.neuroimage.2012.05.043

Gao, X., Gentile, F., & Rossion, B. (2018). Fast periodic stimulation (FPS): A highly effective approach in fMRI brain mapping. *Brain Structure & Function*, *223*, 2433–2454. https://doi.org/10.1007/s00429-018-1630-4

Gao, Z., Goldstein, A., Harpaz, Y., Hansel, M., Zion-Golumbic, E., & Bentin, S. (2013). A magnetoencephalographic study of face processing: M170, gamma-band oscillations and source localization. *Human Brain Mapping*, *34*, 1783–1795. https://doi.org/10.1002/hbm.22028

Gauthier, I., Tarr, M. J., Moylan, J., Skudlarski, P., Gore, J. C., & Anderson, A. W. (2000). The fusiform "face area" is part of a network that processes faces at the individual level. *Journal of Cognitive Neuroscience*, *12*, 495–504. https://doi.org/10.1162/089892900562165

Gentile, F., Ales, J., & Rossion, B. (2017). Being BOLD: The neural dynamics of face perception. *Human Brain Mapping*, *38*, 120–139. https://doi.org/10.1002/hbm.23348

George, N., Evans, J., Fiori, N., Davidoff, J., & Renault, B. (1996). Brain events related to normal and moderately scrambled faces. *Cognitive Brain Research*, *4*, 65–76.

Grech, R., Cassar, T., Muscat, J., Camilleri, K. P., Fabri, S. G., Zervakis, M., … Vanrumste, B. (2008). Review on solving the inverse problem in EEG source analysis. *Journal of NeuroEngineering and Rehabilitation*, *33*, 1–33. https://doi.org/10.1186/1743-0003-5-25

Grill-Spector, K., Weiner, K. S., Kay, K., & Gomez, J. (2017). The functional neuroanatomy of human face perception. *Annual Review of Vision Science*, *3*, 167–196. https://doi.org/10.1146/annurev-vision-102016-061214

Halgren, E., Baudena, P., Heit, G., Clarke, J. M., Marinkovic, K., Chauvel, P., & Clarke, M. (1994). Spatio-temporal stages in face and word processing. 2. Depth-recorded potentials in the human frontal and Rolandic cortices. *Journal of Physiology*, *Paris*, *88*, 51–80.

Halgren, E., Raij, T., Marinkovic, K., Jousmaki, V., & Hari, R. (2000). Cognitive response profile of the human fusiform face area as determined by MEG. *Cerebral Cortex*, *10*, 69–81.

Haxby, J. V., Hoffman, E. A., & Gobbini, M. I. (2000). The distributed human neural system for face perception. *Trends in Cognitive Sciences*, *4*, 223–233.

Henson, R. N., Mouchlianitis, E., & Friston, K. J. (2009). MEG and EEG data fusion: Simultaneous localisation of face-evoked responses. *NeuroImage*, *47*, 581–589. https://doi.org/10.1016/j.neuroimage.2009.04.063

Herrmann, M. J., Ehlis, A. C., Muehlberger, A., & Fallgatter, A. J. (2005). Source localization of early stages of face processing. *Brain Topography*, *18*, 77–85.

Horovitz, S. G., Rossion, B., Skudlarski, P., & Gore, J. C. (2004). Parametric design and correlational analyses help integrating fMRI and electrophysiological data during face processing. *NeuroImage*, *22*, 1587–1595. https://doi.org/10.1016/j.neuroimage.2004.04.018

Hoshiyama, M., Kakigi, R., Watanabe, S., & Miki, K. (2003). Brain responses for the subconscious recognition of faces. *Neuroscience Research*, *46*, 435–442. https://doi.org/10.1016/S0168-0102(03)00121-4

Itier, R. J., Herdman, A. T., George, N., Cheyne, D., & Taylor, M. J. (2006). Inversion and contrast-reversal effects on face processing assessed by MEG. *Brain Research*, *1115*, 108–120.

Itier, R. J., & Taylor, M. J. (2004). N170 or N1? Spatiotemporal differences between object and face processing using ERPs. *Cerebral Cortex*, *14*, 132–142. https://doi.org/10.1093/cercor/bhg111

Jacques, C., & Rossion, B. (2007). Early electrophysiological responses to multiple face orientations correlate with individual discrimination performance in humans. *NeuroImage*, *36*, 863–876.

Jacques, C., Schiltz, C., & Goffaux, V. (2014). Face perception is tuned to horizontal orientation in the N170 time window. *Journal of Vision*, *14*(2), 5, 1-18. https://doi.org/10.1167/14.2.5

Jacques, C., Witthoft, N., Weiner, K. S., Foster, B. L., Rangarajan, V., Hermes, D., … Grill-Spector, K. (2016). Corresponding ECoG and fMRI category-selective signals in human ventral temporal cortex. *Neuropsychologia*, *83*, 14–28. https://doi.org/10.1016/j.neuropsychologia.2015.07.024

Jeffreys, D. (1989). A face-responsive potential recorded from the human scalp. *Experimental Brain Research*, *78*, 193–202. https://doi.org/10.1007/BF00230699

Jeffreys, D. (1996). Evoked potential studies of face and object processing. *Visual Cognition*, *3*, 1–38.

Jiang, F., Badler, J. B., Righi, G., & Rossion, B. (2015). Category search speeds up face-selective fMRI responses in a non-hierarchical cortical face network. *Cortex*, *66*, 69–80.

Jiang, F., Dricot, L., Weber, J., Righi, G., Tarr, M. J., Goebel, R., & Rossion, B. (2011). Face categorization in visual scenes may start in a higher order area of the right fusiform gyrus: Evidence from dynamic

visual stimulation in neuroimaging. *Journal of Neurophysiology*, *106*, 2720–2736. https://doi.org/10.1152/jn.00672.2010

Jonas, J., Descoins, M., Koessler, L., Colnat-Coulbois, S., Sauvée, M., Guye, M., … Maillard, L. (2012). Focal electrical intracerebral stimulation of a face-sensitive area causes transient prosopagnosia. *Neuroscience*, *222*, 281–288. https://doi.org/10.1016/j.neuroscience.2012.07.021

Jonas, J., Jacques, C., Liu-shuang, J., Brissart, H., Colnat-Coulbois, S., & Maillard, L. (2016). A face-selective ventral occipito-temporal map of the human brain with intracerebral potentials. *Proceedings of the National Academy of Sciences of the United States of America*, *113*, E4088–E4097. https://doi.org/10.1073/pnas.1522033113

Jonas, J., Rossion, B., Krieg, J., Koessler, L., Colnat-Coulbois, S., Vespignani, H., … Maillard, L. (2014). Intracerebral electrical stimulation of a face-selective area in the right inferior occipital cortex impairs individual face discrimination. *NeuroImage*, *99*, 487–497. https://doi.org/10.1016/j.neuroimage.2014.06.017

Joyce, C., & Rossion, B. (2005). The face-sensitive N170 and VPP components manifest the same brain processes: The effect of reference electrode site. *Clinical Neurophysiology*, *116*, 2613–2631.

Kanwisher, N., McDermott, J., & Chun, M. M. (1997). The fusiform face area: A module in human extrastriate cortex specialized for face perception. *The Journal of Neuroscience: The Official Journal of the Society for Neuroscience*, *17*, 4302–4311. https://doi.org/10.1098/Rstb.2006.1934

Koessler, L., Cecchin, T., Colnat-Coulbois, S., Vignal, J.-P., Jonas, J., Vespignani, H., … Maillard, L. G. (2015). Catching the invisible: Mesial temporal source contribution to simultaneous EEG and SEEG recordings. *Brain Topography*, *28*, 5–20. https://doi.org/10.1007/s10548-014-0417-z

Koessler, L., Maillard, L., Benhadid, A., Vignal, J. P., Felblinger, J., Vespignani, H., & Braun, M. (2009). Automated cortical projection of EEG sensors: Anatomical correlation via the international 10 – 10 system. *NeuroImage*, *46*, 64–72. https://doi.org/10.1016/j.neuroimage.2009.02.006

Liu, J., Higuchi, M., Marantz, A., & Kanwisher, N. (2000). The selectivity of the occipitotemporal M170 for faces. *Neuroreport*, *11*, 337–341.

Liu-Shuang, J., Torfs, K., & Rossion, B. (2016). An objective electrophysiological marker of face individualisation impairment in acquired prosopagnosia with fast periodic visual stimulation. *Neuropsychologia*, *83*, 100–113. https://doi.org/10.1016/j.neuropsychologia.2015.08.023

Lorenz, S., Weiner, K. S., Caspers, J., Mohlberg, H., Schleicher, A., Bludau, S., … Amunts, K. (2017). Two new cytoarchitectonic areas on the human mid-fusiform gyrus. *Cerebral Cortex*, *27*, 373–385. https://doi.org/10.1093/cercor/bhv225

McCarthy, G., Puce, A., Belger, A., & Allison, T. (1999). Electrophysiological studies of human face perception. II: Response properties of face-specific potentials generated in occipitotemporal cortex. *Cerebral Cortex*, *9*, 431–444.

Miller, J., Patterson, T. U. I., & Ulrich, R. (1998). Jackknife-based method for measuring LRP onset latency differences. *Psychophysiology*, *35*, 99–115.

Miller, K. J., Hermes, D., Pestilli, F., Wig, G. S., & Ojemann, J. G. (2017). Face percept formation in human ventral temporal cortex. *Journal of Neurophysiology*, *118*, 2614–2627. https://doi.org/10.1152/jn.00113.2017

Miller, K. J., Schalk, G., Hermes, D., Ojemann, J. G., & Rao, R. P. N. (2016). Spontaneous decoding of the timing and content of human object perception from cortical surface recordings reveals complementary information in the event-related potential and broadband spectral change. *PLoS Computational Biology*, *12*, e1004660. https://doi.org/10.1371/journal.pcbi.100, https://doi.org/10.1371/journal.pcbi.1004660

Mnatsakanian, E. V., & Tarkka, I. M. (2004). Familiar-face recognition and comparison: Source analysis of scalp-recorded event-related potentials. *Clinical Neurophysiology*, *115*, 880–886. https://doi.org/10.1016/j.clinph.2003.11.027

Mouraux, A., & Iannetti, G. D. (2008). Across-trial averaging of event-related EEG responses and beyond. *Magnetic Resonance Imaging*, *26*, 1041–1054.

Nguyen, V. T., & Cunnington, R. (2014). The superior temporal sulcus and the N170 during face processing: Single trial analysis of concurrent EEG – fMRI. *NeuroImage*, *86*, 492–502. https://doi.org/10.1016/j.neuroimage.2013.10.047

Nichols, T. E., & Holmes, A. P. (2001). Nonparametric permutation tests for functional neuroimaging experiments: A primer with examples. *Human Brain Mapping*, *15*, 1–25. https://doi.org/10.1002/hbm.1058

Pitcher, D., Garrido, L., Walsh, V., & Duchaine, B. C. (2008). Transcranial magnetic stimulation disrupts the perception and embodiment of facial expressions. *The Journal of Neuroscience*, *28*, 8929–8933. https://doi.org/10.1523/JNEUROSCI.1450-08.2008

Pitcher, D., Walsh, V., & Duchaine, B. (2011). The role of the occipital face area in the cortical face perception network. *Experimental Brain Research*, *209*, 481–493. https://doi.org/10.1007/s00221-011-2579-1

Pitcher, D., Walsh, V., Yovel, G., & Duchaine, B. (2007). TMS evidence for the involvement of the right occipital face area in early face processing. *Current Biology*, *17*, 1568–1573. https://doi.org/10.1016/j.cub.2007.07.063

Pizzagalli, D. a., Lehmann, D., Hendrick, A. M., Regard, M., Pascual-Marqui, R. D., & Davidson, R. J. (2002). Affective judgments of faces modulate early activity (∼160 ms) within the fusiform gyri. *NeuroImage*, *16*, 663–677. https://doi.org/10.1006/nimg.2002.1126

Prieto, E. A., Caharel, S., Henson, R., & Rossion, B. (2011). Early (n170/m170) face-sensitivity despite right lateral occipital brain damage in acquired prosopagnosia. *Frontiers in Human Neuroscience*, *5*, 138. https://doi.org/10.3389/fnhum.2011.00138

Privman, E., Nir, Y., Kramer, U., Kipervasser, S., Andelman, F., Neufeld, M. Y., … Malach, R. (2007). Enhanced category tuning revealed by intracranial electroencephalograms in high-order human visual areas. *The Journal of Neuroscience*, *27*, 6234–6342. https://doi.org/10.1523/JNEUROSCI.4627-06.2007

Puce, A., Allison, T., Bentin, S., Gore, J. C., & McCarthy, G. (1998). Temporal cortex activation in humans viewing eye and mouth movements. *The Journal of Neuroscience*, *18*, 2188–2199.

Puce, A., Allison, T., Gore, J. C., & McCarthy, G. (1995). Face-sensitive regions in human extrastriate cortex studied by functional MRI. *Journal of Neurophysiology*, *74*, 1192–1199.

Puce, A., Allison, T., & McCarthy, G. (1999). Electrophysiological studies of human face perception. III: Effects of top-down processing on face-specific potentials. *Cerebral Cortex*, *9*, 445–458.

Rangarajan, V., Hermes, D., Foster, B. L., Weiner, K. S., Jacques, C., Grill-Spector, K., & Parvizi, J. (2014). Electrical stimulation of the left and right human fusiform gyrus causes different effects in conscious face perception. *The Journal of Neuroscience*, *34*, 12828–12836. https://doi.org/10.1523/JNEUROSCI.0527-14.2014

Rosburg, T., Ludowig, E., Dümpelmann, M., Alba-Ferrara, L., Urbach, H., & Elger, C. E. (2010). The effect of face inversion on intracranial and scalp recordings of event-related potentials. *Psychophysiology*, *47*, 147–157. https://doi.org/10.1111/j.1469-8986.2009.00881.x

Rossion, B. (2014). Understanding face perception by means of human electrophysiology. *Trends in Cognitive Sciences*, *18*, 310–318. https://doi.org/10.1016/j.tics.2014.02.013

Rossion, B., Caldara, R., Seghier, M., Schuller, A. M., Lazeyras, F., & Mayer, E. (2003). A network of occipito-temporal face-sensitive areas besides the right middle fusiform gyrus is necessary for normal face processing. *Brain*, *126*, 2381–2395. https://doi.org/10.1093/brain/awg241

Rossion, B., Delvenne, J. F., Debatisse, D., Goffaux, V., Bruyer, R., Crommelinck, M., & Guérit, J. M. (1999). Spatio-temporal localization of the face inversion effect: An event-related potentials study. *Biological Psychology*, *50*, 173–189.

Rossion, B., Gauthier, I., Tarr, M. J., Despland, P., Bruyer, R., Linotte, S., & Crommelinck, M. (2000). The N170 occipito-temporal component is delayed and enhanced to inverted faces but not to inverted objects: An electrophysiological account of face-specific processes in the human brain. *Neuroreport*, *11*, 69–74.

Rossion, B., Hanseeuw, B., & Dricot, L. (2012). Defining face perception areas in the human brain: A large-scale factorial fMRI face localizer analysis. *Brain and Cognition*, *79*, 138–157. https://doi.org/10.1016/j.bandc.2012.01.001

Rossion, B., & Jacques, C. (2008). Does physical interstimulus variance account for early electrophysiological face sensitive responses in the

human brain? Ten lessons on the N170. *NeuroImage*, *39*, 1959–1979. https://doi.org/10.1016/j.neuroimage.2007.10.011

Rossion, B., & Jacques, C. (2011). The N170: Understanding the time-course of face perception in the human brain. In E. S. Kappenman & S. J. Luck (Eds.), *The Oxford handbook of ERP components* (pp. 115–142). New York, NY: Oxford University Press.

Rossion, B., Joyce, C. A., Cottrell, G. W., & Tarr, M. J. (2003). Early lateralization and orientation tuning for face, word, and object processing in the visual cortex. *NeuroImage*, *20*, 1609–1624. https://doi.org/10.1016/j.neuroimage.2003.07.010

Rousselet, G., Husk, J. S., Bennett, P. J., & Sekuler, A. B. (2008). Time course and robustness of ERP object and face differences. *Journal of Vision*, *8*(12), 3, 1–18. https://doi.org/10.1167/8.12.3

Rousselet, G. A., Mace, M. J. M., & Fabre-Thorpe, M. (2004). Animal and human faces in natural scenes: How specific to human faces is the N170 ERP component? *Journal of Vision*, *4*, 13–21.

Sadeh, B., Podlipsky, I., Zhdanov, A., & Yovel, G. (2010). Event-related potential and functional MRI measures of face-selectivity are highly correlated: A simultaneous ERP-fMRI investigation. *Human Brain Mapping*, *31*, 1490–1501. https://doi.org/10.1002/hbm.20952

Sadeh, B., & Yovel, G. (2010). Why is the N170 enhanced for inverted faces? An ERP competition experiment. *NeuroImage*, *53*, 782–789. https://doi.org/10.1016/j.neuroimage.2010.06.029

Salado, A. L., Koessler, L., De Mijolla, G., Schmitt, E., Vignal, J.-P., Civit, T., … Colnat-Coulbois, S. (2018). sEEG is a safe procedure for a comprehensive anatomic exploration of the insula: A retrospective study of 108 procedures representing 254 transopercular insular electrodes. *Operative Neurosurgery*, *14*, 1–8. https://doi.org/10.1093/ons/opx106

Sato, W., Kochiyama, T., Uono, S., Matsuda, K., Usui, K., Inoue, Y., & Toichi, M. (2014). Rapid, high-frequency, and theta-coupled gamma oscillations in the inferior occipital gyrus during face processing. *Cortex*, *60*, 1–17. https://doi.org/10.1016/j.cortex.2014.02.024

Seeck, M., Koessler, L., Bast, T., Leijten, F., Michel, C., Baumgartner, C., … Beniczky, S. (2017). The standardized EEG electrode array of the IFCN. *Clinical Neurophysiology*, *128*, 2070–2077. https://doi.org/10.1016/j.clinph.2017.06.254

Sergent, J., Ohta, S., & Macdonald, B. (1992). Functional neuroanatomy of face and object processing – A positron emission tomography study. *Brain*, *115*, 15–36.

Shibata, T., Nishijo, H., Tamura, R., Miyamoto, K., Eifuku, S., Endo, S., & Ono, T. (2002). Generators of visual evoked potentials for faces and eyes in the human brain as determined by dipole localization. *Brain Topography*, *15*, 51–63.

Sorger, B., Goebel, R., Schiltz, C., & Rossion, B. (2007). Understanding the functional neuroanatomy of acquired prosopagnosia. *NeuroImage*, *35*, 836–852.

Srebro, R. (1985). Localization of visually evoked cortical activity in humans. *Journal of Physiology*, *360*, 233–246.

Swithenby, S. J., Bailey, A. J., Brautigam, S., Josephs, O. E., Jousmaki, V., & Tesche, C. D. (1998). Neural processing of human faces: A magnetoencephalographic study. *Experimental Brain Research*, *118*, 501–510.

Talairach, J., & Bancaud, J. (1973). Stereotaxic approach to epilepsy. Methodology of anatomo-functional stereotaxic investigations. *Progress in Neurological Surgery*, *5*, 297–354. https://doi.org/https://doi.org/10.1159/000394343

Tanskanen, T., Nasanen, R., Montez, T., Paallysaho, J., & Hari, R. (2005). Face recognition and cortical responses show similar sensitivity to noise spatial frequency. *Cerebral Cortex*, *15*, 526–534.

Watanabe, S., Kakigi, R., & Puce, A. (2003). The spatiotemporal dynamics of the face inversion effect: A magneto- and electro-encephalographic study. *Neuroscience*, *116*, 879–895.

Weiner, K. S., Golarai, G., Caspers, J., Chuapoco, M. R., Mohlberg, H., Zilles, K., … Grill-Spector, K. (2014). The mid-fusiform sulcus: A landmark identifying both cytoarchitectonic and functional divisions of human ventral temporal cortex. *NeuroImage*, *84*, 453–465. https://doi.org/10.1016/j.neuroimage.2013.08.068

Weiner, K. S., & Grill-Spector, K. (2010). Sparsely-distributed organization of face and limb activations in human ventral temporal cortex. *NeuroImage*, *52*, 1559–1573. https://doi.org/10.1016/j.neuroimage.2010.04.262

Yang, Y., Qiu, Y., & Schouten, A. C. (2015). Dynamic functional brain connectivity for face perception. *Frontiers in Human Neuroscience*, *9*, 662. https://doi.org/10.3389/fnhum.2015.00662

Yovel, G. (2016). Neural and cognitive face-selective markers: An integrative review. *Neuropsychologia*, *83*, 5–13. https://doi.org/10.1016/j.neuropsychologia.2015.09.026

Zhen, Z., Yang, Z., Huang, L., Kong, X., Wang, X., Dang, X., … Liu, J. (2015). Quantifying interindividual variability and asymmetry of face-selective regions: A probabilistic functional atlas. *NeuroImage*, *113*, 13–25. https://doi.org/https://doi.org/10.1016/j.neuroimage.2015.03.010

How to cite this article: Jacques C, Jonas J, Maillard L, Colnat-Coulbois S, Koessler L, Rossion B. The inferior occipital gyrus is a major cortical source of the face-evoked N170: Evidence from simultaneous scalp and intracerebral human recordings. *Hum Brain Mapp*. 2019;40:1403–1418. https://doi.org/10.1002/hbm.24455

PLOS BIOLOGY

RESEARCH ARTICLE

Neurophysiological evidence for crossmodal (face-name) person-identity representation in the human left ventral temporal cortex

Angélique Volfart[1,2], **Jacques Jonas**[1,3], **Louis Maillard**[1,3], **Sophie Colnat-Coulbois**[1,4], **Bruno Rossion**[1,2,3]*

1 Université de Lorraine, CNRS, CRAN, Nancy, France, **2** Université Catholique de Louvain, Institute of Research in Psychological Science, Institute of Neuroscience, Louvain-La-Neuve, Belgium, **3** Université de Lorraine, CHRU-Nancy, Service de Neurologie, Nancy, France, **4** Université de Lorraine, CHRU-Nancy, Service de Neurochirurgie, Nancy, France

* bruno.rossion@univ-lorraine.fr

OPEN ACCESS

Citation: Volfart A, Jonas J, Maillard L, Colnat-Coulbois S, Rossion B (2020) Neurophysiological evidence for crossmodal (face-name) person-identity representation in the human left ventral temporal cortex. PLoS Biol 18(4): e3000659. https://doi.org/10.1371/journal.pbio.3000659

Academic Editor: Winrich A. Freiwald, The Rockefeller University, UNITED STATES

Received: August 2, 2019

Accepted: March 9, 2020

Published: April 3, 2020

Peer Review History: PLOS recognizes the benefits of transparency in the peer review process; therefore, we enable the publication of all of the content of peer review and author responses alongside final, published articles. The editorial history of this article is available here: https://doi.org/10.1371/journal.pbio.3000659

Data Availability Statement: All EEG and SEEG data, together with a readme text file explaining the structure of the data, are available on a Dryad

Abstract

Putting a name to a face is a highly common activity in our daily life that greatly enriches social interactions. Although this specific person–identity association becomes automatic with learning, it remains difficult and can easily be disrupted in normal circumstances or neurological conditions. To shed light on the neural basis of this important and yet poorly understood association between different input modalities in the human brain, we designed a crossmodal frequency-tagging paradigm coupled to brain activity recording via scalp and intracerebral electroencephalography. In Experiment 1, 12 participants were presented with variable pictures of faces and written names of a single famous identity at a 4-Hz frequency rate while performing an orthogonal task. Every 7 items, another famous identity appeared, either as a face or a name. Robust electrophysiological responses were found exactly at the frequency of identity change (i.e., 4 Hz / 7 = 0.571 Hz), suggesting a crossmodal neural response to person identity. In Experiment 2 with twenty participants, two control conditions with periodic changes of identity for faces or names only were added to estimate the contribution of unimodal neural activity to the putative crossmodal face-name responses. About 30% of the response occurring at the frequency of crossmodal identity change over the left occipito-temporal cortex could not be accounted for by the linear sum of unimodal responses. Finally, intracerebral recordings in the left ventral anterior temporal lobe (ATL) in 7 epileptic patients tested with this paradigm revealed a small number of "pure" crossmodal responses, i.e., with no response to changes of identity for faces or names only. Altogether, these observations provide evidence for integration of verbal and nonverbal person identity-specific information in the human brain, highlighting the contribution of the left ventral ATL in the automatic retrieval of face-name identity associations.

repository: https://doi.org/10.5061/dryad.m8t391m.

Funding: This study was supported by a LUE grant (http://lue.univ-lorraine.fr/en) and an FNRS/FWO grant (HUMVISCAT), grant no. 30991544 (https://www.frs-fnrs.be/fr/financements/credits-et-projets/eos). AV was supported by a grant of the Université de Lorraine (MENESR doctoral grant). The funders had no role in study design, data collection and analysis, decision to publish, or preparation of the manuscript.

Competing interests: The authors have declared that no competing interests exist.

Abbreviations: antCoS, anterior segment of the collateral sulcus; antFG, anterior fusiform gyrus; antMTG/ITG, anterior part of the inferior and middle temporal gyri; antOTS, anterior segment of the occipito-temporal sulcus; antPHG, anterior segment of the parahippocampal gyrus; ATL, anterior temporal lobe; CMS, common mode sense; DRL, driven right leg; EEG, electroencephalography; EOG, electrooculogram; FFT, fast Fourier transform; fMRI, functional magnetic resonance imaging; FPVS, fast periodic visual stimulation; LOT, left occipito-temporal region of interest; RT, response time; SD, semantic dementia; MTL, medial temporal lobe; PTL, posterior temporal lobe; ROI, region of interest; ROT, right occipito-temporal region of interest; SEEG, stereo electroencephalography; SSVEP, steady-state visual evoked potential; TMS, transcranial magnetic stimulation; VOTC, ventral occipito-temporal cortex.

Introduction

Putting a name to a familiar face is a highly common activity in our daily life, which greatly enriches social interactions. For neurotypical adult individuals, this association is often automatic—i.e., names are retrieved even without the intention to do so—and yet quite difficult: often, someone's name cannot be remembered, or can take a few seconds to be evoked from one's face [1–3]. These difficulties increase with ageing, with people being often concerned with a reduced ability to retrieve specific names associated with familiar faces [4–7]. An inability to accurately put a name on a face is particularly salient in patients with Alzheimer disease [8,9], semantic dementia (SD) [10,11], or traumatic brain injury [12,13].

Many studies have described brain-damaged patients with an impaired ability to retrieve a name from a person's face with a preserved ability to provide semantic information about the person (e.g., the person's profession) [14–19]. The reverse pattern of impairment, i.e., impaired access to semantic information with preserved naming of a face, has not been described, to our knowledge. These findings have been interpreted within cognitive models of person recognition, in which person-related semantic representations act as a gateway to name retrieval [20–23].

The neural basis of face-name association remains largely unknown. Rare studies performed in epileptic patients with depth electrodes implanted in the medial temporal lobe (MTL) have revealed single neurons firing selectively to a famous person identity irrespective of the presentation format (e.g., Jennifer Aniston's face and her written name) [24]. However, while these neurons have been defined as "concept cells", they are thought to play a role in creation of associations and recollection of (recent or recently refreshed) conscious episodic memory events rather than supporting long-term semantic associations [25].

At the system level of brain organization, two opposite views can be advanced. On the one hand, verbal and nonverbal person-specific information may be processed separately in the left and right anterior temporal lobe (ATL), respectively, and integrated through re-entrant interhemispheric connections [26,27]. This proposal relies on the consistent observation that the left and right cerebral hemispheres contribute differently to the processing of names and faces, respectively. In neuroimaging, familiar faces activate most strongly the right occipito-temporal cortex, whereas written proper names preferentially activate the left hemisphere [28–32]. Consistent with these studies, group studies of SD patients have shown that the recognition of famous names is relatively more affected by a left anterior temporal atrophy, while famous face recognition deficits are relatively more affected by a right anterior temporal atrophy [11,33,34]. Neuropsychological single-case studies of patients with anterior temporal atrophy [35–38] or focal anterior temporal damage [39] have also found evidence for graded hemispheric dissociations within person-related recognition abilities, i.e., relative differential impairments in accessing person-related information from faces or names depending on the hemispheric side of the lesion. Moreover, the lack of crossmodal adaptation effects to sequences of faces and names with the same identity in functional magnetic resonance imaging (fMRI) [40] has reinforced this view of two separate processing pathways for faces and names in the human brain.

On the other hand, other authors have proposed a semantic "hub" in the bilateral ATLs, integrating modality-specific representations into a shared amodal/transmodal representation [41–45]. This theory was first grounded in the observation of SD patients whose progressive bilateral ATL atrophy has been systematically associated with a severe multimodal semantic impairment [46–48]. According to this view, modality-specific person-related representations stored in different parts of the brain ("spokes") are integrated into a common individual representation in the ATL (hub). Within this bilateral semantic network, between-hemisphere

differences are relative rather than absolute and can be interpreted as a consequence of the differential connectivity with other regions such as language areas and the left hemisphere [49,50]. This "hub-and-spoke" model of semantic processing in the human brain has been supported by a wealth of evidence ranging from clinical observations [41,46,48,51], functional neuroimaging [45,52–55], transcranial magnetic stimulation (TMS) [56,57], and computational simulations [41,58]. Regarding the specific association of familiar faces and names, which is only a subcomponent of person semantics, the hub-and-spoke model predicts modality-specific representations of a person's identity ("spokes"), in addition to an integrated multimodal representation in the bilateral ATL. Supporting this view, neuroimaging studies have provided evidence that the recognition of famous faces and names activates the same regions in the bilateral temporal lobes [28,45,59,60], with potential re-entrant interactions to the cortical face network leading to priming effects between faces and names of the same identity [61,62]. However, the lateralization of these common person-related representations appears inconsistent across studies, i.e., being either unilateral [28,60] or bilateral [45,59,63], possibly because these studies have often used explicit naming tasks, which involve different components of language processing and are thus strongly left lateralized. Most importantly, irrespective of the hemispheric lateralization issue, to our knowledge, no direct evidence has been provided so far for an integrated neural representation of faces and names at the level of a specific person identity. That is, beyond evidence for neural populations responding to both faces and names in addition to unimodal responses, what is critically lacking at present is experimental evidence for neural integration of a specific face and a name identity into a common, i.e., crossmodal, representation.

To provide evidence for such a crossmodal neural representation of person identity, we developed an original crossmodal frequency-tagging paradigm coupled to brain activity recording via both scalp and intracerebral electroencephalography (EEG). Our approach is based on the early observation that the brain's electroencephalographic activity synchronizes exactly with the temporal frequency of a periodic visual stimulus (e.g., a flickering light at 17 Hz generates an EEG response at 17 Hz) [64]. These digitally captured periodic EEG responses, often named steady-state visual evoked potentials (SSVEPs), can be expressed in the frequency domain through Fourier transform [65,66]. Compared to standard recordings of event-related potentials, this approach has substantial advantages in terms of sensitivity (high signal-to-noise ratio) and objectivity (i.e., the response occurs at a frequency predefined by the experimenter and can be quantified easily) [67]. Over the last decade, this "frequency-tagging" or "fast periodic visual stimulation" (FPVS) approach in human EEG has been successfully extended to study higher-level visual functions, in particular using periodic "oddball" stimulation to measure face [68,69] and written words [70] categorization. The term "SSVEP" is not used here because it refers to the type of response obtained rather than the approach, and is a loaded term, with different researchers having different views on what is and what is not a SSVEP (as opposed to a transient event-related potential) [71]. The term "frequency-tagging" is more appropriate, although often used in the context of spatially distinct stimuli flickering at different frequencies [67,72], and this is why the term "FPVS" is preferred here.

Based on these principles and observations, in the present study, we performed a first experiment in which variable pictures of faces and written names of a single famous identity were presented at 4 Hz (i.e., 250-ms stimulus onset asynchrony) while recording brain activity in healthy volunteers with scalp EEG. At every stimulation cycle, either a picture or a name of that same ("base") identity appeared, with the items selected randomly in a large pool of variable pictures and names (Fig 1). Hence, compared to previous studies, the FPVS approach is extended here to a multimodal (i.e., faces and written names) stimulation. Importantly, participants in the study did not have to explicitly associate the names and faces, only perform an

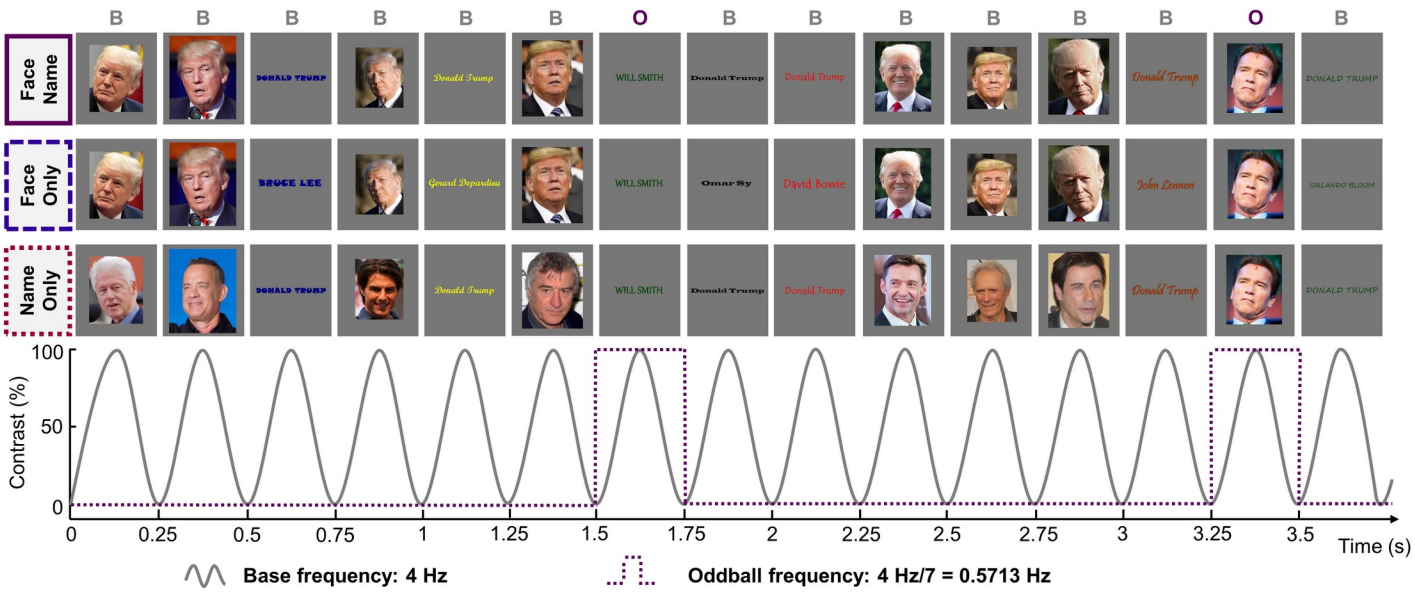

Fig 1. Design of Experiments 1 and 2. Example of a sequence with the identity D. Trump as base stimuli. Experiment 1 included the condition Face Name only (top row), with four famous identities as frequent stimuli. Experiment 2 used two famous identities, but included all 3 conditions: Face Name, Face Only, and Name Only. Visual stimuli (names and faces) are presented at a frequency of 4 Hz with a sinusoidal contrast modulation, and an identity change occurs every seven stimuli (every 0.571 Hz = 4 Hz / 7). For viewing purpose, faces and names are showed at the same position for the three conditions, but the actual order of stimuli was randomized. In Experiment 1, name stimuli were only uppercase and written in more conventional fonts (e.g., Arial, Agency, etc.) than those displayed in the figure. In Experiment 2, name stimuli could be either uppercase or lowercase and were written in less conventional fonts to increase the variability among the stimuli and reduce the potential reliance of the response on low-level visual confounds. Note that face images shown here are not the exact same images as in original paradigms but equivalent images with copyright agreements (CC-BY licenses). Sources (by order of appearance in the figure, left to right, top to bottom) are as follows: https://flic.kr/p/2bnDkJ6; https://flic.kr/p/Mj9V9J; https://flic.kr/p/MBK3za; https://flic.kr/p/MBK4u6; https://flic.kr/p/PeJVCb; https://flic.kr/p/PeJX47; https://flic.kr/p/PeJXHy; https://flic.kr/p/aHvjQc; https://flic.kr/p/NeRpv8; https://flic.kr/p/Ms12cD; https://flic.kr/p/8kTTLh; https://flic.kr/p/7Ybc2J; https://flic.kr/p/DwpstN; https://flic.kr/p/mAWhLD; https://flic.kr/p/nxmqZi.

https://doi.org/10.1371/journal.pbio.3000659.g001

unrelated orthogonal task throughout the stimulation. Every seven items, a different famous identity appeared, either as a face or as a name. If the face and name of the famous base identity are automatically associated during this stimulation sequence, then the occurrence of a different identity among the flow of same-identity stimuli should disrupt this association. Critically, a population of neurons sensitive to person identity from both modalities (written names and face pictures) should therefore adapt/habituate at every stimulation cycle when the given identity is repeated, irrespective of the change of stimulation format and (most importantly) stimulation modality. In this case, identity-oddball responses should emerge in the EEG whether faces or names interrupt this repetition at the periodic "identity-oddball" rate (Fig 1, top row). Consequently, if faces and names of a given identity are automatically integrated into a common crossmodal semantic representation, an electrophysiological identity-oddball response should appear in the EEG spectrum exactly at the frequency of person identity change (4 Hz / 7 = 0.571 Hz), even without any explicit face- or name-related task from our participants.

In a second experiment, having established the presence of neural responses reflecting the putative integration of identity-related faces and names, we ensured that these responses were not due to the mere sum of independent populations of neurons showing identity-oddball responses because of the statistical regularity of the modal identity-oddball response (i.e., a population of face-selective neurons responding to identity-oddball faces falling more often every 7 stimuli than any other regularity in the sequence; e.g., for faces: f1-n1-n1-f1-f1-n1-*f2*-f1-n1-f1-n1-n1-f1-*f3*-n1-n1, etc.). To do that, we added two control conditions to the Face

Name condition (FN), investigating the potential contribution of modality-specific processes to the face-name association response (Fig 1). In the Face Only condition (FO), names of the base identity were replaced by other famous names in order to isolate unimodal face responses that potentially contribute to the neural response observed in the Face Name condition. In the Name Only condition (NO), face images of the base identity were replaced by other famous faces, isolating unimodal name responses potentially contributing to the face-name response. Importantly, a different famous face or name identity was always presented every 7 items in all conditions, and pictures of faces and written names appeared as frequently in all conditions. However, in the two control conditions, automatic association of faces and names of a specific identity was not possible.

Two alternative hypotheses were considered: (1) If face-name association results from the conjoint activation of separated brain regions containing modality-specific person-related representation ("face" regions and "name" regions), then electrophysiological activity in the Face Name condition should not differ from the sum of the electrophysiological responses in the Face Only and Name Only conditions (additive processing; FN = FO + NO). (2) If, on the contrary, a face-name association also emerges from regions coding shared person-related representations, then the electrophysiological response in the Face Name condition should be greater than the sum of the activities in the two control conditions (integrative processing; FN > FO + NO). Given the above debate, the lateralization of the putative specific crossmodal response evoked in the Face Name condition was also of high interest.

Finally, we had the rare opportunity to test this paradigm in seven epileptic patients implanted in the left ventral ATL with depth electrodes (stereo electroencephalography or SEEG), in order to search more directly for local integrated face-name representations, i.e., face-name association responses without modality-specific responses.

Results

As for materials and methods, this section will be divided into three parts: Experiment 1, Experiment 2a in scalp EEG, and Experiment 2b in intracerebral EEG. Our first hypothesis was that face and name representations of the famous base identity are automatically integrated during the Face Name sequence. Therefore, we should observe electrophysiological oddball responses at the frequency of person identity change (4 Hz / 7, i.e., 0.571 Hz) and its harmonics.

Experiment 1

Face-name responses. Consistent with our hypothesis and despite randomly mixing faces and written names (Fig 1), we found clear responses at the frequency of person identity change (4 Hz / 7, i.e., 0.571 Hz and its harmonics). When considering the average of activity across the whole scalp, we found significant oddball responses at harmonics 3, 4, 5, and 6 (1.714 Hz, 2.285 Hz, 2.857 Hz, and 3.428 Hz; $p < 0.01$ for the third harmonic, $p < 0.05$ for the fourth harmonic, and $p < 0.001$ for the fifth and sixth harmonics).

Face-name responses were found over bilateral low occipito-temporal sites, below electrodes PO7 and PO8 (Fig 2). According to this topographical distribution, we defined two bilateral symmetrical occipito-temporal regions of interest (ROIs): electrodes P9, PO9, and PO11 for the left hemisphere (= left occipito-temporal [LOT]); P10, PO10, and PO12 for the right hemisphere (= right occipito-temporal [ROT]); and the middle occipital ROI lying in between (Oz, OIz and Iz), and where responses to the base rate were prominent (Fig 3). When considering only responses on pooled electrodes in the left and right ROIs (average of

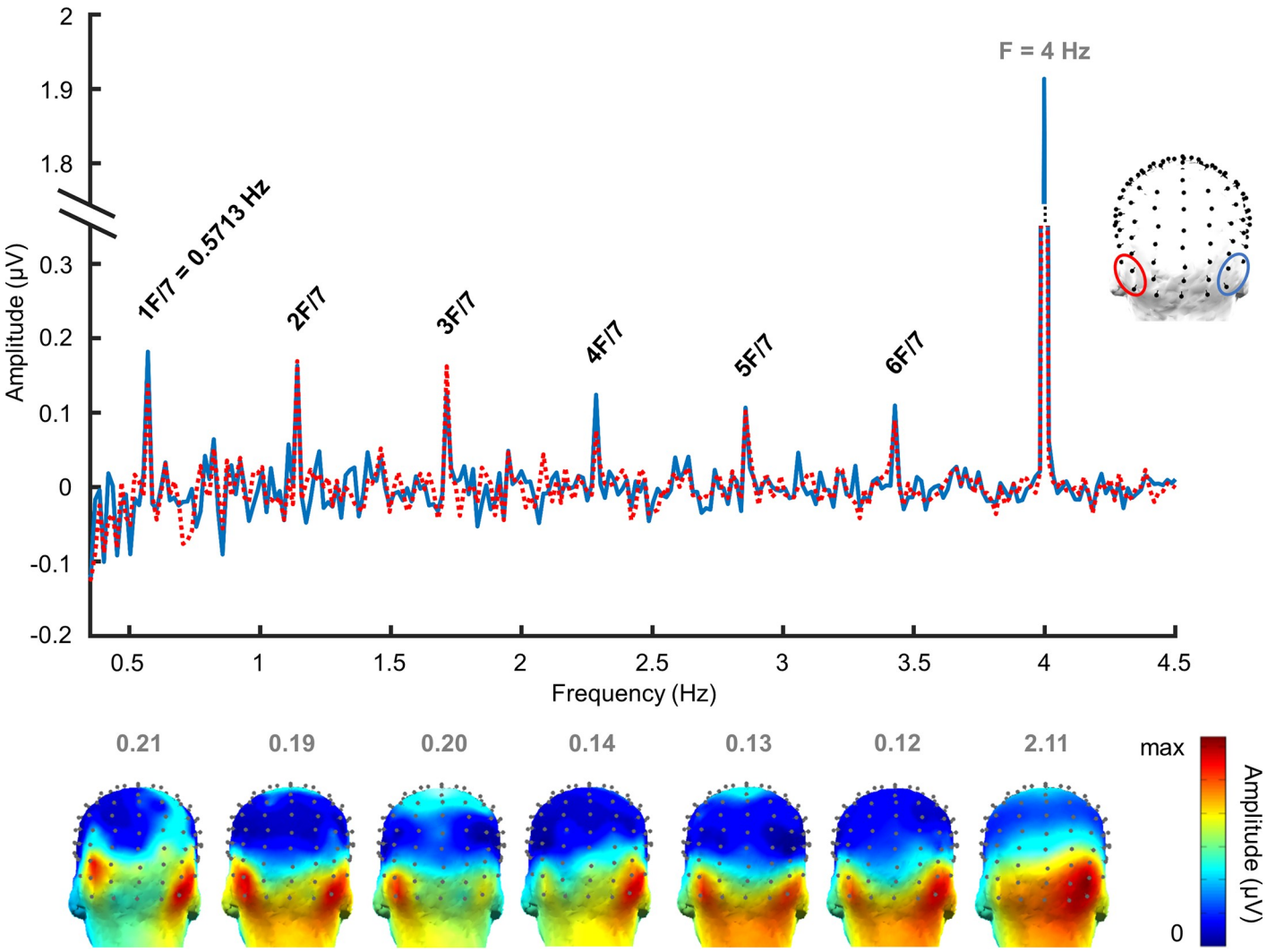

Fig 2. FFT spectrum of EEG responses in Experiment 1. The baseline-corrected FFT spectrum (in μV) in the left and right ROIs (mean amplitude of pooled electrodes) is presented (grand-averaged data, $n = 12$ participants). The location of the ROIs is indicated by the topographical head on the right of the EEG spectrum. Black labels on the FFT spectrum refer to identity-oddball frequencies. All identity-oddball harmonics are significant at $p < 0.05$. The light gray label indicates the base frequency. Below the spectrum, 3D topographical distribution maps of responses are displayed for each identity-oddball harmonic and for the base frequency. Color scales' maxima are shown above each map and indicate the maximal baseline-corrected amplitude in μV at each harmonic of interest. Data underlying this figure are deposited on a Dryad repository: https://doi.org/10.5061/dryad.m8t391m. EEG, electroencephalography; FFT, fast Fourier transform; ROI, region of interest.

https://doi.org/10.1371/journal.pbio.3000659.g002

responses on the 3 electrodes in each ROI), all identity-oddball harmonics were significant in both hemispheres ($p < 0.05$) (Fig 2).

To quantify the periodic response related to person identity change, we computed the sum of six oddball harmonics (0.571 Hz, 1.714 Hz, 2.285 Hz, and so forth) regardless of base identity. We found a significant difference in baseline-corrected amplitudes (μV) between the three ROIs ($F(2,22) = 13.87$, $p = 0.0001$, $d = 2.26$). Whereas no difference was found between face-name responses in the LOT and ROT regions (1.09 μV ± 0.48 and 1.12 μV ± 0.49, respectively; $p = 1$), the amplitude of responses in the middle ROI (0.654 μV ± 0.40) was significantly lower than in occipito-temporal ROIs ($p = 0.0003$ for the difference with the ROT; $p = 0.008$ with the LOT). This effect was not due to variations of the noise level between the middle

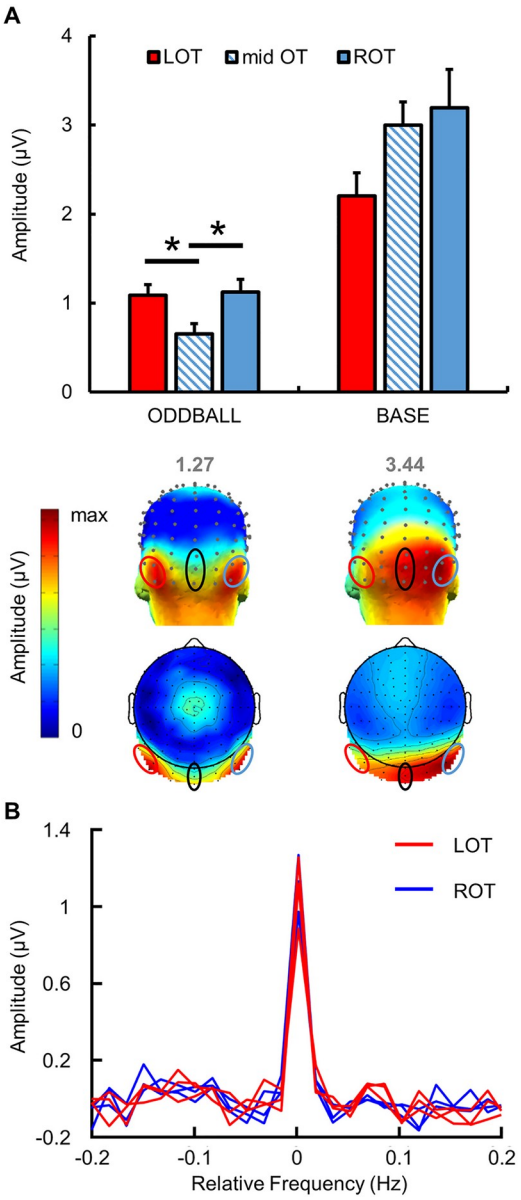

Fig 3. Quantification and scalp topography of EEG responses in Experiment 1. (A) Mean identity-oddball and base responses in μV (baseline-corrected amplitude) at the sum of 6 harmonics for the three ROIs (3 electrodes each) (grand-averaged data, $n = 12$ participants). Error bars indicate standard error of the mean, reflecting variability across participants. Asterisks indicate significant differences with a p-value < 0.05. Below, 3D and 2D topographies of oddball and base responses at the group level. Color scales' maxima are shown above each map, corresponding to the maximal baseline-corrected amplitude value. (B) Chunked segmentation centered on the oddball frequency and summed across six harmonics, with LOT channels in red and ROT channels in blue. Data underlying this figure are deposited on a Dryad repository: https://doi.org/10.5061/dryad.m8t391m. LOT, left occipito-temporal; mid OT, middle occipito-temporal; ROT, right occipito-temporal.

https://doi.org/10.1371/journal.pbio.3000659.g003

occipital ROI and the lateral ROIs: the standard deviation of the noise (standard deviation of amplitudes in the bins surrounding the identity-oddball frequency, i.e., 22 bins) at the electrodes of each ROI was not different between the lateral (left and right) ROIs and the middle occipital ROI ($F(2,6) = 0.935$, $p = 0.443$) (S1 Fig).

Overall, these results confirm the predominance of bilateral occipito-temporal responses at the frequencies of interest when considering the whole group (Fig 3A and 3B).

Impressively, at the individual level, significant responses were found in 100% of participants for the sum of harmonics across all electrodes of the bilateral ROIs and across identities (Z-score range across subjects = 2.59–11.60; all p-values < 0.01) (S2 Fig).

Base frequency responses. A general visual response was expected at 4 Hz, frequency of the base stimulation, thought to reflect general visual synchronization processes. Consistently, there were clear significant base responses ($p < 0.001$) up to the sixth base harmonic (6F = 23.994 Hz) when considering the average of all electrodes. The topographical scalp distribution of base frequency responses showed an overall distribution over the right middle occipital region (Fig 3A).

To quantify base stimulation responses, we computed the sum of the first six base harmonics and contrasted baseline-corrected amplitudes (in μV) in each ROI. A significant difference was found between ROIs ($F(2,22) = 4.92$, $p = 0.017$, $d = 1.34$). Post hoc analysis showed a trend towards statistical difference between the LOT (2.20 μV ± 0.26) and middle ROI (2.99 μV ± 0.26) ($p = 0.059$) and between the LOT and the ROT (3.19 μV ± 0.43) ($p = 0.065$) but no difference between the middle ROI and the ROT ($p = 1$).

Experiment 2a (scalp EEG)

Experiment 1 showed a robust (face-name) oddball response over occipito-temporal sites when a change of identity occurred in the sequence, irrespective of the presentation modality of the base rate and oddball stimuli (i.e., an amodal oddball response). However, we cannot fully exclude that an oddball is generated due to the statistical irregularity in a single modality only, in different populations of neurons coding for facial identity of names and faces separately. If this is the case, the oddball response identified in Experiment 1 should merely be equal to the sum of the two modality-specific violations. Hence, in Experiment 2, we sought to replicate the results of Experiment 1 in the Face Name condition, and added two control conditions (Face Only and Name Only, Fig 1) to be able to determine whether face-name association responses were due to a genuine integrative process (i.e., FN > FO + NO). In this case, we sought to quantify the specific contribution of the integrated response to the overall identity-oddball response. Twenty participants were presented with these three conditions.

First, results in scalp EEG were grand-averaged across subjects, conditions and electrodes to determine the range of significant harmonic frequencies. The first six oddball harmonics (0.571 Hz, 1.714 Hz, and so forth; $p < 0.001$ for the second to the sixth harmonic) and the first nine consecutive base harmonics (4 Hz, 7.998 Hz, and so forth; all p-values < 0.001) were taken into consideration for further analyses.

Comparison between Face Name and control conditions. Grand-averaged data across subjects and electrodes were considered separately for the three conditions. In the Face Name condition, clear oddball responses were found at the second, third, fourth, fifth, and sixth harmonics ($p < 0.05$ for the second harmonic; p-values < 0.001 for the third to fifth harmonics; $p < 0.01$ for the sixth harmonic). In the Face Only condition, only the fifth and sixth oddball harmonics reached significance (respectively, $p < 0.01$ and $p < 0.05$), while in the Name Only condition, no oddball harmonic reached significance. These results show a greater proportion of significant oddball harmonic responses in the Face Name condition relative to the control conditions. Consistently, a significant difference was found between the three conditions at the sum of harmonics ($\chi^2(2) = 10.80$, $p = 0.005$, $d = 2.17$). Post hoc tests demonstrated a larger amplitude at the sum of oddball frequencies in the Face Name condition (0.32 μV ± 0.25) compared to Face Only (0.12 μV ± 0.10, $p = 0.003$) and Name Only (0.09 μV ± 0.13, $p = 0.002$) conditions. No significant difference was found between Face Only and Name Only conditions ($p = 0.39$).

As in Experiment 1, the Face Name condition elicited strong bilateral occipito-temporal responses. The topographical distribution of control conditions was different in that Face Only responses appeared to be strongly right lateralized, while Name Only responses exhibited a bilateral occipito-temporal activation (Fig 4A and 4B). According to these scalp topographies and considering that there was no significant response in the middle occipital ROI of Experiment 1, two bilateral occipito-temporal ROIs were defined: I1, POI1, PO11, PO9 and P9 for the left hemisphere (= LOT); and I2, POI2, PO12, PO10 and P10 for the right hemisphere (= ROT).

When considering only responses on pooled electrodes in the left and right ROIs (average of responses on the 5 electrodes in each ROI), the first to sixth oddball harmonics were significant in both hemispheres (all p-values < 0.001 except the first harmonic in both ROIs, $p < 0.01$) in the Face Name condition. In the Face Only condition, the second to sixth oddball harmonics were significant in both hemispheres (all p-values < 0.001 except the second harmonic in the left ROI, $p < 0.05$). In the Name Only condition, the third to sixth harmonics were significant in both hemispheres (all p-values < 0.05) (S3 Fig).

To quantify the periodic response, baseline-corrected amplitudes at the sum of harmonics were analysed by regions of interest. A two-way ANOVA with repeated measures showed a main effect of condition ($F(2,38) = 5.996$, $p < 0.001$, $d = 2.27$) but no main effect of ROIs ($F(1,19) = 1.026$, $p = 0.324$, $d = 0.46$). Post hoc tests showed significantly larger amplitudes in the Face Name condition compared to the Face Only and Name Only conditions ($p < 0.001$ for both comparisons) but no significant difference between the two control conditions ($p = 0.935$). A significant interaction was also found between ROIs and conditions ($F(2,38) = 3.533$, $p = 0.039$, $d = 0.86$), and post hoc tests showed a significant difference between the left and right ROIs in the Face Only condition ($p = 0.028$) but not in the two other conditions (p-values > 0.05).

These results replicated the findings of Experiment 1, with a bilateral occipito-temporal distribution of person identity responses, and highlighted a strong right lateralization of oddball responses in the Face Only condition. Moreover, the level of noise recorded on the electrodes of the two ROIs did not differ in all 3 conditions (p-value range = 0.30 to 0.98; S1 Fig).

Comparison between Face Name condition and the sum of Face Only and Name Only. Following our hypotheses on the neural organization of face-name association processes, we asked whether the response observed in the Face Name condition could result from the mere addition of the responses in Face Only and Name Only conditions. To answer this question, the uncorrected-baseline amplitudes of the two control conditions were summed at the sum of oddball harmonics across electrodes and then corrected (sum FO + NO). The topography of the sum (FO + NO) appeared to be right lateralized, compared to the bilateral distribution of face-name responses (Fig 5A). However, no significant difference was found between the ROIs at the sum (FO + NO) ($t = -1.208$, $p = 0.242$, $d = -0.294$) (no difference in noise level between left and right ROIs: $p = 0.135$). To highlight the difference in electrophysiological responses between Face Name and the sum (FO + NO), we also subtracted uncorrected-baseline amplitudes of the sum from uncorrected-baseline amplitudes of the Face Name condition [FN–(FO + NO)] and applied a baseline correction. This subtraction showed a left-lateralized selective response for the Face Name condition (Fig 5A).

To quantify this response, corrected-baseline amplitudes of the sum (FO + NO) were compared with amplitudes of the Face Name condition (Fig 5B). A two-way ANOVA with repeated measures showed a main effect of condition ($F(1,19) = 5.003$, $p = 0.037$, $d = 1.02$), revealing a greater amplitude of the effect at the oddball-identity frequency in the Face Name condition compared to the sum (FO + NO). There was no main effect of ROIs ($F(1,19) = 1.031$, $p = 0.323$, $d = 0.46$) and no interaction effect between ROIs and conditions ($F(1,19) = 1.247$, $p = 0.278$, $d = 0.51$). Further analyses (paired t tests) showed that the

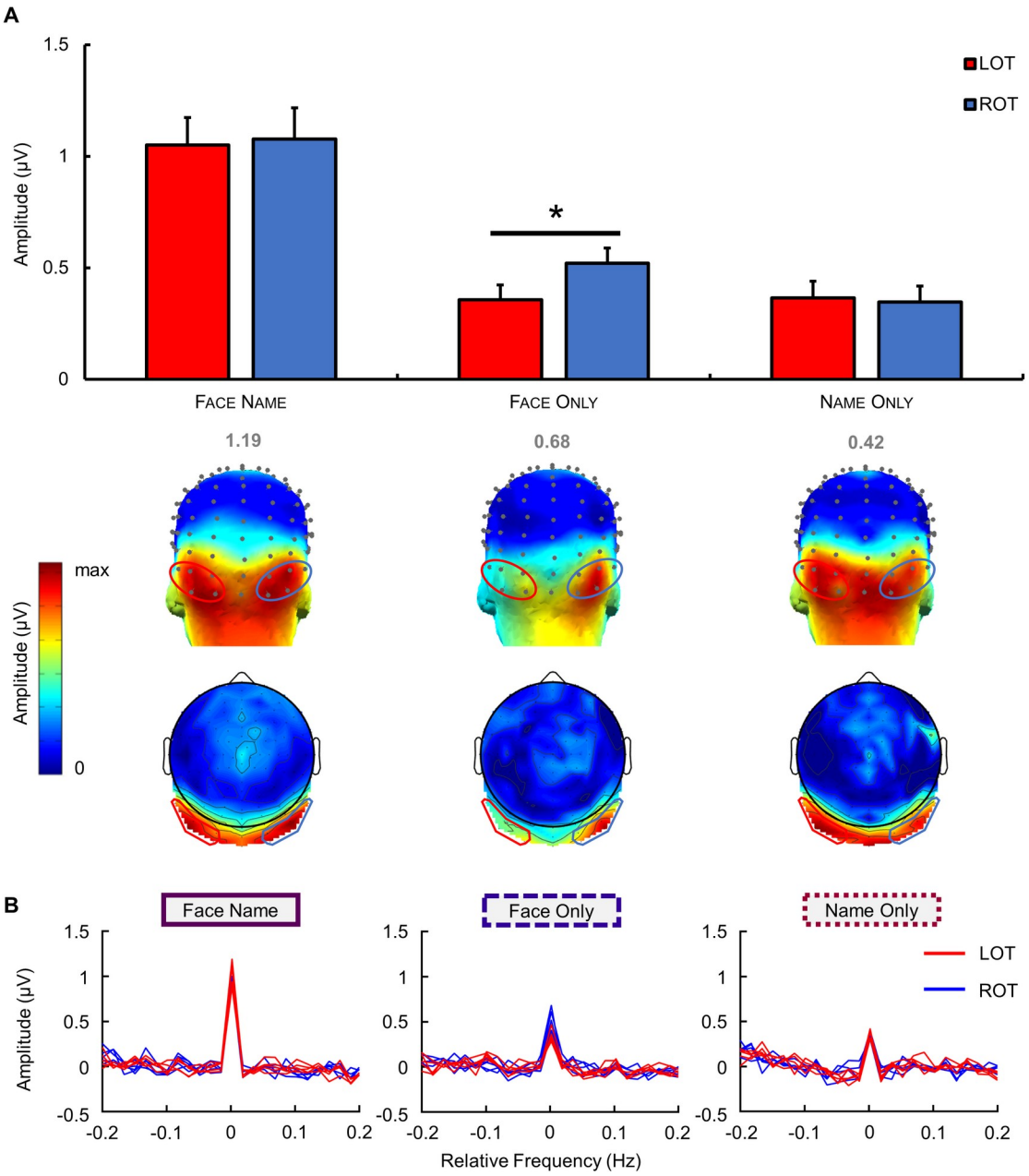

Fig 4. Quantification and scalp topography of EEG responses in each condition of Experiment 2. (A) Mean group-level identity-oddball responses in baseline-corrected amplitude (μV) at the two bilateral ROIs (shown with red and blue ovals on the topographical head to indicate the left and right ROI, respectively) regardless of identity. Error bars indicate standard error from the mean, reflecting variability across participants. Below, 3D and 2D topography maps show the distribution of oddball-identity responses at the sum of oddball harmonics for each condition at the group level (grand-averaged data, $n = 20$ participants). Color scales' maxima are shown above each map, corresponding to the maximal baseline-corrected amplitude in μV. Asterisks indicate significant differences with a p-value < 0.05. (B) Chunked baseline-corrected amplitude spectrum for each condition at the sum of the six oddball harmonics at the group level. The middle of the chunked segment represents the oddball response over the sum of harmonics. LOT channels are represented in red; ROT channels are in blue. Data underlying this figure are deposited on a Dryad repository: https://doi.org/10.5061/dryad.m8t391m. EEG, electroencephalography; LOT, left occipito-temporal; ROI, region of interest; ROT, right occipito-temporal.

https://doi.org/10.1371/journal.pbio.3000659.g004

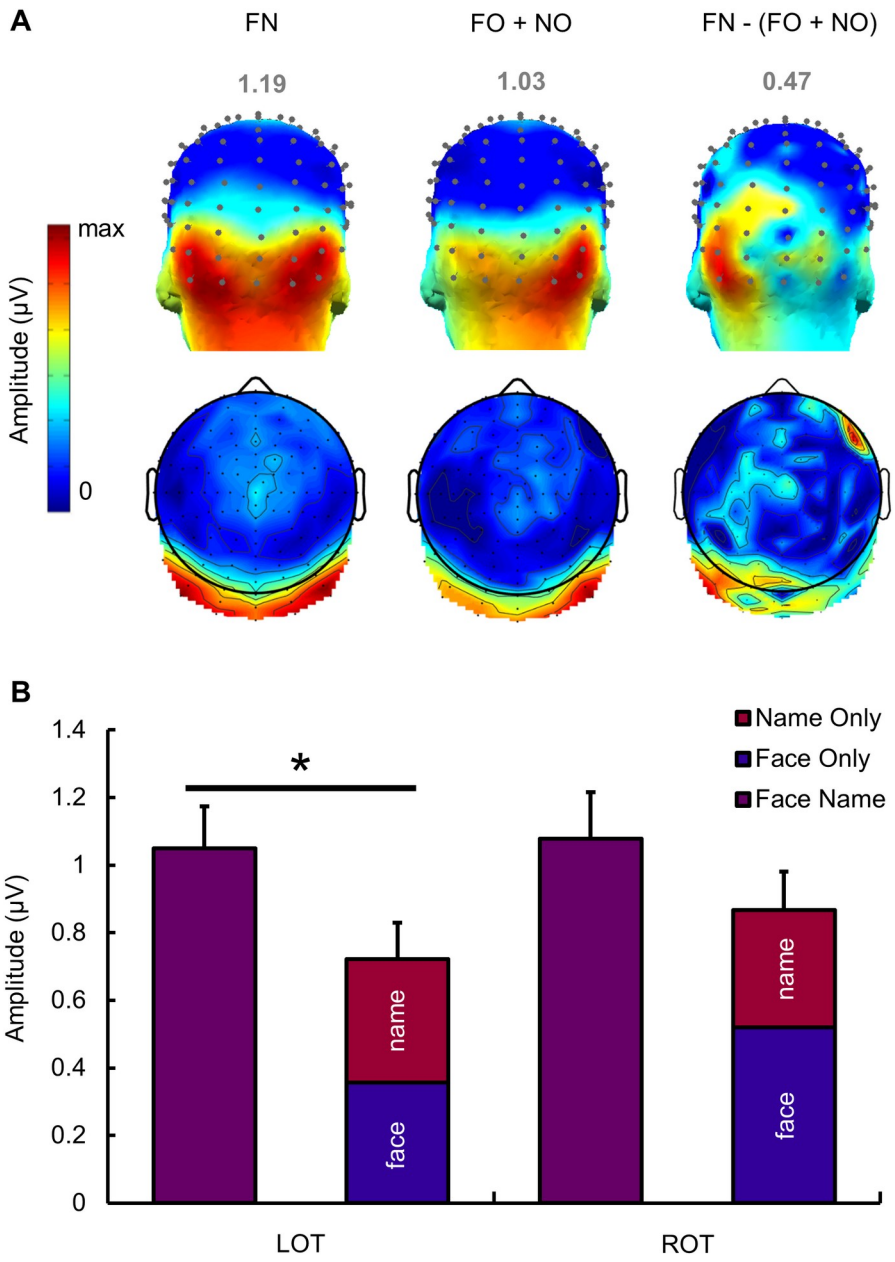

Fig 5. Comparison of responses between the 3 conditions of Experiment 2 in scalp EEG. (A) Three-dimensional (3D) and 2D group-level scalp topographies at the sum of identity-oddball harmonics (baseline-corrected amplitudes in μV) for the Face Name condition, the sum of Face Only and Name Only, and the subtraction of the responses at the sum of control conditions from the response at the Face Name condition. Color scales' maxima are shown above each map and correspond to the maximal amplitude for each condition. Although there is a small area responding at the frequency of interest over the right frontal region in the [FN − (FO + NO)] comparison, it is important to mention that this response is driven by one electrode only (electrode F6), while other electrodes nearby do not show any significant response. (B) Mean baseline-corrected amplitudes in μV at the sum of identity-oddball harmonics for the Face Name condition and the sum of the two control conditions Face Only and Name Only. Error bars indicate standard error from the mean. The asterisk indicates a significant difference at $p < 0.05$. Data underlying this figure are deposited on a Dryad repository: https://doi.org/10.5061/dryad.m8t391m. EEG, electroencephalography; FN, Face Name; FO, Face Only; NO, Name Only.

https://doi.org/10.1371/journal.pbio.3000659.g005

difference between the amplitude of the Face Name condition and the amplitude of the sum (FO + NO) was significant in the LOT ($t = 2.726$, $p = 0.013$) but not in the ROT ($t = 1.509$, $p = 0.148$). It is interesting to note that the amplitude of the response for the sum of control conditions (FO + NO) represented only 68% of the amplitude of the *Face Name* response in the left ROI, while it represented a greater extent (80%) of the Face Name response in the right ROI. That is, thanks to the straightforward quantification of the EEG response afforded by the FPVS approach, we were able to determine that about a third (32%) of the total Face Name response in the left hemisphere and a fifth (20%) of the total Face Name response in the right hemisphere was not explained by the sum of modality-specific representations elicited by control conditions.

Base frequency responses. As in Experiment 1, a general visual response was expected at 4 Hz. Consistently, clear base responses were found in each condition. In the Face Name condition, the first to fifth base harmonics were highly significant (p-values < 0.001). In the Face Only condition, base responses were clearly visible up to the ninth base harmonic (9F = 35.991 Hz; p-values < 0.001). In the Name Only condition, the first to eighth base harmonics were statistically significant (p-values < 0.001, except for the sixth base harmonic: $p < 0.01$).

To quantify base EEG responses, we compared the baseline-corrected amplitudes (in μV) in the three main conditions at the sum of 9 base harmonics across all electrodes. A significant difference was found between conditions ($F(1.386,26.340) = 8.561$, $p = 0.004$). Post hoc tests showed a larger amplitude of the base response in the Face Only condition (1.39 μV ± 0.42) relative to the two other conditions (Face Name: 1.23 μV ± 0.42; Name Only: 1.26 μV ± 0.36; respectively, $p = 0.003$ and $p = 0.0002$).

We also contrasted baseline-corrected amplitudes (in μV) in each ROI for base responses in the 3 conditions. We found a significant effect of ROIs ($F(1,19) = 8.498$, $p = 0.009$, $d = 1.34$), showing a predominance of the response in the right hemisphere. There was also a significant effect of condition ($F(2,38) = 14.325$, $p < 0.001$, $d = 1.74$). Post hoc tests showed that the amplitude at the base frequency in the Face Only condition was greater than in the two other conditions (all p-values < 0.001), but there was no difference between the amplitude at the base frequency in the Face Name and the Name Only conditions ($p = 1$). There was no interaction effect between conditions and ROIs ($F(2,38) = 0.883$, $p = 0.422$, $d = 0.43$). These results suggest that the response at the base frequency was right lateralized, in line with the results of Experiment 1. Accordingly, the topographical scalp distribution of base frequency responses in Experiment 2 showed an overall distribution over the right middle occipital region (S4 Fig).

Experiment 2b (intracerebral EEG)

Seven patients with refractory partial epilepsy were implanted with intracranial electrodes for clinical purposes and were tested with Experiment 2 (three conditions). Across 196 contacts implanted in the gray matter of the left ventral ATL (i.e., located anteriorly to the posterior tip of the hippocampus), we found 7 contacts showing significant responses at the frequency of person identity change (0.571 Hz) in at least one condition in 4 participants. The responses recorded on these 7 contacts and their anatomical locations in the individual anatomy are shown in S5 Fig (see also S6 Fig for their location in the Talairach space). One contact was found significant in the Name Only condition but not in the other Face Name and Face Only conditions (Talairach coordinates: $x = -66$, $y = -14$, $z = -19$; TM'11 in participant 5, located in the anterior part of the inferior and middle temporal gyri [antMTG/ITG]). One contact was found significant in both the Face Name and the Name Only conditions ($x = -39$, $y = -18$, $z = -16$; TM'4 in participant 5, located in the anterior fusiform gyrus [antFG]). Importantly, a

total of 5 contacts were found to elicit a significant response in the Face Name condition but no response in the two control conditions. However, for two of these contacts, the response was not significantly larger in the Face Name condition than when computing the sum of the responses in the other conditions [FN–(FO + NO)] ($z < 1.65$). These two contacts were respectively located in the antFG ($x = -42$, $y = -17$, $z = -16$; TM'5 in participant 5) and anterior segment of the occipito-temporal sulcus (antOTS; $x = -30$, $y = -15$, $z = -27$; TM'2 in participant 6).

Strikingly, three of these 5 contacts showed a "pure" face-name association response, i.e., a significant response in Face Name, no significant response in Face Only and Name Only, and a significant difference between Face Name and the sum (FO + NO). The responses recorded on these three contacts and their anatomical locations are shown in Fig 6 (see S6 Fig for their location in the Talairach space). They were located in a restricted anatomical region in the antFG ($x = -37$, $y = -7$, $z = -27$; TM'1 in participant 2) or its adjacent sulci (anterior segment of the collateral sulcus [antCoS], $x = -33$, $y = -33$, $z = -23$; TB'4 in participant 1; antOTS, $x = -34$, $y = -15$, $z = -25$; TM'3 in participant 6). It is important to note that these results were independent of the number of sequences viewed by the participants. Among the three participants showing pure responses in the Face Name condition, only one (participant 1) was tested twice (total of 12 sequences), while the two other participants were tested only once with the experiment (total of 6 sequences).

In order to assess whether pure face-name responses were specific to the ATL, we also considered responses on the contacts implanted posteriorly to the ATL, in the left posterior temporal lobe (PTL) of the same 7 participants (see S7 Fig for the topographic parcellation of the ventral occipito-temporal cortex [VOTC]). Across the 41 contacts implanted in the gray matter of this region, we found 8 contacts showing significant responses at the identity-oddball frequency in at least one condition in 3 participants, all located in the left fusiform gyrus. The responses recorded on these 8 contacts and their anatomical locations in the individual anatomy are shown in S8 Fig (see also S6 Fig for their location in the Talairach space). Importantly, no pure face-name response was found on any of these contacts. Two contacts were found to be significant in the Face Name condition and not in the Face Only and Name Only conditions, but the difference [FN–(FO + NO)] was not significant ($x = -31$ to -35, $y = -45$, $z = -19$; F'2 and F'3 in participant 2). One contact was significant in the Name Only condition but not in other conditions ($x = -34$, $y = -33$, $z = -21$; F'1 in participant 3). Three contiguous contacts in the same participant were significant in the Face Name and Face Only conditions but not in the Name Only condition ($x = -32$ to -39, $y = -41$, $z = -19$; F'3 to F'5 in participant 4). Two contacts were found to be significant in all 3 conditions ($x = -25$ to -29, $y = -41$, $z = -19$; F'1 and F'2 in participant 4).

Finally, to test whether there were local variations of the noise level that may explain why significant responses were found on some contacts and not on others, for each contact, we compared the standard deviation of the noise between all significant contacts across ATL and PTL ($N = 15$) and their adjacent nonsignificant contact ($N = 12$). There were no statistical differences regardless of the condition (p-value range: 0.84 to 0.96) (S1 Fig).

Discussion

Using an original frequency-tagging approach with mixed modalities of stimulation while recording scalp EEG and intracerebral EEG (SEEG), we found a neural response at the specific frequency at which different famous identities, either as a written name or a face picture, interrupted the successive presentation of a repeated specific identity, also presented in either format. The response was identified objectively, i.e., exactly at the predicted frequency of oddball

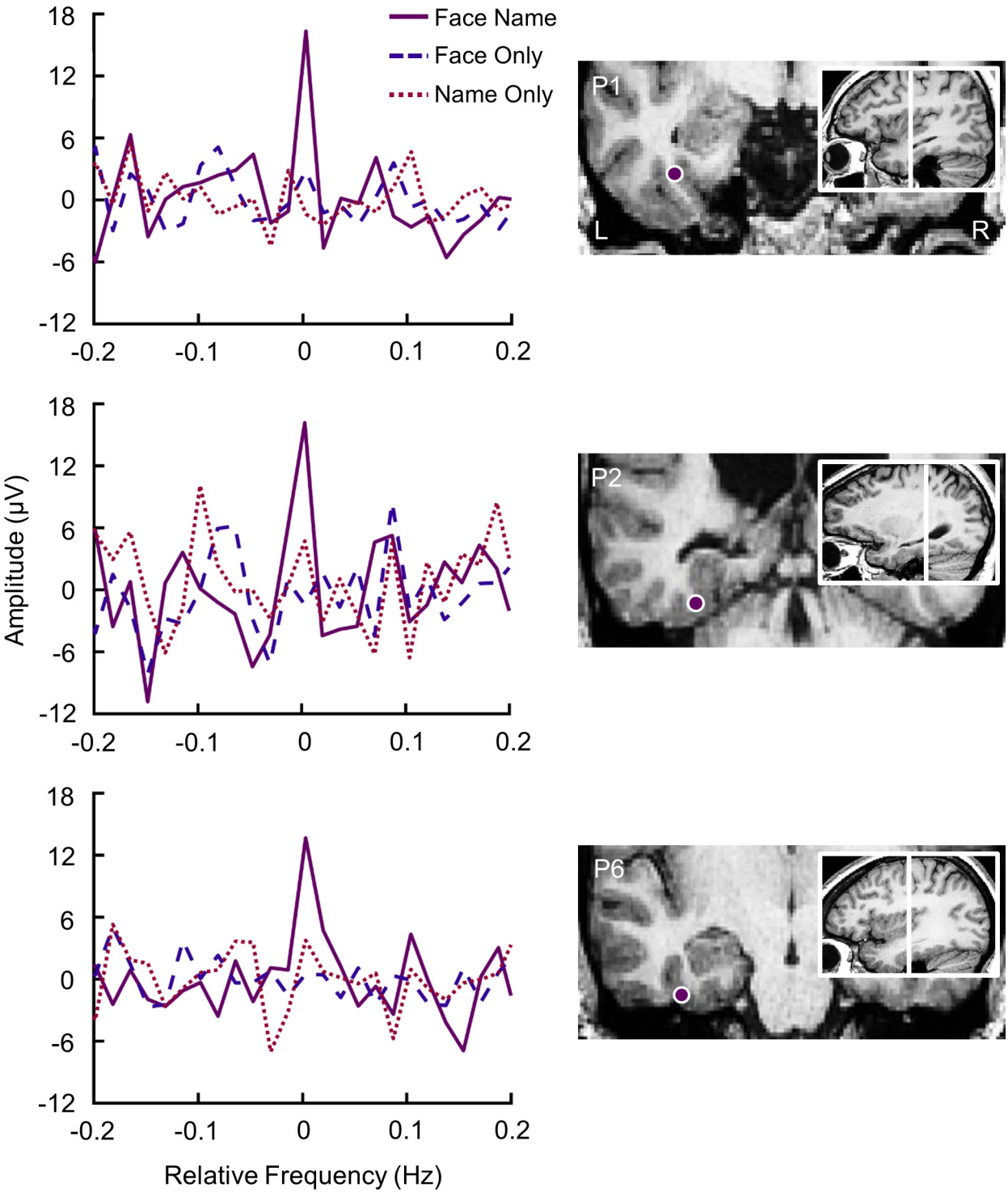

Fig 6. Pure face-name (person identity) intracerebral responses in the ATL. On the left, baseline-subtracted chunked FFT segments depicting oddball responses in Face Name, Face Only, and Name Only conditions as recorded at an individual contact. These contacts show a pure Face Name effect because (1) they show a strong electrophysiological response at the oddball frequency in the Face Name condition and (2) the sum of their responses in the two other conditions is significantly different from the response in the Face Name condition. On the right is shown the location of the individual contact responding selectively to the Face Name condition using a postimplantation CT scan co-registered to a preimplantation MRI. Data underlying this figure are deposited on a Dryad repository: https://doi.org/10.5061/dryad.m8t391m. ATL, anterior temporal lobe; FFT, fast Fourier transform.

https://doi.org/10.1371/journal.pbio.3000659.g006

presentation and its harmonics, over the bilateral occipito-temporal cortex in scalp EEG in Experiment 1. Thanks to another advantage of the fast periodic stimulation approach, i.e., its high signal-to-noise ratio, this response was clearly identified in 100% of the participants for the sum of harmonics across all electrodes of the bilateral ROIs and across the 4 famous identities tested.

To ensure that this crossmodal face-name response was not merely due to the linear superimposition of identity-oddball responses to faces and names generated by separated brain regions containing modality-specific person-related representations, we compared this response to the identity-oddball response elicited in 2 control conditions (Experiment 2, with 2 famous identities and 20 participants). In the Face Only condition, names of the base identity were replaced by other famous names, in order to isolate unimodal face responses that potentially contribute to the neural response observed in the Face Name condition. In the Name Only condition, face images of the base identity were replaced by other famous faces, isolating unimodal name responses potentially contributing to the neural face-name response. Critically, we found a Face Name response in the EEG spectrum significantly above and beyond the sum of the Face Only and Name Only responses [FN > (FO + NO)]. Moreover, thanks to frequency-tagging, we were able to quantify the contribution of the integrated response, which reached up to a third of the total EEG oddball response in the Face Name condition over the left hemisphere. Overall, these observations provide direct evidence for an integrated representation of face and name inputs of specific identities in the human brain. Finally, through intracerebral recordings in the left ventral ATL, we were able to identify a few electrode contacts with a unique response profile, i.e., showing a significant response in the Face Name condition only, suggesting that they capture neural activity associated with a multimodal integrated representation of person identity.

Integrative hub or re-entrant interhemispheric connections?

Our hypotheses on the neural mechanism subtending face-name associations were grounded on two theories of the organization of semantic (here, person-related) knowledge: one that postulates separate modality-specific regions in each hemisphere [26,27], and the other postulating the existence of a common crossmodal region (integrative hub) in addition to modality-specific regions [43–45]. Although a large extent of the oddball EEG response recorded on the scalp (68% and 80% over the left and right hemispheres, respectively) point to modality-specific responses selective to a person identity, our observation of a significant and substantial nonlinearity (i.e., Face Name > Face Only + Name Only) clearly provides support for an integrative hub of face and name identity.

The exact neural sources of this effect, which was found over low occipito-temporal channels, are unknown, and may concern either or both of the PTLs and ATLs. Proponents of the unitary hub theory postulate that both hemispheres contribute to and are activated during multimodal semantic processing [44,45,52,53,55]. While the hub-and-spoke model has been revisited in favor of a graded functionalization of semantic representations according to the functional connectivity of the ATL subregions with other cerebral regions (e.g., more activation of the left hemisphere when language processes are involved) [49,50,73], our protocol did not require an explicit language-related task and used an equal number of verbal (written names) and pictorial (face pictures) stimuli. Hence, according to this view, whether the neural response recorded in scalp EEG originates from the ATL or more posterior regions, it should have engaged both hemispheres in a similar way. Interestingly, Face Name responses were significantly greater than the sum of Face Only and Name Only responses over left occipito-temporal electrodes in scalp EEG. However, there was also a trend for an effect in the same region

of the right hemisphere, and no significant interaction between conditions and hemispheres, so that overall, the EEG results cannot be taken as evidence against the view that both hemispheres equally hold an integrated ("hub") representation of faces and names. A more comprehensive recording of intracerebral responses across the bilateral occipito-temporal cortices with a paradigm as used here should shed more light on this issue of hemispheric lateralization in future investigations.

The role of the (left) ATL

Our SEEG results are consistent with neuroimaging studies that have shown a common locus for famous face and name recognition in the ATL, even though face-name identity association per se was not investigated [28,45,59,60]. Moreover, several studies have found a specific role of the left temporal pole (anterior to the ATL in our study) in retrieving proper names when presented with a famous face or voice [74–76] and in providing semantic information when presented with a famous name [77]. However, these studies provided no direct evidence of an integration of person-related information at the level of identity. Here with SEEG, we recorded few but significant "pure" face-name responses in the left ventral ATL, i.e., not only a significant difference between Face Name and the sum (FO + NO) but a significant response in Face Name with no significant response in Face Only and Name Only.

Admittedly, the likelihood to find 3 pure face-name association responses among 196 ATL contacts sampled may appear to be very low. However, (1) these 3 pure face-name association responses were found in 3 different participants (i.e., in 3 out of 7 participants, in 43% of the participants); (2) the number of significant contacts depends on the size of the functional area (the smaller an area, the less likely it is to be sampled with electrodes and thus to record a significant response); and (3) the number of recorded contacts included in the proportion, and therefore the size of the ROI, is set arbitrary (our ATL region was wide, including lateral regions, i.e., the inferior and middle temporal gyri, and extending posteriorly until the posterior tip of the hippocampus, see S7 Fig). For example, restricting our ROI to the left antFG and adjacent sulci (medial bank of the antOTS and lateral bank of the antCOS), a region that is sampled by 1 or 2 SEEG electrodes per subject, leads to a proportion increase to 11.5% (3/26).

These pure face-name responses show that the left ventral ATL contains representations that are both crossmodal and sensitive to person identity. Presumably, in the Face Name condition, the neural activity must adapt or habituate to both faces and names during the presentation of a repeated identity and show a release from adaptation when a different identity is periodically presented, leading to a face-name oddball response. In the control conditions, the neural activity also adapts or habituates to the repeating faces or names of the specific identity but this adaptation is randomly (and not periodically) interrupted at every change of identity (at every oddball stimuli and at every other face and name replacing the specific identity in the sequence), leading to the absence of oddball response in these conditions. These results show that the left ventral ATL is a neural locus for the integration of a specific face and a name identity into a shared crossmodal representation. Thus, in concordance with studies showing a convergence of sensory information in the ATL [44,78], our results suggest that this ventral anterior temporal region receives visual information from both unimodal face and name regions. Moreover, our findings highlighting the integration of different input stimuli (face pictures and written names) into a semantic concept/identity in the ventral ATL are consistent with previous studies showing the importance of this region in semantic tasks irrespective of the input modality or stimulus category [55,73,79]. Nonetheless, it is important to point out that our findings shedding light on the left ventral ATL do not preclude a similar involvement of its right hemispheric counterpart, which was not explored in SEEG in the present study. We

therefore emphasize again the need for additional intracerebral recordings in larger samples of participants [80,81] in the bilateral ventral ATL in order to clarify its role in crossmodal person-related processing. In addition, recording of electrical activity of individual neurons [82] in the human ATL may provide more direct evidence for integration of identity-related faces and names at the neuronal level and provide useful contrasting information with previously recorded responses in the MTL [24].

The relationship between scalp and intracerebral responses

We found a striking difference between responses recorded on the scalp and intracerebrally with SEEG. In scalp EEG, we found a significant response in the 3 conditions with up to a 32% increase in the amplitude elicited by the Face Name condition compared to the amplitude of the sum of control conditions over the left occipito-temporal cortex (and about 20% over the right homologous region). This shows that the bulk of the response (68% and 80% in the left and right hemispheres, respectively) still originates from separate modalities, suggesting the existence of modality-specific representations of identity in addition to a crossmodal representation. In SEEG, we recorded 5 contacts with a significant response in Face Name only and no significant response in Face Only and Name Only, including 3 contacts with significantly larger responses in Face Name compared to the sum of the two control conditions in the left ventral ATL. One plausible explanation for this discrepancy between the two approaches (recording of pure integrated responses inside the brain but not on the scalp) is that scalp EEG recorded a combination of responses coming from modality-specific regions and pure face-name association responses coming from crossmodal regions coding shared person-related representations.

Clinical relevance of the FPVS approach

Semantic impairments are common in the neurological population, and face-name associations are particularly susceptible to be impaired. As mentioned in the introduction, several neurological conditions are frequently associated with face-name association deficits (e.g., SD, Alzheimer disease, etc.). However, face-name association deficits are difficult to evaluate in these neurological populations since the tests that are commonly used (e.g., the Iowa Famous Faces Test [83–85] or the Boston Famous Faces test [86,87]) require naming and decisional processes in addition to semantic processing. Moreover, these tests require explicit tasks that can be misunderstood by participants who may have comprehension difficulties (e.g., due to a low IQ). Our FPVS-EEG technique provides an objective measure of face-name association processes that do not require to name faces or to ask for an explicit task or an explicit semantic decision or response. FPVS-EEG could therefore be a method of choice to diagnose face-name association deficits in neurological populations, for example, in patients with SD characterized by a degradation of crossmodal anterior temporal regions, in whom the nonlinear pattern found in typical brains (FN > FO + NO) could be reduced or absent, with more linear patterns of responses (FN = FO + NO) observed.

Materials and methods

For clarity purposes, this section is divided in three parts. First, we describe the materials and methods for Experiment 1 (Face Name condition alone, 4 facial identities) administered to normal participants in scalp EEG. In the second and third sections, we describe materials and methods for Experiment 2 (Face Name condition and two control conditions, 2 facial identities) applied to neurotypical participants in scalp EEG and to epileptic participants in intracerebral EEG (SEEG), respectively.

Ethics statement

All subjects gave written informed consent to participate, and the study was approved by the Biomedical Ethical Committee of the University of Louvain (B403201111965) (scalp EEG) and by the Research Ethics Committee of the CHRU-Nancy (2015-A01951-48) (SEEG). The experiments were performed in compliance with the Declaration of Helsinki.

Experiment 1

Participants. Twelve volunteers (6 females, all right-handed, mean age = 22.61 years, standard deviation = 2.13 years) were tested individually and received financial compensation in exchange for their participation. All participants reported normal or corrected-to-normal vision.

Stimuli. Four highly famous male identities, two politicians (Donald Trump and Vladimir Putin) and two actors (Brad Pitt and Johnny Depp), were selected. For each of them, 18 natural photographs (depicting different head orientations, lighting conditions, facial expressions, and background) were selected from the internet. The stimuli were selected to be as variable as possible to minimize repetition effects due to low-level features [88]. For each celebrity, the written names were presented on a gray background in capital letters but were made variable by using 18 different fonts and six different colors. Thirty-six other famous identities were also selected (18 pictures and 18 written names) to create one stimulus per identity (either a face or a name). Names of these other celebrities were also written in 18 fonts, different from those used with the four main identities, and the same six colors were chosen (red, black, green, brown, yellow, and blue). Face pictures were resized to 200 × 250 pixels.

FPVS procedure. Brain activity of each participant was recorded with high-density (128 channels) scalp EEG while participants were seating in front of a computer screen at a distance of 87 cm. To help participants pay attention to the screen before each sequence, a fixation cross was first displayed on the uniform gray background for 2–5 seconds (this duration randomly varied between sequences). A 60-second sequence was then run, plus 2 seconds of fading time before and after the sequence to avoid potential blinks and eye movements due to the sudden appearance or disappearance of flickering stimuli. During the fade-in, the contrast modulation depth of the periodic stimulation progressively increased from 0% to 100% to reach full contrast while it decreased during the fade-out. Across sequences, participants were presented with stimuli through sinusoidal contrast modulation from 0% to 100% at a rate of 4 Hz (= 4 stimuli per second). A relatively low stimulation frequency of 4 Hz (compared to higher stimulation frequencies at 6 Hz used in face categorization studies [88]) was selected based on pilot data and to provide sufficient stimulus duration to extract information necessary to associate specific face and name identities. Within a sequence, each stimulation cycle lasted 250 ms (i.e., 1,000 ms/4) in which an image appeared and disappeared in the middle of the screen as its contrast followed a sinusoidal function (Fig 1). Image size varied randomly at each stimulus presentation cycle across five equidistant steps between 80% and 120%, in order to further reduce the potential impact of low-level adaptation. At 100%, face images subtended about 6.78˚ × 5.47˚ of visual angle, while words subtended on average 13.03˚ × 1.41˚ of visual angle.

The stimulation was repeated once for each of the four famous target identity, representing a total of eight sequences. Each sequence was composed of base and identity-oddball stimuli. Base stimuli were highly variable photographs and written names corresponding to one of the four famous identities (B. Pitt, J. Depp, D. Trump, and V. Putin), while identity-oddball stimuli were variable photographs or names of different identities (Fig 1). Within sequences, all images were randomly selected from the pool of images of their respective types (base stimuli

or identity-oddball stimuli). All images appeared at a frequency of 4 Hz (base frequency, reflecting a general visual processing) and identity-oddball stimuli were displayed every seven stimuli, i.e., every 0.571 Hz (4 Hz / 7; identity-oddball frequency, thought to reflect the disruption from the flow of same-identity stimuli).

Four blocks of eight stimulation sequences were defined prior to the beginning of the experiment, each with a fixed, counterbalanced order of sequences within a block, so that randomization uncertainties due to a small number of participants were avoided. Blocks were administered one after another, every subject being presented with only one block (subject 1 was presented with block 1, subject 2 with block 2, . . . subject 5 with block 1, etc.). Within a block, participants were invited to rest their eyes between every trial.

Participants were aware that they would be presented with famous faces and names, but no further information was given about the procedure. They were asked not to pay particular attention to these stimuli and rather look at the blue fixation cross located in the middle of the screen. Their task was to press the space bar of the keyboard when the fixation cross turned to red. Color changes randomly occurred 8 times for 500 ms within every sequence. This task was orthogonal to the manipulation of interest and was used to ensure that participants maintain a constant level of attention throughout the experiment. Mean accuracy and response time (RT) to the orthogonal task (detecting color changes of the fixation cross) were computed independently for each participant. Behavioral performance was close to ceiling, with a mean accuracy of 98.31% (standard deviation = 2.05%) and mean RTs around 502 ms (standard deviation = 59 ms).

At the end of the experiment, participants were provided with a questionnaire depicting 44 black-and-white faces (the 4 famous base identities, the 36 famous identity-oddball identities, and 4 unknown distractors). This questionnaire was designed to ensure that target identities were well known to the participants. They had to tell if they knew the depicted celebrity (yes, no, uncertain) and for each one, to rate its familiarity on a 5-point scale (ranging from rarely seen to very frequently seen on TV or other media). They also had to tell if they had noticed this face during the experiment or not. Overall, 89.8% (standard deviation = 15%) of the 40 famous faces (4 base identities and 36 identity-oddball stimuli) were rated as known by the participants. Considering base identities only, participants had no difficulty recognizing them, with perfect recognition for D. Trump, J. Depp, and V. Putin (recognized for 100% of the participants), and near perfect recognition for B. Pitt (recognized by 91.6% of the participants; 11/12). None of the four unknown faces (not used in the experiment) were rated as known. When rating face familiarity, participants indicated that they were frequently exposed to these famous people in the media (mean rating of 3.74 on a 5-point scale, with 1 = rarely, 5 = many times; standard deviation = 0.61). D. Trump, J. Depp, and V. Putin were reported as seen by all the participants during testing. Only one participant did not report having seen Brad Pitt during the course of the experiment and this was related to the nonrecognition of this famous face as represented in the black-and-white questionnaire.

EEG recording. EEG was recorded using a 128-channels Biosemi ActiveTwo system. The system uses two additional electrodes for reference (CMS, common mode sense) and ground (DRL, driven right leg). Vertical and horizontal electrooculogram (EOG) was recorded by placing two flat-type electrodes above and below the participant's right eye and two at the outer canthi of the eyes. The EEG and EOG were digitized at a sampling rate of 512 Hz. Recordings were manually initiated when participants showed an artifact-free EEG signal. To facilitate analyses, Biosemi channel labels were later converted to an extended 10–20 system of electrode placement [69].

EEG analysis. Preprocessing of EEG data was carried out using Letswave 5 (https://github.com/NOCIONS/Letswave5), a custom software running over Matlab R2012b

(MathWorks, Natick, MA), and followed procedure developed for frequency tagging studies of face stimuli in a number of published studies [68,71,89]. After importation of raw EEG data files, vertical jumps in the signal due to voltage drift during pauses between trials were corrected for by aligning continuous blocks of recording to the first block. EEG data were band-pass filtered (0.1 to 100-Hz fourth-order zero-phase Butterworth filter) and multi-notch filtered (width 0.5 Hz) to remove 50 Hz's electrical noise on four harmonics. A downsampling to 256 Hz was applied to reduce file size and increase processing speed. The data were then segmented using four distinct stimulation start triggers (one per famous base identity) into epochs from 2 seconds before stimulation to 2 seconds after the end of stimulation (−2 seconds to 66 seconds). A blink detection was applied and a threshold of more than 0.15 blinks per second for each epoch was used in order to apply correction of eye movements when needed [71]. Following this threshold, an ICA (Independent Component Analysis) was computed for three subjects. When needed, noisy electrodes across multiple trials (less than 5% of channels) were linearly interpolated with 3 to 6 pooled neighboring channels. Epochs were then re-referenced to the common average.

Frequency domain analyses were carried out by further segmenting epochs using an integer number of bins of 0.571 Hz cycles beginning 2 seconds after onset of the stimulation sequence (then removing fade-in artifact-prone responses) until approximately 60 seconds, before stimulus fade-out (15.235 bins in total). Resulting epochs were then averaged to improve signal-to-noise ratio. A fast Fourier transform (FFT) was computed and amplitude spectra were extracted. Data were grand-averaged for each channel across participants.

A baseline-subtraction was computed to account for differences in baseline noise across the frequency spectrum and to quantify the electrophysiological responses in microvolts [90]. The difference between the amplitude of the bin of interest and the average of amplitude in the 20 surrounding bins was computed, excluding the immediately adjacent bin in case of remaining spectral leakage, and the local maximum and minimum amplitude bins to avoid projecting the signal in the neighboring bins containing noise. To quantify the responses at the frequency of identity change, we computed the sum of identity-oddball harmonics (0.571 Hz, 1.142, and so on until the sixth harmonic, i.e., 3.427 Hz). To do so, responses on the FFT spectrum were segmented into 6 separate chunks centered on the bin containing the harmonic of interest (see also S9B Fig illustrating the same procedure with SEEG data). Each chunk contained 31 bins (i.e., a chunk length of 0.5208 Hz), with the bin in the middle (the 16th bin, with 15 bins on each side) corresponding to the identity-oddball frequency. The 6 chunks were then summed for each participant (see also S9C Fig), and a grand-average was computed across participants. The quantification of the response at the sum of harmonics was computed following the same principle as for the quantification of responses on the whole FFT spectrum, i.e., with a baseline-subtraction.

In order to determine whether a significant response was present at the frequencies of interest and harmonics, Z-scores were calculated by computing the difference between the amplitude at the bin of interest and the mean amplitude in the 22 surrounding bins (11 bins on either side, no exclusion of the local maximum and minimum amplitude bins) and dividing this value by the standard deviation of amplitudes in the 22 corresponding surrounding bins [68]. An electrode was considered as showing a significant response if the Z-score at the frequency bin of the identity-oddball stimulation exceeded 1.65 (i.e., $p < 0.05$).

Following the analysis of amplitudes, we examined the overall scalp topography at base and identity-oddball frequencies.

Experiment 2a (scalp EEG)

Experiment 1 was designed as a proof of concept and to identify facial identities providing large responses in the paradigm. Experiment 2 used only two facial identities (D. Trump and

V. Putin) and increased variability in written stimuli to counter low-level effects. Most importantly, it added two key control conditions to identify the role of modality-specific representations within the face-name sequence.

Participants. Twenty-two volunteers (10 males, all right-handed) received financial compensation in exchange for their participation in the experiment. One male and one female participant were excluded from the EEG analyses because of excessive artifacts in a large set of electrodes across multiple epochs during data recording. The final sampling of participants (n = 20) had a mean age of 22.96 years (standard deviation = 1.91 years). All participants reported normal or corrected-to-normal vision.

Stimuli. Images and names of two famous identities (D. Trump and V. Putin) were used as base identities. The same 18 natural photographs as in Experiment 1 were used, but the variability among written names was increased by using both uppercase and lowercase letters, and less conventional fonts (e.g., Ravie, Pristina, Segoe Script, etc., instead of Arial, Candara, etc.). A gray background and the same six colors as in Experiment 1 were used for the written stimuli. Seventy-two other famous identities were also selected, 36 being the same as in Experiment 1 so that oddball stimuli were unchanged, and 36 novel ones, serving as base control stimuli. Thirty-six face photographs were used, each depicting a single famous face, with different viewpoints, lighting conditions, background, and facial expressions (18 identity-oddball faces and 18 base control faces). Face pictures were resized to 200 × 250 pixels. Thirty-six written stimuli were created, with 18 using the same design criteria as those of the base identities (= control names) and 18 being written in different fonts (= identity-oddball names).

FPVS procedure. The paradigm and testing conditions were similar to Experiment 1, with the two control conditions added. The experiment consisted of three conditions for each famous base identity, i.e., a total of 6 different sequences (3 conditions × 2 identities).

In the Face Name condition, base and identity-oddball stimuli were similar to those used in Experiment 1, with the exception that only D. Trump and V. Putin appeared as base stimuli and that written stimuli were even more variable in terms of size, color and font (Fig 1). In the Face Only condition, famous base faces were unchanged, but famous base names were replaced by 18 different famous names. Identity-oddball stimuli were the same than in the Face Name condition (Fig 1). This condition aimed at controlling the amount of modality (face)-specific representations that are activated in the face-name association sequence. If a response is observed at the identity-oddball frequency in this condition (0.571 Hz), it cannot reflect the disruption of face-name associative representations (i.e., D. Trump's name with his face) but can reflect the fact that 50% (on average) of the stimuli appearing every 7 stimuli are faces of a different identity than the base face identity (D. Trump). The reverse was done in the Name Only condition in which only famous base names were unchanged, while famous base faces were replaced by 18 different famous faces. Identity-oddball stimuli remained unchanged according to the Face Name condition (Fig 1). The purpose of this condition was to quantify and isolate the amount of modality(name)-specific representations that are elicited by the face-name paradigm. If a response is observed in this condition at the identity-oddball frequency, it can reflect a disruption in the activation of name representations due to the occurrence of different identity names among identity-oddball stimuli.

Each sequence was presented once within a block, and the order of sequences was counterbalanced. Each subject was presented with two blocks, i.e., two presentations per sequence. Within sequences, all images were randomly selected from the pool of images of their respective types (base stimuli or identity-oddball stimuli). All images appeared at a frequency of 4 Hz (base frequency, reflecting a general visual processing) and identity-oddball stimuli appeared every six base stimuli, i.e., every 0.571 Hz. At 100% of their size, face images subtended about 6.78˚ × 5.47˚ of visual angle, while words subtended on average 13.65˚ × 1.62˚ of visual angle.

Mean accuracy and RT to the orthogonal task (detecting color changes of the fixation cross) were computed independently for each participant. We considered behavioral data across identities in the three main conditions: Face Name, Face Only, and Name Only. A one-way ANOVA with repeated measures found no difference between conditions according to accuracy ($F(2,38) = 0.241$, $p = 0.787$) or RTs ($F(2,38) = 0.148$, $p = 0.863$).

Participants also had to complete the same questionnaire as in Experiment 1. Here, 89.25% (standard deviation = 15.75%) of the 40 famous faces were rated as known. The two base identities (D. Trump and V. Putin) were rated as known by all the participants. Overall, some unknown faces were sometimes reported as known, with a 5% occurrence among participants. In these very few cases the supposedly unknown face was globally rated as less frequently seen in the media (mean = 2.83), but the results presented a large variability (standard deviation = 1.61). When asking participants more information about these faces, they reported incorrect information, suggesting confusion and misrecognition of the faces. When rating face familiarity, participants reported a frequent encounter of famous faces in the media (mean = 3.64; standard deviation = 0.53). All the participants reported having seen D. Trump, and only one participant did not rate V. Putin as seen during the testing.

EEG recording and analysis. EEG recordings and analyses were performed exactly as in Experiment 1, considering the Face Name, Face Only, and Name Only conditions, regardless of identity.

Experiment 2b (intracerebral EEG)

Participants. Considering the selective left-lateralized face-name responses observed in scalp EEG and patients' availability, we selected the left ATL as ROI. We recruited 7 participants (6 females, mean age: 30.7 ± 12.5 years, 4 right-handed) undergoing clinical intracerebral evaluation with depth electrodes (SEEG [91]) for refractory partial epilepsy (Epilepsy Unit, University Hospital of Nancy). Participants with at least one intracerebral electrode implanted in the left ventral ATL were included. The ventral ATL was defined as the ventral region located anteriorly to the posterior tip of the hippocampus (see S7 Fig for the topographic parcellation of the VOTC used in this study) [80,81]. The ventral ATL comprises the following anatomical regions: the anterior segment of the parahippocampal gyrus (antPHG), the antCoS, the antFG, the antOTS, and the antMTG/ITG.

Intracerebral EEG recording. Intracerebral electrodes were stereotactically implanted within the participants' brains for clinical purposes, i.e., in order to delineate their seizure onset zones. SEEG avoids the need for large craniotomies as in the more popular implantation of subdural grid electrodes to record intracranial EEG (electrocorticography or ECoG) but offers the possibility to accurately explore mesial structures, deep sulci, and the insula [91]. Due to its intrinsic precision placement features, SEEG may be associated with fewer complications than implantation of subdural grid electrodes [92]. A recent meta-analysis provides strong data regarding the safety of SEEG based on a systematic review of all published complications [92–94]. The implantation scheme is defined individually for each patient according to electro-clinical hypotheses derived from noninvasive investigation; the number of implanted electrodes is minimized, and their location and trajectories are defined strictly based on clinical criteria. After induction of general anesthesia, the stereotactic frame (Leksell model G, Elekta instrument, Stockholm, Sweden) is positioned on the patient's head. A stereotactic CT scan is then performed and fused to the preoperative non-stereotactic MRI using the iPlan Stereotaxy software (Brainlab AG, München, Germany). Electrodes are then implanted according to the following procedure: After reporting the calculated coordinates on the frame, stereotactic guided drilling of the skull is performed and a bone screw is inserted. The

intracerebral electrode (DixiMedical, Besançon, France; diameter of 0.8 mm; 5 to 18 platinum/iridium contacts with 2-mm length, 1.5 mm apart) is inserted and secured to the screw with a tight seal in order to prevent cerebrospinal fluid leak. Fluoroscopic control is performed to rule out major electrode positioning errors before removing the stereotactic frame. A safety margin of 2 mm is respected between the trajectory and the nearby vessels [94].

A total of 196 contacts (mean number per participant = 28; range = 11–39) were distributed over the left ventral ATL of 7 participants, and 41 contacts (mean number per participant = 10; range = 10–11) were implanted over the left PTL in 4 participants. Intracerebral EEG was sampled at a 512 Hz and referenced to either a midline prefrontal scalp electrode (FPz, available in 3 participants) or an intracerebral contact in the white matter (in 4 participants).

FPVS procedure. Stimuli and the FPVS procedure were the same as in Experiment 2 in scalp EEG, except the number of blocks. All participants were administered with at least 6 sequences (2 Face Name, 2 Face Only, and 2 Name Only), corresponding to one session of the experiment. For 4 participants, the experiment was administered twice, corresponding to a total of 12 sequences (4 Face Name, 4 Face Only, and 4 Name Only).

Mean accuracy and RT to the fixation cross task were calculated for each participant. A one-way ANOVA with repeated measures found no difference between conditions according to accuracy ($F(2,16) = 1.019$, $p = 0.383$) or RTs ($F(2,16) = 0.326$, $p = 0.726$).

Intracerebral EEG analysis. SEEG analyses were carried out using the free software Letswave 5 (see https://github.com/NOCIONS/letswave6 for the most recent version) and largely followed procedures used in previous SEEG studies with this approach [80,81]. Segments of SEEG data corresponding to stimulation sequences were extracted. These segments were then cropped to an integer number of 0.571 Hz cycles beginning after the 2-second fade-in and ending before the 2-second fade-out (30,471 bins, approximately 60 seconds). Sequences were averaged in the time domain separately for each condition and each participant. No further preprocessing was applied to the recordings. Subsequently, a FFT was applied to these averaged segments.

Responses significantly above noise level in the frequency domain at the identity-oddball stimulation frequency (0.571 Hz) and its harmonics were determined in each condition as follows: (1) the FFT spectrum was cut into segments of 0.8 Hz centered at the identity-oddball response frequency and the 6 first harmonics, i.e., 0.571 Hz, 1.142 Hz, 1.714 Hz, etc. (S9B Fig); (2) the amplitude values of these 6 FFT segments were summed (S9C Fig); and (3) the summed FFT spectrum was transformed into a Z-score (S9D Fig). Z-scores were computed as the difference between the amplitude at the identity-oddball frequency bin and the mean amplitude of 22 surrounding bins (12 bins on each side, excluding the first bin directly adjacent to the bin of interest) divided by the standard deviation of amplitudes in the corresponding 22 surrounding bins [80]. A contact was considered as showing a significant response in a given condition if the Z-score at the bin of the identity-oddball frequency exceeded 3.1 (i.e., $p < 0.001$ one-tailed: signal > noise; a conservative threshold is used to take into account the number of contacts and harmonics tested).

Identity-oddball amplitude responses were quantified using baseline-subtracted amplitudes. Baseline-corrected amplitudes were computed as the difference between the amplitude at each frequency bin and the average of 22 surrounding bins (12 bins on each side, excluding the first bin directly adjacent to the bin of interest). Amplitude responses were quantified as the sum of the baseline-subtracted amplitudes at the identity-oddball frequencies from the first until the sixth harmonic (0.571 Hz until 3.428 Hz), separately for each condition.

At each contact, the amplitude in the Face Name condition was compared to the sum of amplitudes in the Face Only and Name Only conditions. To do so, for each contact, we summed the 2 FFT spectra corresponding to the conditions Face Only and Name Only (S9E

Fig), and we subtracted this resulting summed FFT spectrum from the FFT spectrum corresponding to the Face Name condition (S9F Fig). Then, to assess the significance of this subtraction, we followed the same procedure as for single conditions: (1) the subtracted FFT spectrum was cut into segments of 0.8 Hz centered at the identity-oddball response frequency and the six first harmonics, i.e., 0.571 Hz, 1.142 Hz, 1.714 Hz, etc. (S9F Fig); (2) the amplitude values of these 6 FFT segments were summed (S9G Fig); and (3) the summed FFT spectrum was transformed into a Z-score (S9H Fig). Z-scores were computed as the difference between the amplitude at the identity-oddball frequency bin and the mean amplitude of 22 surrounding bins (12 bins on each side, excluding the first bin directly adjacent to the bin of interest) divided by the standard deviation of amplitudes in the corresponding 22 surrounding bins [80]. A contact was considered as showing a larger response for the Face Name than for the sum Face Only + Face Name if the Z-score at the frequency bin of the identity-oddball stimulation exceeded 1.65 (i.e., $p < 0.05$, one-tailed).

Contact localization in the individual anatomy. The exact position of each contact in the individual anatomy was determined for each participant by co-registration of the postoperative CT scan with a T1-weighted MRI of the participant's head. To accurately label each contact in the individual anatomy, we used the same topographic parcellation of the VOTC as in previous studies [81,95] (S7 Fig). Major VOTC sulci (collateral sulcus and occipito-temporal sulcus) served as mediolateral landmarks, while coronal reference planes containing given landmarks served as posteroanterior landmarks. A coronal plane including the anterior tip of the parieto-occipital sulcus served as the border of the occipital lobe and PTL. A coronal plane including the posterior tip of the hippocampus served as the border between the PTL and the ATL. Therefore, contacts located anteriorly to the posterior tip of the hippocampus were labeled in the ATL.

All EEG and SEEG data are deposited in a Dryad repository: https://doi.org/10.5061/dryad.m8t391m [96].

Statistical testing

To compare effects between conditions or ROIs, one- or two-way ANOVA with repeated measures (Greenhouse-Geisser corrected when sphericity was violated) and paired *t* tests were computed when assumptions of normality were respected. Bonferroni-corrected post hoc tests were applied when ANOVA showed statistical differences between groups. When assumptions of normality were violated, nonparametric Friedman tests and Wilcoxon signed-rank tests (Bonferroni adjusted for multiple comparisons) were carried out. Effect sizes (Cohen's *d*) are provided.

Supporting information

S1 Fig. Noise comparison across conditions and regions in scalp EEG and SEEG. In Experiment 1, the mean standard deviation of the noise around the identity-oddball frequency is displayed for the left, middle, and right ROIs (3 electrodes in each). In Experiment 2 with scalp EEG, the mean standard deviation of the noise in the left and right ROIs (5 electrodes each) is shown for the 3 conditions: Face Name, Face Only, and Name Only. In Experiment 2 with intracerebral EEG, the mean standard deviation of the noise around the identity-oddball bin is shown for all significant contacts in the ATL and PTL ($N = 15$) and for all their nonsignificant adjacent contacts ($N = 12$) across all the 6 participants showing a significant response in at least one condition, either in the ATL or PTL. Error bars indicate standard deviation of the mean. Data underlying this figure are deposited on a Dryad repository: https://doi.org/10.5061/dryad.m8t391m. ATL, anterior temporal lobe; EEG, electroencephalography; LOT, left

occipito-temporal; mid OT, middle occipito-temporal; PTL, posterior temporal lobe; ROI, region of interest; ROT, right occipito-temporal; SEEG, stereo electroencephalography.
(TIF)

S2 Fig. Scalp EEG responses at the individual level in Experiment 1. Individual participant data for the 12 participants of Experiment 1 are shown at the frequency of person identity change (sum of 6 harmonics), independently of base identity. Each topography and the waveform to its right correspond to the data of one participant. Head plots are scaled from 0 μV (dark blue) to the voltage of the maximal channel (red), separately for each participant. Waveforms show the average of baseline-corrected chunked frequency spectrum of the 6 channels in bilateral occipito-temporal ROIs (P10, PO10, and PO12 for the LOT, and P9, PO9, and PO11 for the ROT), centered on the sum of harmonics, with an *x* axis of relative frequency in Hz and a *y* axis of amplitude (μV). All participants showed a significant response ($p < 0.01$) at the frequency of person identity change in the bilateral ROIs. Data underlying this figure are deposited on a Dryad repository: https://doi.org/10.5061/dryad.m8t391m. EEG, electroencephalography; LOT, left occipito-temporal; ROI, region of interest; ROT, right occipito-temporal.
(TIF)

S3 Fig. FFT spectrum of scalp EEG responses in Experiment 2. Baseline-corrected FFT spectra (in μV) of the responses in the 3 conditions of Experiment 2 are shown at the group level ($n = 20$ participants). The red and blue lines represent the average of the 5 electrodes in the left and right ROIs, respectively; the location of the ROI is indicated by the topographical head on the top of each spectrum. Black labels on the FFT spectrum signal the significant oddball frequencies; the light gray label indicates the base frequency. Data underlying this figure are deposited on a Dryad repository: https://doi.org/10.5061/dryad.m8t391m. EEG, electroencephalography; FFT, fast Fourier transform; ROI, region of interest.
(TIF)

S4 Fig. Scalp EEG responses at the base frequency in Experiment 2. Base frequency responses (sum of the first 9 base harmonics) are shown for each of the 3 conditions: Face Name, Face Only, and Name Only. Above, mean group-level base responses in baseline-corrected amplitude (μV) at the two lateral ROIs regardless of identity. Error bars indicate standard error from the mean, reflecting variability across participants. Asterisks indicate significant differences at $p < 0.05$. Below, topography of the response at the base frequency for each condition. Red and blue ovals show the electrodes included in the left and right ROIs, respectively. The color scale maximum is shown in light gray above each map and corresponds to the maximal baseline-corrected amplitude (in μV) in each condition. Data underlying this figure are deposited on a Dryad repository: https://doi.org/10.5061/dryad.m8t391m. EEG, electroencephalography; LOT, left occipito-temporal; ROI, region of interest; ROT, right occipito-temporal.
(TIF)

S5 Fig. Anatomical location and SEEG responses of the significant contacts in the ATL. Anatomical location and electrophysiological responses of the 7 significant contacts in the ATL in 4 participants (P1, P2, P5, P6) and of their adjacent contacts. The significant contacts are highlighted in red. Significant base responses were determined in the same way as significant identity-oddball responses by (1) epoching the EEG frequency spectrum into segments centered on the first 6 base harmonics (i.e., 4 Hz, 8 Hz, etc.); (2) summing the amplitude values of these 6 frequency spectra segments; and (3) transforming it into a Z-score (difference between the amplitude at the base frequency bin and the mean amplitude of the 22

surrounding bins, divided by the standard deviation of amplitudes in the corresponding 22 surrounding bins). Data underlying this figure are deposited on a Dryad repository: https://doi.org/10.5061/dryad.m8t391m. ATL, anterior temporal lobe; EEG, electroencephalography; SEEG, stereo electroencephalography
(TIF)

S6 Fig. Spatial distribution of significant and nonsignificant intracerebral contacts in the Talairach space. Map of all 237 VOTC recording contacts implanted in the gray matter of the left ATL and PTL across the 7 participants displayed in the Talairach space using a transparent reconstructed cortical surface of the Colin27 brain (left hemisphere, ventral view). Each circle represents a single recording contact. Color-filled circles correspond to significant contacts in at least one condition. Significant contacts are color-coded according to the condition(s) for which we recorded significant responses at the oddball-identity frequency ($p < 0.001$). "Pure FN" contacts are contacts on which the response was significant in the Face Name condition but not in the Face Only and Name Only conditions, and the response in the Face Name condition was larger ($p < 0.05$) than the response in the sum of the two control conditions. "Non pure" FN contacts are contacts on which the response was significant in the Face Name condition but not in the Face Only and Name Only conditions, but the response in the Face Name condition was not significantly larger than the sum of the two control conditions. Note that the more posterior "Pure" FN contact is still located in the ATL (i.e., anterior to the posterior tip of the hippocampus in the individual anatomy). Data underlying this figure are deposited on a Dryad repository: https://doi.org/10.5061/dryad.m8t391m. ATL, anterior temporal lobe; FN, Face Name; FO, Face Only; NO, Name Only; PTL, posterior temporal lobe; VOTC, ventral occipito-temporal cortex.
(TIF)

S7 Fig. Schematic representation of the parcellation scheme of the VOTC. Anatomical regions were defined in each individual hemisphere according to major anatomical landmarks [95]. The ventral temporal sulci (collateral sulcus, occipito-temporal sulcus, and midfusiform sulcus) serve as medial/lateral borders of regions, whereas 2 coronal reference planes containing anatomical landmarks (posterior tip of the hippocampus and anterior tip of the parieto-occipital sulcus) serve as an anterior/posterior boundary for each region. Importantly, the posterior tip of the hippocampus separated the PTL and the ATL, and therefore contacts located anteriorly to the posterior tip of the hippocampus were labeled in the ATL. The anatomical location of each significant contact was determined in the individual brain according to this anatomical subdivision. The schematic locations of these anatomical structures are shown on a reconstructed cortical surface of the Colin27 brain. AntFG, anterior fusiform gyrus; antMTG/ITG, anterior part of the inferior and middle temporal gyri; antPHG, anterior segment of the parahippocampal gyrus; ATL, anterior temporal lobe; CoS, collateral sulcus; HIP, hippocampus; latFG, lateral part of the fusiform gyrus; medFG, medial part of the fusiform gyrus; MFS, midfusiform sulcus; MTG/ITG, inferior and middle temporal gyri; OCC, occipital lobe; OTS, occipito-temporal sulcus; PHG, parahippocampal gyrus; POS, parieto-occipital sulcus; PTL, posterior temporal lobe; VOTC, ventral occipito-temporal cortex.
(TIF)

S8 Fig. Anatomical location and SEEG responses of the significant contacts in the PTL. Anatomical location and electrophysiological responses of the 8 significant contacts in the PTL in 3 participants (P2, P3, P4) and of their adjacent contacts. The significant contacts are highlighted in red. Significant base responses were determined in the same way as significant identity-oddball responses by (1) epoching the EEG frequency spectrum into segments

centered on the first 6 base harmonics (i.e., 4 Hz, 8 Hz, etc.); (2) summing the amplitude values of these 6 frequency spectrum segments; and (3) transforming it into a Z-score (difference between the amplitude at the base frequency bin and the mean amplitude of the 22 surrounding bins, divided by the standard deviation of amplitudes in the corresponding 22 surrounding bins). Data underlying this figure are deposited on a Dryad repository: https://doi.org/10.5061/dryad.m8t391m. EEG, electroencephalography; SEEG, stereo electroencephalography; PTL, posterior temporal lobe.
(TIF)

S9 Fig. Illustration of the identification procedure of significant intracerebral contacts from the raw FFT spectrum. (A) The anatomical location of the contact that is illustrated in this example is shown in both coronal and sagittal views and indicated by a green dot. (B) Intracerebral frequency-domain responses recorded in this individual contact in the Face Name condition. Significant responses were determined by first segmenting the EEG frequency spectrum into 6 segments centered at the identity-oddball frequency and its harmonics. These 6 segments are illustrated by 6 gray bars on the *x* axis and correspond to the length of each frequency spectrum segment. (C) Pattern of response of the 6 individual frequency segments is shown as gray lines. These segments were then summed, resulting in the green spectrum. The 0 mark represents the identity-change frequency. (D) Z-score transformation of the summed FFT spectrum. Z-score was computed as the difference between the amplitude at the identity-change frequency and the mean amplitude of the 22 surrounding bins, divided by the standard deviation of the 22 surrounding bins. The dashed line indicates the threshold of 3.1 ($p < 0.001$) that was used in intracerebral EEG to detect significant responses. (E) Computation of the subtraction between the Face Name condition and the sum of the two control conditions: Face Only and Name Only. First, raw FFT spectra of the Face Only and Name Only conditions were summed. This sum was then subtracted from the raw FFT spectrum of the Face Name condition. (F) Intracerebral frequency-domain responses resulting from the subtraction [Face Name − (Face Only + Name Only)]. Significant responses in this subtraction were determined by first segmenting the EEG frequency spectrum into 6 segments centered at the identity-oddball frequency and its harmonics. These 6 segments are illustrated by 6 gray bars on the *x* axis that correspond to the length of each segment. (G) Pattern of response of the 6 individual segments is shown as gray lines. Because these responses resulted from the subtraction of two conditions (Face Only and Name Only) from one condition (Face Name), only the identity-oddball amplitude remains positive, while the amplitude of the surrounding bins is mostly negative. These segments were then summed, resulting in the green spectrum. As a consequence of the subtraction process, only the frequency of interest has a positive amplitude. The 0 mark represents the identity-change frequency. (H) Z-score transformation of the summed FFT spectrum. The dashed line indicates the threshold of 1.65 ($p < 0.05$) that was used in intracerebral EEG to detect significant responses at the subtraction [Face Name − (Face Only + Name Only)]. In this example, the Z-score at the identity-oddball frequency exceeds 1.65, indicating that the face-name response is not only explained by the sum of modality-specific responses. Data underlying this figure are deposited on a Dryad repository: https://doi.org/10.5061/dryad.m8t391m. EEG, electroencephalography; FFT, fast Fourier transform; FN, Face Name; FO, Face Only; NO, Name Only.
(TIF)

Author Contributions

Conceptualization: Angélique Volfart, Bruno Rossion.

Data curation: Angélique Volfart, Jacques Jonas, Louis Maillard, Sophie Colnat-Coulbois.

Formal analysis: Angélique Volfart.

Funding acquisition: Bruno Rossion.

Investigation: Angélique Volfart, Jacques Jonas.

Methodology: Angélique Volfart, Bruno Rossion.

Project administration: Jacques Jonas, Bruno Rossion.

Resources: Bruno Rossion.

Supervision: Jacques Jonas, Bruno Rossion.

Validation: Bruno Rossion.

Visualization: Angélique Volfart, Jacques Jonas, Bruno Rossion.

Writing – original draft: Angélique Volfart, Jacques Jonas, Bruno Rossion.

Writing – review & editing: Angélique Volfart, Jacques Jonas, Louis Maillard, Sophie Colnat-Coulbois, Bruno Rossion.

References

1. Brédart S. Names and Cognitive Psychology. In: Hough C, editor. The Oxford Handbook of Names and Naming. Oxford, UK: Oxford University Press; 2016. pp. 476–487.
2. Brédart S. The cognitive psychology and neuroscience of naming people. Neurosci Biobehav Rev. 2017; 83: 145–154. https://doi.org/10.1016/j.neubiorev.2017.10.008 PMID: 29038031
3. Young AW, Hay DC, Ellis AW. The faces that launched a thousand slips: Everyday difficulties and errors in recognizing people. Br J Psychol. 1985; 76: 495–523. https://doi.org/10.1111/j.2044-8295.1985.tb01972.x PMID: 4075060
4. Maylor EA. Recognizing and naming faces: aging, memory retrieval, and the tip of the tongue state. J Gerontol. 1990; 45: 215–226.
5. Evrard M. Ageing and lexical access to common and proper names in picture naming. Brain Lang. 2002; 81: 174–179. https://doi.org/10.1006/brln.2001.2515 PMID: 12081390
6. James LE. Specific effects of aging on proper name retrieval: Now you see them, now you don't. J Gerontol Ser B. 2006; 61: 180–183. https://doi.org/10.1093/geronb/61.3.P180 PMID: 16670188
7. Kljajevic V, Erramuzpe A. Proper name retrieval and structural integrity of cerebral cortex in midlife: A cross-sectional study. Brain Cogn. 2018; 120: 26–33. https://doi.org/10.1016/j.bandc.2017.11.003 PMID: 29253727
8. Greene JDW, Hodges JR. Identification of famous faces and famous names in early Alzheimer's disease: Relationship to anterograde episodic and general semantic memory. Brain. 1996; 119: 111–128. https://doi.org/10.1093/brain/119.1.111 PMID: 8624675
9. Calabria M, Sabio A, Martin C, Hernández M, Juncadella M, Gascón-Bayarri J, et al. The missing link between faces and names: Evidence from Alzheimer's disease patients. Brain Cogn. 2012; 80: 250–256. https://doi.org/10.1016/j.bandc.2012.07.002 PMID: 22940399
10. Calabria M, Miniussi C, Bisiacchi PS, Zanetti O, Cotelli M. Face–name repetition priming in semantic dementia: A case report. Brain Cogn. 2009; 70: 231–237. https://doi.org/10.1016/j.bandc.2009.02.005 PMID: 19285772
11. Snowden JS, Thompson JC, Neary D. Knowledge of famous faces and names in semantic dementia. Brain. 2004; 127: 860–872. https://doi.org/10.1093/brain/awh099 PMID: 14985259
12. Miceli G, Capasso R, Daniele A, Esposito T, Magarelli M, Tomaiuolo F. Selective deficit for people's names following left temporal damage: an impairment of domain-specific conceptual knowledge. Cogn Neuropsychol. 2000; 17: 489–516. https://doi.org/10.1080/02643290050110629 PMID: 20945192
13. Milders MW, Deelman B, Berg I. Retrieving familiar people's names in patients with severe closed-head injuries. J Clin Exp Neuropsychol. 1999; 21: 171–185. https://doi.org/10.1076/jcen.21.2.171.932 PMID: 10425515
14. Semenza C, Zettin M. Generating proper names: A case of selective inability. Cogn Neuropsychol. 1988; 5: 711–721. https://doi.org/10.1080/02643298808253279

15. Lucchelli F, De Renzi E. Proper Name Anomia. Cortex. 1992; 28: 221–230. https://doi.org/10.1016/s0010-9452(13)80050-0 PMID: 1499308

16. Otsuka Y, Suzuki K, Fujii T, Miura R, Endo K, Kondo H, et al. Proper name anomia after left temporal subcortical hemorrhage. Cortex. 2005; 41: 39–47. https://doi.org/10.1016/s0010-9452(08)70176-x PMID: 15633705

17. Martins IP, Farrajota L. Proper and common names: A double dissociation. Neuropsychologia. 2007; 45: 1744–1756. https://doi.org/10.1016/j.neuropsychologia.2006.12.016 PMID: 17303198

18. Kurimoto M, Takaiwa A, Nagai S, Hayashi N, Endo S. Anomia for people's names after left anterior temporal lobe resection—case report. Neurol Med Chir (Tokyo). 2010; 50: 36–40.

19. Semenza C. The neuropsychology of proper names. Mind Lang. 2009; 24: 347–369.

20. Bruce V, Young A. Understanding face recognition. Br J Psychol. 1986; 77: 305–327. https://doi.org/10.1111/j.2044-8295.1986.tb02199.x PMID: 3756376

21. Valentine T, Bredart S, Lawson R, Ward G. What's in a name? Access to information from people's names. Eur J Cogn Psychol. 1991; 3: 147–176. https://doi.org/10.1080/09541449108406224

22. Neuner F, Schweinberger SR. Neuropsychological impairments in the recognition of faces, voices, and personal names. Brain Cogn. 2000; 44: 342–366. https://doi.org/10.1006/brcg.1999.1196 PMID: 11104530

23. Hanley JR. An appreciation of Bruce and Young's (1986) serial stage model of face naming after 25 years: Face naming. Br J Psychol. 2011; 102: 915–930. https://doi.org/10.1111/j.2044-8295.2011.02032.x PMID: 21988392

24. Quian Quiroga R, Reddy L, Kreiman G, Koch C, Fried I. Invariant visual representation by single neurons in the human brain. Nature. 2005; 435: 1102–1107. https://doi.org/10.1038/nature03687 PMID: 15973409

25. Quian Quiroga R. Concept cells: the building blocks of declarative memory functions. Nat Rev Neurosci. 2012; 13: 587–597. https://doi.org/10.1038/nrn3251 PMID: 22760181

26. Gainotti G. The format of conceptual representations disrupted in semantic dementia: A position paper. Cortex. 2012; 48: 521–529. https://doi.org/10.1016/j.cortex.2011.06.019 PMID: 21807363

27. Gainotti G. Implications of recent findings for current cognitive models of familiar people recognition. Neuropsychologia. 2015; 77: 279–287. https://doi.org/10.1016/j.neuropsychologia.2015.09.002 PMID: 26359717

28. Nielson KA, Seidenberg M, Woodard JL, Durgerian S, Zhang Q, Gross WL, et al. Common neural systems associated with the recognition of famous faces and names: An event-related fMRI study. Brain Cogn. 2010; 72: 491–498. https://doi.org/10.1016/j.bandc.2010.01.006 PMID: 20167415

29. Sugiura M, Sassa Y, Watanabe J, Akitsuki Y, Maeda Y, Matsue Y, et al. Cortical mechanisms of person representation: Recognition of famous and personally familiar names. NeuroImage. 2006; 31: 853–860. https://doi.org/10.1016/j.neuroimage.2006.01.002 PMID: 16478667

30. Nakamura K, Kawashima R, Sato N, Nakamura A, Sugiura M, Kato T, et al. Functional delineation of the human occipito-temporal areas related to face and scene processing: A PET study. Brain. 2000; 123: 1903–1912. https://doi.org/10.1093/brain/123.9.1903 PMID: 10960054

31. Gorno-Tempini ML, Price CJ. Identification of famous faces and buildings: A functional neuroimaging study of semantically unique items. Brain. 2001; 124: 2087–2097. https://doi.org/10.1093/brain/124.10.2087 PMID: 11571224

32. Gainotti G. Laterality effects in normal subjects' recognition of familiar faces, voices and names. Perceptual and representational components. Neuropsychologia. 2013; 51: 1151–1160. https://doi.org/10.1016/j.neuropsychologia.2013.03.009 PMID: 23542500

33. Snowden JS, Thompson JC, Neary D. Famous people knowledge and the right and left temporal lobes. Behav Neurol. 2012; 25: 35–44. https://doi.org/10.3233/BEN-2012-0347 PMID: 22207421

34. Snowden JS, Harris JM, Thompson JC, Kobylecki C, Jones M, Richardson AM, et al. Semantic dementia and the left and right temporal lobes. Cortex. 2018; 188–203. https://doi.org/10.1016/j.cortex.2017.08.024 PMID: 28947063

35. Cosseddu M, Gazzina S, Borroni B, Padovani A, Gainotti G. Multimodal face and voice recognition disorders in a case with unilateral right anterior temporal lobe atrophy. Neuropsychology. 2018; 32: 920–930. https://doi.org/10.1037/neu0000480 PMID: 30080078

36. Gainotti G. Different patterns of famous people recognition disorders in patients with right and left anterior temporal lesions: A systematic review. Neuropsychologia. 2007; 45: 1591–1607. https://doi.org/10.1016/j.neuropsychologia.2006.12.013 PMID: 17275042

37. Gainotti G, Barbier A, Marra C. Slowly progressive defect in recognition of familiar people in a patient with right anterior temporal atrophy. Brain. 2003; 126: 792–803. https://doi.org/10.1093/brain/awg092 PMID: 12615639

38. Gainotti G, Ferraccioli M, Marra C. The relation between person identity nodes, familiarity judgment and biographical information. Evidence from two patients with right and left anterior temporal atrophy. Brain Res. 2010; 1307: 103–114. https://doi.org/10.1016/j.brainres.2009.10.009 PMID: 19836361

39. Busigny T, de Boissezon X, Puel M, Nespoulous J-L, Barbeau EJ. Proper name anomia with preserved lexical and semantic knowledge after left anterior temporal lesion: A two-way convergence defect. Cortex. 2015; 65: 1–18. https://doi.org/10.1016/j.cortex.2014.12.008 PMID: 25617826

40. Harris RJ, Rice GE, Young AW, Andrews TJ. Distinct but overlapping patterns of response to words and faces in the fusiform gyrus. Cereb Cortex. 2016; 26: 3161–3168. https://doi.org/10.1093/cercor/bhv147 PMID: 26157025

41. Rogers TT, Lambon Ralph MA, Garrard P, Bozeat S, McClelland JL, Hodges JR, et al. Structure and deterioration of semantic memory: A neuropsychological and computational investigation. Psychol Rev. 2004; 111: 205–235. https://doi.org/10.1037/0033-295X.111.1.205 PMID: 14756594

42. Patterson K, Nestor PJ, Rogers TT. Where do you know what you know? The representation of semantic knowledge in the human brain. Nat Rev Neurosci. 2007; 8: 976–987. https://doi.org/10.1038/nrn2277 PMID: 18026167

43. Lambon Ralph MA. Neurocognitive insights on conceptual knowledge and its breakdown. Philos Trans R Soc B Biol Sci. 2014; 369: 20120392. https://doi.org/10.1098/rstb.2012.0392 PMID: 24324236

44. Lambon Ralph MA, Jefferies E, Patterson K, Rogers TT. The neural and computational bases of semantic cognition. Nat Rev Neurosci. 2017; 18: 42–55. https://doi.org/10.1038/nrn.2016.150 PMID: 27881854

45. Rice GE, Hoffman P, Binney RJ, Lambon Ralph MA. Concrete versus abstract forms of social concept: an fMRI comparison of knowledge about people versus social terms. Philos Trans R Soc B Biol Sci. 2018; 373: 20170136. https://doi.org/10.1098/rstb.2017.0136 PMID: 29915004

46. Coccia M, Bartolini M, Luzzi S, Provinciali L, Lambon Ralph MA. Semantic memory is an amodal, dynamic system: Evidence from the interaction of naming and object use in semantic dementia. Cogn Neuropsychol. 2004; 21: 513–527. https://doi.org/10.1080/02643290342000113 PMID: 21038218

47. Jefferies E, Lambon Ralph MA. Semantic impairment in stroke aphasia versus semantic dementia: a case-series comparison. Brain. 2006; 129: 2132–2147. https://doi.org/10.1093/brain/awl153 PMID: 16815878

48. Hoffman P, Evans GAL, Lambon Ralph MA. The anterior temporal lobes are critically involved in acquiring new conceptual knowledge: Evidence for impaired feature integration in semantic dementia. Cortex. 2014; 50: 19–31. https://doi.org/10.1016/j.cortex.2013.10.006 PMID: 24268323

49. Rice GE, Hoffman P, Lambon Ralph MA. Graded specialization within and between the anterior temporal lobes. Ann N Y Acad Sci. 2015; 1359: 84–97. https://doi.org/10.1111/nyas.12951 PMID: 26502375

50. Hoffman P, Lambon Ralph MA. From percept to concept in the ventral temporal lobes: Graded hemispheric specialisation based on stimulus and task. Cortex. 2018; 101: 107–118. https://doi.org/10.1016/j.cortex.2018.01.015 PMID: 29475076

51. Mayberry EJ, Sage K, Lambon Ralph MA. At the edge of semantic space: the breakdown of coherent concepts in semantic dementia is constrained by typicality and severity but not modality. J Cogn Neurosci. 2010; 23: 2240–2251. https://doi.org/10.1162/jocn.2010.21582 PMID: 21126159

52. Rice GE, Lambon Ralph MA, Hoffman P. The roles of left versus right anterior temporal lobes in conceptual knowledge: an ALE meta-analysis of 97 functional neuroimaging studies. Cereb Cortex. 2015; 25: 4374–4391. https://doi.org/10.1093/cercor/bhv024 PMID: 25771223

53. Visser M, Jefferies E, Lambon Ralph MA. Semantic processing in the anterior temporal lobes: a meta-analysis of the functional neuroimaging literature. J Cogn Neurosci. 2010; 22: 1083–1094. https://doi.org/10.1162/jocn.2009.21309 PMID: 19583477

54. Visser M, Embleton KV, Jefferies E, Parker GJM, Lambon Ralph MA. The inferior, anterior temporal lobes and semantic memory clarified: Novel evidence from distortion-corrected fMRI. Neuropsychologia. 2010; 48: 1689–1696. https://doi.org/10.1016/j.neuropsychologia.2010.02.016 PMID: 20176043

55. Visser M, Jefferies E, Embleton KV, Lambon Ralph MA. Both the middle temporal gyrus and the ventral anterior temporal area are crucial for multimodal semantic processing: distortion-corrected fMRI evidence for a double gradient of information convergence in the temporal lobes. J Cogn Neurosci. 2012; 24: 1766–1778. https://doi.org/10.1162/jocn_a_00244 PMID: 22621260

56. Pobric G, Jefferies E, Lambon Ralph MA. Anterior temporal lobes mediate semantic representation: mimicking semantic dementia by using rTMS in normal participants. Proc Natl Acad Sci U S A. 2007; 104: 20137–20141. https://doi.org/10.1073/pnas.0707383104 PMID: 18056637

57. Pobric G, Jefferies E, Lambon Ralph MA. Amodal semantic representations depend on both anterior temporal lobes: Evidence from repetitive transcranial magnetic stimulation. Neuropsychologia. 2010; 48: 1336–1342. https://doi.org/10.1016/j.neuropsychologia.2009.12.036 PMID: 20038436

58. Chen L, Lambon Ralph MA, Rogers TT. A unified model of human semantic knowledge and its disorders. Nat Hum Behav. 2017; 1: 0039. https://doi.org/10.1038/s41562-016-0039 PMID: 28480333

59. Chedid G, Wilson MA, Provost J-S, Joubert S, Rouleau I, Brambati SM. Differential involvement of the anterior temporal lobes in famous people semantics. Front Psychol. 2016; 7: 1333. https://doi.org/10.3389/fpsyg.2016.01333 PMID: 27625630

60. Gorno-Tempini ML, Price CJ, Josephs O, Vandenberghe R, Cappa SF, Kapur N, et al. The neural systems sustaining face and proper-name processing. Brain. 1998; 121: 2103–2118. https://doi.org/10.1093/brain/121.11.2103 PMID: 9827770

61. Amado C, Kovács P, Mayer R, Ambrus GG, Trapp S, Kovács G. Neuroimaging results suggest the role of prediction in cross-domain priming. Sci Rep. 2018; 8: 10356. https://doi.org/10.1038/s41598-018-28696-0 PMID: 29985455

62. Ambrus GG, Amado C, Krohn L, Kovács G. TMS of the occipital face area modulates cross-domain identity priming. Brain Struct Funct. 2019; 224: 149–157. https://doi.org/10.1007/s00429-018-1768-0 PMID: 30291480

63. Joassin F, Meert G, Campanella S, Bruyer R. The associative processes involved in faces-proper names versus animals-common names binding: A comparative ERP study. Biol Psychol. 2007; 75: 286–299. https://doi.org/10.1016/j.biopsycho.2007.04.002 PMID: 17521799

64. Adrian ED, Matthews BH. The Berger rhythm: potential changes from the occipital lobes in man. Brain. 1934; 57: 355–385.

65. Regan D. Some characteristics of average steady-state and transient responses evoked by modulated light. Electroencephalogr Clin Neurophysiol. 1966; 20: 238–248. https://doi.org/10.1016/0013-4694(66)90088-5 PMID: 4160391

66. Regan D. Human Brain Electrophysiology: Evoked Potentials and Evoked Magnetic Fields in Science and Medicine. Elsevier. 1989.

67. Norcia AM, Appelbaum LG, Ales JM, Cottereau BR, Rossion B. The steady-state visual evoked potential in vision research: A review. J Vis. 2015; 15: 4. https://doi.org/10.1167/15.6.4 PMID: 26024451

68. Liu-Shuang J, Norcia AM, Rossion B. An objective index of individual face discrimination in the right occipito-temporal cortex by means of fast periodic oddball stimulation. Neuropsychologia. 2014; 52: 57–72. https://doi.org/10.1016/j.neuropsychologia.2013.10.022 PMID: 24200921

69. Rossion B, Torfs K, Jacques C, Liu-Shuang J. Fast periodic presentation of natural images reveals a robust face-selective electrophysiological response in the human brain. J Vis. 2015; 15: 1–18. https://doi.org/10.1167/15.1.18 PMID: 25597037

70. Lochy A, Van Reybroeck M, Rossion B. Left cortical specialization for visual letter strings predicts rudimentary knowledge of letter-sound association in preschoolers. Proc Natl Acad Sci U S A. 2016; 113: 8544–8549. https://doi.org/10.1073/pnas.1520366113 PMID: 27402739

71. Retter TL, Rossion B. Uncovering the neural magnitude and spatio-temporal dynamics of natural image categorization in a fast visual stream. Neuropsychologia. 2016; 91: 9–28. https://doi.org/10.1016/j.neuropsychologia.2016.07.028 PMID: 27461075

72. Regan D, Heron JR. Clinical investigation of lesions of the visual pathway: a new objective technique. J Neurol Neurosurg Psychiatry. 1969; 32: 479. https://doi.org/10.1136/jnnp.32.5.479 PMID: 5360055

73. Visser M, Lambon Ralph MA. Differential contributions of bilateral ventral anterior temporal lobe and left anterior superior temporal gyrus to semantic processes. J Cogn Neurosci. 2011; 23: 3121–3131. https://doi.org/10.1162/jocn_a_00007 PMID: 21391767

74. Grabowski TJ, Damasio H, Tranel D, Boles Ponto LL, Hichwa RD, Damasio AR. A role for left temporal pole in the retrieval of words for unique entities. Hum Brain Mapp. 2001; 13: 199–212. PMID: 11410949

75. Tranel D. The left temporal pole is important for retrieving words for unique concrete entities. Aphasiology. 2009; 23: 867. https://doi.org/10.1080/02687030802586498 PMID: 20161625

76. Waldron EJ, Manzel K, Tranel D. The left temporal pole is a heteromodal hub for retrieving proper names. Front Biosci. 2014; 6: 50–57.

77. Schneider B, Heskje J, Bruss J, Tranel D, Belfi AM. The left temporal pole is a convergence region mediating the relation between names and semantic knowledge for unique entities: Further evidence from a "recognition-from-name" study in neurological patients. Cortex. 2018; 109: 14–24. https://doi.org/10.1016/j.cortex.2018.08.026 PMID: 30273798

78. Binney RJ, Parker GJM, Lambon Ralph MA. Convergent connectivity and graded specialization in the rostral human temporal lobe as revealed by diffusion-weighted imaging probabilistic tractography. J Cogn Neurosci. 2012; 24: 1998–2014. https://doi.org/10.1162/jocn_a_00263 PMID: 22721379

79. Binney RJ, Embleton KV, Jefferies E, Parker GJM, Lambon Ralph MA. The ventral and inferolateral aspects of the anterior temporal lobe are crucial in semantic memory: evidence from a novel direct comparison of distortion-corrected fMRI, rTMS, and semantic dementia. Cereb Cortex. 2010; 20: 2728–2738. https://doi.org/10.1093/cercor/bhq019 PMID: 20190005

80. Jonas J, Jacques C, Liu-Shuang J, Brissart H, Colnat-Coulbois S, Maillard L, et al. A face-selective ventral occipito-temporal map of the human brain with intracerebral potentials. Proc Natl Acad Sci U S A. 2016; 113: 4088–4097. https://doi.org/10.1073/pnas.1522033113 PMID: 27354526

81. Lochy A, Jacques C, Maillard L, Colnat-Coulbois S, Rossion B, Jonas J. Selective visual representation of letters and words in the left ventral occipito-temporal cortex with intracerebral recordings. Proc Natl Acad Sci. 2018; 115: 7595–7604.

82. Quian Quiroga R, Panzeri S. Extracting information from neuronal populations: information theory and decoding approaches. Nat Rev Neurosci. 2009; 10: 173–185. https://doi.org/10.1038/nrn2578 PMID: 19229240

83. Damasio H, Grabowski TJ, Tranel D, Hichwa RD, Damasio AR. A neural basis for lexical retrieval. Nature. 1996; 380: 499–505. https://doi.org/10.1038/380499a0 PMID: 8606767

84. Tranel D. Impaired naming of unique landmarks is associated with left temporal polar damage. Neuropsychology. 2006; 20: 1–10. https://doi.org/10.1037/0894-4105.20.1.1 PMID: 16460217

85. Drane DL, Ojemann JG, Phatak V, Loring DW, Gross RE, Hebb AO, et al. Famous face identification in temporal lobe epilepsy: Support for a multimodal integration model of semantic memory. Cortex. 2013; 49: 1648–1667. https://doi.org/10.1016/j.cortex.2012.08.009 PMID: 23040175

86. Albert MS, Butters N, Levin J. Temporal gradients in the retrograde amnesia of patients with alcoholic Korsakoff's disease. Arch Neurol. 1979; 36: 211–216. https://doi.org/10.1001/archneur.1979.00500400065010 PMID: 426664

87. Tranel D, Damasio H, Damasio AR. A neural basis for the retrieval of conceptual knowledge. Neuropsychologia. 1997; 35: 1319–1327. https://doi.org/10.1016/s0028-3932(97)00085-7 PMID: 9347478

88. Zimmermann FGS, Yan X, Rossion B. An objective, sensitive and ecologically valid neural measure of rapid human individual face recognition. R Soc Open Sci. 2019; 6: 181904. https://doi.org/10.1098/rsos.181904 PMID: 31312474

89. Quek GL, Liu-Shuang J, Goffaux V, Rossion B. Ultra-coarse, single-glance human face detection in a dynamic visual stream. NeuroImage. 2018; 176: 465–476. https://doi.org/10.1016/j.neuroimage.2018.04.034 PMID: 29678757

90. Retter TL, Rossion B. Visual adaptation provides objective electrophysiological evidence of facial identity discrimination. Cortex. 2016; 80: 35–50. https://doi.org/10.1016/j.cortex.2015.11.025 PMID: 26875725

91. Talairach J, Bancaud J. Stereotaxic approach to epilepsy: methodology of anatomo-functional stereotaxic investigations. Prog Neurol Surg. 1973; 5: 297–354. https://doi.org/10.1159/000394343

92. Mullin JP, Shriver M, Alomar S, Najm I, Bulacio J, Chauvel P, et al. Is SEEG safe? A systematic review and meta-analysis of stereo-electroencephalography–related complications. Epilepsia. 2016; 57: 386–401. https://doi.org/10.1111/epi.13298 PMID: 26899389

93. Bourdillon P, Ryvlin P, Isnard J, Montavont A, Catenoix H, Mauguière F, et al. Stereotactic electroencephalography is a safe procedure, including for insular implantations. World Neurosurg. 2017; 99: 353–361. https://doi.org/10.1016/j.wneu.2016.12.025 PMID: 28003163

94. Salado AL, Koessler L, De Mijolla G, Schmitt E, Vignal J-P, Civit T, et al. sEEG is a safe procedure for a comprehensive anatomic exploration of the insula: a retrospective study of 108 procedures representing 254 transopercular insular electrodes. Oper Neurosurg. 2017; 14: 1–8.

95. Jonas J, Jacques C, Liu-Shuang J, Brissart H, Colnat-Coulbois S, Maillard L, et al. A face-selective ventral occipito-temporal map of the human brain with intracerebral potentials. Proc Natl Acad Sci. 2016; 113: E4088–E4097. https://doi.org/10.1073/pnas.1522033113 PMID: 27354526

96. Volfart A, Jonas J, Maillard LG, Colnat-Coulbois S, Rossion B. Data from: Neurophysiological evidence for crossmodal (face-name) person-identity representation in the human left ventral temporal cortex. Dryad Digit Repos. 2020. https://doi.org/10.5061/dryad.m8t391m

NeuroImage 221 (2020) 117174

Contents lists available at ScienceDirect

NeuroImage

journal homepage: www.elsevier.com/locate/neuroimage

The neural basis of rapid unfamiliar face individuation with human intracerebral recordings

Corentin Jacques[a,1], Bruno Rossion[a,b,c,1,*], Angélique Volfart[a,b], Hélène Brissart[b,c], Sophie Colnat-Coulbois[b,d], Louis Maillard[b,c], Jacques Jonas[b,c]

[a] Psychological Sciences Research Institute and Institute of Neuroscience, Université Catholique de Louvain (UCLouvain), 1348 Louvain-la-Neuve, Belgium
[b] Université de Lorraine, CNRS, CRAN, F-54000 Nancy, France
[c] Université de Lorraine, CHRU-Nancy, Service de Neurologie, F-54000 Nancy, France
[d] Université de Lorraine, CHRU-Nancy, Service de Neurochirurgie, F-54000 Nancy, France

ARTICLE INFO

Keywords:
Face recognition
SEEG
Fast periodic visual stimulation
Ventral occipito-temporal cortex
Fusiform gyrus

ABSTRACT

Rapid individuation of conspecifics' faces is ecologically important in the human species, whether the face belongs to a familiar or unfamiliar individual. Here we tested a large group ($N = 69$) of epileptic patients implanted with intracerebral electrodes throughout the ventral occipito-temporal cortex (VOTC). We used a frequency-tagging visual stimulation paradigm optimized to objectively measure face individuation with direct neural recordings. This enabled providing an extensive map of the significantly larger neural responses to upright than to inverted unfamiliar faces, i.e. reflecting visual face individuation processes that go beyond physical image differences. These high-level face individuation responses are both distributed and anatomically confined to a strip of cortex running from the inferior occipital gyrus all along the lateral fusiform gyrus, with a large right hemispheric dominance. Importantly, face individuation responses are limited anteriorly to the bilateral anterior fusiform gyrus and surrounding sulci, with a near absence of significant responses in the extensively sampled temporal pole. This large-scale mapping provides original evidence that face individuation is supported by a distributed yet anatomically constrained population of neurons in the human VOTC, and highlights the importance of probing this function with face stimuli devoid of associated semantic, verbal and affective information.

1. Introduction

Face individuation (FID) occurs when the face of a unique individual elicits a specific behavioral and/or neural response that is reliably distinct from the response to other individuals. Individuation of *unfamiliar* faces is critical in the human species for three main reasons. First, in humans, recognition of conspecifics' identity is based primarily on the face (Sheehan and Nachman, 2014). Second, in most human societies, people are constantly exposed to unfamiliar faces in their natural or digital environment. Third, recognizing familiar people based on their faces requires to pick out idiosyncratic features of these faces when we first encounter them or when they have not yet been encoded in long-term memory, i.e. when they are unfamiliar.

Although non-human animal species can be trained to behaviorally individuate pictures of unfamiliar faces of conspecifics or even of humans, their performance is often limited and strictly image-dependent (e.g., fish: Newport et al., 2016; wasps: Sheehan and Tibbetts, 2011). By comparison, human adults naturally excel at individuating unfamiliar human faces (Rossion, 2018), having acquired this ability without formal training throughout development (Carey, 1992; Hills and Lewis, 2018). Their individuation of unfamiliar faces is fast (e.g., within 1–2 fixations and a few hundreds of milliseconds; Hsiao and Cottrell, 2008; Jacques et al., 2007) and automatic (i.e., occurring without the intention to do so and being able to suppress it; Liu-Shuang et al., 2014; Palermo and Rhodes, 2007; Yan et al., 2019).

Given the importance of faces for social interactions in the human species, understanding the neural basis of human FID must be a major scientific goal in cognitive neuroscience. Using pictures of unfamiliar faces is critical to achieve this goal since they are not associated with semantic information, affect or verbal labels, therefore allowing to isolate the contribution of *visual* processes to FID (Rossion, 2018). Neurophysiological studies have reported face-selective neurons in the infero-temporal cortex of the macaque monkey that fire at a different spike rate to pictures of different (monkey and human) unfamiliar

* Corresponding author at: CRAN, UMR 7039, CNRS - Université de Lorraine, Pavillon Krug, Hôpital Central, CHRU Nancy - University Hospital of Nancy, 29 Avenue du Maréchal de Lattre de Tassigny, 54000 Nancy, France.
E-mail address: bruno.rossion@univ-lorraine.fr (B. Rossion).
[1] These authors contributed equally

https://doi.org/10.1016/j.neuroimage.2020.117174
Received 25 February 2020; Received in revised form 19 May 2020; Accepted 14 July 2020
Available online 17 July 2020

faces, suggesting that face identity is coded in terms of distributed patterns of spike rates in small local neuronal populations (Baylis et al., 1985; Chang and Tsao, 2017; Leopold et al., 2006; also Young and Yamane, 1992 with familiar faces). However, similarly to other non-human animal species, macaque monkeys are poor at behavioral FID tasks and may rely essentially on low-level image-based statistics (Parr et al., 2008; Rossion and Taubert, 2019). Moreover, their performance differ qualitatively from humans at such tasks (e.g., no effect of picture-plane inversion of the stimuli; see Bruce, 1982; Griffin, 2020) such that this species does not provide an adequate model of human FID (Rossion and Taubert, 2019). In humans, neurons firing for specific facial identities have been recorded in the medial temporal lobe, but this firing occurs only to highly familiar faces, irrespective of the presentation format (e.g., Jennifer Aniston's face and her written name) (Quian Quiroga et al., 2005). Moreover, these neurons fire relatively late (about 300 ms onset) and are thought to play a role in recollecting conscious episodic multimodal memory events rather than in the FID process *per se* (Quian Quiroga, 2012; Rey et al., 2020).

At the system level of neural organization in humans, lesions causing a selective impairment in face identity recognition, i.e. prosopagnosia (Bodamer, 1947), are located in the ventral occipito-temporal cortex (VOTC), with a right hemispheric lesion being both necessary and sufficient to cause such impairment in most individuals (Barton, 2008; Bouvier and Engel, 2006; Meadows, 1974; Sergent and Signoret, 1992). Providing that correct response times are considered, these patients are also systematically impaired at unfamiliar face matching tasks (Farah, 1990). While the brain structures involved remain necessarily coarsely defined in lesion studies, recent studies have reported that focal intracerebral stimulation of the face-selective regions in the right VOTC generate transient impairments in face identity recognition (Jonas et al., 2015, 2012), including unfamiliar face matching (Jonas et al., 2014). In typical adults, functional magnetic resonance imaging (fMRI) studies have used fMRI-adaptation and multivariate pattern analysis (MVPA) to define the neural basis of FID. On the one hand, fMRI-adaptation takes advantage of the reduced neural response to a repeated stimulus ('repetition suppression') (Grill-Spector et al., 2006; Grill-Spector and Malach, 2001). Repetition suppression effects for unfamiliar individual face pictures have been found in pre-defined face-selective regions of the VOTC such as the inferior occipital gyrus (IOG, or "Occipital Face Area", OFA) and the lateral section of middle fusiform gyrus (latFG or "Fusiform Face Area", FFA; Eger et al., 2004; Ewbank et al., 2013; Gauthier et al., 2000; Gilaie-Dotan et al., 2010; Hermann et al., 2017; Hughes et al., 2019; Rostalski et al., 2019; Schiltz and Rossion, 2006). On the other hand, MVPA approaches rely on the decoding of differences between the patterns of activity evoked by different individual faces across multiple voxels. However, the decoding accuracies in this approach, often for simple image-based discriminations, are rather modest and found in inconsistent brain regions across studies (Anzellotti et al., 2014; Goesaert and Op de Beeck, 2013; Kriegeskorte et al., 2007; Natu et al., 2010; Nestor et al., 2011; see the critical view in Kanwisher, 2017).

Overall, fMRI studies have either focused on specific regions of interest or investigated response patterns at a local scale (i.e., region-of-interest analyses in repetition suppression; searchlight analyses in MVPA), rather than considering the whole VOTC. Similarly, the majority of human intracranial EEG studies that have investigated FID using repetition suppression (Engell and McCarthy, 2014; Puce et al., 1999) or MVPA (Davidesco et al., 2014; Ghuman et al., 2014) have either focused on specific anatomical regions (Davidesco et al., 2014; Engell and Mccarthy, 2014; Ghuman et al., 2014; see Puce et al., 1999 for an exception) or combined data from different regions (Davidesco et al., 2014). In addition, despite its strengths (i.e., non-invasiveness, high spatial resolution and large spatial coverage), fMRI provides indirect neural recordings associated with large fluctuations of signal-to-noise ratio across brain regions, making it difficult to fairly assess the FID function across the entire VOTC. In particular, due to severe magnetic susceptibility artifacts arising from the ear canals (Axelrod and Yovel, 2013; Jonas et al., 2015; Rossion et al., 2018; Wandell, 2011), fMRI is limited in exploring VOTC regions located anteriorly to the middle fusiform gyrus, i.e. in the anterior temporal lobe (ATL). Although intracranial EEG studies do not suffer from regional variations in signal-to-noise ratio, previous investigations have not localized, quantified, and compared FID neural responses across anatomical regions of the human VOTC.

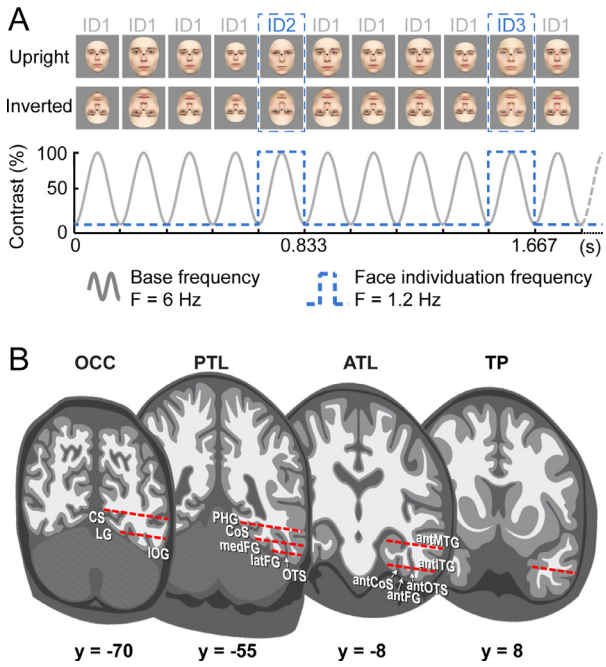

Fig. 1. Fast periodic visual stimulation (FPVS) paradigm and SEEG method. **A.** In the paradigm used here (from Liu-Shuang et al., 2014), face images are presented by sinusoidal contrast modulation at a rate of six stimuli per second (6 Hz) in sequences of 65 s. In each sequence, a base face (here ID1) is randomly selected within a pool of 25 male or 25 female faces and repeated throughout the sequence. At a fixed interval of every 5th base face (i.e. at the frequency of 6 Hz/5 = 1.2 Hz), a different unfamiliar facial identity (selected from the 24 remaining faces of the same gender) is presented (e.g. ID2, ID3, etc.). To avoid pixel-wise overlap, face size is randomly varied between 77% and 123% at every stimulation cycle. In a given sequence, faces are either presented all upright or all in the inverted orientation. **B.** Schematic coronal representation of the typical trajectories of depth electrodes implanted in the VOTC. Electrodes consist of 8–15 contiguous recording contacts (red rectangles) spread along the electrode length, along the medio-lateral axis. Acronyms: TP: temporal pole; ATL: anterior temporal lobe; PTL: posterior temporal lobe; OCC: occipital lobe; PHG: parahippocampal gyrus; CoS: collateral sulcus; FG: fusiform gyrus; ITG: inferior temporal gyrus; MTG: middle temporal gyrus; OTS: occipito-temporal sulcus; CS: calcarine sulcus; IOG: inferior occipital gyrus; LG: lingual gyrus; ant: anterior; lat: lateral; med: medial. (For interpretation of the references to colour in this figure legend, the reader is referred to the web version of this article.)

Here, we provide a comprehensive map of direct neural responses of FID measured in the whole human VOTC. To achieve this, we use a validated frequency-tagging paradigm to capture the FID function in a large group (N = 69) of epileptic patients implanted with intracerebral (i.e., depth) electrodes across the VOTC (stereotaxic-electroencephalography, SEEG, Talairach and Bancaud, 1973), allowing to measure local neural activity from the cortex. In this paradigm (Liu-Shuang et al., 2014, reviewed in Rossion et al., 2020), the picture of an unfamiliar face identity devoid of external features ("base face" = ID1) is randomly selected from a large set of face identities, and repeated at a constant rate of 6 Hz for about one minute. During this face stimulation sequence, other unfamiliar face identities (ID2, ID3, ID4, etc.) are inserted among the base face at regular intervals as every 5th face (Fig. 1A). As a result, a change of face identity occurs periodically at 6 Hz/5, i.e. 1.2 Hz, while

observers complete an orthogonal task. Responses measured in the EEG (on the scalp) or SEEG (inside the brain) exactly at the 1.2 Hz identity change frequency and its harmonics (i.e., 2.4 Hz, etc.) index FID. Combined with electroencephalography, this paradigm has many advantages: it is highly sensitive (i.e., high signal-to-noise ratio and significant effects in >90% of individuals tested during a few minutes), objective (i.e., providing responses at experimentally-defined frequencies), and reliable (i.e., with stable responses within and between recording sessions, Dzhelyova et al., 2019; see Rossion et al., 2020 for an extensive review of 20 published studies with this paradigm with scalp EEG recordings).

Here, we extensively cover the bilateral VOTC by sampling a total of 3825 recording contacts in the gray matter from 69 participants tested with this paradigm (Fig. 1B). We quantify the 1.2 Hz FID response at each recording contact and map this response across the VOTC to define the neural basis of human unfamiliar FID. Importantly, in order to isolate high-level FID effects, i.e. effects that go beyond mere physical differences between images, we compare the FID responses to upright and inverted faces tested in separate stimulation sequences. Since picture-plane inversion is known to largely impair FID (Yin, 1969; Rossion, 2008 for review) and severely reduces scalp EEG responses in the paradigm used here (Liu-Shuang et al., 2014), we expect this manipulation to substantially decrease the FID response in the critical regions subtending face individuation.

2. Materials and methods

2.1. Participants

The study included 69 participants (32 females, mean age: 32.3 ± 8 years, 63 right-handed and 6 left-handed) undergoing clinical intracerebral evaluation with depth electrodes (SEEG, Talairach and Bancaud, 1973) for refractory partial epilepsy in the Epilepsy Unit of the University Hospital of Nancy. They were included in the study if they had at least one intracerebral electrode implanted in the ventral occipito-temporal cortex. All participants tested in SEEG gave written consent to participate to the study, which was part of a protocol approved by the human investigation committee of the University Hospital of Nancy.

Intellectual efficiency (IQ, WAIS-IV) was assessed in 58 participants, with an average IQ score of 88.8 ± 14.8. All but 11 participants performed the electronic version of the Benton Face Recognition Test (BFRT-c; Rossion and Michel, 2018; see Benton and Van Allen, 1968 for the original version of the test) before the SEEG exploration. Their average score at the BFRT-c was of 42.1 ± 4.5, although 13 participants had scores below normal range (i.e., <39; range 32–52; see distribution of BFRT-c scores in Fig. S1). Average response time to perform the BFRT-c was about 6 min (360.4 s ± 165.8, range 146–1016 s; see distribution of BFRT-c reaction times in Fig. S1A). A subset of these participants (N = 32; 46%) also performed a behavioral delayed matching task (as described in Busigny and Rossion, 2010, experiment 4) with upright and inverted faces. Accuracy and response times were comparable to older control participants reported in the literature (Busigny and Rossion, 2010) and response times were correlated with age, IQ and visuospatial processing speed (as assessed by the subtest Code of the WAIS) (Table S1). They displayed a large face inversion effect in accuracy (upright faces: 87 ± 9.5%; inverted faces: 71.4 ± 11.6%, one-tailed t-test: t(31) = 10.2, p < 0.001) and correct response times (upright faces: 1959 ± 480 ms; inverted faces: 2219 ± 496 ms, one-tailed t-test: t(31) = 6.3, p < 0.001). Every single participant of this subsample showed better performance for upright than inverted faces (Fig. S1B).

2.2. Intracerebral electrode implantation and SEEG recording

Intracerebral electrodes (Dixi Medical, Besançon, France) were stereotactically implanted in the patient's brain for purely clinical purposes, i.e., in order to delineate the seizure onset zone (Talairach and Bancaud, 1973). The sites of electrode implantation were determined based on non-invasive data collected during an earlier phase of the investigation. Each 0.8 mm diameter intracerebral electrode contains 8–15 independent recording contacts of 2 mm in length separated by 1.5 mm from edge to edge (Fig. 1B, for details about the electrode implantation procedure, see Salado et al., 2018). The exact anatomical location of each recording contact was determined by coregistration of post-operative non-stereotactic CT-scan with a pre-operative T1-weighted MRI. A total of 484 electrode arrays were implanted in the VOTC of the 69 participants. These electrodes contained 3825 individual recording contacts in the gray matter (left hemisphere: 2031; right hemisphere: 1794). Intracerebral EEG was recorded at a 512 Hz sampling rate referenced to either a midline prefrontal scalp electrode (FPz, in 59 participants) or an intracerebral contact in the white matter (in 10 participants).

2.3. Face individuation fast periodic visual stimulation (FPVS) paradigm

2.3.1. Stimuli

We used full-front colored photographs of 25 male and 25 female faces with a neutral expression, taken under standardized conditions with respect to lighting, background, and distance from the camera (Fig. 1A for examples of faces; same stimuli as in Liu-Shuang et al., 2014). External features such as hair and ears were cropped out. Inverted (upside-down) versions of these faces were generated by vertically flipping each image.

2.3.2. Experimental procedure

Participants viewed sequences of face images (Fig. 1A) presented at a rate of 6 Hz through sinusoidal contrast modulation. In separate sequences, faces were either presented in the upright orientation or in the inverted orientation. Faces were of the same sex within a sequence. A sequence lasted 65 s, consisting of 60 s of stimulation at full-contrast followed by 5 s of "fade-out", where contrast gradually decreased. In every sequence, the base face was one randomly selected face identity (within the 25 faces of one sex set) and repeated throughout at 6 Hz (e.g., identity 1, ID1). At fixed intervals of every 1/5 face, a different facial identity (selected from the 24 remaining faces of the same sex set) was shown (ID2, ID3, ID4, etc.). Thus, face identity changes occurred a frequency of 6 Hz/5, i.e., 1.2 Hz (Fig. 1A). As a result, EEG amplitude at this frequency (1.2 Hz) and its harmonics (i.e. integer multiples: 2.4 Hz, 3.6 Hz, etc.) was used as an index of the visual system's discrimination of individual faces. To avoid confounding changes of face identity with changes of local pixel intensity (e.g., blue eyes vs. brown eyes), face size varied randomly between 77% and 123% at every 6 Hz stimulation cycle to minimize the overlap between the spatial location of a given facial landmark across cycles. During the stimulation, participants fixated a small black cross presented continuously at the center of the stimuli and had to detect brief (500 ms) color-changes of this fixation cross (black to red), occurring randomly 8 times in each sequence. Due to equipment malfunction, the behavioral data at color-change detection is missing for 11 participants. In the remaining 58 participants, accuracy at detecting the color change of the fixation cross was near ceiling for both the upright (96.7 ± 4.3%; range: 61 to 100%) and inverted (95.1 ± 5.7%; range: 60 to 100%) conditions, with no significant difference between conditions (p = 0.2, 2-tailed paired permutation test). Participants were slightly and significantly slower to respond to the color change in the upright (471 ± 56 ms) compared to inverted (457 ± 50 ms) condition (p = 0.011, 2-tailed paired permutation test).

Half of the participants (N = 34) were presented with 4 sequences (2 sequences per face orientation, one with male faces, one with female faces, i.e. around 5 min of experiment, including short breaks). Twenty-two participants viewed 8 sequences (4 in each face orientation), 3 participants viewed 12 sequences (6 per face orientation) and 10 participants viewed only 2 sequences (1 per face orientation). These

differences across participants were due to the particular clinical context in which the experiment took place. Since the study does not compare across individual participants, we considered all the collected data for analysis. No participant had seizures in the 2 h preceding FPVS recordings.

2.4. SEEG signal processing and analyses

SEEG signal processing and analyses were largely similar to those in previous studies with this approach (Jonas et al., 2016; Lochy et al., 2018) but is reported in full in the present study.

2.4.1. Frequency domain processing

We analyzed segments of SEEG corresponding to stimulation sequences (69-second segments, −2 s to +67 s). The 69 s data segments were cropped to contain an integer number of 1.2 Hz cycles beginning 2 s after the onset of the sequence until approximately 60 s, before stimulus fade-out (69 identity change cycles ≈ 58 s). Sequences were then averaged in the time-domain, separately for each condition and each participant. No further pre-processing was applied to the recordings. Subsequently, a Fast Fourier Transform (FFT) was applied to these averaged segments and amplitude spectra (see examples in Fig. 2A) were extracted for all contacts.

2.4.2. Face individuation (FID) responses

The FPVS approach used here allows identifying two distinct types of responses: (1) a general visual stimulation response at the base stimulation frequency (6 Hz) and its harmonics (e.g., 12 Hz, 18 Hz, etc.), as well as (2) a face individuation response at 1.2 Hz and its harmonics (FID response, Fig. 1A). In the current study, we will focus on the FID response. The significance of FID responses relative to noise was determined as follows (Fig. 2). First, the FFT spectrum was cut into segments centered at the identity change frequency and harmonics, i.e., 1.2 Hz, 2.4 Hz, 3.6 Hz and 4.8 Hz (no responses were found above 6 Hz) and surrounded by 25 neighboring bins on each side. Next, the amplitude values of these 4 segments of FFT spectra were summed. Finally, the summed FFT spectrum was transformed into a Z-score. Z-scores were computed as the difference between the amplitude at the center identity change frequency bin and the mean amplitude of 48 surrounding bins (25 bins on each side, excluding the 2 bins directly adjacent to the bin of interest, i.e., 48 bins), divided by the standard deviation of amplitudes in the corresponding 48 surrounding bins. A recording contact was labeled as an FID contact if the Z-score of the FID response at the identity change frequency bin exceeded 3.1 (i.e., $p < 0.001$ one-tailed), in the upright, in the inverted condition or in both conditions. A one-tailed test was used as the search is restricted to recording contacts showing larger signal than noise (Dzhelyova et al., 2019; Jonas et al., 2016; Liu-Shuang et al., 2016; Lochy et al., 2018).

2.4.3. Classification of FID contacts in UP and INV contacts

For the proportion analysis, FID contacts were further split in 2 sets of contacts: (1) the contacts that showed a significant FID response in the upright condition, regardless of the responses in the inverted condition (*UP contacts*, Fig. 3, left); (2) the contacts that showed a significant FID response in the inverted condition, regardless of the responses in the upright condition (*INV contacts*, Fig. 3, right). Some contacts exhibited significant responses in both upright and inverted conditions such that the two sets overlapped (Fig. 3, bottom; Fig. 4A).

2.4.4. Quantification of response amplitude

Amplitude quantification was performed on all FID contacts (i.e., significant FID response either for upright or inverted condition) independently for the upright and inverted conditions, following a similar procedure as described above for defining significant contacts. Specifically, we first computed baseline-subtracted amplitudes in the frequency domain as the difference between the amplitude at each frequency bin and the average of 48 corresponding surrounding bins (up to 25 bins on each side, i.e., 50 bins, excluding the 2 bins directly adjacent to the bin of interest, i.e., 48 bins). Then, FID response amplitude was quantified for each significant FID contact as the sum of the baseline-subtracted amplitudes at the first 4 harmonics of the identity change frequency (i.e. 1.2, 2.4, 3.6 and 4.8 Hz). Amplitude was quantified independently for the upright and inverted conditions. In addition, the effect of face inversion was computed for each contact as the amplitude difference between upright and inverted conditions. Contacts located in the same individually defined anatomical region (see section "Contact localization in the individual anatomy" below) were grouped, separately for the left and the right hemisphere. In each anatomical region, we statistically compared group-level FID amplitude differences between hemispheres using general linear mixed effect models implemented in the lme4 package (Bates et al., 2015) in R v4.0.0. Statistical models were fitted using REML and *p*-values were obtained using Satterthwaite's approximation for degrees of freedom. Models included a random intercept per participant to account for both inter-participants variability and non-independence of contacts within a participant. The significance of the face inversion effect was tested at group-level for each region and each hemisphere by comparing amplitudes in the upright vs. inverted conditions using general linear mixed effect models with a random intercept for factors 'contacts' nested in 'participants'. Each set of tests was corrected for multiple comparisons using Benjamini-Hochberg false discovery rate correction (Benjamini and Hochberg, 1995). Note that the FID responses amplitude quantification in the middle temporal gyrus and inferior temporal gyrus (MTG/ITG) and temporal pole were not performed as there were too few contacts in these regions to obtain reliable measures (Table 1).

Table 1
Number of contacts showing significant FID responses (in upright and/or inverted conditions) in each anatomical region. The corresponding number of subjects in which these contacts were found is indicated in parenthesis. For each region, the larger anatomical subdivision is indicated in parenthesis. Acronyms: VMO: ventro-medial occipital cortex; IOG: inferior occipital gyrus; medFG: medial fusiform gyrus and collateral sulcus; latFG: lateral fusiform gyrus and occipito-temporal sulcus; MTG/ITG: the inferior and middle temporal gyri; antCoS: anterior collateral sulcus; antOTS: anterior occipito-temporal sulcus; antFG: anterior fusiform gyrus; antMTG/ITG: anterior middle and inferior temporal gyri; TP: temporal pole; OCC: occipital lobe; PTL: posterior temporal lobe; ATL: anterior temporal lobe.

Regions	Left hemisphere	Right hemisphere
VMO (OCC)	23 (4)	15 (5)
IOG (OCC)	11 (5)	33 (8)
medFG (PTL)	11 (7)	16 (6)
latFG (PTL)	22 (10)	33 (9)
MTG/ITG (PTL)	1 (1)	4 (3)
antCOS (ATL)	12 (7)	14 (9)
antFG (ATL)	6 (4)	15 (6)
antOTS (ATL)	23 (11)	10 (4)
antMTG/ITG (ATL)	19 (6)	13 (6)
TP	10 (3)	4 (3)
Total	138	157

2.5. Contact localization in the individual anatomy

The exact position of each contact relative to brain anatomy was determined in each participant's own brain by coregistrating the post-operative CT-scan with a T1-weighted MRI of the patient's head. Contacts located in the white matter were excluded from the analyses. To accurately assign an anatomical label to each contact, we used the same topographic parcellation of the VOTC as in Jonas et al. (2016) and Lochy et al. (2018), which is close to the parcellation proposed by Kim et al. (2000). Major VOTC sulci (collateral sulcus, CoS; midfusiform sul-

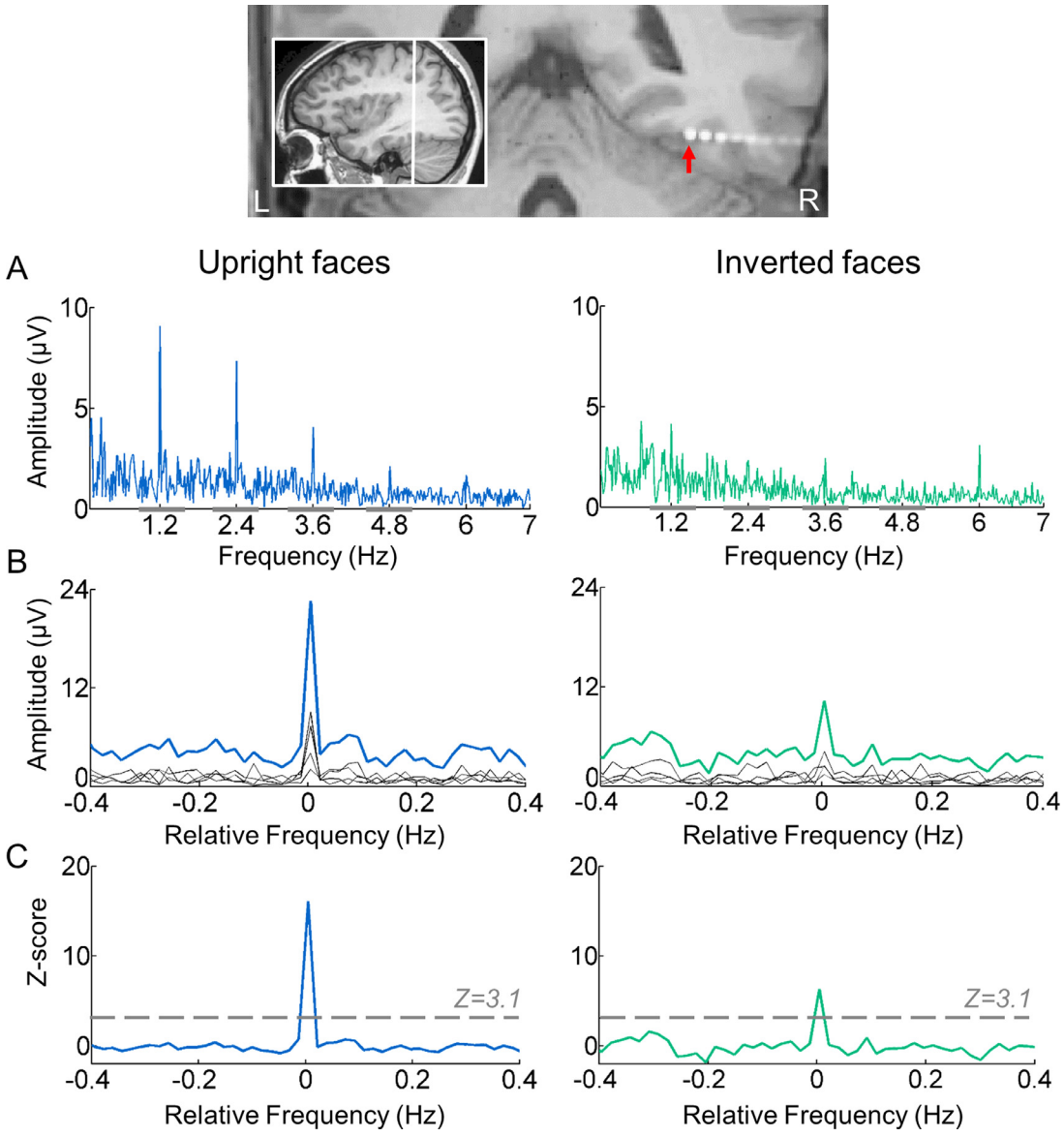

Fig. 2. Objective and high signal-to-noise ratio FID responses recorded in the VOTC. **A.** SEEG frequency-domain responses recorded at an individual recording contact in the upright (left) and inverted (right) conditions. The anatomical location of the contact (in the right latFG) is shown in a coronal MRI slice (indicated by a red arrow). FID responses are found at the exact face identity change frequency and harmonics (1.2, 2.4, 3.6, and 4.8 Hz) in both upright and inverted conditions, albeit with a higher amplitude in the upright condition. **B.** Significant selective responses were determined by first segmenting the FFT spectrum into four segments centered at the frequency of face identity change and its harmonics up to 4.8 Hz. Individual FFT segments are shown in gray (see horizontal gray bars on the X axis in A, representing the length of each FFT segment). The four segments, containing both the signal and the surrounding noise, were then summed (colored line). The 0 mark corresponds to the face identity change frequency. **C.** Z-score transformation of the summed FFT spectrum for statistical purpose and computed as the difference between the amplitude at the identity change frequency bin and the mean amplitude of 48 surrounding bins (25 bins on each side, excluding the 2 bins directly adjacent to the bin of interest, i.e., 48 bins), divided by the standard deviation of amplitudes in the 48 surrounding bins. The Z score at the face identity change frequency exceeds 3.1 ($p < 0.001$) in the upright condition (left) and in the inverted condition (right). This contact was therefore classified as an UP contact and as an INV contact. (For interpretation of the references to colour in this figure legend, the reader is referred to the web version of this article.)

cus, MFS; and occipito-temporal sulcus, OTS) served as medio-lateral landmarks while coronal reference planes containing given landmarks served as postero-anterior landmarks (Fig. S2). A coronal plane including the anterior tip of the parieto-occipital sulcus served as the border of the occipital lobe (OCC) and posterior temporal lobe (PTL). A coronal plane including the posterior tip of the hippocampus served as the border between the PTL and the anterior temporal lobe (ATL). A coronal plane including the limen insulae served as the border between the ATL and the temporal pole (TP). Hence, we located contacts in the ATL if they were located anteriorly to the posterior tip of the hippocampus (i.e., anteriorly to a Y Talairach coordinate around −40) and posteriorly to the limen insulae.

2.6. Group visualization, proportion and amplitude analyses in Talairach space

For group analyses and visualization, anatomical MRI were spatially normalized in order to determine the Talairach coordinates of VOTC intracerebral contacts. The cortical surface used to display group maps was obtained from segmenting the Colin27 brain from AFNI (Cox, 1996), which is aligned to the Talairach space. We performed two separate group analyses using Talairach transforms.

First, we used Talairach transformed coordinates to compute the local proportion of FID intracerebral contacts across the VOTC. Unlike in the amplitude quantification analysis, proportions were computed

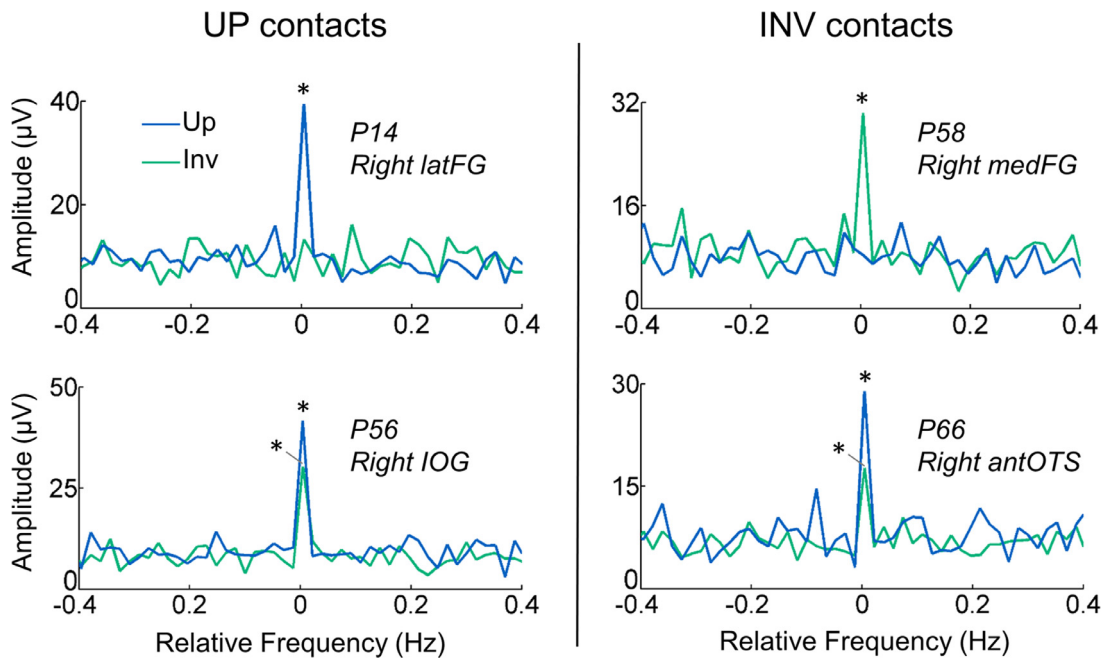

Fig. 3. Classification of FID contacts in UP and INV contacts for the proportion analysis. Example of summed segmented FFT spectra for the upright and inverted conditions in 4 recording contacts, illustrating the classification of FID contacts in UP and INV contacts (left and right columns respectively). Top-row: Contacts significant only either in the upright (left, UP contacts) or in the inverted (right, INV contacts) conditions. Bottom row: example contacts with a significant FID response in both conditions being classified as both UP and INV contacts. * Indicates statistically significant responses ($Z > 3.1$, $p < 0.001$).

separately for UP contacts (i.e. contacts with significant FID response in the upright condition, independently of the inverted condition) and INV contacts (i.e. contacts with significant FID response in the inverted condition, independently of the upright condition). For ventral views of the VOTC, local proportion of contacts was computed in volumes (i.e. 'voxels') of size 15 × 15 × 100 mm (respectively for the X: left – right, Y: posterior – anterior, and Z: inferior – superior dimensions) by steps of 3 × 3 × 100 mm over the whole VOTC. A large voxel size in the Z dimension enabled collapsing across contacts along the inferior-superior dimension, in order to increase statistical power and provide a compact visualization of the VOTC. Additional views of the lateral VOTC were generated by running the same analyses using voxels of size 20 × 20 × 15 mm by steps of 3 × 3 × 3 mm along the X, Y and Z dimensions respectively. For each voxel, we extracted the following information across all participants in our sample: (1) number of recorded contacts located within the voxel; (2) number of significant UP and INV contacts. From these values, for each voxel we computed the proportion of significant contacts as the number of UP or INV contacts within the voxel divided by the total number of recorded contacts located in that voxel. Then, for each voxel we determined whether the proportions of significant UP or INV contacts were significantly above zero using a bootstrap procedure, as follows: (1) within each voxel, sample as many contacts as the number of recorded contacts, with replacement; (2) for this bootstrap sample, determine the proportion of UP or INV contacts and store this value; (3) repeat steps (1) and (2) 5000 times to generate a distribution of bootstrap proportions; and (4) estimate the *p*-value as the fraction of bootstrap proportions equal to zero. In addition, we statistically compared the proportion VOTC maps for UP vs. INV contacts in the same manner as described above but using, for each voxel, the difference between the number of UP vs. INV contacts in relation to the number of recorded contacts. With the UP vs. INV difference map, we also statistically determined interhemispheric differences by comparing this UP-INV difference of proportion across corresponding voxels of the left vs. right hemispheres, again using a permutation test.

Second, we used the same mapping approach to compute the local FID response amplitude across the VOTC. Here, we plotted the mean baseline-subtracted amplitude across all the FID contacts (i.e. responding significantly either in the upright or inverted conditions) within each 15 × 15 × 100 mm voxel (for the ventral view) or 20 × 20 × 15 mm (for the lateral view) over the cortical surface. Mapping the FID response amplitude in the upright and inverted conditions therefore uses the same set of contacts. We also statistically compared the amplitude maps for upright and inverted conditions by applying a paired-sample permutation test (2-tailed, 5000 permutations) to the amplitude in the sample of contacts within each voxel.

3. Results

3.1. Spatial distribution of face individuation (FID) contacts in the VOTC

Following Fast Fourier Transform of SEEG data, high signal-to-noise FID responses were identified in the VOTC at exactly the identity change frequency (1.2 Hz) and harmonics (Fig. 2 shows an example contact in one participant) in the upright and inverted conditions. Significant FID responses were determined by grouping the first four harmonics (i.e. summing 1.2, 2.4, 3.6 and 4.8 Hz, Fig. 2B) and computing a z-score transform ($z > 3.1$, $p < 0.001$, Fig. 2C). In total, we found 295 contacts showing a significant FID response in either the upright or the inverted condition in 63 individual brains (among 3825 contacts implanted in the VOTC of 69 participants). When using a slightly less conservative threshold of $z > 2.745$ ($p < 0.003$) which was FDR-corrected (Benjamini and Hochberg, 1995) at $p < 0.05$, more FID contacts were identified but the pattern of results and data interpretation were extremely similar (Fig. S3).

The proportion of these FID contacts was significantly higher in the right (8.8%, 157/1794) than in the left hemisphere (6.8%, 138/2031, $p = 0.02$, 2-tailed permutation test). Among these 295 contacts, 161 were significant only in the upright condition, 75 only in the inverted condition, and 59 in both conditions (see examples in Figs. 2 and 3). For some of the analyses (i.e. proportion), FID contacts were further split in 2 sets based on the significance in the upright and inverted conditions: (1) UP contacts (i.e. showing a significant FID response in the upright

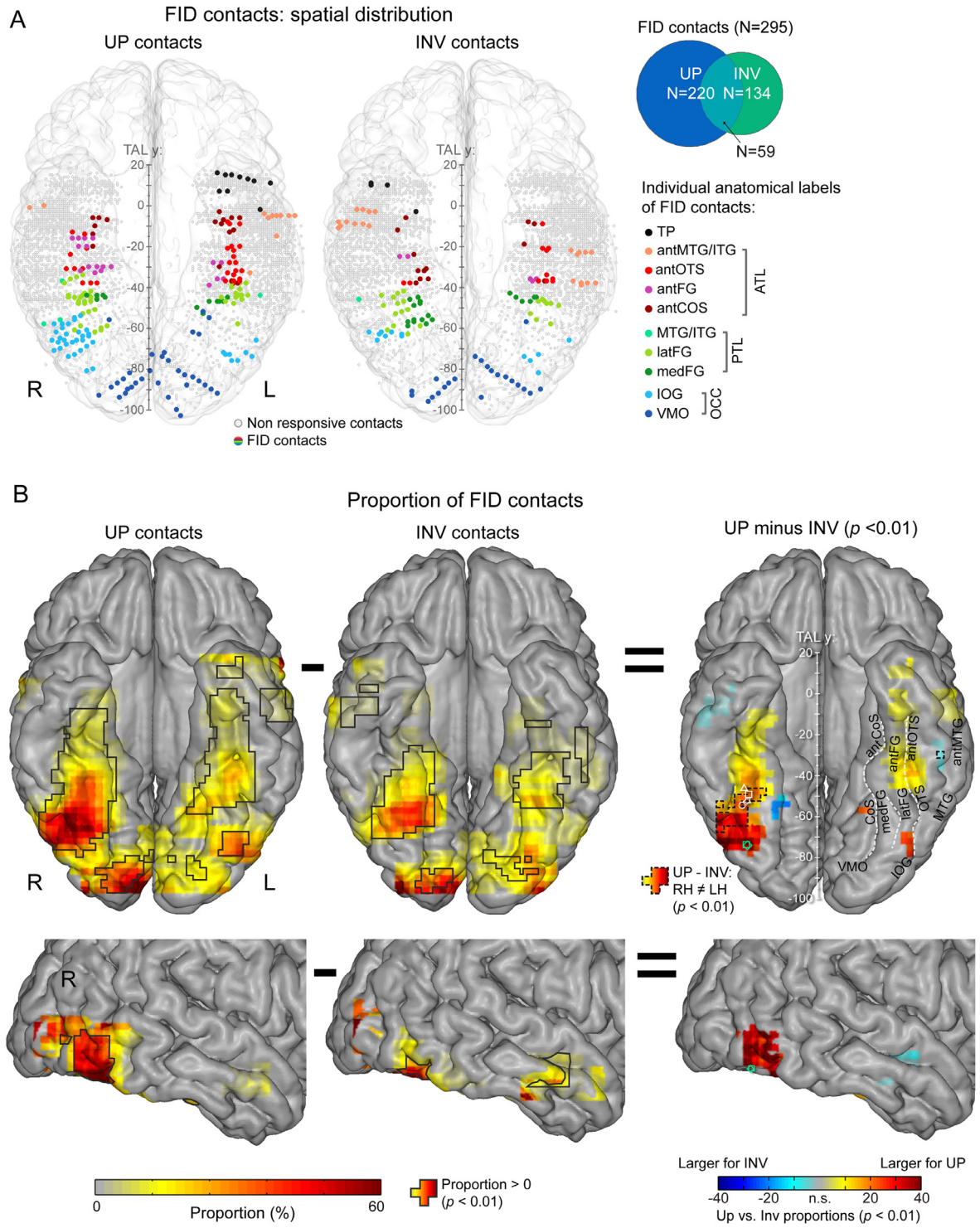

Fig. 4. Spatial distribution and proportions of UP and INV FID contacts in Talairach space. **A.** Map of all 3825 VOTC recording contacts across the 69 individual brains displayed in the Talairach space using a transparent reconstructed cortical surface of the Colin27 brain (ventral view). Each circle represents a single recording contact. Color-filled circles correspond to FID contacts, either defined as UP contacts (left map, $N = 220$, see Venn diagram inset on the right) or INV contacts (right map, $N = 134$). UP and INV contacts are color-coded according to their anatomical location in the original individual anatomy (see legend on the right). White-filled circles correspond to contacts on which no significant FID responses was recorded. For visualization purposes, individual contacts are displayed larger than their actual size (2 mm in length). Values along the Y axis of the Talairach coordinate system (antero-posterior) are shown near the interhemispheric fissure. **B.** Ventral and right lateral maps of the local proportion of UP contacts (left) and INV contacts (middle) relative to number of recorded contacts, and statistical comparison between the local proportions of UP and the local proportion of INV contacts across VOTC (right, only significant differences of proportions at $p < 0.01$ are displayed). For left and middle maps, black solid contours outline proportions significantly above zero at $p < 0.01$. For the ventral map on the right, the dashed black contour lines show the location of the proportion difference between UP and INV contacts that are significantly ($p < 0.01$) larger in one hemisphere. This indicates that the higher proportion of UP compared to INV contacts in the IOG and latFG is significantly larger in the right hemisphere. The coordinates of published peak location of face-selective regions are show in white for fMRI-defined FFA (star: Berman et al., 2010, circle: Gao et al., 2018, square: Zhen et al., 2015), in green for fMRI-defined OFA (square: Zhen et al., 2015, diamond: Pitcher et al., 2011b) and the mean coordinates for latFG face-selective responses in a recent SEEG study are displayed with a white triangle (Jonas et al., 2016). (For interpretation of the references to colour in this figure legend, the reader is referred to the web version of this article.)

condition, regardless of the inverted condition, Fig. 3 left), and (2) INV contacts (i.e. showing a significant FID response in the inverted condition, regardless of the upright condition, Fig. 3 right). Some contacts exhibited significant responses in both upright and inverted conditions so that the 2 sets of contacts overlapped (Fig. 3 bottom; Fig. 4A).

Each significant FID contact was located and labeled according to the participant's individual anatomy (Table 1) using a topographic parcellation of the VOTC (Fig. S2; as in Jonas et al., 2016; Lochy et al., 2018). Moreover, to perform group visualization and analyses, the coordinates of each contact were transformed in the Talairach space (Fig. 4A). In the occipital lobe (OCC), FID responses were recorded in the inferior occipital gyrus (IOG) and in a large portion of the ventro-medial occipital cortex (VMO, Table 1, Fig. 4A). In the posterior temporal lobe (PTL), numerous FID responses were recorded in the lateral fusiform gyrus and adjacent occipito-temporal sulcus (latFG), as well as to a lesser extent in the medial fusiform gyrus and adjacent collateral sulcus (medFG), but very few in the lateral temporal cortex (inferior and middle temporal gyri, MTG/ITG). In the ATL (anterior to the posterior tip of the hippocampus, around Talairach y coordinate = −40, Fig. 4A), FID responses were observed in several distinct regions: along the anterior segments of the collateral sulcus (antCoS) and occipito-temporal sulcus (antOTS, located laterally to the CoS), in the anterior fusiform gyrus (antFG, located between the antCoS and the antOTS) and more laterally in the anterior part of the middle and inferior temporal gyri (antMTG/ITG). Finally, few FID responses were also found in the TP. Most of FID responses extended from approximately −100 to −5 along the antero-posterior Y axis in Talairach coordinates (Fig. 4A).

We investigated the spatial distribution of FID contacts separately for UP and INV contacts. Fig. 3 shows examples of these 2 contact types. There were 220 UP contacts and 134 INV contacts (59 contacts in common between the 2 orientations, see Fig. 3 bottom and Fig. 4A Venn diagram). Overall, the proportion of UP contacts (i.e. number of UP contacts divided by the number of recorded contacts) was significantly higher than INV contacts (UP = 220/3825 = 5.75% vs. INV = 134/3825 = 3.5%, $p < 0.0001$, 2-tailed permutation test). Both types of contacts were widely distributed across the VOTC (Fig. 4A).

3.2. Right VOTC shows higher proportion of UP FID contacts

To quantify and visualize the spatial distribution of UP and INV contacts at a more local level, we used Talairach transformed coordinates to compute the proportion of each type of contact (i.e. UP and INV) relative to the number recorded contacts in smaller volumes (i.e. 'voxels') (Fig. 4B, see also Fig. S4 for the left hemisphere lateral views). Computing such proportions allows taking into account the local variation in the number of recorded contacts across the VOTC. These proportion maps show that for both types of contacts, proportions significantly above zero ($p < 0.01$) are found in the VMO and in the bilateral FG. For UP contacts, we also observed significant proportions in the ventral and lateral IOG, especially in the right hemisphere, and in more anterior portions of the bilateral temporal lobe (Fig. 4B, see the solid black contour lines on the left and middle maps). Statistically comparing proportion maps for UP vs. INV contacts reveals a significantly higher ($p < 0.01$) proportion of UP contacts in the right hemisphere between approximately −80 mm to −10 mm along the postero-anterior axis of the Talairach space (i.e. y-dimension, Fig. 4B, right). More precisely, the significantly higher proportion of UP contacts started from the right IOG (mean Talairach antero-posterior y-coordinate of IOG contacts = -65 ± 6 mm) over ventral and lateral aspects (Fig. 4B, right), continuing anteriorly all along the right latFG (mean Talairach y-coordinate = -49 ± 8 mm), and up to the antFG (-25 ± 7 mm), antOTS (-28 ± 10 mm) and antCOS (-22 ± 12 mm). Notably, as depicted in Fig. 4B, this strip of cortex in the right hemisphere includes the mean peak coordinate of the FFA (in the latFG) as identified in fMRI in a meta-analysis (Berman et al., 2010, [39, −52, −15]), in a probabilistic atlas (Zhen et al., 2015, [38, −49, −18] converted from MNI to Talairach space), in a recent fMRI face lo-

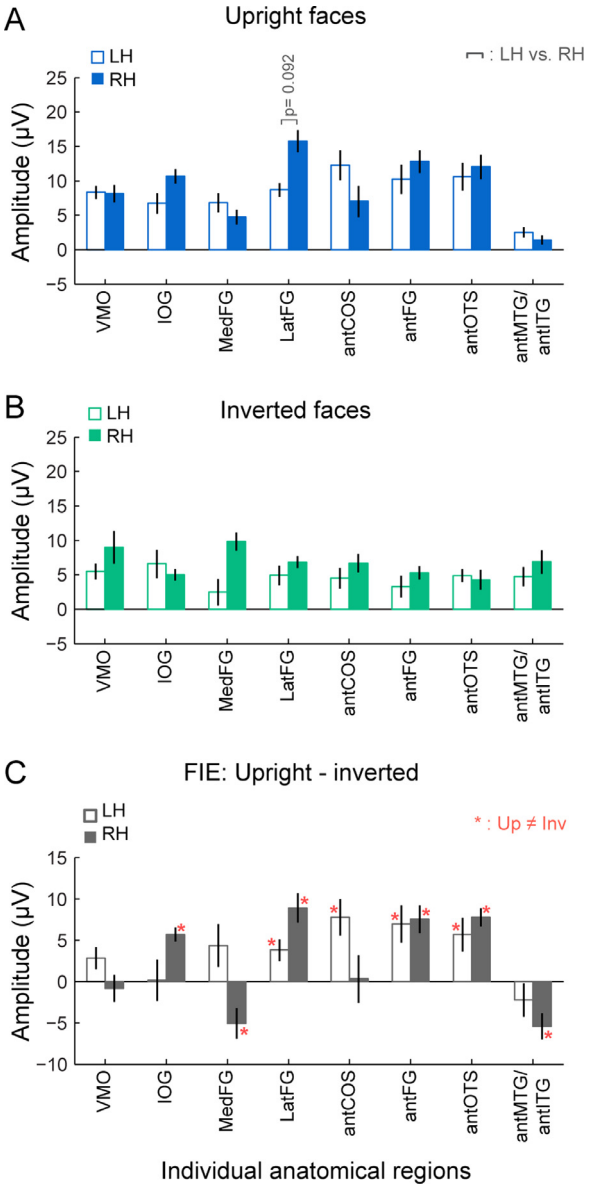

Fig. 5. Amplitude quantification in FID contacts. **A.** FID response amplitudes in the upright face condition over all FID contacts ($N = 295$), for each anatomical region (i.e. as defined in the individual native anatomy) and separately for the left and right hemispheres (LH and RH respectively). Amplitudes are quantified as the mean of the amplitudes across recording contacts within a given anatomical region. Error bars are standard error of the mean across contacts. **B.** Same convention as for panel A but displaying amplitudes in the inverted face condition for the same contacts (FID contacts, $N = 295$). **C.** Face inversion effect. Amplitude difference between upright and inverted face conditions are computed in each FID contact and averaged by anatomical region and hemisphere. Asterisks in red indicate significant (FDR-corrected) amplitude difference between upright and inverted face conditions, computed separately for each region and hemisphere using linear mixed models. Note that the mean amplitudes of FID responses in the MTG/ITG and TP are not reported as there were too few contacts in these regions to obtain reliable measures. (For interpretation of the references to colour in this figure legend, the reader is referred to the web version of this article.)

calizer using a frequency-tagging procedure similar to the present study (Gao et al., 2018, [42, −54, −14]), as well as the mean coordinate of the face-selective responses in the latFG in a recent intracerebral recording study (Jonas et al., 2016, [41, −45, −16]). This strip of cortex also includes the mean coordinates of the OFA in the inferior occipital gyrus as reported in a review (Pitcher et al., 2011b, [39, −74, −10]) or in a probabilistic atlas (Zhen et al., 2015, [39, −73, −13] converted from MNI to Talairach space). In the left hemisphere, we also found a higher proportion of UP contacts in the ATL and in a small portion of the IOG. Interestingly, the proportion of significant UP and INV contacts did not differ in the VMO. To statistically establish interhemispheric differences in the local proportions of UP vs. INV contacts, we compared this difference in proportion (i.e. UP vs. INV contacts) in corresponding voxels across hemispheres, restricting the comparison to voxels showing a significant difference between UP and INV contacts. This revealed that the difference in proportion of UP vs. INV contacts was significantly higher in the right hemisphere in portions of the IOG and latFG (Fig. 4B right, see the dashed black contour lines on the ventral map). Note that the proportion analyses yield virtually the same results whether or not the 13 participants with a BFRT-c score below the normal range were included in the analyses (Fig. S5).

3.3. Right hemispheric predominance of upright FID response amplitudes

We also quantified response amplitudes of the significant FID contacts ($N = 295$). Unlike in the proportion analysis, this was performed by measuring the response amplitude for the upright and inverted conditions over the whole set of FID contacts (i.e. no longer splitting in UP and INV contacts). To do so, we summed the baseline-subtracted amplitude over the first 4 harmonics of the face identity change frequency (i.e. 1.2, 2.4, 3.6 and 4.8 Hz) for each significant FID contact (see Methods for details). We then calculated the mean amplitudes across FID contacts in each anatomical region, separately for the upright and inverted conditions (Fig. 5) and compared amplitudes across hemisphere using linear mixed model statistics. Note that the mean amplitudes of FID responses in the MTG/ITG and TP are not reported as there were too few contacts in these regions to obtain reliable measures (Table 1). In the upright condition (Fig. 5A), the largest FID response was recorded in the right latFG, followed by the right antFG, the left antCOS, the right antOTS and the right IOG. Only the latFG showed a trend for significant hemispheric difference ($p = 0.09$, FDR corrected, $p = 0.01$ uncorrected), despite a large difference in the amplitude between left and right hemispheres for this region (Fig. 5A; the amplitude in the left latFG was 45% smaller than in the right latFG; computed as 100*(R-L) / R). When combining the two regions in the posterior temporal lobe with the highest proportions of FID contacts (i.e. the latFG and IOG), the amplitude in the right hemisphere was significantly higher than in the left hemisphere (13.22 μV vs. 8.04 μV, $p = 0.021$). In the inverted face condition, the overall amplitudes across the VOTC was reduced compared to the upright condition (Fig. 5B) and the largest responses were found in the right medFG, followed by the right VMO. No significant interhemispheric differences were found in the inverted face condition.

Next, we quantified the face inversion effect in each region by subtracting the response amplitude in inverted condition from the response in the upright condition for each contact and then averaging across contacts (Fig. 5C). FID responses were significantly higher in the upright compared to inverted conditions in several regions: the right IOG (mean amplitude difference between upright and inverted ± S.D. = 5.7 μV ± 4.8, $p < 0.0001$, FDR-corrected, Fig. 5C; percentage of amplitude reduction for INV vs. UP = −53%, computed as 100*(UP-INV) / UP), the left and right latFG (respectively 3.8 μV ± 6.1, $p < 0.005$ and 8.9 μV ± 10.1, $p < 0.0002$, i.e. −44% and −56% of reduction for inverted faces), the left and right antFG (7.5 μV ± 6.5, $p < 0.05$ and 6.9 μV ± 5.5, $p < 0.0005$; -68% and −59% of reduction for inverted faces), the left antCOS (3.8 μV ± 6.1, $p < 0.01$; −63%), and the left and right antOTS (5.7 μV ± 9.8, $p < 0.01$ and 7.8 μV ± 3.5, $p < 0.0005$; −54% and −65% respectively). We also found the opposite pattern with significantly larger FID responses for inverted compared to upright faces in the right medFG (−5.1 μV ± 7.4, $p < 0.01$, + 108%) and right antMTG/ITG (−5.4 μV ± 5.7, $p = 0.0015$, +384%). The face inversion effect measured in the IOG and latFG was larger in the right compared to left hemisphere (65% smaller in the left hemisphere when combining the two regions). However, owing to the high variability of amplitude values across patients ($n = 13$ and $n = 12$ for left and right hemisphere, respectively) in these regions, this difference did not reach significance.

As in the proportion analyses above, we also examined the distribution of response amplitudes without a priori regional grouping by generating VOTC maps of the amplitudes of all FID contacts ($N = 295$) in the Talairach space. FID amplitudes were displayed either at the level of each individual contact (Fig. 6A) or averaged within voxels projected to the cortical surface (Fig. 6B, see also Fig. S4 for the left hemisphere lateral views). As expected from the previously described regional aver-

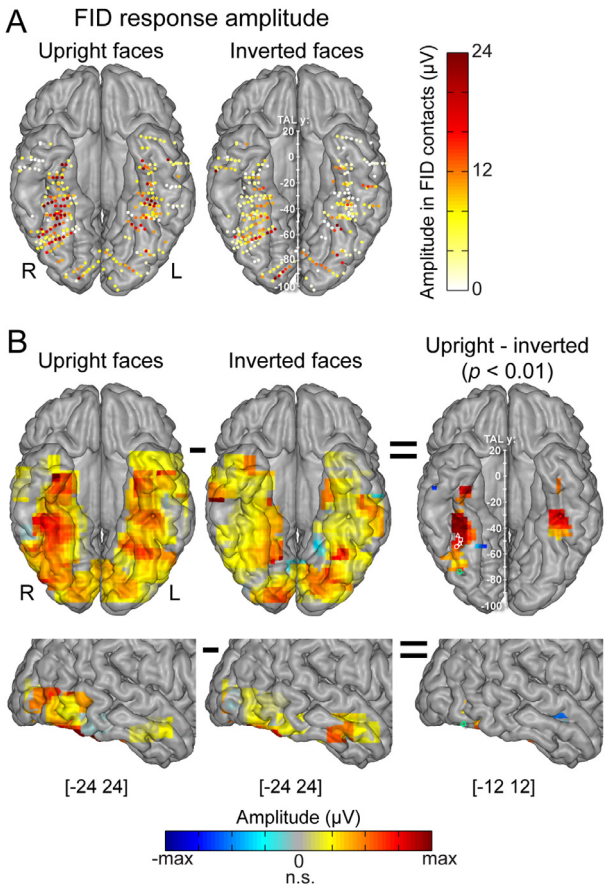

Fig. 6. Spatial distribution and response amplitude over FID contacts in the Talairach space. **A.** Map of all FID contacts ($N = 295$) across 69 individual brains displayed in the Talairach space. Each circle represents a single contact color-coded according to its FID response amplitude in the upright face (left) or inverted face (right) condition. For visualization purposes, individual contacts are displayed larger than their actual size (2 mm in length). **B.** Ventral and right lateral maps showing smoothed response amplitude over FID contacts displayed over the VOTC cortical surface for the upright face (left) and inverted face (middle) conditions, and maps of the significant amplitude difference ($p < 0.01$) between upright and inverted face conditions (right). The coordinates of published peak location of face-selective regions are show in white for fMRI-defined FFA (star: Berman et al., 2010, circle: Gao et al., 2018, square: Zhen et al., 2015), in green for fMRI-defined OFA (square: Zhen et al., 2015, diamond: Pitcher et al., 2011b) and the mean coordinates for latFG face-selective responses in a recent SEEG study are displayed with a white triangle (Jonas et al., 2016). (For interpretation of the references to colour in this figure legend, the reader is referred to the web version of this article.)

ages, the highest response amplitude was located in the right latFG in the upright condition. A statistical comparison of upright and inverted amplitude maps revealed significantly higher responses for upright faces predominantly in the right hemisphere, stretching along the postero-anterior axis starting from the right IOG, to the right latFG, and up to the ATL region (Fig. 6B, right). Similarly to the significantly higher proportion of UP contacts in the right hemisphere (Fig. 4B, right), this face inversion effect amplitude difference also extended from approximately −75 mm to −7 mm on the antero-posterior Y axis of the Talairach space. This strip of cortex in the right hemisphere showing a face inversion effect in amplitude includes the mean peak coordinate of the FFA (Berman et al., 2010; Gao et al., 2018; Zhen et al., 2015), the mean coordinate of the face-selective responses in the latFG in a recent SEEG study (Jonas et al., 2016) and the mean coordinates of the OFA (Pitcher et al., 2011b; Zhen et al., 2015) (Fig. 6B, right). We also found significantly higher amplitudes in the upright condition in the left hemisphere, restricted to the anterior portion of the latFG and posterior portions of the antCOS, antFG and antOTS (Fig. 6B and 5C). Interestingly, while there were clear responses over the posterior VOTC (VMO), these responses were of similar magnitude in the upright and inverted conditions, as indicated by an absence of significant difference across conditions in this region (Fig. 6B, see also Fig. 5C). As for the proportion analyses, note that the amplitude analyses yield virtually the same results whether or not the 13 participants with a BFRT-c score below the normal range were included in the analyses (Fig. S5 and Fig. S6).

Last, we further investigated whether the neural processes involved in generating FID responses in the upright and inverted conditions were qualitatively different by correlating the response amplitude in the two conditions across regions ($N = 18$ across the 2 hemispheres) and FID contacts ($N = 295$). The resulting correlations were weak: Pearson $r = -0.18$ ($p = 0.47$, randomization test where the null distribution is generated by randomly shuffling the pairing of amplitudes) and 0.14 ($p < 0.0063$), respectively for correlations using regions or contacts. Although the correlation using all FID contacts was significantly different from zero, it has very low explanatory power, accounting for only 2% of shared variance.

4. Discussion

We report an original neural cartography of unfamiliar face individuation across the human VOTC, using data collected in a large sample of individuals implanted with intracerebral electrodes. To our knowledge, only a handful of studies reported human intracranial recordings during unfamiliar FID. Specifically, Puce et al. (1999) showed amplitude decreases of low-frequency late ECoG (Electrocorticography) responses in the ATL to repeated presentations of faces, while Engell and McCarthy (2014) described high-frequency activity decreases over the middle FG at an earlier latency with a subset of the same data. Using MVPA, Ghuman et al. (2014) found significant decoding of individual face images and features in 4 patients with recordings over the middle FG, and Davidesco et al. (2014) were able to decode 14 different images of faces in the posterior ventral and lateral occipito-temporal cortex using data recorded in 14 patients with both ECoG and SEEG.

While the current observations generally agree with these previous findings, the present investigation goes well beyond these studies by mapping neurophysiological FID responses across the whole human VOTC, sampling both gyri and sulci thanks to the SEEG approach, in a large number of individual brains (Rossion et al., 2018). Importantly, the strengths of the current FPVS paradigm enable to capture neural responses directly reflecting visual face identity processing. Hence, not only does this paradigm have high validity, objectivity, sensitivity, and reliability, but it also offers control for individuation based on low-level features through the speed and large number of variable individual discriminations occurring during a sequence, the requirement to generalize across stimulus size (Dzhelyova and Rossion, 2014; Liu-Shuang et al., 2014), and most importantly, through the comparison to the exact same stimulation with faces presented in the inverted orientation (Rossion et al., 2020).

Our comprehensive intracerebral mapping of the VOTC reveals four key findings characterizing the FID function in the human brain. First, we find a robust face inversion effect as demonstrated by a larger proportion of significant contacts and higher FID response amplitudes for upright than inverted faces. Second, the face inversion effect is spatially distributed yet confined to a relatively narrow strip of cortex extending from the right posterior VOTC (IOG and latFG) to bilateral ATL regions. Third, our study identifies clear FID responses in the anterior FG and surrounding sulci, up to 3 cm more anterior than the latFG. Fourth, almost no FID responses are found in very anterior ATL regions, including the temporal pole, despite extensive sampling of this region.

4.1. The effect of stimulus inversion on face individuation

Picture-plane inversion dramatically affects behavioral individuation of faces in humans (Rossion, 2008; Yin, 1969), therefore allowing to isolate high-level neural processes subtending FID, i.e. processes that go beyond the discrimination of physical differences between face images (which are strictly identical regardless of orientation). Interestingly, our extensive spatial sampling reveals substantial differences across brain regions in terms of the FID response amplitude and the proportion of significant contacts for upright and inverted faces. On recording contacts located closely to or in low-level visual cortical regions (“VMO”), there was little to no difference between FID responses to upright and inverted faces, suggesting that the small effects found in these regions are based on low-level visual cues. In contrast, multiple higher-order cortical regions, i.e., in the posterior and anterior ventral temporal cortex, showed a robust reduction of amplitude and proportion of significant contacts for inverted compared to upright faces. These findings directly contradict the view that unfamiliar faces are individuated by low-level visual processes/cues in the human brain similarly for upright and inverted faces (Hancock et al., 2000; Megreya & Burton, 2006; Burton, 2013). Moreover, according to a quantitative view of the face inversion effect (e.g., Murphy et al., 2020; Sekuler et al., 2004), the decrease of amplitude for inverted faces should be uniformly observed, and proportional across brain regions (i.e., no interaction between inversion and cortical localization). Instead, the large differences in the face inversion effect observed between regions as described above, as well as the null or very weak correlation between FID amplitude for upright and inverted faces across electrode contacts, rather fully support a qualitative view of this effect (Rossion, 2008).

The reduction of amplitude for inverted faces was most prominent in the right hemisphere, where it ranged from 53% (IOG) to 65% (antOTS). Intriguingly, the magnitude of the face inversion effect observed in the right IOG and latFG (−53% and −56% respectively) is in striking correspondence with scalp EEG results over the right hemisphere in neurotypical adult participants, showing a 53% decrease in FID response amplitude with inversion (Rossion et al., 2020). The location of this effect is also largely in line with fMRI-adaptation studies reporting significantly larger repetition suppression for upright than inverted faces in well-defined bilateral face-selective regions of the latFG (i.e., the FFA) and, to a lesser extent, of the IOG (OFA; Gilaie-Dotan et al., 2010; Mazard et al., 2006; Yovel and Kanwisher, 2005). The role of the right IOG in FID has sometimes been related to the processing of low-level facial features due to the lack of a behavioral inversion effect when stimulating this region with transcranial magnetic stimulation (TMS) (Pitcher et al., 2011a). In contrast with this view, our data unambiguously shows a robust and right lateralized effect of inversion on FID in this region.

Inversion also largely modulated FID responses in the ATL (antCOS, antFG, and antOTS), reaching up to −65% in the right antOTS. To our knowledge, such effects have not been reported, most likely owing to the large signal drop-out in these ventral ATL regions in fMRI (Axelrod and Yovel, 2013; Rossion et al., 2018; Wandell, 2011). In ad-

dition, there was no inversion effect in more medial regions (medFG) or more lateral regions of the VOTC (MTG/ITG, antMTG/ITG), with the right medFG even exhibiting the opposite pattern of larger FID responses to inverted than to upright faces. Larger responses to inverted compared to upright faces (regardless of identity) have been observed previously in fMRI over medial regions of the VOTC such as the parahippocampal gyrus or medial fusiform gyrus (Aguirre et al., 1999; Gilaie-Dotan et al., 2010; Haxby et al., 1999; Rosenthal et al., 2016), with one study reporting larger repetition suppression effects for inverted than for upright individual unfamiliar faces in the parahippocampal gyrus (Gilaie-Dotan et al., 2010). Since these regions typically show reduced responses to faces relative to visual objects in fMRI (Aguirre et al., 1999; Haxby et al., 1999), these effects have been interpreted in terms of the recruitment of processing resources from object perception systems for inverted faces (see also Rosenthal et al., 2016). Our findings with direct recordings of neural activity in VOTC support these observations.

4.2. A confined distribution of cortical face individuation responses in the right hemisphere

While individuation of inverted faces is not necessarily based on low-level visual cues, comparing upright and inverted faces nevertheless allows to isolate high-level processes, i.e. going beyond physical differences between stimuli. Hence, in the remaining of the discussion, we focus on the differential FID maps for this comparison. The large-scale proportion and the amplitude maps (Figs. 4 and 6), which largely agree with each other, indicate that unfamiliar FID in humans is not limited to a local brain region but is instead achieved by widely distributed populations of neurons. Specifically, high-level unfamiliar FID is supported by a strip of cortex in the right VOTC including the right IOG, the right latFG and the right ATL region just anterior to the latFG (antCOS, antFG and antOTS), as well as the latter region in the left hemisphere. Face-selective activations typically identified in fMRI studies in the IOG (OFA, Gauthier et al., 2000; Pitcher et al., 2011b; Zhen et al., 2015) and latFG (FFA, Berman et al., 2010; Gao et al., 2018; Kanwisher et al., 1997; Zhen et al., 2015; pFUS and mFUS, Weiner and Grill-Spector, 2012; see also Jonas et al., 2016 for latFG face-selective responses in SEEG) fall within this strip of cortex (Figs. 4B and 6B). This is supported by the similarity both in terms of the anatomical location in individual brains in the current study and in terms of mean Talairach coordinates. As mentioned earlier, these two functional regions are known to be involved in FID, based on fMRI-adaptation effects. However, although these effects are often found bilaterally in these regions (see Rossion, 2014 for review), lesion studies, as well as effects of transcranial and intracranial stimulation on FID clearly point to a right hemisphere dominance of these regions (Bouvier and Engel, 2006; Jonas et al., 2018, 2014; Meadows, 1974; Pitcher et al., 2007). Such right hemispheric dominance is clearly supported by the present direct recordings of intracerebral neurophysiological responses, in line with effects observed on the scalp in the same paradigm (Liu-Shuang et al., 2014; Rossion et al., 2020). The lack of strong right hemispheric lateralization of this effect in fMRI may be due to the slow temporal dynamics of the fMRI responses, which favors a spread of responses to the other hemisphere.

Importantly, despite their wide cortical distribution, high-level unfamiliar FID responses are not found everywhere in the occipito-temporal cortex. Rather, they are anatomically confined to the right IOG, the right latFG and extending to the bilateral ATL. Whether this cortical strip appears continuous due to the averaging methods across individual brains or reflects a genuine functional organization cannot be determined with the present dataset. Again, fMRI-adaptation studies have investigated the sensitivity to individual face identities within focal face-selective regions of the IOG and latFG spatially segregated in each participant's brain (e.g., Eger et al., 2004; Ewbank et al., 2013; Gauthier et al., 2000; Hermann et al., 2017; Hughes et al., 2019; Rostalski et al., 2019; Schiltz and Rossion, 2006). The variable localizations of these fMRI regions-of-interest across individual brains coupled with a superimposition of neural activity across brains as performed here could result in a visually artificial continuous strip subtending the FID function. Alternatively, fMRI studies may only identify the tip(s) of the iceberg(s), i.e. local regions with the highest density of neurons sensitive to face identity, these neurons being nevertheless distributed continuously all along the IOG, latFG and the ATL. In other words, the FID function may well be truly continuously distributed along the (right) IOG, latFG and ATL, with local clusters of neuronal populations being most critical for the function. Supporting this latter point, rare transient behavioral disruptions of FID due to intracerebral electrical stimulation appears to be confined to regions showing the largest face-selective and FID responses (Jonas et al., 2018, 2014).

4.3. The role of the anterior fusiform gyrus and surrounding sulci in FID

Our investigation identified regions anterior to the latFG/FFA as being involved in unfamiliar FID. Hence, the cortical maps showed that FID responses extended anteriorly and bilaterally in the ATL, up to about 3 cm beyond the anterior part of the latFG (i.e. starting at Talairach y coordinate around −40) but not covering the most anterior part of the ATL (i.e. anterior to around $y = -7$ Talairach coordinate; see the discussion below). This region corresponds anatomically to the anterior fusiform gyrus and its 2 adjacent sulci, antCOS and antOTS (for simplicity, we will refer to this region as antFG+sulci). The effects of inversion are particularly large (i.e., 65%) in this antFG+sulci region, except in the right antCOS. While FID is strictly right lateralized in the posterior temporal lobe (IOG and latFG), FID is found bilaterally in the antFG+sulci, pointing to a functional difference from posterior FID regions.

Since the antFG+sulci is located at the heart of the largest VOTC magnetic susceptibility artifact in fMRI (e.g., Axelrod and Yovel, 2013; Jonas et al., 2015; Rossion et al., 2018; Wandell, 2011), its contribution to FID and face processing in general has been largely unexplored. In fact, this region lies more anteriorly than the reported location of the most anterior face-selective activation in the latFG measured with fMRI (FFA1 / mFus; Pinsk et al., 2009; Weiner et al., 2014). It is also more anterior and lateral than the antFG region showing above chance decoding of individual faces as reported in a MVPA-fMRI study (Nestor et al., 2016). However, the antFG+sulci region has been singled out as showing categorical differences between unfamiliar and familiar faces during an orthogonal task in an early Positron Emission Tomography study (Rossion et al., 2001) and has been associated with reduced cortical volume in low performers at face identity recognition (Behrmann et al., 2007). Intracerebral electrical stimulation of this region in the right hemisphere can also lead to temporary selective familiar face identity recognition impairments (Jonas et al., 2015). The present findings suggest that this transient interruption could be due to a failure to individuate faces based on visual representations rather than access to specific semantic information about people.

4.4. Lack of temporal pole FID responses: an effect of un*familiarity*?

Despite extensive sampling of the ATL up to the temporal pole, FID responses are weak and rare in the most anterior part of the ATL (anterior to around −7 Talairach y coordinate) and in the temporal pole (except in the left hemisphere in the proportion map). Over the last decade, ATL regions, in particular in the temporal pole, have been attributed a prominent role in face processing (Avidan et al., 2014; Axelrod and Yovel, 2013; Rajimehr et al., 2009; Von Der Heide et al., 2013). Some studies, relying primarily on fMRI-MVPA reports of above chance unfamiliar face identity decoding in this region, have even claimed it as a primary locus of face identity recognition (Anzellotti et al., 2014; Kriegeskorte et al., 2007). However, the localization of decoding effects is inconsistent across these studies, these effects are usually just above chance level and may not be specific to identity (e.g., decoding between a single male and female face picture in Kriegeskorte et al., 2007). Most importantly, cortical damage to this region is not typically

associated with prosopagnosia – an impairment of face identity recognition limited to the visual modality – but rather with multimodal semantic memory impairments, as in the right hemispheric fronto-temporal variant of semantic dementia (Busigny et al., 2009; Evans et al., 1995; Gainotti et al., 2008; Lambon Ralph, 2014). Together with the present findings based on an extensive spatial sampling of the FID function in the ATL, this suggests that the temporal pole is not critical for visual face identity recognition. Instead, this region may be involved in the association of semantic information with specific face identities, including verbal labels (Collins et al., 2016; Rice et al., 2018; Von Der Heide et al., 2013). If this reasoning is correct, the same frequency-tagging approach as used here but with pictures of familiar(ized) faces (Verosky et al., 2020) should reveal an increased contribution of ATL regions including the temporal poles.

4.5. Potential limitations and future extensions

Although we isolated high-level visual responses supporting FID by comparing upright and inverted faces, the present frequency-tagging paradigm is based on the repetition of the exact same image (at different sizes) of a full-front face identity, interrupted periodically by other facial identities also presented at a full-front view. Hence, we did not evaluate FID responses across natural changes of viewing conditions, e.g. in head rotation and lighting direction (O'Toole et al., 2006; Rossion and Michel, 2018; Tarr and Bülthoff, 1998). Scalp EEG data collected with this paradigm show that the FID response to unfamiliar faces remains robust through random variations in head pose (e.g., head tilted down, looking upward, to the side, etc.) throughout the stimulation sequence (Damon et al., 2020). The FID response is also strong when head orientation varies randomly in depth (i.e. full-front faces, profile, $\frac{3}{4}$ profile faces, etc.) but decreases linearly over the right occipito-temporal cortex with increasing viewpoint variation (Rossion et al., 2020), indicating that this response is viewpoint-dependent to some extent. Exploring the neural basis of this viewpoint-dependency with the present intracerebral recording approach would be highly valuable, in particular to evaluate whether there is a progressive increase of invariance to changes in viewing conditions in FID responses from posterior (IOG) to more anterior (latFG or antFG) regions in the human brain (see Ramirez, 2018).

An important issue to consider is that the data reported here was collected on a specific clinical population, namely patients with long-term drug-resistant epilepsy. Most participants tested here have temporal lobe epilepsy which may cause (visual) recognition deficits. Neuropsychological studies have shown that this population, on average, suffers from increased difficulties at encoding and recognizing familiar faces (Drane et al., 2013). However, there is also a wide interindividual variability in this function in the normal population (Jenkins et al., 2018), and there is currently no evidence that these face identity encoding and recognition processes are qualitatively different in temporal lobe epilepsy patients than in the normal population. Moreover, to our knowledge, there is no evidence that temporal lobe epilepsy patients have difficulties to individuate *unfamiliar* faces (Chiaravalloti and Glosser, 2004). A subset of 32 participants of our sample performed a behavioral delayed face matching task (experiment 4 of Busigny and Rossion, 2010) and showed large, normal range, face inversion effects both in accuracy rates and response times (Fig. S1). Also, most of our participants (84%) were tested at the Benton Face Recognition Test-c (Rossion and Michel, 2018), reaching an average performance in the normal range. While 13 participants showed a score below normal range (<39), the outcome of the proportion and amplitude analyses reported here was not affected by the inclusion of these participants (Fig. S5 and S6). This supports the view that lower performance (and higher reaction times) at explicit behavioral tasks of face individuation in some of these temporal lobe epilepsy patients are not due to specific face individuation deficits. Instead, these difficulties may be due to lower levels of education and general cognitive impairments (see Benton et al., 1983; Schretlen et al., 2001 for BFRT performance; see also Fig. S1 for performance at the face matching task in the present sample).

Another related issue is that of the potential neuro-functional reorganization of face processing in this population of temporal lobe epilepsy patients. Here, contrary to weakly substantiated claims of such reorganization (Mogi et al., 2019; Riley et al., 2015), our observations of large neural face inversion effects, right hemispheric lateralization and confined localization of FID responses in the IOG and latFG in our sample of patients are in general agreement with multiple sources of evidence from lesion studies, neuroimaging and effects of intracerebral or transcranial stimulation as reviewed in the introduction. In addition, there is a close correspondence between the present findings from temporal lobe epilepsy patients in SEEG and normal controls tested with the exact same experimental paradigm in scalp EEG. Specifically, the magnitude of the face inversion effect in the two key regions of the right IOG and latFG (53% and 56% reduction respectively) is strikingly similar to the effect found on the scalp over the right occipito-temporal region (53% reduction; Rossion et al., 2020). As for the right hemispheric lateralization index, it is at least as large in these two regions here (37% and 45% right IOG and latFG respectively) as it is on the scalp in neurotypical individuals (27%; Rossion et al., 2020). These observations do not only strengthen the validity of the present findings, but also neurophysiological data recordings in temporal lobe epilepsy patients to understand human face recognition and brain function in general.

A future extension of this study would be to determine *when* and *how* unfamiliar FID is achieved in the human brain. Answering the question of the time-course of FID could be potentially addressed by analyzing the present data in the time-domain (Rossion et al., 2020). However, unlike the frequency-domain approach used here, which provides an objective compact measure of the function, the temporal decomposition of the response yields numerous deflections over time (Dzhelyova and Rossion, 2014; Rossion et al., 2020). Inside the brain, these local field potentials occur with opposite polarities in interlocked time-courses depending on the recording sites and reference electrode (e.g., Barbeau et al., 2008), making it extremely challenging to combine participants to obtain an intelligible representation across the whole neural circuitry. Determining *how* (i.e., neural mechanisms) unfamiliar FID is achieved in the human brain would require recording at lower-levels of neural organization to capture the activity of single units in humans (Quian Quiroga, 2012; Rey et al., 2020). Importantly, the findings of the present study indicate that the neuronal code for human face individuation is unlikely to be cracked by focusing on small local populations of neurons but will rather require recordings at multiple VOTC locations, preferentially in the right hemisphere.

5. Summary and conclusions

In summary, our large scale human intracerebral investigation shows that fast, automatic and high-level unfamiliar face individuation in humans is achieved by neural populations distributed within a strip of cortex running from the IOG and latFG to the antFG and surrounding sulci, with a right hemispheric dominance. These observations fully support the qualitative view of the face inversion effect. They also highlight the importance of probing the neural basis of human FID with unfamiliar faces in order to isolate visual processes subtending this function from the contribution of associated semantic, affective and verbal information.

CRediT authorship contribution statement

Corentin Jacques: Conceptualization, Methodology, Software, Formal analysis, Visualization, Writing - original draft, Writing - review & editing. **Bruno Rossion:** Conceptualization, Methodology, Project administration, Writing - original draft, Supervision, Funding acquisition, Writing - review & editing. **Angélique Volfart:** Investigation, Formal

analysis, Visualization. **Hélène Brissart:** Investigation, Formal analysis. **Sophie Colnat-Coulbois:** Resources, Investigation. **Louis Maillard:** Resources, Project administration, Funding acquisition. **Jacques Jonas:** Conceptualization, Methodology, Investigation, Resources, Visualization, Writing - original draft, Writing - review & editing.

Acknowledgments

We thank the participants for their involvement in the study. We thank Joan Liu-Shuang for her contribution to the research design and SEEG data collection. This work is supported by an EOS grant "HUMVISCAT" 30991544.

Supplementary materials

Supplementary material associated with this article can be found, in the online version, at doi:10.1016/j.neuroimage.2020.117174.

References

Aguirre, G.K., Singh, R., D'Esposito, M., 1999. Stimulus inversion and the responses of face and object-sensitive cortical areas. Neuroreport 10, 189–194.

Anzellotti, S., Fairhall, S.L., Caramazza, A., 2014. Decoding representations of face identity that are tolerant to rotation. Cereb. Cortex 24, 1988–1995. doi:10.1093/cercor/bht046.

Avidan, G., Tanzer, M., Hadj-Bouziane, F., Liu, N., Ungerleider, L.G., Behrmann, M., 2014. Selective dissociation between core and extended regions of the face processing network in congenital prosopagnosia. Cereb. Cortex 24, 1565–1578. doi:10.1093/cercor/bht007.

Axelrod, V., Yovel, G., 2013. The challenge of localizing the anterior temporal face area: a possible solution. Neuroimage 81, 371–380. doi:10.1016/j.neuroimage.2013.05.015.

Barbeau, E.J., Taylor, M.J., Regis, J., Marquis, P., Chauvel, P., Liégeois-Chauvel, C., 2008. Spatio temporal dynamics of face recognition. Cereb. Cortex 18, 997–1009. doi:10.1093/cercor/bhm140.

Barton, J.J.S., 2008. Structure and function in acquired prosopagnosia: lessons from a series of 10 patients with brain damage. J. Neuropsychol. 2, 197–225. doi:10.1348/174866407×214172.

Bates, D., Mächler, M., Bolker, B., Walker, S., 2015. Fitting Linear Mixed-Effects Models Using lme4. J. Stat. Softw 67, 1–48. doi:10.18637/jss.v067.i01.

Baylis, G.C., Rolls, E.T., Leonard, C.M., 1985. Selectivity between faces in the responses of a population of neurons in the cortex in the superior temporal sulcus of the monkey. Brain Res 342, 91–102.

Behrmann, M., Avidan, G., Gao, F., Black, S., 2007. Structural imaging reveals anatomical alterations in inferotemporal cortex in congenital prosopagnosia. Cereb. Cortex 17, 2354–2363. doi:10.1093/cercor/bhl144.

Benjamini, Y., Hochberg, Y., 1995. Controlling the false discovery rate: a practical and powerful approach to multiple testing. J. R. Stat. Soc. Ser. B 57, 289–300.

Benton, A.L., Sivan, A.B., Hamsher, K., Varney, N.R., Spreen, O., 1983. Contributions to Neuropsychological Assessment: A Clinical Manual, Oxford Uni. Oxford University Press, New York ed..

Benton, A.L., Van Allen, M.W., 1968. Impairment in facial recognition in patients with cerebral disease. Trans. Am. Neurol. Assoc. 93, 38–42.

Berman, M.G., Park, J., Gonzalez, R., Polk, T.A., Gehrke, A., Knaffla, S., Jonides, J., 2010. Evaluating functional localizers: the case of the FFA. Neuroimage 50, 56–71. doi:10.1016/j.neuroimage.2009.12.024.

Bodamer, J., 1947. Die-Prosop-agnosie. Arch. Psychiatr. Nervenkrankh 179, 6–54.

Bouvier, S.E., Engel, S.A., 2006. Behavioral deficits and cortical damage loci in cerebral achromatopsia. Cereb. Cortex 16, 183–191.

Bruce, C., 1982. Face recognition by monkeys: absence of an inversion effect. Neuropsychologia 20, 515–521. doi:10.1016/0028-3932(82)90025-2.

Busigny, T., Robaye, L., Dricot, L., Rossion, B., 2009. Right anterior temporal lobe atrophy and person-based semantic defect: a detailed case study. Neurocase 15, 485–508. doi:10.1080/13554790902971141.

Burton, M., 2013. Why has research in face recognition progressed so slowly? The importance of variability. Q. J. Exp. Psychol. 66, 1467–1485. doi:10.1080/17470218.2013.800125.

Busigny, T., Rossion, B., 2010. Acquired prosopagnosia abolishes the face inversion effect. Cortex 46, 965–981. doi:10.1016/j.cortex.2009.07.004.

Carey, S., 1992. Becoming a face expert. Philos. Trans. R. Soc. Lond. B. Biol. Sci. 335, 93–95. doi:10.1098/rstb.1992.0012.

Chang, L., Tsao, D.Y., 2017. The code for facial identity in the primate brain. Cell 169, 1013–1028. doi:10.1016/j.cell.2017.05.011.

Chiaravalloti, N.D., Glosser, G., 2004. Memory for faces dissociates from memory for location following anterior temporal lobectomy. Brain Cogn 54, 35–42. doi:10.1016/s0278-2626(03)00257-4.

Collins, J.A., Koski, J.E., Olson, I.R., 2016. More than meets the eye: the merging of perceptual and conceptual knowledge in the anterior temporal face area. Front. Hum. Neurosci. 10, 189. doi:10.3389/fnhum.2016.00189.

Cox, R.W., 1996. AFNI: software for analysis and visualization of functional magnetic resonance neuroimages. Comput. Biomed. Res. 29, 162–173. doi:10.1006/cbmr.1996.0014.

Damon, F., Leleu, A., Rekow, D., Poncet, F., Baudouin, J.Y., 2020. Expertise for conspecific face individuation in the human brain. Neuroimage 204, 116218. doi:10.1016/j.neuroimage.2019.116218.

Davidesco, I., Zion-Golumbic, E., Bickel, S., Harel, M., Groppe, D.M., Keller, C.J., Schevon, C.a., McKhann, G.M., Goodman, R.R., Goelman, G., Schroeder, C.E., Mehta, A.D., Malach, R., 2014. Exemplar selectivity reflects perceptual similarities in the human fusiform cortex. Cereb. Cortex 24, 1879–1893. doi:10.1093/cercor/bht038.

Drane, D.L., Ojemann, J.G., Phatak, V., Loring, D.W., Gross, R.E., Hebb, A.O., Silbergeld, D.L., Miller, J.W., Voets, N.L., Saindane, A.M., Barsalou, L., Meador, K.J., Ojemann, G.A., Tranel, D., 2013. Famous face identification in temporal lobe epilepsy: support for a multimodal integration model of semantic memory. Cortex 49, 1648–1667. doi:10.1016/j.cortex.2012.08.009.

Dzhelyova, M., Jacques, C., Dormal, G., Michel, C., Schiltz, C., Rossion, B., 2019. High test-retest reliability of a neural index of rapid automatic discrimination of unfamiliar individual faces. Vis. cogn. 27, 127–141. doi:10.1080/13506285.2019.1616639.

Dzhelyova, M., Rossion, B., 2014. The effect of parametric stimulus size variation on individual face discrimination indexed by fast periodic visual stimulation. BMC Neurosci 15, 87. doi:10.1186/1471-2202-15-87.

Eger, E., Schyns, P.G., Kleinschmidt, A., 2004. Scale invariant adaptation in fusiform face-responsive regions. Neuroimage 22, 232–242.

Engell, A.D., McCarthy, G., 2014. Repetition suppression of face-selective evoked and induced EEG recorded from human cortex. Hum. Brain Mapp. 35, 4155–4162. doi:10.1002/hbm.22467.

Evans, J.J., Heggs, A.J., Antoun, N., Hodges, J.R., 1995. Progressive prosopagnosia associated with selective right temporal lobe atrophy. A new syndrome? Brain 118, 1–13. doi:10.1093/brain/118.1.1, Pt 1.

Ewbank, M.P., Henson, R.N., Rowe, J.B., Stoyanova, R.S., Calder, A.J., 2013. Different neural mechanisms within occipitotemporal cortex underlie repetition suppression across same and different-size faces. Cereb. Cortex 23, 1073–1084. doi:10.1093/cercor/bhs070.

Farah, M.J., 1990. Visual agnosia: disorders of object recognition and what they tell us about normal vision., Visual agnosia: disorders of object recognition and what they tell us about normal vision. Issues in the Biology of Language and Cognition. The MIT Press, Cambridge, MA, US.

Gainotti, G., Ferraccioli, M., Quaranta, D., Marra, C., 2008. Cross-modal recognition disorders for persons and other unique entities in a patient with right fronto-temporal degeneration. Cortex 44, 238–248. doi:10.1016/j.cortex.2006.09.001.

Gao, X., Gentile, F., Rossion, B., 2018. Fast periodic stimulation (FPS): a highly effective approach in fMRI brain mapping. Brain Struct. Funct. doi:10.1007/s00429-018-1630-4.

Gauthier, I., Tarr, M.J., Moylan, J., Skudlarski, P., Gore, J.C., Anderson, A.W., 2000. The fusiform "face area" is part of a network that processes faces at the individual level. J. Cogn. Neurosci. 12, 495–504. doi:10.1162/089892900562165.

Ghuman, A.S., Brunet, N.M., Li, Y., Konecky, R.O., Pyles, J.A., Walls, S.A., Destefino, V., Wang, W., Richardson, R.M., 2014. Dynamic encoding of face information in the human fusiform gyrus. Nat. Commun. 5, 1–10. doi:10.1038/ncomms6672.

Gilaie-Dotan, S., Gelbard-Sagiv, H., Malach, R., 2010. Perceptual shape sensitivity to upright and inverted faces is reflected in neuronal adaptation. Neuroimage 50, 383–395. doi:10.1016/j.neuroimage.2009.12.077.

Goesaert, E., Op de Beeck, H.P., 2013. Representations of facial identity information in the ventral visual stream investigated with multivoxel pattern analyses. J. Neurosci. 33, 8549–8558. doi:10.1523/JNEUROSCI.1829-12.2013.

Griffin, J.W., 2020. Quantifying the face inversion effect in nonhuman primates: a phylogenetic meta-analysis. Anim. Cogn. 23, 237–249. doi:10.1007/s10071-019-01340-8.

Grill-Spector, K., Henson, R., Martin, A., 2006. Repetition and the brain: neural models of stimulus-specific effects. Trends Cogn. Sci. 10, 14–23. doi:10.1016/j.tics.2005.11.006.

Grill-Spector, K., Malach, R., 2001. fMR-adaptation: a tool for studying the functional properties of human cortical neurons. Acta Psychol. (Amst). 107, 293–321.

Hancock, P.J.B., Bruce, V., Burton, A.M., 2000. Recognition of unfamiliar faces. Trends Cogn. Sci. 4, 330–337. doi:10.1016/S1364-6613(00)01519-9.

Haxby, J.V., Ungerleider, L.G., Clark, V.P., Schouten, J.L., Hoffman, E.A., Martin, A., 1999. The effect of face inversion on activity in human neural systems for face and object perception. Neuron 22, 189–199.

Hermann, P., Grotheer, M., Kovacs, G., Vidnyanszky, Z., 2017. The relationship between repetition suppression and face perception. Brain Imaging Behav 11, 1018–1028. doi:10.1007/s11682-016-9575-9.

Hills, P.J., Lewis, M.B., 2018. The development of face expertise: evidence for a qualitative change in processing. Cogn. Dev. 48, 1–18. doi:10.1016/j.cogdev.2018.05.003.

Hsiao, J.H., Cottrell, G., 2008. Two fixations suffice in face recognition. Psychol. Sci. 19, 998–1006. doi:10.1111/j.1467-9280.2008.02191.x.

Hughes, B.L., Camp, N.P., Gomez, J., Natu, V.S., Grill-Spector, K., Eberhardt, J.L., 2019. Neural adaptation to faces reveals racial outgroup homogeneity effects in early perception. Proc. Natl. Acad. Sci. 116, 14532–14537. doi:10.1073/pnas.1822084116.

Jacques, C., d'Arripe, O., Rossion, B., 2007. The time course of the inversion effect during individual face discrimination. J. Vis. 7 (8), 1–9. doi:10.1167/7.8.3.Introduction, 3.

Jenkins, R., Dowsett, A.J., Burton, A.M., 2018. How many faces do people know? Proc. Biol. Sci. 285. doi:10.1098/rspb.2018.1319.

Jonas, J., Brissart, H., Hossu, G., Colnat-Coulbois, S., Vignal, J.-.P., Rossion, B., Maillard, L., 2018. A face identity hallucination (palinopsia) generated by intracerebral stimulation of the face-selective right lateral fusiform cortex. Cortex 99, 296–310. doi:10.1016/j.cortex.2017.11.022.

Jonas, J., Descoins, M., Koessler, L., Colnat-Coulbois, S., Sauvée, M., Guye, M., Vignal, J.-.P., Vespignani, H., Rossion, B., Maillard, L., 2012. Focal electrical intracerebral stimulation of a face-sensitive area causes transient prosopagnosia. Neuroscience 222, 281–288. doi:10.1016/j.neuroscience.2012.07.021.

Jonas, J., Jacques, C., Liu-shuang, J., Brissart, H., Colnat-coulbois, S., Maillard, L., Rossion, B., 2016. A face-selective ventral occipito-temporal map of the human brain with intracerebral potentials. Proc. Natl. Acad. Sci. U.S.A. 113, E4088–E4097. doi:10.1073/pnas.1522033113.

Jonas, J., Rossion, B., Brissart, H., Frismand, S., Jacques, C., Hossu, G., Colnat-Coulbois, S., Vespignani, H., Vignal, J.P., Maillard, L., 2015. Beyond the core face-processing network: Intracerebral stimulation of a face-selective area in the right anterior fusiform gyrus elicits transient prosopagnosia. Cortex 72, 140–155. doi:10.1016/j.cortex.2015.05.026.

Jonas, J., Rossion, B., Krieg, J., Koessler, L., Colnat-Coulbois, S., Vespignani, H., Jacques, C., Vignal, J.P., Brissart, H., Maillard, L., 2014. Intracerebral electrical stimulation of a face-selective area in the right inferior occipital cortex impairs individual face discrimination. Neuroimage 99, 487–497. doi:10.1016/j.neuroimage.2014.06.017.

Kanwisher, N., 2017. The Quest for the FFA and Where It Led. J. Neurosci. 37, 1056–1061. doi:10.1523/JNEUROSCI.1706-16.2016.

Kanwisher, N., McDermott, J., Chun, M.M., 1997. The fusiform face area: a module in human extrastriate cortex specialized for face perception. J. Neurosci. 17, 4302–4311. doi:10.1098/Rstb.2006.1934.

Kim, J.-J., Crespo-Facorro, B., Andreasen, N.C., O'Leary, D.S., Zhang, B., Harris, G., Magnotta, V.A., 2000. An MRI-Based Parcellation Method for the Temporal Lobe. Neuroimage 11, 271–288. doi:10.1006/nimg.2000.0543.

Kriegeskorte, N., Formisano, E., Sorger, B., Goebel, R., 2007. Individual faces elicit distinct response patterns in human anterior temporal cortex. Proc. Natl. Acad. Sci. U.S.A. 104, 20600–20605.

Lambon Ralph, M.A., 2014. Neurocognitive insights on conceptual knowledge and its breakdown. Philos. Trans. R. Soc. Lond. B. Biol. Sci. 369, 20120392. doi:10.1098/rstb.2012.0392.

Leopold, D.A., Bondar, I.V., Giese, M.A., 2006. Norm-based face encoding by single neurons in the monkey inferotemporal cortex. Nature 442, 572–575. doi:10.1038/nature04951.

Liu-Shuang, J., Norcia, A.M., Rossion, B., 2014. An objective index of individual face discrimination in the right occipito-temporal cortex by means of fast periodic oddball stimulation. Neuropsychologia 52, 57–72. doi:10.1016/j.neuropsychologia.2013.10.022.

Liu-Shuang, J., Torfs, K., Rossion, B., 2016. An objective electrophysiological marker of face individualisation impairment in acquired prosopagnosia with fast periodic visual stimulation. Neuropsychologia 83, 100–113. doi:10.1016/j.neuropsychologia.2015.08.023.

Lochy, A., Jacques, C., Maillard, L., Colnat-Coulbois, S., Rossion, B., Jonas, J., 2018. Selective visual representation of letters and words in the left ventral occipito-temporal cortex with intracerebral recordings. Proc. Natl. Acad. Sci. U.S.A. 115, E7595–E7604. doi:10.1073/pnas.1718987115.

Mazard, A., Schiltz, C., Rossion, B., 2006. Recovery from adaptation to facial identity is larger for upright than inverted faces in the human occipito-temporal cortex. Neuropsychologia 44, 912–922. doi:10.1016/j.neuropsychologia.2005.08.015.

Meadows, J.C., 1974. The anatomical basis of prosopagnosia. J. Neurol. Neurosurg. Psychiatry..

Megreya, A.M., Burton, A.M., 2006. Unfamiliar faces are not faces: Evidence from a matching task. Mem. Cognit. 34, 865–876. doi:10.3758/BF03193433.

Mogi, T., Tsunoda, T., Yoshino, A., 2019. Altered upright face recognition and presence of face inversion effect in temporal lobe epilepsy: an event-related potential study. Psychiatry Clin. Neurosci. 73, 269–276. doi:10.1111/pcn.12829.

Murphy, J., Gray, K.L.H., Cook, R., 2020. Inverted faces benefit from whole-face processing. Cognition 194, 104105. doi:10.1016/j.cognition.2019.104105.

Natu, V.S., Jiang, F., Narvekar, A., Keshvari, S., Blanz, V., O'Toole, A.J., 2010. Dissociable neural patterns of facial identity across changes in viewpoint. J. Cogn. Neurosci. 22, 1570–1582. doi:10.1162/jocn.2009.21312.

Nestor, A., Plaut, D.C., Behrmann, M., 2016. Feature-based face representations and image reconstruction from behavioral and neural data. Proc. Natl. Acad. Sci. U. S. A. 113, 416–421. doi:10.1073/pnas.1514551112.

Nestor, A., Plaut, D.C., Behrmann, M., 2011. Unraveling the distributed neural code of facial identity through spatiotemporal pattern analysis. Proc. Natl. Acad. Sci. U.S.A. 108, 9998–10003. doi:10.1073/pnas.1102433108.

Newport, C., Wallis, G., Reshitnyk, Y., Siebeck, U.E., 2016. Discrimination of human faces by archerfish (Toxotes chatareus). Sci. Rep. 6, 27523. doi:10.1038/srep27523.

O'Toole, A.J., Jiang, F., Roark, D., Abdi, H., 2006. Predicting human performance for face recognition. In: Chellappa, R., Zhao, W. (Eds.), Face Processing: Advanced Models and Methods. Academic Press, New York, pp. 293–320.

Palermo, R., Rhodes, G., 2007. Are you always on my mind? A review of how face perception and attention interact. Neuropsychologia 45, 75–92. doi:10.1016/j.neuropsychologia.2006.04.025.

Parr, L.A., Heintz, M., Pradhan, G., 2008. Rhesus monkeys (Macaca mulatta) lack expertise in face processing. J. Comp. Psychol. 122, 390–402. doi:10.1037/0735-7036.122.4.390.

Pinsk, M.A., Arcaro, M., Weiner, K.S., Kalkus, J.F., Inati, S.J., Gross, C.G., Kastner, S., 2009. Neural representations of faces and body parts in macaque and human cortex: a comparative FMRI study. J. Neurophysiol. 101, 2581–2600. doi:10.1152/jn.91198.2008.

Pitcher, D., Duchaine, B., Walsh, V., Yovel, G., Kanwisher, N., 2011a. The role of lateral occipital face and object areas in the face inversion effect. Neuropsychologia 49, 3448–3453. doi:10.1016/j.neuropsychologia.2011.08.020.

Pitcher, D., Walsh, V., Duchaine, B., 2011b. The role of the occipital face area in the cortical face perception network. Exp. Brain Res. 209, 481–493. doi:10.1007/s00221-011-2579-1.

Pitcher, D., Walsh, V., Yovel, G., Duchaine, B., 2007. TMS evidence for the involvement of the right occipital face area in early face processing. Curr. Biol. 17, 1568–1573. doi:10.1016/j.cub.2007.07.063.

Puce, A., Allison, T., McCarthy, G., 1999. Electrophysiological studies of human face perception. III: effects of top-down processing on face-specific potentials. Cereb. Cortex 9, 445–458.

Quian Quiroga, R., 2012. Concept cells: the building blocks of declarative memory functions. Nat. Rev. Neurosci. 13, 587–597. doi:10.1038/nrn3251.

Quian Quiroga, R., Reddy, L., Kreiman, G., Koch, C., Fried, I., 2005. Invariant visual representation by single neurons in the human brain. Nature 435, 1102–1107. doi:10.1038/nature03687.

Rajimehr, R., Young, J.C., Tootell, R.B.H., 2009. An anterior temporal face patch in human cortex, predicted by macaque maps. Proc. Natl. Acad. Sci. U.S.A. 106, 1995–2000. doi:10.1073/pnas.0807304106.

Ramirez, F.M., 2018. Orientation Encoding and Viewpoint Invariance in Face Recognition: inferring Neural Properties from Large-Scale Signals. Neuroscientist 24, 582–608. doi:10.1177/1073858418769554.

Rey, H.G., Gori, B., Chaure, F.J., Collavini, S., Blenkmann, A.O., Seoane, P., Seoane, E., Kochen, S., Quian Quiroga, R., 2020. Single neuron coding of identity in the human hippocampal formation. Curr. Biol. 30, 1152–1159. doi:10.1016/j.cub.2020.01.035, e3.

Rice, G.E., Caswell, H., Moore, P., Hoffman, P., Lambon Ralph, M.A., 2018. The roles of left versus right anterior temporal lobes in semantic memory: a neuropsychological comparison of postsurgical temporal lobe epilepsy patients. Cereb. Cortex 28, 1487–1501. doi:10.1093/cercor/bhx362.

Riley, J.D., Fling, B.W., Cramer, S.C., Lin, J.J., 2015. Altered organization of face-processing networks in temporal lobe epilepsy. Epilepsia 56, 762–771. doi:10.1111/epi.12976.

Rosenthal, G., Sporns, O., Avidan, G., 2016. Stimulus dependent dynamic reorganization of the human face processing network. Cereb. Cortex 27, 4823–4834. doi:10.1093/cercor/bhw279.

Rossion, B., Retter, T.L., Liu-Shuang, J., 2020. Understanding human individuation of unfamiliar faces with oddball fast periodic visual stimulation and electroencephalography. Eur J Neurosci. Accepted Author Manuscript. doi:10.1111/ejn.14865.

Rossion, B., 2018. Damasio's error - Prosopagnosia with intact within-category object recognition. J. Neuropsychol. 12, 357–388. doi:10.1111/jnp.12162.

Rossion, B., 2014. Understanding face perception by means of prosopagnosia and neuroimaging. Front. Biosci. Elit. 6, 258–307.

Rossion, B., 2008. Picture-plane inversion leads to qualitative changes of face perception. Acta Psychol. (Amst). 128, 274–289. doi:10.1016/j.actpsy.2008.02.003.

Rossion, B., Jacques, C., Jonas, J., 2018. Mapping face categorization in the human ventral occipito-temporal cortex with direct neural intracranial recordings. Ann. N.Y. Acad. Sci. doi:10.1111/nyas.13596.

Rossion, B., Michel, C., 2018. Normative accuracy and response time data for the computerized Benton Facial Recognition Test (BFRT-c). Behav. Res. Methods 50, 2442–2460. doi:10.3758/s13428-018-1023-x.

Rossion, B., Schiltz, C., Robaye, L., Pirenne, D., Crommelinck, M., 2001. How does the brain discriminate familiar and unfamiliar faces?: a PET study of face categorical perception. J. Cogn. Neurosci. 13, 1019–1034. doi:10.1162/089892901753165917.

Rossion, B., Taubert, J., 2019. What can we learn about human individual face recognition from experimental studies in monkeys? Vision Res. 157, 142–158. doi:10.1016/j.visres.2018.03.012.

Rostalski, S.-.M., Amado, C., Kovács, G., 2019. Repetition suppression for noisy and intact faces in the occipito-temporal cortex. Front. Psychol. 10, 1348. doi:10.3389/fpsyg.2019.01348.

Salado, A.L., Koessler, L., De Mijolla, G., Schmitt, E., Vignal, J.-.P., Civit, T., Tyvaert, L., Jonas, J., Maillard, L.G., Colnat-Coulbois, S., 2018. sEEG is a safe procedure for a comprehensive anatomic exploration of the insula: a retrospective study of 108 procedures representing 254 transopercular insular electrodes. Oper. Neurosurg. 14, 1–8. doi:10.1093/ons/opx106.

Schiltz, C., Rossion, B., 2006. Faces are represented holistically in the human occipito-temporal cortex. Neuroimage 32, 1385–1394. doi:10.1016/j.neuroimage.2006.05.037.

Schretlen, D.J., Pearlson, G.D., Anthony, J.C., Yates, K.O., 2001. Determinants of benton facial recognition test performance in normal adults. Neuropsychology. doi:10.1037/0894-4105.15.3.405.

Sekuler, A.B., Gaspar, C.M., Gold, J.M., Bennett, P.J., 2004. Inversion leads to quantitative, not qualitative, changes in face processing. Curr. Biol. 14, 391–396.

Sergent, J., Signoret, J.L., 1992. Functional and anatomical decomposition of face processing - evidence from prosopagnosia and pet study of normal subjects. Philos. Trans. R. Soc. London Ser. B-Biological Sci. 335, 55–62.

Sheehan, M.J., Nachman, M.W., 2014. Morphological and population genomic evidence that human faces have evolved to signal individual identity. Nat. Commun. 5, 4800. doi:10.1038/ncomms5800.

Sheehan, M.J., Tibbetts, E.A., 2011. Specialized face learning is associated with individual recognition in paper wasps. Science 334 (80–), 1272–1275. doi:10.1126/science.1211334.

Talairach, J., Bancaud, J., 1973. Stereotaxic approach to epilepsy. Methodology of anatomo-functional stereotaxic investigations. Prog. Neurol. Surg. 5, 297–354. doi:10.1159/000394343.

Tarr, M.J., Bülthoff, H.H., 1998. Image-based object recognition in man, monkey and machine. Cognition 67, 1–20.

Verosky, S.C., Zoner, K.A., Marble, C.W., Sammon, M.M., Babarinsa, C.O., 2020. Familiarization increases face individuation measured with fast periodic visual stimulation. Biol. Psychol. 153, 107883. doi:10.1016/j.biopsycho.2020.107883.

Von Der Heide, R.J., Skipper, L.M., Olson, I.R., 2013. Anterior temporal face patches:

a meta-analysis and empirical study. Front. Hum. Neurosci. 7, 17. doi:10.3389/fnhum.2013.00017.

Wandell, B.A., 2011. The neurobiological basis of seeing words. Ann. N.Y. Acad. Sci. 1224, 63–80. doi:10.1111/j.1749-6632.2010.05954.x.

Weiner, K.S., Golarai, G., Caspers, J., Chuapoco, M.R., Mohlberg, H., Zilles, K., Amunts, K., Grill-Spector, K., 2014. The mid-fusiform sulcus: a landmark identifying both cytoarchitectonic and functional divisions of human ventral temporal cortex. Neuroimage 84, 453–465. doi:10.1016/j.neuroimage.2013.08.068.

Weiner, K.S., Grill-Spector, K., 2012. The improbable simplicity of the fusiform face area. Trends Cogn. Sci. 16, 251–254. doi:10.1016/j.tics.2012.03.003.

Yan, X., Liu-Shuang, J., Rossion, B., 2019. Effect of face-related task on rapid individual face discrimination. Neuropsychologia 129, 236–245. doi:10.1016/j.neuropsychologia.2019.04.002.

Yin, R.K., 1969. Looking at upside-down faces. J. Exp. Psychol. Percept. Perform. 81, 141–145.

Young, M.P., Yamane, S., 1992. Sparse Population Coding of Faces in the Inferotemporal Cortex. Science 256 (80–), 1327–1331.

Yovel, G., Kanwisher, N., 2005. The neural basis of the behavioral face-inversion effect. Curr. Biol. 15, 2256–2262.

Zhen, Z., Yang, Z., Huang, L., Kong, X., Wang, X., Dang, X., Huang, Y., Song, Y., Liu, J., 2015. Quantifying interindividual variability and asymmetry of face-selective regions: a probabilistic functional atlas. Neuroimage 113, 13–25. doi:10.1016/j.neuroimage.2015.03.010.

OXFORD

Cerebral Cortex, July 2020;30: 4026–4043

doi: 10.1093/cercor/bhaa022
Advance Access Publication Date: 16 March 2020
Original Article

ORIGINAL ARTICLE

Spatially Dissociated Intracerebral Maps for Face- and House-Selective Activity in the Human Ventral Occipito-Temporal Cortex

Simen Hagen[1], Corentin Jacques[2], Louis Maillard[1,3], Sophie Colnat-Coulbois[1,4], Bruno Rossion[1,2,3] and Jacques Jonas[1,3]

[1]Université de Lorraine, CNRS, CRAN, Nancy F-54000, France, [2]Psychological Sciences Research Institute, Institute of Neuroscience, University of Louvain, Louvain-La-Neuve B-1348, Belgium, [3]Université de Lorraine, CHRU-Nancy, Service de Neurologie, Nancy F-54000, France and [4]Université de Lorraine, CHRU-Nancy, Service de Neurochirurgie, Nancy F-54000, France

Address correspondence to Bruno Rossion, CRAN UMR 7039, CNRS - Université de Lorraine, Pavillon Krug, Hôpital Central, CHRU de Nancy, Nancy 54000, France. Email: bruno.rossion@univ-lorraine.fr

Abstract

We report a comprehensive mapping of the human ventral occipito-temporal cortex (VOTC) for selective responses to frequency-tagged faces or landmarks (houses) presented in rapid periodic trains of objects, with intracerebral recordings in a large sample ($N = 75$). Face-selective contacts are three times more numerous than house-selective contacts and show a larger amplitude, with a right hemisphere advantage for faces. Most importantly, these category-selective contacts are spatially dissociated along the lateral-to-medial VOTC axis, respectively, consistent with neuroimaging evidence. At the minority of "overlap" contacts responding selectively to both faces and houses, response amplitude to the two categories is not correlated, suggesting a contribution of distinct populations of neurons responding selectively to each category. The medio-lateral dissociation also extends into the underexplored anterior temporal lobe (ATL). In this region, a relatively high number of intracerebral recording contacts show category-exclusive responses (i.e., without any response to baseline visual objects) to faces but rarely to houses, in line with the proposed role of this region in processing people-related semantic information. Altogether, these observations shed novel insight on the neural basis of human visual recognition and strengthen the validity of the frequency-tagging approach coupled with intracerebral recordings in epileptic patients to understand human brain function.

Key words: anterior temporal lobe, face categorization, frequency-tagging, fusiform gyrus, SEEG

Introduction

The human visual system is highly efficient at transforming retinal input into meaningful categories, as exemplified by the ease of detecting highly variable human faces among other variable nonface objects (i.e., generic face categorization). Categorizing visual stimuli as faces is a challenging brain function since, besides the inherent variability in face and nonface object identity, each instance of a face or an object can produce an infinite number of retinal inputs, resulting from changes in, for example, size (distance), position, lighting, or orientation. The neural basis of human face categorization has been studied extensively in functional magnetic resonance imaging (fMRI) studies, which consistently report larger responses to faces in the lateral parts of the middle fusiform gyrus (latFG) and in the

inferior occipital gyrus (IOG) of the ventral occipito-temporal cortex (VOTC) (Puce et al. 1995; Kanwisher et al. 1997; Haxby et al. 2000; see Grill-Spector et al. 2017 for recent review).

These indirect measures of face-selective neural activity can be complemented by direct intracranial recordings of brain activity in human epileptic patients (Allison et al. 1994, 1999; Halgren et al. 1994; Engell and McCarthy 2010; Vidal et al. 2010; Ghuman et al. 2014; Jonas et al. 2016; Kadipasaoglu et al. 2016; see Rossion et al. 2018 for review). These investigations are valuable by the high temporal resolution that they afford but also because they provide direct neural measures without substantial regional variations in signal-to-noise ratio. Moreover, they provide direct links with the causal effects of electrical stimulation (e.g., Jonas et al. 2012; Parvizi et al. 2012). However, these investigations remain rare and are often limited in terms of the number of individual brains sampled as well as their spatial range of investigation, which is determined by strict clinical criteria. Moreover, the exact location/source of the neurophysiological recordings remains uncertain (Katzner et al. 2009; Herreras 2016). This important approach for human neuroscience research therefore requires further validation by testing large cohort of patients with objective quantification of responses of interest across wide cortical regions, documenting similarities and differences with other measures (Rossion et al. 2018).

In this context, a recent study isolated face categorization responses with a frequency-tagging approach (fast period visual stimulation [FPVS]) applied to 28 patients implanted with intracerebral (i.e., depth) electrodes across the VOTC (Jonas et al. 2016). Although face-selective responses were found across the whole VOTC, replicating previous intracranial observations with more traditional stimulation approaches (e.g., Allison et al. 1999), clusters of high-amplitude face-selective contacts with a peak in the right lateral section of the middle fusiform gyrus were found, supporting fMRI observations (i.e., evidence for the "fusiform face area", "FFA" with a direct neural measure). Moreover, face-selective responses were found in several regions of the ventral anterior temporal lobe (ATL), an underexplored region in fMRI due to severe magnetic susceptibility artifacts (Wandell 2011; Axelrod and Yovel 2013; Rossion et al. 2018). Notably, up to 40% of population-level neural responses in the ATL showed responses to faces without any significant response to nonface objects (i.e., "face-exclusive" contacts; Jonas et al. 2016).

Although this frequency-tagging approach has substantial advantages in terms of sensitivity, objectivity, and quantification, these observations raise at least two important unresolved issues. First, to what degree does the wide distribution of face-selective responses in the human VOTC reflect a lack of specificity of this approach? That is, could this wide distribution be due to the recording of neural activity from distant sources in intracerebral recordings (Herreras 2016; Dubey and Ray 2019), or to the additional contribution of non-category-selective responses triggered by the mere periodic repetition of the same kinds of items in a continuous stream of variable nonface objects, or else to a combination of these two factors? Second, are face-exclusive contacts found predominantly in the ATL truly category-selective—in particular limited to faces due to their rich network of semantic associations (Collins et al. 2016; Rice et al. 2018)—or do they rather reflect some kind of generic "oddball" responses to rare periodic events in such stimulation sequences? These issues are important to resolve not only to inform about the neural basis of face categorization and visual categorization in general but also to better understand the validity and limitations of the frequency-tagging approach in the context of human intracerebral recordings.

The current study directly addresses these issues in a very large group of individual human brains ($N = 75$) implanted with intracerebral electrodes. Subjects viewed variable objects images presented periodically at 6 Hz with either variable face or house images interleaved as every fifth image in separate sequences (Fig. 1). Hence, both face-selective and house-selective neural responses were objectively identified and quantified at the face stimulation frequency (6 Hz/5 = 1.2 Hz) and harmonics in different stimulation sequences. Pictures of houses provide a robust test to the issues at stake because it is known that houses, as spatial landmarks or places, are associated with responses in the medial regions of the VOTC such as the collateral sulcus (COS), the lingual sulcus, and the parahippocampal gyrus (PHG) (Epstein and Kanwisher 1998; Weiner and Grill-Spector 2010; Epstein et al. 2014; Kadipasaoglu et al. 2016). Moreover, faces and houses evoke quantitatively and qualitatively different category-selective responses in scalp EEG (Jacques et al. 2016a). Hence, we hypothesized that face- and house-selective responses (i.e., discriminating faces or houses from a variety of other visual objects) would elicit largely spatially distinct maps in the VOTC, with a predominance in lateral and medial temporal regions, respectively. Moreover, we took advantage of an extensive sampling of the ATL to test whether this spatial dissociation extends to these anterior regions. Finally, based on growing evidence for the role of the ATL in person recognition and semantics (e.g., Gainotti 2013; Rice et al. 2018), we hypothesized exclusive responses in the ATL to be truly category-specific, and with no or little response to houses on these contacts. Such findings would not only shed important insight on the neural basis of human face categorization but would also strengthen the validity and the frequency-tagging approach combined with human intracerebral recordings in temporal epileptic patients to understand brain function.

Materials and Methods

Participants

The study included 75 patients (35 females, mean age: 32.3 ± 8.4 years, 68 right-handed) undergoing clinical intracerebral evaluation with depth electrodes (stereoelectroencephalography [SEEG]) for refractory partial epilepsy, studied in the Epilepsy Unit of the University Hospital of Nancy between 2013 and 2017. Patients were included in the study if they had at least one intracerebral electrode implanted in the VOTC (Fig. 1C). The data on periodic faces from 28 of the 75 patients were included in the study of Jonas et al. (2016). They all gave written consent to participate to the study, which was part of a protocol approved by the ethics committee of the University Hospital of Nancy.

Intracerebral Electrode Implantation and Recording

Intracerebral electrodes were stereotactically implanted within the participants' brains for clinical purposes, that is, to delineate their seizure-onset zones and to functionally map the surrounding cortex in the perspective of an eventual epilepsy surgery (Bédos Ulvin et al. 2017). Each 0.8-mm-diameter intracerebral electrode contains 8–15 independent recording contacts of 2 mm in length separated by 1.5 mm from edge to edge (for details about the electrode implantation procedure, see Salado et al. 2017). Intracerebral EEG was sampled at a 512 Hz with a

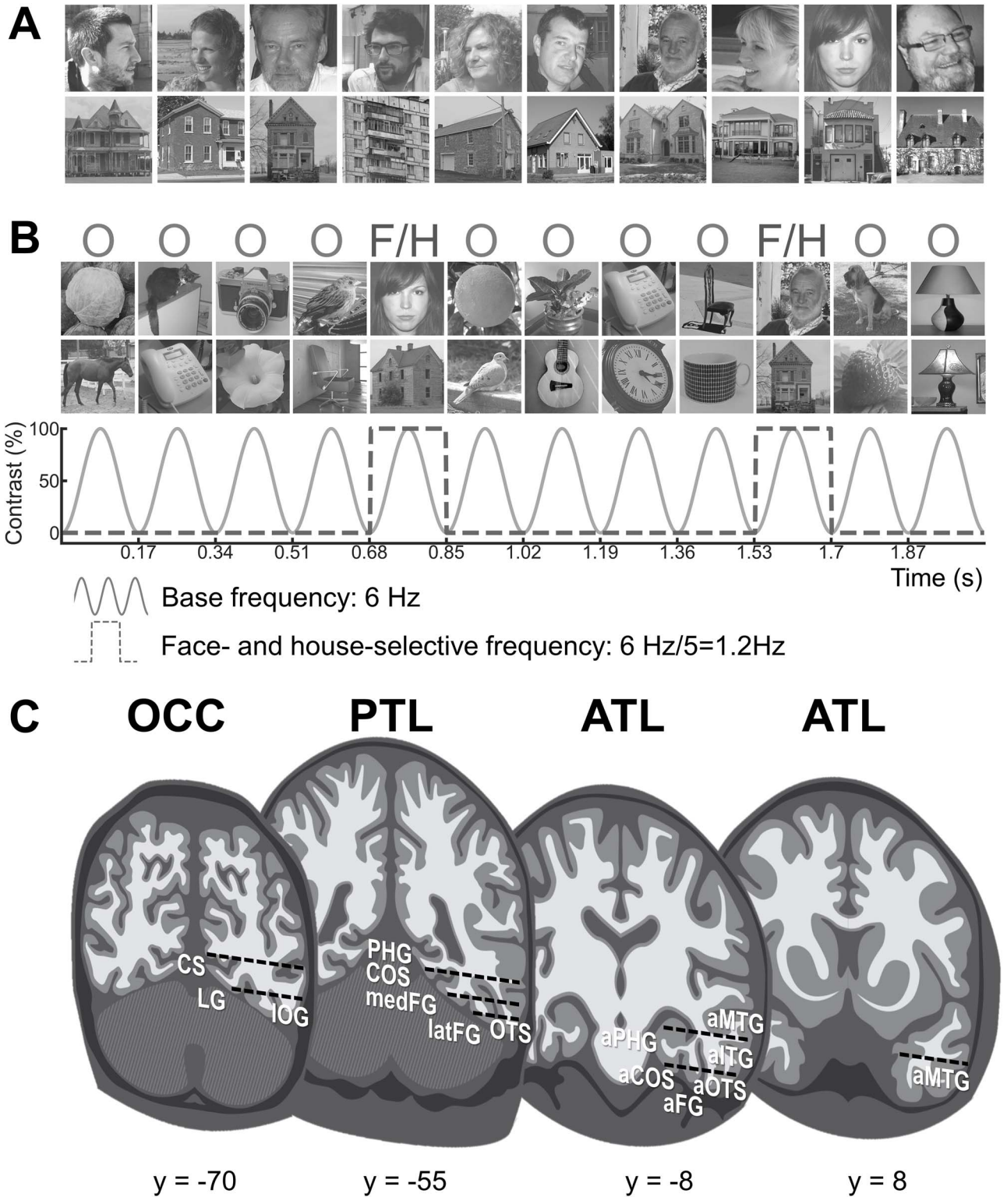

Figure 1. FPVS and SEEG methods. (*A*) Example of natural images of faces and houses used in the experiment (actual face images not shown for copyright reasons). (*B*) Images of living or nonliving objects were presented by sinusoidal contrast modulation at a rate of 6 stimuli per second (6 Hz) with different images of either faces or houses presented in separate sequences every 5 stimuli (i.e., appearing at the frequency of 6 Hz/5 = 1.2 Hz). (*C*) Schematic coronal representation of the typical trajectories of depth electrodes implanted in the VOTC (adapted from Jonas et al. 2016). Electrodes consist of 8–15 contiguous recording contacts (black rectangles) spread along the electrode length, along the medio-lateral axis. Acronyms: ITG, inferior temporal gyrus; MTG, middle temporal gyrus; OTS, occipito-temporal sulcus; CS, calcarine sulcus; LG, lingual gyrus; a, anterior; lat, lateral; med, medial.

256-channel amplifier and referenced to either a midline prefrontal scalp electrode (FPz, available in 66 participants) or an intracerebral contact in the white matter (in nine participants). The data were not re-referenced. Contacts located in brain lesions visible on structural MRI were excluded from any analysis ($n = 67$; 1.83% of all contacts).

Fast Periodic Visual Stimulation Paradigm

Stimuli

We used 200 grayscale natural images of various nonface objects (from 14 nonface categories: cats [$n = 9$], dogs [$n = 5$], horses [$n = 5$], birds [$n = 24$], flowers [$n = 15$], fruits [$n = 28$], vegetables [$n = 21$], houseplants [$n = 15$], phones [$n = 13$], chairs [$n = 15$], cameras [$n = 6$], dishes [$n = 15$], guitars [$n = 15$], lamps [$n = 14$]), 50 grayscale natural images of faces, and 50 grayscale natural images of houses (see Fig. 1 for examples of stimuli). Each image contained an unsegmented object, face, or house near the center, which differed in terms of size, viewpoint, lighting conditions, and background. Images were equalized for mean pixel luminance and contrast (i.e., standard deviation across pixels). Faces (or houses) represented 20% of the stimuli. Since they appeared one out of five stimuli (20%), images of faces (or houses) were repeated the same amount of time than images of nonface objects. In a recording sequence, there were 227 cycles displaying objects, and at each cycle an image was sampled randomly from the 200 object stimuli. In contrast, there were 75 cycles displaying faces or houses, and at each cycle an image was sampled randomly from the 50 face or 50 house stimuli, respectively.

Experimental Procedure

Participants viewed continuous sequences of natural images of objects presented at a fast rate of 6 Hz through sinusoidal contrast modulation. In separate sequences, images of either faces or houses were presented periodically as every fifth stimulus so that the frequency of face/house presentation was 1.2 Hz (i.e., 6 Hz/5) (see Fig. 1, see also Videos 1 and 2 for an example of visual stimulation). All images were randomly selected from their respective categories. A sequence lasted 70 s: 66 s of stimulation at full-contrast flanked by 2 s of fade-in and fade-out, where contrast gradually increased or decreased, respectively. During one sequence, there were 75 presentations of faces or houses and 227 presentations of objects. During the sequences, participants were instructed to fixate a small black cross which was presented continuously at the center of the stimuli and to detect brief (500 ms) color changes (black to red) of this fixation cross. All but 19 participants saw the same number of sequences of face and houses (minimum 1 sequence per condition). The average number of sequences across all patients was 2.67 and 2.37 of face and house sequences, respectively. No participant had seizures in the 2 h preceding FPVS recordings.

Frequency-Domain Processing

Signals corresponding to the face and house conditions were processed the same way. Segments of SEEG corresponding to stimulation sequences were extracted (74-s segments, −2 to +72 s). The 74-s data segments were cropped to contain an integer number of 1.2-Hz cycles beginning 2 s after the onset of the sequence (right at the end of the fade-in period) until approximately 65 s, that is, before stimulus fade-out (75 face cycles ≈63 s). No artifact rejection was performed since EEG artifacts generate broadband noise in the frequency domain that locate mostly outside the narrow frequency bins containing the signal measurements (1.2 Hz and associated harmonics; Regan 1989; Jonas et al. 2016). Sequences of recorded voltage (i.e., time domain) were averaged separately for each participant and condition. Averaging sequences in the time domain before the fast Fourier transform (FFT) increases signal-to-noise ratio by canceling out non-phase-locked noise. Subsequently, FFT was applied to the full length of the cropped averaged time sequences. The amplitude spectra were extracted for all contacts by taking the modulus of the Fourier coefficients at each frequency bin normalized (by dividing) by half of the number of time samples in the time series. No normalization was performed on the time series prior to running the FFT. The long recording sequence resulted in a spectrum with a high-frequency resolution of 0.0159 (1/63 s). No data segments were excluded from the analysis. No other processing was performed to the data.

Selective Responses

The FPVS approach used here allows identifying and separating two distinct types of responses in both conditions: 1) a base response occurring at the base stimulation frequency (6 Hz) and its harmonics as well as 2) a selective response at 1.2 Hz and its harmonics (face-selective or house-selective response). In both face and house conditions, selective responses significantly above noise level at the face/house frequency (1.2 Hz) and its harmonics were determined as follows: 1) the FFT spectrum was cut into four segments centered at the face/house frequency and harmonics, from the first until the fourth (1.2 Hz until 4.8 Hz), and surrounded by 25 neighboring bins on each side (Fig. 2A); 2) the amplitude values in these four segments of FFT spectra were summed (Fig. 2B); 3) the summed FFT spectrum was transformed into a Z-score (Fig. 2C). Z-scores were computed as the difference between the amplitude at the face/house frequency bin and the mean amplitude of 48 surrounding bins (25 bins on each side, excluding the 2 bins directly adjacent to the bin of interest, i.e., 48 bins) divided by the standard deviation of amplitudes in the corresponding 48 surrounding bins. A contact was considered as showing a selective response in a given condition if the Z-score at the frequency bin of face or house stimulation exceeded 3.1 (i.e., $P < 0.001$ one-tailed: signal > noise).

Classification of Significant Contacts

Based on the pattern of discrimination responses across the two conditions (i.e., significant or not), we labeled each significant contact as follows: 1) contacts showing a significant face discrimination response, but not a significant house discrimination response, were defined as "face" (+face, −house); 2) contacts showing a significant house response, but not a significant face discrimination response, were defined as "house" (−face, +house); and 3) contacts showing significant discrimination responses to both faces and houses were defined as "overlap" (+face, +house).

Quantification of Response Amplitude

Baseline-corrected amplitudes were computed as the difference between the amplitude at each frequency bin and the average of 48 corresponding surrounding bins (up to 25 bins on each side, i.e., 50 bins, excluding the 2 bins directly adjacent to the bin of interest, i.e., 48 bins). Face- and house-selective responses were quantified separately as the sum of the

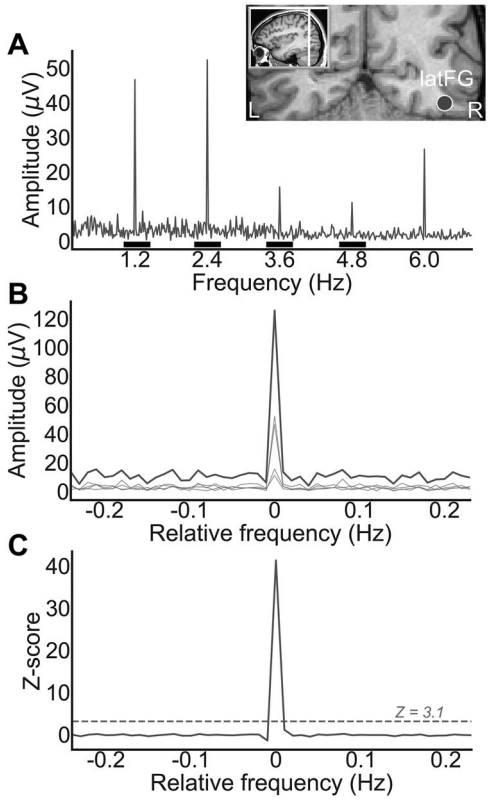

Figure 2. Intracerebral selective responses recorded in the VOTC. (*A*) Intracerebral EEG frequency-domain responses recorded at an individual recording contact (raw FFT amplitude) located in the right latFG in a single participant during a face sequence. The anatomical location of the contact is shown in a coronal MRI slice. Face-selective responses are observed at 1.2 Hz and harmonics. (*B*) Significant face-selective responses were determined by first segmenting the FFT spectrum into four segments centered at the frequency of face stimulation and its harmonics up to 4.8 Hz (i.e., 1.2, 2.4, 3.6, and 4.8 Hz). Individual FFT segments are shown in light-gray (horizontal gray bars on the *x*-axis in A represents the length of each FFT segment). The four segments, containing both the signal and the surrounding noise, were then summed (dark gray line). The 0 mark corresponds to the face stimulation frequency. (*C*) Z-score transformation of the summed FFT spectrum for statistical purpose. The Z-score at the face frequency exceeds 3.1 ($P < 0.001$), indicating that this contact shows a significant face-selective response. The same procedure was used to identify house-selective responses.

baseline-subtracted amplitudes at the face/house frequency from the 1st until the 14th (1.2 Hz until 16.8 Hz), excluding the 5th and 10th harmonics (6 and 12 Hz) that coincided with the base frequency (Jonas et al. 2016). Base response amplitudes were quantified separately as the sum of the baseline-subtracted amplitudes at the base frequency from the first until the fourth (6 Hz until 24 Hz), separately for face and house sequences.

Contact Localization in the Individual Anatomy

The exact position of each contact in the individual anatomy was determined by fusing the postoperative CT scan with a T1-weighted MRI. Contacts inside the gray matter were anatomically labeled in the individual anatomy using the same topographic VOTC parcellation as in Jonas et al. (2016) and Lochy et al. (2018) based on anatomical landmarks (Supplementary Fig. 1). Major VOTC sulci (COS and occipito-temporal sulcus) served as medio-lateral divisions. Postero-anterior divisions were the anterior tip of the parieto-occipital sulcus for the border between occipital and temporal lobes and the posterior tip of the hippocampus for the border between the posterior temporal lobe (PTL) and ATL (Kim et al. 2000). We did not include the temporal pole in our analyses (i.e., contacts anterior to the limen insulae, Ding et al. 2009). Therefore, we considered contacts in the ATL if they were located anteriorly to the posterior tip of the hippocampus and posterior to the limen insulae.

Proportion and Amplitude Maps in Talairach Space

In a separate analysis, anatomical MRIs were spatially normalized to determine Talairach coordinates of intracerebral contacts (for transformation procedure, see Koessler et al. 2009). Talairach coordinates of the intracerebral contacts were used to perform group analyses and visualization. The cortical surface used to display group maps was obtained from segmentation of the Collin27 brain from AFNI (Cox 1996) which is aligned to the Talairach space. Using Talairach coordinates, we computed the local proportion and amplitudes of the discrimination intracerebral contacts across the VOTC. Local proportion and amplitudes of contacts were computed in volumes (i.e., "voxels") of size $15 \times 15 \times 200$ mm (for the X, left–right; Y, posterior–anterior; and Z, inferior–superior dimensions, respectively) by steps of $3 \times 3 \times 200$ mm over the whole VOTC. A large voxel size in the Z dimension was used to collapse across contacts along the inferior–superior dimension. For each voxel, we extracted the following information across all participants in our sample: 1) the number of recorded contacts located within the voxel; 2) the number of contacts showing a significant response for each type of discrimination; and 3) the mean amplitudes in the significant contacts. For each voxel and each type of discrimination (i.e., face, house, overlap), we computed the proportion of significant contacts over recorded contacts (proportions are crucial here since sampling differs across regions), as well as the mean amplitudes over/in the significant contacts. To ensure reliability and reproducibility, we only considered voxels in which at least two participants showed significant responses. Then, for each voxel, we determined whether the proportion/amplitudes of significant contacts was significantly above zero using a bootstrap procedure in the following way: 1) sampling contacts from the voxel (the same number as the number of recorded contacts in the voxel) with replacement; 2) determining the proportion of significant contacts for this bootstrap sample and storing this value; and 3) repeating steps (1) and (2) 5000 times to generate a distribution of bootstrap proportions and to estimate the *P*-value as the fraction of bootstrap proportions equal to zero.

Bayesian Estimation

Bayesian estimation was used as a statistical tool for direct comparisons between conditions (for information on Bayesian estimation, see Kruschke 2013, 2014). This method assigns credibility to different parameter values (e.g., parameter = mean difference of face and house amplitudes in latFG) according to their consistency with the data. The more consistent the data is with a parameter value, the more credible that parameter value is (and vice versa for parameter values not consistent with the data). The posterior probability distribution expresses the probability of parameter values given the data, from which we computed 95% high-density confidence interval (95% HDI), reflecting the 95% most likely parameter values given the data.

A separate decision criterion was applied to yield a discrete decision as to whether there was evidence for a difference larger than 0. Specifically, a 95% HDI excluding a difference of 0 was interpreted as sufficient evidence for a difference (i.e., 0 was not among the 95% most likely values given the data), whereas a 95% HDI including a difference of 0 was interpreted as insufficient evidence for a difference (i.e., 0 was among the 95% most likely values given the data).

Continuous data (e.g., amplitudes, Talairach coordinates) was described by a normal distribution with the parameters mean and standard deviation. A noninformative prior distribution was specified by a uniform distribution. All dichotomous data (described as proportions) was described by a binominal distribution with the parameter theta. A noninformative prior distribution was specified using a beta distribution with shape parameters $a = 1$ and $b = 1$. A No-U-Turn sampler (NUTS) Markov chain Monte Carlo (MCMC) algorithm, implemented using the Pystan package (Carpenter et al. 2017) in the Python programming language, was used to estimate the posterior probability distribution. For each estimation, four chains were initialized, and each provided 100 000 samples. The burn-in period consisted of 50 000 samples. The chains were checked for convergence by inspecting the overlap of the different chains as plotted in trace plots and density plots of the parameter values sampled in each chain.

Results

Following Fourier transform of SEEG data, high SNR selective responses (for faces and/or houses) were identified in the VOTC exactly at the face/house presentation frequency (1.2 Hz) and harmonics (see Fig. 2A for an example in the face condition). Significant selective responses were determined based on a combination of the first four harmonics (i.e., 1.2, 2.4, 3.6, and 4.8 Hz, Fig. 2B) and a Z-score transform ($z > 3.1, P < 0.001$, Fig. 2C).

We found 1154 contacts with category-selective responses (for faces and/or houses) in 71 participants (among 3588 contacts implanted in the VOTC of 75 participants; i.e., 32% of recorded contacts). Among these contacts, 46.6% were selective to faces only (face contacts, 537/1154, participants = 65) and 15.8% were selective to houses only (house contacts, 182/1154, participants = 47). The remaining 37.7% contacts were selective to both faces and houses (overlap contacts, 435/1154, participants = 54). An example of the response profile of each contact type is shown in Figure 3. Each contact was localized in the individual anatomy using a topographic parcellation of the VOTC and in the Talairach space to perform group analyses and visualization (Fig. 3; see Supplementary Fig. 1 for the parcellation; Table 1 for contact count by hemisphere and region).

Latero-Medial Spatial Dissociation Between Face and House Contacts

Bayesian estimation was used for subsequent inferential analysis (e.g., Kruschke 2013). For each contrast we report the difference in central tendencies and a 95% posterior high-density confidence interval (HDI), which indicates the 95% most likely parameter values given the data (e.g., difference of mean face and house amplitudes in latFG). For a given contrast, a 95% HDI excluding a difference of 0 was interpreted as sufficient evidence for a difference (i.e., 0 was not among the 95% most likely values given the data), whereas a 95% HDI including a difference of 0 was interpreted as insufficient evidence for a difference (i.e., 0 was among the 95% most likely values given the data). See the Methods section for additional information on this approach.

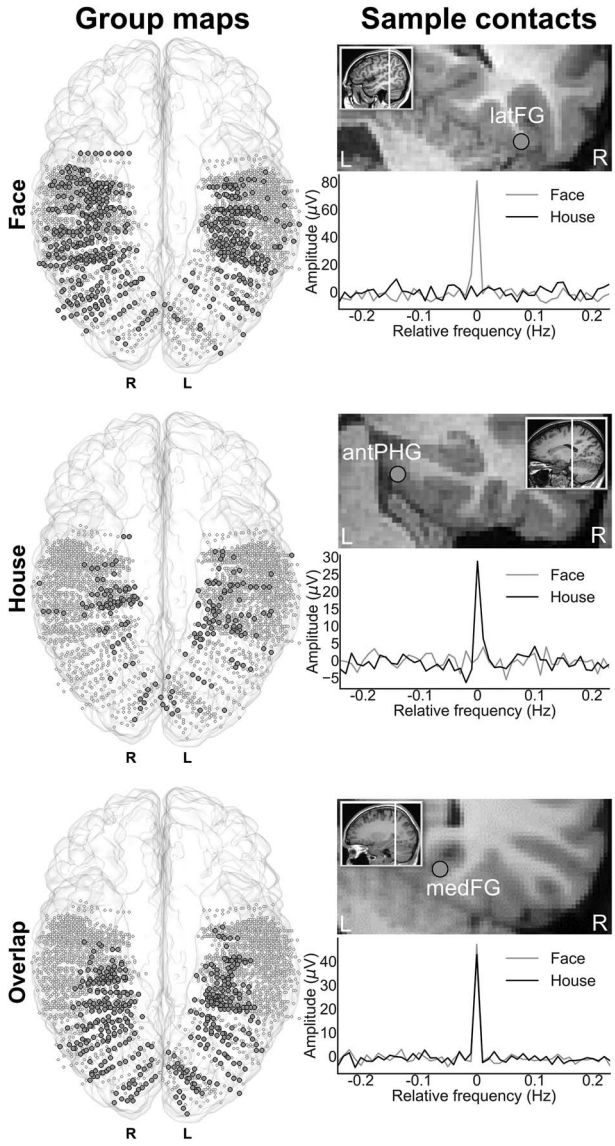

Figure 3. Classification and distribution of three types of selective contacts. Left: Maps of all 3588 VOTC recording contacts across the 75 individual brains displayed in the Talairach space using a transparent reconstructed cortical surface of the Colin27 brain. Each circle represents a single contact. Dark-gray-filled circles correspond to selective contacts. Light-gray-filled circles correspond to contacts on which no selective responses were recorded. Right: Examples of baseline-corrected FFT spectra for each contact type (three individual contacts in three different participants). Top: face contact selective to faces only; middle: house contact selective to houses only; bottom: overlap contact selective to both faces and houses. Their anatomical location is illustrated in the respective coronal MRI slices. The letters below each hemisphere (R, L) refers to the hemispheric side.

Overall there was a larger proportion of significant face than house contacts ($prop_{diff} = (537/3588) - (182/3588) = 9.89\%$, 95% HDI = [8.52, 11.27]). Moreover, for faces, there was a higher proportion of significant contacts in the right as compared with the left hemisphere ($prop_{diff} = (314/1682) - (223/1906) = 6.97\%$, 95% HDI = [4.61, 9.31]). In contrast, for houses, there was an equal proportion of significant contacts in the right and the

Table 1 Number of selective contacts and corresponding number of participants (in parentheses) in each anatomical region

Regions	Left hemisphere			Right hemisphere		
	Faces	Houses	Overlap	Faces	Houses	Overlap
VMO	14(4)	15(6)	49(7)	25(6)	13(6)	33(4)
IOG	15(8)	5(2)	22(8)	37(11)	0(0)	39(11)
Total OCC	**29 (8)**	**20 (6)**	**71 (9)**	**62 (13)**	**13 (6)**	**72 (12)**
PHG	0(0)	1(1)	2(1)	0(0)	5(4)	1(1)
medFG	12(8)	23(11)	55(19)	17(10)	6(3)	48(14)
latFG	34(16)	10(8)	23(11)	43(15)	2(2)	32(13)
MTG/ITG	27(8)	6(4)	5(4)	27(10)	5(1)	3(1)
Total PTL	**73 (19)**	**40 (16)**	**85 (20)**	**87 (21)**	**18 (8)**	**84 (18)**
antPHG	0(0)	7(6)	1(1)	0(0)	6(4)	0(0)
antCOS	48(23)	17(10)	26(17)	41(16)	36(18)	31(14)
antFG	8(5)	2(1)	7(5)	7(3)	2(1)	16(6)
antOTS	43(20)	10(6)	23(12)	54(21)	6(3)	17(7)
antMTG/ITG	22(10)	4(4)	0(0)	63(16)	1(1)	2(1)
Total ATL	**121 (32)**	**40 (20)**	**57 (22)**	**165 (29)**	**51 (20)**	**66 (19)**

left hemispheres ($prop_{diff}$ = (82/1682) − (100/1906) = −0.37%, 95% HDI = [−1.8, 1.09]). Finally, there was a larger proportion of face than house contacts in the occipital lobe (OCC) ($prop_{diff}$ = (91/381) − (33/381) = 15.22%, 95% HDI = [10.04, 20.28]), PTL ($prop_{diff}$ = (160/660) − (58/660) = 15.45%, 95% HDI = [11.51, 19.36]), and the ATL ($prop_{diff}$ = (286/2547) − (91/2547) = 7.65%, 95% HDI = [6.24, 9.08]).

To visualize and quantify the proportions of face and house contacts at a group level, local proportions were computed and projected on the cortical surface (Fig. 4A). Consistent with previous work (e.g., Spiridon et al. 2006; Kadipasaoglu et al. 2016), we observed a medio-lateral spatial dissociation between house- and face-selective contacts. The lateral regions of the VOTC contained the largest proportion of face contacts, while the medial regions contained the largest proportion of house contacts (Fig. 4A). This was confirmed statistically by comparing the percentage of house and face contacts along the X Talairach axis (12 equally spaced bins with size 6 mm), which was computed separately for each contact type by dividing the number of contacts in each bin by the total number of contacts for that specific contact type across all bins and converting to percentage (Fig. 5A; each curve sums to 100). This showed that the center of mass for house contacts ($mean_{talx}$ = 28.39 mm) was more medial than that of face contacts ($mean_{talx}$ = 38.79 mm; $mean_{diff}$ = 10.40 mm, 95% HDI = [8.17, 12.61]; Fig. 5A).

Next, we compared the relative proportion of face and house contacts within anatomical regions (e.g., latFG: face or house contacts/total of face and house contacts). A larger proportion of face than house contacts was observed in the IOG ($prop_{diff}$ = (52/57) − (5/57) = 82.46%, 95% HDI = [67.64, 89.16]), latFG ($prop_{diff}$ = (77/89) − (12/89) = 73.03%, 95% HDI = [60.58, 80.81]), MTG/ITG ($prop_{diff}$ = (54/65) − (11/65) = 66.15%, 95% HDI = [50.35, 76.13]), antFG ($prop_{diff}$ = (15/19) − (4/19) = 57.90%, 95% HDI = [25.09, 75.18]), antCOS ($prop_{diff}$ = (89/142) − (53/142) = 25.35%, 95% HDI = [13.64, 35.93]), antOTS ($prop_{diff}$ = (97/113) − (16/113) = 71.68%, 95% HDI = [60.70, 78.94]), and antMTG/ITG ($prop_{diff}$ = (85/90) − (5/90) = 88.89%, 95% HDI = [79.01, 93.13]; Fig. 6A). In contrast, a larger proportion of house than face contacts were observed in the PHG ($prop_{diff}$ = (0/6) − (6/6) = −100%, 95% HDI = [−96.64, −37.69]) and the antPHG ($prop_{diff}$ = (0/13) − (13/13) = −100%, 95% HDI = [−98.27, −65.03]). Finally, an equal proportion of face and house contacts was observed in the ventromedial occipital (VMO) ($prop_{diff}$ = (39/67) − (28/67) = 16.42%, 95% HDI = [−0.6, 32.01]) and the medFG ($prop_{diff}$ = (29/58) − (29/58) = 0%, 95% HDI = [−17.66, 17.67]). As illustrated in Figure 6A, there was also a medial to lateral organization within OCC, PTL, and ATL, as indicated by a decrease (or increase) in the proportion of house (or face) contacts moving from medial to lateral regions (logistic regression, where b reflects a change in the odds of significant contacts moving from medial to lateral regions [negative reflects a decrease and increase in house and face contacts, respectively]: OCC: b = −2.1, 95% HDI = [−3.26, −1.09]; PTL: b = −1.11, 95% HDI = [−1.55, −0.69]; ATL: b = −0.85, 95% HDI = [−1.1, −0.63]). Thus, in terms of proportions, house and face contacts were organized across medial and lateral regions, respectively, and were found in both posterior and anterior parts of the VOTC. The anterior parts largely followed the patterns of the more posterior regions of the VOTC.

We next quantified the selective response amplitudes recorded in face and house contacts. For each contact, we summed the baseline-subtracted amplitudes over harmonics of the 1.2 Hz face/house-selective response (from the 1st until the 14th, i.e., 1.2 Hz until 16.8 Hz, excluding the 5th and 10th harmonics, i.e., 6 and 12 Hz that coincided with the base frequency). Overall, the mean face-selective amplitude in face contacts was larger than the mean house-selective amplitude in house-selective contacts ($mean_{diff}$ = 20.60–15.56 = 5.04 μV, 95% HDI = [2.62, 7.48]). Moreover, for both faces and houses, there was a higher selective amplitude in the right than the left hemisphere (faces: $mean_{diff}$ = 22.27–18.24 = 4.03 μV, 95% HDI = [0.48, 7.58]; houses: $mean_{diff}$ = 17.49–13.97 = 3.52 μV, 95% HDI = [0.35, 6.66]). These observations are consistent with recordings on the scalp (Jacques et al. 2016a).

To visualize and quantify the selective amplitudes of face and house contacts at a finer spatial scale and group level, local average amplitudes were computed and projected on the cortical surface (Fig. 4B). Amplitudes also showed a medio-lateral dissociation between house- and face-selective contacts (Fig. 4B). This was confirmed statistically by first computing the mean selective response amplitude within each X Talairach bin (12 equally spaced bins with size of 6 mm) separately for each contact type (Fig. 5B). Using the amplitude, for each contact type, we generated a distribution of Talairach coordinates proportional to the mean selective amplitude in each bin.

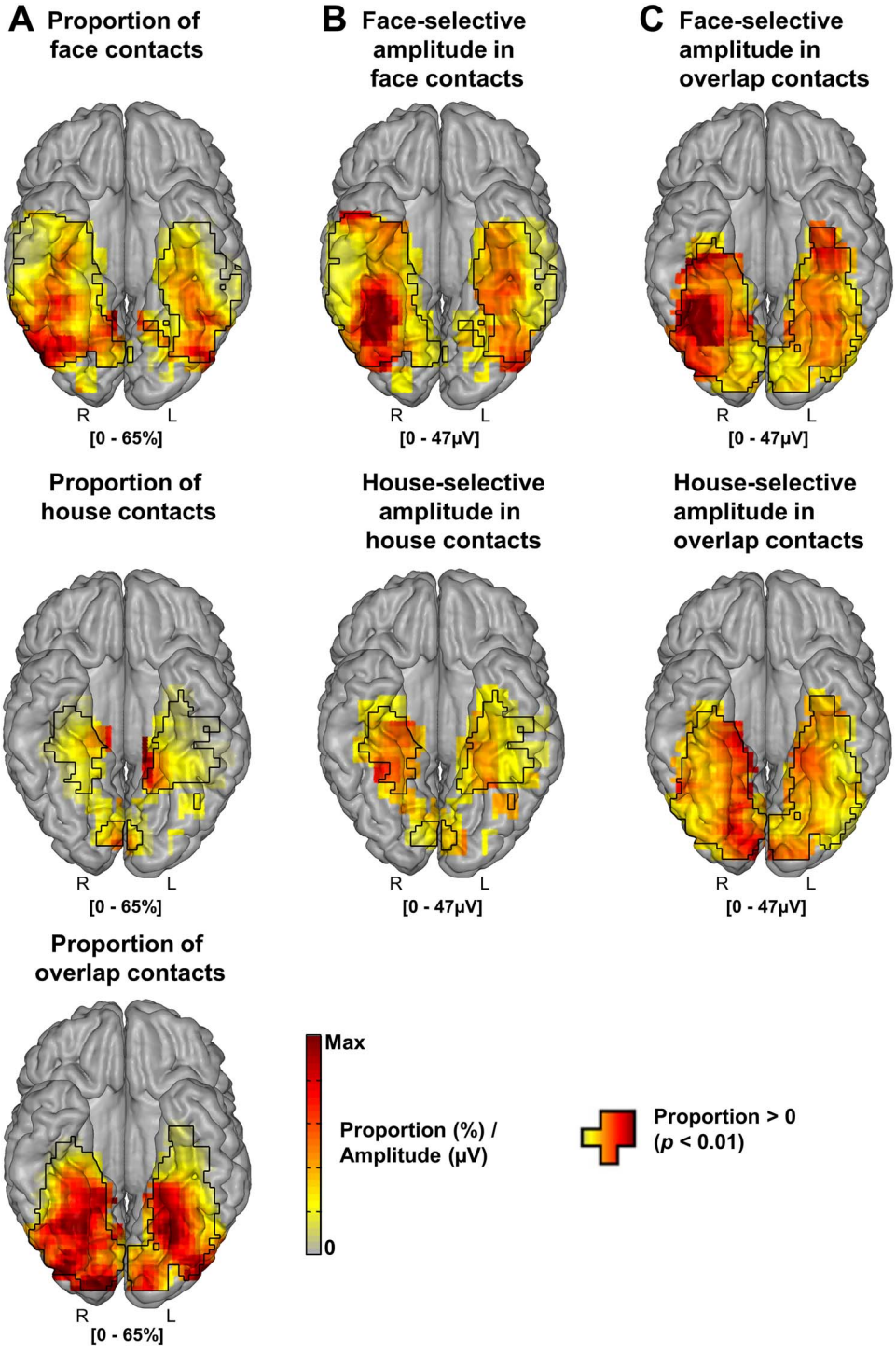

Figure 4. Proportion and amplitude maps. (*A*) Maps of the local proportion of selective contacts relative to recorded contacts across VOTC for each contact type (face, house, overlap), displayed on the cortical surface. (*B*) Maps of the local mean selective response amplitudes for face and house contacts. (*C*) Maps of the local mean face- and house-selective response amplitudes in overlap contacts. Local proportions and amplitudes were computed in 15 × 15 voxels (for *x*- and *y*-dimensions, respectively) using contacts collapsed over the Z dimension (inferior–superior) for better visualization. For the sake of replicability, only voxels containing significant responses from at least two individual brains were considered. Black contours outline proportions and amplitude significantly above zero. The letters below each hemisphere (R, L) refers to the hemispheric side.

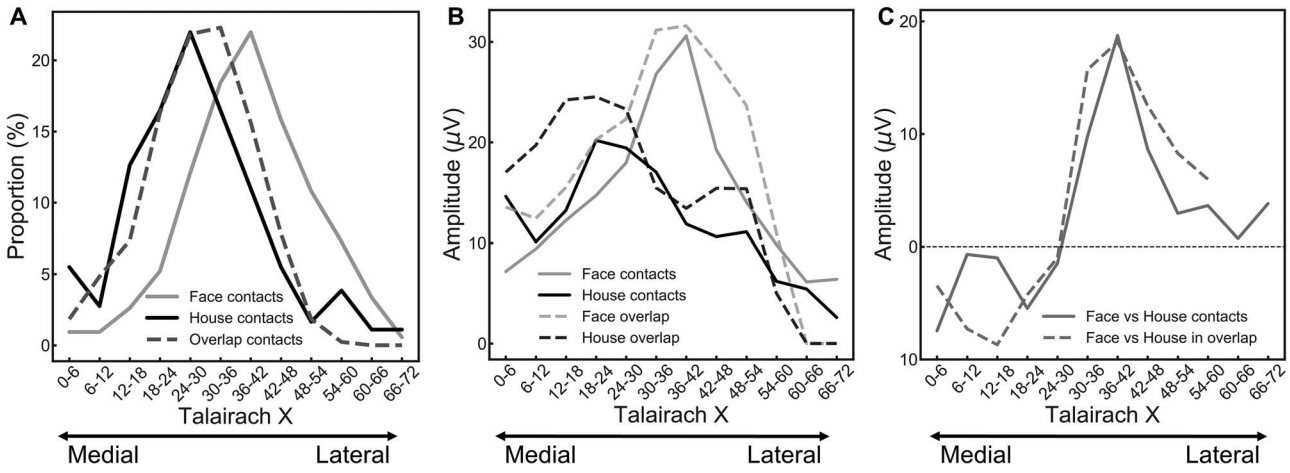

Figure 5. Medio-lateral organization to faces and houses across 6 equally spaced bins (width = 6 mm) along the Talairach coordinates. (*A*) Percentage of contacts as a function of Talairach coordinates and contact type (hemispheres collapsed). The percentages were normalized by dividing the number of contacts in each bin by the total contacts across all bins separately for each contact type, before converting to percentage (each curve sums to 100). (*B*) Average selective response amplitudes to faces and houses as a function of X Talairach in face and house contacts (solid lines) and overlap contacts (dashed lines). (*C*) Face and house amplitude bias in face and house contacts (solid line) and overlap contacts (dashed line). Bias was computed by subtracting the average house-selective from average face-selective amplitude within each bin. Thus, amplitudes below and above 0 indicate house and face amplitude bias, respectively.

Specifically, for each X Talairach bin, we generated a number of data points (with coordinates matching the center of the X Talairach bin) that was directly proportional to the mean selective amplitudes in that bin (e.g., for amplitude = 2 we generated 2 coordinate data points; for amplitude = 4 we generated 4 coordinate data points; and so on). In the resulting distribution of X Talairach coordinates across bins, the mode reflects the X Talairach coordinate with the highest amplitudes (unlike the mode for the count data, which reflects the X Talairach coordinate with the highest density of contacts). Direct statistical comparison of the house- and face-scaled coordinate data revealed that the house-selective amplitudes centered more medially ($mean_{talx}$ = 29.66 mm) than did the face-selective amplitudes ($mean_{talx}$ = 35.14 mm, $mean_{diff}$ = 5.48, 95% HDI = [1.69, 9.27]; Fig. 5B). This medio-lateral dissociation was also found in individual participants showing face- and house-selective responses in the same anatomical regions (higher face-selective responses in lateral regions and higher house-selective responses in medial regions, Supplementary Fig. 2).

Next, we directly compared face and house amplitudes within anatomical regions. Maximum face-selective response amplitudes for face contacts were recorded in the latFG (Fig. 6B), where, consistently with Jonas et al. (2016), the response was larger in the right than the left hemisphere ($mean_{diff}$ = 36.5 μV, 95% HDI = [19.77, 53.26], see Fig. 4B top). This difference was not found in proportion of face contacts (Fig. 4A top), as analyzed by statistically comparing the proportion in right and left latFG voxels ($P < 0.01$, permutation test). Direct comparisons between face- and house-selective response amplitudes within each anatomical region (hemisphere collapsed, Fig. 6B) showed that faces evoked larger response in the IOG ($mean_{diff}$ = 6.73 μV, 95% HDI = [1.64, 11.76]), latFG ($mean_{diff}$ = 26.22 μV, 95% HDI = [10.51, 41.95]), antOTS ($mean_{diff}$ = 12.37 μV, 95% HDI = [7.63, 17.1]), and antMTG/ITG ($mean_{diff}$ = 5.53 μV, 95% HDI = [0.85, 10.14]). In contrast, houses evoked larger amplitudes in the PHG ($mean_{diff}$ = −17.91 μV, 95% HDI = [−21.72, −14.1]) and antPHG ($mean_{diff}$ = −14.17 μV, 95% HDI = [9.03, 19.24]), since there were no face contacts in these regions (thus relative to 0). Finally, houses and faces evoked equal amplitudes in the VMO ($mean_{diff}$ = 2.01 μV, 95% HDI = [−2.58, 6.59]), medFG ($mean_{diff}$ = −4.15 μV, 95% HDI = [−8.99, 0.69]), MTG/ITG ($mean_{diff}$ = 2.48 μV, 95% HDI = [−1.05, 6.0]), antCOS ($mean_{diff}$ = −1.65 μV, 95% HDI = [−5.53, 2.24]), and antFG ($mean_{diff}$ = 6.92 μV, 95% HDI = [−13.52, 26.89]). Overall, the amplitude patterns were largely consistent with the patterns observed in the proportion data.

Spatial Dissociation Between Face and House Contacts is Maintained in the ATL

We examined whether the well-known face/house spatial dissociations extend into the ATL, largely affected by a magnetic artifact in fMRI. Figure 7A shows the distribution of face and house contacts in the ATL as a function of X Talairach (medio-lateral) and Y Talairach (postero-anterior) axes, where the darkness of the lines indicate the density of the respective contacts (face and house densities are relative to itself). A medio-lateral dissociation was confirmed statistically in the ATL by comparing mean X Talairach coordinates for face and house contacts, which showed that the center of mass for house contacts ($mean_{talx}$ = 31.42 mm) was more medial than that of face contacts ($mean_{talx}$ = 40.34 mm; $mean_{diff}$ = 8.92 mm, 95% HDI = [6.36, 11.45]; Fig. 7A), which is in agreement with our proportion and amplitude analyses across ATL anatomical regions (see above). Moreover, a comparison of the mean Y Talairach (postero-anterior) coordinates for face and house contacts showed that the center of mass for house contacts ($mean_{taly}$ = −23.11 mm) was more posterior than that of face contacts ($mean_{taly}$ = −18.80 mm; $mean_{diff}$ = −4.31 mm, 95% HDI = [1.94, 6.67]; Fig. 7A).

Next, we examined the medio-lateral and postero-anterior dissociation between houses and faces in specific anatomical regions of the ATL. To do so, we combined the Talairach coordinates and the anatomical locations of face and house contacts in the ATL. We considered the *x*-coordinates in the different ATL anatomical regions to examine in which region the medio-lateral transition of the ATL is likely to occur (Fig. 7B). Only the antCOS, containing both numerous face and house contacts,

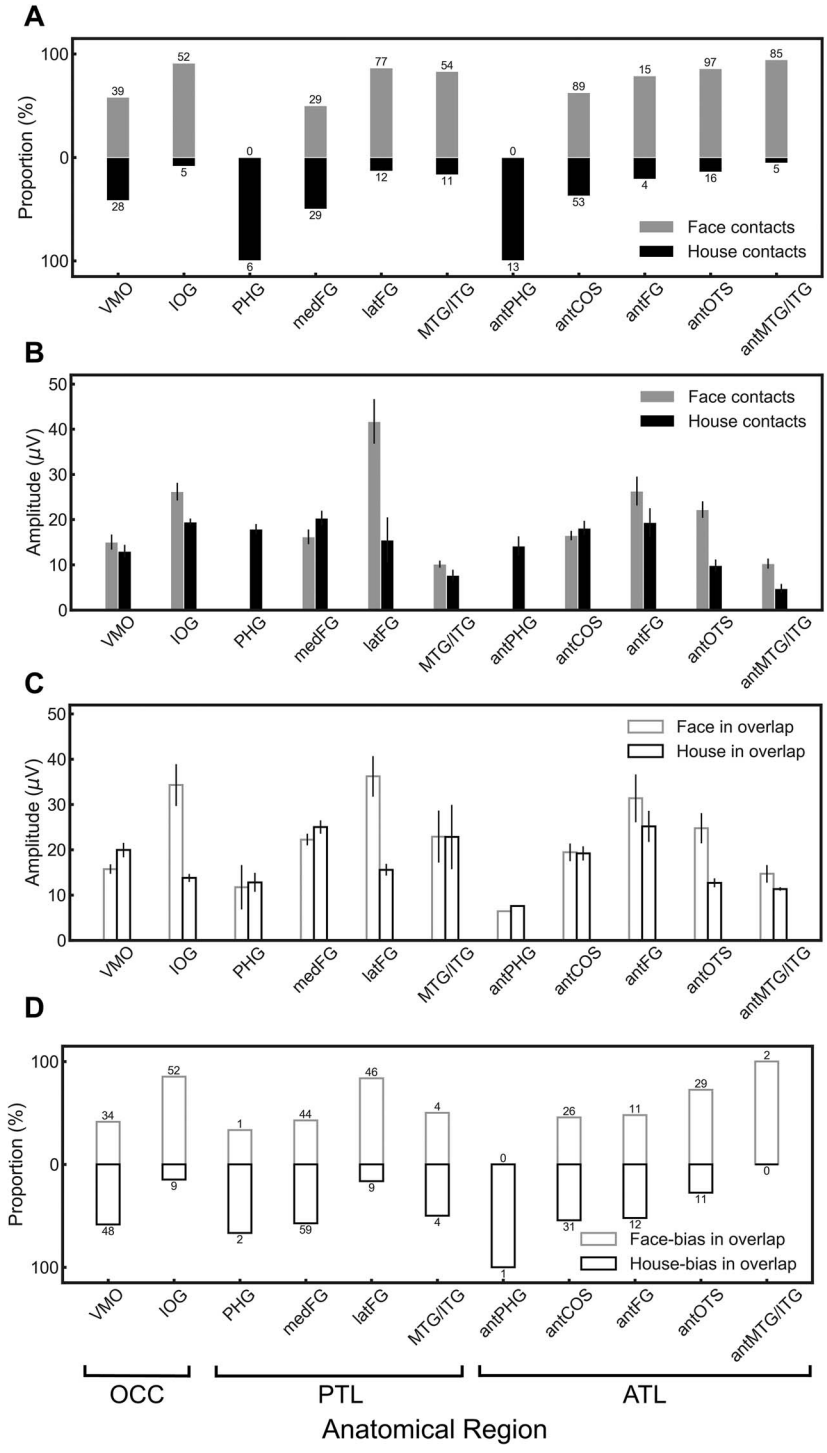

Figure 6. Quantification of proportions and selective amplitudes in each anatomical region (hemispheres collapsed). (*A*) Relative percentage of face and house contacts were computed in each region as the number of face (or house) contact out of the total of face and house contacts in that region. (*B*) Selective response amplitudes were quantified in each region as the average of the selective response amplitudes across contacts, separately for face and house contacts. (*C*) Selective response amplitudes were quantified in each region as the average of the response amplitudes across contacts, separately for face- and house-selective response amplitudes in overlap contacts. (*D*) Relative proportion of face- and house-biased overlap contacts were computed in each region as the number of face (or house) biased contact out of the total of overlap contacts in that region. Face and house bias were computed in each overlap contact by subtracting the house- from the face-selective response amplitudes. An overlap contact with positive value was categorized as a face-biased overlap contact, whereas one with a negative value was categorized as a house-biased overlap contact. Error bars represent SEMs. The number of significant contacts in each region is indicated by the number on top of each proportion bar.

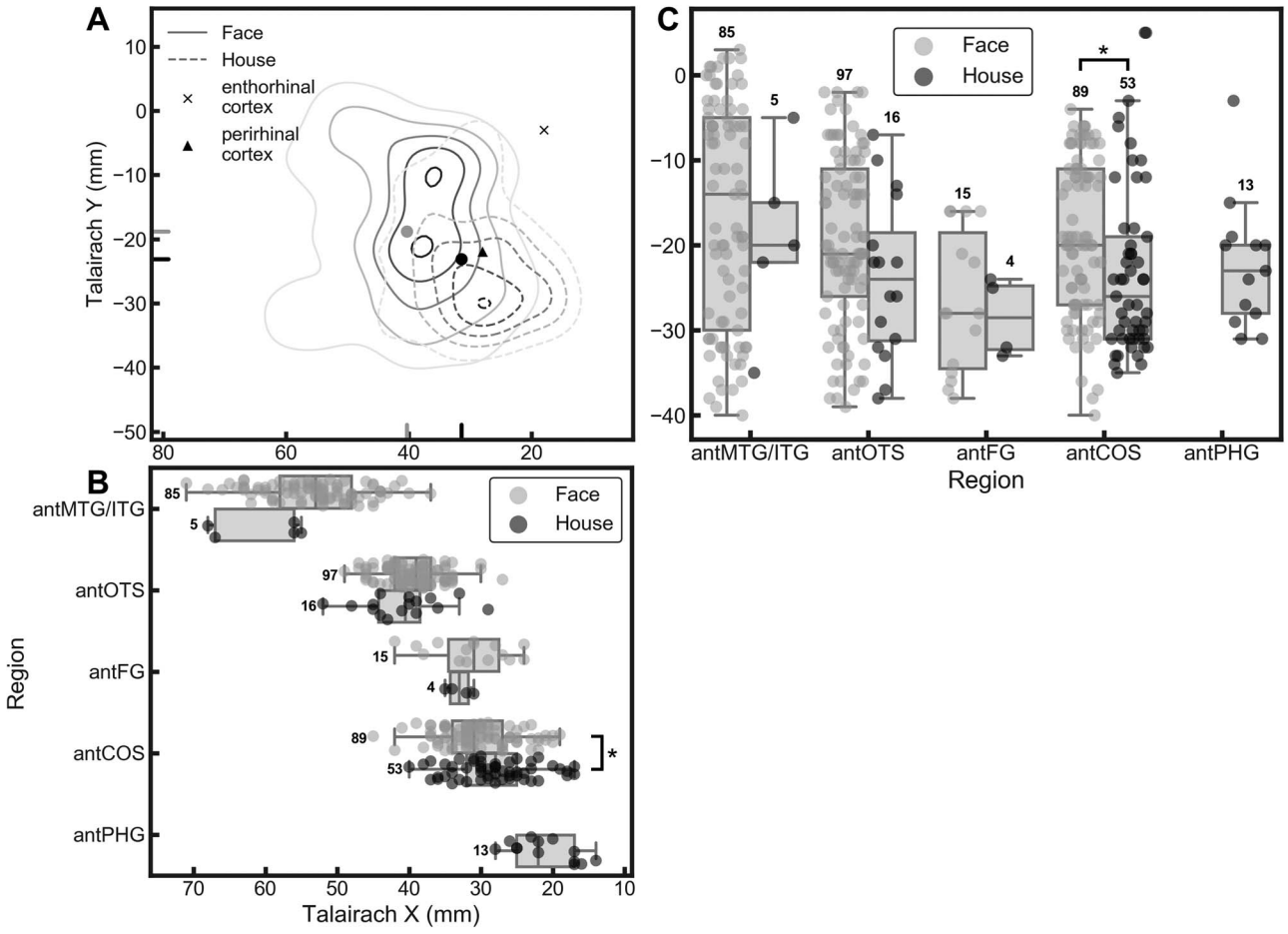

Figure 7. Spatial dissociation between face and house contacts in the ATL. (*A*) Contour plot showing distribution of face and house contacts along the medio-lateral (*x*-axis) and postero-lateral axis (*y*-axis). Each distribution is computed relative to itself and darker contours indicate larger density of contacts. The central mass for each distribution is plotted as a solid dot within the contour plot and as a vertical line on the *x*- and *y*-axis (light gray: face; dark gray: house). The central mass coordinates of the entorhinal and perirhinal cortices extracted from the Brede Database are plotted within the figure. (*B*) *x*-coordinates of face and house contacts in the different ATL anatomical regions. The boxplot displays three quartiles (Q1, median, Q2), and the whiskers extend to points that lie within 1.5 interquartile range (IQRs) of the lower and upper quartile. ∗Indicates that the 95% HDI did not include 0. The number next to the error bar indicates the number of contacts. Note that darker of contacts (relative to legend) indicate larger density along the X Talairach. (*C*) *y*-coordinates of face and house contacts in the different ATL anatomical regions. Same convention as for panel B.

showed a medio-lateral dissociation, with the central mass of houses ($mean_{talx} = 28.26$ mm) being more medial than the central mass of faces ($mean_{talx} = 30.47$ mm; $mean_{diff} = 2.21$ mm, 95% HDI = [0.3, 4.13]; Fig. 7A). No other regions in the ATL contained a medio-lateral dissociation (all 95% HDIs included 0). This shows that the antCOS is an anatomical landmark between face- and house-selective regions in the ATL. Second, we examined postero-anterior dissociations within regions of the ATL (*y*-coordinates of face and house contacts in the different ATL anatomical regions, Fig. 7C). Again, a dissociation was found only in the antCOS, where the central mass of houses ($mean_{taly} = -23.02$ mm) was more posterior than that of face contacts ($mean_{taly} = -19.03$ mm; $mean_{diff} = 3.99$ mm, 95% HDI = [0.56, 7.38]; Fig. 7A). This dissociation was not found in any other regions (all 95% HDIs included 0). The antPHG, containing only house contacts, did not show very anterior house contacts (except one, Fig. 7C). As it is shown in Fig. 7C, while face-selective contacts are distributed all along the postero-anterior axis of the antMTG/ITG, antOTS, antFG, and antCOS, the house contacts are clustered in the posterior parts of the (medial) antCOS and the antPHG (Fig. 7A,C).

Dissociations Between Face and House Amplitudes in Overlap Contacts

A large portion of contacts responded to both faces and houses (overlap contacts, Fig. 3). They were equally distributed in both hemispheres ($prop_{diff} = (213/1906) - (222/1682) = -2.02\%$, 95% HDI = [−0.11 4.17]), and local proportion maps showed a wide distribution across OCC and PTL (without a clear medial or lateral bias) while density was low in the ATL (Fig. 4A). We first characterize the spatial location of overlap contacts along the X Talairach axis (medio-lateral). The statistical comparison of the normalized percentages of overlap contacts with that of faces and houses (the contact count in each bin divided by the sum within contact type and converted to percentage) showed that the central mass of overlap contacts ($mean_{talx} = 28.96$ mm) differed from that of face ($mean_{diff} = 9.83$ mm; HDI = [8.43, 11.26]),

but not house contacts ($mean_{diff} = -0.57$ mm; HDI = [−2.78, 1.62]; Fig. 5A).

What do the overlap contacts represent? Since these contacts are selective to both faces and houses, they could reflect domain-general responses that originate in mechanisms that discriminate both face and house stimuli (or a repeating category among less frequently repeated categories). According to this account, overlap contacts should have similar response profiles to both face and house stimuli. Alternatively, the overlap contacts could reflect dissociated face- and house-selective responses originating from distinct neural sources close to the same contact. In this latter scenario, one would expect faces and houses to evoke dissociated responses (e.g., spatially dissociated maximum amplitudes; noncorrelated amplitudes). To disentangle these accounts, we quantified and compared in each overlap contact the selective responses evoked separately by faces and houses (sum over harmonics, as for face and house contacts and computed local amplitude maps).

We first examined their amplitudes along the X Talairach axis. Notably, the house and face amplitude profiles of the overlap contacts mirrored the profiles measured for house and face contacts in two ways. First, following the same approach as with house and face contacts (generating the x-coordinates proportional to its mean amplitude, see above) revealed that the house-selective amplitudes centered more medially ($mean_{talx} = 25.95$ mm) than did the face-selective amplitudes ($mean_{talx} = 32.31$ mm, $mean_{diff} = 6.36$ mm, 95% HDI = [3.29, 9.50]; Fig. 5B). Second, within each bin, we subtracted the mean amplitude between house and face responses (dashed line) within the overlap contacts, as well as between house and face contacts (solid line) (Fig. 5C). There was a strong correlation between the bias reflected by the solid and dashed lines ($r = 0.87$, $n = 12$, 95% HDI = [0.48, 0.99]; X Talairach bins with no data [i.e., 60–66, 66–72 for overlap] was set to 0 to indicate neither face nor house bias). For both analyses, we found similar results with house-biased amplitudes centered more medially and face-biased amplitudes more laterally. Such similarity is consistent with the claim that the house and face sources measured by the overlap contacts originate medially and laterally, respectively.

Second, we computed maps separately for face- and house-selective response amplitudes in overlap contacts (Fig. 4C). At local levels, faces evoked maximum amplitude in the same lateral regions (especially the right IOG and right latFG) as in face contacts, whereas houses evoked maximum amplitude in some of the same medial regions as in house contacts (Fig. 4C). Direct comparisons between face and house response amplitudes within each anatomical region showed that faces evoked larger responses than houses in the IOG ($mean_{diff} = 20.51$ µV, 95% HDI = [11.03, 30.03]), latFG ($mean_{diff} = 20.62$ µV, 95% HDI = [11.73, 29.55]), and antOTS ($mean_{diff} = 12.07$ µV, 95% HDI = [4.65, 19.47]; Fig. 6C). In contrast, houses evoked larger response amplitudes than faces in the VMO ($mean_{diff} = -4.21$ µV, 95% HDI = [−7.59, −0.82]). Equal amplitudes were found in the medFG ($mean_{diff} = -2.74$ µV, 95% HDI = [−5.87, 0.39]), MTG/ITG ($mean_{diff} = 0.09$ µV, 95% HDI = [−11.84, 12.13]), antCOS ($mean_{diff} = 0.22$ µV, 95% HDI = [−3.78, 4.24]), and antFG ($mean_{diff} = 6.20$ µV, 95% HDI = [−7.56, 19.97]). Finally, there were too few contacts to estimate the mean amplitudes in the PHG ($n = 3$), antPHG ($n = 1$), and antMTG/ITG ($n = 2$). Collectively, these patterns largely mirrored that of the face and house contacts (compare Fig. 4B,C; compare Fig. 6B,C).

Third, we computed the proportion of face-biased contacts (selective response amplitude face > house) and house-biased contacts (selective response amplitude house > face) among all overlap contacts across regions (Fig. 6D). We compared the relative proportion of face- and house-biased contacts within local regions (e.g., latFG: face- or house-biased contacts/total of overlap contacts). A larger proportion of face- than house-biased contacts was observed in the IOG ($prop_{diff} = (52/61) - (9/61) = 70.49\%$, 95% HDI = [54.62, 79.83]), latFG ($prop_{diff} = (46/55) - (9/55) = 67.27\%$, 95% HDI = [50.03, 77.63]), and antOTS ($prop_{diff} = (29/40) - (11/40) = 45\%$, 95% HDI = [22.91, 61.04]; Fig. 6D). In contrast, a larger proportion of house than face contacts were observed in the VMO ($prop_{diff} = (34/82) - (48/82) = -17.07\%$, 95% HDI = [−31.34, −1.67]) and medFG ($prop_{diff} = (44/103) - (59/103) = -14.56\%$, 95% HDI = [−27.53, −0.73]). An equal proportion of face and house contacts was observed in the MTG/ITG ($prop_{diff} = (4/8) - (4/8) = 0\%$, 95% HDI = [−41.32, 41.35]), antCOS ($prop_{diff} = (26/57) - (31/57) = -8.77\%$, 95% HDI = [−26.17, 9.43]), and antFG ($prop_{diff} = (11/23) - (12/23) = -4.35\%$, HDI = [−30.93, 23.36]). Finally, there were too few contacts to estimate the relative proportions in the PHG ($n = 3$), antPHG ($n = 1$), and antMTG/ITG ($n = 2$). Importantly, across regions, the proportions of face- and house-biased contacts correlated strongly with the respective proportions of face and house contacts (compare Fig. 6A,D; $r = 0.87$, $n = 11$, 95% HDI = [0.48, 0.99]).

Finally, we correlated face- and house-selective response amplitudes computed at the individual contact level. Across all overlap contacts, the face- and house-selective response amplitudes (1.2 Hz and harmonics) correlated weakly ($r = 0.16$, $n = 435$, 95% HDI = [0.07, 0.25]; Fig. 8A), despite that the exact same contacts showed an almost perfect correlation to the base responses (i.e., 6 Hz and harmonics; $r = 0.98$, $n = 435$, 95% HDI = [0.96, 1], Fig. 8C). This suggests that while the base response was largely generated by the same neural populations, the selective response at the same contacts was generated largely by dissociated neural populations. Even after removing face- and house-selective amplitudes higher than z = 3 (Z-score computed separately, 18 "outlier" contacts removed), the correlation of category-selective response remained weak (i.e., $r = 0.26$, $n = 417$, 95% HDI = [0.17, 0.36], Fig. 8B) and substantially lower than the correlation for base responses.

Taken together, these results showed that overlap contacts reflected to a large extent dissociated face- and house-selective responses that are both captured by a common contact, typically located between face- and house-selective regions.

Category-Exclusive Responses

A previous SEEG-FPVS study (Jonas et al. 2016) found contacts in the ATL that exhibited exclusive responses to faces, that is, significant face responses without any significant general visual response to nonface objects at the base frequency. However, due to their anterior location, it could be speculated that these responses (rather than being face-exclusive) reflected a domain-general response to a predictable event (oddball faces) among nonpredictable events (base objects). If the latter account is correct, then the face-exclusive contacts should also be selective to houses (i.e., overlap contacts with similar selective responses for both categories). To detect exclusive contacts in our sample, we assessed the significance of the base response (6 Hz and harmonics) on each selective contacts (face, house, overlap)

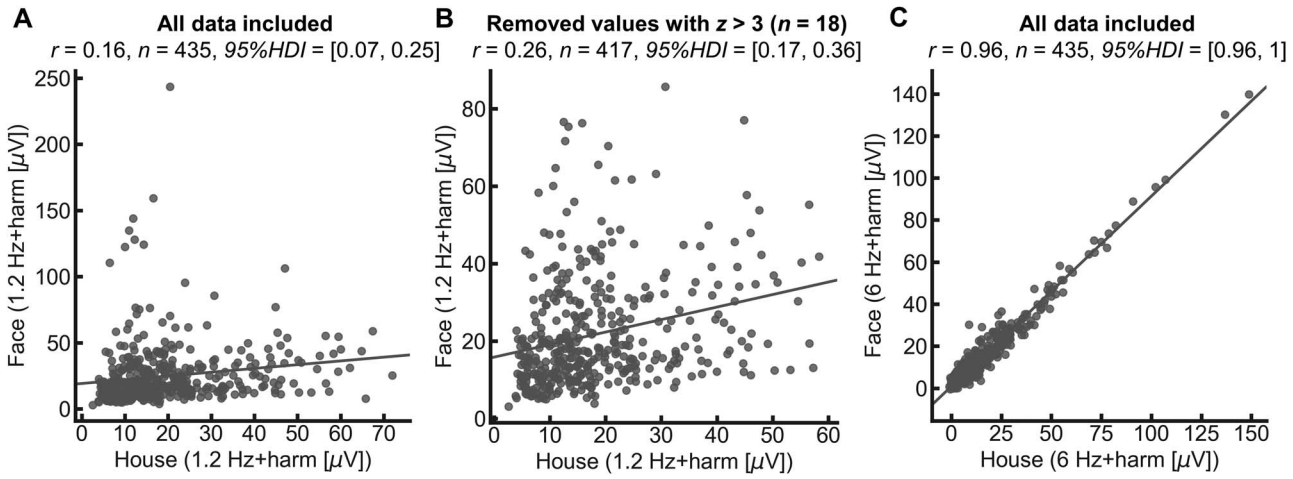

Figure 8. Amplitude correlations with overlap contacts. (*A*) Correlation between the face (*y*-axis)- and house (*x*-axis)-selective response amplitudes within the overlap contacts. (*B*) Correlation between the face (*y*-axis)- and house (*x*-axis)-selective response amplitudes within the overlap contacts, after removing contacts with a selective amplitude higher than z = 3 (18 contacts removed). (*C*) Correlation between the base response amplitudes in the face sequences (*y*-axis) and the base response amplitudes in the house sequences (*x*-axis) within the overlap contacts.

using the same method as for the discrimination responses (epoching the FFT spectrum into segments centered at the base frequency and harmonics, from the first until the fourth, i.e., 6 Hz until 24 Hz, summing the four FFT segments, transforming the summed FFT spectrum into a Z-score). A selective contact was considered as exclusive if the base response was nonsignificant in both the face and the house conditions (Z-score < 3.1).

In total, we found 225 exclusive contacts (19.50% of significant contacts; 6.34% of total recorded; 59 unique patients). Consistent with Jonas et al. (2016), most of these contacts were located in the ATL (160/225 = 71.11%). We found exclusive contacts specific to one category (face-exclusive = 160; house-exclusive = 41) as well as exclusive contacts responsive to both categories (overlap-exclusive = 24). An example of each contact is shown in Figure 9. Most of the exclusive contacts were specific to one category ([160 + 41]/225 = 89.33%). Out of the total number of exclusive contacts, there was a much larger proportion of face-exclusive than house-exclusive contacts ($prop_{diff}$ = (160/225) − (41/225) = 52.89%, 95% HDI = [44.44, 59.98]) and a larger proportion of house-exclusive than overlap-exclusive contacts ($prop_{diff}$ = (41/225) − (24/225) = 7.56%, 95% HDI = [1.05, 14.01]). Out of the number of total selective contacts within each contact type (e.g., face, house, and overlap contact), there was no difference in the proportion of face- and house-exclusive contacts ($prop_{diff}$ = (160/537) − (41/182) = 7.27%, 95% HDI = [−0.31, 14.03]). However, the proportions of face- and house-exclusive contacts were larger than the proportion of overlap contacts (face vs. overlap: $prop_{diff}$ = (160/537) − (24/435) = 24.28%, 95% HDI = [19.74, 28.56]; house vs. overlap: $prop_{diff}$ = (41/182) − (24/435) = 17.01%, 95% HDI = [10.94, 23.74]). The spatial distribution of each exclusive contact type (face, house, overlap) at group level is shown in Figure 9.

Thus, the finding of mostly category-exclusive contacts contradicts the claim that the exclusive contacts reflect domain-general responses to a predictable event, but rather suggest a change in response profile of category-specific (e.g., face, house) processes toward anterior regions.

Discussion

The Functional Specificity of the FPVS-SEEG Approach

Testing 28 patients with the same paradigm as used here but with faces as the only category of interest, Jonas et al. (2016) reported clusters of high-amplitude face-selective contacts with a peak in the right latFG, supporting the dominant role of this region in face categorization as identified previously with fMRI (e.g., Kanwisher et al. 1997). They also reported a wide distribution of face-selective responses across the VOTC, including the underexplored ATL. These findings are largely replicated here with a much larger group of patients (N = 75), providing a much denser sampling of the VOTC (3588 contacts in the gray matter in the present study compared with 1678 contacts in Jonas et al. (2016)). Most importantly, the present study goes well beyond previous evidence by showing that the wide distribution of face-selective responses in the human VOTC does not reflect a lack of specificity of the FPVS-SEEG approach (i.e., responses to any highly familiar category appearing periodically in a continuous stream of various nonface objects and/or responses from very distant sources), for several reasons. First, although face- and house-selective responses are found in the VOTC, they elicit largely spatially distinct VOTC maps, both in amplitude and proportion of significant contacts, in lateral regions for faces and in medial regions for houses. This observation is consistent with observations of fMRI studies that have directly contrasted the two categories (e.g., Spiridon et al. 2006, Tootell et al. 2008, Weiner and Grill-Spector 2010, Nasr et al. 2011, Gomez et al. 2015) but also with the findings of an intracranial (electrocorticography [ECoG]) study focusing on more restricted regions and with smaller sample tested (Kadipasaoglu et al. 2016). Second, most (62.4%) of the significant contacts were selective to one category only, either faces or houses. Third, the wide distribution of face-selective responses was still present when considering only the contacts selective to faces and not to houses. Fourth, there was a higher proportion of significant face than house contacts and a higher amplitude recorded on face contacts (consistent with observations made on the scalp on neurotypical observers tested with the same

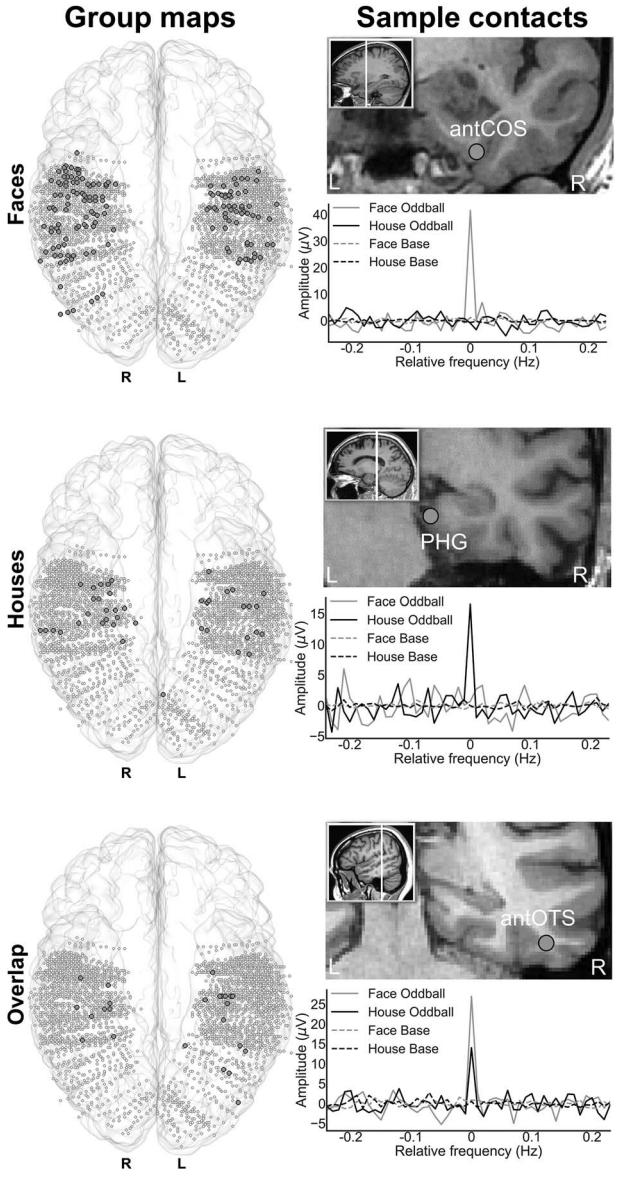

Figure 9. Classification and distribution of three types of exclusive discrimination contacts. Left: Maps of all 3588 VOTC recording contacts across the 75 individual brains displayed in the Talairach space using a transparent reconstructed cortical surface of the Colin27 brain. Each circle represents a single contact. Dark-gray-filled circles correspond to selective contacts. These were contacts that showed a significant selective response (to faces only, houses only or both), but no significant response to other objects at the base frequency. Light-gray-filled circles correspond to contacts on which no exclusive responses were recorded. Right: Examples of summed FFT spectra showing both selective and base responses for each contact type (three individual contacts in three different participants). Top: face-exclusive contact selective to faces only with no base responses; middle: house-exclusive contact selective to houses only with no base responses; bottom: overlap-exclusive contact selective to both faces and houses with no base responses. Their anatomical location is illustrated in the respective coronal MRI slices.

approach, Jacques et al. 2016a), as well as a specifically higher proportion in the right than in the left hemisphere only for face contacts. This last result is in agreement with the long-standing observation of a right hemispheric dominance for faces (Meadows 1974; see Rossion 2014). Altogether, these observations show that selective responses recorded with the SEEG-FPVS approach are specific to the tested category and not merely due or related to the periodic repetition of any category in a continuous stream of various nonface objects (Quek and Rossion 2017).

Spatial Dissociation Between Face- and House-Selective Responses Extends to the ATL

Previous fMRI and intracranial EEG studies comparing face- and house-selective responses found a medio-lateral dissociation in the posterior VOTC only (fMRI: Spiridon et al. 2006; Nasr et al. 2011; intracranial EEG: Jacques et al. 2016b; Kadipasaoglu et al. 2016). A recent fMRI study showed that place-selective voxels in the medial VOTC are not found anteriorly to the anterior tip of the midfusiform sulcus, that is, not anteriorly to the latFG and medFG (Weiner et al. 2018). Here we found that this spatial dissociation extends to the ATL, mostly because house selectivity extends into the antPHG and antCOS (at least in their posterior parts, as indicated by the group maps; Figs 3 and 4). By combining the individual anatomy and the Talairach coordinates, we found a medio-lateral dissociation within the antCOS, showing that this sulcus is an anatomical landmark between face- and house-selective regions in the ATL (houses, antPHG and medial part of the antCOS; faces, lateral part of the antCOS, antOTS, antFG, antMTG/ITG). Within the antCOS, we also found a postero-lateral dissociation, with house contacts being clustered in the posterior part of the antCOS. Moreover, in the antPHG, containing only house contacts, these contacts are not located very anteriorly. These observations are probably explained by the fact that the anterior parts of the (medial) antCOS and antPHG are known to be the location of the perirhinal cortex and entorhinal cortex, respectively (Van Hoesen 1995; Van Hoesen et al. 2000), both belonging to the medial temporal lobe (MTL) memory system. This suggests that, along the postero-anterior axis of the (medial) antCOS and antPHG, these are a transition from a high-level visual area (house-selective) to the MTL memory system involved in episodic memory. These results also help clarifying the relationship between the face-selective responses found in the antCOS belonging to the cortical face network (the present data, Tsao et al. 2008; Rajimehr et al. 2009; Rossion et al. 2012; Tanji et al. 2012; Jonas et al. 2016) and the perirhinal cortex involved in episodic memory (e.g., see Collins and Olson 2014). The present data suggest that these regions are spatially segregated: while the face-selective responses are located all along the lateral part of the antCOS, the perirhinal cortex is restricted to the medial and anterior part of the antCOS.

This spatial dissociation in the ATL has not been found in fMRI studies, probably because the signal dropout affects both face- and house-selective responses in this region (e.g., Spiridon et al. 2006; Nasr et al. 2011). Intracranial EEG studies using ECoG with a high SNR in the ATL also failed to find such dissociation in anterior regions of the temporal lobe (Jacques et al. 2016b; Kadipasaoglu et al. 2016). For example, despite a wide sampling across the VOTC, Kadipasaoglu et al. (2016) did not report category-selective responses anteriorly to the anterior tip of the middle fusiform sulcus, in the ATL (for faces or houses). This could be because ECoG electrodes as used by Kadipasaoglu et al. (2016) are restricted to the gyral surface and may therefore be less sensitive to ATL category-selective responses located mainly in sulci, as captured here with the SEEG approach.

The Overlap Between Face-Selective and House-Selective Responses

In the current FPVS paradigm, responses to face stimulation measured at 1.2 Hz and harmonics are "face-selective" responses, that is, responses that reflect a contrast with nonface objects presented in the FPVS sequence. This contrast response is generalized across widely variable exemplars, providing a generic face categorization response in the human brain (see Rossion et al. 2018). However, interestingly, a proportion of contacts that measured a selective response to faces also recorded significant selective responses to houses. These responses could either 1) reflect domain-general processes that originate in populations of neurons that discriminate any repeated category among other categories or 2) reflect functionally distinct populations of neurons whose responses are measured at the same recording contacts. Consistent with the latter account, the low correlation between the amplitude of face- and house-selective responses in the overlap contacts provides no evidence that these responses originate from the same domain-general underlying process. Moreover, the spatial dissociation between the response amplitudes to faces and houses in overlap contacts closely matched that of face and house contacts (Figs 4 and 5), providing further evidence that the overlap contacts reflect dissociated face- and house-selective responses.

In the case of dissociated face- and house-selective responses projecting to the same contact, two main scenarios could be considered. First, category selectivity could gradually decrease, so that adjacent category-selective populations of neurons could be partly intermingled (Spiridon et al. 2006; Kadipasaoglu et al. 2016). Second, face- and house-selective neurons could be located in spatially distinct but nearby anatomical regions, and some recording contacts may measure responses generated by both regions due to volume conduction of the electrical field (Buzsáki et al. 2012; Herreras 2016). Current fMRI findings on spatial organization of category selectivity in VOTC is compatible with both scenarios, with evidence for spatially separated face-selective and house-selective regions but with potentially graded selectivity along the medio-lateral axis (Spiridon et al. 2006; Tootell et al. 2008). It is important to note that some fMRI studies may have artificially increased the spatial dissociation between face- and house-selective regions since they directly contrasted faces and house stimuli (e.g., Tootell et al. 2008; Nasr et al. 2011). Further investigation will be needed to disentangle the different scenarios.

How local electrophysiological activities recorded with intracranial electrodes (using SEEG or ECoG) is a matter of debate (e.g., Yoshor et al. 2007; Zaveri et al. 2009; Wennberg 2010; Dubey and Ray 2019). This issue is not specific to the present FPVS approach and concerns intracranial EEG studies in general. Here, according to one of the scenarios outlined above, some responses could be related to volume conduction from distant source. For example, a recent ECoG study in the monkey visual cortex showed that the spatial spread was around 3 mm (Dubey and Ray 2019). However, despite this uncertainty, the FPVS-SEEG approach as used here is able to provide distinct and valid category-selective maps across the whole VOTC, even if different sources could project to the same electrode (Fig. 4). Moreover, it validates with a direct measure of neural activity the predominant face-selective activation in the right latFG found in human neuroimaging, the so-called fusiform face area (FFA), where the highest face-selective response amplitude was found. Further support that our approach allows measuring local neural sources comes from the observation that the sites where impairments of face perception and/or recognition are observed following intracerebral electrical stimulation are systematically the sites that record the largest FPVS face-selective response amplitudes among all the implanted electrodes (Jonas et al. 2014, 2018).

The Neural Basis of Face Categorization

Considering here only the contacts that showed a face-selective response without any house-selective response (46.6% of significant contacts), they were widely distributed across the VOTC, with the largest amplitude responses in the middle section of the right lateral FG as previously observed, that is, corresponding to the FFA in neuroimaging (Kanwisher et al. 1997), but also in the IOG and the ATL of the right hemisphere (Fig. 4). The wide distribution of face-selective responses refers to the numerous brain regions showing a high face-selective response amplitude and/or a high proportion of face-selective responses. These regions include the IOG, the latFG, the antFG, the antOTS, and the antCoS bilaterally, that is, a large a part of the human VOTC running all along the fusiform gyrus from the OCC to the ATL. These regions are thought to form a highly interconnected face-selective network (Gschwind et al. 2011; Pyles et al. 2013; Duchaine and Yovel 2015).

Nevertheless, it is important to stress that a wide distribution as found here or in previous large-scale studies (e.g., Allison et al. 1999 with ECoG) contrasts with the spatially separated clusters identified by fMRI studies (Rossion et al. 2018). Two hypotheses can be considered. On the one hand, the present approach may artificially increase the width of the distribution of face-selective responses. Our data visualization, showing maps with the superposition of all significant recording contacts across participants (Fig. 3), may enhance the impression of distributed responses (relative to fMRI studies showing maps averaged across participants). This impression is further increased by the large interindividual variability of the location of face-selective areas across individuals (e.g., Rossion et al. 2012; Zhen et al. 2015; Gao et al. 2018). To control for this bias, in the present study, we reported "proportion" maps of significant contacts (out of total recorded contacts), which were not reported previously (Jonas et al. 2016), highlighting the regions with the highest probability of face-selective responses. Moreover, as discussed above, there is a possibility that some overlap contacts in the present study may capture responses arising from distant source due to volume conduction of the electrical field. The combination of these two factors (data visualization and volume conduction) may explain discrepancies with fMRI findings and offer a potential explanation for rare (among nonsignificant) and weak face-selective responses in some regions (e.g., MTG/ITG, antMTG/ITG, medFG, i.e., regions lateral or medial to the fusiform gyrus) which are usually not disclosed in fMRI studies. On the other hand, fMRI may not be sensitive enough to record all face-selective responses of the VOTC. fMRI provides only a hemodynamic (indirect) measure of neural activity, and therefore smaller, scattered, face-selective responses in the VOTC may be entirely missed by fMRI studies that identify only sufficiently large clusters of activation near blood vessels. In contrast, our approach provides electrophysiological face-selective responses with a very high SNR (FPVS) on small electrodes implanted directly inside the gray matter (SEEG). Moreover, fMRI is affected by severe magnetic susceptibility artifacts that cause a strong

signal dropout in the ATL, so that our approach identified many more face-selective regions in the ATL (antCOS, antOTS, antFG, antMTG/ITG).

In the present study, we report intracranial maps both for amplitude and proportion of significant contacts in the VOTC for the first time (Fig. 4). We believe that both types of analyses are important and informative. First, both analyses showed largely overlapping results, thus reinforcing each other. Amplitude and proportion of face-selective responses were maximal in the IOG and all along the fusiform gyrus (latFG, the antFG, the antOTS, and the antCOS bilaterally), reinforcing the extent of the face-selective network, centered on the lateral fusiform gyrus. Second, both types of analyses provide complementary information. For example, while the right latFG showed the largest face-selective response amplitude, the bilateral IOG showed the highest proportion (Fig. 4). The right IOG is a region where high face-selective responses are usually observed in fMRI (Haxby et al. 2000; Rossion et al. 2003; Duchaine and Yovel 2015; Grill-Spector et al. 2017), whose lesion can produce prosopagnosia (Rossion et al. 2003; Bouvier and Engel 2006) and whose transient inactivation either by transcranial electrical stimulation (TMS; Pitcher et al. 2007; Ambrus et al. 2017) or intracerebral electrical stimulation (Jonas et al. 2012) can cause difficulties of face identity recognition. The amplitude recorded on a given SEEG contact depends on several factors including the distance between the source and the electrode, the spatial configuration of the cortical source, etc. (Herreras 2016). Therefore, if all conditions are not met to record the largest amplitude possible, the proportion analysis can still identify an important region of the cortical face network independently of the response amplitude.

Face-Exclusive Responses in the ATL

Importantly, the wide distribution of face-selective responses refers also to the fact that these responses largely extend to the ATL (Jonas et al. 2016), a region that is difficult to image with fMRI due to strong magnetic artifacts caused by the proximity of the ear canals (Wandell 2011; Axelrod and Yovel 2013; Rossion et al. 2018). In this region, face contacts largely outnumbered house contacts (286 vs. 91). This region also showed the highest proportion of so-called "exclusive" contacts (Jonas et al. 2016), that is, contacts exhibiting significant categorization response (1.2 Hz and harmonics) without a general visual stimulation response to other objects at the base frequency (6 Hz and harmonics).

Given the anterior location of these exclusive contacts, it was unknown whether they reflected a post-visual categorization process evoked by any category or if they were truly part of a face-selective process. For example, it is well known that a post-visual categorization system(s) is capable of monitoring events that differ in frequency, as, for example, reflected in the robust P300 scalp EEG component located on posterior parietal channels (e.g., Kutas et al. 1977; Donchin 1981). Consistent with Jonas et al. (2016), here we identified a large proportion of exclusive responses (19.5% of all significant contacts) that were mostly located in the ATL (71.11% of all exclusive contacts). It is important to note that the criteria to define a contact as exclusive were stricter in the present study than in Jonas et al. (2016) (no base response for the preferred category but also no selective and base responses for the nonpreferred category). Contrary to a general oddball detector account, we found that most of the exclusive contacts were responsive to either only faces or only houses (89.3% of all exclusive contacts). Notably, most of the exclusive contacts (71.1%) responded to faces only.

The current study thus provides additional evidence that response profiles in the ATL are qualitatively different than in the more posterior brain regions. These results suggest that the ATL is involved in the highest stages of face categorization for which faces should be processed independently of the context and for which face information should be shared with other modality-specific regions in order to build a common person-related representation (face–name–voice association, linking information specific to an individual face, etc.). This hypothesis is consistent with a "hub" theory of semantic cognition in which the ATL integrates modality-specific representations into a shared crossmodal representation (Lambon Ralph 2014; Rice et al. 2018). The response profile evolving from category-selective to category-exclusive along the postero-anterior axis may reflect that regions of the temporal lobe become gradually crossmodal as direct connections from early visual areas become sparser and connections with other modality-specific regions increase (voice, name, etc.).

In summary, our large-scale intracerebral recording study provides a global mapping of the human VOTC for selective responses to frequency-tagged faces presented in rapid periodic trains of nonface objects. Face- and house-selective contacts were spatially dissociated along the medial to lateral VOTC axis, even across overlap contacts which appeared to measure spatially distinct populations of neurons responding selectively to each category, and this dissociation was present up to the ATL. A high proportion of intracerebral recording contacts in the ATL show exclusive responses to faces, indicating that this region is particularly important for higher-order face-related processes independent of general visual responses. Altogether, these observations shed light on the neural basis of human face categorization and strengthen the validity of the frequency-tagging approach coupled with intracerebral recordings in epileptic patients to understand visual categorization and human brain function in general.

Supplementary Material

Supplementary material is available at *Cerebral Cortex* online.

Funding

Lorraine Université d'Excellence program, a 2018 project from the Région Grand Est; FNRS (Fonds de la Recherche Scientifique) - EOS (The Excellence of Science) project (ID: 30991544).

Conflict of Interest

None declared.

References

Allison T, McCarthy G, Nobre A, Puce A, Belger A. 1994. Human extrastriate visual cortex and the perception of faces, words, numbers, and colors. *Cereb Cortex*. 4:544–554.

Allison T, Puce A, Spencer DD, McCarthy G. 1999. Electrophysiological studies of human face perception. I: potentials generated in occipitotemporal cortex by face and non-face stimuli. *Cereb Cortex*. 9:415–430.

Ambrus GG, Dotzer M, Schweinberger SR, Kovács G. 2017. The occipital face area is causally involved in the formation of identity-specific face representations. *Brain Struct Funct*. 222:4271–4282.

Axelrod V, Yovel G. 2013. The challenge of localizing the anterior temporal face area: a possible solution. *NeuroImage*. 81:371–380.

Bédos Ulvin LB, Jonas J, Brissart H, Colnat-Coulbois S, Thiriaux A, Vignal JP, Maillard L. 2017. Intracerebral stimulation of left and right ventral temporal cortex during object naming. *Brain Lang*. 175:71–76.

Bouvier SE, Engel SA. 2006. Behavioral deficits and cortical damage loci in cerebral achromatopsia. *Cereb Cortex*. 16: 183–191.

Buzsáki G, Anastassiou CA, Koch C. 2012. The origin of extracellular fields and currents—EEG, ECoG, LFP and spikes. *Nat Rev Neurosci*. 13:407.

Carpenter B, Gelman A, Hoffman MD, Lee D, Goodrich B, Betancourt M, Brubaker M, Guo J, Li P, Riddell A. 2017. Stan: a probabilistic programming language. *J Stat Softw*. 76:1–32.

Collins JA, Koski JE, Olson IR. 2016. More than meets the eye: the merging of perceptual and conceptual knowledge in the anterior temporal face area. *Front Hum Neurosci*. 10:189.

Collins JA, Olson IR. 2014. Beyond the FFA: the role of the ventral anterior temporal lobes in face processing. *Neuropsychologia*. 61:65–79.

Cox RW. 1996. AFNI: software for analysis and visualization of functional magnetic resonance neuroimages. *Comput Biomed Res*. 29:162–173.

Ding SL, Van Hoesen GW, Cassell MD, Poremba A. 2009. Parcellation of human temporal polar cortex: a combined analysis of multiple cytoarchitectonic, chemoarchitectonic, and pathological markers. *J Comp Neurol*. 514:595–623.

Donchin E. 1981. Surprise!... surprise? *Psychophysiology*. 18:493–513.

Dubey A, Ray S. 2019. Cortical Electrocorticogram (ECoG) is a local signal. *J Neurosci*. 39:4299–4311.

Duchaine B, Yovel G. 2015. A revised neural framework for face processing. *Annu Rev Vis Sci*. 1:393–416.

Engell AD, McCarthy G. 2010. The relationship of gamma oscillations and face-specific ERPs recorded subdurally from occipitotemporal cortex. *Cereb Cortex*. 21:1213–1221.

Epstein RA, Bar M, Kveraga K. 2014. Neural systems for visual scene recognition. In: *Scene vision*, pp. 105–134.

Epstein R, Kanwisher N. 1998. A cortical representation of the local visual environment. *Nature*. 392:598.

Gainotti G. 2013. Is the right anterior temporal variant of prosopagnosia a form of 'associative prosopagnosia' or a form of 'multimodal person recognition disorder'? *Neuropsychol Rev*. 23:99–110.

Gao X, Gentile F, Rossion B. 2018. Fast periodic stimulation (FPS): a highly effective approach in fMRI brain mapping. *Brain Struct Funct*. 223:2433–2454.

Ghuman AS, Brunet NM, Li Y, Konecky RO, Pyles JA, Walls SA, Destefino V, Wang W, Richardson RM. 2014. Dynamic encoding of face information in the human fusiform gyrus. *Nat Commun*. 5:5672.

Gomez J, Pestilli F, Witthoft N, Golarai G, Liberman A, Poltoratski S, Yoon J, Grill-Spector K. 2015. Functionally defined white matter reveals segregated pathways in human ventral temporal cortex associated with category-specific processing. *Neuron*. 85:216–227.

Grill-Spector K, Weiner KS, Kay K, Gomez J. 2017. The functional neuroanatomy of human face perception. *Annu Rev Vis Sci*. 3:167–196.

Gschwind M, Pourtois G, Schwartz S, Van De Ville D, Vuilleumier P. 2011. White-matter connectivity between face-responsive regions in the human brain. *Cereb Cortex*. 22:1564–1576.

Halgren E, Baudena P, Heit G, Clarke M, Marinkovic K. 1994. Spatio-temporal stages in face and word processing. 1. Depth recorded potentials in the human occipital and parietal lobes. *J Physiol*. 88:1–50.

Haxby JV, Hoffman EA, Gobbini MI. 2000. The distributed human neural system for face perception. *Trends Cogn Sci*. 4:223–233.

Herreras O. 2016. Local field potentials: myths and misunderstandings. *Front Neural Circuit*. 10:101.

Jacques C, Retter TL, Rossion B. 2016a. A single glance at natural face images generate larger and qualitatively different category-selective spatio-temporal signatures than other ecologically-relevant categories in the human brain. *NeuroImage*. 137:21–33.

Jacques C, Witthoft N, Weiner KS, Foster BL, Rangarajan V, Hermes D, Miller KJ, Parvizi J, Grill-Spector K. 2016b. Corresponding ECoG and fMRI category-selective signals in human ventral temporal cortex. *Neuropsychologia*. 83:14–28.

Jonas J, Brissart H, Hossu G, Colnat-Coulbois S, Vignal JP, Rossion B, Maillard L. 2018. A face identity hallucination (palinopsia) generated by intracerebral stimulation of the face-selective right lateral fusiform cortex. *Cortex*. 99:296–310.

Jonas J, Descoins M, Koessler L, Colnat-Coulbois S, Sauvée M, Guye M, Vignal JP, Vespignani H, Rossion B, Maillard L. 2012. Focal electrical intracerebral stimulation of a face-sensitive area causes transient prosopagnosia. *Neuroscience*. 222:281–288.

Jonas J, Jacques C, Liu-Shuang J, Brissart H, Colnat-Coulbois S, Maillard L, Rossion B. 2016. A face-selective ventral occipitotemporal map of the human brain with intracerebral potentials. *Proc Natl Acad Sci U S A*. 113:E4088–E4097.

Jonas J, Rossion B, Krieg J, Koessler L, Colnat-Coulbois S, Vespignani H, Jacques C, Vignal JP, Brissart H, Maillard L. 2014. Intracerebral electrical stimulation of a face-selective area in the right inferior occipital cortex impairs individual face discrimination. *NeuroImage*. 99:487–497.

Kadipasaoglu CM, Conner CR, Whaley ML, Baboyan VG, Tandon N. 2016. Category-selectivity in human visual cortex follows cortical topology: a grouped icEEG study. *PLoS One*. 11:e0157109.

Kanwisher N, McDermott J, Chun MM. 1997. The fusiform face area: a module in human extrastriate cortex specialized for face perception. *J Neurosci*. 17:4302–4311.

Katzner S, Nauhaus I, Benucci A, Bonin V, Ringach DL, Carandini M. 2009. Local origin of field potentials in visual cortex. *Neuron*. 61:35–41.

Kim JJ, Crespo-Facorro B, Andreasen NC, ÓLeary DS, Zhang B, Harris G, Magnotta VA. 2000. An MRI-based parcellation method for the temporal lobe. *NeuroImage*. 11:271–288.

Koessler L, Maillard L, Benhadid A, Vignal JP, Felblinger J, Vespignani H, Braun M. 2009. Automated cortical projection of EEG sensors: anatomical correlation via the international 10–10 system. *NeuroImage*. 46:64–72.

Kruschke JK. 2013. Bayesian estimation supersedes the t test. *J Exp Psychol Gen*. 142:573.

Kruschke JK. 2014. *Doing Bayesian data analysis: a tutorial with R, JAGS, and Stan*. Academic Press.

Kutas M, McCarthy G, Donchin E. 1977. Augmenting mental chronometry: the P300 as a measure of stimulus evaluation time. *Science*. 197:792–795.

Lambon Ralph MA. 2014. Neurocognitive insights on conceptual knowledge and its breakdown. *Philos Trans R Soc B*. 369:20120392.

Lochy A, Jacques C, Maillard L, Colnat-Coulbois S, Rossion B, Jonas J. 2018. Selective visual representation of letters and words in the left ventral occipito-temporal cortex with intracerebral recordings. *Proc Natl Acad Sci U S A*. 115: E7595–E7604.

Meadows JC. 1974. The anatomical basis of prosopagnosia. *J Neurol Neurosurg Psychiatry*. 37:489–501.

Nasr S, Liu N, Devaney KJ, Yue X, Rajimehr R, Ungerleider LG, Tootell RB. 2011. Scene-selective cortical regions in human and nonhuman primates. *J Neurosci*. 31: 13771–13785.

Parvizi J, Jacques C, Foster BL, Withoft N, Rangarajan V, Weiner KS, Grill-Spector K. 2012. Electrical stimulation of human fusiform face-selective regions distorts face perception. *J Neurosci*. 32:14915–14920.

Pitcher D, Walsh V, Yovel G, Duchaine B. 2007. TMS evidence for the involvement of the right occipital face area in early face processing. *Curr Biol*. 17:1568–1573.

Puce A, Allison T, Gore JC, McCarthy G. 1995. Face-sensitive regions in human extrastriate cortex studied by functional MRI. *J Neurophysiol*. 74:1192–1199.

Pyles JA, Verstynen TD, Schneider W, Tarr MJ. 2013. Explicating the face perception network with white matter connectivity. *PLoS One*. 8:e61611.

Quek GL, Rossion B. 2017. Category-selective human brain processes elicited in fast periodic visual stimulation streams are immune to temporal predictability. *Neuropsychologia*. 104:182–200.

Rajimehr R, Young JC, Tootell RB. 2009. An anterior temporal face patch in human cortex, predicted by macaque maps. *Proc Natl Acad Sci U S A*. 106:1995–2000.

Regan D. 1989. *Human brain electrophysiology: Evoked potentials and evoked magnetic fields in science and medicine*. Amsterdam, The Netherlands: Elsevier.

Rice GE, Caswell H, Moore P, Hoffman P, Lambon Ralph MA. 2018. The roles of left versus right anterior temporal lobes in semantic memory: a neuropsychological comparison of postsurgical temporal lobe epilepsy patients. *Cereb Cortex*. 28:1487–1501.

Rossion B. 2014. Understanding face perception by means of prosopagnosia and neuroimaging. *Front Biosci (Elite Ed)*. 6:258–307.

Rossion B, Caldara R, Seghier M, Schuller AM, Lazeyras F, Mayer E. 2003. A network of occipito-temporal face-sensitive areas besides the right middle fusiform gyrus is necessary for normal face processing. *Brain*. 126:2381–2395.

Rossion B, Hanseeuw B, Dricot L. 2012. Defining face perception areas in the human brain: a large-scale factorial fMRI face localizer analysis. *Brain Cogn*. 79:138–157.

Rossion B, Jacques C, Jonas J. 2018. Mapping face categorization in the human ventral occipitotemporal cortex with direct neural intracranial recordings. *Ann N Y Acad Sci*. 1426:5–24.

Salado AL, Koessler L, De Mijolla G, Schmitt E, Vignal JP, Civit T, Tyvaert L, Jonas J, Maillard LG, Colnat-Coulbois S. 2017. sEEG is a safe procedure for a comprehensive anatomic exploration of the insula: a retrospective study of 108 procedures representing 254 transopercular insular electrodes. *Oper Neurosurg*. 14:1–8.

Spiridon M, Fischl B, Kanwisher N. 2006. Location and spatial profile of category-specific regions in human extrastriate cortex. *Hum Brain Mapp*. 27:77–89.

Tanji K, Iwasaki M, Nakasato N, Suzuki K. 2012. Face specific broadband electrocorticographic spectral power change in the rhinal cortex. *Neurosci Lett*. 515:66–70.

Tsao DY, Moeller S, Freiwald WA. 2008. Comparing face patch systems in macaques and humans. *Proc Natl Acad Sci U S A*. 105:19514–19519.

Tootell RB, Devaney KJ, Young JC, Postelnicu G, Rajimehr R, Ungerleider LG. 2008. fMRI mapping of a morphed continuum of 3D shapes within inferior temporal cortex. *Proc Natl Acad Sci U S A*. 105:3605–3609.

Vidal JR, Ossandón T, Jerbi K, Dalal SS, Minotti L, Ryvlin P, Kahane P, Lachaux JP. 2010. Category-specific visual responses: an intracranial study comparing gamma, beta, alpha, and ERP response selectivity. *Front Hum Neurosci*. 4:195.

Yoshor D, Ghose GM, Bosking WH, Sun P, Maunsell JH. 2007. Spatial attention does not strongly modulate neuronal responses in early human visual cortex. *J Neurosci*. 27:13205–13209.

Van Hoesen GW. 1995. Anatomy of the medial temporal lobe. *Magn Reson Imaging*. 13:1047–1055.

van Hoesen GW, Augustinack JC, Dierking J, Redman SJ, Thangavel R. 2000. The parahippocampal gyrus in Alzheimer's disease: clinical and preclinical neuroanatomical correlates. *Ann N Y Acad Sci*. 911:254–274.

Wandell BA. 2011. The neurobiological basis of seeing words. *Ann N Y Acad Sci*. 1224:63–80.

Weiner KS, Barnett MA, Witthoft N, Golarai G, Stigliani A, Kay KN, Gomez J, Natu VS, Amunts K, Zilles K *et al*. 2018. Defining the most probable location of the parahippocampal place area using cortex-based alignment and cross-validation. *NeuroImage*. 170:373–384.

Weiner KS, Grill-Spector K. 2010. Sparsely-distributed organization of face and limb activations in human ventral temporal cortex. *NeuroImage*. 52:1559–1573.

Wennberg R. 2010. On electrical potentials observed at a distance from intracranial electrode contacts. *Clin Neurophysiol*. 121:259.

Zaveri HP, Duckrow RB, Spencer SS. 2009. Concerning the observation of an electrical potential at a distance from an intracranial electrode contact. *Clin Neurophysiol*. 10: 1873–1875.

Zhen Z, Yang Z, Huang L, Kong XZ, Wang X, Dang X, Huang Y, Song Y, Liu J. 2015. Quantifying interindividual variability and asymmetry of face-selective regions: a probabilistic functional atlas. *NeuroImage*. 113:13–25.

Received: 20 September 2019 | Revised: 23 January 2020 | Accepted: 3 February 2020

DOI: 10.1002/hbm.24952

WILEY

RESEARCH ARTICLE

Fast periodic visual stimulation to highlight the relationship between human intracerebral recordings and scalp electroencephalography

Corentin Jacques[1,2] | Jacques Jonas[3,4] | Louis Maillard[3,4] | Sophie Colnat-Coulbois[3,5] | Bruno Rossion[1,3,4†] | Laurent Koessler[3,4†]

[1]Psychological Sciences Research Institute and Institute of Neuroscience, Université Catholique de Louvain (UCLouvain), Louvain-la-Neuve, Belgium

[2]Center for Developmental Psychiatry, Department of Neurosciences, KULeuven, Belgium

[3]Université de Lorraine, CNRS, CRAN, F-54000, Nancy, France

[4]Université de Lorraine, CHRU-Nancy, Service de Neurologie, F-54000, Nancy, France

[5]Université de Lorraine, CHRU-Nancy, Service de Neurochirurgie, F-54000, Nancy, France

Correspondence
Bruno Rossion, CRAN, UMR 7039, CNRS - Université de Lorraine, Pavillon Krug (1er étage - entrée CC-1), Hôpital Central, Nancy, France.
Email: bruno.rossion@univ-lorraine.fr

Funding information
Fédération Wallonie-Bruxelles, Grant/Award Number: ARC 13/18-053; Fondation Louvain; Fonds National de la Recherche - FNRS, Grant/Award Number: PDR T.0207.16

Abstract

Despite being of primary importance for fundamental research and clinical studies, the relationship between local neural population activity and scalp electroencephalography (EEG) in humans remains largely unknown. Here we report simultaneous scalp and intracerebral EEG responses to face stimuli in a unique epileptic patient implanted with 27 intracerebral recording contacts in the right occipitotemporal cortex. The patient was shown images of faces appearing at a frequency of 6 Hz, which elicits neural responses at this exact frequency. Response quantification at this frequency allowed to objectively relate the neural activity measured inside and outside the brain. The patient exhibited typical 6 Hz responses on the scalp at the right occipitotemporal sites. Moreover, there was a clear spatial correspondence between these scalp responses and intracerebral signals in the right lateral inferior occipital gyrus, both in amplitude and in phase. Nevertheless, the signal measured on the scalp and inside the brain at nearby locations showed a 10-fold difference in amplitude due to electrical insulation from the head. To further quantify the relationship between the scalp and intracerebral recordings, we used an approach correlating time-varying signals at the stimulation frequency across scalp and intracerebral channels. This analysis revealed a focused and right-lateralized correspondence between the scalp and intracerebral recordings that were specific to the face stimulation is more broadly distributed in various control situations. These results demonstrate the interest of a frequency tagging approach in characterizing the electrical propagation from brain sources to scalp EEG sensors and in identifying the cortical sources of brain functions from these recordings.

KEYWORDS

face perception, frequency tagging, inferior occipital gyrus, intracerebral electrophysiology, occipitotemporal, SEEG, source imaging, vision

†Bruno Rossion and Laurent Koessler contributed equally to this work.

1 | INTRODUCTION

Since its first report and validation in humans (Adrian & Matthews, 1934) scalp electroencephalography (EEG) has been widely used to study dynamic neurofunctional processes and their pathology in large-scale brain networks (Lopes da Silva, 2013; Nunez & Srinivasan, 2005; Regan, 1989). Given that EEG noninvasively provides information about the unfolding of brain processes at the millisecond time resolution, understanding the relationship between scalp EEG signals and their source(s) at the cortical level is important for fundamental research. It is also of primary importance for clinical studies, in particular for the neurological study of epileptic patients, in order to define and localize brain sources of epileptic seizures (Coito et al., 2019; Gavaret, Badier, Marquis, Bartolomei, & Chauvel, 2004; Koessler et al., 2010). Unfortunately, knowledge about the relationship between scalp EEG signals and their cortical source(s) remains severely limited, for several reasons. First, scalp EEG signals are attenuated by the electrical resistance of head tissues, which remain unknown in human in vivo (especially the skull resistivity) and very difficult to estimate noninvasively and during in vivo measurements (Goncalves et al., 2003; Koessler et al., 2017; Malmivuo & Suihko, 2004). Second, the distance from brain sources to scalp sensors reduce the amplitude of EEG signal, making it difficult to capture and estimate brain sources at the deepest portions of sulci or the medial brain structures (Koessler et al., 2015; Seeber, Cantonas, Sesia, Visser-vandewalle, & Michel, 2019; see also Pizzo et al., 2019 in MEG). Third and perhaps most importantly, many brain sources (often co-activated in interlocked time-courses) contribute to EEG recording. Electrical signals generated by these co-activated sources are mixed when measured on the scalp with EEG sensors, making it difficult to assign a specific source to a specific EEG signal characteristic (nonlinear relationship; Kovach, Oya, & Kawasaki, 2018) and requiring to solve an undetermined inverse problem (Grech et al., 2008; Kaiboriboon, Luders, Hamaneh, Turnbull, & Lhatoo, 2012; Michel et al., 2004).

In humans, the relationship between scalp EEG signals and their cortical sources can be potentially addressed by comparing simultaneous scalp and intracranial EEG recordings. These rare studies derive from invasive investigations performed mainly with foramen ovale or subdural electrodes (e.g., Alarcon et al., 1994; Lantz, Holub, Ryding, & Rosen, 1996; Van Der Loo, Congedo, Plazier, Van De Heyning, & De Ridder, 2007; Wennberg & Cheyne, 2014) and more rarely with intracerebral electrodes (Alarcon et al., 1994; Gavaret, Dubarry, Carron, & Bartolomei, 2016; Koessler et al., 2015). In the latter case, intracerebral EEG (also named stereoelectroencephalography, SEEG) records electrical activity directly from specific brain areas with high anatomical accuracy by means of implanted multicontact electrodes. This technique is used in the presurgical evaluation of drug-resistant epilepsies (Chauvel, Gonzalez-Martinez, & Bulacio, 2019; Talairach & Bancaud, 1973). Beyond its clinical significance, the recorded signal can be analyzed in parallel for research purposes (e.g., Allison, Puce, Spencer, McCarthy, & Belger, 1999; Barbeau et al., 2008; Halgren et al., 1994; Jacques et al., 2016; Jonas et al., 2016).

The few studies which investigated the relationship between simultaneously recorded scalp EEG and SEEG signals relied on event-related potential (ERP) approaches, in which brain activity is recorded to the sudden occurrence of an event (external or internal such as epileptic spikes) and then averaged in the time domain (Dubarry et al., 2014; Jacques et al., 2019; Koessler et al., 2015; Merlet et al., 1998; Rosburg et al., 2010). At least two main factors make it difficult to perform these studies and therefore seriously limit their availability. First, relating scalp to intracerebral EEG requires a high signal-to-noise ratio (SNR) on the scalp, which typically results in long-duration experiments to collect data from a large number of events (exogenous or endogenous; Luck, 2014). SNR is particularly an issue in these clinical settings where recordings can take place over several days without the possibility to fix or replace noisy scalp electrodes. Second, the amplitude and shape of evoked responses in the time domain are difficult to relate across scalp and intracerebral EEG because of the diversity and the unknown spatiotemporal dynamic of activated sources within the brain (Lopes da Silva, 2019).

One approach to overcome these difficulties would be to use a stimulus presentation technique that provides high SNR and allows to more objectively characterize the signal to be compared across recordings. A potentially powerful approach that fits these criteria is the frequency tagging approach where a stimulus is presented at a (relatively fast) fixed frequency rate, for instance, a flickering light, eliciting a neural response exactly at this frequency rate which can be therefore objectively tracked and quantified in simultaneously recorded scalp EEG and SEEG signals. This approach was discovered shortly after the first descriptions of EEG recordings in humans (Adrian & Matthews, 1934), that is, well before the first ERP recordings (Dawson, 1951; see Regan, 1972). It was already considered at the time as offering a powerful mean to understand the nature and the source(s) of EEG recordings, as stated by Adrian (1944):

> "All the messages which reach the cortex will produce their own electrical accompaniment, and this can be recorded well enough if electrodes can be placed on the surface of the brain. But if we can get no nearer than the scalp, the potential changes generated in any group of nerve cells will usually be obscured by those of other groups nearby, and the record will then show us nothing… Fortunately this difficulty can be overcome, in part at least, by making all the cells work in unison. This can be done, as far as vision is concerned, by making the field more or less uniform and lighting it with a flickering light. The nerve cells are then forced to work in unison at the frequency of the flicker, and we can record their electrical activity through the skull up to frequencies of about 30 a second. This gives us a method of tracing the visual messages in the brain, for by means of the flicker rhythm they can be made easy to recognize" (Adrian, 1944, p. 361).

Thanks to the subsequent application of Fourier analysis to EEG recordings (Regan, 1966), these "frequency-tagged" neural responses

can be investigated in the frequency domain in various sensory modalities in neurotypical adults, but also in developmental and clinical populations (Regan, 1989; see Norcia, Appelbaum, Ales, Cottereau, & Rossion, 2015 for a recent review in vision research). The main advantages of this approach are its objectivity (i.e., responses are identified at a frequency known by the experimenter) and high sensitivity (i.e., high SNR) (Norcia et al., 2015; Regan, 1989; Rossion, 2014). Moreover, by carefully manipulating the nature of the stimulus property that is periodically modulated, sensory processes, but also higher-level brain processes such as face or word categorization for instance (e.g., Lochy, Van Belle, & Rossion, 2015; Rossion & Boremanse, 2011), can be selectively tracked in all modalities.

Despite these advantages, to our knowledge, the frequency-tagging approach has never been applied to simultaneous EEG and intracerebral recordings in order to shed light on the relationship between the two types of signals.[1] Here we report simultaneous frequency-tagged scalp and intracerebral EEG responses in a unique epileptic patient implanted with three intracerebral electrodes (27 recording contacts) in the right occipitotemporal (OT) cortex and equipped simultaneously with 27 scalp electrodes on the scalp surface. Thanks to a fast periodic (6 Hz) visual stimulation with highly salient stimuli (faces), we objectively relate the quantified face-evoked responses observed inside and outside the brain. Specifically, we address the following questions: (a) How do objectively related signals recorded simultaneously inside the brain and on the scalp differ in terms of amplitude and SNR? and (b) Can frequency-tagging significantly improve the precise identification of the sources of activity recorded on the scalp?

2 | MATERIALS AND METHODS

The epileptic patient, as well as the recording settings, are identical to those reported in Jacques et al. (2019). The patient has also been described in Jonas et al. (2014). Therefore, a shortened version of the methods is reported here.

2.1 | Case description

KV is a right-handed female suffering from refractory occipital epilepsy related to a focal cortical dysplasia involving the right lingual gyrus and posterior collateral sulcus. The patient was 32 year-old at the time of testing. Her case was also reported as evidence of strong face identity repetition suppression effects in the lateral cortex of right IOG using fast periodic visual stimulation (FPVS) with unfamiliar faces (Jonas et al., 2014).

2.2 | Simultaneous intracerebral—Scalp EEG recordings

The patient underwent simultaneous intracerebral and scalp EEG recordings. The co-locations of these electrodes are shown in Figure 1. The originality of electrode placements is a relatively dense spatial coverage of the occipital-temporal cortex with both intracerebral (27 intracerebral contacts) and surface electrodes (including sO1, sOz, sO2, sPO7, sPO8, sP9, sP10, sP5, sP6).

2.2.1 | Intracerebral electrodes

The patient was stereotactically implanted with three intracerebral multicontact electrodes targeting the right ventral OT cortex, according to a well-defined and previously described procedure (Jonas et al., 2016; Salado et al., 2018). Each intracerebral electrode consists of a cylinder of 0.8 mm diameter and contains 8–11 independent recording contacts of 2 mm in length separated by 1.5 mm from edge to edge and by 3.5 mm center to center (DIXI Medical, Besançon, France). Electrodes D and L (eight recording contacts each: D1–D8 and L1–L8) sampled the right inferior occipital gyrus and posterior collateral sulcus. Electrode F (11 contacts, F1–F11) was more anterior and went from the right inferior temporal gyrus to the lingual gyrus. All intracerebral contacts except D8 were in direct contact with the gray matter. The recording surface of contact D8 was located ~2 mm from the cortical surface, likely within the meninges (Figure 1c,d).

2.2.2 | Scalp electrodes

Simultaneous scalp EEG recordings were acquired with 28 Ag/AgCl electrodes of 10 mm diameter placed according to the 10–20 system (Figure 1, Seeck et al., 2017) using sterile procedures, with a particular spatial coverage of bilateral OT regions. Some of the posterior electrodes were slightly displaced relative to the 10–20 positions due to the presence of depth electrodes. Scalp electrode positions were determined using a 3D digitizer system (3 space Fastrak, Polhemus, Colchester, VT).

2.2.3 | Recordings

Simultaneous SEEG—scalp EEG signals were recorded at a 1,024 Hz sampling rate with a 128-channel amplifier (SD LTM 128 Headbox; Micromed, Italy). The reference electrode was a prefrontal midline scalp electrode (sFPz). The recording of the periodic visual stimulation experiment reported here was performed 2 days after the scalp electrode placement. Due to the low diameter of the skull defect at the penetration points of intracerebral electrodes (1.2 mm) and the low electrical conductivity of the guidance screw (titanium), no leakage of current was observed in scalp EEG recordings.

2.3 | FPVS

2.3.1 | Rationale

The main aspects of the procedure for this experiment have been previously described in three different studies comparing the

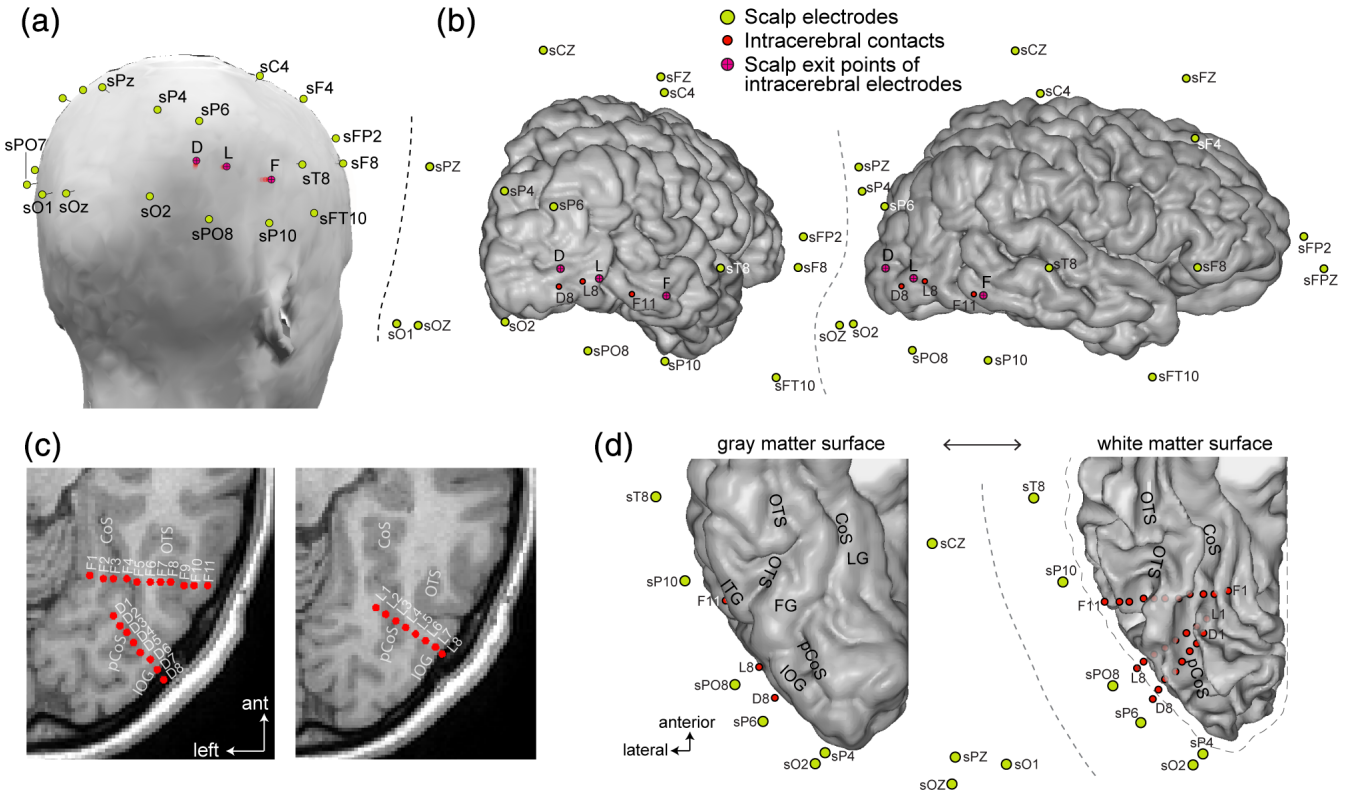

FIGURE 1 Simultaneous recording of scalp and intracerebral EEG. (a) Scalp view from the posterior right hemisphere showing the position of the scalp recording electrodes (shown in green) and the location on the scalp of the exit point of the three intracerebral electrodes (D, L, F, shown as red dots). (b) Three/quarter posterior and profile views of 3D reconstruction of the patient's right hemisphere cortical surface, showing the locations of the intracerebral electrodes (in red, only the most external contacts D8, L8, and F11 appear on the cortical surface) and the locations of the scalp electrodes (green). (c) Axial views of the posterior half of the right hemisphere of the patient, showing the locations of intracerebral contacts in the right OT cortex. Electrode L was slightly superior to D and F electrodes. All intracerebral contacts except D8 were in direct contact with the gray matter. Contact D8 was located ~2 mm from the cortical surface. (d) 3D ventral views of the posterior half of the right hemisphere of the patient, showing the anatomical location of the intracerebral contacts and scalp electrodes. The plots show the gray matter cortical surface (left) and the corresponding white matter surface (right, the gray matter surface is represented as a dotted gray outline). Since intracerebral contacts penetrate the brain tissue, contacts are only visible when stripping away the gray matter and keeping only white matter surface. Acronyms: IOG: inferior occipital gyrus, OTS: occipitotemporal sulcus, (p)CoS: (posterior) collateral sulcus, FG, fusiform gyrus, LG: lingual gyrus

presentation of trains of different faces to identical faces at a fixed frequency rate (Jonas et al., 2014; Rossion & Boremanse, 2011; Rossion, Prieto, Boremanse, Kuefner, & Van Belle, 2012). From a methodological perspective, this FPVS approach—which leads to so-called steady-state visual evoked potentials (SSVEPs, Regan, 1989, Regan, 1966)—has multiple advantages: objectivity of definition and quantification of the response of interest, high SNR, short duration of the experiment, and recording of the response of interest during a simple incidental task (Regan, 1989; Rossion, 2014), making it a tool of choice for the study of patients implanted with intracerebral electrodes. Here, faces were presented at a 6 Hz rate because this frequency rate provides the largest repetition suppression effect on the scalp over the right OT cortex (Alonso-Prieto, Van Belle, Liu-Shuang, Norcia, & Rossion, 2013), as well as in face-selective areas of the right inferior occipital gyrus and middle section of the lateral fusiform gyrus (Gentile & Rossion, 2014).

2.3.2 | Stimuli

Full-front color face pictures of 18 unfamiliar individuals (7° × 10° of visual angle for the base face size) equalized for global luminance were used. These face stimuli were the same as used in previous studies (Alonso-Prieto et al., 2013; Rossion & Boremanse, 2011) and taken from a well-known set of laser-scanned faces from the Tubingen Max Planck Institute (MPI) database of laser-scanned (Cyberware TM) human heads. They were cropped to remove external features (hair and ears) but their overall shape was preserved.

2.3.3 | Procedure

In each condition, a face stimulus appeared and disappeared (sinusoidal contrast modulation) on the screen, at a stimulation rate of six faces per second (one face every 166.66 ms; Figure 2). A trigger was

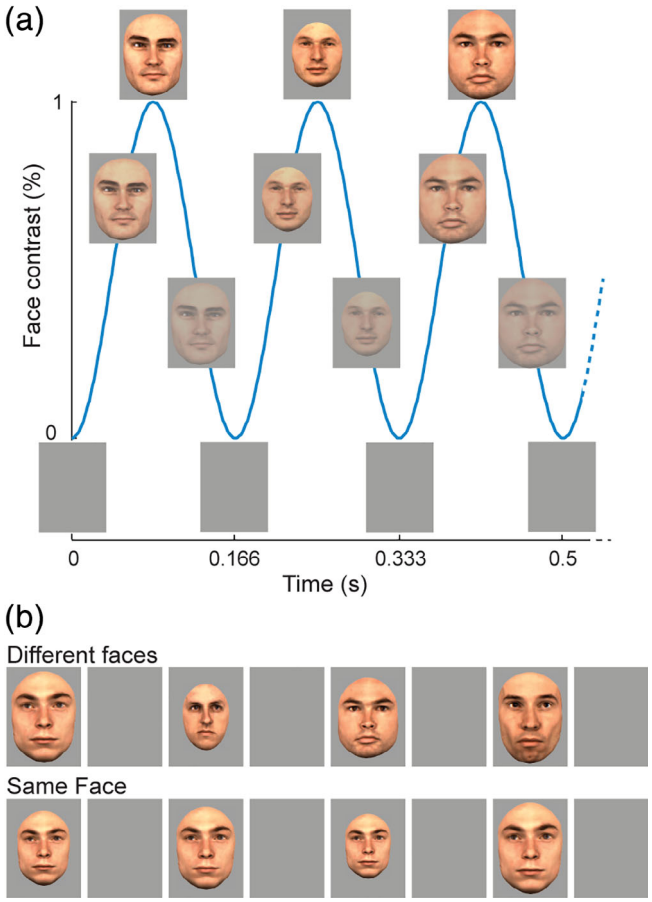

FIGURE 2 Fast periodic visual stimulation procedure and experimental design. (a) Faces were presented in sequences of 70 s using a sinusoidal contrast modulation at a rate of 6 Hz. Here, the "different faces" condition is shown, with the face of a different individual presented at full contrast every 0.167 s (1/6 s). The size of faces changed at every cycle. (b) The two conditions used in the study, in which either a different face was presented at every cycle throughout the duration of the FPVS sequence (top) or the same face was repeated for the whole sequence (bottom)

sent to the parallel port of the EEG recording computer at each minimal level of visual stimulation (gray background), using a photodiode placed on the left upper corner of a laptop monitor. In the *same face* condition, a randomly selected face picture was presented repeatedly during the whole stimulation duration (70 s). In the *different faces* condition, the sequence started with the repeated presentation of a randomly selected face picture for the first 15 s, after which the face identity changed at every cycle for the remainder of the sequence (i.e., from 16 to 70 s, see Rossion et al., 2012). In these *different faces* condition, 18 individual faces of the same sex were used and presented in random order. The same face identity never appeared twice in a row, so that the face identity change rate was always 6 Hz. To minimize repetition suppression effects due to low-level visual cues, the face stimulus changed substantially in size with each presentation, that is, at a rate of 6 Hz, in all conditions (random face size between 82 and 118% of base face size). The experiment consisted of four sequences of 70 s: each condition (same face or different faces) was repeated two times (face gender: male or female). The order of conditions was randomized. During each 70 s run, the patient was instructed to fixate on a small black cross located centrally on the face, slightly below the bridge of the nose. The fixation cross changed color (black to red) briefly (200 ms) 6 to 8 times during each run and the patient was instructed to report the color changes by pressing a response key.

2.4 | Data processing and analyses

2.4.1 | Frequency domain analyses

All analyses were performed using Letswave 5 (Mouraux & Iannetti, 2008) and MATLAB v7.8 (The Mathworks, Inc.). Segments of 50 s of recording during visual stimulation (i.e., 300 face stimulation cycles at 6.0 Hz) from 17 to 67 seconds were considered for analysis. These segments were cropped to contain an exact integer number of 6 Hz cycles. Segments were averaged in the time domain separately for each condition and a Fast Fourier Transform (FFT) was applied to these averaged segments to compute the amplitude and phase spectra at a high spectral resolution of 1/50 = 0.02 Hz. SNR was computed from the amplitude spectra as the ratio between the amplitude at each frequency bin and the average amplitude of the corresponding 20 neighboring bins (up to 11 bins on each side, i.e., 22 bins, but excluding the 2 bins directly adjacent to the bin of interest, i.e., 20 bins, e.g., Rossion et al., 2012). Significant responses above noise level at the stimulation frequency at each channel were defined by computing Z-scores on the amplitude spectra, using the mean and *SD* of the 20 neighboring bins around the frequency of interest (e.g., Liu-Shuang, Norcia, & Rossion, 2014). Statistical comparisons between conditions were similarly made by computing Z-scores on amplitude spectra obtained by subtracting the spectra measured in the *same face* condition from the spectra measured in the *different faces* condition.

2.4.2 | Time domain analyses

For this and further analyses, we only used data from the *different faces* condition which generated the largest responses both in scalp and intracerebral recordings. Each recording sequence from 17 to 67 s relative to sequence onset was divided into epochs of 1 s duration centered on the appearance of a face. Epochs containing blinks were rejected and remaining epochs were averaged and the mean amplitude was centered on zero (dc correction).

2.4.3 | Correlation between intracerebral and scalp EEG signals

We examined the relationship between visually-driven signal recorded at intracerebral contacts relative to scalp electrodes by correlating the

variations of the 6 Hz response amplitude over time across all scalp electrodes and intracerebral contacts (Figure 3).

We first applied a Morlet wavelet transform on the raw signal to compute the time-varying amplitude envelope of the electrophysiological signal around 6 Hz. The parameters of the mother wavelet (central frequency: 6 Hz, full width at half maximum [FWHM] in the frequency-domain = 0.8 Hz; FWHM in the time domain = 0.47 s) were chosen to provide a relatively high frequency resolution while preserving the dynamic in the amplitude variation over time. We kept the amplitude envelope from 15 to 69 s from each recording sequence and divided the envelope from each sequence in 9 segments of 6 s, resulting in 18 segments in total (2 sequences with 9 segments). Then, for each intracerebral contact, the signal in each segment was correlated (Pearson's coefficient) with the corresponding segment in each scalp electrode and the correlations were averaged across the 18 segments, resulting in a 27 (intracerebral) × 27 (scalp) correlation matrix. We also computed the across-segments *SD* of the correlation coefficients. We determined whether correlations were significantly different from zero using a randomization procedure in which, for each electrode, we randomly shuffled (5,000 times) the order of the 6 s segments prior to computing correlations and averaging the correlations across segments. For each intracerebral contact correlated with all scalp electrodes, we determined significance using a cluster-based correction (cluster-mass) for multiple comparisons (Maris & Oostenveld, 2007; Pernet, Latinus, Nichols, & Rousselet, 2015) with a cluster-forming threshold of $p < .05$. Note that the wavelet analysis used here removes the phase information so that the correlations across channels are only determined by the variation of amplitude across time at each channel. Disregarding the phase information for this inter-channel correlation analysis is crucial to avoid correlations being driven by simple phase coherence across channels triggered by a common stimulation.

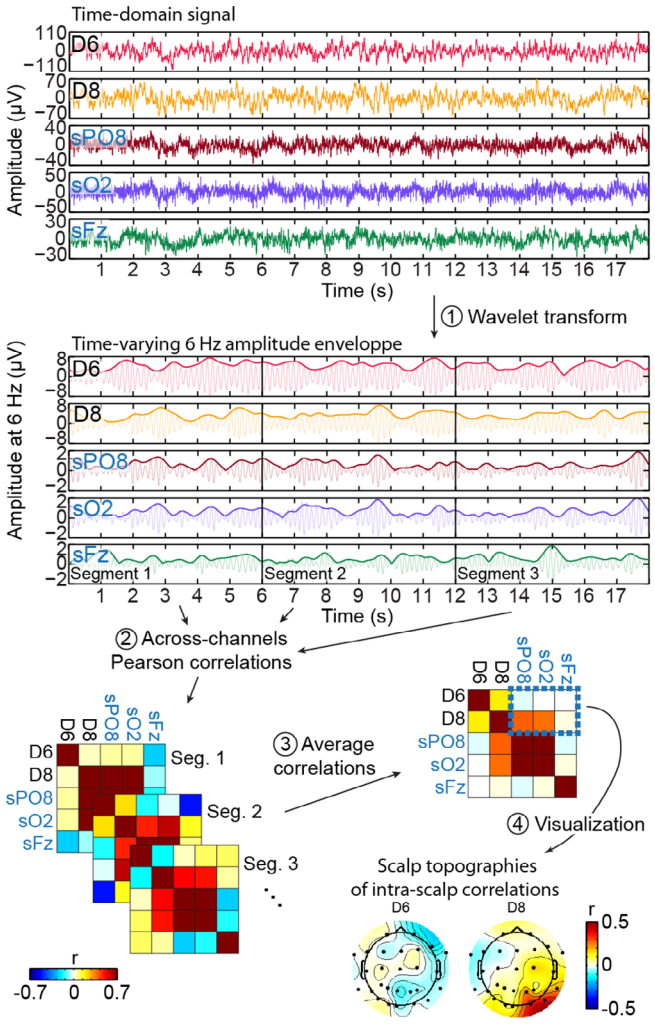

FIGURE 3 Procedure for correlating scalp and intracerebral 6 Hz signals during periodic face stimulation. (1) we apply a wavelet transform to the raw signal (top: 18 s of recording at two example intracerebral contacts –D6, D8- and three scalp electrodes – sPO8, sO2, sFz) to extract the variation of signal amplitude overtime at the 6 Hz frequency corresponding to the stimulation frequency (bottom: raw (s)EEG signal band-pass filtered from 5.9 to 6.1 Hz for illustration and 6 Hz wavelet amplitude envelope). This amplitude envelope is divided into segments of 6 s duration. (2) The signal in each segment is Pearson correlated across all channels. Here we show across-channels correlation matrices for the three segments displayed above. (3) Correlation coefficients computed for different segments are averaged and (4) correlations between individual intracerebral contacts and all scalp electrodes are visualized as scalp topographies. Last, statistics are performed to isolate significant correlations between intracerebral and scalp signals

Even if we observe significant scalp-intracerebral correlations, they could still occur because scalp and intracerebral channels are sensitive to the same electrophysiological responses (i.e., generated by a common cortical territory) unrelated to the FPVS stimulation. To determine whether the pattern of scalp-intracerebral correlations obtained using the original signal at the stimulation frequency during FPVS (*Ori@6 Hz*) is specific to the signal with visual stimulation, we compared this correlation pattern with patterns obtained in several control situations: (a) *NotchOri@6 Hz*: Pattern of scalp-intracerebral correlations with the visually-driven signal filtered-out from the original signal using a narrow notch filter (butterworth notch filter order 4: [5.9–6.1] Hz); (b) *Ori@4 Hz*: Pattern of correlations on the original signal using the amplitude envelope at another frequency than the stimulation frequency (i.e., 4 Hz); (c) *Rest@6 Hz*: Pattern of correlations obtained in (S)EEG recording where no periodic visual stimulation was presented and the patient was resting with eyes open. In this third control situation (rest), sections of the amplitude envelope corresponding to eye blinks were removed prior to computing the correlations. Correlations during rest were computed using 44 segments of 6 s.

We also used further benchmark tests for the control situations to evaluate the effect of notch filtering and of using a different analysis frequency on the correlation patterns. We reasoned that if the difference in the correlation patterns obtained in the *Ori@6 Hz* versus the control situations is due to the notch filtering or to the use of a different analysis frequency rather than to FPVS, then we should observe similar differences when applying notch filtering or using a different frequency on signal which does not contain a visually-driven

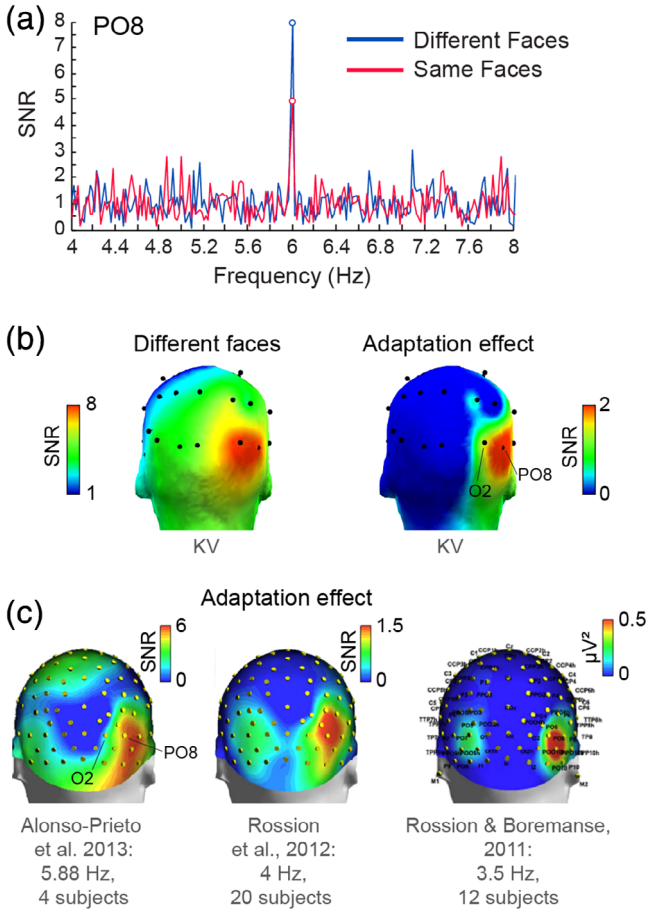

FIGURE 4 Scalp response to faces during FPVS in patient KV and healthy participants. (a). SNR transformation of the frequency amplitude spectrum (4 to 8 Hz) at one right-hemispheric OT scalp electrodes (SPO8) in patient KV. A response with high SNR is observed specifically at the 6 Hz stimulation frequency. (b) Patient KV's scalp topographical distribution showing the 6 Hz SNR response to faces in the "different face" condition (left) and the effect of identity adaptation/repetition suppression ("different faces" minus "same face," right). Both topographies display the largest response focused on the right OT region. (c) Scalp topographies in healthy normal participants (averages over different groups of participant) from multiple studies showing a dominance of the right hemispheric OT cortex in the effect of identity adaptation across multiple stimulation frequencies. In panel b, we purposely used the same colormap as in the topographies shown in panel c for best comparison

periodic response. The benchmark situations to evaluate the effect of notch-filtering on the patterns of correlations were the following: (a) *NotchOri@4 Hz*: correlations using amplitude envelope at 4 Hz when the original signal has been notched filtered at 4 Hz ([3.9–4.1] Hz); (b) *NotchRest@6 Hz*: correlations using amplitude envelope at 6 Hz when the signal during rest has been notched filtered at 6 Hz ([5.9–6.1] Hz). The benchmark situation to evaluate the effect of using the amplitude envelope at a different frequency was the following: (c) *Rest@4 Hz*: correlations using the amplitude envelope at 4 Hz from the signal recorded during rest.

The pattern of correlations in the original, control and benchmark situations were summarized and statistically compared by computing an index of right-hemispheric lateralization: we subtracted the correlations averaged over left-hemispheric OT scalp electrodes from the correlations averaged over corresponding electrodes in the right hemisphere (sO2, sPO8, sP4, and sP10). These indices were compared against zero and against each other using a permutation test (10,000 permutations).

3 | RESULTS

3.1 | Patient KV shows a significant and typical synchronization to 6 Hz face identity stimulation on the scalp

Fast periodic face stimulation generated robust and significant (z-score > 2.33, $p < .01$, one-tailed) visual responses over patient KV's scalp as evidenced by the distinct peak in the EEG spectrum at the 6 Hz stimulation frequency (Figure 4a). As in typical subjects (Alonso-Prieto et al., 2013; Rossion et al., 2012; Rossion & Boremanse, 2011), the EEG response in the *different faces* condition was clearly strongest over right OT electrodes (largest at sO2: 0.67 μV and sPO8: 0.63 μV). In addition, scalp topographies of the identity adaptation effect (i.e., larger amplitudes in the *different faces* relative to the *same face* conditions) revealed an even more focused positive difference at right OT electrodes (Figure 4b) with a maximum at sPO8 (0.23 μV). The adaptation effect was statistically significant at two scalp electrodes, sPO8 and sP10 (z-scores: 3.870 and 3.02, respectively; *ps* < .01, two-tailed). These observations largely replicate findings from healthy subjects using a similar experimental procedure (Alonso-Prieto et al., 2013; Rossion et al., 2012; Rossion & Boremanse, 2011; see also Liu-Shuang et al., 2014; Figure 4c), and suggest that patient KV's electrophysiological responses related to (unfamiliar) face individuation are typical. Further, this demonstrates that significant functional responses can be obtained from the scalp with the FPVS approach in single epileptic patient tested for a few minutes only.

3.2 | Corresponding spatial location of maximal response amplitude to faces between scalp and intracerebral EEG recordings

A detailed report of periodic intracerebral responses recorded in the *same face* and *different faces* conditions in patient KV's right OT cortex is described in Jonas et al. (2014). Here, for comparison with scalp recordings, we will summarize responses measured in the *different faces* condition and the effect of identity adaptation.

In intracerebral recordings, we found robust responses to the visual presentation of different faces at the 6 Hz stimulation frequency (Figure 5a,b) in ventral and lateral sections of the occipital and posterior temporal cortex. SEEG Responses were significantly above noise (all *zs* > 3.45, *ps* < .001) for all contacts except three adjacent

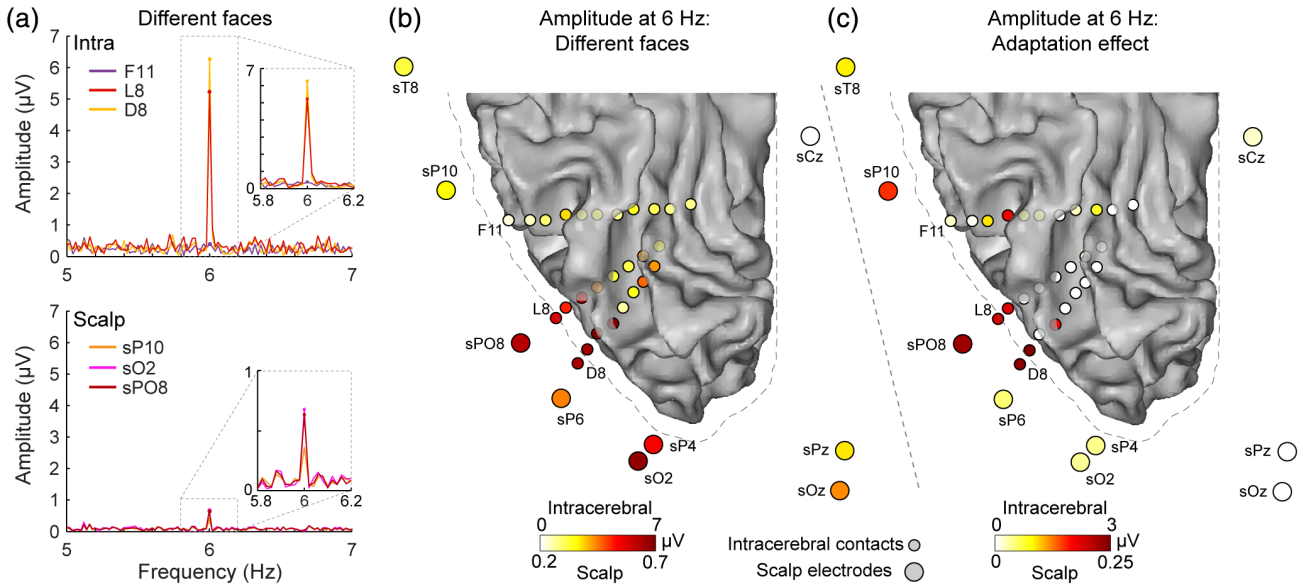

FIGURE 5 Intracerebral and scalp responses to faces in FPVS. (a) Amplitude spectrum (5–7 Hz) measured during FPVS at 6 Hz in the "different faces" condition at the three most external intracerebral contacts of electrodes F, D, and L (top), and at three right OT scalp electrodes closest to the intracerebral contacts shown above (bottom). The plots are displayed at the same amplitude scale to visualize the difference of amplitude between intracerebral and scalp recording of the same visual response. (b) Ventral view of the posterior half of the patient KV's right hemisphere (white matter surface, the gray matter surface is shown as a dotted gray outline) together with intracerebral contacts (small circles) and selected surrounding scalp electrodes (large circles). Channels are colored as a function of the amplitude of response at 6 Hz in the "different faces" condition. Note the difference in the color scale used for scalp and intracerebral data. (c) Same convention as for panel B but representing the effect of identity adaptation

contacts of electrode F (F9 to F11). The largest responses were measured in contacts located in the posterior section of the collateral sulcus (D1 to D5 and L1 to L5, amplitude range: 0.7 to 6.9 μV, mean amplitude: 2.8 μV, Figure 5b) and the lateral section of the inferior occipital gyrus (D6 to D8 and L6 to L8, amplitude range: 4.4 to 7.6 μV, mean amplitude: 5.8 μV). Responses in electrode F, going through the CoS (F1 to F5), occipitotemporal sulcus (F6 to F10) and posterior inferior temporal gyrus (F11) were overall much weaker (amplitude range: 0.4 to 2.5 μV, mean amplitude: 1.3 μV). SEEG responses also displayed a significant face identity adaptation effect (larger response in the *different faces* condition; $z > 2.33$, $p < .01$ Figure 5c) at contacts in or near the right lateral IOG (D5, D7, D8, L7, and L8: mean amplitude for different faces: 5.8 μV, mean amplitude for same face: 3.2 μV) or more anterior contacts in the CoS (F3) or in the OTS above the lateral fusiform gyrus (F7, F8, ~8 mm from the cortical surface of the lateral fusiform gyrus).

Importantly, there is a correspondence in the spatial location of intracerebral contacts and scalp electrodes showing the strongest response in the *different faces* condition, or the strongest effect of adaptation. First, in the *different faces* condition (Figure 5b), the scalp electrodes displaying the strongest scalp EEG responses were the closest to the intracerebral contacts in lateral IOG (sPO8, sO2, sP6, sP4 scalp electrodes; Euclidean distance to D8 = 27, 26, 32, and 43 mm, respectively; Euclidean distance to L8 = 28, 35, 33, and 46 mm, respectively). Second, the adaptation effect in intracerebral recording was maximally measured at two separate cortical locations: around the lateral IOG (D5, D7, D8, L7, and L8 contacts) and more anteriorly in the OTS above the lateral fusiform gyrus (F7, F8 contacts). Interestingly, this pattern of intracerebral response was associated with a maximal adaptation effect on the scalp over slightly more anterior electrodes (e.g., sP10) compared to the response in the *different faces* condition: scalp electrode sPO8 was closest to intracerebral contacts in the lateral IOG and scalp electrode sP10 was closest to intracerebral contacts in the lateral fusiform gyrus compared to contacts in lateral IOG (Euclidean distances from sP10 = 35 mm to F8, 45 mm to L8, and 51 mm to D8).

3.3 | Strong amplitude and SNR attenuation in scalp compared to intracerebral EEG

While we observed a spatial correspondence of the largest responses in scalp and intracerebral recordings, the amplitude measured on the scalp was very much attenuated relative to the intracerebral signal (Figure 5a, compare top and bottom plots). Indeed, relative to intracerebral contacts D8 and L8 where the amplitude at 6 Hz in the *different faces* condition was 6.3 and 5.2 μV respectively, the amplitudes at the closest scalp electrodes sO2 and sPO8 were 0.67 and 0.63 μV respectively, which is between 7.7 and 9.9 times smaller than the corresponding intracerebral signal. Interestingly, the SNR at the stimulation frequency (i.e., 6 Hz) was less attenuated than the absolute signal amplitude when comparing scalp to intracerebral recordings. SNR

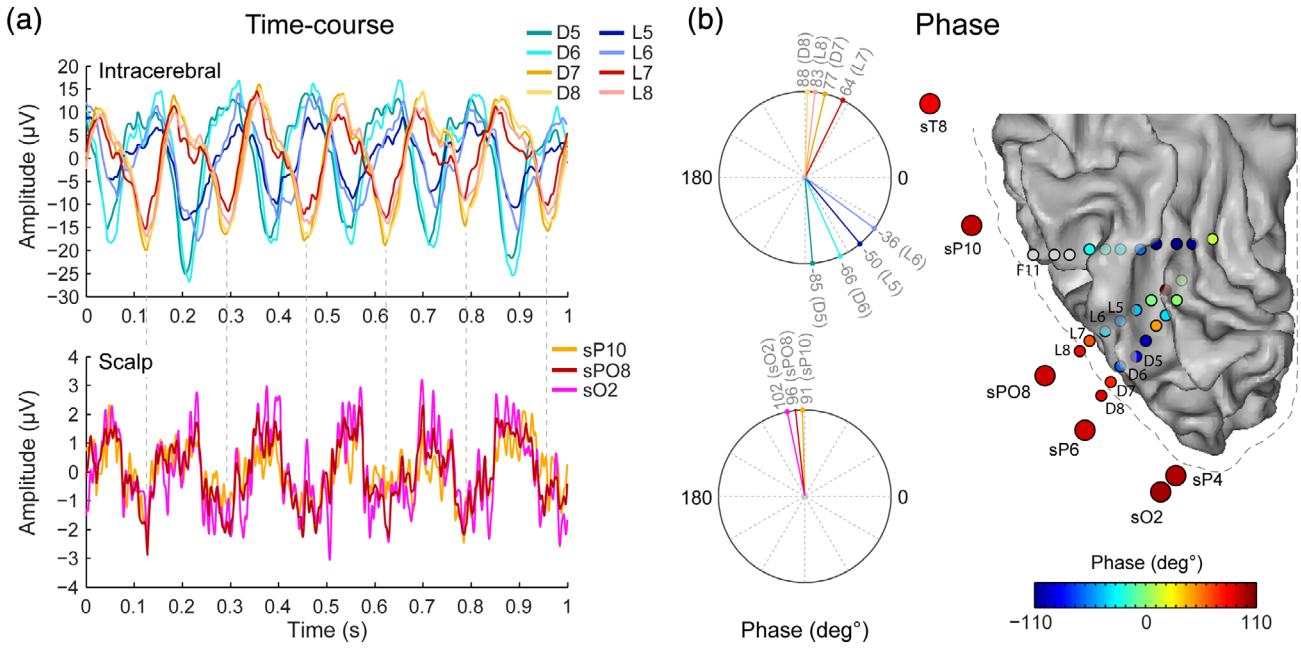

FIGURE 6 Time domain and phase responses in intracerebral and scalp FPVS responses. (a) Time domain representation of the FPVS responses to faces ("different faces" condition) in eight lateral intracerebral contacts of the L and D electrodes (top) and in three scalp electrodes over the right OT cortex (bottom) in the vicinity of the intracerebral contacts shown on top. We highlight these eight intracerebral contacts since they are the closest to scalp right OT electrodes, showed the highest 6 Hz response amplitude, and exhibited the closest correspondence with signal measured at right OT scalp electrodes. Plots were obtained by cutting the recordings during FPVS sequences in segments of 1 s and averaging over these segments. The waveforms manifest a sudden phase shift from most external contacts (D7–8, L7–8) to more internal contacts (D5-6, L5-6). (b) Left: Polar plot representations of the phase of responses at channels shown in panel a (see panel A for channel legend). Right: Ventral white-matter surface view of the posterior half of the patient KV's right hemisphere together with intracerebral contacts (small circles) and selected surrounding scalp electrodes (large circles). Channels are colored as a function of the phase of the response at 6 Hz in the "different faces" condition. Intracerebral contacts in gray (F9 to F11) showed no significant response to faces

was between 2 and 3.5 times lower in scalp (SNR = 8.3 and 8.1 for sO2 and sPO8, respectively) compared to intracerebral (SNR = 29 and 16.7 for D8 and L8, respectively) recordings. This is due to the signal amplitude being comparatively more attenuated from intracerebral to scalp recordings than the mean noise amplitude in frequency bins around 6 Hz (mean noise at D8/L8 = 0.26 μV; mean noise at sO2/sPO8 = 0.08 μV; ratio of intracerebral to scalp noise = 3.4).

3.4 | Focal correspondence between intracerebral and scalp EEG signals over the right occipitotemporal cortex

3.4.1 | Phase investigation

For the remainder of the analyses, we will focus on the signal measured in the *different faces* condition, as it generated the strongest responses over the right OT cortex, in contrast to the *same face* condition which generated low responses over OT regions and a maximal response over medial occipital regions (Supplementary Figure S1) as in previous publications (Alonso-Prieto et al., 2013; Rossion et al., 2012; Rossion & Boremanse, 2011). This latter condition is therefore sub-optimal to investigate the relationship between intracerebral and scalp responses in the OT region. Moreover, this avoids relying on a post hoc subtraction of conditions (i.e., adaptation effect), which provided an optimal opportunity to investigate the relationship between simultaneously recorded intracerebral and scalp EEG.

To further characterize the relationship between intracerebral and scalp recordings, we computed the phase of the signal at the stimulation frequency for intracerebral and scalp channels and visualized the signal in the time domain (Figure 6). Phase provides additional information about response timing and allows to further characterize the relationship between neighboring recording sites. For instance, perfect phase alignment or phase-reversal (i.e., 180° difference) at two separate recording sites is indicative of a common neural source generating the signal measured at the two sites. This revealed that although lateral contacts of the D and L electrodes (D5–D8 and L5–L8) all exhibited strong visual responses at the stimulation frequency (Figures 5 and 6), only the four most lateral contacts (D7–D8, L7–L8) were in phase with the signal measured at nearby scalp electrodes (Figure 6). The signal of adjacent—more medial—contacts (D5–D6, L5–L6) was out of phase relative to the more lateral contacts. This is clear when visualizing data in the time domain (Figure 6a), where the crests and troughs of the responses measured at the most lateral intracerebral contacts (D7–D8, L7–L8) are temporally aligned with responses measured at the scalp, but misaligned with signal measured

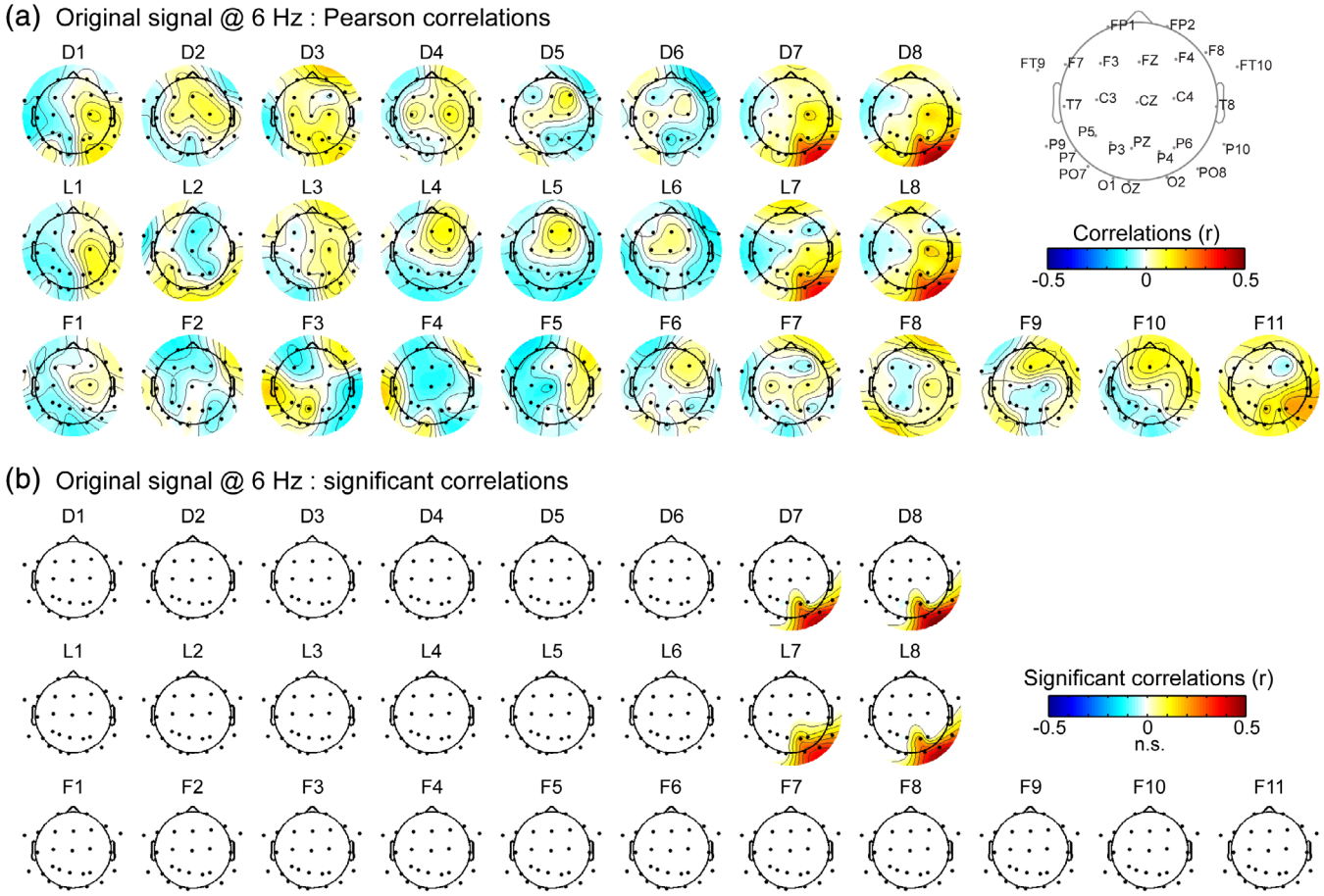

FIGURE 7 Correlations between intracerebral and scalp signals during FPVS. (a) Scalp topographical maps of the unthresholded Pearson correlation coefficients between the signal around 6 Hz measured at each intracerebral contact and each scalp electrode. Each map represents the correlations of one intracerebral contact with all scalp electrodes. Different intracerebral electrodes (D, L, F) are shown in rows and adjacent recording contacts are shown in columns (see Figure 1 for anatomical location of the contacts). (b) Topographical maps showing only significant correlation coefficients ($p < .05$, cluster-based correction for multiple comparisons). White indicates no significant correlation

at more medial contacts (D5–D6, L5–L6). This is also reflected in the phase of the frequency spectra (Figure 6b), where the phase values are similar between D8/L8 and right OT scalp electrodes (sO2, sPO8, sP10, mean phase difference: 11°), but very dissimilar between contiguous contacts D5–D6 and D7–D8 (mean phase difference: 158°) and between L5–L6 and L7–L8 (mean phase difference: 116°). The observation of only a partial phase opposition between these two groups of intracerebral contacts (i.e., rather than a phase difference close to 180°) suggests that the signal measured at these two groups arises from partly distinct generators. Only one of these neural generators, the generator contributing to the signal at lateral IOG contacts (D7–D8, L7–L8), also contributes to the EEG signal measured at OT scalp electrodes.

3.4.2 | Correlation investigation

To directly and formally quantify the relationship between scalp and intracerebral signals, we correlated the variations of the 6 Hz response amplitude over time across all scalp and intracerebral contacts (Figure 3, methods). As a reminder, this analysis disregards phase information so that only coordinated temporal variation of amplitude across channels could result in meaningful correlation coefficients. This was done to avoid correlations (positive or negative) driven simply by phase coherence across channels triggered by a common visual stimulation.

While the temporal variations of the amplitude of the 6 Hz response were strongly correlated between contacts D5–D6/L5–L6 and between contacts D7–D8/L7–L8, the 6 Hz signal was not correlated between these two groups of adjacent contacts. Specifically, correlations were high between contacts D5, D6, L5, and L6 (both within electrode: r = 0.84 ± 0.07 and 0.82 ± 0.13 for D5–D6 and L5–L6, respectively, and across the D and L electrodes: r = 0.5 ± 0.26 and 0.42 ± 0.22 for D5–L5 and D6–L6, respectively) and between contacts D7, D8, L7, and L8 (within electrode: r = 0.97 ± 0.03 and 0.76 ± 0.16 for D7–D8 and L7–L8, respectively, and across the D and L electrodes: r = 0.5 ± 0.23 and 0.68 ± 0.16 for D7–L7 and D8–L8, respectively). In contrast, there was no meaningful correlation between signals at immediately adjacent contacts D6–D7 (r = 0.08 ± 0.28) and L6–L7 (r = 0.02 ± 0.27). Thus, these analyses support our

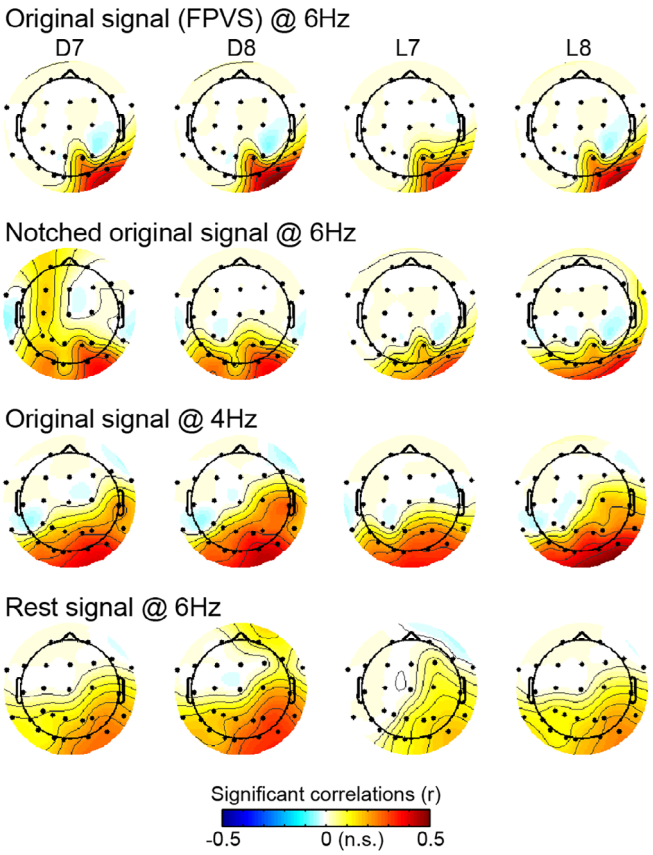

FIGURE 8 Correlations between scalp and intracerebral signals during FPVS and control situations. Topographical maps of significant correlations ($p < .05$, cluster-based correction for multiple comparisons) between signal at four intracerebral contacts in the lateral IOG and scalp electrodes. Maps of correlations are shown when using the original signal at around 6 Hz during FPVS (Ori@6 Hz, top row), when using signal in which the visually-driven signal has been filtered-out (NotchOri@6 Hz, second row), when using another frequency (4 Hz) than the stimulation frequency (Ori@4 Hz, third row), and when using 6 Hz signal recorded during rest (Rest@6 Hz, bottom row)

view that despite the partial phase opposition between contacts D5–D6/L5–L6 and contacts D7–D8/L7–L8 (Figure 6), the signal measured at these two groups of contacts arises from different cortical generators.

In addition, these analyses confirmed and refined our observation above that signal measured at right OT scalp electrodes arises mainly from regions in the lateral IOG around contacts D7–D8 and L7–L8 rather than from more medial cortical regions around contacts D5–D6, L5–L6. Indeed, we observed a very focal pattern of positive correlations between contacts D/L 7–8 and right OT scalp electrodes closest to the location of the corresponding intracerebral contacts (Figure 7a). Statistical analyses indicated that the 6 Hz signal at each of these four intracerebral contacts was significantly correlated with a cluster of 4 to 5 scalp electrodes. D7, D8, L7, and L8 were each significantly correlated with sPO8, sO2, sP10, and sP4, and L7 was also significantly correlated with sP6. Among these channels, Pearson's coefficients ranged from 0.32 (*SD* across segments: ± 0.25) to 0.37 ± 0.23 for sPO8, from 0.28 ± 0.28 to 0.36 ± 0.22 for sO2, from 0.19 ± 0.22 to 0.25 ± 0.19 for sP4 and from 0.17 ± 0.29 to 0.21 ± 0.31 for sP10. In contrast, correlations of the same scalp electrodes with intracerebral contacts D5–D6, L5–L6 were around zero (range of correlations: −0.11 ± 0.25 to −0.02 ± 0.22). Moreover, these positive correlations were restricted to the right hemisphere: the correlations for contacts D7–D8, L7–L8 with electrodes in the OT left hemisphere (sO1, sPO7, sP9, sP7) ranged from −0.08 to 0.11 (mean r = 0.01 ± 0.24).

Correlations were slightly but significantly higher ($t[8] = 7.6$, $p < .001$) for the most external contact (D8, L8, mean r across channels: 0.28) relative to the immediately adjacent more internal contact (D7, L7, mean r across channels: 0.25).

Over the more anterior F electrode, only the signal from F11 tended to be correlated with surrounding scalp electrodes (Figure 7a, sP10: r = 0.2 ± 0.25; sP6: r = 0.2 ± 0.3; sPO8: r = 0.18 ± 0.33; sT8: r = 0.14 ± 0.3). However, these correlations did not reach significance at the cluster level.

3.5 | Focal and right-lateralized intracerebral-scalp correlations are specific to the FPVS signal

The observed correlations suggest that these scalp and intracerebral channels pick up electrophysiological responses coming from the same cortical region responding to the periodic visual stimulation. However, these correlations may also be driven by a general electrophysiological activity (i.e., unrelated to the stimulation) coming from cortical territories to which both intracerebral contacts and scalp electrodes are sensitive to, given their spatial proximity. If this is the case, we should observe the same correlation pattern with or without the presence of a visually-driven response in the recorded electrophysiological signal. We, therefore, compared the patterns of scalp-intracerebral correlations obtained at the stimulation frequency during periodic visual stimulation (*Ori@6 Hz*) with a series of "control" situations: (a) *NotchOri@6 Hz*: Pattern of correlations when the visually-driven signal has been selectively filtered-out; (b) *Ori@4 Hz*: Pattern of correlations at another frequency than the stimulation frequency (4 Hz); (c) *Rest@6 Hz*: Pattern of correlations obtained using 6 Hz signal recorded during a rest period. These analyses revealed that intracerebral-scalp correlations were more focal when a visually-driven periodic response was present in the electrophysiological signal. Specifically, in the three control conditions, while the patterns of scalp correlations measured for intracerebral contacts D7–D8 and L7–L8 were overall similar to the one observed at 6 Hz using the original signal, these patterns were all more widespread and included significant correlations on the scalp both in the right and the left hemisphere (Figure 8). This observation was reflected in the larger number of scalp electrodes significantly correlated with each intracerebral contacts—D7, D8, L7, and L8—in the three control situations (mean number of significant scalp electrodes across D7, D8, L7, and L8 = 9.25 to 14.5, Figure 9a) compared to the original FPVS condition

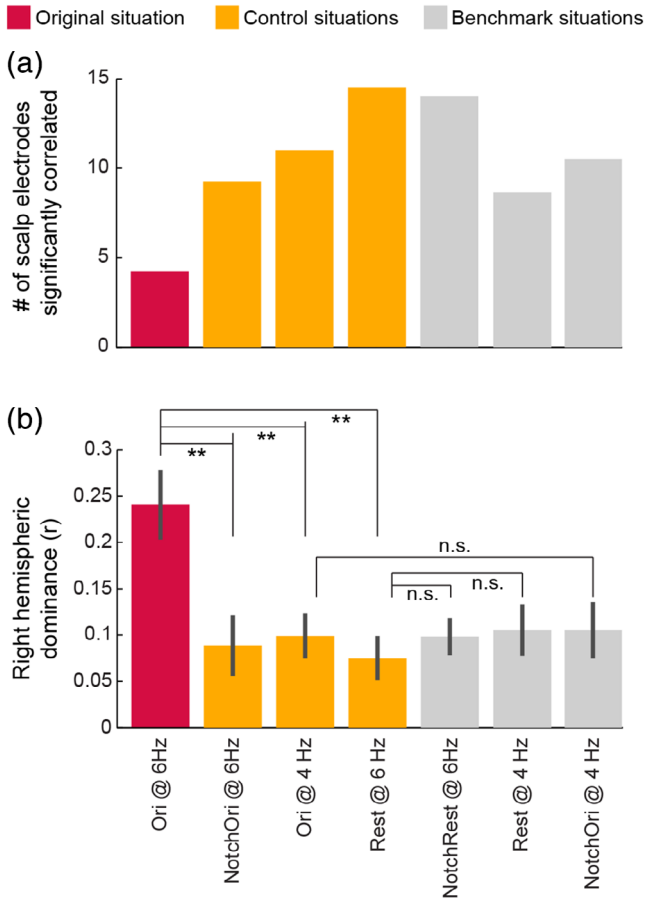

FIGURE 9 Scalp-intracerebral correlations are more focal and right-lateralized during the periodic presentation of faces. (a) The bars represent the number of scalp electrodes significantly correlated with intracerebral signal averaged over contacts D7, D8, L7, L8 in the original, control, and benchmark situations. A lower number means fewer scalp electrodes were significantly correlated with intracerebral signal. (b). The bars represent the difference in scalp-intracerebral correlations between posterior right- and left-lateralized scalp electrodes in the original, control, and benchmark situations. Correlations between scalp electrode and intracerebral contacts D7, D8, L7, L8 were first averaged across intracerebral contacts, then averaged separately for right and left posterior scalp electrodes, and finally averaged correlations in the two groups were subtracted (right minus left). Error bars represent the *SE* of the mean across the 18 segments used to compute correlations. The correlations are higher in the right hemisphere for all comparisons but the right-hemisphere dominance is significantly larger (all *p*'s < .005) for the original FPVS condition. In contrast, the comparisons across control and corresponding benchmark situations are not significant

(*Ori@6 Hz*: 4.25 significant scalp electrodes). In addition, the right hemispheric dominance of the correlations pattern when using the original signal at 6 Hz was assessed and compared to control conditions by subtracting the correlations averaged over left-hemispheric OT scalp channels from the correlations averaged over corresponding electrodes in the right hemisphere (sO2, sPO8, sP4, sP10). This revealed that, while scalp correlations were significantly stronger in the right than in the left hemisphere in all conditions (all *p*'s < .02, one-tailed permutation test, Figure 9b), the right hemispheric dominance was significantly stronger when using the signal at 6 Hz in the original signal where periodic visual stimulation is present (*Ori@6 Hz*: right hemispheric dominance = 0.24 ± 0.16) compared to the three control situations (0.09 ± 0.14, 0.1 ± 0.1, 0.1 ± 0.13, all *p*'s < .005, one-tailed permutation test). In contrast, there was no significant difference among any of the control and additional benchmark situations (*p*'s > 0.5, Figure 9b, see methods for benchmark situations).

4 | DISCUSSION

This study shows that a few minutes of periodic visual stimulation suffice to generate a robust signal, objectively identifiable at the exact frequency of stimulation (and harmonics) in the frequency spectrum of both SEEG and EEG signals recorded simultaneously. Here we find in the single epileptic patient tested that the response peaks over the right occipitotemporal scalp region, as in neurotypical participants tested with this paradigm (Figure 4), suggesting the generalizability of the present observations to the normal population. By combining FPVS with correlation analyses we thus provide an original approach to investigate the relationship between functional brain electrophysiological activity measured simultaneously inside the brain and on the scalp.

Quantification of the 6 Hz response in the frequency domain is straightforward and reveals a tenfold decrease of amplitude at 6 Hz between the most external intracerebral contacts and the nearest scalp EEG electrodes (i.e., 25–30 mm), providing unique information about skull attenuation of electrophysiological activity (Oostendorp, Delbeke, & Stegeman, 2000; Wendel, Vaisanen, Seemann, Hyttinen, & Malmivuo, 2010). The choice of the 6 Hz stimulation frequency was dictated by previous studies showing robust responses at this frequency for face stimulation, in particular when different face identities are presented at every stimulation cycle (Alonso-Prieto et al., 2013). Note that this attenuation might even be underestimated, given that the intracranial sampling was limited and that larger responses might have been found at other nearby locations inside the brain. Nevertheless, the attenuation in SNR between intracerebral and surface EEG responses was of "only" 2–3.5. This reduced ratio indicates that the electrophysiological noise, as computed as in the present study, is significantly larger inside than outside the brain. A major factor contributing to this reduction of the ratio between amplitudes and SNR is that, rather than being computed over a pre-stimulus baseline as in standard ERP studies, electrophysiological noise is computed here within a small theta range frequency around the signal of interest that is, 6 Hz (Meigen & Bach, 1999; Rossion et al., 2012; Srinivasan, Russell, Edelman, & Tononi, 1999). Hence, EEG noise is "free" of alpha activity, environmental noise, eye and muscle artifacts, and so forth which typically greatly contaminate scalp EEG signals (Luck, 2014). Additionally, the cortical surface to which an EEG scalp electrode is sensitive to is likely larger than that of an SEEG electrode. Noise in scalp EEG might thus be smaller

compared to SEEG by virtue of averaging uncorrelated electrophysiological "noise" over a larger surface.

The narrow band of the 6 Hz signal allows objective and finer-grained tracking of the phase and identification of the intracerebral electrodes generating that signal on the scalp. Using FPVS in relation with our correlation approach, we found that activity recorded over right OT scalp regions directly relates to the activity measured at intracerebral contacts located in the inferior occipital gyrus either in the cortex (D7, L7, L8) or in the meninges (D8). This latter intracerebral contact likely receives electrical field propagation from the nearby cortex (i.e., about 2 mm distance) (Zaveri, Duckrow, & Spencer, 2009). This strongly suggests that one major neural source for the 6 Hz FPVS signal measured on the scalp is located in the inferior occipital gyrus at or near contacts D7–D8 and L7–L8. Other sources in neighboring location likely also contribute to the measured scalp activity, but they could not be captured here due to the limited intracerebral sampling in the clinical case. Nevertheless, the main contribution of lateral brain sources to scalp EEG by comparison to medial sources is in line with previous studies in epilepsy and especially in mesial temporal lobe epilepsy (Koessler et al., 2015; Merlet et al., 1998).

The identification of the right OT scalp region is similar to our findings in a previous study measuring the relationship between the face-evoked N170 potential on the scalp and in the cortex in the same epileptic patient (Jacques et al., 2019). However, this relationship was relatively more widespread on the scalp in the previous ERP study (see Figures 5 and 6 in Jacques et al., 2019) compared to the current study. Specifically, in the previous study, significant correlations involved up to six scalp electrodes (right OT and medial occipital) when correlating N170 latency and up to 11 scalp electrodes (bilateral OT and medial occipital) when correlating N170 amplitude, while the relationship found here with the frequency-tagging approach was restricted to four scalp electrodes (Figure 7).

Notwithstanding this comparison across studies of the spatial spread of the correlations on the scalp, it should be noted that differences in the experimental design, in the type of signal used to compute the correlations and in the analyses schemes prevent a more formal comparison across the current and the previous study. For instance, in the current study, the use of FPVS allows taking into account the amplitude variations in a relatively narrow frequency range (i.e., around 6 Hz), which is less affected by ongoing broadband EEG noise (mostly in the theta and alpha range) compared to when using the ERP signal as in the previous study. Such broadband noise in the ERP signal may be correlated across a large cortical surface (e.g., Buzsáki, 2002; Klimesch, 1999; Miller, Foster, & Honey, 2012), therefore being picked up simultaneously by intracerebral contacts in the IOG and by many posterior scalp electrodes, resulting in a broad correlation pattern on the scalp. Therefore, while the cortical regions involved in generating the N170 and the 6 Hz FPVS face signals are likely similar given the overall similarity in the scalp topographies of the correlations (irrespective of their spatial spread) across the two studies, the FPVS approach allows revealing a more focused relationship between scalp and intracerebral recordings.

In addition, we demonstrate that the relationship between scalp and intracerebral channels at 6 Hz is significantly more focal and right-lateralized during FPVS as compared to rest EEG or during stimulation but considering a frequency range outside the stimulation frequency (i.e., around 4 Hz). Hence, this relationship is specific to the stimulation frequency and cannot be attributed to general factors such as an increase of arousal during visual stimulation for instance. Moreover, other benchmark control situations (Figure 9) further indicate that the specificity of this relationship during FPVS is not driven by analyses or testing parameters. Note that since we did not stimulate with other frequencies, whether 6 Hz provides the tightest correlation between scalp and intracerebral activity cannot be determined in the present study—although this is likely given the particularly large response that it generates in this paradigm (Alonso-Prieto et al., 2013).

A peculiar observation is the broader pattern of correlations for control situations, such as when using a different frequency of analysis (i.e., Ori@4 Hz), compared to when using FPVS. One might have expected no or reduced correlations in control situations when no visual response is present in the signal at the frequency of analyses. The observation of a correlation for the control situations likely stems from the close spatial proximity between scalp right OT electrodes and the most lateral intracerebral contacts, which makes it likely that these recording channels are sensitive to a similar cortical territory. This would result in correlations across channels inside the brain and on the scalp stemming from the fact that they are sensitive to the same ongoing cortical EEG activity unrelated to a visual response (i.e., "noise"). As indicated above, this EEG "noise" in the theta and alpha range (e.g., Buzsáki, 2002; Klimesch, 1999; Miller et al., 2012) is more likely to correlate across a larger brain surface than neural signal related to the visual stimulation, therefore being measured over a broader scalp surface. This would yield patterns of correlations that are more broadly distributed on the scalp over both hemispheres. This phenomenon is also likely to take place in the control situation where the visually-driven signal at 6 Hz was removed using a very narrow notch filter (i.e., NotchOri@6 Hz). In this particular situation, one possibility is that when the visually-driven 6 Hz signal is filtered out, the variations of the wavelet amplitude envelope across time (which is used to obtain the correlations) are related to other frequencies around 6 Hz (i.e., theta range) that fall within the frequency bandwidth of the wavelet at 6 Hz (full width at half maximum in the frequency-domain at 6 Hz is 0.8 Hz), resulting in broad scalp correlation patterns. In contrast, when visually-driven signal at 6 Hz is present (Ori@6 Hz), it completely dominates over surrounding frequencies in the amplitude envelope, allowing to reveal the more local neural activity specifically related to face periodic stimulation.

Several studies (Cosandier-Rimele, Merlet, Badier, Chauvel, & Wendling, 2008; Ebersole, 1997; Ramantani et al., 2014; Tao, Ray, Hawes-Ebersole, & Ebersole, 2005) have shown that a large cortical surface from 6 to 30 cm^2 is required to generate detectable scalp EEG signals. According to a recent computational study (Cosandier-Rimele et al., 2008), a cortical surface of 26cm^2 is required to obtain a SNR equal to eight in scalp EEG, corresponding roughly to the SNR

observed in our study. However, the FPVS approach is known to generate extremely high SNR responses on the scalp, so that more focal sources in the lateral section of the inferior occipital gyrus, corresponding to smaller cortical patches, may have been sufficient to generate this response. While fMRI studies indicate that the (right) IOG plays a key role in (unfamiliar) face individuation responses in the human brain (e.g., Gauthier, Tarr, Moylan, Skudlarski, & Gore, 2000; Schiltz et al., 2006), these responses are not confined to this region but extend to more anterior regions of the lateral fusiform gyrus. Although these regions may also contribute to the signal recorded on the scalp, the cortical orientation of the lateral fusiform gyrus makes it unlikely for this region to majorly contributes to the EEG measured over lateral OT cortex scalp regions (Jacques et al., 2019).

While simultaneous scalp and intracerebral studies very often rely on relatively complex signal processing methods (e.g., blind source separation) to extract biomarkers from scalp background activity (Koessler et al., 2015; Pizzo et al., 2019), the spontaneous visibility (i.e., even without averaging method or baseline correction method) of the scalp responses during FPVS highlights the interest of this approach to clarify the scalp EEG correlates of focal cortical generators. Therefore, compared to signal analysis performed in time domain and on spontaneous activity (like epileptic spikes or seizures), FPVS in combination with our correlation approach may represent a major tool in order to understand and characterize the link between cortical source activity and scalp EEG signals. Moreover, our observation of robust intracerebral vs. scalp EEG correlations with just two sequences of stimulation (2 × 50 s of data) is a clear advantage over more conventional stimulation approach in clinical settings where these recordings take place. Given that we report data from a single patient implanted with three intracerebral electrode arrays, this approach should be further validated to ensure its applicability in different experimental research domains and settings. Nevertheless, the frequency-tagging approach is readily used to measure a wide range of responses in the visual domain (e.g., to luminance or contrast changes, but also visual words, quantities, or objects, Norcia et al., 2015) and in other modalities (e.g., low-level and high-level auditory responses: Fujiki, Jousmaki, & Hari, 2002; Nozaradan, Peretz, Missal, & Mouraux, 2011; somatosensory responses: Colon, Legrain, Huang, & Mouraux, 2015), as well as their modulation by attentional factors (Chen, Seth, Gally, & Edelman, 2003; Colon et al., 2015; Morgan, Hansen, & Hillyard, 1996; Yan, Liu-Shuang, & Rossion, 2019). This suggests that the original approach introduced here could be extended to larger samples of individual brains and other brain functions, pending appropriate adaptation in the stimulation and analyses parameters. Moreover, this approach could be extended to understand functional connectivity between intracerebral contacts in close or remote regions with a wider sampling across the brain.

ACKNOWLEDGMENTS

This work was supported by the Belgian Fonds National de la Recherche Scientifique (FNRS –PDR T.0207.16), Fédération Wallonie-Bruxelles under Grant No. ARC 13/18–053, and the Fondation Louvain.

DATA AVAILABILITY STATEMENT

The data that support the findings of this study are available from the corresponding author upon reasonable request.

ORCID

Corentin Jacques https://orcid.org/0000-0001-8917-4346

ENDNOTE

[1] A recent study recorded 48-channel ECoG and 27-channel scalp-EEG data simultaneously during light flickering in a single patient (Wittevrongel et al., 2018). However, due to insufficient quality of the simultaneously recorded scalp-EEG (dried conductive gel, as well as the influence of scarred and swollen tissue with the particularly invasive ECoG procedure), the patient's scalp-EEG was excluded from further analysis.

REFERENCES

Adrian, E. (1944). Brain rythms. *Nature*, *153*, 360–362.

Adrian, E., & Matthews, B. (1934). The Berger rhythm: Potential changes from the occipital lobes in man. *Brain*, *57*, 355–385.

Alarcon, G., Guy, C. N., Binnie, C. D., Walker, S. R., Elwes, R. D., & Polkey, C. E. (1994). Intracerebral propagation of interictal activity in partial epilepsy: Implications for source localisation. *Journal of Neurology, Neurosurgery, and Psychiatry*, *57*, 435–449. https://doi.org/10.1136/jnnp.57.4.435

Allison, T., Puce, A., Spencer, D. D., McCarthy, G., & Belger, A. (1999). Electrophysiological studies of human face perception. I: Potential generated in occiptotemporal cortex by face and non-face stimuli. *Cerebral Cortex*, *9*, 415–430.

Alonso-Prieto, E., Van Belle, G., Liu-Shuang, J., Norcia, A. M., & Rossion, B. (2013). The 6 Hz fundamental stimulation frequency rate for individual face discrimination in the right occipito-temporal cortex. *Neuropsychologia*, *51*, 2863–2875. https://doi.org/10.1016/j.neuropsychologia.2013.08.018

Barbeau, E. J., Taylor, M. J., Regis, J., Marquis, P., Chauvel, P., & Liégeois-Chauvel, C. (2008). Spatio temporal dynamics of face recognition. *Cerebral Cortex*, *18*, 997–1009. https://doi.org/10.1093/cercor/bhm140

Buzsáki, G. (2002). Theta oscillations in the hippocampus. *Neuron*, *33*, 325–340. https://doi.org/10.1016/s0896-6273

Chauvel, P., Gonzalez-Martinez, J., & Bulacio, J. (2019). Presurgical intracranial investigations in epilepsy surgery. *Handbook of Clinical Neurology*, *161*, 45–71. https://doi.org/10.1016/B978-0-444-64142-7.00040-0

Chen, Y., Seth, A. K., Gally, J. A., & Edelman, G. M. (2003). The power of human brain magnetoencephalographic signals can be modulated up or down by changes in an attentive visual task. *Proceedings of the National Academy of Sciences of the United States of America*, *100*, 3501–3506. https://doi.org/10.1073/pnas.0337630100

Coito, A., Biethahn, S., Tepperberg, J., Carboni, M., Roelcke, U., Seeck, M., … Vulliemoz, S. (2019). Interictal epileptogenic zone localization in patients with focal epilepsy using electric source imaging and directed functional connectivity from low-density EEG. *Epilepsia Open*, *4*, 281–292. https://doi.org/10.1002/epi4.12318

Colon, E., Legrain, V., Huang, G., & Mouraux, A. (2015). Frequency tagging of steady-state evoked potentials to explore the crossmodal links in spatial attention between vision and touch. *Psychophysiology*, *52*, 1498–1510. https://doi.org/10.1111/psyp.12511

Cosandier-Rimele, D., Merlet, I., Badier, J. M., Chauvel, P., & Wendling, F. (2008). The neuronal sources of EEG: Modeling of simultaneous scalp

and intracerebral recordings in epilepsy. *NeuroImage*, *42*, 135–146. https://doi.org/10.1016/j.neuroimage.2008.04.185

Dawson, G. D. (1951). A summation technique for detecting small signals in a large irregular background. *The Journal of Physiology*, *115*, 2p–3p.

Dubarry, A., Badier, J., Fonseca, A. T., Gavaret, M., Carron, R., Bartolomei, F., … Bénar, C. G. (2014). Simultaneous recording of MEG, EEG and intracerebral EEG during visual stimulation: From feasibility to single-trial analysis. *NeuroImage*, *99*, 548–558. https://doi.org/10.1016/j.neuroimage.2014.05.055

Ebersole, J. S. (1997). Defining epileptogenic foci: past, present, future. *Journal of Clinical Neurophysiology: Official Publication of the American Electroencephalographic Society.*, *14*, 470–483.

Fujiki, N., Jousmaki, V., & Hari, R. (2002). Neuromagnetic responses to frequency-tagged sounds: A new method to follow inputs from each ear to the human auditory cortex during binaural hearing. *The Journal of Neuroscience*, *22*, RC205.

Gauthier, I., Tarr, M.J., Moylan, J., Skudlarski, P., Gore, J.C., & Anderson, A W. (2000). The fusiform "face area" is part of a network that processes faces at the individual level. *Journal of Cognitive Neuroscience 12*, 495–504. https://doi.org/10.1162/089892900562165

Gavaret, M., Badier, J.-M., Marquis, P., Bartolomei, F., & Chauvel, P. (2004). Electric source imaging in temporal lobe epilepsy. *Journal of Clinical Neurophysiology*, *21*, 267–282.

Gavaret, M., Dubarry, A., Carron, R., & Bartolomei, F. (2016). Simultaneous SEEG-MEG-EEG recordings overcome the SEEG limited spatial sampling. *Epilepsy Research*, *128*, 68–72. https://doi.org/10.1016/j.eplepsyres.2016.10.013

Gentile, F., & Rossion, B. (2014). Temporal frequency tuning of cortical face-sensitive areas for individual face perception. *NeuroImage*, *90*, 256–265. https://doi.org/10.1016/j.neuroimage.2013.11.053

Goncalves, S. I., de Munck, J. C., Verbunt, J. P. A., Bijma, F., Heethaar, R. M., & Lopes da Silva, F. (2003). In vivo measurement of the brain and skull resistivities using an EIT-based method and realistic models for the head. *IEEE Transactions on Bio-Medical Engineering*, *50*, 754–767.

Grech, R., Cassar, T., Muscat, J., Camilleri, K. P., Fabri, S. G., Zervakis, M., … Vanrumste, B. (2008). Review on solving the inverse problem in EEG source analysis. *Journal of Neuroengineering and Rehabilitation*, *5*, 25. https://doi.org/10.1186/1743-0003-5-25

Halgren, E., Baudena, P., Heit, G., Clarke, J. M., Marinkovic, K., & Clarke, M. (1994). Spatio-temporal stages in face and word processing. I. Depth-recorded potentials in the human occipital, temporal and parietal lobes. *Journal of Physiology*, *88*, 1–50.

Jacques, C., Jonas, J., Maillard, L., Colnat-Coulbois, S., Koessler, L., & Rossion, B. (2019). The inferior occipital gyrus is a major cortical source of the face-evoked N170: Evidence from simultaneous scalp and intracerebral human recordings. *Human Brain Mapping*, *40*, 1403–1418. https://doi.org/10.1002/hbm.24455

Jacques, C., Witthoft, N., Weiner, K. S., Foster, B. L., Rangarajan, V., Hermes, D., … Grill-Spector, K. (2016). Corresponding ECoG and fMRI category-selective signals in human ventral temporal cortex. *Neuropsychologia*, *83*, 14–28. https://doi.org/10.1016/j.neuropsychologia.2015.07.024

Jonas, J., Jacques, C., Liu-shuang, J., Brissart, H., Colnat-coulbois, S., & Maillard, L. (2016). A face-selective ventral occipito-temporal map of the human brain with intracerebral potentials. *Proceedings of the National Academy of Sciences of the United States of America*, *113*, E4088–E4097. https://doi.org/10.1073/pnas.1522033113

Jonas, J., Rossion, B., Krieg, J., Koessler, L., Colnat-Coulbois, S., Vespignani, H., … Maillard, L. (2014). Intracerebral electrical stimulation of a face-selective area in the right inferior occipital cortex impairs individual face discrimination. *NeuroImage*, *99*, 487–497. https://doi.org/10.1016/j.neuroimage.2014.06.017

Kaiboriboon, K., Luders, H. O., Hamaneh, M., Turnbull, J., & Lhatoo, S. D. (2012). EEG source imaging in epilepsy- -practicalities and pitfalls. *Nature Reviews. Neurology*, *8*, 498–507. https://doi.org/10.1038/nrneurol.2012.150

Klimesch, W. (1999). EEG alpha and theta oscillations reflect cognitive and memory performance: A review and analysis. *Brain Research. Brain Research Reviews*, *29*, 169–195.

Koessler, L., Benar, C., Maillard, L., Badier, J. M., Vignal, J. P., Bartolomei, F., … Gavaret, M. (2010). Source localization of ictal epileptic activity investigated by high resolution EEG and validated by SEEG. *NeuroImage*, *51*, 642–653. https://doi.org/10.1016/j.neuroimage.2010.02.067

Koessler, L., Cecchin, T., Colnat-Coulbois, S., Vignal, J.-P., Jonas, J., Vespignani, H., … Maillard, L. G. (2015). Catching the invisible: Mesial temporal source contribution to simultaneous EEG and SEEG recordings. *Brain Topography*, *28*, 5–20. https://doi.org/10.1007/s10548-014-0417-z

Koessler, L., Colnat-Coulbois, S., Cecchin, T., Hofmanis, J., Dmochowski, J. P., Norcia, A. M., & Maillard, L. G. (2017). In-vivo measurements of human brain tissue conductivity using focal electrical current injection through intracerebral multicontact electrodes. *Human Brain Mapping*, *38*, 974–986. https://doi.org/10.1002/hbm.23431

Kovach, C. K., Oya, H., & Kawasaki, H. (2018). The bispectrum and its relationship to phase-amplitude coupling. *NeuroImage*, *173*, 518–539. https://doi.org/10.1016/j.neuroimage.2018.02.033

Lantz, G., Holub, M., Ryding, E., & Rosen, I. (1996). Simultaneous intracranial and extracranial recording of interictal epileptiform activity in patients with drug resistant partial epilepsy: Patterns of conduction and results from dipole reconstructions. *Electroencephalography and Clinical Neurophysiology*, *99*, 69–78. https://doi.org/10.1016/0921-884x

Liu-Shuang, J., Norcia, A. M., & Rossion, B. (2014). An objective index of individual face discrimination in the right occipito-temporal cortex by means of fast periodic oddball stimulation. *Neuropsychologia*, *52*, 57–72. https://doi.org/10.1016/j.neuropsychologia.2013.10.022

Lochy, A., Van Belle, G., & Rossion, B. (2015). A robust index of lexical representation in the left occipito-temporal cortex as evidenced by EEG responses to fast periodic visual stimulation. *Neuropsychologia*, *66*, 18–31. https://doi.org/10.1016/j.neuropsychologia.2014.11.007

Lopes da Silva, F. (2013). EEG and MEG: Relevance to neuroscience. *Neuron*, *80*, 1112–1128. https://doi.org/10.1016/j.neuron.2013.10.017

Lopes da Silva, F. H. (2019). Intracerebral sources reconstructed on the basis of high-resolution scalp EEG and MEG. *Brain Topography*, *32*, 523–526. https://doi.org/10.1007/s10548-019-00717-9

Luck, S. J. (2014). *An introduction to the event-related potential technique* (2nd ed.). Cambridge, MA: MIT Press.

Malmivuo, J. A., & Suihko, V. E. (2004). Effect of skull resistivity on the spatial resolutions of EEG and MEG. *IEEE Transactions on Bio-Medical Engineering*, *51*, 1276–1280. https://doi.org/10.1109/TBME.2004.827255

Maris, E., & Oostenveld, R. (2007). Nonparametric statistical testing of EEG- and MEG-data. *Journal of Neuroscience Methods*, *164*, 177–190. https://doi.org/10.1016/j.jneumeth.2007.03.024

Meigen, T., & Bach, M. (1999). On the statistical significance of electrophysiological steady-state responses. *Documenta Ophthalmologica. Advances in Ophthalmology*, *98*, 207–232. https://doi.org/10.1023/a:1002097208337

Merlet, I., Garcia-Larrea, L., Ryvlin, P., Isnard, J., Sindou, M., & Mauguiere, F. (1998). Topographical reliability of mesio-temporal sources of interictal spikes in temporal lobe epilepsy. *Electroencephalography and Clinical Neurophysiology*, *107*, 206–212. https://doi.org/10.1016/s0013-4694

Michel, C. M., Murray, M. M., Lantz, G., Gonzalez, S., Spinelli, L., & Grave de Peralta, R. (2004). EEG source imaging. *Clinical Neurophysiology*, *115*, 2195–2222.

Miller, K. J., Foster, B. L., & Honey, C. J. (2012). Does rhythmic entrainment represent a generalized mechanism for organizing computation

in the brain? *Frontiers in Computational Neuroscience*, *6*, 85. https://doi.org/10.3389/fncom.2012.00085

Morgan, S. T., Hansen, J. C., & Hillyard, S. A. (1996). Selective attention to stimulus location modulates the steady-state visual evoked potential. *Proceedings of the National Academy of Sciences of the United States of America*, *93*, 4770–4774. https://doi.org/10.1073/pnas.93.10.4770

Mouraux, A., & Iannetti, G. D. (2008). Across-trial averaging of event-related EEG responses and beyond. *Magnetic Resonance Imaging*, *26*, 1041–1054.

Norcia, A. M., Appelbaum, L. G., Ales, J. M., Cottereau, B. R., & Rossion, B. (2015). The steady-state visual evoked potential in vision research: A review. *Journal of Vision*, *15*(6), 41–46. https://doi.org/10.1167/15.6.4

Nozaradan, S., Peretz, I., Missal, M., & Mouraux, A. (2011). Tagging the neuronal entrainment to beat and meter. *The Journal of Neuroscience*, *31*, 10234–10240. https://doi.org/10.1523/JNEUROSCI.0411-11.2011

Nunez, P. L., & Srinivasan, R. (2005). *Electric fields of the brain: The neurophysics of EEG*. Oxfor University Press: Oxfor University.

Oostendorp, T. F., Delbeke, J., & Stegeman, D. F. (2000). The conductivity of the human skull: Results of in vivo and in vitro measurements. *IEEE Transactions on Bio-Medical Engineering*, *47*, 1487–1492. https://doi.org/10.1109/TBME.2000.880100

Pernet, C. R., Latinus, M., Nichols, T. E., & Rousselet, G. A. (2015). Cluster-based computational methods for mass univariate analyses of event-related brain potentials/fields: A simulation study. *Journal of Neuroscience Methods*, *250*, 85–93. https://doi.org/10.1016/j.jneumeth.2014.08.003

Pizzo, F., Roehri, N., Medina Villalon, S., Trebuchon, A., Chen, S., Lagarde, S., … Bénar, C. G. (2019). Deep brain activities can be detected with magnetoencephalography. *Nature Communications*, *10*, 971. https://doi.org/10.1038/s41467-019-08665-5

Ramantani, G., Dumpelmann, M., Koessler, L., Brandt, A., Cosandier-Rimele, D., Zentner, J., … Maillard, L. G. (2014). Simultaneous subdural and scalp EEG correlates of frontal lobe epileptic sources. *Epilepsia*, *55*, 278–288. https://doi.org/10.1111/epi.12512

Regan, D. (1966). Some characteristics of average steady-state and transient responses evoked by modulated light. *Electroencephalography and Clinical Neurophysiology*, *20*, 238–248.

Regan, D. (1972). Evoked potentials to changes in the chromatic contrast and luminance contrast of checkboard stimulus patterns. *Advances in Experimental Medicine and Biology*, *24*, 171–187. https://doi.org/10.1007/978-1-4684-8231-7_17

Regan, D. (1989). *Human brain electrophysiology: Evoked potentials and evoked magnetic fields in science and medicine*. New York: Elsevier.

Rosburg, T., Ludowig, E., Dümpelmann, M., Alba-Ferrara, L., Urbach, H., & Elger, C. E. (2010). The effect of face inversion on intracranial and scalp recordings of event-related potentials. *Psychophysiology*, *47*, 147–157. https://doi.org/10.1111/j.1469-8986.2009.00881.x

Rossion, B. (2014). Understanding face perception by means of human electrophysiology. *Trends in Cognitive Sciences*, *18*, 310–318. https://doi.org/10.1016/j.tics.2014.02.013

Rossion, B., & Boremanse, A. (2011). Robust sensitivity to facial identity in the right human occipito-temporal cortex as revealed by steady-state visual-evoked potentials. *Journal of Vision*, *11*, 11. https://doi.org/10.1167/11.2.16

Rossion, B., Prieto, E. A., Boremanse, A., Kuefner, D., & Van Belle, G. (2012). A steady-state visual evoked potential approach to individual face perception: Effect of inversion, contrast-reversal and temporal dynamics. *NeuroImage*, *63*, 1585–1600. https://doi.org/10.1016/j.neuroimage.2012.08.033

Salado, A. L., Koessler, L., De Mijolla, G., Schmitt, E., Vignal, J.-P., Civit, T., … Colnat-Coulbois, S. (2018). sEEG is a safe procedure for a comprehensive anatomic exploration of the insula: A retrospective study of 108 procedures representing 254 Transopercular insular electrodes. *Operative Neurosurgery*, *14*, 1–8. https://doi.org/10.1093/ons/opx106

Schiltz, C., Sorger, B., Caldara, R., Ahmed, F., Mayer, E., Goebel, R., & Rossion, B. (2006). Impaired face discrimination in acquired prosopagnosia is associated with abnormal response to individual faces in the right middle fusiform gyrus. *Cerebral Cortex*, *16*, 574–586.

Seeber, M., Cantonas, L., Sesia, T., Visser-vandewalle, V., & Michel, C. M. (2019). Subcorticalelectrophysiological activity is detectable with high-density EEG sourceimaging. *Nature Communications 10*, 1–7. https://doi.org/10.1038/s41467-019-08725-w

Seeck, M., Koessler, L., Bast, T., Leijten, F., Michel, C., Baumgartner, C., … Beniczky, S. (2017). The standardized EEG electrode array of the IFCN. *Clinical Neurophysiology*, *128*, 2070–2077. https://doi.org/10.1016/j.clinph.2017.06.254

Srinivasan, R., Russell, D. P., Edelman, G. M., & Tononi, G. (1999). Increased synchronization of neuromagnetic responses during conscious perception. *The Journal of Neuroscience*, *19*, 5435–5448.

Talairach, J., & Bancaud, J. (1973). Stereotaxic approach to epilepsy. Methodology of anatomo-functional stereotaxic investigations. *Progress in Neurological Surgery*, *5*, 297–354. https://doi.org/https://doi.org/10.1159/000394343

Tao, J. X., Ray, A., Hawes-Ebersole, S., & Ebersole, J. S. (2005). Intracranial EEG substrates of scalp EEG interictal spikes. *Epilepsia*, *46*, 669–676. https://doi.org/10.1111/j.1528-1167.2005.11404.x

Van Der Loo, E., Congedo, M., Plazier, M., Van De Heyning, P., & De Ridder, D. (2007). Correlation between independent components of scalp EEG and intra-cranial EEG (iEEG) time series. *International Journal of Bioelectromagnetism*, *9*, 270–275.

Wendel, K., Vaisanen, J., Seemann, G., Hyttinen, J., & Malmivuo, J. (2010). The influence of age and skull conductivity on surface and subdermal bipolar EEG leads. *Computational Intelligence and Neuroscience*, *2010*, 397272–397277. https://doi.org/10.1155/2010/397272

Wennberg, R., & Cheyne, D. (2014). EEG source imaging of anterior temporal lobe spikes: Validity and reliability. *Clinical Neurophysiology: Official Journal of the International Federation of Clinical Neurophysiology*, *125*, 886–902. https://doi.org/10.1016/j.clinph.2013.09.042

Wittevrongel, B., Khachatryan, E., Fahimi Hnazaee, M., Camarrone, F., Carrette, E., De Taeye, L., … Van Hulle, M. M. (2018). Decoding steady-state visual evoked potentials from electrocorticography. *Frontiers in Neuroinformatics*, *12*, 65. https://doi.org/10.3389/fninf.2018.00065

Yan, X., Liu-Shuang, J., & Rossion, B. (2019). Effect of face-related task on rapid individual face discrimination. *Neuropsychologia*, *129*, 236–245. https://doi.org/10.1016/j.neuropsychologia.2019.04.002

Zaveri, H. P., Duckrow, R. B., & Spencer, S. S. (2009). Concerning the observation of an electrical potential at a distance from an intracranial electrode contact. *Clinical Neurophysiology*, *120*, 1873–1875. https://doi.org/10.1016/j.clinph.2009.08.001

SUPPORTING INFORMATION

Additional supporting information may be found online in the Supporting Information section at the end of this article.

How to cite this article: Jacques C, Jonas J, Maillard L, Colnat-Coulbois S, Rossion B, Koessler L. Fast periodic visual stimulation to highlight the relationship between human intracerebral recordings and scalp electroencephalography. *Hum Brain Mapp*. 2020;41:2373–2388. https://doi.org/10.1002/hbm.24952

Neuropsychologia 147 (2020) 107583

Contents lists available at ScienceDirect

Neuropsychologia

journal homepage: http://www.elsevier.com/locate/neuropsychologia

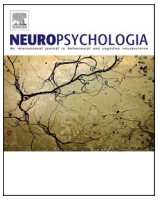

Typical visual unfamiliar face individuation in left and right mesial temporal epilepsy

Angélique Volfart [a,b], Jacques Jonas [a,c], Louis Maillard [a,c], Thomas Busigny [b], Bruno Rossion [a,b,c,1,*], Hélène Brissart [a,c,1]

[a] Université de Lorraine, CNRS, CRAN, F-54000, Nancy, France
[b] Université Catholique de Louvain, Institute of Research in Psychological Science, Louvain-La-Neuve, Belgium
[c] Université de Lorraine, CHRU-Nancy, Service de Neurologie, F-54000, Nancy, France

ARTICLE INFO

Keywords:
Mesial temporal lobe epilepsy
Face individuation
Neuropsychology
Anterior temporal lobe

ABSTRACT

Patients with chronic mesial temporal lobe epilepsy have difficulties at identifying familiar faces as well as at explicit old/new face recognition tasks. However, the extent to which these difficulties can be attributed to visual individuation of faces, independently of general explicit learning and semantic memory processes, is unknown. We tested 42 mesial temporal lobe epilepsy patients divided into two groups according to the side of epilepsy (left and right) and 42 matched controls on an extensive series of individuation tasks of unfamiliar faces and control visual stimuli, as well as on face detection, famous face recognition and naming, and face and non-face learning. Overall, both patient groups had difficulties at identifying and naming famous faces, and at explicitly learning face and non-face images. However, there was no group difference in accuracy between patients and controls at the two most widely used neuropsychological tests assessing visual individuation of unfamiliar faces (Benton Facial Recognition Test and Cambridge Face Memory Test). While patients with right mesial temporal lobe epilepsy were slowed down at all tasks, this effect was not specific to faces or even high-level stimuli. Importantly, both groups showed the same profile of response as typical participants across various stimulus manipulations, showing no evidence of qualitative processing impairments. Overall, these results point to largely preserved visual face individuation processes in patients with mesial temporal lobe epilepsy, with semantic and episodic memory difficulties being consistent with the localization of the neural structures involved in their epilepsy (anterior temporal cortex and hippocampus). These observations have implications for the prediction of neuropsychological outcomes in the case of surgery and support the validity of intracranial electroencephalographic recordings performed in this population to understand neural mechanisms of human face individuation, notably through intracranial electrophysiological recordings and stimulations.

1. Introduction

Face identity recognition is critical for social interactions in the human species and constitutes one of the most impressive functions of the adult human brain. Unfortunately, face identity recognition is also frequently affected in a variety of neurological conditions, e.g. following acquired brain damage (Benton and Van Allen, 1972; Valentine et al., 2006; Barton, 2008), surgery for temporal glioma (Papagno et al., 2017), Alzheimer's disease (Tippett et al., 2003; Pal et al., 2019), fronto-temporal semantic dementia (Luzzi et al., 2017; Pozueta et al., 2019), or temporal lobe epilepsy (Seidenberg et al., 2002; Drane et al., 2013).

Recognizing the identity of familiar people based on their faces requires first and foremost to decode the idiosyncratic visual features of these faces (i.e. face individuation). Efficient face individuation is often required when we first encounter people or when they have not yet been encoded in long-term memory, i.e. when they are unfamiliar. Since most human societies are characterized by the presence of numerous individuals and a tendency to change the number of individuals over time, visual individuation of *unfamiliar* faces occurs frequently and is key to our social interactions (Rossion, 2018).

In neurotypical individuals, the neural basis of visual face individuation has been primarily investigated with functional MRI (fMRI). In

* Corresponding author. Université de Lorraine, CNRS, CRAN - University Hospital of Nancy, 29 Avenue du Maréchal de Lattre de Tassigny, 54000 Nancy, France.
E-mail address: bruno.rossion@univ-lorraine.fr (B. Rossion).
[1] Equal contribution.

https://doi.org/10.1016/j.neuropsychologia.2020.107583
Received 23 April 2020; Received in revised form 7 July 2020; Accepted 5 August 2020
Available online 7 August 2020
0028-3932/

List of abbreviations

BFRT-c	Benton Facial Recognition Test computerized
CFMT	Cambridge Face Memory Test
iEEG	intracranial electroencephalography
fMRI	functional magnetic resonance imaging
FRI	face recognition index
HR	head rotation
LD	lighting direction
MTLE	mesial temporal lobe epilepsy
NAI	name access index
NC	normal controls
RT	response times
SEEG	stereotaxic electroencephalography
VOTC	ventral occipito-temporal cortex
WAIS	Wechsler Adult Intelligence Scale

particular, fMRI-adaptation studies have found face individuation effects in pre-defined face-selective regions of the posterior ventral occipito-temporal cortex (VOTC) such as the inferior occipital gyrus ("Occipital Face Area") and the middle fusiform gyrus ("Fusiform Face Area") (Gauthier et al., 2000; Schiltz et al., 2006; Davies-Thompson et al., 2009; Ewbank et al., 2013; Fox et al., 2013; Hermann et al., 2017; Hughes et al., 2019; Rostalski et al., 2019). These studies usually use pictures of unfamiliar faces to rule out the automatic involvement of affective and semantic memory processes, as well as name retrieval. In contrast, the processing of familiar (i.e. famous and personally familiar) faces has been consistently shown to involve more anterior regions of the VOTC, such as the anterior and medial temporal regions (Sergent et al., 1992; Gorno-Tempini et al., 1998; Leveroni et al., 2000; Gorno--Tempini and Price, 2001; Elfgren et al., 2006; Gobbini and Haxby, 2007; Natu and O'Toole, 2011; Sugiura et al., 2011; Von Der Heide et al., 2013; Duchaine and Yovel, 2015; Ramon et al., 2015, Rice et al., 2018b), in line with episodic, semantic and emotional contents evoked by familiar faces (Brambati et al., 2010; Sugiura et al., 2011; Ross and Olson, 2012).

Mesial temporal lobe epilepsy (MTLE) is the most frequent focal epilepsy referred for epilepsy surgery (Schuele and Lüders, 2008; Spencer and Huh, 2008; Tatum, 2012; see also Ladino et al., 2014). Intracranial electroencephalographic (iEEG) recordings have shown that MTLE frequently affects the temporal pole, the amygdala, the head and body of the hippocampus, the rhinal cortex, and the ventral anterior temporal cortex (including the anterior parts of the fusiform and inferior temporal gyri) (Maillard et al., 2004). These structures are typically involved in anterior temporal lobectomy, one of the most frequent surgical procedure in refractory MTLE (Brotis et al., 2019). Several studies have shown that patients with MTLE are impaired at recognizing familiar faces (Seidenberg et al., 2002; Viskontas et al., 2002; Glosser et al., 2003; Griffith et al., 2006). More precisely, left-sided MTLE has been more consistently related to difficulties at *naming* famous faces, while right-sided MTLE has been frequently linked to difficulties at *judging familiarity*, or providing *semantic* information about a face (Gainotti, 2007; Drane et al., 2008, 2013). A similar pattern of famous face identification difficulties has also been found in MTLE patients following ATL resection (Glosser et al., 2003; Drane et al., 2008, 2013; Lambon Ralph et al., 2012, Rice et al., 2018a). Additionally, these patients exhibit difficulties at explicitly encoding and subsequently recognizing pictures of unfamiliar faces, regardless of the epileptogenic focus side (Milner, 1968; Chiaravalloti and Glosser, 2004).

The extent to which famous face recognition difficulties in MTLE can be attributed to the process of visual individuation of faces, independently of general explicit learning and semantic memory processes, remains unknown. Clarifying this issue is important both for clinical and fundamental research. From a clinical standpoint, a comprehensive view of the neuropsychological performance of epileptic patients before epilepsy surgery is critical to predict the neurocognitive outcome after surgery (Potter et al., 2009; Sherman et al., 2011; Helmstaedter, 2013). Indeed, post-operative cognitive outcome depends, among other variables, on the relationship between the location of the epileptogenic zone (i.e. the region to be resected to cure the patient) and the pre-operative neuropsychological profile. According to the model of functional adequacy, the postoperative decline is expected to be high when there is adequacy between the brain region planned to be resected and high pre-operative performance on the cognitive functions supported by this region (Chelune, 1995; Helmstaedter, 2004). At the level of fundamental research, there is increasing evidence for limitations of animal models, in particular the macaque brain, to understand the neural mechanisms of human face (identity) recognition (Rossion and Taubert, 2019; Griffin, 2020). In this context, iEEG recordings of face processing in human epileptic patients may become increasingly informative (e.g. Allison et al., 1999; Davidesco et al., 2014; Jonas et al., 2016; see Rossion et al., 2018 for review). Therefore, a comprehensive view of face recognition performance in these patients is needed to validate the results obtained with iEEG recordings. This issue of potential deficits in visual individuation of faces in MTLE patients remains unsolved, mainly because very few studies have assessed face individuation with unfamiliar faces in these patients (Hermann et al., 1997; Seidenberg et al., 1998; Glosser et al., 2003; Chiaravalloti and Glosser, 2004; Griffith et al., 2006), and these studies have used only a single test (most often the Benton Facial Recognition Test, BFRT, Benton and Van Allen, 1968). While these studies found that both left and right MTLE patients performed in the normal range at this test, with sometimes a trend towards higher scores for left MTLE patients, they never recorded response times (RT) at this task, an important variable to consider in individual face matching tasks (Delvenne et al., 2004; Rossion and Michel, 2018).

In the present study, we went well beyond the state-of-the-art by testing 42 MTLE patients and their matched controls on a series of individuation tasks with unfamiliar faces and control visual stimuli and by reporting both accuracy and response times. The entire cohort of participants was also tested with a face detection task, face and non-face explicit learning tasks, and a famous face recognition and naming task, in order to provide a comprehensive overview of their face recognition performance.

2. Materials and methods

2.1. Participants

Forty-three consecutive pre-surgical patients with refractory MTLE were prospectively enrolled between 2013 and 2017 at the University Hospital of Nancy. The inclusion criteria were: (1) age above 18 years; (2) left or right MTLE as assessed by non-invasive examinations (structural MRI, EEG-video, positron emission tomography, single photon emission computed tomography) for all patients and stereotaxic-EEG (SEEG) for 24 out of 42 patients (when non-invasive examinations were inconclusive about the location of the epileptogenic focus); (3) normal basic visual functions (as measured by the Visual Object and Space Perception battery).

Among the 43 patients screened, one patient was later excluded because of insufficient data about the location of the epileptic focus. Therefore, 42 patients were included in the subsequent analyses (21 males, 21 females; mean age 37.05 $\pm$ 11.68). Thirty-nine patients were right-handed (93%) and three patients were left-handed (7%) as measured by the Edinburgh Handedness Inventory (Oldfield, 1971). All but 2 (left) MTLE patients had their intellectual efficiency assessed through the WAIS-R or WAIS-IV (Wechsler Adult Intelligence Scale) and showed a normal IQ (>70). All patients gave written informed consent and the study (ATENA-F, trial N°2013-A00515-40, ClinicalTrials.gov identifier NCT02888925) was approved by the local ethical committee

(CPP Est III, 13.05.02).

Two groups of patients were distinguished according to the lateralization of the epileptogenic focus: a left MTLE group (17 patients, 9 females; mean age 36.41 ± 12.49) and a right MTLE group (25 patients, 12 females; mean age 37.48 ± 11.34). The side of the epileptogenic focus was assessed by non-invasive examinations (structural MRI, EEG-video, positron emission tomography, single photon emission computed tomography) and, when available, SEEG recordings (24/42 patients). The two patient groups were not statistically different on gender, age at inclusion, handedness, educational level, age at epilepsy onset, duration of epilepsy, number of antiepileptic drugs, structural status of the hippocampus (presence or not of hippocampal sclerosis), or total IQ (Table 1). However, left MTLE patients were significantly faster in processing speed (as measured by the Coding test from the WAIS) than right MTLE patients (Table 1).

Patients were matched individually to normal controls (NC) on age range (±5 years), gender, handedness, and level of education (<12, 12 to 14 or > 14 academic years). Of these 42 NC, 37 were included in the present protocol (ATENA-F, N° 2013-A00515-40) and 5 were controls from a previous single-case study (Jonas et al., 2018) who were tested with the same tasks as in the present study. We constituted two NC groups: the left NC group matched to left MTLE patients (17 controls, 9 females; mean age 35.88 ± 12.44), and the right NC group matched to right MTLE patients (25 controls, 12 females; mean age 37.12 ± 11.92). None of the control participants had a history of neurological or psychiatric disease, drug or alcohol abuse, nor did they have cognitive complaints. All NC gave written consent before their inclusion and received financial compensation for their participation in the study.

2.2. Neuropsychological tests

2.2.1. General procedure

Participants were assessed with a set of seven behavioral experiments. The order of administration was the same for each participant: (1) the electronic version of the Benton Face Recognition Test-computerized (BFRT-c); (2) Old/New face recognition task; (3) Old/New recognition task with birds; (4) Face and car delayed matching task with upright and inverted orientations; (5) Mooney face test; (6) Famous face identification test (CELEB); and (7) Cambridge Face Memory Test (CFMT). Testing lasted for approximately 2 h.

The behavioral tasks were created and tested using E-prime 1.1, except for the CFMT test, running in Java, and the CELEB task running with its own software (https://www.ipsp.ucl.ac.be/recherche/projets/Celeb/setup.exe). Participants were seated in front of a computer screen, at a distance of about 50 cm. In all tests but the BFRT-c and CELEB, participants had to respond by pressing a button on the keyboard. In the BFRT-c, participants had to respond by clicking with the mouse on on-screen images. In the CELEB, the experimenter was responsible for pressing a button on the keyboard when the participant correctly named the famous face and for writing down semantic information when the name was not automatically retrieved by the participant.

Table 1
Demographic and clinical characteristics of MTLE patients. Values are shown as mean ± standard deviation or as the number of patients per category. Independent t-tests, Mann-Whitney U and chi-square's results are shown. Statistical comparisons in bold are significant at p < .05.

Characteristics		Left MTLE (n=17)	Right MTLE (n=25)	Statistical comparisons
Gender (N)	Male	8	13	χ=0.099, p=.753
	Female	9	12	V_{Cramer}= 0.049
Age at inclusion (years)		36.41 ± 12.49	37.48 ± 11.34	t=−0.288, p=.775 d_{Cohen}= 0.135
Handedness (N left/right)		2/15	1/24	χ=0.920, p=.338 V_{Cramer}= 0.148
Educational Level (N)	< 12 academic years	7	13	χ=2.293, p=.318 V_{Cramer}= 0.234
	12-14 academic years	3	7	
	> 14 academic years	7	5	
Age at epilepsy onset (years)		19.88 ± 16.65	14.56 ± 9.95	U=181, p=.419 d_{Cohen}= 0.251
Duration of epilepsy (years)		16.53 ± 12.8	22.92 ± 13.94	U=157, p=.155 d_{Cohen}= 0.450
Number of anti-epileptic drugs (N)		2.18 ± 1.13	2.28 ± 0.89	U=185.5, p=.440 d_{Cohen}= 0.215
Presence of hippocampal sclerosis (N yes/no)		7/10	13/12	χ=0.475, p=.491 V_{Cramer}= 0.106
Total IQ		100.13 ± 17.87	90.28 ± 11.39	U=126, p=.085 d_{Cohen}= 0.565
Processing speed (percentile Coding test)		48.2 ± 32.1	27.4 ± 23.17	**U=117, p=.047 d_{Cohen}= 0.816**

2.2.2. Face detection

Mooney face test. This test assesses the ability to categorize a visual stimulus as a "face" without being able to rely on local features (i.e. requiring to perceive the stimulus as a global configuration; Moore and Cavanagh, 1998; Rossion et al., 2011). The stimuli and procedure were the same as those used in experiment 16 of Busigny et al. (2010).

Stimuli. Eighty Mooney faces (two-tone, thresholded, black and white) were selected from the dataset created by Schurger and colleagues (http://www.princeton.edu/artofscience/gallery/view.php%3Fid=77.html) and based on Mooney's original stimuli (Mooney, 1957). When a Mooney face is presented upside-down, the face is usually not perceived.

Procedure. Mooney faces were individually presented upright and upside-down in the middle of the screen. They were randomly displayed in two blocks of 80 trials. The subject had to decide whether the image depicted a face or not. We considered a correct response when participants pressed the button "yes" for upright Mooney faces (80 trials), and "no" for upside-down Mooney faces (80 trials). Every response was followed by the apparition of a central cross (300 ms) and a gray screen (300 ms).

One control participant (matched with a left MTLE patient) was not tested with this task because of technical issues.

2.2.3. Face and non-face individuation

Benton Facial Recognition Test-computerized (BFRT-c). This test, developed by Benton and Van Allen (1968), is the oldest unfamiliar face matching test in neuropsychology, used in numerous clinical and experimental studies. It requires to match simultaneously presented pictures of unfamiliar faces, against distractor faces. It was performed in a computerized version (Rossion and Michel, 2018).

Stimuli. As in the original test, stimuli were grayscale male or female face photographs with neutral expressions and unfamiliar to the participants.

Procedure. A full-front target was always presented in the upper part of the screen with six probes organized in two rows below it. Participants were instructed to match as fast as possible the face at the top of the screen to the face(s) presented among distractors The experiment was composed of 22 trials split into two parts (6 trials in Part 1 and 16 in Part 2). In Part 1, targets and probes were all full-front stimuli taken under the same lighting conditions, and participants were instructed to match the target face with the same identical face presented among five distractors. In Part 2, targets were full-front while probes were pictures taken under different lighting conditions (8 items, lighting direction or LD items) and head orientations (8 items, head rotation or HR items) and participants were instructed to match the target face to 3 different exemplars of the same face among 3 distractors. Each trial was separated

from the following one by a blank interval of 500 ms. Accuracy was scored on a total of 54, and the total time taken by participants to complete the test was measured in seconds (Rossion and Michel, 2018).

Cambridge Face Memory Test (CFMT). The CFMT was originally developed by Duchaine and Nakayama (2006) to evaluate face identity recognition difficulties of developmental origin and has become one of the most widely used tests in the literature. It requires to explicitly encode pictures of six individual faces that have to be matched to pictures of the same individuals, against distractor faces. The stimuli and procedure used here were the same as those used in Duchaine and Nakayama (2006).

Stimuli. The stimuli were 52 faces of young men with cropped hair and neutral expressions taken under different viewpoints and lightings. Six individuals were designated as targets (with 12 images for each target face) while the other 46 individuals were used as distractors.

Procedure. The CFMT starts with a brief practice (3 trials) followed by a learning step in which participants are asked to learn six unfamiliar target faces. Each target face is first presented under three different viewpoints and participants have to subsequently recognize it among two distractors (6 target faces x 3 trials each, i.e. 18 trials). In this first step, target faces in the forced-choice task are identical to the studied items. In a second step, participants are asked to perform the same task with novel images of the target faces in which viewpoints and lighting conditions are different from the learning step (30 trials). In the last step, participants have to perform the task while Gaussian noise is added on target and distractor faces to obscure facial features (24 trials). Total accuracy on the CFMT is scored on 72. Note that three right MTLE patients were not tested with this task because of time constraints.

Face and car delayed matching task with upright and inverted orientations. This task also requires matching individual face and non-face items against a distractor, across orientation changes, and with a brief delay between the presentation of the stimuli to match. The stimuli and procedure are identical to experiment 4 in Busigny and Rossion (2010).

Stimuli. One full-front and one 3/4 profile grayscale photographs of 36 individuals (18 females) and 36 cars were used. The target picture was always a full-front picture, and the probe a left 3/4 profile picture.

Procedure. Each trial began with a white screen (1000 ms), followed by the target (2000 ms) and a blank interval (1000 ms). After this interval, two 3/4 profile probes were presented. Participants were instructed to find the probe that corresponded to the previously shown target. Each trial was presented both at upright and upside-down orientations. In total, the experiment consisted of 144 trials (36 per condition and orientation). As in Busigny and Rossion (2010), an index of inversion effect was computed to quantify the performance decrease related to inversion by combining both accuracy and correct response times. This was done by first calculating the inverse efficiency, i.e. the average response times of the correct trials divided by accuracy in each condition (face upright, face inverted, car upright and car inverted). The index of inversion effect for faces and cars was then calculated using the following formula: (Inverse efficiency Upright - Inverse efficiency Inverted)/(Inverse efficiency Upright + Inverse efficiency Inverted).

2.2.4. Old/New individual recognition tasks with face and non-face items

These tasks evaluate the ability to encode a series of individual faces or birds in a separate test, and then to recognize these items against distractors in a subsequent recognition stage.

Old/New faces. The stimuli and procedure was identical to experiment 3 in Busigny et al. (2010).

Stimuli. Stimuli were 60 color uncropped unfamiliar face pictures (30 females, 30 males). Thirty faces were selected as targets, while the 30 other faces were used as distractors (matched with the target in gender, hairstyle, and skin color).

Procedure. Participants were first presented with each of the 30 target faces for 4 seconds and were asked to explicitly learn them. Next, in a forced-choice recognition task, participants were presented with 30 pairs of faces (= 30 trials). For each pair, one face had been learned during the first step while the other face was a similar-looking distractor. Participants were instructed to select the learned face.

Old/New birds. The procedure was the same as for the Old/New faces test except that faces were replaced by images of birds. Birds' images were presented in grayscale to avoid simple matching based on color differences (color varying substantially across birds in the original images). Distractor items were matched with the target in general appearance, all pairs depicting birds from the same bird family, thus making it difficult to rely on a verbal strategy to retrieve the target item.

2.2.5. Famous face recognition and naming

CELEB test. This test assesses (French) famous face identification through naming, retrieval of semantic knowledge, and multiple-choice face-to-name matching (Busigny et al., 2014). An advantage of this test is that it provides two indexes evaluating famous face identification and naming independently. The same procedure as in Busigny et al. (2014) was used.

Stimuli. Sixty photographs of famous faces without external facial cues were presented. They were mostly from the French-speaking community (singers, actors, politicians, etc.). Stimuli were displayed on a black background in the middle of the screen.

Procedure. Each famous face was displayed for 30 seconds and the participant had to name the person (naming step). If naming was correct, the next face was presented; if not, the subject performed 2 additional steps on this face (description and designation steps). First, the subject had 30 additional seconds to give as much information as possible, i.e. occupation, age, nationality, etc. (description step). Second, after these 30 seconds, the participant was provided with a multiple-choice and asked to find the correct name among four distractors (designation step). A face was considered to be correctly identified if the participant correctly named the face (naming step) or if the face was well-described *and* correctly-designated. At the end of the task, a final step was performed for all faces that were not correctly identified (knowledge step). Here, the experimenter provided the correct name and asked the participants if they know this person. If the person was not known, it was removed from the calculation of indexes.

Scores and indexes. Three scores were computed. The denomination score was the number of correctly-named faces. The recognition score represented the total of recognized faces, i.e. the number of correctly-named faces plus the number of faces correctly-described *and* correctly-designated. The knowledge score was the total of famous faces that were really known to participants. Based on these three scores, two indexes were computed. The Facial Recognition Index (FRI), representing the ability to recognize famous people from their face, corresponded to the recognition score divided by the knowledge score (multiplied by 100). The Name Access Index (NAI), representing the ability to retrieve a proper name based on a face, corresponded to the denomination score divided by the recognition score (multiplied by 100) (Busigny et al., 2014). Response times were recorded for the naming step only (correctly-named faces).

2.3. Statistical analysis

Statistical analyses were conducted using the SPSS software (IBM SPSS Statistics, Version 20.0; Armonk, NY: IBM Corp.). All tests were two-sided, and the alpha-level was set at $p < .05$. Analyses were carried out using chi-square tests for categorical variables and two independent samples t-tests or non-parametric Mann-Whitney U-tests for continuous variables, depending on whether the data were or were not normally distributed (as assessed by the Shapiro-Wilk test). Estimation of effect size is reported using Cramer's V for categorical variables and Cohen's d for continuous variables.

3. Results

3.1. Group level

The results are summarized in Fig. 1. All data and statistical results are available in Table 2. The following analysis focuses on the comparison of accuracy and correct RT between left and right MTLE patients and their respective NC (Fig. 1, Table 2). Direct comparisons between right and left MTLE patients are also reported (Fig. 1, Table 2).

3.1.1. Face detection

Left and right MTLE patients did not differ in accuracy rates from their respective NC groups at the Mooney face test. Whereas left MTLE patients were not different from their NC in RT, right MTLE patients showed significantly longer RT.

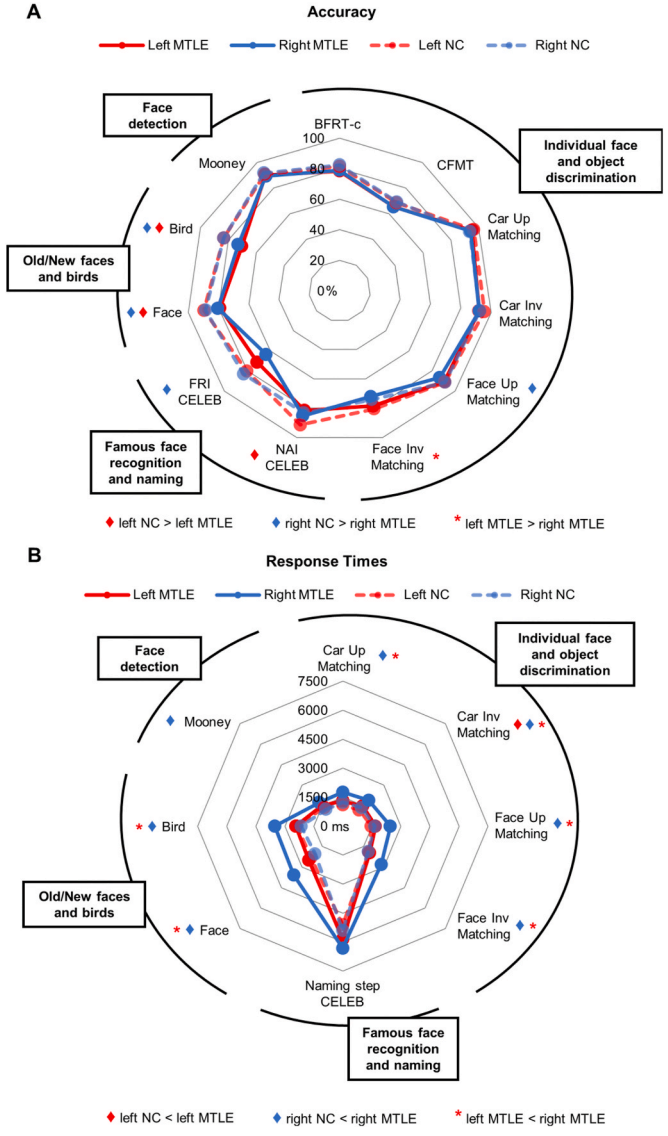

Fig. 1. Accuracy and correct RT of patients and NC in the face and object recognition tasks. Significant differences between patient groups and their respective NC groups, and between left and right patient groups on independent t-tests or Mann-Whitney U tests ($p < .05$) are noted with diamonds and asterisks, respectively. A. Accuracy is reported in percentages. BFRT-c and CFMT total scores were converted in percentages for visual purposes. B. RT are reported in milliseconds. BFRT-c is not represented because response times were measured in seconds.

3.1.2. Unfamiliar face and non-face individuation

Left and right MTLE patients did not differ in accuracy at the BFRT-c and CFMT from their respective NC groups. At the delayed matching task with pictures of cars, both patient groups showed normal accuracy performance compared to their NC group. For faces, left MTLE patients performed in the normal range in accuracy. Right MTLE patients had a slightly (i.e. 4%) but significantly lower accuracy at matching upright faces only. However, there was no interaction with stimulus inversion, both patient groups showing normal face inversion indexes.

Right MTLE patients were significantly slower than their NC group on all measures (BFRT-c; delayed matching task with faces and cars, both orientations). In contrast, left MTLE patients were only slower on the delayed matching task with inverted cars. Interestingly, in both patient groups, RT on the BFRT-c correlated with the Coding test of the WAIS assessing visuospatial processing speed ($r = -0.56$, $p = .02$, and $r = -0.51$, $p = .01$, for left and right MTLE groups respectively) (Tables 3 and 4).

3.1.3. Old/New recognition tasks

Both patient groups had lower accuracy than their NC on the old/new tasks, both with face and bird stimuli. Right MTLE patients were also significantly slower than their NC on these two tasks while left MTLE were unimpaired (Table 2).

3.1.4. Famous face recognition and naming

Right MTLE patients showed lower performance than their NC in identifying famous people from their face (FRI, CELEB test) but had no difficulty in naming those that they could identify (NAI, CELEB test). In contrast, left MTLE patients did not differ in identifying famous people from their face but showed lower performance than their NC in naming famous faces. Right and left MTLE did not differ from their respective NC groups in RT on naming (correctly-named famous faces).

3.2. Interim summary

The latter finding that left MTLE patients had difficulties at naming famous faces, while right MTLE patients were impaired at identifying famous persons from their face, is consistent with previous studies (Drane et al., 2008, 2013). Moreover, both left and right MTLE patients were impaired at explicitly learning face and bird images, in line with visual episodic memory deficits in MTLE (Chiaravalloti and Glosser, 2004; Helmstaedter, 2013). However, a novel aspect of the present study is that left and right MTLE patients had no difficulties at individuating pictures of unfamiliar faces (BRFT-c, CFMT, face matching), at least when accuracy only is considered. Right MTLE performed more slowly than NC in all tasks (except at naming famous faces in the CELEB test, after identification). This slowing down was not specific to faces since it was always found for both face and non-face items, without any evidence of a more severe effect for faces. Moreover, right MTLE patients were also significantly slower than the left MTLE patients at the general Coding test.

3.3. Interindividual variability in unfamiliar face and non-face individuation tasks

Although no clear difference was found between patients and controls in unfamiliar face individuation tasks at the group level, there was an increase of interindividual variability in patients as compared to their NC for some of these tasks (BFRT-c, face and car delayed matching task and CFMT), as shown by Levene's tests. Left and right MTLE patients had more variable accuracy on the delayed matching task with upright cars than their respective NC ($F = 4.175$, $p = .049$, and $F = 4.879$, $p = .032$, respectively). Right MTLE patients also had more variable response times on the BFRT-c ($F = 8.793$, $p = .005$), delayed matching with upright and inverted cars ($F = 7.659$, $p = .008$, and $F = 7.056$, $p = .011$, respectively) and with inverted faces ($F = 5.551$, $p = .023$).

Table 2
Performance of patients and controls on face and non-face recognition tasks. Values are shown as mean ± standard deviation. Independent t-tests' or Mann-Whitney U's results, as well as effect sizes (Cohen's d), are shown for each comparison between left MTLE/left NC groups and right MTLE/right NC groups. Significant values at $p < .05$ (two-tailed) are shown in bold. Acc = accuracy, RT = response times, Up = upright, Inv = inverted.

Cognitive tasks			Left MTLE (n=17)	Left NC (n=17)	Comparison MTLE/NC	Right MTLE (n=25)	Right NC (n=25)	Comparison MTLE/NC	Comparison left/right MTLE
Mooney Face Test		Acc (%)	90.08 ± 4.7	90.76 ± 5.8	U=116.5, p=.482 d_{Cohen}= 0.246	89.27 ± 7.1	91.64 ± 4.7	U=246.5, p=.200 d_{Cohen}= 0.368	U=212.5, p=1 d_{Cohen}= 0
		RT (ms)	1528 ± 749	1364 ± 913	U=99, p=.183 d_{Cohen}= 0.477	1728 ± 725	1232 ± 671	**U=176, p=.008** d_{Cohen}= 0.808	U=164.5, p=.219 d_{Cohen}= 0.387
BFRT-c		Acc (/54)	42.35 ± 2.4	44.06 ± 2.9	t=−1.821, p=.078 d_{Cohen}= 0.624	42.64 ± 4.8	44.56 ± 3.4	t=−1.631, p=.110 d_{Cohen}= 0.461	t=−0.255, p=.800 d_{Cohen}= 0.080
		RT (s)	275 ± 81	243 ± 80	t=1.176, p=.248 d_{Cohen}= 0.403	397 ± 255	246 ± 82	**U=176, p=.008** d_{Cohen}= 0.808	U=148.5, p=.101 d_{Cohen}= 0.523
Delayed Matching Task	Cars	Acc Up (%)	95.09 ± 8.0	96.55 ± 3.3	U=131.5, p=.637 d_{Cohen}= 0.154	94.34 ± 3.9	93.55 ± 7.9	U=278.5, p=.501 d_{Cohen}= 0.187	U=146.5, p=.082 d_{Cohen}= 0.541
		Acc Inv (%)	92.15 ± 9.4	95.58 ± 4.0	U=113.5, p=.276 d_{Cohen}= 0.373	92.32 ± 6.3	92.55 ± 10.2	U=256.5, p=.267 d_{Cohen}= 0.311	U=200.5, p=.755 d_{Cohen}= 0.095
		RT Up (ms)	1305 ± 528	1096 ± 227	U=118, p=.361 d_{Cohen}= 0.317	1756 ± 785	1238 ± 279	**U=151, p=.002** d_{Cohen}= 0.989	**U=97, p=.003** d_{Cohen}= 1.027
		RT Inv (ms)	1469 ± 563	1188 ± 258	**U=77, p=.020** d_{Cohen}= 0.870	1887 ± 799	1360 ± 298	**U=159, p=.003** d_{Cohen}= 0.929	**U=117, p=.014** d_{Cohen}= 0.816
		Index	8.39 ± 5.5	4.68 ± 3.8	**t=2.277, p=.030** d_{Cohen}= 0.781	5.49 ± 4.3	5.42 ± 4.7	t=0.057, p=.955 d_{Cohen}= 0.016	t=1.900, p=.065 d_{Cohen}= 0.597
	Faces	Acc Up (%)	90.51 ± 8.3	91.32 ± 5.3	U=139, p=.848 d_{Cohen}= 0.065	86.79 ± 7.5	91.32 ± 7.9	**U=193, p=.02** d_{Cohen}= 0.694	U=145.5, p=.084 d_{Cohen}= 0.549
		Acc Inv (%)	78.43 ± 10.7	80.55 ± 6.9	t=−0.687, p=.497 d_{Cohen}= 0.236	72.10 ± 9.0	74.22 ± 8.6	t=−0.843, p=.403 d_{Cohen}= 0.238	**t=2.064, p=.046** d_{Cohen}= 0.649
		RT Up (ms)	1682 ± 605	1475 ± 550	U=110, p=.235 d_{Cohen}= 0.416	2463 ± 2298	1649 ± 480	**U=178, p=.009** d_{Cohen}= 0.794	**U=124, p=.023** d_{Cohen}= 0.747
		RT Inv (ms)	1958 ± 715	1909 ± 713	U=133, p=.692 d_{Cohen}= 0.136	2814 ± 2324	1856 ± 394	**U=174, p=.007** d_{Cohen}= 0.144	**U=119, p=.017** d_{Cohen}= 0.796
		Index	14.34 ± 6.2	15.35 ± 10.7	t=−0.336, p=.740 d_{Cohen}= 0.115	16.44 ± 9.9	16.53 ± 10.1	t=−0.031, p=.975 d_{Cohen}= 0.009	t=−0.846, p=.403 d_{Cohen}= 0.266
CELEB		FRI (%)	71.27 ± 20.2	80.29 ± 19.1	U=102, p=.143 d_{Cohen}= 0.519	63.65 ± 24.3	83.15 ± 17.2	**U=150.5, p=.002** d_{Cohen}= 0.993	t=1.065, p=.293 d_{Cohen}= 0.335
		NAI (%)	81.65 ± 18.0	91.41 ± 5.7	**U=85.5, p=.042** d_{Cohen}= 0.744	85.20 ± 9.1	83.31 ± 13.4	U=311, p=.977 d_{Cohen}= 0.008	U=205, p=.847 d_{Cohen}= 0.059
		RT (ms)	5848 ± 2809	5117 ± 1148	U=136, p=.770 d_{Cohen}= 0.101	6321 ± 2447	5409 ± 1992	t=1.444, p=.155 d_{Cohen}= 0.408	U=177, p=.363 d_{Cohen}= 0.284
CFMT	Intro	Acc (/18)	17.00 ± 1.8	17.76 ± 0.6	U=122.5, p=.308 d_{Cohen}= 0.262	16.90 ± 2.1	17.44 ± 1.1	U=232, p=.289 d_{Cohen}= 0.270	U=167, p=.516 d_{Cohen}= 0.366
	No Noise	Acc (/30)	18.24 ± 4.4	19.18 ± 4.4	t=−0.621, p=.539 d_{Cohen}= 0.213	17.95 ± 5.4	18.96 ± 5.0	t=−0.661, p=.512 d_{Cohen}= 0.193	t=0.173, p=.863 d_{Cohen}= 0.056
	Noise	Acc (/24)	11.94 ± 4.1	12.35 ± 4.0	t=−0.294, p=.771 d_{Cohen}= 0.101	12.20 ± 4.7	13.40 ± 4.2	t=−0.905, p=.370 d_{Cohen}= 0.264	t=−0.200, p=.843 d_{Cohen}= 0.064
	Total	Acc (/72)	47.18 ± 9.1	49.41 ± 8.0	t=−0.759, p=.453 d_{Cohen}= 0.260	47.10 ± 10.9	49.80 ± 8.8	t=−0.945, p=.350 d_{Cohen}= 0.276	t=0.026, p=.979 d_{Cohen}= 0.008
Old/New Tasks	Faces	Acc (%)	79.12 ± 11.5	89.66 ± 7.2	**t=-3.206, p=.003** d_{Cohen}= 1.099	80.40 ± 10.8	88.54 ± 8.3	**U=170.5, p=.005** d_{Cohen}= 0.846	U=197.5, p=.699 d_{Cohen}= 0.119
		RT (ms)	2484 ± 1184	2325 ± 900	U=142, p=.931 d_{Cohen}= 0.030	3583 ± 2114	2034 ± 549	**U=131, p<.001** d_{Cohen}= 1.149	**U=128, p=.030** d_{Cohen}= 0.709
	Birds	Acc (%)	70.39 ± 8.2	83.34 ± 6.5	**t=-5.099, p<.001** d_{Cohen}= 1.749	72.92 ± 8.4	83.37 ± 9.1	**t=-4.208, p<.001** d_{Cohen}= 1.190	t=−0.964, p=.341 d_{Cohen}= 0.303
		RT (ms)	2433 ± 710	2374 ± 1029	U=119, p=.380 d_{Cohen}= 0.305	3514 ± 1715	2152 ± 606	**U=108, p<.001** d_{Cohen}= 1.356	**U=108, p=.007** d_{Cohen}= 0.907

To further understand the nature of this interindividual variability in unfamiliar face and non-face individuation tasks (BFRT-c, CFMT, face and car delayed matching task), we correlated the patients' performance (accuracy and RT) on these tasks with their demographic and clinical characteristics (all correlations are found in Tables 3 and 4 for left and right MTLE patients respectively). Note that in the following analysis, we did not correct our statistical threshold for multiple comparisons ($6 \times 13 = 78$ comparisons for each patient group) because this led to a highly conservative threshold (FDR-corrected). This analysis should be interpreted with caution because of the weak statistical power due to the small sample of subjects, especially in the left MTLE group. However, we report confidence intervals for each correlation in Tables 3 and 4. In right MTLE patients, duration of epilepsy was significantly and negatively correlated with accuracy at the BFRT-c and delayed matching with upright faces and cars, and inverted cars (Tables 3 and 4). In left MTLE patients, no correlation was found between epilepsy duration and any of these individuation tasks. Total IQ was positively correlated with several scores in both left (delayed matching with faces) and right (BFRT-c, delayed matching with upright faces and inverted cars, face inversion index, CFMT) MTLE patients, indicating that patients with a lower IQ also had lower performance on these tasks.

There were also significant negative correlations of RT in the BFRT-c with total IQ and the Coding test in both left and right MTLE patients. A significant positive correlation was also found between age at inclusion and BFRT-c RT in right MTLE patients only (Table 4), indicating that older patients had longer RT. RT in the delayed matching task with faces and cars were not correlated with IQ or processing speed, except for the RT at matching upright faces which were correlated with processing speed in left MTLE patients only.

3.4. Do MTLE patients differ qualitatively from normal controls?

Although no clear difference was found between patients and controls in unfamiliar face individuation tasks at the group level (i.e. at a

Table 3
Correlations in left MTLE patients. Correlations of clinical and demographic variables with the accuracy scores and response times at the face and non-face individuation tasks in left MTLE patients. Pearson r and associated p-values are displayed, as well as 95% confidence intervals. Values in bold are significant at $p < .05$ (not corrected for multiple comparisons). Acc = accuracy, RT = response times, $CI_{95\%}$ = 95% confidence intervals.

Correlations in left MTLE patients			Age at inclusion	Age at epilepsy onset	Epilepsy duration	Number of antiepileptic drugs	Total IQ	Processing speed (percentile Coding test)
BFRT-c		Acc	r = 0.169, p = .517 $CI_{95\%}$ = -0.339/0.601	r = -0.023, p = .930 $CI_{95\%}$ = -0.498/0.463	r = 0.195, p = .453 $CI_{95\%}$ = -0.315/0.618	r = 0.315, p = .218 $CI_{95\%}$ = -0.195/0.691	r = -0.261, p = .312 $CI_{95\%}$ = -0.682/0.290	r = 0.003, p = .991 $CI_{95\%}$ = -0.510/0.514
		RT	r = 0.051, p = .846 $CI_{95\%}$ = -0.440/0.519	r = 0.273, p = .289 $CI_{95\%}$ = -0.239/0.666	r = -0.305, p = .234 $CI_{95\%}$ = -0.685/0.206	r = -0.046, p = .861 $CI_{95\%}$ = -0.515/0.444	r = -0.497, p = .042 $CI_{95\%}$ = -0.804/0.020	r = -0.557, p = .020 $CI_{95\%}$ = -0.832/-0.062
Delayed Matching Task	Cars	Acc Up	**r = -0.544, p = .024 $CI_{95\%}$ = -0.812/-0.086**	**r = -0.751, p = .0005 $CI_{95\%}$ = -0.905/-0.423**	r = 0.446, p = .073 $CI_{95\%}$ = -0.044/0.763	r = 0.331, p = .194 $CI_{95\%}$ = -0.178/-0.009	r = 0.341, p = .180 $CI_{95\%}$ = -0.207/0.726	r = 0.202, p = .437 $CI_{95\%}$ = -0.346/0.647
		Acc Inv	**r = -0.488, p = .047 $CI_{95\%}$ = -0.785/-0.009**	**r = -0.577, p = .015 $CI_{95\%}$ = -0.828/-0.133**	r = 0.274, p = .287 $CI_{95\%}$ = -0.238/0.667	r = 0.220, p = .396 $CI_{95\%}$ = -0.291/0.634	r = 0.358 p = .158 $CI_{95\%}$ = -0.189/0.735	r = 0.257, p = .319 $CI_{95\%}$ = -0.294/0.680
		RT Up	**r = 0.531, p = .028 $CI_{95\%}$ = 0.068/0.806**	r = 0.455, p = .066 $CI_{95\%}$ = -0.033/0.768	r = -0.074, p = .778 $CI_{95\%}$ = -0.536/0.422	r = -0.368, p = .146 $CI_{95\%}$ = -0.721/0.137	r = -0.037, p = .888 $CI_{95\%}$ =-0.539/0.484	r = -0.306, p = .232 $CI_{95\%}$ = -0.707/0.245
		RT Inv	r = 0.431, p = .084 $CI_{95\%}$ = -0.063/0.755	r = 0.287, p = .264 $CI_{95\%}$ = -0.225/0.674	r = 0.048, p = .855 $CI_{95\%}$ = - 0.443/0.517	r = 0.351, p = .167 $CI_{95\%}$ = -0.156/0.711	r = -0.030, p = .909 $CI_{95\%}$ = -0.534/0.490	r = -0.315, p = .218 $CI_{95\%}$ = -0.712/0.235
		Index	**r = -0.560, p = .019 $CI_{95\%}$ = -0.820/-0.108**	**r = -0.612, p = .009 $CI_{95\%}$ = -0.844/-0.186**	r = 0.250, p = .333 $CI_{95\%}$ = -0.262/0.652	r = 0.058, p = .825 $CI_{95\%}$ = -0.435/0.524	r = -0.142, p = .587 $CI_{95\%}$ = -0.610/0.399	r = -0.165, p = .527 $CI_{95\%}$ = -0.624/0.379
	Faces	Acc Up	r = -0.127, p = .627 $CI_{95\%}$ = -0.573/0.377	r = -0.125, p = .633 $CI_{95\%}$ = -0.571/0.378	r = 0.039, p = .882 $CI_{95\%}$ = -0.450/0.510	r = -0.104, p = .691 $CI_{95\%}$ = -0.557/0.396	**r = 0.492, p = .045 $CI_{95\%}$ = -0.027/0.802**	**r = 0.598, p = .011 $CI_{95\%}$ = 0.123/0.850**
		Acc Inv	r = -0.120, p = .646 $CI_{95\%}$ = -0.568/0.383	r = -0.159, p = .542 $CI_{95\%}$ = -0.594/0.348	r = 0.090, p = .731 $CI_{95\%}$ = -0.408/0.547	r = 0.004, p = .988 $CI_{95\%}$ = -0.477/0.484	**r = 0.545, p = .024 $CI_{95\%}$ = 0.045/0.826**	**r = 0.650, p = .005 $CI_{95\%}$ = 0.206/0.872**
		RT Up	r = 0.199, p = .444 $CI_{95\%}$ = -0.311/0.620	r = 0.295, p = .250 $CI_{95\%}$ = -0.216/0.679	r = -0.189, p = .467 $CI_{95\%}$ = -0.614/0.321	r = -0.232, p = .370 $CI_{95\%}$ = -0.641/0.280	r = -0.291, p = .257 $CI_{95\%}$ = -0.699/0.260	**r = -0.545, p = .024 $CI_{95\%}$ = -0.826/-0.045**
		RT Inv	r = 0.119, p = .649 $CI_{95\%}$ = -0.383/0.567	r = 0.263, p = .308 $CI_{95\%}$ = -0.249/0.660	r = -0.225, p = .385 $CI_{95\%}$ = -0.637/0.287	r = -0.273, p = .289 $CI_{95\%}$ = -0.666/0.239	r = -0.186, p = .475 $CI_{95\%}$ = -0.637/0.361	r = -0.331, p = .194 $CI_{95\%}$ = -0.721/0.218
		Index	r = -0.100, p = .702 $CI_{95\%}$ = -0.554/0.400	r = -0.069, p = .792 $CI_{95\%}$ = -0.532/0.426	r = -0.008, p = .975 $CI_{95\%}$ = -0.487/0.474	r = -0.260, p = .313 $CI_{95\%}$ = -0.658/0.252	r = -0.133, p = .611 $CI_{95\%}$ = -0.604/0.407	r = 0.088, p = .737 $CI_{95\%}$ = -0.444/0.574
CFMT Total		Acc	r = -0.172, p = .509 $CI_{95\%}$ = -0.603/0.336	r = -0.329, p = .197 $CI_{95\%}$ = -0.699/0.180	r = 0.260 p = .313 $CI_{95\%}$ = -0.252/0.658	r = -0.131, p = .616 $CI_{95\%}$ = -0.575/0.373	r = 0.206, p = .428 $CI_{95\%}$ = -0.342/0.650	r = 0.370, p = .144 $CI_{95\%}$ = -0.175/0.742

quantitative level), we explored the possibility that they differ qualitatively (i.e. accuracy or RT pattern across items). We therefore performed an item-by-item analysis on the second part of the BFRT-c (matching the target with its 3 corresponding probes). We focused on the BRFT-c for two main reasons: (1) normative data from 307 participants are available with this test, including mean accuracy and RT for each item (Rossion and Michel, 2018); (2) the BFRT-c is characterized by a large variability in difficulty across items (Rossion and Michel, 2018).

In the normative study of the test (Rossion and Michel, 2018), mean accuracy scores and RT across 307 typical participants were computed for each of the 16 items of the second part of the BFRT-c, ranking the items from the easiest to the most difficult. Here, we followed the same procedure as in Rossion and Michel (2018) and considered the mean accuracy score and mean RT for each item of this second part (n = 16) in both patient and NC groups. Consistent with the results observed in Rossion and Michel (2018) (these results are shown in Figs. 2A and 3A), items with changes in head rotation (HR items) showed higher accuracy scores and lower RT than items with changes in lighting direction (LD items) in both left and right MTLE patients and in their NC (Fig. 2B and C for accuracy; Fig. 3B and C for RT). To statistically assess that the difference between LD and HR items was the same across patients and their matched NC, we calculated two indexes reflecting the difference in accuracy or response times between these two types of items for each participant. We subtracted the mean accuracy score of LD items from the mean accuracy score of HR items and divided it by the mean accuracy of all items. We followed the same principle with RT, but subtracted the mean RT of HR items from the mean RT of LD items, to obtain a positive index. We then compared the accuracy and RT difference indexes of the patients and their NC. No difference was found between the right MTLE patients and their NC (accuracy: t = -0.780, p = .439; RT: t = 1.298, p = .202), or between the left MTLE patients and their NC (accuracy: t = -0.454, p = .653; RT: t = -0.554, p = .584). The same comparison performed between MTLE patients and the 307 participants of the normative data did not reveal any difference between groups (accuracy

Table 4
Correlations in right MTLE patients. Correlations of clinical and demographic variables with the accuracy scores and response times at the face and non-face individuation tasks in right MTLE patients. Pearson r and associated p-values are displayed, as well as 95% confidence intervals. Values in bold are significant at $p < .05$ (not corrected for multiple comparisons). Acc = accuracy, RT = response times, $CI_{95\%}$ = 95% confidence intervals.

Correlations in right MTLE patients			Age at inclusion	Age at epilepsy onset	Epilepsy duration	Number of antiepileptic drugs	Total IQ	Processing speed (percentile Coding test)
BFRT-c		Acc	r = -0.274, p = .185 $CI_{95\%}$ = -0.604/0.136	r = 0.285, p = .167 $CI_{95\%}$ = -0.124/0.611	r = -0.425, p = .034 $CI_{95\%}$ = -0.702/-0.036	r = 0.034, p = .872 $CI_{95\%}$ = -0.366/0.423	r = 0.454, p = .023 $CI_{95\%}$ = 0.072/0.720	r = 0.163, p = .436 $CI_{95\%}$ = -0.248/0.524
		RT	r = 0.476, p = .016 $CI_{95\%}$ = 0.099/0.733	r = 0.070, p = .739 $CI_{95\%}$ = -0.334/0.453	r = 0.340, p = .096 $CI_{95\%}$ = -0.064/0.648	r = 0.294, p = .154 $CI_{95\%}$ = -0.114/0.617	r = -0.478, p = .016 $CI_{95\%}$ = -0.734/-0.102	r = -0.512, p = .009 $CI_{95\%}$ = -0.754/-0.146
Delayed Matching Task	Cars	Acc Up	**r = -0.563, p = .003 $CI_{95\%}$ = -0.784/-0.216**	r = 0.159, p = .448 $CI_{95\%}$ = -0.252/0.521	**r = -0.569, p = .003 $CI_{95\%}$ = -0.787/-0.224**	r = 0.140, p = .504 $CI_{95\%}$ = -0.270/0.507	r = 0.197, p = .345 $CI_{95\%}$ = -0.215/0.549	r = -0.077, p = .714 $CI_{95\%}$ = -0.458/0.328
		Acc Inv	**r = -0.537, p = .006 $CI_{95\%}$ = -0.769/-0.180**	r = 0.277, p = .180 $CI_{95\%}$ = -0.133/0.606	**r = -0.636, p = .0006 $CI_{95\%}$ = -0.824/-0.322**	r = -0.345, p = .091 $CI_{95\%}$ = -0.651/0.058	**r = 0.400, p = .047 $CI_{95\%}$ = 0.006/0.687**	r = 0.309, p = .133 $CI_{95\%}$ = -0.098/0.627
		RT Up	**r = 0.650, p = .0004 $CI_{95\%}$ = 0.343/0.831**	r = -0.017, p = .936 $CI_{95\%}$ = -0.409/0.381	**r = 0.543, p = .005 $CI_{95\%}$ = 0.188/0.772**	r = 0.339, p = .097 $CI_{95\%}$ = -0.065/0.647	r = -0.256, p = .217 $CI_{95\%}$ = -0.763/-0.165	r = -0.382, p = .059 $CI_{95\%}$ = -0.675/0.015
		RT Inv	**r = 0.669, p = .0002 $CI_{95\%}$ = 0.372/0.842**	r = 0.005, p = .981 $CI_{95\%}$ = -0.391/0.399	**r = 0.544, p = .005 $CI_{95\%}$ = 0.190/0.773**	r = 0.313, p = .128 $CI_{95\%}$ = -0.094/0.630	r = -0.232, p = .256 $CI_{95\%}$ = -0.574/0.180	r = -0.385, p = .057 $CI_{95\%}$ = -0.677/0.012
		Index	r = 0.042, p = .842 $CI_{95\%}$ = -0.359/0.430	r = -0.152, p = .468 $CI_{95\%}$ = -0.516/0.259	r = 0.150, p = .474 $CI_{95\%}$ = -0.260/0.515	r = 0.066, p = .754 $CI_{95\%}$ = -0.338/0.449	r = -0.141, p = .501 $CI_{95\%}$ = -0.508/0.269	r = -0.153, p = .465 $CI_{95\%}$ = -0.517/0.258
	Faces	Acc Up	r = -0.328, p = .109 $CI_{95\%}$ = -0.640/0.077	r = 0.225, p = .279 $CI_{95\%}$ = -0.187/0.569	**r = -0.429, p = .032 $CI_{95\%}$ = -0.705/-0.041**	r = -0.185, p = .376 $CI_{95\%}$ = -0.541/0.227	**r = 0.668, p = .0003 $CI_{95\%}$ = 0.371/0.841**	**r = 0.413, p = .040 $CI_{95\%}$ = 0.021/0.695**
		Acc Inv	r = -0.260, p = .209 $CI_{95\%}$ = -0.594/0.151	r = 0.173, p = .408 $CI_{95\%}$ = -0.238/0.532	r = -0.333, p = .104 $CI_{95\%}$ = -0.643/0.071	r = -0.241, p = .546 $CI_{95\%}$ = -0.581/0.170	r = -0.016, p = .939 $CI_{95\%}$ = -0.408/0.381	r = 0.036, p = .864 $CI_{95\%}$ = -0.364/0.425
		RT Up	r = 0.382, p = .059 $CI_{95\%}$ = -0.015/0.675	r = 0.042, p = .842 $CI_{95\%}$ = -0.359/0.430	r = 0.281, p = .174 $CI_{95\%}$ = -0.128/0.608	r = 0.083, p = .693 $CI_{95\%}$ = -0.323/0.463	r = -0.238, p = .252 $CI_{95\%}$ = -0.579/0.173	r = -0.319, p = .120 $CI_{95\%}$ = -0.634/0.087
		RT Inv	**r = 0.432, p = .031 $CI_{95\%}$ = 0.044/0.706**	r = 0.051, p = .809 $CI_{95\%}$ = -0.351/0.437	r = 0.315, p = .125 $CI_{95\%}$ = -0.091/0.631	r = 0.185, p = .376 $CI_{95\%}$ = -0.227/0.541	r = -0.226, p = .277 $CI_{95\%}$ = -0.570/0.186	r = -0.326, p = .112 $CI_{95\%}$ = -0.639/0.079
		Index	r = -0.003, p = .989 $CI_{95\%}$ = -0.398/0.393	r = 0.065, p = .757 $CI_{95\%}$ = -0.339/0.449	r = 0.049, p = .816 $CI_{95\%}$ = -0.353/0.436	r = 0.244, p = .240 $CI_{95\%}$ = -0.167/0.583	**r = 0.408, p = .043 $CI_{95\%}$ = 0.015/0.692**	r = 0.234, p = .260 $CI_{95\%}$ = -0.177/0.576
CFMT Total		Acc	r = -0.181, p = .386 $CI_{95\%}$ = -0.560/0.260	r = -0.016, p = .939 $CI_{95\%}$ = -0.435/0.408	r = -0.141, p = .501 $CI_{95\%}$ = -0.531/0.298	r = -0.194, p = .353 $CI_{95\%}$ = -0.569/0.248	**r = 0.413, p = .040 $CI_{95\%}$ = -0.010/0.711**	r = 0.307, p = .135 $CI_{95\%}$ = -0.132/0.645

indexes: t = -0.390, p = .697 and t = 1.350, p = .189 for the comparison of the normative data with left and right MTLE patients, respectively; RT indexes: t = 1.445, p = .149 and t = -0.414, p = .682 for left and right MTLE patients, respectively).

Moreover, mean accuracy scores correlated negatively with mean RT in both left and right MTLE patients (r = -0.760, p < .001, and r = -0.793, p < .001, respectively), as well as in left and right NC (r = -0.864, p < .001, and r = -0.880, p < .001, respectively), indicating that items with the highest accuracy scores were also the ones with the shortest response times (see Figs. 2 and 3), as found in normative data (Rossion and Michel, 2018).

Finally, we calculated the inverse efficiency of each item for both patient and NC groups to take into consideration speed-accuracy trade-offs. This was done by dividing the RT by mean accuracy for each item in each group (Townsend and Ashby, 1978, 1983; see also Bruyer and Brysbaert, 2011). There was a strong positive correlation across items between patients and NC, for both left and right MTLE patients (r = 0.91, p < .001 and r = 0.90, p < .001, respectively), indicating that items that were better succeeded (high accuracy and low RT) in NC were also those that were better succeeded in MTLE patients (Fig. 4A and B). Results of both MTLE patient groups were also similar to the results of the large normative sample of 307 younger participants (Rossion and Michel, 2018) as shown by strong positive correlations between inverse efficiency scores of left MTLE and normative data (r = 0.90, p < .001), and right MTLE and normative data (r = 0.97, p < .001) (Fig. 4C). Altogether, these results show that MTLE patients do not differ qualitatively from normal controls at unfamiliar face individuation.

4. Discussion

The present study is the first to systematically assess a range of face and non-face recognition abilities in patients presenting with left or right MTLE. Our main findings are that: (1) MTLE patients present with famous face identification and learning difficulties, in line with previous

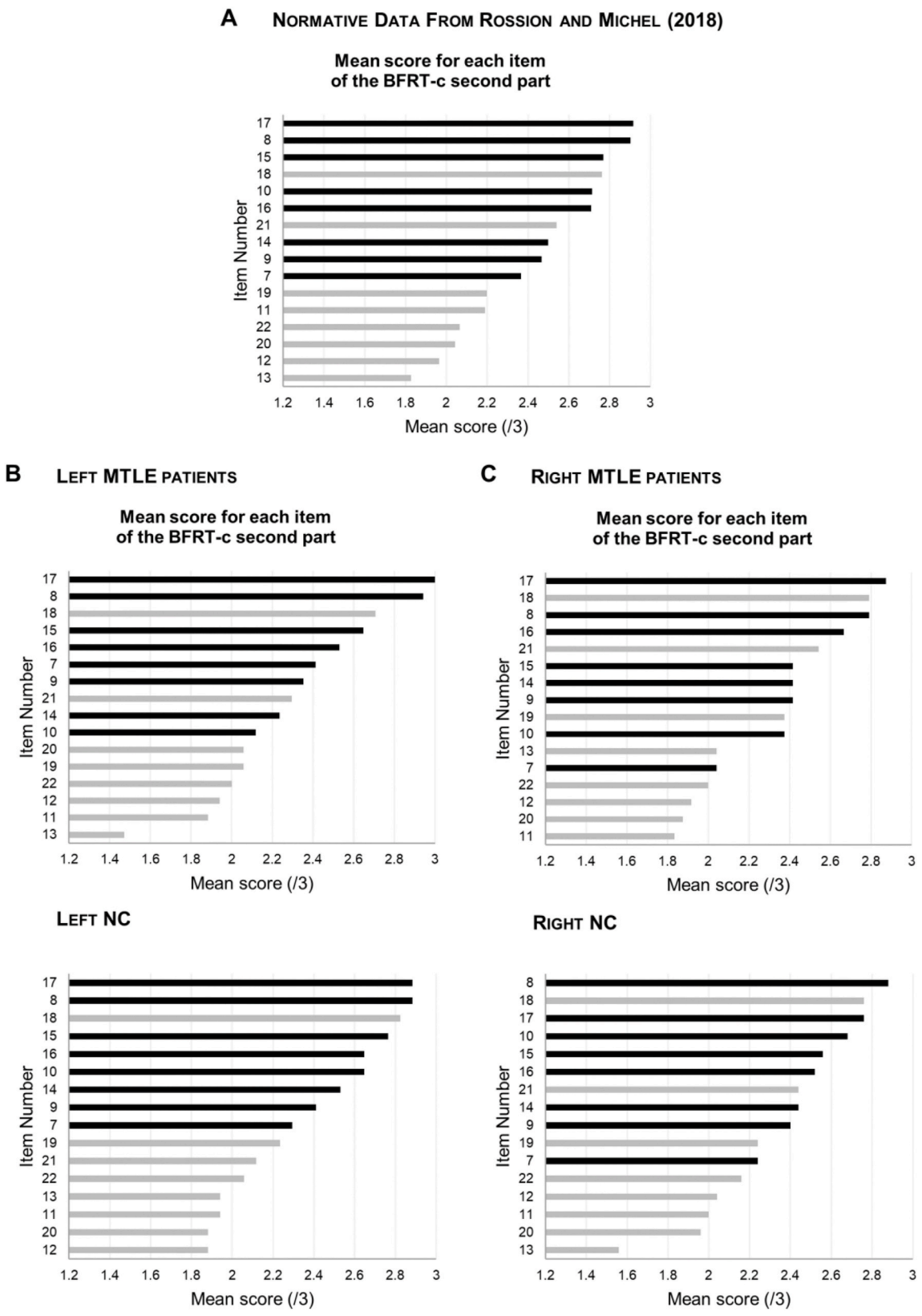

Fig. 2. Mean accuracy scores per item of the second part of the BFRT-c. Items are ordered from the highest to the lowest score. Light gray represents LD items, dark gray represents HR items. **A.** Normative data on 307 young adult participants from Rossion and Michel (2018). **B.** Mean accuracy scores per item in the left MTLE patients and their matched NC. **C.** Mean accuracy scores per item in the right MTLE patients and in their matched NC.

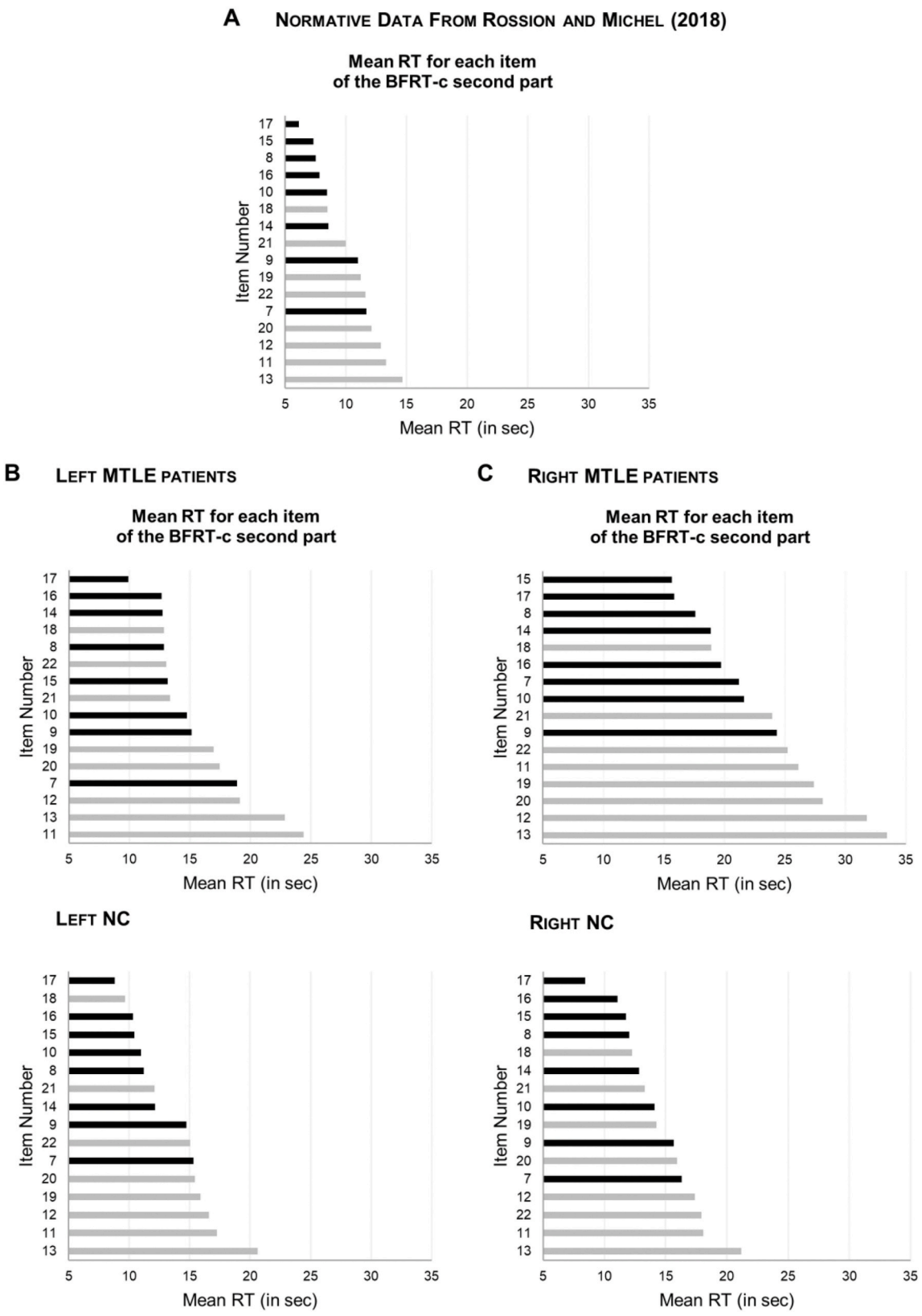

Fig. 3. Mean response times per item of the second part of the BFRT-c. Items are shown from the fastest to the slowest RT. Light gray represents LD items, dark gray represents HR items. **A.** Normative data on 307 young adult participants from Rossion and Michel (2018). **B.** Mean RT per item in the left MTLE patients and their matched NC. **C.** Mean RT per item in the right MTLE patients and in their matched NC.

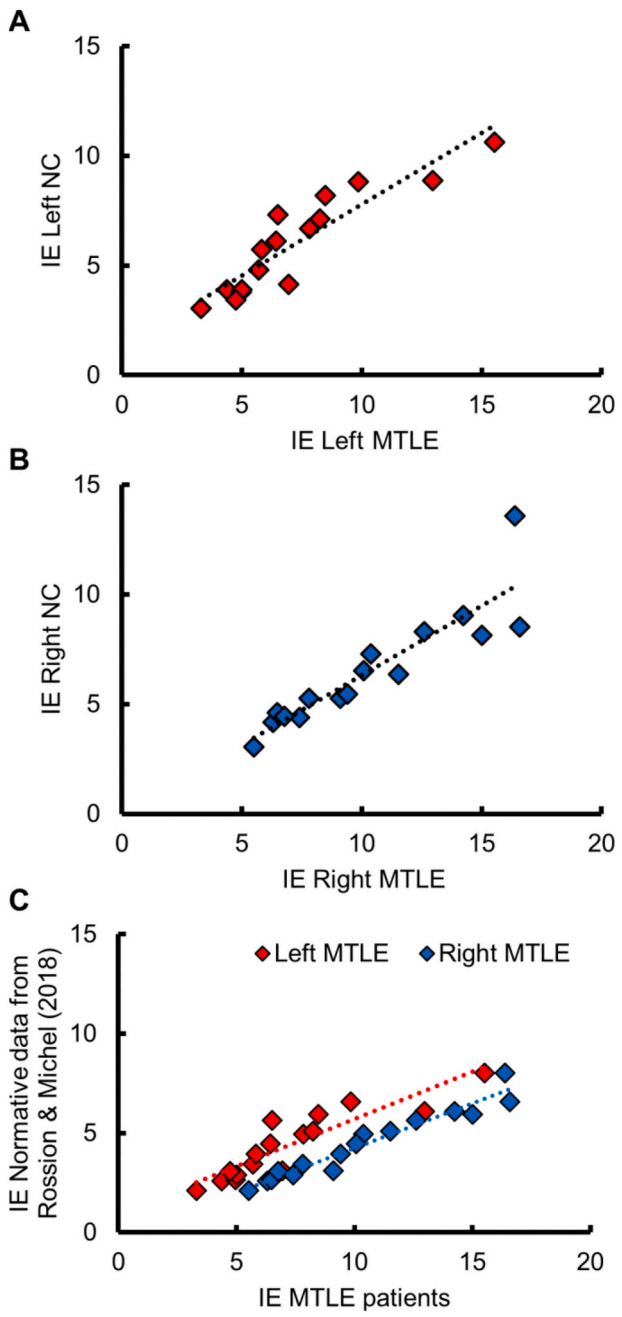

Fig. 4. Correlations of inverse efficiency scores for each item of the second part of the BFRT-c. Each data point represents one of the 16 items of the second part of the BFRT-c. **A.** Correlation between inverse efficiency scores of left MTLE and their respective NC. **B.** Correlation between inverse efficiency scores of right MTLE and their respective NC. **C.** Correlation between inverse efficiency scores of left and right MTLE and inverse efficiency scores of 307 neurotypical participants from the normative data in Rossion and Michel (2018). IE = inverse efficiency.

evidence (Chiaravalloti and Glosser, 2004; Drane et al., 2008, 2013); (2) despite this, left and right MTLE patient groups do not differ on accuracy scores at unfamiliar face individuation tasks compared to their respective NC groups; (3) MTLE patients do not differ qualitatively from NC at unfamiliar face individuation; and (4) right MTLE patients show a general increase of RT in all tasks, suggesting a slowdown at explicit behavioral tasks for visual material, unspecific to unfamiliar face individuation.

4.1. Unfamiliar face individuation is preserved in MTLE patients

The most important and original finding of our study is that at the group level both left and right MTLE patients do not differ in accuracy compared to their NC on unfamiliar face and non-face individuation tasks (BFRT-c, CFMT, and delayed face and car matching task). Importantly, there was no difference in accuracy between patient and NC groups on the two most widely used neuropsychological tests to investigate face recognition in the scientific literature, i.e. the BFRT and CFMT (Benton et al., 1983; Duchaine and Nakayama, 2006). Only a significant 4% decrease in accuracy at matching upright faces was found in right MTLE patients at the delayed matching task. However: (1) this decrease, even if it is significant, remains very small (91.32% of correct responses in right NC compared to 86.79% in right MTLE patients), (2) it may be due to the nature of a task that, contrary to the BFRT-c, requires to hold individual face representations in memory for 1000 ms, and (3) total IQ might play a role in this small decrease, knowing that we found a strong positive correlation between IQ and accuracy at matching upright faces in right MTLE patients and that these patients had a mean IQ 10 points lower than left MTLE patients (even though the difference was not significant).

Although patient and NC groups did not differ on accuracy scores at the group level, some of the scores were correlated across individuals with clinical and demographic characteristics (Tables 3 and 4). In right MTLE patients, both the upright face matching and the BFRT-c accuracy scores were negatively correlated with epilepsy duration, suggesting that a slightly lower performance at these two face individuation tasks in some individuals could be associated with a longer epilepsy duration. More generally, total IQ was positively correlated with several scores in both left (delayed matching with upright and inverted faces) and right (BFRT-c, delayed matching with upright faces and inverted cars, face inversion index, CFMT) MTLE patients, suggesting that their performance may be related to difficulties to understand the instructions of explicit behavioral tasks.

4.2. MTLE patients do not differ qualitatively from normal controls

In the delayed face and car matching task, MTLE patients showed a classical face inversion effect (i.e. lower accuracy and higher RT for inverted faces compared to upright faces) with the same magnitude as their NC (similar index of face inversion effect between MTLE patients and their NC). Face inversion is known to dramatically affect behavioral individuation of faces in neurotypical human adults (Yin, 1969; Freire et al., 2000; see Rossion, 2008 for review) and this effect is abolished in brain-damaged prosopagnosic patients (as reviewed in Busigny and Rossion, 2010). A preserved face inversion effect in left and right MTLE patients therefore provides strong evidence that this clinical population is not qualitatively impaired at unfamiliar face individuation. Moreover, the magnitude of the face inversion effect was higher than for non-face stimuli, as is also observed in neurotypical human adults (Busigny and Rossion, 2010; Rossion and Curran, 2010).

We further explored potential qualitative differences using the BFRT-c data. The normative study of Rossion and Michel (2018) showed higher accuracy and lower RT on HR items than on LD items. However, the well-known prosopagnosic patient PS, although she achieved a borderline score of 39/54 (Busigny and Rossion, 2010), showed almost no advantage for HR items compared to LD items at the BFRT-c (Liu-Shuang et al., 2016; Rossion and Michel, 2018). Importantly, the same profile as in normative data was found here in left and right MTLE as well as in their respective NC. Moreover, items that were better performed (high accuracy and low RT) by MTLE patients were also those that were better performed by their respective NC and by the normative population (N = 307, Rossion and Michel, 2018).

4.3. Semantic and episodic memory in MTLE patients

As in previous studies, we found that MTLE patients had lower performance at famous face recognition compared to normal controls (Seidenberg et al., 2002; Viskontas et al., 2002; Glosser et al., 2003; Griffith et al., 2006). Specifically, left MTLE patients were impaired at naming famous faces while right MTLE patients were impaired at explicitly recognizing famous faces (i.e. both by naming and providing semantic information from a face), consistently with previous studies (Drane et al., 2008, 2013). Since the very same patients were not impaired at individuating unfamiliar faces, their famous face recognition deficit does not appear to be due to visual face individuation, but rather to semantic memory impairment. This hypothesis is consistent with the functions of the ventral anterior and polar temporal cortex, which is affected in MTLE (Maillard et al., 2004). Numerous neuroimaging and lesion studies have provided evidence for a strong involvement of the bilateral ventral anterior temporal cortex and temporal pole in semantic processing (Rice et al., 2015, 2018; Hoffman and Lambon Ralph, 2018). In particular, lesion studies (in patients after surgical resection of the anterior temporal lobe or presenting with a neurodegenerative disease such as semantic dementia) found relative differences in semantic performance depending on the side of the lesion (Snowden et al., 2004, 2012; Butler et al., 2009, Rice et al., 2018a). Damage to the left ventral anterior and polar temporal regions has been shown to cause relatively more difficulties with verbal semantic processing (as naming) while damage to the right ventral anterior and polar temporal regions leads to more relative difficulties with non-verbal semantics (as recognizing famous faces). The differential involvement of left and right anterior temporal lobes in semantics is consistent with our results showing greater difficulties at naming famous faces in left MTLE patients and greater difficulties at explicitly recognizing famous faces in right MTLE patients.

Interestingly, we also found that both left and right MTLE patients had lower performance (around 10% less in accuracy compared to NC) at explicitly encoding and retrieving visual items. This decrease in performance affected both face and non-face (birds) items, showing that this impairment was not specific to faces. These results are consistent with well-known visual episodic memory deficits in this population (Helmstaedter, 2013; Brissart et al., 2018; Ono et al., 2019), related to dysfunctions of the hippocampus and rhinal cortex, which are always affected (to a greater or lesser extent) in MTLE. Moreover, the fact that both left and right MTLE patients present with visual learning difficulties is consistent with the view that there is no strict relationship between the lateralization of the epileptogenic focus and the performance at memorizing visual information (Lee et al., 2002; Saling, 2009).

4.4. Response times increase in right MTLE patients

Right MTLE patients showed a general increase of RT in virtually all tasks that were tested in the present study. RT is an important variable to consider in individual face matching tasks, as it may reveal impairments beyond accuracy measures, for instance in patients with prosopagnosia (Davidoff and Landis, 1990; Farah, 1990; Delvenne et al., 2004). However, and importantly, RT increases in right MTLE patients in the present study were not specific to the type of stimuli (increase in RT for face and non-face items) or to the task (increase in RT for detection, individuation, and learning tasks). Right MTLE patients were also slowed down compared to left MTLE patients at a simple visuospatial task, evaluating general processing speed. Specifically for the BFRT-c, the performance on the Coding test was negatively correlated with the RT at this task, suggesting that the slowing down of right MTLE patients at the BFRT-c was partly related to a general slowing down in visuospatial processing speed rather than to difficulties at individuating unfamiliar faces. This is supported by the fact that the Coding test was not correlated with the RT on other face or non-face individuation tasks that require less visuospatial processing compared to the BFRT-c (2 images to explore in the delayed matching task, 3 in the CFMT, as compared to 6 in the BFRT-c).

Overall, our observations suggest that the general increase of RT in right MTLE patients does not reflect impairment at unfamiliar face individuation *per se* but rather a general slowdown at all visual tasks, related to the right hemispheric lateralization of epilepsy. Cerebral asymmetry in RT in brain-damaged populations has been previously demonstrated (see Benton, 1986). A plausible explanation for this asymmetry relies on the more prominent role of the right hemisphere in sustaining visuospatial attention. According to this hypothesis, the right hemisphere has a crucial role in maintaining directed attention towards a task (Heilman and Van Den Abell, 1979; Mesulam, 1981; Whitehead, 1991; Thiebaut de Schotten et al., 2011), and right-lateralized damage is thus more susceptible to cause attentional deficits (Mesulam, 1981). Consistently, early studies have shown that patients with right-lateralized lesions had increased RT on simple visual reaction tasks (e.g., pressing a button when a light appeared) compared to patients with left-lateralized lesions (Arrigoni and De Renzi, 1964; De Renzi and Faglioni, 1965; see Benton, 1986).

Another possibility to explain the slower RT of right MTLE patients is related to intellectual efficiency. Although the difference was not significant, right MTLE patients exhibited on average a 10 points lower total IQ than left MTLE patients, which could be of importance when understanding instructions of the tasks and responding appropriately to them. This is in line with numerous studies showing a strong association between processing speed and intellectual efficiency and indicating that lower IQ scores are associated with longer response times during simple reaction tasks or choice reaction tasks (Deary et al., 2001; Schweizer, 2001; Jensen, 2006; Sheppard and Vernon, 2008; see also Frischkorn et al., 2019). Hence, the general slowing-down observed in our population of right MTLE patients could be related to an alteration of visuospatial attentional networks or to more general cognitive factors (i.e. as measured by the IQ score; see Table 4) rather than visual face individuation processing *per se*.

A promising avenue to clarify this issue with MTLE patients in future studies is the use of implicit measures of face individuation, as provided by EEG frequency tagging (Norcia et al., 2015). In particular, sensitive and objective measures of unfamiliar face individuation can be obtained in a few minutes of testing with an oddball paradigm (Liu-Shuang et al., 2014; reviewed in Rossion et al., 2020) showing high test-retest reliability (Dzhelyova et al., 2019) and specific sensitivity to severe impairment in face identity recognition (i.e. prosopagnosia, Liu-Shuang et al., 2016). If the slowing down of right MTLE patients is not specific to visual individuation of faces *per se*, this population should present with typical frequency-tagged EEG responses in this paradigm.

4.5. The validity of iEEG recordings to understand visual face recognition

Over the last decade, iEEG recordings (either with subdural electrodes in electrocorticography, or with depth intracerebral electrodes in SEEG) in patients with epilepsy have become increasingly used to understand the neural basis of face recognition, and in particular the mechanisms of visual face individuation (Allison et al., 1999; Davidesco et al., 2014; Engell and McCarthy, 2014; Ghuman et al., 2014; Jonas et al., 2016; Kadipasaoglu et al., 2016; Hagen et al., 2020; Jacques et al., 2020; Rangarajan et al., 2020). Since iEEG recordings are performed in patients with drug-resistant epilepsy and MTLE is the most frequent focal epilepsy referred for epilepsy surgery (Schuele and Lüders, 2008; Spencer and Huh, 2008; see also Ladino et al., 2014), MTLE patients are the most included patients in iEEG studies. Therefore, it is legitimate to ask whether iEEG recordings in epileptic patients provide a valid model to understand normal face recognition (Rossion et al., 2018). Several sources of evidence provide support for the validity of human iEEG to inform about normal visual face individuation. For example, despite mixed evidence of general decreases of neuroimaging signal in some regions (Riley et al., 2015), MTLE patients appear to show a typical localization of posterior cortical face-selective activations in fMRI

(Jacques et al., 2016; Weiner et al., 2016). Moreover, in this population, the largest face-selective responses in iEEG are found in the lateral section of the right middle fusiform gyrus (Jonas et al., 2016; Hagen et al., 2020), as in typical brains in fMRI (Kanwisher et al., 1997). The present behavioral study significantly adds to these sources of evidence by showing that left and right MTLE patients have normal quantitative and qualitative performance at individuating unfamiliar faces, suggesting that these patients present with a typical neurofunctional organization of face individuation.

Funding

The work is supported by the University Hospital of Nancy in France, and the first author, AV, is supported by a doctoral grant from the MESRI, also in France.

Declarations of interest

None.

CRediT authorship contribution statement

Angélique Volfart: Data curation, Formal analysis, Methodology, Visualization, Writing - original draft, Writing - review & editing. **Jacques Jonas:** Conceptualization, Funding acquisition, Investigation, Supervision, Writing - original draft, Writing - review & editing. **Louis Maillard:** Funding acquisition, Investigation, Writing - original draft. **Thomas Busigny:** Conceptualization, Methodology. **Bruno Rossion:** Conceptualization, Funding acquisition, Supervision, Writing - original draft, Writing - review & editing. **Hélène Brissart:** Conceptualization, Data curation, Supervision, Writing - original draft.

Acknowlegdments

We thank Julie Gamper, Mylène Romilly, Marion Beringer, Clémentine Castro, Hélène Romary, Natacha Forthoffer for their help in data collection, and Justine David for her help with the item-by-item analysis.

References

Allison, T., Puce, A., Spencer, D.D., McCarthy, G., 1999. Electrophysiological studies of human face perception. I: potentials generated in occipitotemporal cortex by face and non-face stimuli. Cerebr. Cortex 9, 415–430.
Arrigoni, G., De Renzi, E., 1964. Constructional apraxia and hemispheric locus of lesion. Cortex 1, 170–197.
Barton, J.J.S., 2008. Structure and function in acquired prosopagnosia: lessons from a series of 10 patients with brain damage. J. Neuropsychol. 2, 197–225.
Benton, A., 1986. Reaction time in brain disease: some reflections. Cortex 22, 129–140.
Benton, A.L., Sivan, A.B., Hamsher, K., Varney, N.R., Spreen, O., 1983. Benton Facial Recognition: Stimulus and Multiple Choice Pictures. Psychological Assessment Resources Inc. Lutz, FL.
Benton, A.L., Van Allen, M.W., 1968. Impairment in facial recognition in patients with cerebral disease. Cortex 4 (4), 344–358.
Benton, A.L., Van Allen, M.W., 1972. Prosopagnosia and facial discrimination. J. Neurol. Sci. 15, 167–172.
Brambati, S.M., Benoit, S., Monetta, L., Belleville, S., Joubert, S., 2010. The role of the left anterior temporal lobe in the semantic processing of famous faces. Neuroimage 53, 674–681.
Brissart, H., Volfart, A., Forthoffer, N., 2018. Les troubles cognitifs des patients épileptiques. Neuropsychologie des épilepsies de l'adulte: Approche clinique et pratique. De Boeck Supérieur, pp. 32–59.
Brotis, A.G., Giannis, T., Kapsalaki, E., Dardiotis, E., Fountas, K.N., 2019. Complications after anterior temporal lobectomy for medically intractable epilepsy: a systematic review and meta-analysis. Stereotact. Funct. Neurosurg. 97, 69–82.
Bruyer, R., Brysbaert, M., 2011. Combining speed and accuracy in cognitive psychology: is the inverse efficiency score (IES) a better dependent variable than the mean reaction time (RT) and the percentage of errors (PE)? Psychol. Belg. 51, 5–13.
Busigny, T., Joubert, S., Felician, O., Ceccaldi, M., Rossion, B., 2010. Holistic perception of the individual face is specific and necessary: evidence from an extensive case study of acquired prosopagnosia. Neuropsychologia 48, 4057–4092.
Busigny, T., Prairial, C., Nootens, J., Kindt, V., Engels, S., Verplancke, S., et al., 2014. CELEB : une batterie d'évaluation de la reconnaissance des visages célèbres et de l'accès aux noms propres. Rev. Neuropsychol. 6, 69–81.
Busigny, T., Rossion, B., 2010. Acquired prosopagnosia abolishes the face inversion effect. Cortex 46, 965–981.
Butler, C.R., Brambati, S.M., Miller, B.L., Gorno-Tempini, M.-L., 2009. The neural correlates of verbal and nonverbal semantic processing deficits in neurodegenerative disease. Cognit. Behav. Neurol. 22, 73–80.
Chelune, G.J., 1995. Hippocampal adequacy versus functional reserve: predicting memory functions following temporal lobectomy. Arch. Clin. Neuropsychol. 10, 413–432.
Chiaravalloti, N.D., Glosser, G., 2004. Memory for faces dissociates from memory for location following anterior temporal lobectomy. Brain Cognit. 54, 35–42.
Davidesco, I., Zion-Golumbic, E., Bickel, S., Harel, M., Groppe, D.M., Keller, C.J., et al., 2014. Exemplar selectivity reflects perceptual similarities in the human fusiform cortex. Cerebr. Cortex 24, 1879–1893.
Davidoff, J., Landis, T., 1990. Recognition of unfamiliar faces in prosopagnosia. Neuropsychologia 28, 1143–1161.
Davies-Thompson, J., Gouws, A., Andrews, T.J., 2009. An image-dependent representation of familiar and unfamiliar faces in the human ventral stream. Neuropsychologia 47, 1627–1635.
De Renzi, E., Faglioni, P., 1965. The comparative efficiency of intelligence and vigilance tests in detecting hemispheric cerebral damage. Cortex 1, 410–433.
Deary, I.J., Der, G., Ford, G., 2001. Reaction times and intelligence differences: a population-based cohort study. Intelligence 29, 389–399.
Delvenne, J.-F., Seron, X., Coyette, F., Rossion, B., 2004. Evidence for perceptual deficits in associative visual (prosop)agnosia: a single-case study. Neuropsychologia 42, 597–612.
Drane, D.L., Ojemann, G.A., Aylward, E., Ojemann, J.G., Johnson, L.C., Silbergeld, D.L., et al., 2008. Category-specific naming and recognition deficits in temporal lobe epilepsy surgical patients. Neuropsychologia 46, 1242–1255.
Drane, D.L., Ojemann, J.G., Phatak, V., Loring, D.W., Gross, R.E., Hebb, A.O., et al., 2013. Famous face identification in temporal lobe epilepsy: support for a multimodal integration model of semantic memory. Cortex 49, 1648–1667.
Duchaine, B., Yovel, G., 2015. A revised neural framework for face processing. Annu Rev Vis Sci 1, 393–416.
Duchaine, B.C., Nakayama, K., 2006. The Cambridge Face Memory Test: results for neurologically intact individuals and an investigation of its validity using inverted face stimuli and prosopagnosic participants. Neuropsychologia 44, 576–585.
Dzhelyova, M., Jacques, C., Dormal, G., Michel, C., Schiltz, C., Rossion, B., 2019. High test-retest reliability of a neural index of rapid automatic discrimination of unfamiliar individual faces. Vis. Cognit. 27, 127–141.
Elfgren, C., van Westen, D., Passant, U., Larsson, E.-M., Mannfolk, P., Fransson, P., 2006. fMRI activity in the medial temporal lobe during famous face processing. Neuroimage 30, 609–616.
Engell, A.D., McCarthy, G., 2014. Face, eye, and body selective responses in fusiform gyrus and adjacent cortex: an intracranial EEG study. Front. Hum. Neurosci. 8, 642.
Ewbank, M.P., Henson, R.N., Rowe, J.B., Stoyanova, R.S., Calder, A.J., 2013. Different neural mechanisms within occipitotemporal cortex underlie repetition suppression across same and different-size faces. Cerebr. Cortex 23, 1073–1084.
Farah, M.J., 1990. Visual Agnosia: Disorders of Object Recognition and what They Tell Us about Normal Vision. MIT Press, Cambridge, Massachusetts.
Fox, C.J., Iaria, G., Duchaine, B.C., Barton, J.J.S., 2013. Residual fMRI sensitivity for identity changes in acquired prosopagnosia. Front. Psychol. 4, 756.
Freire, A., Lee, K., Symons, L.A., 2000. The face-inversion effect as a deficit in the encoding of configural information: direct evidence. Perception 29, 159–170.
Frischkorn, G.T., Schubert, A.-L., Hagemann, D., 2019. Processing speed, working memory, and executive functions: independent or inter-related predictors of general intelligence. Intelligence 75, 95–110.
Gainotti, G., 2007. Different patterns of famous people recognition disorders in patients with right and left anterior temporal lesions: a systematic review. Neuropsychologia 45, 1591–1607.
Gauthier, I., Tarr, M.J., Moylan, J., Skudlarski, P., Gore, J.C., Anderson, A.W., 2000. The fusiform 'face area' is part of a network that processes faces at the individual level. J. Cognit. Neurosci. 12, 495–504.
Ghuman, A.S., Brunet, N.M., Li, Y., Konecky, R.O., Pyles, J.A., Walls, S.A., et al., 2014. Dynamic encoding of face information in the human fusiform gyrus. Nat. Commun. 5, 5672.
Glosser, G., Salvucci, A.E., Chiaravalloti, N.D., 2003. Naming and recognizing famous faces in temporal lobe epilepsy. Neurology 61, 81–86.
Gobbini, M.I., Haxby, J.V., 2007. Neural systems for recognition of familiar faces. Neuropsychologia 45, 32–41.
Gorno-Tempini, M.L., Price, C.J., 2001. Identification of famous faces and buildings: a functional neuroimaging study of semantically unique items. Brain 124, 2087–2097.
Gorno-Tempini, M.L., Price, C.J., Josephs, O., Vandenberghe, R., Cappa, S.F., Kapur, N., et al., 1998. The neural systems sustaining face and proper-name processing. Brain 121, 2103–2118.
Griffin, J.W., 2020. Quantifying the face inversion effect in nonhuman primates: a phylogenetic meta-analysis. Anim. Cognit. 23, 237–249.
Griffith, H.R., Richardson, E., Pyzalski, R.W., Bell, B., Dow, C., Hermann, B.P., et al., 2006. Memory for famous faces and the temporal pole: functional imaging findings in temporal lobe epilepsy. Epilepsy Behav. 9, 173–180.
Hagen, S., Jacques, C., Maillard, L.G., Colnat-Coulbois, S., Rossion, B., Jonas, J., 2020. Spatially dissociated intracerebral maps for face- and house-selective activity in the human ventral occipito-temporal cortex. Cerebr. Cortex 30 (7), 4026–4043.

Heilman, K.M., Van Den Abell, T., 1979. Right hemispheric dominance for mediating cerebral activation. Neuropsychologia 17, 315–321.
Helmstaedter, C., 2004. Neuropsychological aspects of epilepsy surgery. Epilepsy Behav. 5, 45–55.
Helmstaedter, C., 2013. Cognitive outcomes of different surgical approaches in temporal lobe epilepsy. Epileptic Disord. 15, 221–239.
Hermann, B.P., Seidenberg, M., Schoenfeld, J., Davies, K., 1997. Neuropsychological characteristics of the syndrome of mesial temporal lobe epilepsy. Arch. Neurol. 54, 369–376.
Hermann, P., Grotheer, M., Kovács, G., Vidnyánszky, Z., 2017. The relationship between repetition suppression and face perception. Brain Imaging Behav 11, 1018–1028.
Hoffman, P., Lambon Ralph, M.A., 2018. From percept to concept in the ventral temporal lobes: graded hemispheric specialisation based on stimulus and task. Cortex 101, 107–118.
Hughes, B.L., Camp, N.P., Gomez, J., Natu, V.S., Grill-Spector, K., Eberhardt, J.L., 2019. Neural adaptation to faces reveals racial outgroup homogeneity effects in early perception. Proc. Natl. Acad. Sci. Unit. States Am. 116, 14532–14537.
Jacques, C., Rossion, B., Volfart, A., Brissart, H., Colnat-Coulbois, S., Maillard, L., Jonas, J., 2020. The neural basis of rapid unfamiliar face individuation with human intracerebral recordings. Neuroimage 221, 117174.
Jacques, C., Witthoft, N., Weiner, K.S., Foster, B.L., Rangarajan, V., Hermes, D., et al., 2016. Corresponding ECoG and fMRI category-selective signals in human ventral temporal cortex. Neuropsychologia 83, 14–28.
Jensen, A.R., 2006. Clocking the Mind: Mental Chronometry and Individual Differences. Elsevier.
Jonas, J., Brissart, H., Hossu, G., Colnat-Coulbois, S., Vignal, J.-P., Rossion, B., et al., 2018. A face identity hallucination (palinopsia) generated by intracerebral stimulation of the face-selective right lateral fusiform cortex. Cortex 99, 296–310.
Jonas, J., Jacques, C., Liu-Shuang, J., Brissart, H., Colnat-Coulbois, S., Maillard, L., et al., 2016. A face-selective ventral occipito-temporal map of the human brain with intracerebral potentials. Proc. Natl. Acad. Sci. U. S. A. 113, 4088–4097.
Kadipasaoglu, C.M., Conner, C.R., Whaley, M.L., Baboyan, V.G., Tandon, N., 2016. Category-selectivity in human visual cortex follows cortical topology: a grouped icEEG study. PloS One 11, e0157109.
Kanwisher, N., McDermott, J., Chun, M.M., 1997. The fusiform face area: a module in human extrastriate cortex specialized for face perception. J. Neurosci. 17, 4302–4311.
Ladino, L.D., Moien-Afshari, F., Téllez-Zenteno, J.F., 2014. A comprehensive review of temporal lobe epilepsy. In: neurological Disorders. Clinical Methods. iConcept Press 1–35.
Lambon Ralph, M.A., Ehsan, S., Baker, G.A., Rogers, T.T., 2012. Semantic memory is impaired in patients with unilateral anterior temporal lobe resection for temporal lobe epilepsy. Brain 135, 242–258.
Lee, T.M.C., Yip, J.T.H., Jones-Gotman, M., 2002. Memory deficits after resection from left or right anterior temporal lobe in humans: a meta-analytic review. Epilepsia 43, 283–291.
Leveroni, C.L., Seidenberg, M., Mayer, A.R., Mead, L.A., Binder, J.R., Rao, S.M., 2000. Neural systems underlying the recognition of familiar and newly learned faces. J. Neurosci. 20, 878–886.
Liu-Shuang, J., Norcia, A.M., Rossion, B., 2014. An objective index of individual face discrimination in the right occipito-temporal cortex by means of fast periodic oddball stimulation. Neuropsychologia 52, 57–72.
Liu-Shuang, J., Torfs, K., Rossion, B., 2016. An objective electrophysiological marker of face individualisation impairment in acquired prosopagnosia with fast periodic visual stimulation. Neuropsychologia 83, 100–113.
Luzzi, S., Baldinelli, S., Ranaldi, V., Fabi, K., Cafazzo, V., Fringuelli, F., et al., 2017. Famous faces and voices: differential profiles in early right and left semantic dementia and in Alzheimer's disease. Neuropsychologia 94, 118–128.
Maillard, L., Vignal, J.-P., Gavaret, M., Guye, M., Biraben, A., McGonigal, A., et al., 2004. Semiologic and electrophysiologic correlations in temporal lobe seizure subtypes. Epilepsia 45, 1590–1599.
Mesulam, M.-M., 1981. A cortical network for directed attention and unilateral neglect. Ann. Neurol. 10, 309–325.
Milner, B., 1968. Visual recognition and recall after right temporal-lobe excision in man. Neuropsychologia 6, 191–209.
Mooney, C.M., 1957. Age in the development of closure ability in children. Can. J. Psychol. 11, 219–226.
Moore, C., Cavanagh, P., 1998. Recovery of 3D volume from 2-tone images of novel objects. Cognition 67, 45–71.
Natu, V., O'Toole, A.J., 2011. The neural processing of familiar and unfamiliar faces: a review and synopsis: neural correlates of familiar and unfamiliar face perception. Br. J. Psychol. 102, 726–747.
Norcia, A.M., Appelbaum, L.G., Ales, J.M., Cottereau, B.R., Rossion, B., 2015. The steady-state visual evoked potential in vision research: a review. J. Vis. 15, 4.
Oldfield, R.C., 1971. The assessment and analysis of handedness: the Edinburgh inventory. Neuropsychologia 9, 97–113.
Ono, S.E., de Carvalho Neto, A., Joaquim, M.J.M., dos Santos, G.R., de Paola, L., Silvado, C.E.S., 2019. Mesial temporal lobe epilepsy: revisiting the relation of hippocampal volumetry with memory deficits. Epilepsy Behav. 100, 106516.
Pal, S., Sengupta, P., Ghosal, M., Pal, A., Acharya, R., Biswas, D., 2019. Storage, degradation, and new connectivity of face-related semantic memory in Alzheimer's Disease. Ann. Indian Acad. Neurol. 22, 170–174.
Papagno, C., Mattavelli, G., Casarotti, A., Bello, L., Gainotti, G., 2017. Defective recognition and naming of famous people from voice in patients with unilateral temporal lobe tumours. Neuropsychologia 116, 194–204.
Potter, J.L., Schefft, B.K., Beebe, D.W., Howe, S.R., Yeh, H., Privitera, M.D., 2009. Presurgical neuropsychological testing predicts cognitive and seizure outcomes after anterior temporal lobectomy. Epilepsy Behav. 16, 246–253.
Pozueta, A., Lage, C., García-Martínez, M., Kazimierczak, M., Bravo, M., López-García, S., et al., 2019. Cognitive and behavioral profiles of left and right semantic dementia: differential diagnosis with behavioral variant frontotemporal dementia and Alzheimer's disease. J Alzheimers Dis 72, 1129–1144.
Ramon, M., Vizioli, L., Liu-Shuang, J., Rossion, B., 2015. Neural microgenesis of personally familiar face recognition. Proc. Natl. Acad. Sci. U. S. A. 112, 4835–4844.
Rangarajan, V., Jacques, C., Knight, R.T., Weiner, K.S., Grill-Spector, K., 2020. Diverse temporal dynamics of repetition suppression revealed by intracranial recordings in human ventral temporal cortex. Cerebr. Cortex, bhaa173.
Rice, G.E., Caswell, H., Moore, P., Hoffman, P., Lambon Ralph, M.A., 2018a. The roles of left versus right anterior temporal lobes in semantic memory: a neuropsychological comparison of postsurgical temporal lobe epilepsy patients. Cerebr. Cortex 28 (4), 1487–1501.
Rice, G.E., Hoffman, P., Binney, R.J., Lambon Ralph, M.A., 2018b. Concrete versus abstract forms of social concept: an fMRI comparison of knowledge about people versus social terms. Philos Trans R Soc B Biol Sci 373, 20170136.
Rice, G.E., Lambon Ralph, M.A., Hoffman, P., 2015. The roles of left versus right anterior temporal lobes in conceptual knowledge: an ALE meta-analysis of 97 functional neuroimaging studies. Cerebr. Cortex 25, 4374–4391.
Riley, J.D., Fling, B.W., Cramer, S.C., Lin, J.J., 2015. Altered organization of face-processing networks in temporal lobe epilepsy. Epilepsia 56, 762–771.
Ross, L.A., Olson, I.R., 2012. What's unique about unique entities? An fMRI investigation of the semantics of famous faces and landmarks. Cerebr. Cortex 22 (9), 2005–2015.
Rossion, B., 2008. Picture-plane inversion leads to qualitative changes of face perception. Acta Psychol. 128, 274–289.
Rossion, B., 2018. Humans are visual experts at unfamiliar face recognition. Trends Cognit. Sci. 22, 471–472.
Rossion, B., Curran, T., 2010. Visual expertise with pictures of cars correlates with RT magnitude of the car inversion effect. Perception 39, 173–183.
Rossion, B., Dricot, L., Goebel, R., Busigny, T., 2011. Holistic face categorization in higher-level cortical visual areas of the normal and prosopagnosic brain: towards a non-hierarchical view of face perception. Front. Hum. Neurosci. 4, 225.
Rossion, B., Jacques, C., Jonas, J., 2018. Mapping face categorization in the human ventral occipitotemporal cortex with direct neural intracranial recordings. Ann. N. Y. Acad. Sci. 1426 (1), 5–24.
Rossion, B., Michel, C., 2018. Normative accuracy and response time data for the computerized Benton Facial Recognition Test (BFRT-c). Behav. Res. Methods 50, 2442–2460.
Rossion, B., Retter, T., Liu-Shuang, J., 2020. Understanding human individuation of unfamiliar faces with oddball fast periodic visual stimulation and electroencephalography. Eur JNeurosci. https://doi.org/10.1111/ejn.14865.
Rossion, B., Taubert, J., 2019. What can we learn about human individual face recognition from experimental studies in monkeys? Vis. Res. 157, 142–158.
Rostalski, S.-M., Amado, C., Kovács, G., Feuerriegel, D., 2019. Measures of repetition suppression in the Fusiform Face Area are inflated by co-occurring effects of statistically learned visual associations. bioRxiv 803163.
Saling, M.M., 2009. Verbal memory in mesial temporal lobe epilepsy: beyond material specificity. Brain 132, 570–582.
Schiltz, C., Sorger, B., Caldara, R., Ahmed, F., Mayer, E., Goebel, R., et al., 2006. Impaired face discrimination in acquired prosopagnosia is associated with abnormal response to individual faces in the right middle fusiform gyrus. Cerebr. Cortex 16, 574–586.
Schuele, S.U., Lüders, H.O., 2008. Intractable epilepsy: management and therapeutic alternatives. Lancet Neurol. 7, 514–524.
Schweizer, K., 2001. Preattentive processing and cognitive ability. Intelligence 29, 169–186.
Seidenberg, M., Griffith, R., Sabsevitz, D., Moran, M., Haltiner, A., Bell, B., et al., 2002. Recognition and identification of famous faces in patients with unilateral temporal lobe epilepsy. Neuropsychologia 40, 446–456.
Seidenberg, M., Hermann, B., Wyler, A.R., Davies, K., Dohan, F.C., Leveroni, C., 1998. Neuropsychological outcome following anterior temporal lobectomy in patients with and without the syndrome of mesial temporal lobe epilepsy. Neuropsychology 12, 303–316.
Sergent, J., Ohta, S., MacDonald, B., 1992. Functional neuroanatomy of face and object processing: a positron emission tomography study. Brain 115, 15–36.
Sheppard, L.D., Vernon, P.A., 2008. Intelligence and speed of information-processing: a review of 50 years of research. Pers. Indiv. Differ. 44, 535–551.
Sherman, E.M.S., Wiebe, S., Fay-McClymont, T.B., Tellez-Zenteno, J., Metcalfe, A., Hernandez-Ronquillo, L., et al., 2011. Neuropsychological outcomes after epilepsy surgery: systematic review and pooled estimates. Epilepsia 52, 857–869.
Snowden, J.S., Thompson, J.C., Neary, D., 2004. Knowledge of famous faces and names in semantic dementia. Brain 127, 860–872.
Snowden, J.S., Thompson, J.C., Neary, D., 2012. Famous people knowledge and the right and left temporal lobes. Behav. Neurol. 25, 35–44.
Spencer, S., Huh, L., 2008. Outcomes of epilepsy surgery in adults and children. Lancet Neurol. 7, 525–537.
Sugiura, M., Mano, Y., Sasaki, A., Sadato, N., 2011. Beyond the memory mechanism: person-selective and nonselective processes in recognition of personally familiar faces. J. Cognit. Neurosci. 23, 699–715.
Tatum, W.O., 2012. Mesial temporal lobe epilepsy. J. Clin. Neurophysiol. 29, 10.
Thiebaut de Schotten, M., Dell'Acqua, F., Forkel, S.J., Simmons, A., Vergani, F., Murphy, D.G.M., et al., 2011. A lateralized brain network for visuospatial attention. Nat. Neurosci. 14, 1245–1246.

Tippett, L.J., Blackwood, K., Farah, M.J., 2003. Visual object and face processing in mild-to-moderate Alzheimer's disease: from segmentation to imagination. Neuropsychologia 41, 453–468.
Townsend, J.T., Ashby, F.G., 1978. Methods of modeling capacity in simple processing systems. In: Castellan, N.J., Restle, F. (Eds.), Cognitive Theory. Lawrence Erlbaum Associates, Hillsdale, New Jersey, pp. 199–239.
Townsend, J.T., Ashby, F.G., 1983. The Stochastic Modeling of Elementary Psychological Processes. Cambridge University Press.
Valentine, T., Powell, J., Davidoff, J., Letson, S., Greenwood, R., 2006. Prevalence and correlates of face recognition impairments after acquired brain injury. Neuropsychol. Rehabil. 16, 272–297.
Viskontas, I.V., McAndrews, M.P., Moscovitch, M., 2002. Memory for famous people in patients with unilateral temporal lobe epilepsy and excisions. Neuropsychology 16, 472–480.
Von Der Heide, R.J., Skipper, L.M., Olson, I.R., 2013. Anterior temporal face patches: a meta-analysis and empirical study. Front. Hum. Neurosci. 7, 17.
Weiner, K.S., Jonas, J., Gomez, J., Maillard, L., Brissart, H., Hossu, G., et al., 2016. The face-processing network is resilient to focal resection of human visual cortex. J. Neurosci. 36, 8425–8440.
Whitehead, R., 1991. Right hemisphere processing superiority during sustained visual attention. J. Cognit. Neurosci. 3, 329–334.
Yin, R.K., 1969. Looking at upside-down faces. J. Exp. Psychol. 81, 141–145.